Modelling Climate Changes, Biogenic Emissions and Tropospheric Chemistry in Southeast Asia

Justin Sentian
BSc. (Hons), MSc.(Res)

A thesis submitted to the University of Lancaster for the degree of Doctor Philosophy

July 2009

Lancaster Environmental Centre
University of Lancaster

Dedicated to my wonderful wife, Marcella and my beautiful children: Anne, Fredyll and Pio. Thank you for everything. I love you!

....I am sure that God, who began this good work in you, will carry it on until it is finished on the Day of Christ Jesus.

Phil. 1:6

Declaration

I declare that this thesis consists of original work undertaken solely by myself at Lancaster University between 2006 and 2009. When the work of other author is referred, it has been properly acknowledged and referenced.

04 June 2009

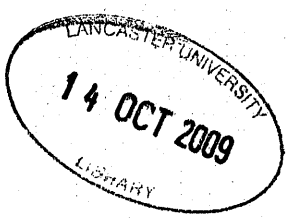

Acknowledgement

First and foremost, I would like to thank God for giving me the strength and fortitude to complete this thesis. When my To-Do list piled up higher and higher and there was no end in sight, He was the one who helped me through all of the stressful times.

I owe my most sincere gratitude to Dr. Robert MacKenzie and Prof. Nick Hewitt who gave me the opportunity to work with them, and for their continuous support, patience, motivation, enthusiasm, and immense knowledge. Their guidance helped me throughout the research and writing of this thesis. I would like to thank the thesis panel committee, Prof. Nick Chappell and Dr. Alan Blackburn for their encouragement and insightful comments. My sincere thanks also goes to Dr. David Hein of the Met Office for his invaluable support in the use of the PRECIS model, Dr. Juliette Lathiere for providing the BVOCEM model and Dr Oliver Wild and Thomas Pugh for the use of the CiTTyCAT model. I also must say thanks to Andy, Chuansen, Kirsti, Ben, Annette, Liawas, Sheena and all the Malaysian friends for their friendly advice, help and support.

My deepest gratitude goes to my family for their unflagging love and support throughout my life; this dissertation would have been simply impossible without them. A special thanks goes out to my loving wife for her help in so many ways, and also to my three beautiful children for giving me a quiet space to write. Mostly, however, I would like to thank my loving parents, brothers, sisters and my in laws for their endless support and prayers.

Abstract

A regional climate model (PRECIS) and a biogenic emission model (BVOCEM) were used to investigate the impact of climate changes on biogenic emissions during northeast monsoon (Dec-Jan-Feb, DJF) and southwest monsoon (Jun-(July)-Aug, JJA) in both the A2 and B2 transient climate scenarios of the IPCC in Southeast Asia. The investigation also explored the regional climate change and biogenic emissions response to future landcover changes, both alone and in combination with atmospheric forcing. Consequently, a tropsopheric chemistry model (CiTTyCAT) was used to investigate the relative impact of climate changes and biogenic emissions on tropospheric chemistry, particularly ozone in both seasons and climate scenarios. A warming across the region occurred, with the largest temperature increase apparent over land areas during DJF and JJA in both the A2 (3.0°C and 3.1°C) and B2 (2.6°C and 2.1°C) climate scenarios. These temperature changes were statistically significant at the 95% level in both climate scenarios across the domain with the exception during DJF (B2 scenario) in some areas over the South China Sea and the Philippines Sea. The increase in solar radiation was also reflected in the increase of surface temperature and decreased cloud fraction in both seasons in the A2 and B2 scenarios. Future changes in other climatic variables, such as precipitation and boundary layer, have shown a high degree of variability. The combined effect of atmospheric forcing and landcover forcing was observed to increase the surface temperature significantly in both climate scenarios. However, the effects of future landcover forcing alone in both seasons in the A2 and B2 climate scenarios were observed to be small and produced cooling temperatures.

Projected climate changes in the present-day landcover scenario in both A2 and B2, with the exclusion of the CO_2 activity factor, showed an increase in isoprene emissions by 27% (A2) and 13% (B2) in 2100 relative to 2008. In the same scenario, but with the inclusion of future CO_2 concentrations of 560 ppm, isoprene emissions were found to be inhibited by 8% (A2) and 19% (B2) respectively. The inhibitory effects of elevated CO_2 on isoprene emissions was much larger than that of climate change alone. Meanwhile, the combined effects of climate change and future landcover forcing with the inclusion of the CO_2 activity factor accounted for the decrease of future isoprene emissions by 66% (A2) and 60% (B2) respectively.

Landcover forcing alone accounted for the decrease of isoprene emissions by 5% (A2) and 6% (B2) with the CO_2 activity factor, and conversely the increase of isoprene emissions by 9% (A2) and 5% (B2) without the CO_2 activity factor. The CO_2 inhibitory effect was more important than the combined effects of climate changes and landcover forcings on isoprene emissions. These results suggest that future emissions of isoprene in the region is largely buffered by a number of competing factors, which is certainly an important consideration when estimating the global isoprene budget.

In the present-day landcover scenario, the combined impact of climate changes and biogenic emissions (with the CO_2 activity factor) in 2100, surface O_3 concentrations in urban (Bangkok) and remote (Danum) areas increased in both climate scenarios. In Bangkok, in the A2 scenario, the surface O_3 increased by 16% ((January) and 21% (July); while in the B2 scenario, O_3 increased by 15% (January) and 18% (July) respectively. In Danum, in the A2 scenario, the O_3 increased by 43% (January) and 28% (July); while in the B2 scenario, O_3 increased by 13% (January) and 27% (July). In the future landcover scenario, the combined impact of climate changes and biogenic emissions resulted in a further increase in surface O_3 concentrations in both seasons in the A2 and B2 climate scenarios in Danum (between 38% and 77%) and Bangkok (between 12% and 21%). In both locations, biogenic emissions accounted for a larger effect on the increase of surface O_3 concentrations in both seasons in the A2 and B2 climate scenarios than that of climate changes. In Bangkok, the combined impact of climate changes and biogenic emissions in the present-day and future landcover scenarios were found to decrease OH concentrations in both seasons in A2 and B2 climate scenarios. The OH suppression was largely due to the oxidation of isoprene by OH radicals. This OH suppression was much greater in future landcover scenario than in the present-day landcover sceanrio. However, in Danum, the combined impact of climate change and biogenic emissions in the present-day and future landcover scenarios were observed to increase OH concentrations in both seasons in the A2 and B2 climate scenarios. The increases were largely attributed to climate changes, although the suppression of OH concentrations was also found to be due to biogenic emissions.

Table of Content

2 TROPOSPHERIC CHEMISTRY AND CLIMATE CHANGE

3 CLIMATE CHANGES IN SOUTHEAST ASIA

5 BIOGENIC EMISSION IN RESPONSE TO LANDCOVER AND CLIMATE CHANGES IN SOUTHEAST ASIA

6 CLIMATE CHANGE AND LAND COVER CHANGE EFFECT ON THE TROPOSPHERIC CHEMISTRY IN SOUTHEAST ASIA

List of Figures

List of Tables

List of Appendices

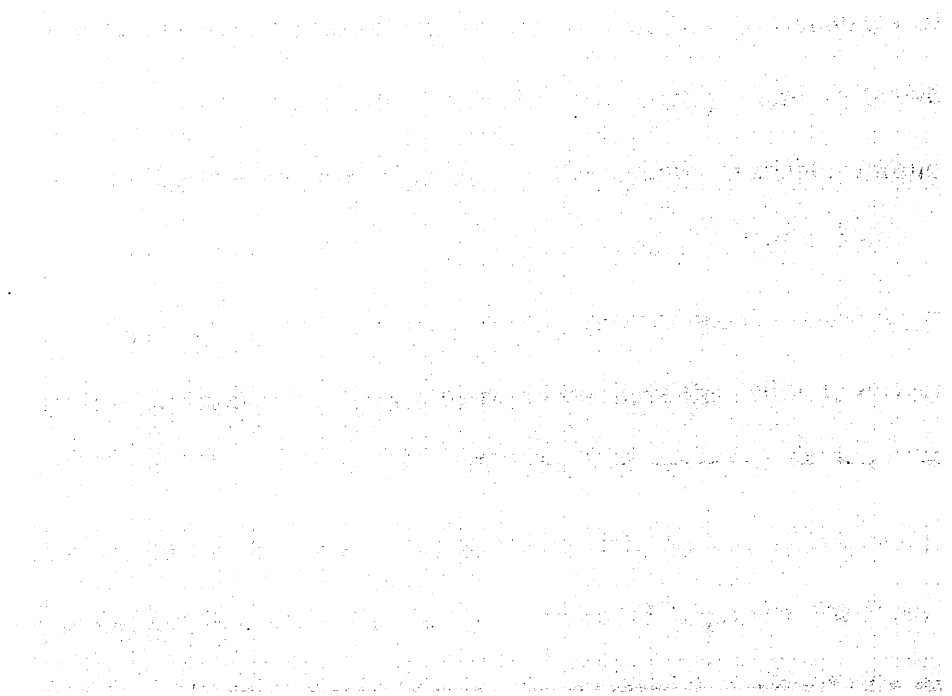

Chapter 1

INTRODUCTION

1.1 Introduction

Tropospheric chemistry plays a significant role in determining the behaviour and composition of the troposphere. The emission of chemically active gases and aerosols is the main forcing agent for tropospheric chemistry. Climatically active gases can be grouped into two sets, namely the long-lived gaseous species (e.g. CO_2, CH_4, N_2O, CFCs, etc.) and the short-lived reactive gaseous species (e.g. O_3, CO, NO_x, Volatile Organic Compounds (VOCs), SO_2, OH, HO_2, etc.). Apart from CO_2 and water vapour, other greenhouse gases (GHGs) that are significantly important in climate-chemistry interactions are CH_4, N_2O, and O_3. These GHGs in the atmosphere are very important because they capture and recycle energy emitted by the Earth surface through their ability to absorb and re-emit infrared radiation, defining the primary characteristic of the greenhouse effect. Therefore, concentration changes of these GHGs in the atmosphere can modify the balance of energy transfers between the atmosphere and Earth's surface. Change in the energy available through this modification to the Earth-atmosphere system is measured as radiative forcing (IPCC, 1994; 2007-Chapter 2). Other short-lived reactive gaseous species, although they do not produce directly radiative forcing effects, do still have the ability to influence the global radiation budget. For example, the chemical reactions of two precursor pollutants, VOCs and NO_x, in the presence of ultraviolet light (sunlight) can produce tropospheric O_3, a GHG. Tropospheric O_3, is estimated to provide the third largest increase in direct radiative forcing since the pre-industrial era, behind CO_2 and CH_4 (IPCC, 2007-Chapter 2; USEPA, 2002).

Based on the its contribution to the radiative forcing from the pre-industrial (1750) to present time (2005) (IPCC, 2007-Chapter 2) (Figure 1.1), in term of global average, CO_2 has been recognised as the most important GHGs (1.46 W/m^2), followed by CH_4 (0.48 W/m^2), O_3 (0.35 W/m^2), CFC-12 (0.17 W/m^2), and N_2O (0.15 W/m^2) (IPCC, 2007). Other chemically reactive gases such as CO, NO_x, and NMHC are considered as indirect GHGs, as these species compounds are reactively involved in tropospheric chemistry, thus affecting some GHGs such as O_3 and CH_4.

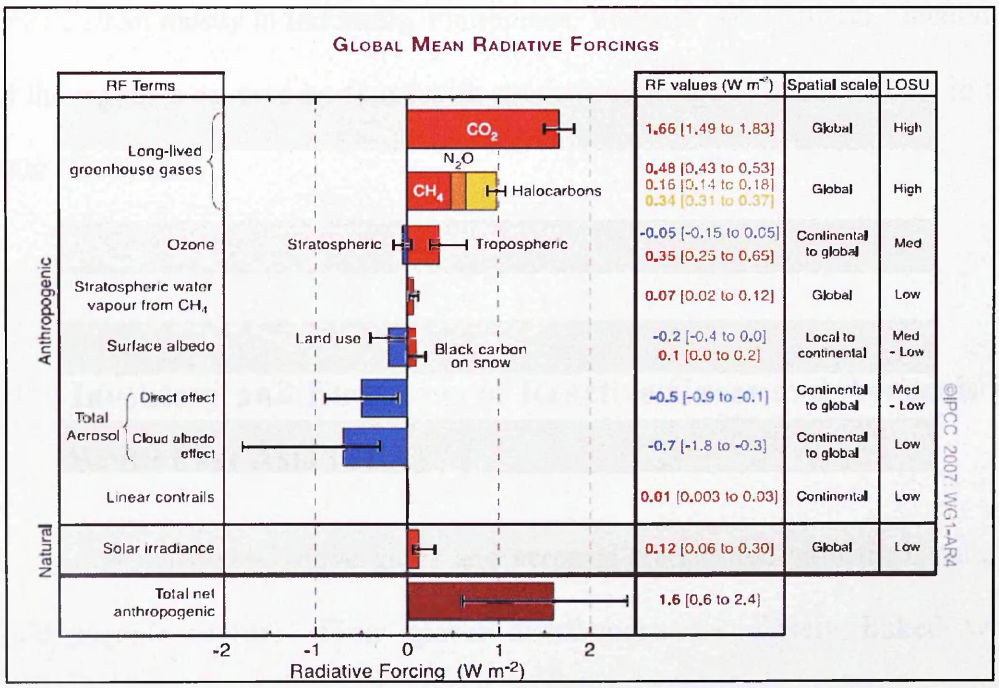

Figure 1.1: The global mean radiative forcing of the climate system between 1750 and 2005 (*Adapted from IPCC (2007-Chapter 2)*).

In the following section, the potential sources of the GHGs and their current emissions estimate, along with some other short-lived reactive gases such as CO, NO_x and VOCs, will be described. Aerosol, extremely small particles or liquid droplets often composed of sulphur compounds, carbonaceous combustion products, crustal materials and other human induced pollutants, is also described as it plays important

roles in the tropospheric chemistry-climate system through heterogenous reactions and its effect on the radiative transfer through the atmosphere (IPCC, 2001; 2007-Chapter 2).

In this work, the area of study is Southeast Asia (SEA), which is a subregion of Asia consisting of eleven countries, Brunei, Cambodia, Indonesia, Laos, Malaysia, Myanmar, Philippines, Singapore, Thailand, Timor Leste and Vietnam. The region total land area is about 4,855,688 km^2 with a population of about 565 million in mid-2006 (PRB, 2006) mostly in Indonesia, Philippines, Vietnam and Thailand. Generally, most of the region is covered by forest with estimate coverage of about 48.6% in the year 2000 (FAO, 2006).

1.2 Inventory and Emissions of Reactive Gases and Aerosols in South East Asia (SEA)

Chemically and radiatively active gases and aerosols are emitted both from natural and anthropogenic sources. Their global distributions are closely linked with demographic and economic development, and changes in technology. At local and regional scales, emissions of these gases and aerosols have been a great concern with regard to local and regional air quality deterioration, and its effect on the regional climate (IPCC, 2001; 2007-Chapter 2). In fact, there is an emerging interest and priority to improve the current understanding of the interaction between climate change and regional air quality in light of the increase of potential sources of these important chemical species such as biomass burning and urban development, as well as from natural sources (Jacob *et al.*, 2005). Therefore, an inventory of emissions into

the atmosphere, particularly of climatically reactive gases and aerosols, is important to support climate and atmospheric modelling studies, as well as observations on the ground.

For SEA, one of the most comprehensive emission inventories is based on Streets *et al.* (2003), though this inventory has not taken into consideration the emissions from natural sources. Another emission inventory data set for SEA in 2000, from *EDGAR* 32FT2000 (NEAA, 2005), which is based on the EDGAR 3.2 estimates for 1995, is also available in various formats including in 1° x 1° gridded files. As shown in Table 1.1, the EDGAR emission inventory has relatively higher values for all emissions, with the exception of Non-Methane Volatile Organic Compounds (NMVOCs), which is due to overestimation of emissions from burning of agricultural wastes (NEAA, 2005), and emission inventory from Streets *et al.* (2003a) has not considered emission from biomass burning.

Table 1.1 Summary of gas and aerosol emissions in SEA in 2000 (Gg/year)

Country	CH_4	N_2O	NO_x	CO	NMVOC	BC	OC
Brunei	50 (98)	- (1)	20 (26)	15 (425)	43 (151)	0	0
Cambodia	708 (636)	- (11)	89 (144)	1707 (3090)	305 (278)	14	89
Indonesia	6443 (10625)	- (223)	1317 (2413)	23105 (43300)	6903 (6253)	206	1138
Laos	387 (470)	- (14)	96 (269)	2547 (5840)	486 (475)	18	129
Malaysia	869 (1206)	- (29)	494 (728)	5552 (8730)	1424 (2204)	26	151
Myanmar	2691 (2823)	- (71)	226 (610)	8446 (14700)	1671 (1282)	65	421
Philippines	2563 (2125)	- (60)	326 (488)	4102 (4600)	1398 (824)	36	192
Singapore	85 (60)	- (3)	185 (977)	138 (286)	81 (161)	3	2
Thailand	3567 (3670)	- (83)	1086 (1246)	10815 (9840)	3052 (1669)	72	364
Vietnam	2907 (3408)	- (88)	283 (427)	9248 (7990)	1390 (1115)	88	432
Total	**20,270 (25,121)**	**- (583)**	**4,122 (7,328)**	**65,675 (98,801)**	**16,753 (14,412)**	**528**	**2,918**

Note: BC = black carbon; OC = organic carbon : BC & OC are included in $PM_{2.5}$ & PM_{10}

Source: Extracted from Streets et al. (2003a) and in brackets ( ) from EDGAR 32FT (NEAA, 2005)

1.2.1 Methane

Methane (CH_4), which is second only to CO_2 in terms of contribution to radiative forcing, is a chemically reactive gas that is extremely important in tropospheric chemistry due to its central role in atmospheric oxidation chemistry. Emissions of CH_4 from anthropogenic sources are mainly from the harnessing of biological processes such as paddy fields, enteric fermentation (ruminant animals), extraction of fossil fuel (natural gas, coal, and petroleum), landfills, and biomass burning (IPCC, 1995). Wetlands have been singled out as the main source of CH_4 emissions from natural sources (Hein *et al.*, 1997; Lelieveld *et al.*, 1998; Houweling *et al.*, 1999). In SEA, the total anthropogenic emissions of CH_4 are estimated to be about 20.27 Tg in 2000, mostly from rice cultivation, animals, biofuel combustion, biomass burning, wastewater treatment, and landfills (Streets *et al.*, 2003a). The inventory from EDGAR32FT2000 (NEAA, 2005) has shown a slightly higher value of 25.12 Tg, which is about 8.0% of the global anthropogenic emissions. With an annual growth of about 0.4%, the global average of CH_4 surface abundance from all sources (anthropogenic and natural emissions) in 1998 was 1745 ppb, corresponding to a total burden of about 4850 Tg CH_4 (Prather *et al.*, 2001), and slightly increasing to 1783 ppb in 2004 (IPCC, 2007-Chapter2; WMO, 2006).

The emissions of CH_4 from biological processes are assumed to be formed under anaerobic conditions (anoxic), but a recent proposal by Keppler *et al.* (2006) is that significant amounts of CH_4 are emitted directly from plants and detached leaves under oxic conditions. This newly-identified source of CH_4 has very significant implications on the global methane budget and its role in past and future climate changes. Based on this finding, Keppler *et al.* (2006) estimated the CH_4 source strength to be 62–

236 Tg/yr for living plants, and 1–7 Tg/yr for plant litter (1 Tg = 10^{12} g). This proposed new source of CH_4 is contentious and is not used in the present study. The loss of CH_4 in the troposphere is predominantly through chemical processes by oxidation of OH, which is responsible for the removal of approximately 500 Tg CH_4/year (almost 90% of the total sink) (Wuebbles and Hayhoe, 2002) as well as through soil sinks and stratospheric loss (Prather *et al.*, 2001).

1.2.2 Nitrous Oxide

Nitrous oxide (N_2O) is also an important GHG, which is produced by microbial processes in soils and fertiliser application, and has a long lifetime (IPCC, 1995). N_2O is believed to be responsible for 6% of the total radiative forcing from anthropogenic forcing (Graedel and Crutzen, 1993). The IPCC Third Assessment Report (IPCC 2001) estimated a radiative forcing value due to N_2O of 0.15 Wm^{-2}, which has taken into account the slightly increased of N_2O since the IPCC Second Assessment Report. Anthropogenic sources of N_2O include biomass burning, combustion of fossil fuel, production of industrial nitric acids, and substantial emissions from agricultural activities through nitrogen-based fertiliser application (Matson *et al.*, 1999; Becker *et al.*, 2000; NEAA, 2005). Substantial emissions of N_2O are also produced from natural sources through microbial processes in soils (Akiyama and Tsuruta, 2003). Based on the EDGAR32FT2000 emission inventory, N_2O emissions from anthropogenic sources in SEA are estimated to be about 583 Gg/yr, which is about 4.8% of the global emissions (NEAA, 2005). Meanwhile, the global average surface abundance of N_2O from all sources was estimated to be about 314 ppb in 1998, which corresponds to a global burden of 1510 Tg N (Prather *et al.*, 2001), and increased to 318.6 ppb in 2004 at the rate of 0.8 ppb/year (WMO, 2006). The major sink of N_2O in the

atmosphere is through photodissociation in the stratosphere, which accounts for about 90% (Volk *et al.*, 1997; Prinn and Zander, 1999). The emissions of N_2O from soils are regulated by temperature and soil moisture, and therefore its variability is subject to climate conditions (Frolking *et al.*, 1998; Parton *et al.*, 1994).

1.2.3 Tropospheric Ozone

Tropospheric ozone (O_3) is a radiatively active GHG produced as a secondary species through photochemical reactions in the atmosphere (Houghton *et al.*, 1996; Portmann *et al.*, 1997; Roelofs *et al.*, 1997; van Dorland *et al.*, 1997; Shine and Forster, 1999). Ozone plays an important role in the chemistry of the troposphere, as it controls the oxidation capacity of the atmosphere (Thompson, 1992; Brasseur *et al.*, 1998; Fuglestvedt, 1999) and so affects the lifetimes of other GHGs such as CH_4 (Prather *et al.*, 2001). Due to its short lifetime in the troposphere, its temporal and spatial distribution is highly variable (EC, 2003; Naik *et al.*, 2005). As the chemistry of the tropospheric O_3 is very much dependent on its precursors, therefore the emissions of the precursors are highly responsible for tropospheric O_3 forcing. IPCC (2001; 2007-Chapter 2) has reported the annual global average value of tropospheric O_3 for total-sky conditions is between 0.28 to 0.43 Wm^{-2}, while the normalised forcing is between 0.033 to 0.056 Wm^{-2}, which in terms of magnitude is comparable with the studies by Berntsen *et al.* (1997) and Shine and Forster (1999). In the near future (2050), the average global tropospheric O_3 forcings since pre-industrial times is projected to increase, particularly in Asia, due to population growth and rapid development, but estimate of the forcing due to differences in model input such as the latitudinal distributions, emissions inventories, or model processes such as transport (IPCC, 2001). For example van Dorland *et al.* (1997) and Brasseur *et al.* (1998) has projected

a higher globally averaged total tropospheric O_3 forcing of 0.66 Wm^{-2} and 0.63 Wm^{-2} compared to the earlier study by Chalita *et al.* (1996) of 0.43 Wm^{-2}. In the year 2100, Stevenson *et al.* (2005) has projected a tropospheric O_3 forcing of 0.48 Wm^{-2}.

The current estimate of the tropospheric O_3 burden is about 370 Tg, which is equivalent to a mean abundance of about 50 ppb (Prather *et al.*, 2001; Park *et al.*, 1999). From satellite measurements, it has been observed that O_3 mixing ratios increase in the extratropical upper troposphere, indicating the high efficiency of O_3 production through photochemical reactions (EC, 2003) as well as O_3 flux from the stratosphere (Fehsenfeld and Liu, 1993; Murphy and Fahey, 1994; Gettelmen *et al.*, 1997; McLinden *et al.*, 2000). However, recent studies based on measurements and modelling analyses have indicated a reduction of stratospheric O_3 flux to troposphere of about 30% since the early 1970s to the mid 1990s (Fusco and Logan, 2003). The production of tropospheric O_3 through photochemical reactions is very much dependent on the emission of its precursors, such as CO, NO_x, CH_4 and volatile organic compounds (VOCs), which are emitted primarily from anthropogenic and natural sources. Apart from through photolysis (see Chapter 2), tropospheric O_3 is lost through deposition and the rate of uptake is influenced by temperature and soil moisture (Emberson *et al.*, 1996; Fuhrer, 1996). The amount of tropospheric O_3 lost through heterogenous chemistry (cloud chemistry) is still uncertain (Reichardt *et al.*, 1996; Heikes *et al.*, 1996; Davies *et al.*, 1998). However, loss of O_3 driven by heterogeneous chemistry in the marine boundary layer, correlated with BrO_x radicals (BrO_x = Br + BrO) has been observed (Barrie *et al.*, 1988; Haussmann and Platt, 1994).

1.2.4 Carbon Monoxide

Carbon monoxide (CO) is not a GHG, having no significant radiative effect, but plays a very important role in tropospheric chemistry through reaction with OH, which subsequently affects the rates of production or destruction of GHGs, in particular, CH_4 and O_3. The typical mixing ratio of CO is in the range of 40 ppb (remote)–200 ppb (urban), with a chemical lifetime of 30–90 days (Seinfeld and Pandis, 1998). Most CO emissions are derived from anthropogenic sources and so are heavily weighetd to the northern hemisphere (Prather *et al.*, 2001). Hauglustaine *et al.* (1998) and Bergamaschi *et al.* (2000) have estimated the global emissions of CO, derived both from natural and anthropogenic sources, to be about 2100 Tg/yr and 2860 Tg/yr respectively. Based on OxComp model calculations for the year 2000, the global emissions of CO were estimated to be about 2780 Tg/yr (Prather *et al.*, 2001). In the TAR IPCC report, emissions of CO in SEA were estimated to be about 44 Tg/yr, which is about 4% of the global emissions (Prather *et al.*, 2001). Based on the emission inventory in SEA by Streets *et al.* (2003a), CO abundance has been estimated to be about 65.7 Tg/yr. Meanwhile, the estimation from the EDGAR32FT2000 inventory has shown a higher value of about 98.8 Tg, or about 9.1% of the global anthropogenic emissions (NEAA, 2005). The major sources of CO emissions in SEA from anthropogenic origins are biomass burning, combustion of fossil fuels, and waste burning (NEAA, 2005).

1.2.5 Nitrogen Oxides

Similarly to CO, nitrogen oxides (NO_x) ($NO_x = NO_2 + NO$) does not directly affect the Earth's radiative balance, but plays a very important role in regulating the

production of tropospheric O_3, which is a GHG. NO_x is primarily emitted into the atmosphere as NO and oxidised very quickly into NO_2. The detail of NO_x chemistry in the troposphere is described in Chapter 2. Globally, the NO_x emissions from anthropogenic sources in 2000 are estimated to be about 32,600 Tg N/yr, of which 33% is emitted from fossil fuel combustions (Prather *et al.*, 2001). In the last two decades, emissions from fossil fuel combustion, such as transportation activities and power plants, have dominated the emissions of NO_x (Ehhalt, 1999; Holland *et al.*, 1999; Penner *et al.*, 1999). In the tropics, apart from the combustion of fuel, other important sources of emissions are biomass burning (Andreae, 1993; Lee *et al.*, 1997; Prather *et al.*, 2001), soil microbial emissions (Yenger and Levy, 1995; Jaegle *et al.*, 2005; Stewart *et al.*, 2007), and lightning, which is abundant in the deep convective thunderstorms of the Inter-Tropical Convergence Zone (ITCZ) (Olivier *et al.*, 1998; Schumann and Huntrieser, 2007) and Tropical Warm Pool of SEA. A previous study by Bond *et al.* (2002), using satellite lightning measurement from the Lightning Image Sensor (LIS), found that lightning NO_x production in the tropics is highest over land masses, due to the intense convection caused by solar heating. On an annual basis, this study concluded that about 23% of the global NO_x production by lightning is produced in the tropics. Lightning NO_x is produced in the upper troposphere, and so is not considered in the atmospheric chemistry modelling reported below, which focuses on the planetary boundary layers.In SEA, based on emission inventories of Streets *et al.* (2003a) and EDGAR32FT2000 (NEAA, 2005), the abundance of anthropogenic emissions of NO_x is estimated to be about 4.1Tg/yr and 7.3 Tg/yr respectively. Based on EDGAR32FT2000, the NO_x emissions in SEA are about 5.8% of the global anthropogenic NO_x emissions. The main sources of NO_x emissions are biomass burning, transportation, and power plants (NEAA, 2005).

1.2.6 Anthropogenic Non-Methane Volatile Organic Compounds

NMVOCs play very important roles in tropospheric chemistry, particularly in the urban environment, where high concentrations of these compounds are observed. These compounds generally have short lifetimes (i.e hours to days) and therefore have small direct radiative forcing. However, their most important roles in tropospheric chemistry are their involvement in photochemistry (Derwent, 1995; Atkinson, 2000; Prather *et al.*, 2001; Rappenglucka *et al.*, 2005) and organic aerosol production (Seinfeld and Pandis, 1998; Castro *et al.*, 1999; Kleindienst *et al.*, 1999; Prather *et al.*, 2001), which are linked to climate change. Significant emissions of anthropogenic NMVOCs are mostly concentrated in the northern hemisphere (Prather *et al.*, 2001). A wide range of NMVOCs with strong diurnal and seasonal variations have been observed in urban environments with typical mixing ratios of 100–1999 ppb C (Singh, 1999). In 1990, the global emissions of NMVOCs were estimated to be about 142 Tg/yr (Middleton, 1995), and in 2000 the abundance of these compounds was found to increase to 186.3 Tg/yr (NEAA, 2005). The major contributor to the global emissions of these compounds is transport, which contributes 18% of the total emission. Based on the emission inventory of Streets *et al.* (2003a), the emission of NMVOCs in 2000 in SEA from anthropogenic sources was estimated to be about 16.8 Tg/yr. Hydrocarbons from the alkane, alkene, and aromatic groups dominate the NMVOC emissions in SEA. The estimate from the EDGAR32FT2000 inventory is slightly lower, at about 14.4 Tg/yr, which is about 7.7% of the global anthropogenic emission (NEAA, 2005). In SEA, the main sources of emissions are from transportation, oil production, and biomass burning activities (Streets *et al.*, 2003a; NEAA, 2005).

1.2.7 Biogenic Volatile Organic Compounds (BVOCs)

Plants emit hydrocarbon compounds, most of which are extremely reactive in the troposphere with relatively short lifetimes-ranging from 1–2 hours to greater than a day (Guenther *et al.*, 1995). Generally, biogenic emissions can be grouped into three categories, namely (a) isoprenoid compounds, such as hemiterpenes (e.g. isoprene), monoterpenes (e.g. α-pinene, limonene, etc.) and sesquiterpenes (e.g. β-caryophyllene); (b) other VOCs such as alkenes, aldehydes, organic acids and esters, alcohols, ketones, alkanes, organic sulphur, and halogenated compounds; and (c) other compounds that can be emitted from plants such as NO, CO and organic particles. Considerable studies on biogenic VOC emissions from various types of ecosystems have been carried out in light of the recognition of the importance of biogenic VOCs to tropospheric chemistry (Fehsenfeld *et al.*, 1992; Seinfeld and Pandis, 1998). Isoprene and the monoterpenes, which have atmospheric lifetimes of considerably less than a day, are very important in tropospheric photochemistry. Isoprene in particular is an extremely reactive gas, and plays a dominant role in photochemistry and regulation of the oxidant balance of the troposphere, including O_3 production (Poison *et al.*, 2000; Monson & Holland, 2001). Through its capability to regulate the oxidant balance, it also affects the atmospheric chemical composition and lifetimes of many radiatively active species affecting the climate such as CH_4 and other reactive gases such as CO (Collins *et al.*, 2000).

Globally, it has been estimated that about 1150 Tg C/yr of biogenic hydrocarbons are emitted from plants (Seinfeld and Pandis, 1998), mainly from trees although shrubs and non-woody plants may also emit some hydrocarbon compounds (Wiedinmyer *et al.*, 2004). Isoprene has been singled out as the dominant biogenic trace gas emission,

and is estimated to constitute half of the global biogenic emissions (Guenther *et al.*, 1995; Wiedinmyer *et al.*, 2004). It has been observed that biogenic emission sources are concentrated in the tropics and subtropics due to the high temperature and light regimes, and high leaf area indices (Guenther *et al.*, 1995; Lerdau and Keller, 1997; Guenther *et al.*, 1999; Geron *et al.*, 2002; Greenberg *et al.*, 2004; Geron *et al.*, 2006). Despite being the single largest source of biogenic VOC emissions, estimated to consist of more than 80% of the total global isoprene emissions (Guenther *et al.*, 1997; Lerdau *et al.*, 1997), tropical ecosystems are still relatively unknown in this respect largely because of their extremely high species diversity, inaccessibility, and lack of tree canopy access facilities (Lerdau and Throop, 2000). Recent attempts to establish databases for tropical species have been limited to Costa Rica (Geron *et al.*, 2002), Panama (Lerdau & Keller, 1997; Lerdau & Throop, 2000), Puerto Rico (Lerdau & Keller, 1997, China (Klinger *et al.*, 2002), central Africa (Klinger *et al.*, 1998, Guenther *et al.*, 1999), and southern Africa (Guenther *et al.*, 1996; Harley *et al*, 2004). So far, in the SEA region, there is very little information available on biogenic VOC emissions from tropical forests. In this study I will utilise preliminary results from the OP3 campaign, which was based in Malasyian Borneo (Hewitt *et al.*, 2009 manuscript submitted), and which constitute the first comprehensive measurements in and above SEA rainforest.

Environmental conditions, mainly temperature, radiation, vegetation type, and foliar area control biogenic VOC emissions, thus making them very sensitive to climate change and landuse change (Lathiere *et al.*, 2005). Urbanisation and deforestation (for timber extraction and agricultural expansion) have dominated the landscape in most tropical regions in last few decades of the 20th century. The tremendous landuse

change in this region has significantly affected vegetation cover, distribution and type, thus influencing regional biogenic VOC emissions. A previous study by Ganzeveld and Lelieveld (2004) on the impact of deforestation in Amazonia for grazing expansion has predicted a significant decrease in maximum isoprene emission fluxes, mainly due to a decrease in the isoprene emission factor and in the foliar density. However, conversion of tropical forest to other some crops (e.g. oil palm) – can result in significant increases in isoprene emissions (Owen *et al.*, private communication; Hewitt *et al.*, 2009).

1.2.8 Aerosols

Tropospheric aerosols also have anthropogenic and natural sources, and are derived from primary (direct emission of particles) and secondary (indirectly through gas-particle conversion) sources. The presence of aerosols in the troposphere is very important to the climate-chemistry system, as aerosols directly scatter incoming solar radiation; are capable of providing surface area for the reaction of reactive gases, act as cloud condensation nuclei (CCN), and affect primary photochemical reactions through scattering and absorption of radiation (Turco, 1999; Rosenfeld, 2000; Penner *et al.*, 2001; Ramaswamy *et al.* 2001). A variety of anthropogenic aerosol types exist in the atmosphere such as water-soluble inorganic species (e.g sulphate), carbonaceous aerosols (e.g. organic carbon and black carbon), mineral dust and sea salt. Most of the anthropogenic aerosols originate from industrial dust and biomass burning, and have components such as soot, trace metals, and partially oxidized organic matter (Heintzenberg, 1989; Querol *et al.*, 1995; Dickerson *et al.*, 1997; Cachier, 1998). Primary biogenic aerosols, which are mainly emitted from forest vegetation, comprise many different types of particles such as pollen, spores, bacteria,

algae, fungi, excrement, etc. (Artaxo *et al.*, 1994; Andreae and Crutzen, 1997; Echalar *et al.*, 1998).

In terms of aerosol abundance in the atmosphere, the total emission of aerosols (diameter <25 μm) from anthropogenic and natural sources are 1065–1325 Tg/yr and 1363–3550 Tg/yr respectively (Turco, 1999). Globally, primary particles such as sea salt and mineral dust (soil), which are derived from natural sources, are the most abundant aerosols in the atmosphere, with estimated emissions of 3340 Tg/yr and 2150 Tg/yr respectively, followed by carbonaceous aerosols (150 Tg/yr) and industrial dust (100 Tg/yr) (Prather *et al.*, 2001). Carbonaceous aerosols, which are mainly organic carbon and black carbon, are largely emitted from biomass burning (Cachier *et al.*, 1995; Artaxo *et al.*, 1998) and fossil fuel combustion (Penner *et al.*, 1993; Cooke and Wilson, 1996; Echalar *et al.*, 1998; Cooke *et al.*, 1999; Scholes and Andrae, 2000). In tropical regions such as SEA, where biomass burning occurs frequently every year, carbonaceous aerosol emissions are expected to be significant. Based on Streets *et al.* (2003a), the emissions of carbonaceous aerosols in term of organic carbon and black carbon in SEA are estimated to be about 2.9 Tg/yr and 0.5 Tg/yr respectively, which are about 28% and 20.9 % of the total emissions of organic carbon and black carbon in Asia (see Table 1.1).

Different types of aerosols have different effects on climate forcing. In modelling studies over East Asia by Giorgi *et al* (2002) using a coupled regional climate-chemistry/aerosol model has found that sulphate aerosols (inorganic aerosol) induce a negative radiative forcing at the top of the atmosphere (TOA) with maximum negative values of up to -8 Wm^{-2} (winter) and -10 Wm^{-2} (summer). In other studies,

the direct effect of organic carbon (OC) aerosols from fossil fuel was found to induce negative radiative forcings of -0.04Wm^{-2} (Penner *et al.*, 1998) and -0.02Wm^{-2} (Cooke *et al.*, 1999). Black carbon (BC) aerosol, on the other hand, found to induce a positive radiative forcing at TOA and a negative radiative forcing at the surface (Wu *et al.*, 2004). Earlier studies by Hansen *et al.* (1998) showed that BC from fossil fuel and biomass burning induced posititve radiative forcing of +0.27Wm^{-2} at TOA. Other studies on the assessment of BC from fossil fuel alone have found to induce positive radiative forcings of +0.17 Wm^{-2} (Cooke *et al.*, 1999) and +0.20 Wm^{-2} (Grant *et al.*, 1999) at TOA.

1.3 Sources of Emissions in SEA

The rapid population and economic growth in the SEA region (Figure 1.2 and Figure 1.3) will have significantly contributed to the regional and global emissions of reactive gases and aerosols due to increasing anthropogenic emissions (van Aardenne *et al.*, 1999; Streets *et al*, 2002; Streets *et al.*, 2003a), and the widespread occurrence of biomass burning (Crutzen and Andreae, 1990; Roths and Harris, 1996; Christopher *et al.*, 1998; Goldammer, 1999; Siegert *et al.*, 2001; Thompson *et al.*, 2001; Streets *et al.*, 2003b). Large biogenic emissions from remaining tropical rainforests (Kirchoff and Rasmussen, 1990; Guenther *et al.*, 1995), may have combined with anthropogenic emissions to produce a greater oxidising capacity (Crutzen *et al.*, 1985; Sanhueza *et al.*, 1999). Total anthropogenic emissions of reactive gases and aerosols from Asia, including the SEA region, have exceeded those from North America or Europe at the end of the 20th century, and have now become a major source of anthropogenic emissions on a global scale (Pochanart *et al.*, 2004a).

In tropical regions such as SEA, tropospheric chemical composition is influenced by monsoonal flow, associated movements of the Inter-tropical Convergence Zone (ITCZ) and more active photochemistry (Lobert and Harris, 2002; Pochanart *et al.*, 2003; Pochanart *et al.*, 2004a). In SEA, the emissions of chemically reactive gases, particularly the GHGs, are mainly from anthropogenic sources (Tan, 2006). In the following sections, emissions of chemically reactive gases and aerosols in SEA from anthropogenic and natural sources are described. Though emissions from biomass burning are mainly due to human activities such as agricultural activities, it has been specifically separated, as biomass burning activities on a large scale occur periodically, and have a significant effect on the tropospheric chemistry in the region.

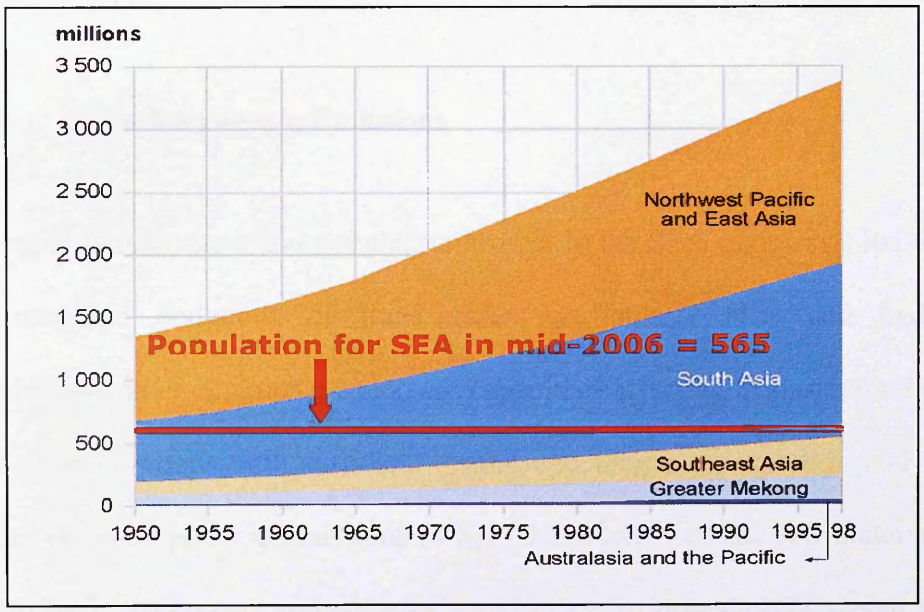

Figure 1.2: Population growth in SEA and other regions in Asia.
(Source: UNEP(2000); PRB (2006))

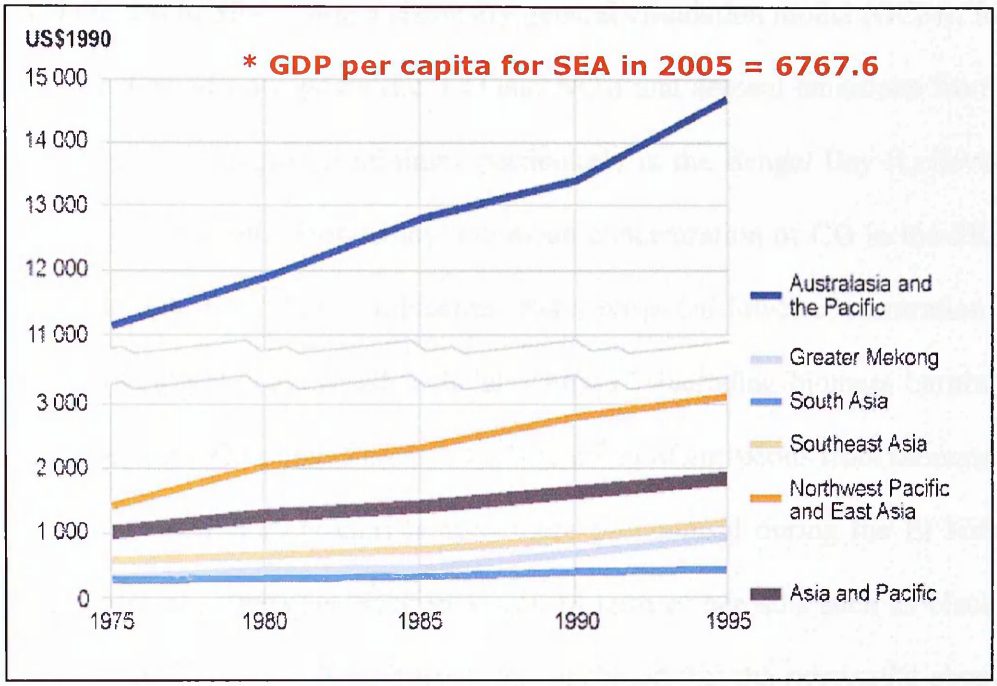

Figure 1.3: Economic growth in SEA and other regions in Asia.
(Source: UNEP(2000); IMF (2006))

1.3.1 Anthropogenic Emissions

The rapid development and population growth in the SEA region has led to growing anthropogenic emissions of trace gases, particularly NO_x and hydrocarbons (Kunhikrishnan *et al.*, 2004), which are capable of affecting tropospheric GHGs. The lack of observations with sufficient spatial and temporal resolution and modelling studies of anthropogenic emissions in SEA have hindered the full understanding of tropospheric trace gases and aerosols, particularly in relation to regional air quality and climate changes. The mean tropospheric NO_x in the SEA region from 1997–1998 has been calculated through numerical modelling (MATCH-MPIC) and from satellite observation (GOME), and was estimated to be about 2.84×10^{14} molecules/cm^2 and 3.49×10^{14} molecules/cm^2 respectively (Kunhikrishnan *et al.*, 2004). Another modelling study in the Asian region from January to March 1999, coinciding with the

SW monsoon in SEA, using a chemistry general circulation model (GCM), found that the attribution of trace gases (i.e. CO and NO_x) and aerosol emissions from SEA to the Indian Ocean region is minimal, particularly in the Bengal Bay (Lelieveld *et al.*, 2002). From the sensitivity study, the mean concentration of CO in the SEA region based on "only fossil fuel combustion" has a projected lower concentration value of between 5–30 ppbv compared with "all sources" (including biomass burning) which is between 100–225 ppbv (Figure 1.4). The effect of emissions from biomass burning on this region (Indian Ocean) is even more pronounced during the El Niño period (Connors *et al.*, 1996)(See Section 1.3.2). In term of aerosols such as black carbon, sulphate, and organic carbon, it has been concluded that the substantial abundance of these aerosols in the Bengal Bay is attributed mainly to anthropogenic sources, and originates mainly from the Indian sub-continent (Lelieveld *et al.*, 2002).

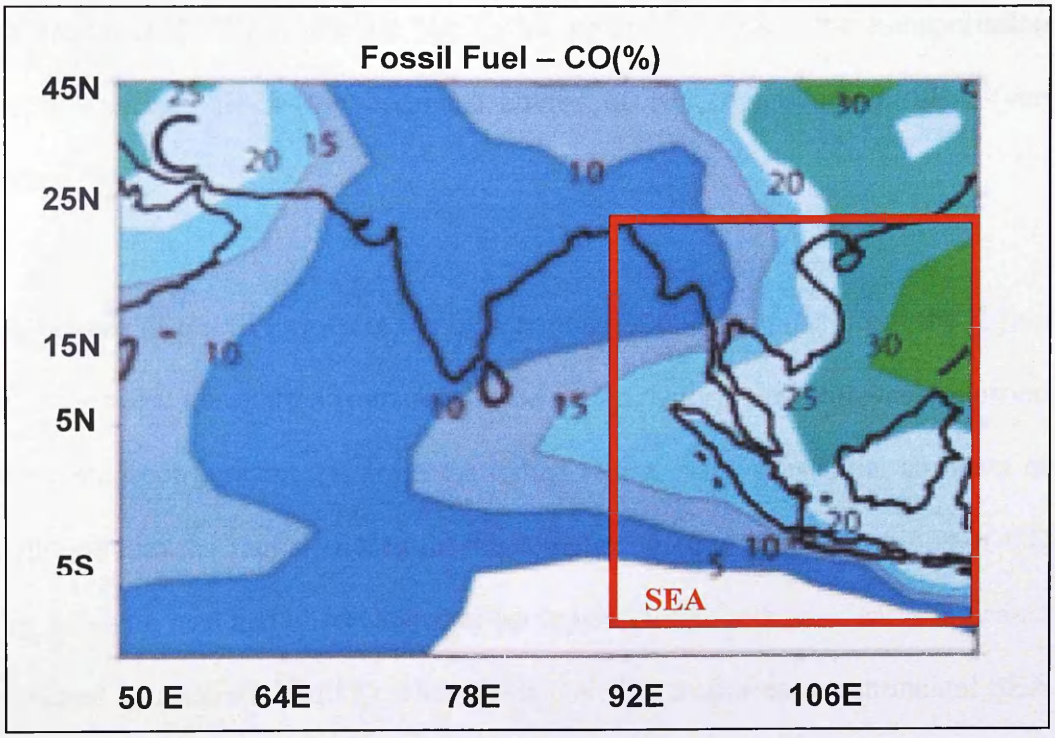

Figure 1.4: Percentage of CO contribution from fossil fuel combustion in SEA from the total anthropogenic source (note: the biomass burning emission was included as anthropogenic emission) (*adapted from* Lelieveld *et al.*, 2002)

Based on the emission inventories of anthropogenic NO_x (excluding biomass burning) in 2000, the transportation sector (air, sea, and land transportation) has the highest share of emissions in SEA (Streets *et al.*, 2003a; NEAA, 2005). Emissions of NO_x from transportation sectors, mainly from automobile emissions, are known to contribute to local air pollution and photochemical smog. Calculations of road emissions with the 3-D chemical transport model MOZART-2 model show that the concentrations of O_3 and its precursors (NO_x, CO, hydrocarbons) are considerably enhanced in response to current surface traffic (Horowitz *et al.*, 2003). In polluted urban environments, oxidation of anthropogenic hydrocarbons in the troposphere also enhances the production of CO (Bruhl and Crutzen, 1999), for example through methane oxidation by OH (Seinfeld and Pandis, 1998). In SEA, based on the global emissions produced by road vehicles of 381 Tg/yr CO and 25 Tg/yr NO_x, a major change was observed when road emissions increased to about 2–5 molecules $m^{-2}s^{-1}$. In the future (2010–2020), under the "no further control scenario", the transportation sector is projected to be the dominant source of NO_x emissions in SEA (van Aardenne, 1999).

The emissions of reactive gases in the SEA region not only originate from the region itself, but are also transported from outside the region. During the southwest monsoon (summer monsoon), air masses from the Indian Ocean bring substantial amounts of air pollution into the region. Based on the comparison between observations of CO mixing ratios on land and observations in the Indian Ocean, this has clearly indicated an increased concentration of CO when oceanic air is transported to continental SEA (Novelli *et al.*, 1998; Lobert and Harris, 2002; Pochanart *et al.*, 2003; Lawrence, 2004). Similar observations were also made during the northeast monsoon (winter

monsoon), where heavily polluted air masses from northeast Asia (China, Korea, Japan and Siberia) contributed to the significant increase of air pollutants in SEA (Newell and Evans, 2000; Porchanart *et al.*, 2001; 2003). Figure 1.5 shows the schematic of pollutant transport pathways for near-surface flow over the Indian Ocean during SW and NW monsoons that could affect the anthropogenic emissions in SEA region.

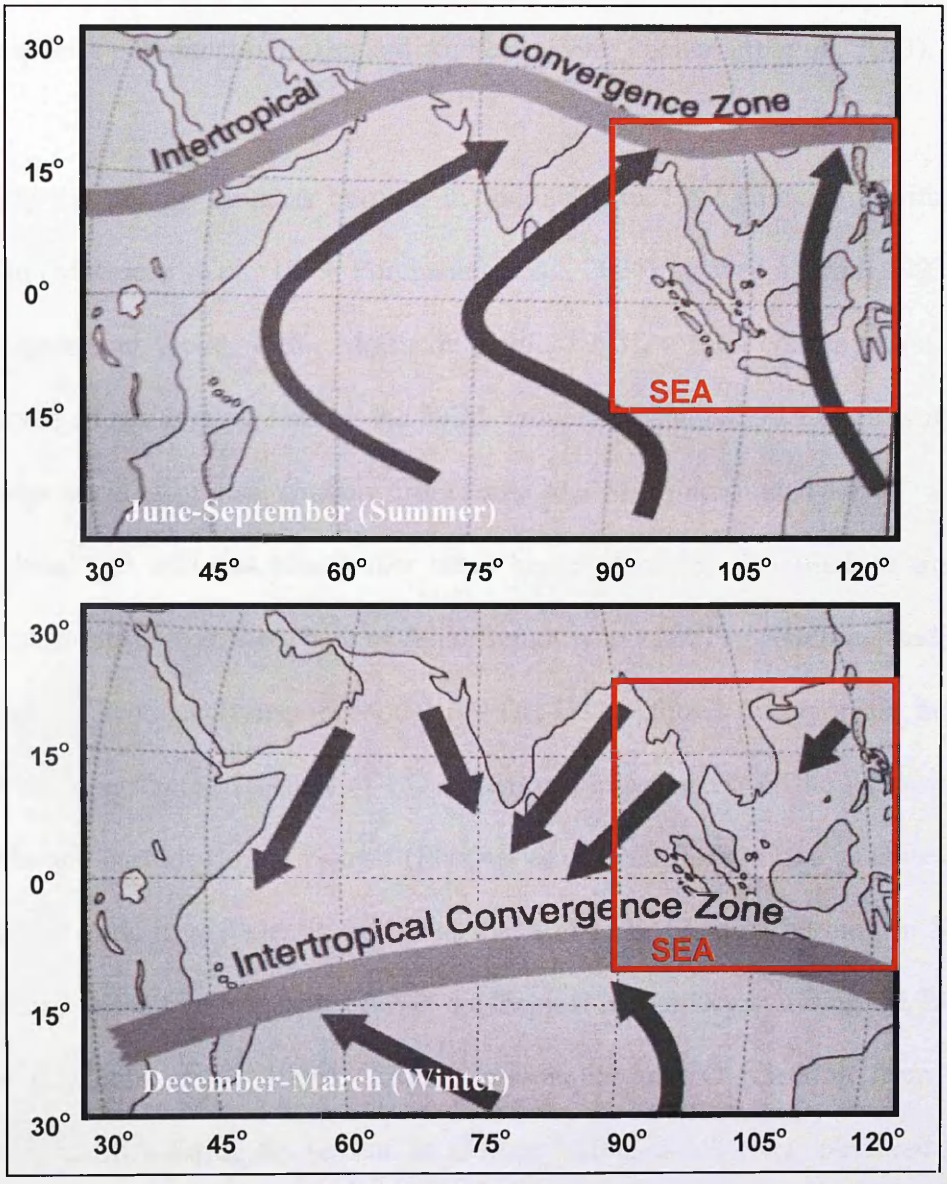

Figure 1.5: Pollutants transport pathways for near-surface flow over the Indian Ocean during summer monsoon (SW monsoon) and winter monsoon (NE monsoon) (*adapted from* Lawrence, 2004).

1.3.2 Biomass Burning Emissions

In SEA, there is a high variability of observed chemically reactive gases and aerosol emissions, both annually and seasonally, as the sources of emissions are localised. Furthermore, the large inter-annual variation of trace gases and aerosols from biomass burning, for example, is characterised by its close connection to the El-Niño/Southern Oscillation (ENSO) events (Bell and Halpert, 1998; Gutman *et al.*, 2000; Matsueda *et al.*, 2002). In the tropics, biomass burning is well known as a major source of atmospheric pollutants (Crutzen and Andreae, 1990; Pocharnart *et al.*, 2003).

During the intense biomass burning in Indonesia in 1997 coinciding with the dry season (Matsueda *et al.*, 1999; Porchanart *et al.*, 2004), as well as from 1993 to 1996 (Matsueda and Inoue, 1996; Matsueda *et al.*, 1998), a high concentration CO was observed in the region. During the PEM-Tropics B Campaign, CO emissions from biomass burning in Asia (mainly from India and SEA) accounted for about 40% of the global CO, and was almost four times higher than the CO emissions from fossil fuel combustion over the whole of Asia (Staudt *et al.*, 2001). Modelling studies using a Global Chemical Transport Model (GFDL GTM) found that biomass burning in SEA has contributed 20–30% of CO to regional emissions over the western tropical pacific and eastern Bay of Bengal (Phadnis *et al.*, 2002). From the satellite (MAPS) measurements, it was clearly observed that CO from biomass burning in SEA was enhanced in the free troposphere over the tropical Indian Ocean during the El Niño in 1994 (Connors *et al.*, 1996). Strong seasonality of CO injection from biomass burning in SEA during dry season in 1997 as well as in 1994 was observed from the long-term observation program using passenger aircraft of Japan Airlines (JAL) between Australia and Japan. For example, in October 28 in 1997, during the intense

biomass burning in Indonesia, CO maximum level of more than 300 ppb was observed in SEA from a JAL airliner (Matsueda and Inoue, 1996; Matsueda *et al.*, 1998; Matsueda *et al.*, 1999). Further investigation by Matsueda *et al.* (2002) on the widespread emission of CO from the biomass burning based on the major forest fire in Indonesia in 1997 using a 3-D global chemical transport model (CTM) developed by national Institute of Advanced Industrial Science and Technology (AIST) in Japan has concluded that biomass burning in SEA was mainly responsible for the large injection of CO into the upper troposphere over the western pacific in 1997 as shown in Figure 1.6. Similar finding has been concluded in another study on the CO transport in SEA using a global 3-D chemical transport model (GEOS-CHEM) for March 2001 by Wang *et al.* (2004) as shown in Figure 1.7.

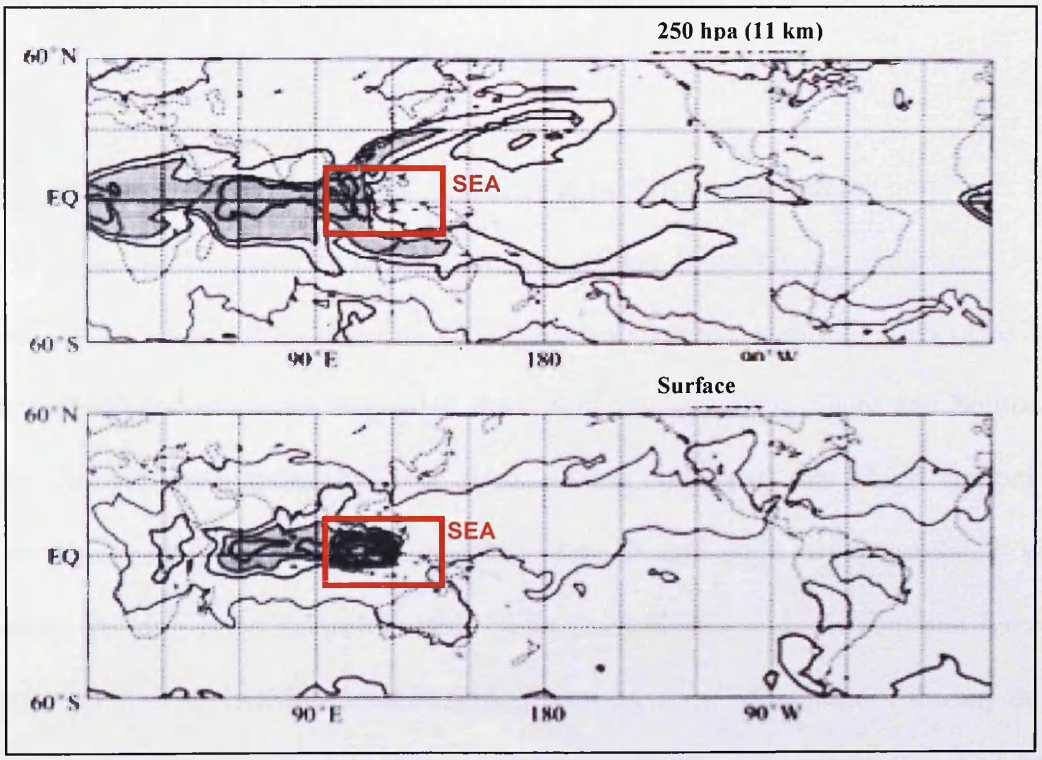

Figure 1.6: Simulated CO distribution at 250 hpa and surface air on October 28, 2007 for emission site of southern Kalimantan of Indonesia. The shaded areas indicate high concentration of CO up to 100 ppb (*adapted from* Matsueda *et al.*, 2002).

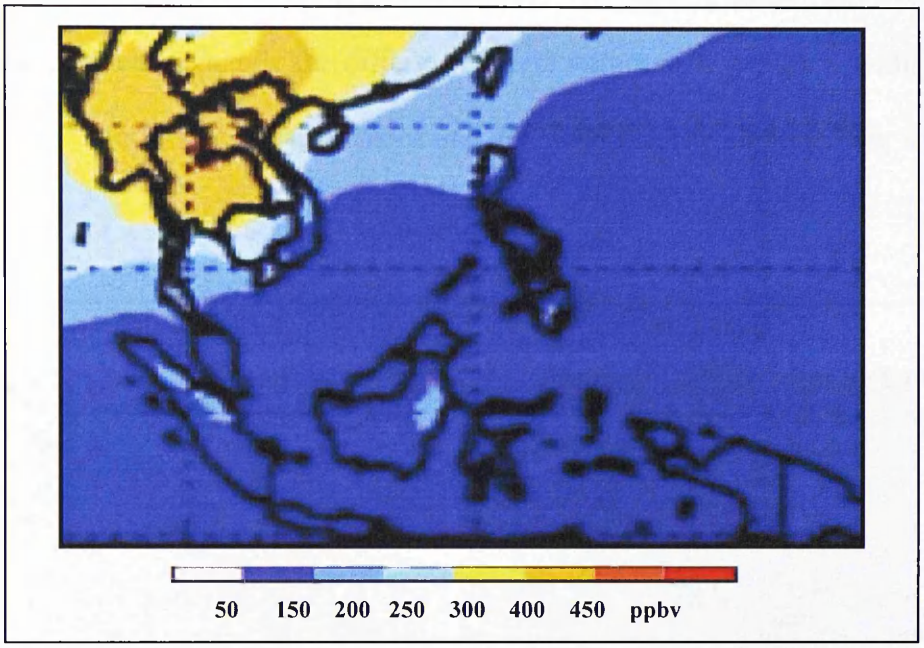

Figure 1.7: Calculated CO mixing ratios average for March 2001 in SEA using a global 3-D chemical transport model (GEOS-CHEM) (1^{o} x 1^{o} resolution) (*adapted from* Wang *et al.*, 2004) .

Apart from fossil fuel combustion, the seasonal occurrence of biomass burning is also responsible for NO_x emissions into the atmosphere (Crutzen and Andreae, 1990). Modelling studies by Phadnis *et al.* (2002) have shown that about 20–30% of NO_x in the northern Indian Ocean originated from biomass burning in South and Southeast Asia. Recent investigation by Tie *et al.* (2006) concluded that high amount of tropospheric NO_2 column in Indonesia, Vietnam and Laos was correlated with biomass burning activities in Indonesia in September 2007 and Vietnam and Laos in April 2007. The GOME measurement of tropospheric NO_2 column during those particular months were 5-10 x 10^{14} molecules/cm^2 in Vietnam and Laos and 10-20 x 10^{14} molecules/cm^2 in Indonesia. The spatial and seasonal measurements (GOME) in SEA were generally found to be consistent with the model results using MOZART-2 particularly in Vietnam and Laos (Figure 1.8). However, there were some visible

discrepancies between the model (MOZART-2) and measurement (GOME) in Indonesian region but generally the differences were within 50%, which is within the uncertainty of both GOME measurement and MOZART-2 calculations (Tie *et al.*, 2006).

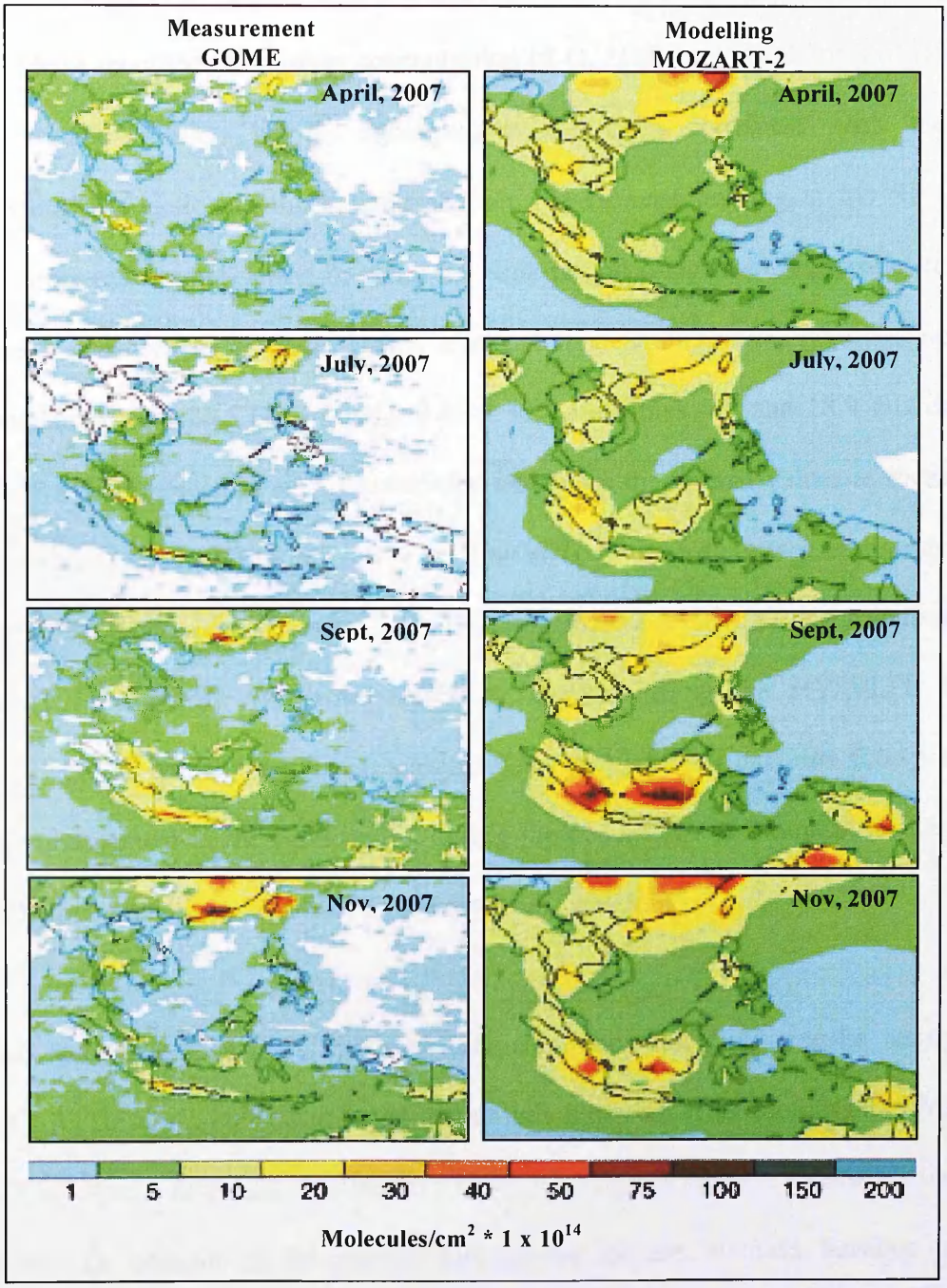

Figure 1.8: Tropospheric column NO_2 in SEA from the measurement (GOMES) and modelling calculations (MOZART-2) in April, July, September and November 2007. (*adapted from* Tie *et al.*, 2006)

The occurrence of biomass burning, combined with the modified circulation that occurs during the El Niño events, for example, has been attributed to the large enhancement of tropospheric O_3 in Singapore (Yonemura, *et al.*, 2002a), Kuala Lumpur, Malaysia (Yonemura *et al.*, 2002b) and Watukosek, Indonesia (Fujiwara *et al.*, 1999; Fujiwara *et al.* 2003) in September to November 1999. Observations in Singapore have recorded the highest concentration of O_3 (112 ppbv) at 8 km altitude on 23rd October 2002. The O_3 enhancement has been correlated with the photochemical production in the air masses from the biomass burning in the SEA region. During the normal period or weak La Niña period (August to September to 1999), the tropospheric O_3 averages at two observation sites in Indonesia (Watukosek and Kototabang) were 25.5 DU or about 6.86 x 10^{15} molecules/cm^2 and 18.9 DU or about 5.08 x 10^{15} molecules/cm^2 respectively, which are the normal values at these sites (Fujiwara *et al.*, 2003) [*note: 1 Dobson Unit (DU) is equivalent to a horizontal density of 2.69 x 10^{14} molecules/cm^2 at standard temperature (273.16K) and standard pressure (101.325 kPa)*]. Backward trajectory analyses using the HYSPLIT 4 (HYbrid Single-Particle Lagrangian Integrated Trajectory) Model has also shown a large O_3 enhancement in the SEA region during the occurrence of biomass burning between February and May in 1998 (Yonemura *et al.*, 2002a).

A recent study based on GOME measurements and modelling results using MOZART-2 (Tie *et al.*, 2006) has found that emission of NO_x from biomass burning in SEA in April, July and November 1997 has significantly enhanced the tropospheric O_3 column in the region. During the intense biomass burning in Indonesia in 1997, the tropospheric column O_3 has been observed to increase between 35-40 DU (or 0.9 – 1.1 x 10^{17} molecules/cm^2). This observation has been captured

well by MOZART-2 model as shown in Figure 1.9 despite some differences of between 5-10 DU, though these differences were thought to be not significant in recognizing the uncertainty of about 5 DU in TOMS/MLS (Tie *et al.*, 2006). Observation in September 2007, when there were extensive forest fires in Indonesia, the total tropospheric NO_x increased by more than 80% and the tropospheric column O_3 by 30-40% (Figure 1.10). The impact of NO_x emission from biomass burning to the enhancement of tropospheric column O_3, however, was not observed in middle and higher latitude such as in central and eastern Asia (i.e China, Korea and Japan).

Intense aerosol emissions in the form of particulate matter have been identified as one of the main pollutants from biomass burning activities. It was estimated that the global emissions of total particulate matter (TPM) from biomass burning are 36–154 Tg/year (Crutzen and Andreae, 1990). In SEA, during the intense biomass burning in the last quarter of 1997, trajectory modelling results have shown the particulate matter (PM_{10}) surge to peak at 416 $\mu g/m^3$ in Kuala Lumpur on 19 September 1997 (Koe *et al.*, 2001), which exceeded the Malaysian Ambient Air Quality Guideline Standard of 150 $\mu g/m^3$ (24-hr average). For the same period, similar trends of high concentrations of particulate matter were also observed in a number of trajectories, as well as at the ground measurements in Kuantan (Malaysia), Singapore, Jambi and Palembang (Indonesia). Measurements of an aerosol index from TOMS instrument-which can detect UV-absorbing aerosols but is less sensitive to pure scattering aerosols such as sea salt and sulfate aerosol and so allows a more accurate comparison for absorbing aerosols such as biomass carbonaceous aerosols - has shown an enhancement of aerosol index (> 0.7) during the investigation of biomass burning emission in Indonesia in 1997 (Figure 1.11) (Chandra *et al.*, 2002; Generoso *et al.*, 2003).

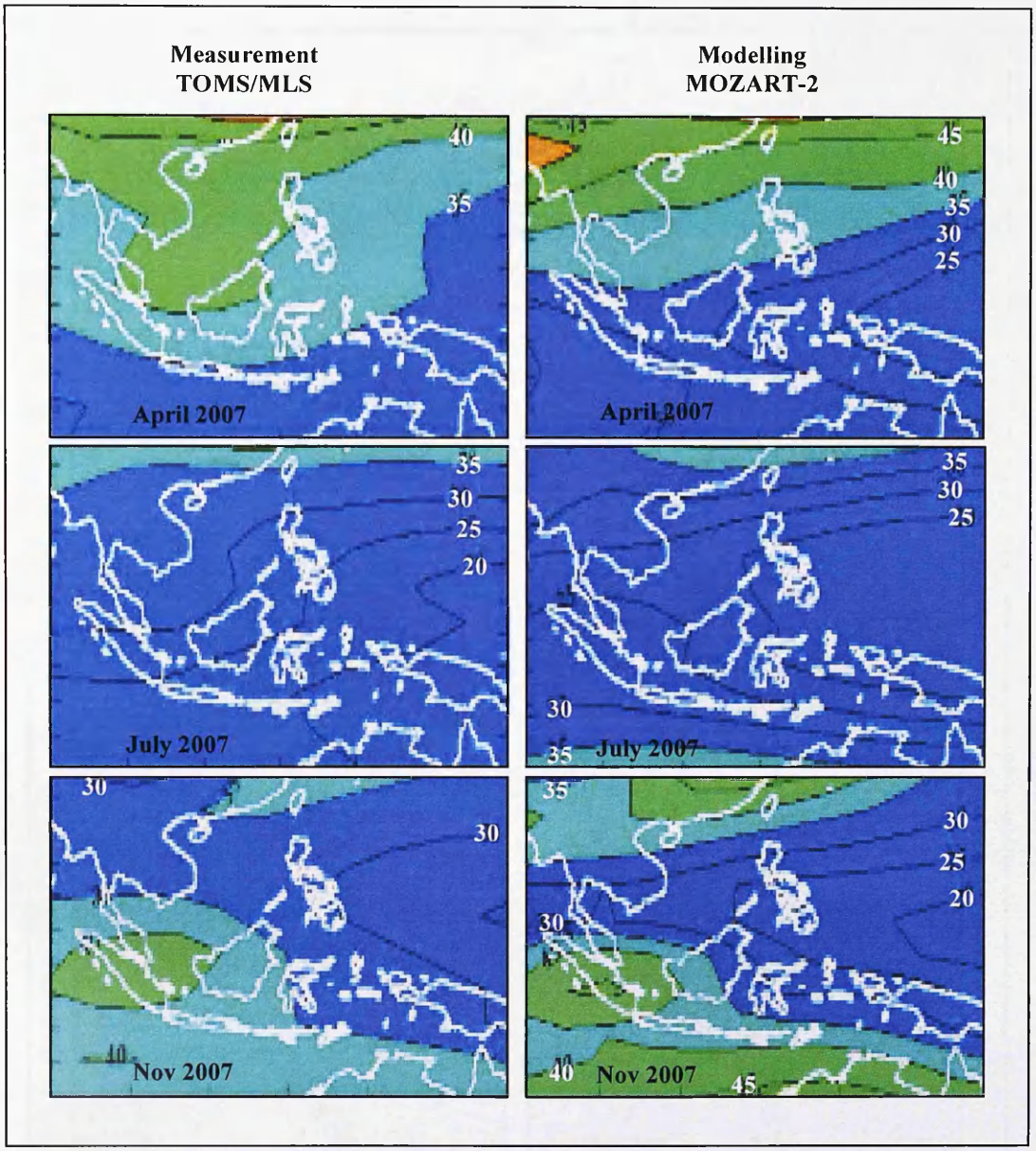

Figure 1.9: Tropospheric column O_3 in SEA from the measurement (TOMS/MLS) and modelling calculations (MOZART-2) in April, July, and November 2007. (*adapted from* Tie *et al.*, 2006)

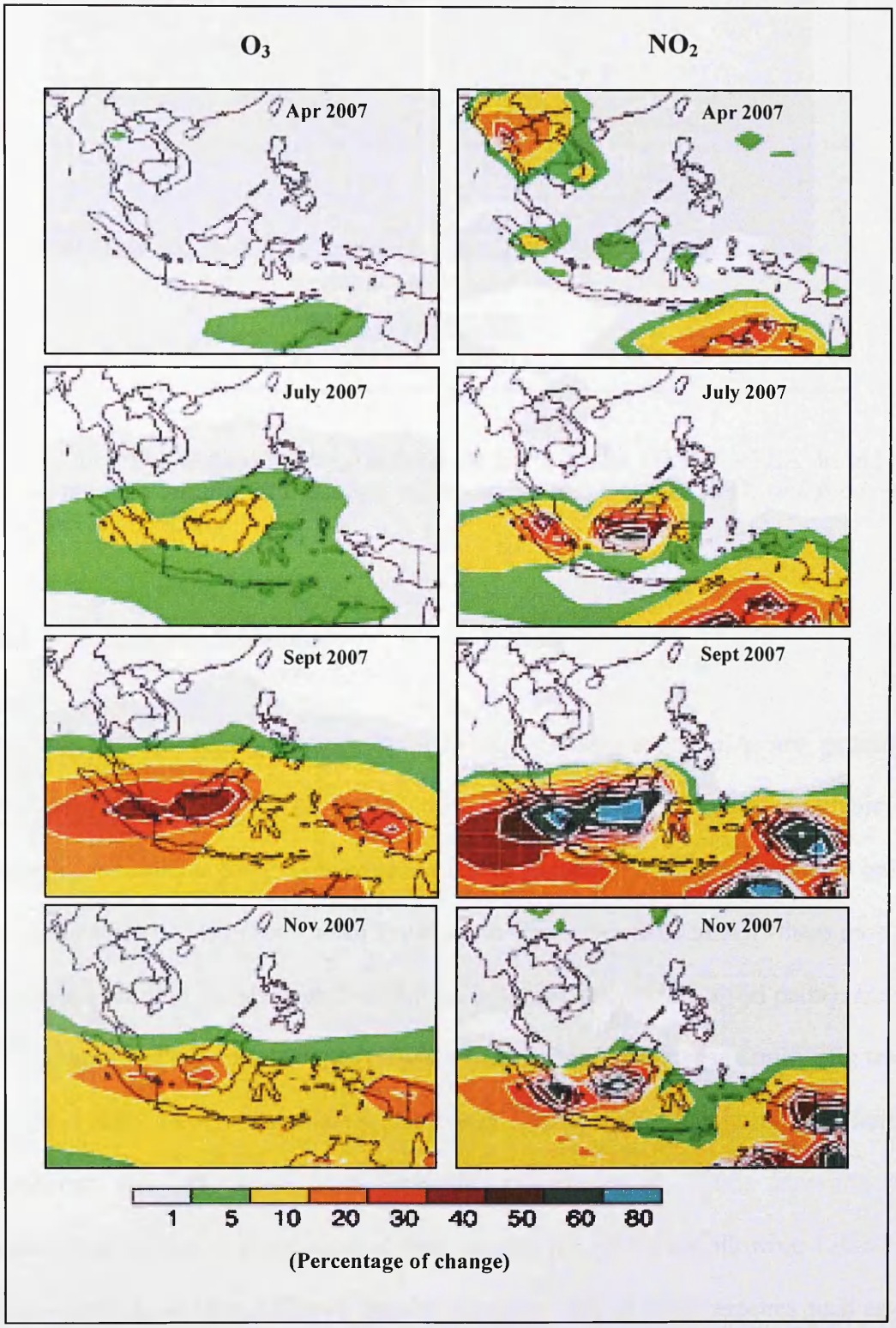

Figure 1.10: Impact of biomass burning NO_x emissions on tropospheric column O_3 in SEA from the modelling calculations (MOZART-2) in April, July, and November 2007. (*adapted from* Tie *et al.*, 2006)

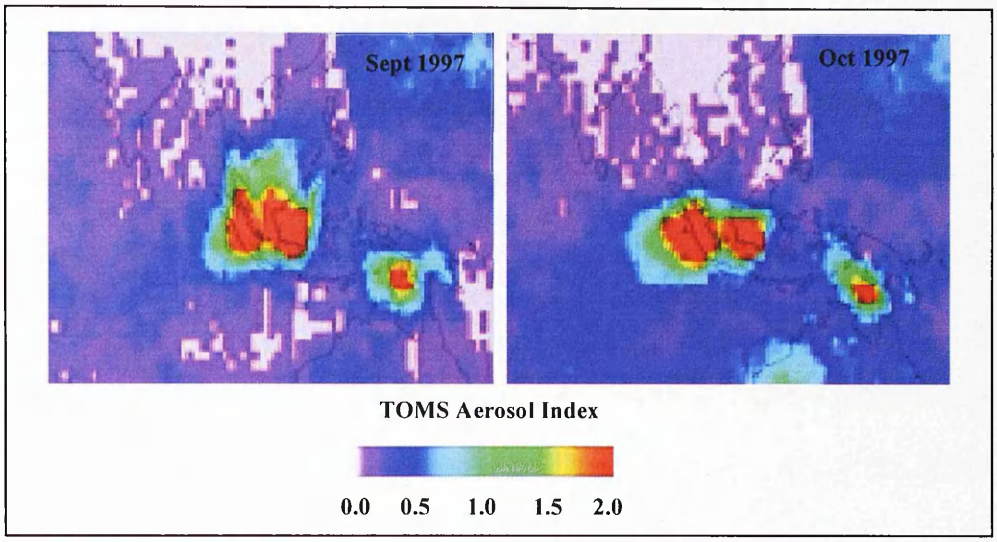

Figure 1.11: The aerosol index (AI) from the Earth-Probe TOMS in SEA during the intense biomass burning in Indonesia in September and October 1997. (*adapted from* Generoso *et al.*, 2003)

1.3.3 Biogenic Emissions

Biogenic volatile organic compound (BVOC) emissions in SEA are generally unknown (See Section 1.2.7). So far, there is very little information available on biogenic emissions in the tropical region of SEA. Recent BVOC measurements on 95 species of trees/plants in the Yunan Province in China (north of SEA), where most of the species are also widely found in SEA such as *Elaeis guineensis* (oil palm), *Hevea brasiliensis* (rubber tree), *Mangifera indica* (mango tree), Moraceae family (fig tree), Palmae (palm trees), *Parashorea chinensis* (hard tree), Bambusoideae family (bamboos), etc. have found high variability (Geron *et al.*, 2006). Isoprene and monoterpene emissions from some of these species are shown in following Table 1.2. These studies have also indicated that the emission rates of monoterpenes such as α-pinene and β-pinene from *H. brasiliensis* are 2–13% higher than earlier studies in southern China by Klinger *et al.* (2002).

The oil palm (*E. guineensis*) and rubber tree (*H. brasiliensis*) are common crops in SEA. Malaysia and Indonesia have the largest plantations of oil palm and rubber in the world (FAO, 2006). Considering the large land cover of oil palms and rubber trees in the region, and at the same time, rapid conversion of forested area into plantations, there are potentially significant impacts to biogenic VOC emissions. In an earlier study by Steiner *et al.* (2002) in the northern part of SEA it was estimated that the human-induced land cover changes, characterised by the conversion of about 30% of the forested area into cropland, led to a decrease of 30% in isoprene and 40% in monoterpene annual emissions.

Table 1.2 Isoprene emissions from selected plants in SEA

Families	**Species (Common Name)**	**EF^E ($\mu g\ C\ g^{-1}h^{-1}$)**		**EF^L ($\mu g\ C\ g^{-1}h^{-1}$)**	
		Isoprene	Monoterpene	Isoprene	Monoterpene
Anacardiaceae	*Mangifera indica* (mango)	25–130	-	-	-
Arecaceae	*Calamus gracilis*	146	-	-	-
	Elaeis guineensis	28	-	3-22	0.0
	(oil palm)	5.5*	0.15*		
Euphorbiaceae	*Hevea brasiliensis* (rubber tree)	0.0	-	0.0	0.4-2.7
Moraceae	*Ficus altissima*	22–118	-	-	-
	Ficus annulata	0-57	-	4–14	0.11
	Ficus auriculata	15	-	4–82	0.2–3.1
	Ficus esquiroliana	98–190	-	-	-
	Ficus fistulosa	49	-	22–31	1.2
	Ficus maclelandii	49	-	28–66	0.0
	Ficus microphylla	50–57	-	-	-
	Ficus regiolosa	39–60	-	-	-

EF^E = Emission factor determined from the EPA cuvette and PID system
EF^L = Emission factor determined from the Lancaster cuvette and GC/FID system

Source: Extracted from Geron *et al.* (2006)

* = *Emission fluxes above the oil palm plantation during the OP3 measurement campaign in Borneo*
Source: Extracted from Nemitz *et al.* (2008)

1.4 Climate-Atmospheric Chemistry Models

The chemistry-climate system is controlled by a large number of complex chemical and physical processes in the atmosphere. In light of the complex and non-linear interactions between the atmospheric chemistry and climate, numerical models are pivotal in carrying out any study. Numerical models, which have been increasingly developed over the past 15 years, have tremendously improved our understanding of the global and regional chemistry-climate interactions. Further, in order for policy-makers to effectively address the impact of climatically reactive gases to regional and global climate changes and vice versa, it is important to provide accurate and reliable assessments that are based on accurate physical models, which account for the interactions between atmospheric components and climate. Tropospheric chemistry models are used to project emissions, transport, chemical reactions and conversions of tropospheric gases. Meanwhile, climate models are used to simulate the dynamics and thermodynamics of the atmosphere and oceans. In order for these two models to interact, coupling of these models is required as demanded by the physics of the processes involved (Wang and Prinn, 1999). Coupling can be on-line or , as in this study, off-line. Tropospheric climate-chemistry models are useful tools for the understanding of pollutant dynamics in the atmosphere, and how the climate might evolve or respond to the changes of future atmospheric chemical compositions and vice versa.

1.4.1 Climate Models

General circulation models (GCMs) with global coverage have been the primary tools used in climate studies. The current resolutions of GCMs of 200–500 km are capable

of simulating the global climate of the recent past reasonably well. However, due to their low resolution, the model results produce apparent errors of as much as ±5°C in temperature, and -40% to +60% in precipitation for regional climates (IPCC, 2001; Leung *et al.*, 2003; Fowell, 2006). In order to provide a more realistic response of regional climate changes to radiative forcings, particularly in areas with complex orography, coastline, and landuse patterns, higher resolution regional climate models should be considered (IPCC, 2001; IPCC, 2007-Chapter 11).

A regional climate model (RCM) is a higher resolution model that covers a limited area of the globe. RCMs are comprehensive physical models, which include the components of the climate system of the atmosphere and land surface, as well as the representation of the important processes within the climate system. In RCMs the physical processes that take place on much smaller spatial scale than the GCM model grid are taken into account using parameterizations, where the process is represented by relationships between the area or time averaged effect of such sub-grid scale processes and the large scale flow (Jones *et al.*, 2004). In this manner, the RCMs produce high resolution simulations for region of interest the simulations being consistent with the large-scale simulations from the GCM. There are a number of reasons why RCMs are necessary in the investigation of regional climate change. (Jones *et al.*, 2004). RCMs simulate current climate more realistically, particular in mountainous areas and closer to the coastline on scales of 100 km or less (Figure 1.12 and Figure 1.13). RCMs also represent smaller islands in climate change simulations, and so resolve better the difference in thermal inertia between land and ocean (Figure 1.14). Another interesting feature of RCMs is their capability to simulate better extreme changes of weather such as heavy rainfall events. RCMs can also provide an

indication of mesoscale weather features such as cyclones and hurricanes, which is absent in the driving GCM (Figure 1.15).

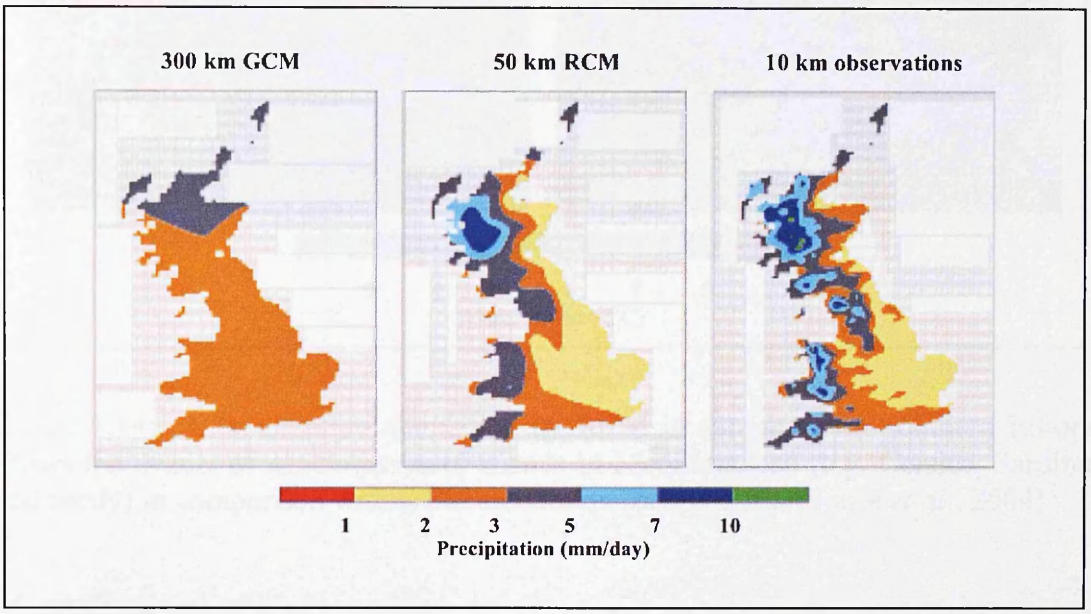

Figure 1.12: A more realistic simulation by RCM of enhanced rainfall (mm/day) over the mountains of the western part over Great Britain in winter (*adapted from* Hulme *et al.*, 2002).

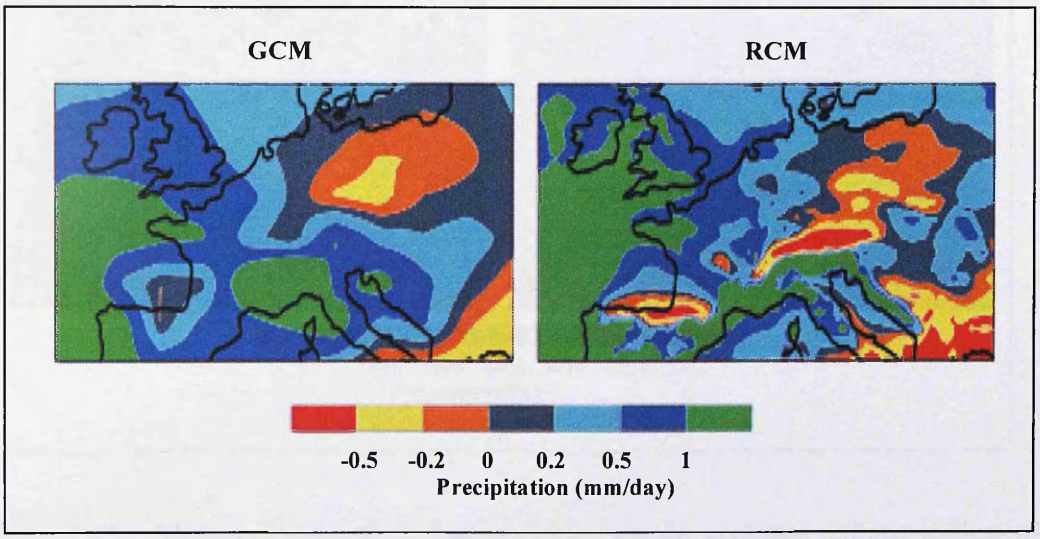

Figure 1.13: More detail on precipitation changes in winter (between now and the 2080s) simulated by RCM over the Pyreenees and Alps in Europe (*adapted from* Durman *et al.*, 2001).

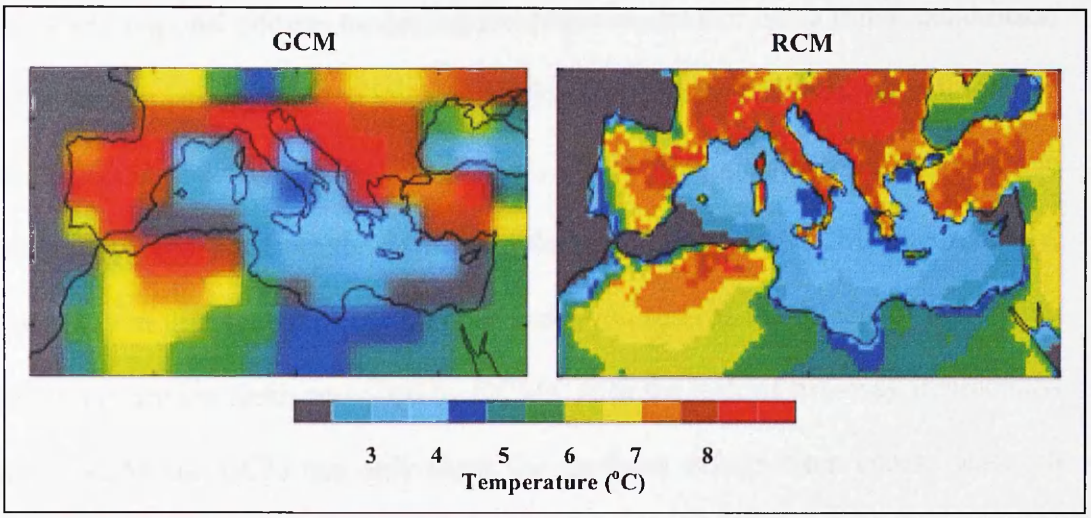

Figure 1.14: A temperature simulation by RCM in summer over southern Europe shows the details of simulation over islands in Mediterranean (e.g. Corsica, Sardinia and Sicily) in comparison with GCM simulation (*adapted from* Jones *et al.*, 2004).

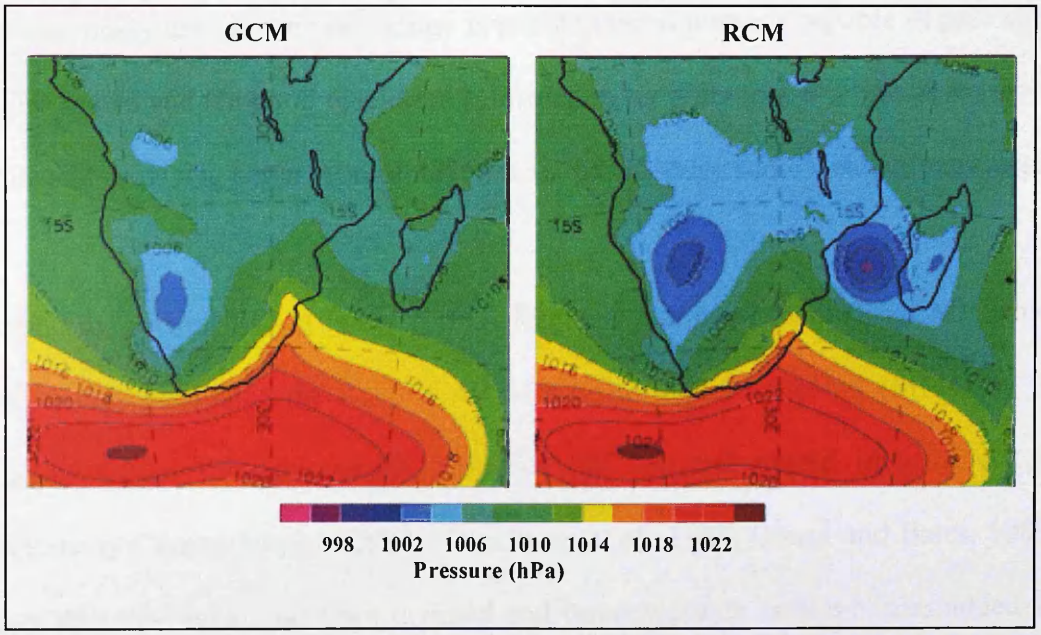

Figure 1.15: Mesoscales weather features, such as the pressure pattern indicating a cyclone in the Mozambique Channel are clearly illustrated in the RCM but absent in the driving GCM (adapted from Hudson and Jones, 2002).

The RCMs can be nested into a GCM either one-way or two-way, but to date the usual nested regional climate modelling technique consists of using initial conditions, time-dependent lateral meteorological conditions, and surface boundary conditions, to drive RCMs in one-way mode (Giorgi *et al.*, 2001). The one-way nesting technique doesn't allow feedback from the RCMs simulation to the driving GCM. Theoretically, the one-way nesting technique could pose limitation such as the effects of systematic errors in the driving fields provided by GCMs. Also the lack of two-way interactions between RCM and GCM can only show the feedback effects from coarse scales to fine scales but in the real atmosphere, feedbacks derive from different regions and interact with each other (Giorgi *et al.*, 2001). Despite the setbacks in terms of dependency on input from the GCM driving model, the lack of two-way nesting with its driving model, as well as its computational cost, RCMs are still developing rapidly and are widely used in climate change investigations as they are capable of providing higher spatial and temporal resolution information for a number of climatic variables while still providing better representation than the GCM for some weather extremes.

Among the earliest RCMs is the NCAR Regional Climate Model (RegCM), which was initially built upon the PSU/NCAR Mesoscale Model version 4 (MM4) by the National Center for Atmospheric Research (NCAR) and nested into the NCAR Community Climate Model (CCM) (Dickinson *et al.*, 1989; Giorgi and Bates, 1989). Since then, the model has been updated and improved with new modules added for use in chemistry-climate interaction studies (Giorgi *et al.*, 1993; 1999: 2002). Meanwhile, the Canadian Regional Climate Model (CRCM), which was developed based on the dynamic core of the Compressible Community Mesoscale model (MC^2), is nested one way on the second generation Canadian GCM (GCMii) and with an

execution resolution of 45 km (Laprise *et al.*, 1997; Caya and Laprise, 1999). This model has been tested and widely used in a number of regional climate studies (Bouchet *et al.*, 1999; Barrette and Laprise, 2002; Anderson *et al.*, 2003; Laprise *et al.*, 2003; Girard and Bekcic, 2005). The Climate High Resolution Model (CHRM) is another regional climate model that has been used in a number of climate studies in Europe for example by Luthi *et al.* (1996) and Vidale *et al.* (2003). This model is developed based on the High Resolution Model (HRM) version 1.6 of the German Weather Service, DWD. The PRECIS RCM, which was used in the present study was developed by the Hadley Centre with a resolution of 25 km x 25 km is capable of producing a high resolution climate model with reasonable computational requirements (Jones *et al.*, 2004) and has been used in a number of climate change impact studies in South Asia (see Bhaskaran *et al.*, 1998; Hassel and Jones, 1999; Islam and Mannan, 2005; Challinor *et al.*, 2006; Kumar *et al.*, 2006), East Asia (see Erda *et al.*, 2005; Wang and Shallcross, 2005), Europe (see Moberg and Jones, 2004; Lalas *et al.*, 2005), Africa (see Hudson and Jones, 2002; Arnell *et al.*, 2003; Beraki, 2005), and North America and South America (see Martineu, 2005; Marengo and Ambrizzi, 2006).

1.4.2 Atmospheric Chemistry Models

The integration of individual atmospheric processes and their interactions can be better understood through mathematical modelling. Atmospheric chemistry models have been widely used over the last 20 years for various objectives, mainly to study the transport and chemistry of trace gases and aerosols in the atmosphere, as well as to project and assess future changes in the chemical composition of the atmosphere and its effect on climate change. Basically, atmospheric chemistry models are

developed based on Lagrangian or Eulerian models (Seinfeld and Pandis, 1998). The Lagrangian models simulate the chemical composition of a given air parcel advected with the local wind. Usually no mass exchange occurs between the air parcel and its surroundings except for species emissions. The Eulerian models describe the concentrations in an array of fixed computational cells, and species emissions can enter and leave the cell with the wind. All atmospheric chemistry models are characterized by their dimensionality (Seinfeld and Pandis, 1998; Rhode, 1999).

CiTTyCAT (Cambridge Tropospheric Trajectory Model of Chemistry and Transport) is a zero-D Lagrangian atmospheric chemistry model that simulates the interaction of a range of chemical compounds in the lower atmosphere. This model, which was developed by Wild (1995) was used in the present work for the investigation of the climate changes feedback on tropospheric chemistry in SEA. This chemistry model has been used in a number of tropospheric chemistry simulation studies such as by Evans *et al.* (2000); Methven *et al.* (2001); Emmerson (2002); Donovan *et al* (2005) and Ryder (2005). Chemical Transport Models (CTMs), which typically have modules to treat pollutant emission, transport, chemical conversion, and removal, are also widely used to simulate air pollutants within 3-D and time-dependent framework (Russell, 1997; Roelofs and Lelieveld, 1997; Wang *et al.*, 1998; Crutzen *et al.*, 1999; Wild and Prather, 2000; Horowitz *et al.*, 2003). These models also rely on meteorological fields generated from global climate models to drive the models for long-term trends and impact studies (Wang *et al.*, 1998; Horowitz *et al.*, 2003), or from regional climate models for simulating short-term trends and evaluating model performance during specific periods (Byun and Ching, 1999; Klonecki *et al.*, 2003). For example, GEOS-CHEMs, a 3-D model, is driven by assimilated meteorological

observations from the Goddard Earth Observing System (GEOS) of the NASA Global Modelling and Assimilation Office (GMAO) with a temporal resolution of 6 hours (*http://www-as.harvard.edu/chemistry/trop/geos/ index.html*). This model has been widely used in a number of atmospheric studies (see Bey *et al.*, 2001; Liu, 2004; Park *et al.*, 2006). STOCHEM is another 3-D CTM developed by the Hadley Centre, which is driven by meteorology field data from the Hadley Centre GCM. The details of this model are described by Collins *et al.* (1997; 1999) and also widely used in a number of studies related to atmospheric chemistry and modelling (see Collins *et al.*, 2000; Derwent *et al.*, 2006)

1.4.3 Climate-Chemistry Models

The chemistry of the troposphere is dominated by the responses of the atmosphere to a variety of emission sources, both anthropogenic and natural. Emissions of chemically and radiatively important trace gases from these sources are crucial input to the climate-chemistry models. In the modelling studies, emissions of long-lived gases, which are the key determinant changes in radiative forcing such as CO_2, CH_4, N_2O, and CFCs are included along with several short-lived trace gases such as NO_x, SO_2, and CO. Different scenarios of emissions are normally employed in modelling studies to capture the atmospheric chemistry sensitivity to climate changes, which can also be linked to existing and/or proposed policies for control of emissions of aerosols and climatically important trace gases. The output of the models can be utilised to drive other regional or global models (i.e. terrestrial ecosystem models, etc.) that can give feedback to the climate models, chemistry models, and natural emission models (Prinn *et al.*, 1999).

The most advanced climate-chemistry modelling studies use 3-D climate-chemistry models, where climate and atmospheric chemistry are fully coupled, and which can be used to simulate both the climatological and atmospheric chemical processes simultaneously(Adams *et al.*,1999; Kiehl *et al.*, 2000; Koch *et al.*, 2001; Jacobson, 2001). However, one of the limiting factors to using these models is the computational resource requirement, which is very high. Various component of the models are integrated and the interactions within the climate system and chemistry system are executed by exchanging simulated state parameters among component models (Yu, 2004). The back-and-forth passing of simulated parameters between the models system constitutes a coupling interface, where these coupling interfaces are responsible for coordinating and processing information flow among component models and this normally require high-performance computational tools (Yu and Mechoso, 1999) Processing and analyzing the huge amounts of output from long-term simulations of coupled climate-chemistry model can also be time-consuming and difficult.

A recent approach in climate-chemistry modelling is to extend the GCMs to become Earth System Models or integrated models, where global dynamics, chemistry, biology, and oceans are interactively coupled. For example, the MIT Integrated Global System Model (IGSM), which was developed at the Massachusetts Institute of Technology was designed for analysing global environmental changes due to anthropogenic causes, quantifying the uncertainties associated with projected changes, and assessing the cost and effectiveness of proposed mitigation measures on climate change (Sokolov *et al.*, 2005). The model includes an economic model for analysis of GHGs and aerosol precursors and mitigating measure proposals, atmospheric chemistry and climate model, and terrestrial ecosystems model. In this

integrated model, the emission model outputs are used to drive the coupled atmospheric chemistry-climate model, and meanwhile the climate model outputs are used to drive the terrestrial ecosystems model to project the land vegetation changes, land CO_2 fluxes, and soil composition, which give feedback to the coupled chemistry-climate and natural emissions models. This modelling approach has been used to study the effects of ozone damage on carbon sequestration and its effect on climate change policies (Felzer *et al.*, 2005) and climate changes for the 21st century in response to the increasing emissions of GHGs and aerosols (Dutkiewicz *et al.*, 2005).

1.5 Modelling Climate Changes and Tropospheric Chemistry in SEA

The broad focus of the present study is to investigate the regional climate changes based on a number of emission scenarios, and to subsequently investigate the regional atmospheric chemistry changes based on feedback from regional climate change modelling results. Further investigation of feedback from the regional climate-chemistry system in response to the changes of land cover and emissions are also to be carried out. Figure 1.16 shows the conceptual framework of this study. The study area covers most of the SEA region with a domain of 33° latitude x 55° longitude (approximately 2.20 x 10^7 km^2) (see Figure 3.1). The domain to be studied is at the upper end of regional studies considering the operational definition of the "regional scale" as areas between 10^4 and 10^7 km^2 (Giorgi *et al.*, 2001). Regional- and local-scale forcings such as complex topography, land-cover characteristics, atmospheric aerosols, radiatively active gases, inland water bodies, ocean-land contrast, sea ice, snow, and ocean current distributions, which modulate the spatial and temporal structure of the regional climate signal are embedded within the global scale

circulations regimes that can influence the global scale circulation features (Giorgi *et al.*, 2001).

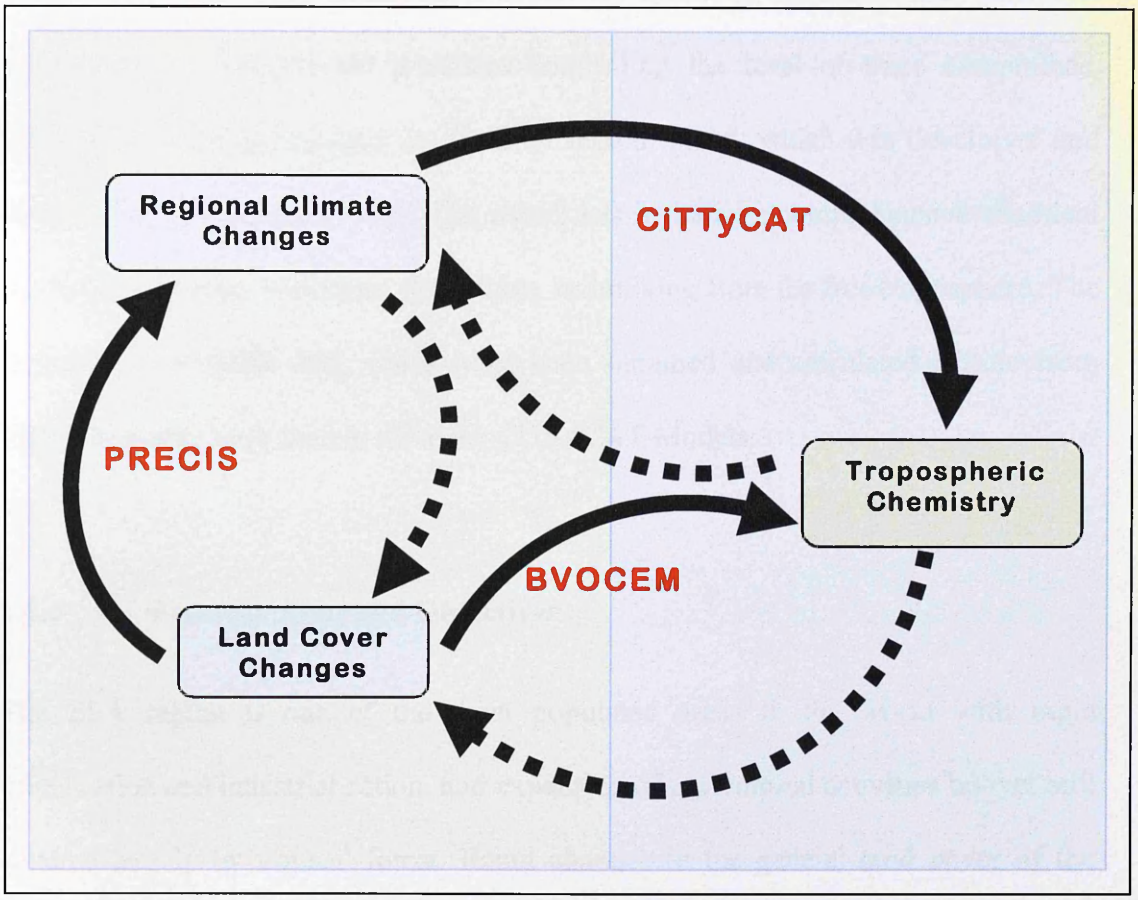

Figure 1.16: Conceptual framework of relationship between land cover-climate-tropospheric chemistry system. The dotted line relationships were not investigated in the present study.

For the projection of climate changes in the region, PRECIS-RCM (Providing REgional Climates for Impact Studies - Regional Climate Model), a regional climate modelling system developed by the Hadley Centre (Jones *et al.*, 2004) was used. The PRECIS RCM was used to downscale output from the global circulation model (GCM), for both recent and future climates. The RCM is nested within the coarse-scale global model to simulate the climate over the SEA region at a finer spatial and

temporal resolution. Emission scenarios were constructed based on the Intergovernmental Panel on Climate Change (IPCC) emission scenarios (IPCC, 2001) as an input to the PRECIS. Meanwhile, a simple chemical transport model, CiTTyCAT (Cambridge Tropospheric Trajectory model of Chemistry and Transport) was used to investigate the processes controlling the level of trace compounds, including aerosol components, in the SEA region model, which was developed and described by Wild *et al.* (1996). The model has included a comprehensive chemical mechanism scheme, emissions, deposition, and mixing from the free troposphere. The meteorological fields data, which have been obtained and calculated offline from PRECIS model, were used to drive the CiTTyCAT Models.

1.5.1 Research Aims and Objectives

The SEA region is one of the most populated areas in the world with rapid urbanization and industrialization, and expansion of agricultural activities but yet still covered largely by tropical forest. Rapid changes to the general land cover of the region, coupled with the increase in anthropogenic emissions and naturally high levels of biogenic emissions have been the impetus of this study. The objective of this study is to project the future regional climate in SEA based on IPCC emission scenarios using the PRECIS regional climate model. Interactions between the regional climate change and tropospheric chemistry are also investigated by using the meteorological field output data from the regional climate model to drive CiTTyCAT, a tropospheric chemistry model. This study is also extended to investigate the effects of land cover changes on the regional climate-tropospheric chemistry system at the regional scale.

Improved knowledge on climate-chemistry interactions in less-studied areas such as SEA is necessary for the evaluation of which mechanisms are important to be incorporated into models. These mechanisms include chemistry, emissions, land surface, and atmospheric dynamics. This region in particular is forecast to experience the largest increase of O_3 forcings in association with its rapid increase of population and extensive economic activities (Dorland *et al.*, 1997; Brasseur *et al.*, 1998). A high rate of land cover change, such as rainforest conversion to other types of land use mainly agriculture, was reported to be between 20–60% from 1981–1990 in SEA (WRI, 1994; O'Brien, 2000), and intensive anthropogenic land-use change in SEA may cause greater changes to the local radiative forcing than that of all the anthropogenic greenhouse gases together (IPCC, 2001).

This study is motivated by four scientific questions. First, what spatial patterns of climate changes are predicted by a state-of-the-art regional climate model over SEA? secondly, based on the projected future climate changes, what would be the projected spatial patterns of secondary tropospheric pollutants, especially ozone in the region? Thirdly, in light of the interactions between climate changes and tropospheric chemistry, what one-way feedbacks (climate change feedbacks on tropospheric chemistry) arise from the new chemical environment? Finally, what is the role of land cover changes to the regional climate-chemistry system?

1.5.2 Outline of the Study

This thesis, underlined by the abovementioned aims and objectives, is organized as follows:

The details of the tropospheric chemistry of the chemically reactive gases and aerosols, and the climate-chemistry interactions, and the effect of land surface change on the climate-chemistry system are discussed qualitatively in Chapter 2. Specific reference is made of the perturbation effects of tropospheric chemical composition on climate change, and also the climate change feedbacks on tropospheric chemistry. Chapter 3 and Chapter 4 describe the details of the regional climate model (PRECIS) runs used in this study, which has focused on the investigation of the regional climate change and the importance of land cover changes to the regional climate changes. Chapter 5 describes the investigations of landcover changes and climate-change effects to the regional biogenic emissions. In Chapter 6, the impacts of climate change, landcover changes and biogenic emissions on tropospheric chemistry will be described. Chapter 7 summarises the main conclusions of this study and its implications, and discussion of future investigations.

Chapter 2

TROPOSPHERIC CHEMISTRY AND CLIMATE CHANGES

2.1 Introduction

The perturbation in atmospheric abundance of climate active gases and aerosols, both by human and natural activities, either directly or through emissions of their precursors, is well recognised. Changes in the distribution of these tropospheric gases and aerosols through chemical transformations have been known to affect the dynamics of the chemistry-climate system, such as the changes of temperature in the troposphere (Stevenson *et al.*, 2000). Conversely, climate changes affect the chemical and physical processes that determine atmospheric composition through changes in temperature, water vapour, short wave radiation, and other factors (Ravishankara and Liu, 2003). The emissions of GHGs, reactive gases, and aerosol have been discussed in Chapter 1. In this Chapter, atmospheric chemistry processes are reviewed.

2.2 Atmospheric Chemistry of Reactive Gases and Aerosols

The lifetimes of most atmospheric species are strongly affected by atmospheric concentrations of oxidant species, which play vital roles in tropospheric chemistry as they have the capability to control the chemistry and chemical composition of the troposphere (Guicherit and Roemer, 2000). In polluted atmospheres, important oxidants, which have a greater oxidation potential than oxygen, are formed through chemical reactions among the primary pollutants. The abundance of oxidants such as tropospheric OH radicals largely defines the oxidising capacity of the atmosphere, as

they are capable of reacting with hundreds of emissions from anthropogenic and natural sources (Thompson, 1992). Other reactive oxidants such as O_3, nitrate (NO_3) radicals, excited state atomic oxygen (O^1D), hydroperoxyl (HO_2) radicals, organic peroxy (RO_2) radicals, hydrogen peroxides (H_2O_2), ground state atomic oxygen (O^3P), and organic peroxides (ROOH) are also important to the tropospheric oxidising capacity (Fuglestvedt *et al.*, 1999; Thompson, 1992).

One of the most important roles played by O_3 is the generation of OH radicals, which are responsible for initiating the oxidation of a wide variety of atmospheric trace constituents (Thompson, 1992). OH is formed when O_3 undergoes photolysis to form excited oxygen, $O(^1D)$ (R1). Subsequently $O(^1D)$ will either be deactivated to ground-state oxygen $O(^3P)$ and be rapidly oxidised to reform O_3 (R2 & R3), or will react with vapour (H_2O) to produce OH radicals (R4) (Atkinson *et al.*, 1997; DeMore *et al.*, 1997).

$$O_3 + h\nu \rightarrow O(^1D) + O_2 \qquad (R1)$$

$$O(^1D) + M \rightarrow O(^3P) + M \qquad (R2)$$

$$O(^3P) + O_2 + M \rightarrow O_3 + M \qquad (R3)$$

$$O(^1D) + H_2O \rightarrow 2OH \qquad (R4)$$

Photolysis of O_3 is the main route for OH radicals production in the atmosphere and the OH production process itself depends on the quantum yield for $O(^1D)$ production. In the lower troposphere, where H_2O is present at mixing ratio of up to 10^4 ppm (1%) and the rate constant of reaction R4 is larger than reaction R2 by a factor of 10, most of the generated $O(^1D)$ reacts with H_2O to produce OH (Seinfeld and Pandis, 1998). At room temperature (278K) and 50% relative humidity, approximately 0.2 OH

radicals are formed per $O(^1D)$ atom generated from the O_3 photolysis. As the H_2O mixing ratio decreases with altitudes in the troposphere, and at the same time the O_3 mixing ratio generally increases, therefore the production of OH radical concentration through reaction R4 will be diminished (Dentener and Crutzen, 1993).

Away from sources of reactive organic compounds and nitrogen oxides, the OH radicals will also react with O_3 (R5) to produce HO_2, which subsequently reacts with O_3 to reform OH radicals (R6), and also, the combination of two HO_2 radicals will produce H_2O_2 (R7), either in the atmosphere or inside cloud droplets (Graedel and Weschler, 1981).

$$OH + O_3 \rightarrow HO_2 + O_2 \qquad (R5)$$

$$HO_2 + O_3 \rightarrow OH + 2O_2 \qquad (R6)$$

$$HO_2 + HO_2 \xrightarrow{M} H_2O_2 + O_2 \qquad (R7)$$

The OH radical is extremely reactive, and is the most important oxidizing agent in the gas phase (Graedel, 1978; Thompson, 1992). The concentration of OH radicals in the troposphere is mainly controlled by chemical cycling of the hydrogen oxide family and the nitrogen oxide family both of which, in turn, depend on the ratio of reactive organic compounds to nitrogen oxides in the air parcel. The OH radical and other radicals are also responsible for the transformation and initiation of the removal of many important tropospheric trace gases, which will be further highlighted in the following sections.

2.2.1 Chemically Reactive Gases

Chemically active gaseous pollutants emitted into the lower levels of the troposphere can be transported for long distances in the atmosphere, and play a major role in atmospheric chemistry. The regional atmospheric chemistry of chemically active gases such as NO_x, CO, and VOCs are known to affect the regional climate by influencing the emission rates and residence times of GHGs such as O_3. In the following sections, important chemical reactions of reactive gases in the troposphere will be discussed briefly.

2.2.1.1 Chemistry of NO_x in the troposphere

In the troposphere, NO_x is emitted from anthropogenic and natural sources (see Chapter 1: Section 1.2.5). Nitric oxide (NO) is emitted to the atmosphere from anthropogenic and natural sources, and rapidly oxidised into NO_2 by a number of oxidants, primarily O_3 and radicals such as HO_2 and RO_2 (R8–R10) (Atkinson, 2000).

$$NO + O_3 \rightarrow NO_2 + O_2 \qquad (R8)$$

$$NO + HO_2 \rightarrow NO_2 + OH \qquad (R9)$$

$$NO + RO_2 \rightarrow NO_2 + RO \qquad (R10)$$

Where RO and RO_2 are –oxy and –peroxy radicals formed from the oxidation of reactive organic compounds. During daytime, NO_2 is photolysed to reform NO and $O(^3P)$ (R11), where $O(^3P)$ will combine rapidly with O_2 to form O_3 (R3):

$$NO_2 + h\nu \rightarrow NO + O(^3P) \qquad (R11)$$

$$O(^3P) + O_2 + M \rightarrow O_3 + M \qquad (R3)$$

So, reactions R3, R8 and R11 form a rapid cycle with a characteristic timescale of only a few minutes. These reactions define what is called the photostationary state for O_3. Reactions R9 and R10, on the other hand, produce NO_2 without consuming O_3, and so constitute a source of NO_2 (or O_3). When reactions R9 and R10 occur alongside reactions R1 and R4-R7, O_3 production occurs.

In polluted conditions, another important reaction involving NO_x is the reaction of NO_2 with O_3 to form nitrate (NO_3) radicals (R12), which play an important role in night-time chemistry due to their high reactivity (Atkinson, 2000). During daytime, NO_3 will rapidly dissociate to NO and NO_2 (R13 & R14), but at night-time, NO_3 will react again with NO_2 to form dinitrogen pentoxide (N_2O_5) (R15) (Wayne *et al.*, 1991; Carslaw *et al.*, 1997; Allan *et al.*, 1999; Atkinson, 2000; Wayne, 2000). In this case, the reaction with NO_3 becomes a night sink of NO_2.

$$NO_2 + O_3 \rightarrow NO_3 + O_2 \qquad \text{(R12)}$$

$$NO_3 + h\nu \rightarrow NO_2 + O(^3P) \qquad \text{(R13)}$$

$$NO_3 + h\nu \rightarrow NO + O_2 \qquad \text{(R14)}$$

$$NO_3 + NO_2 + M \rightleftharpoons N_2O_5 + M \qquad \text{(R15)}$$

During night-time, the heterogeneous hydrolysis of N_2O_5 will lead to the formation of nitric acid (HNO_3) (R16) (Mentel *et al.*, 1996), which is an alternative pathway to HNO_3 formation, besides the gas-phase oxidation of NO_2 by OH radicals (R17) during daytime (Ehhalt *et al.*, 1991; Atkinson, 2000). Nitric acid ($HONO_2$) will be removed in the atmosphere through wet and dry deposition, and uptake of N_2O_5 by aerosols (Jacob, 2000; Wesley and Hicks, 2000). Additional homogeneous oxidation of NO by OH will lead to the formation of nitrous acid (HONO) (R18) during night-

time, which is also attributed to the heterogeneous hydrolysis of NO_2 on aerosol and particulate matter surfaces (Lammel and Cape, 1996; Jacob, 2000).

$$N_2O_5 + H_2O\ (aq) \rightarrow 2HNO_3 \qquad (R16)$$

$$NO_2 + OH + M \rightarrow HNO_3 + M \qquad (R17)$$

$$NO + OH + M \rightarrow HONO + M \qquad (R18)$$

Formation of HONO provides a reservoir for OH that can be released when an air parcel next experiences daylight, because HONO is rapidly photolysed at visible wavelengths.

2.2.1.2 Chemistry of tropospheric ozone

Ozone (O_3) has been recognised as one of the most important oxidants in the troposphere (Thompson, 1992). Interest in this oxidant, particularly its distribution at the global and regional scale, has been enormous, mainly due to its toxicity but also because O_3 is an effective GHG in the middle and upper troposphere (Lacis *et al.*, 1990; Wang *et al.*, 1980). This is in contrast to CO_2 and water vapour, which are also GHGs, abundant in the atmosphere, but which are not chemically reactive, and therefore their abundance in the lower atmosphere is not defined by chemical processes (IPCC, 2001).

The net effect of the photostationary state for O_3 is neither to generate nor destroy O_3, and therefore, for ozone to accumulate, an additional pathway is needed to convert NO to NO_2. The photochemical oxidation of VOCs, such as hydrocarbons and aldehydes provides that pathway (Finlayson-Pitts & Pitts, 2000; Seinfeld & Pandis,

1998). The degradation of VOCs (including CH_4) will lead to the formation of intermediate RO_2 and HO_2 radicals, which will react with NO to form NO_2 (R19 & R9). Subsequently, photolysis of NO_2 will lead to the net formation of O_3 (R11 & R3) (Atkinson, 2000; Wayne, 2000). The net result of this chain of reactions is that NO_x is acting as a very important precursor of O_3 formation in the troposphere.

$RO_2 + NO \rightarrow RO + NO_2$ (R19)

$HO_2 + NO \rightarrow OH + NO_2$ (R9)

$2(NO_2 + h\nu \rightarrow NO + O(^3P))$ (R11)

$2(O(^3P) + O_2 + M \rightarrow O_3 + M)$ (R3)

Net: $RO2 + HO2 + 2O_2 \xrightarrow{NO, M, h\nu} RO + OH + 2O_3$

Much of the tropospheric O_3 production is balanced by other photochemical reactions that involve O_3 destruction, mainly through catalytic destruction cycles, involving radicals such as OH and HO_2 (R5 & R6). Photolytic destruction (R1) is an additional loss process for O_3 (Atkinson, 2000; Wayne, 2000). Another significant sink of tropospheric O_3 is through uptake by vegetation, which in term of magnitude is found to be comparable with the influx of O_3 from the stratosphere into troposphere (IPCC, 2001). The rate of O_3 uptake by vegetation is driven by environmental conditions that influence stomatal opening and closure (with high uptake through open stomata) and not merely O_3 concentration. A number of studies have investigated the uptake of O_3 by various types of crops and plants (Emberson *et al.*, 2000; Mikkelsen *et al.*, 2000; Fowler *et al.*, 2001; Manes *et al.*, 2007) and their response to the exposure to O_3 concentrations (Fuhrer *et al.*, 1997; Tuovinen, 2000). As the scope of these studies are limited to certain species of plants and crops and mostly in mid- and high-latitude, the estimates of O_3 uptake by vegetation are highly varied and still largely

unknown. In the polar marine boundary layer, under certain environmental conditions, O_3 loss is observed notably at the end of Arctic winter through reactions involving halogen radicals and aerosol though the contribution to the global O_3 loss is expected to be small (Oum *et al.*, 1998; Dickerson *et al.*, 1999; Impey *et al.*, 1999; Platt and Moortgat, 1999; Prados *et al.*, 1999; Vogt *et al.*, 1999).

2.2.1.3 Chemistry of tropospheric methane

In the free troposphere, the major loss of CH_4 is through oxidation by OH radicals (R20) to form methyl (CH_3) radicals (e.g. Levy, 1971; Bruhl and Crutzen, 1999). In the troposphere, the methyl radicals react solely with O_2 to yield methyl peroxy (CH_3O_2) radicals (R21) (e.g. Atkinson *et al.*, 1992):

$$CH_4 + OH \rightarrow CH_3 + H_2O \qquad (R20)$$

$$CH_3 + O_2 + M \rightarrow CH_3O_2 + M \qquad (R21)$$

Subsequently, methyl peroxy radicals can react with NO, NO_2, HO_2 radicals, and other organic peroxy (RO_2) radicals in the troposphere. In the presence of NO, the reaction will lead to the formation of methoxy (CH_3O) radicals (R22). The only important reaction involving methoxy radicals in the troposphere is the reaction with O_2 to form HCHO and HO_2 radicals (R23). HCHO is subsequently destroyed by photolysis and reaction with OH to form HCO (R24 & R25), whereby HCO is further oxidised to form CO (R26) (Seinfeld and Pandis, 1998)

$$CH_3O_2 + NO \rightarrow CH_3O + NO_2 \qquad (R22)$$

$$CH_3O + O_2 \rightarrow HCHO + HO_2 \qquad (R23)$$

$$HCHO + h\nu \rightarrow H + HCO \qquad (R24)$$

$$HCHO + OH \rightarrow HCO + H_2O \quad \text{(R25)}$$

$$HCO + O_2 \rightarrow CO + HO_2 \quad \text{(R26)}$$

Methyl peroxy (CH_3O_2) radicals will also react with NO_2 and HO_2 to form methyl peroxynitrate (R27) and methyl hydroperoxide (R28), which are subsequently photolysed, or react with OH radicals to form formaldehyde (R29–R32).

$$CH_3O_2 + NO_2 + M \rightleftharpoons CH_3OONO_2 + M \quad \text{(R27)}$$

$$CH_3O_2 + HO_2 \rightarrow CH_3OOH + O_2 \quad \text{(R28)}$$

$$CH_3OOH + h\nu \rightarrow CH_3O + OH \quad \text{(R29)}$$

$$CH_3OOH + OH \rightarrow CH_3O_2 + H_2O \quad \text{(R30)}$$

$$CH_3OOH + OH \rightarrow CH_2OOH + H_2O \quad \text{(R31)}$$

$$CH_2OOH \rightarrow HCHO + OH \quad \text{(R32)}$$

The formaldehyde products in these chain reactions will be photolysed and react with OH to form formyl radicals (HCO), and subsequently this radical is oxidised by O_2 to form CO. The major termination steps of the CH_4 chain reactions are the formation of nitric acid and hydrogen peroxide (R17 & R33) (Stockwell, 1995). The termination reaction involves the removal of radicals from the reaction mixture.

$$NO_2 + OH + M \rightarrow HNO_3 + M \quad \text{(R17)}$$

$$HO_2 + HO_2 \rightarrow H_2O_2 + O_2 \quad \text{(R33)}$$

2.2.1.4 Chemistry of carbon monoxide

Carbon monoxide (CO) in the troposphere mainly originates from anthropogenic sources (see Chapter 1: Section 1.1.4) plays an important role in the formation of O_3.

Carbon monoxide is also produced from the photolysis of HCHO and reaction with OH and its subsequent reactions (R24-R26) (DeMore *et al.*, 1997). The most important removal process of CO in the troposphere is oxidation by OH radicals (R34). In the presence of sufficient NO_x(e.g. Bangkok, see Chapter 6), the oxidation of CO will lead to the formation of O_3 (R9, R11 & R3):

$$CO + OH (+ O_2) \rightarrow CO_2 + HO_2 \quad (R34)$$

$$NO + HO_2 \rightarrow NO_2 + OH \quad (R9)$$

$$NO_2 + h\nu \rightarrow NO + O(^3P) \quad (R11)$$

$$O(^3P) + O_2 + M \rightarrow O_3 + M \quad (R3)$$

In the presence of low concentrations of NO_x (e.g. Danum, see Chapter 6), O_3 destruction will dominate the chain reactions through oxidation by HO_2 radicals (R6) (Bruhl and Crutzen, 1999):

$$HO_2 + O_3 \rightarrow 2O_2 + OH \quad (R6)$$

In the perturbed environment where the trend of emissions of CO and CH_4 are increasing, the resultant OH depletion has been predicted to lengthen the lifetimes of CO and CH_4 (Wang and Prinn, 1999). The abundance of CO and CH_4 in the troposphere therefore has a great implication on the current understanding of the CH_4 budget, as well as its importance to the tropospheric oxidising capacity.

2.2.1.5 Chemistry of biogenic volatile organic compounds (BVOCs)

Isoprene (2-methyl-1,3-butadiene or $CH_2=C(CH_3)CH=CH_2$ or C_5H_8) is one of the most important BVOCs in the atmosphere (see Section 1.2.7 and Chapter 5), as it is

an extremely reactive hydrocarbon released in huge quantities by both natural and anthropogenic sources. Anthropogenic sources are believed to be from transport, while natural emissions arise mainly from terrestrial vegetation, particularly in the tropics (Guenther *et al.*, 1995; Guenther *et al.*, 2006). Isoprene plays an important role in atmospheric photochemistry, as it is a large source of hydroperoxy (HO_2) and organic peroxy (RO_2) radicals, which can react with mainly anthropogenic NO_x to stimulate O_3 production in the lower atmosphere (Levy *et al.*, 1999; Lee and Wang, 2006). In remote areas where NO_x emissions are limited, isoprene can act as a sink of OH and O_3 by sequestering NO_x as isoprene nitrates and thereby suppressing O_3 formation (Kang *et al.*, 2004), and also by direct ozonolysis of isoprene (von Kuhlmann *et al.*, 2004; Fiore *et al.*, 2005). Oxidation of isoprene in the atmosphere is initiated by OH, O_3, NO_3 or halogen radicals and involves thousands of intermediate species (Saunders *et al.*, 1997; Pöschl *et al.*, 2000), which has important implications to local and regional air quality, as well as to climate change through the production of GHGs such as O_3 (IPCC, 2001).

Examples of OH-initiated reactions of the main isoprene degradation pathways are shown in Figure 2.2. A number of possible isomers are formed and further degraded in the presence of high and low NO_x conditions to produce species such as peroxy radicals and peracetic acid, as well as multi-functional C_5-nitrates, which can generally be lost by dry and wet deposition (von Kuhlmann, 2001; Fan and Zhang, 2004). Meanwhile, isoprene ozonolysis produces two primary ozonides, which are subsequently decomposed to yield five activated carbonyl oxides (Criegee intermediates – labelled as CI1-CI5 in Figure 2.2) (Zhang and Zhang, 2002; Zhang *et al.*, 2002; Fan and Zhang, 2004). Initiation by NO_3 produces nitrooxyalkyl radicals,

which are subsequently oxidised to form eight nitrooxyalkyl peroxy radicals (labelled as ISON1-ISON8 in Figure 2.3), which in the presence of NO, eight nitrooxyalkoxy radicals are produced (labelled as ISN1-ISN8) (Fan and Zhang, 2004). Isoprene oxidation by halogen radicals such as Cl also produces six chloroalkyenyl peroxy radicals (labelled as ISOCl1-ISOCl6 in Figure 2.4) and subsequently leads to the formation of six chlorokenyl alkoxy radicals (labelled as ISCl1-ISCl6) in the presence of NO (Zhang *et al.*, 2002; Fan and Zhang, 2004). Depending on the type of oxidants, (i.e. OH, O_3, NO_3, or Cl) stable products such as methyl vinyl ketone ($CH_3C(O)CHCH_2$, MVK), methacrolein ($CH_2=C(CH_3)CHO$; MACR), 3-methyl furan, formaldehyde, etc. are produced (von Kuhlmann, 2001; Fan and Zhang, 2004).

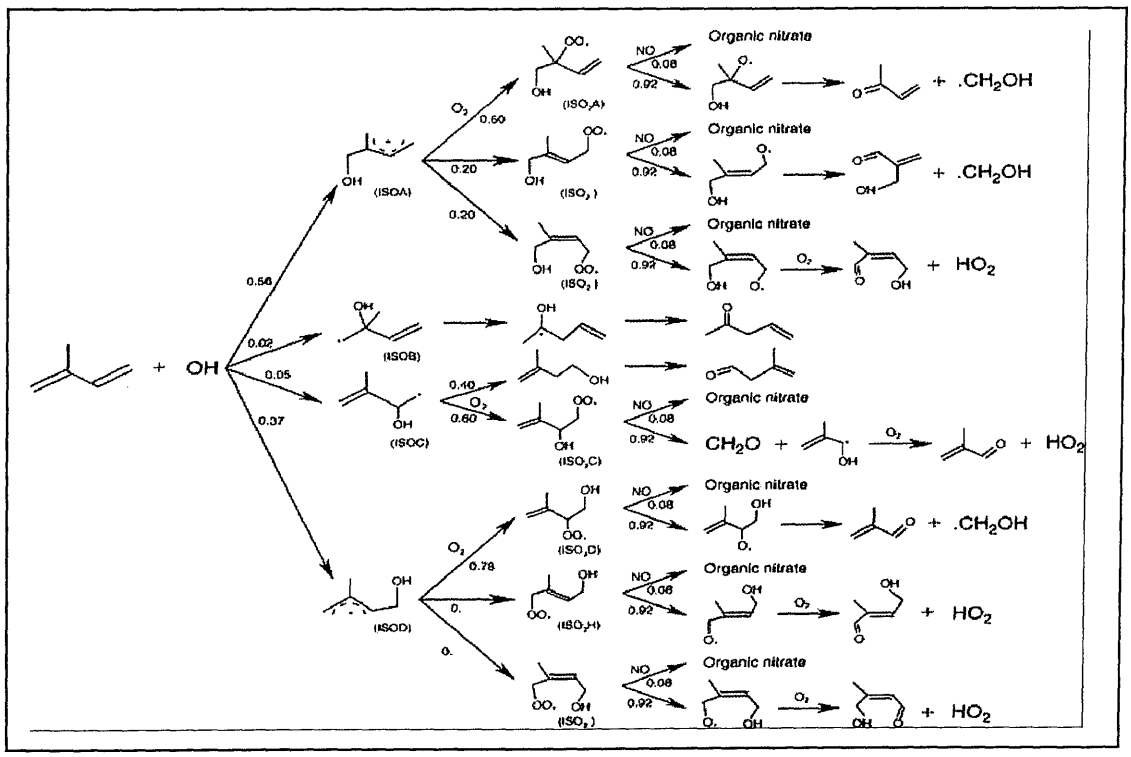

Figure 2.1. Simplified schematic showing the reaction pathways of isoprene initiated by OH (*Adapted from Fan and Zhang (2004)*)

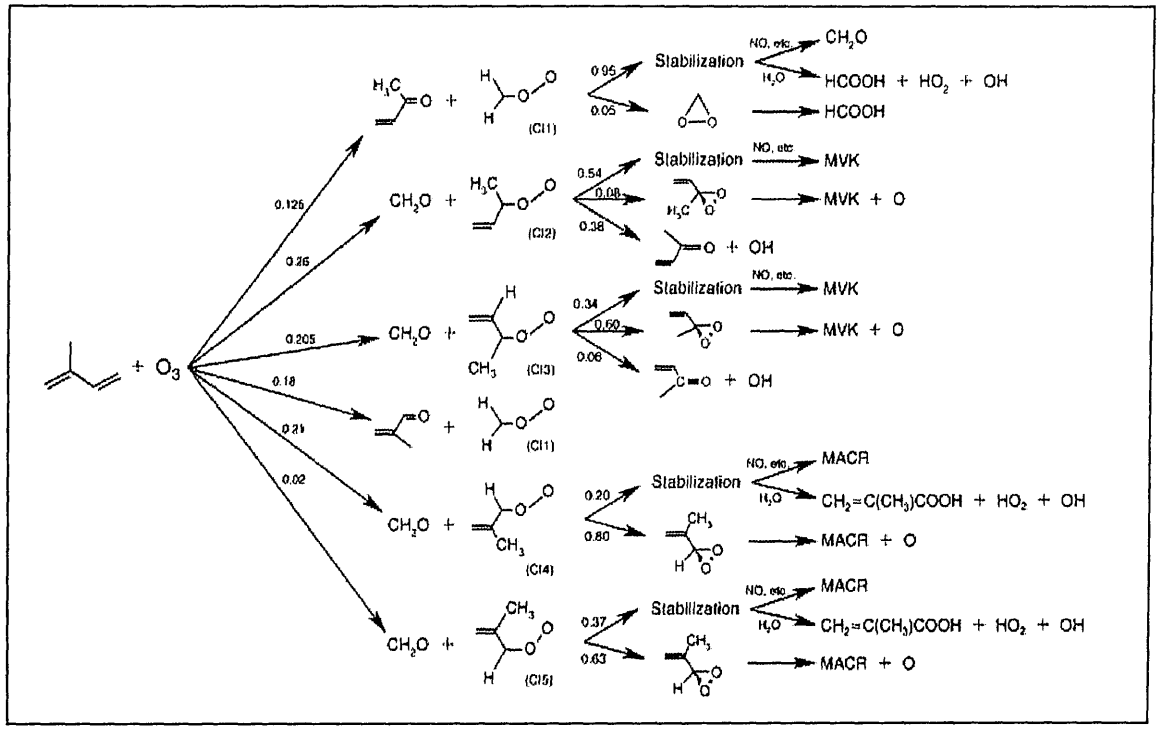

Figure 2.2. Simplified schematic showing the reaction pathways of isoprene initiated by O_3 (*Adapted from Fan and Zhang (2004)*)

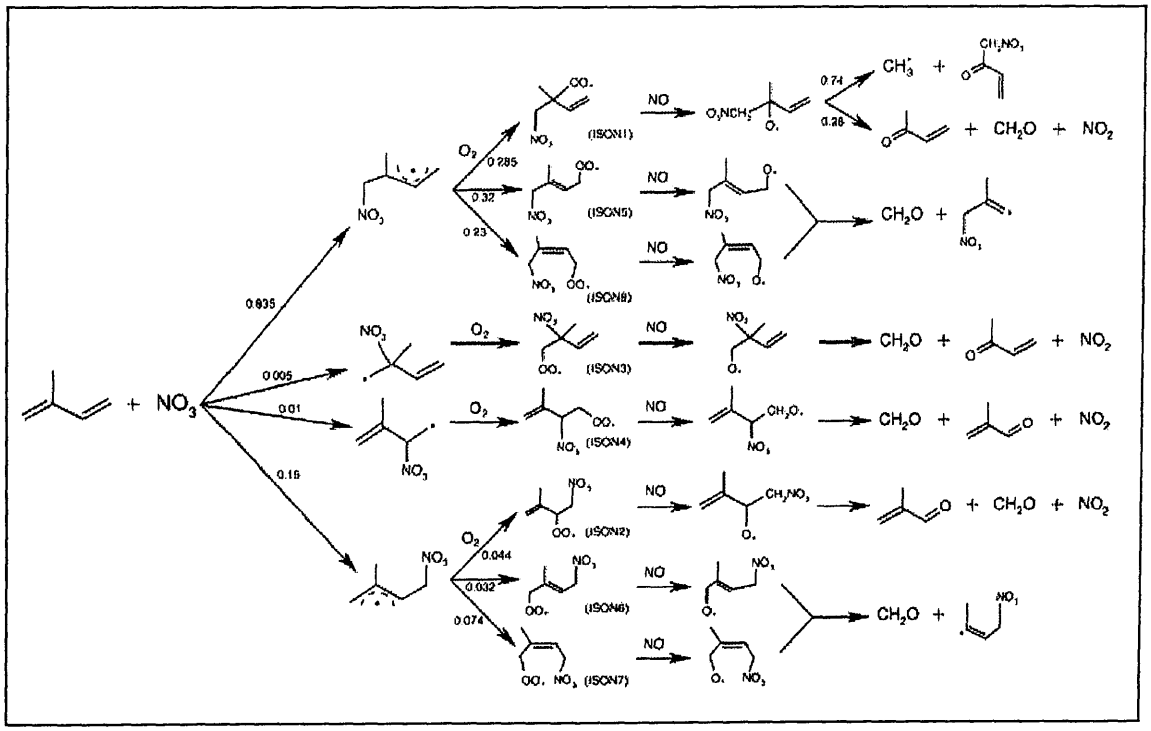

Figure 2.3. Simplified schematic showing the reaction pathways of isoprene initiated by NO_3 (*Adapted from Fan and Zhang (2004)*)

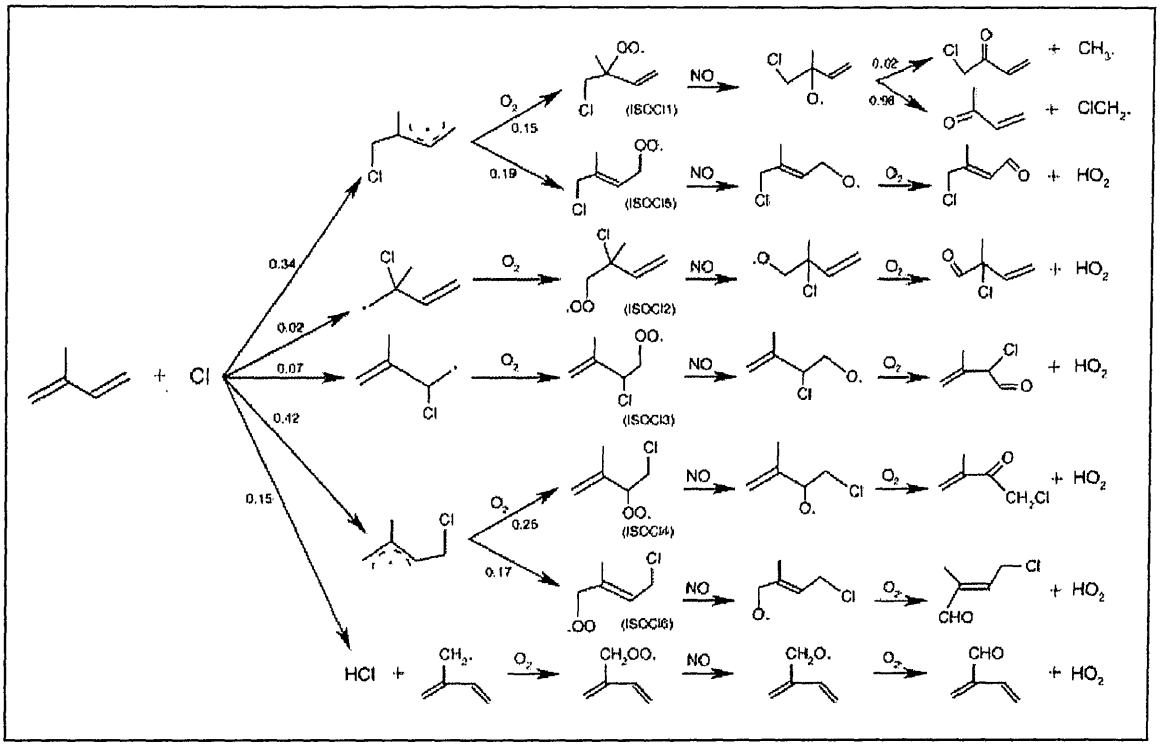

Figure 2.4. Simplified schematic showing the reaction pathways of isoprene initiated by Cl (*Adapted from Fan and Zhang (2004)*)

2.2.2 Aerosols

An aerosol, is a suspension of solid and concentrated liquid particles present in the atmosphere but distinct from the dilute water droplets and ice crystals found in clouds (e.g. Jacob, 2000); the atmospheric aerosol also plays important roles in atmospheric chemistry. Similar to gaseous pollutants, aerosols are also emitted from natural and anthropogenic sources; 90% of the global atmospheric aerosol flux of about 3440 Tg per year originates from natural sources (Andreae, 1995; IPCC, 1995). It is conventional to categorise atmospheric aerosols into three modes depending on the particles sizes (e.g Seinfeld and Pandis (1998)). In the nucleation mode (radius <0.01 μm), particles are formed from gas-to-particle conversion such as oxidation and

condensation of SO_2, NO_x, and VOCs. The accumulation mode (0.01–1 μm) arises from coagulation and condensational growth of nucleation mode particles. Aerosols in this mode have been of particular interest for a number of reasons, such as their tendency to remain in the atmosphere for relatively long times (i.e. a few days), their efficient interaction with solar radiation, and their optimum size as cloud condensation nuclei (CCN) and as ice nuclei (IN) (Charlson *et al.*, 1990; Penner *et al.*, 2001; Ramasamy *et al.*, 2001). The coarse mode (radius > 1 μm), arises when aerosol particles are formed mechanically, such as blown dust and sea spray.

The aerosols in the atmosphere are more regional in nature due to their regional distribution of sources, short lifetime and variability of aerosols properties (Kaufman *et al.*, 2002; 2005). By using aerosol optical thickness (AOT) as a measurement of aerosols concentration in the atmosphere column, Kaufman *et al* (2005) have shown the global distribution of aerosol from all sources and anthropogenic sources as shown in Figure 2.5. As also shown in Figure 2.6, coarse aerosol were observed at higher concentration in Asia (mainly in China and India) and Sahara-Saudi Arabia regions, which are mainly originated from urban haze and dust from the Saharan desert. Aerosol polarisation index was also calculated for Asia region as shown in Figure 2.7, which is derived from the measurement of polarisation of scattered solar light (data from POLDER Instrument flown on ADEOS-1, February 2007) and is sensitive only to the presence of fine aerosol particles. This observation has also indicated the high concentration of fine aerosols particle in China and India mainly from anthropogenic sources (Kaufman *et al.* 2002).

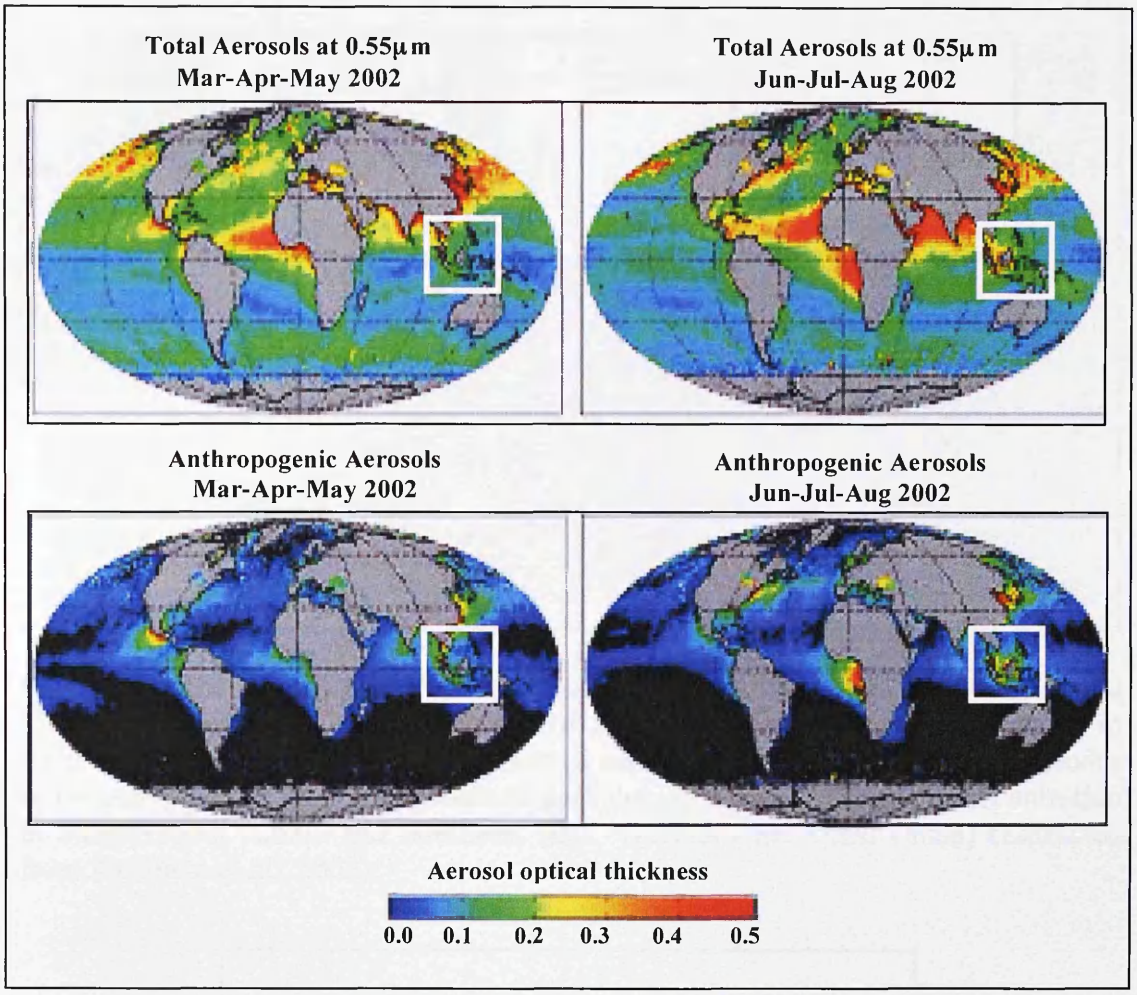

Figure 2.5: Global distribution of total aerosol optical thickness (AOT) and anthropogenic aerosols optical thickness (AOT) derived from MODIS measurements (Mar-Apr-May 2002 and Jun-Jul-Aug 2002) (extracted from Kaufman *et al.*, 2005).

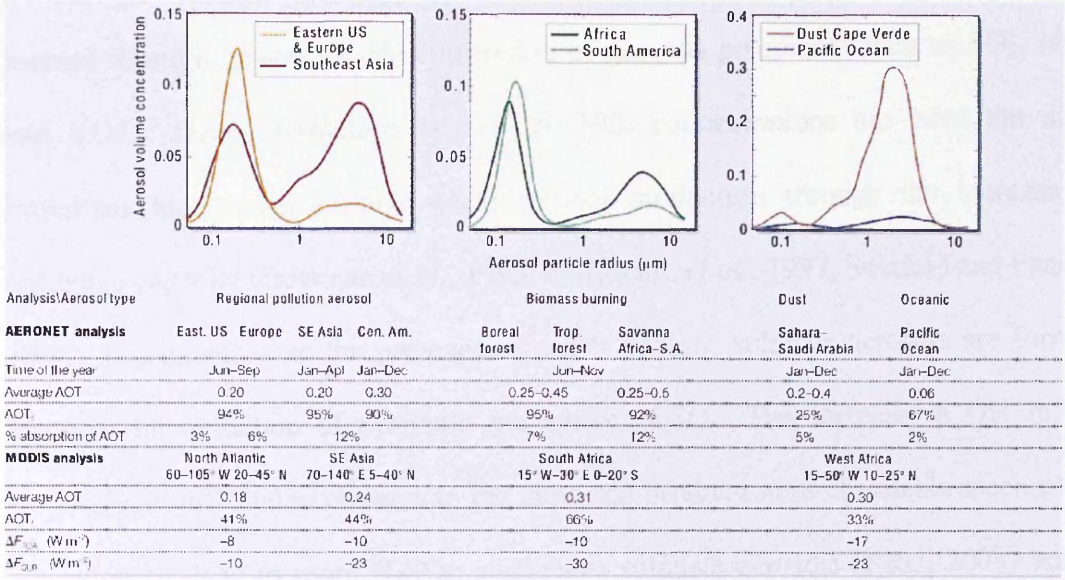

Analysis\Aerosol type	Regional pollution aerosol				Biomass burning			Dust	Oceanic
AERONET analysis	East. US	Europe	SE Asia	Cen. Am.	Boreal forest	Trop. forest	Savanna Africa-S.A.	Sahara-Saudi Arabia	Pacific Ocean
Time of the year	Jun–Sep		Jan–Apl	Jan–Dec		Jun–Nov		Jan–Dec	Jan–Dec
Average AOT	0.20		0.20	0.30	0.25–0.45		0.25–0.5	0.2–0.4	0.06
AOT,	94%		95%	90%	95%		92%	25%	67%
% absorption of AOT	3%	6%	12%		7%		12%	5%	2%
MODIS analysis	North Atlantic 60–105° W 20–45° N		SE Asia 70–140° E 5–40° N		South Africa 15° W–30° E 0–20° S			West Africa 15–50° W 10–25° N	
Average AOT	0.18		0.24		0.31			0.30	
AOT,	41%		44%		66%			33%	
ΔF_{TOA} (W m^{-2})	–8		–10		–13			–17	
$\Delta F_{Surface}$ (W m^{-2})	–10		–23		–30			–23	

Figure 2.6: The aerosol properties based on two types of analysis (AERONET and MODIS analyses). High concentration of fine aerosol particles were observed in Eastern US, Europe, Africa, South America and Southeast Asia (which also includes India and China), while coarse aerosols particles were observed higher concentration in Sahara-Saudi Arabia and Southeast Asia (includes India and China) (Extracted from Kaufman *et al.*, 2002).

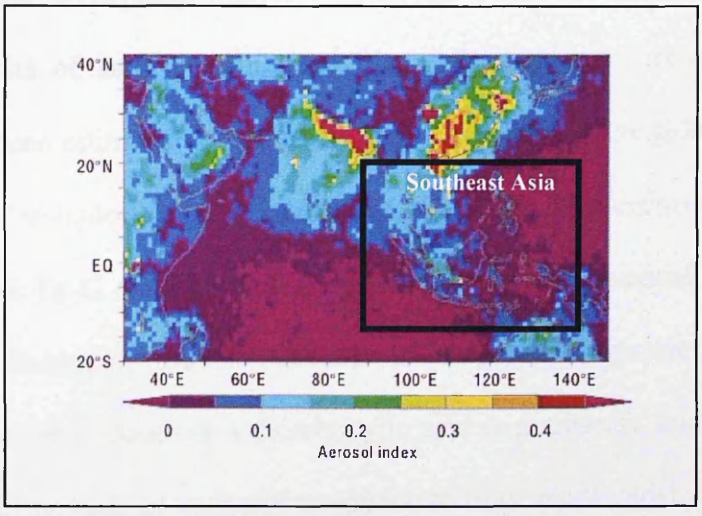

Figure 2.7: Aerosol polarisation index for Asia derived from measurements of polarisation of scattered solar light (POLDER Instruments flown on ADEOS-1 February 1997) and is sensitive only to the presence of fine particles (Extracted from Kaufman *et al.*, 2002).

A large fraction of the aerosols in the troposphere are emitted directly as particles, or formed through gas-to-particle conversion of gaseous precursors such as SO_2, NO_x, and VOCs. Ozone formation in elevated NO_x concentrations has been the most important mechanism of high yield aerosol production through the increase in oxidative capacity (Bowman *et al.*, 1995; Hoffmann *et al.*, 1997; Seinfeld and Pandis, 1998). For example, in the presence of water vapour, sulphate aerosols are formed through the oxidation of SO_2 into gas phase H_2SO_4. The increase in OH in the troposphere will lead to changes in the rates and production of chemicals species that consequently lead to more H_2SO_4, and hence sulphate aerosols (NRC, 2003) which play an important role in the halogen and sulphur budgets of the atmosphere (Andreae and Crutzen, 1997).

Production of aerosols through oxidation of biogenic volatile organic compounds (BVOCs) such as terpenes into low volatility compounds has been linked to the indirect results of anthropogenic activities. Production of aerosols through this process has been estimated to consist of as much as 80% of the global organic aerosol production (Kanakidou, 2000). Guenther *et al.*, (1995) have estimated that about 30% of over 1000 Tg C emissions of BVOCs annually are potential aerosol precursor substances. Secondary organic aerosols (SOAs) are a mixture of low volatility products, such as a mono- or a dicarboxylic acid (e.g. pinonic acid) and a product of higher volatility such as carbonyl compounds (e.g. pinon-aldehyde) (Odum *et al.*, 1996; Hoffman *et al.*, 1997; Seinfeld and Pankow, 2003). The hygroscopic properties of SOAs strongly affect the formation of CCN, which influences the size and concentration of cloud droplets and the radiative properties of the clouds (Bonn *et al.*, 2004). In terms of mass production, the main precursors of SOA are believed to be monoterpenes (78%), followed by sesquiterpenes (22%) (Chung and Seinfeld, 2002),

which are expected to be highest in the tropics as the emissions of BVOCs (i.e. monoterpenes) are temperature dependent (Guenther *et al.*, 1995). Products of α-pinene oxidation such as hydroperoxides (e.g. APINAOOH-low volatiles and C_{96}OOH-high volatiles) were found to contribute about 63% of the global average of SOA (Bonn *et al.*, 2004). These results are highly uncertain because the chemistry causing SOA production is highly uncertain.

In the unpolluted marine environment, sulphate aerosols are formed through heterogeneous chemical reactions of naturally emitted marine biogenic DMS (Dimethylsulphide), which is also responsible for the formation of CCN (Charlson *et al.*, 1987). Sea spray aerosol particles, also emitted from the marine environment, are a potential source of reactive gaseous halogens, which are responsible for photochemical hydrocarbon oxidation, O_3 destruction, and are other reactions in the marine boundary layer (Vogt *et al.*, 1999; Sander and Crutzen, 1996; Sander *et al.*, 1996; Andreae and Crutzen, 1997; Keene *et al.*, 1998). Mineral dust aerosols originating from natural and anthropogenic sources can also act as a sink for acidic trace gases, such as SO_2 and HNO_3 (Dentener *et al.*, 1996; Li-Jones and Prospero, 1998), and at the same time, mineral dust aerosols coated with sulphate or nitrate are capable of forming CCN (Levin *et al.*, 1996). The treatment in PRECIS of aerosol production from SO_2 and DMS is discussed in Section 3.2.2.3 (Chapter 3). Cloud processes in PRECIS are discussed in Section 3.2.2.2.3 in Chapter 3.

In the polluted atmosphere, aerosols also have a substantial influence on smog chemistry. Accumulation mode aerosols (radius between 0.01-1 μm) have the ability to modify and scatter UV radiation very efficiently, and for this reason, in polluted environments, the turbidity of the atmosphere can (Dickerson *et al.*, 1997). In the

boundary layer, production of O_3 is found to be affected by the abundance and type of aerosols and by solar zenith angles. Previous study by Kondragunta *et al.* (1997) during pollution episodes over the eastern United States in summer has observed that O_3 production in boundary layer increased by up to 23 ppb and 50 ppb for scattering aerosols with a single scattering albedo of 0.96 and 1.0 respectively. Conversely absorbing aerosols with a single scattering albedo of 0.75 were found to decrease O_3 production by up to 34 ppb; and as much as 55 ppb for highly absorbing soot aerosols with a single scattering albedo of 0.45. In another study in India, during severe air pollution, O_3 pollution was found to be surprisingly low with values between 34 to 126 ppb in New Delhi despite the NO_x levels reach as high as 272 ppb due to the presence of light-absorbing soot aerosol particles (Singh *et al.*, 1997). These results show that the O_3 production is very sensitive to the aerosol loading and refractive index, which affects the aerosol radiative properties.

Oxidant concentrations in the troposphere are also known to alter the surface of aerosol particles, which in turn can affect the ability of aerosols to induce nucleation of droplets in the formation of clouds (Mauldin *et al.*, 1997; NRC, 2003). Clouds affect tropospheric chemistry by providing surfaces for heterogeneous chemistry to take place (Jacob, 2000), by scavenging soluble trace gases and aerosols (Liu *et al.*, 2001), and by scattering and absorbing incoming solar radiation that can modify the actinic flux, and thus, the photolysis frequency of chemical species at the upper level of clouds (Lefer *et al.*, 2003; Mauldin *et al.*, 1997). Clouds also play an important role in providing sources of key chemical species such as hydrogen oxide radicals in the upper troposphere through convective transport. In the tropics, deep convective clouds flush the upper troposphere and bring in a new source of NO_x (lightning) (Pickering *et al.*, 1998) and provide a large source of hydrogen oxides (HO_x= OH +

HO_2) from reservoirs such as H_2O_2, CH_3OOH and HCHO (Prather and Jacob, 1997). This physical process produces a photochemical imbalance and increases the net O_3 production in the upper troposphere.

Recent modelling studies by Liu *et al.* (2006) using a global 3-D chemical transport model (GEOS-CHEM) found that clouds are responsible for a small (ca. 5%) decrease in global mean photolysis frequencies for $O(^1D)$ and NO_2 in the troposphere. Earlier modelling studies by Tang *et al.* (2003) found that radical OH concentrations and the photolysis frequencies of NO_2 decreased by 23% and 20% respectively below clouds, and were enhanced by about 30% and 25% respectively above 1 km in the troposphere in the Asian-Pacific Rim during the TRACE-P period (February–April 2001). These results indicate that clouds play important roles in the vertical redistribution of photochemical activities, thus influencing tropospheric chemistry.

2.3 Interactions between Atmospheric Chemistry and Climate

Radiative forcing is a tool to estimate the relative importance to climate change (i.e. changes in surface temperature, precipitation, etc.) of changes in the concentrations of radiatively active gases and aerosols (Ramaswamy *et al.*, 2001; Mickley *et al.*, 2002) Since the onset of industrialisation, the radiative forcing due to all well-mixed GHGs has been the main contributor to the positive forcing (warming) which was estimated to be 2.43 W/m^2; radiative forcing due to GHGs also has the highest level of scientific understanding compared to other radiative forcings (Ramaswamy *et al.*, 2001). For tropospheric O_3 alone, the estimate of global annual mean radiative forcing is a few tenths of $1 W/m^2$ (IPCC, 1994). A number of modelling studies to estimate the global average radiative forcing for O_3 since pre-industrial times to 2050 projected an

increase to 0.43 W/m^2 (Chalita *et al.*, 1996), 0.66 W/m^2 (Dorland *et al.*, 1997), 0.63 W/m^2 (Brasseur *et al.*, 1998) and between 0.40 to 0.78 W/m^2 (Gauss *et al.*, 2003). It is also forecast that the largest increases of O_3 forcings may occur in Asia, in association with the rapid increase in population and development (Dorland *et al.*, 1997; Brasseur *et al.*, 1998). In the tropics, the radiative forcing of tropospheric O_3 is projected to increase by 10 to 20%, with a 40 Tg increase in CO emissions, and a 6 to 8-fold increase in the case of a 1 Tg increase in NO_x surface emissions (Berntsen *et al.*, 2002).

IPCC (1995; 2007-Chapter 2) has also reported a global mean direct forcing of -0.4 W/m^2 for sulphates, -0.2 W/m^2 for carbonaceous biomass burning, -0.1 W/m^2 for fossil fuel organic carbon, and +0.2 W/m^2 for fossil black carbon aerosols since pre-industrial times. Meanwhile, the indirect forcing is estimated to be in the range of 0 to -2.0 W/m^2 (Ramanathan *et al.*, 2001). In comparison with anthropogenic GHGs radiative forcing of +2.5 W/m^2, the anthropogenic aerosol radiative forcing appear to be comparable in magnitude but opposite in sign, which signifies that aerosols may have largely offset the warming effects of greenhouse gases (Charlson *et al.*, 1992; Kiehl and Briegleb, 1993). Recent modelling studies by Giorgi *et al.* (2002 and 2003) on the direct and indirect effects of anthropogenic sulphates and fossil fuel aerosols on the regional climate over East Asia have estimated that direct forcing was dominant over the winter monsoon season, while indirect forcing was dominant in the summer monsoon season.

2.3.1 Tropospheric Chemistry Effects on Climate Change

2.3.1.1 Chemically reactive gases

The increased emissions of chemically reactive gases such as CH_4, CO, NMHCs, and NO_x are the main drivers for tropospheric changes of O_3. The production of O_3 depends non-linearly on the concentration of its precursors such as NO_x, CO, and NMHCs. The complex nonlinear photochemistry relation between O_3, NO_x and VOC can be illustrated by isopleth plots (Sillman, 1999) as shown in Figure 2.8. This diagram has indicated the two possible of regimes with different O_3-NO_x-VOC sensitivity, namely the NO_x sensitive regime (with relatively low NO_x and high VOC) and VOC sensitive regime (NO_x saturated). Under the NO_x sensitive regime, O_3 increases with increasing NO_x but shows little changes in response to increasing VOC. Meanwhile under VOC sensitive regime, O_3 decreases with increasing NO_x and increases with increasing VOC. The ridge line (dotted line) in the diagram is representing the maximum O_3 concentration versus NO_x and VOC as well as separating the two regimes, NO_x sensitive and VOC sensitive regimes. Urban regimes (e.g Bangkok) are typically VOC sensitive, whilst remote rainforest regions (e.g Danum) are extremely NO_x sensitive.

Several studies have indicated the importance of O_3 as a radiatively active gas through interactions with short wave and long wave radiation, and through control of local stratospheric temperatures (Wang *et al.*, 1980; Lacis *et al.*, 1990; Forster and Shine, 1997). In the absence of dense clouds, a large fraction of the incident solar radiation (short wave) penetrates the atmosphere and reaches the surface. At the earth's surface, most of the radiation (long wave) emitted by the earth's surface is absorbed by the atmosphere but, because the atmosphere is a good absorber, it is also a good emitter

(Kirchhoff's law) and reemits a large portion of the absorbed energy back to the surface (this phenomenon is called "green house effect"). In a cloud-free, atmosphere absorbs solar radiation (short-wave) only weakly but at the higher altitudes, the shorter wavelengths are absorbed by atmospheric gases including O_3. Strong absorption by ozone at stratopause (about 50 km) produces the temperature maximum at this height. The spectral absorptivities shown in Figure 2.9 clearly show the absorption of various atmospheric gases. An atmosphere "window" appears in the absorption spectrum near the peak in the spectrum of terrestrial radiation (~10 μm) allowing longwave radiation to escape to space under cloud-free conditions (Ritter, 2006).

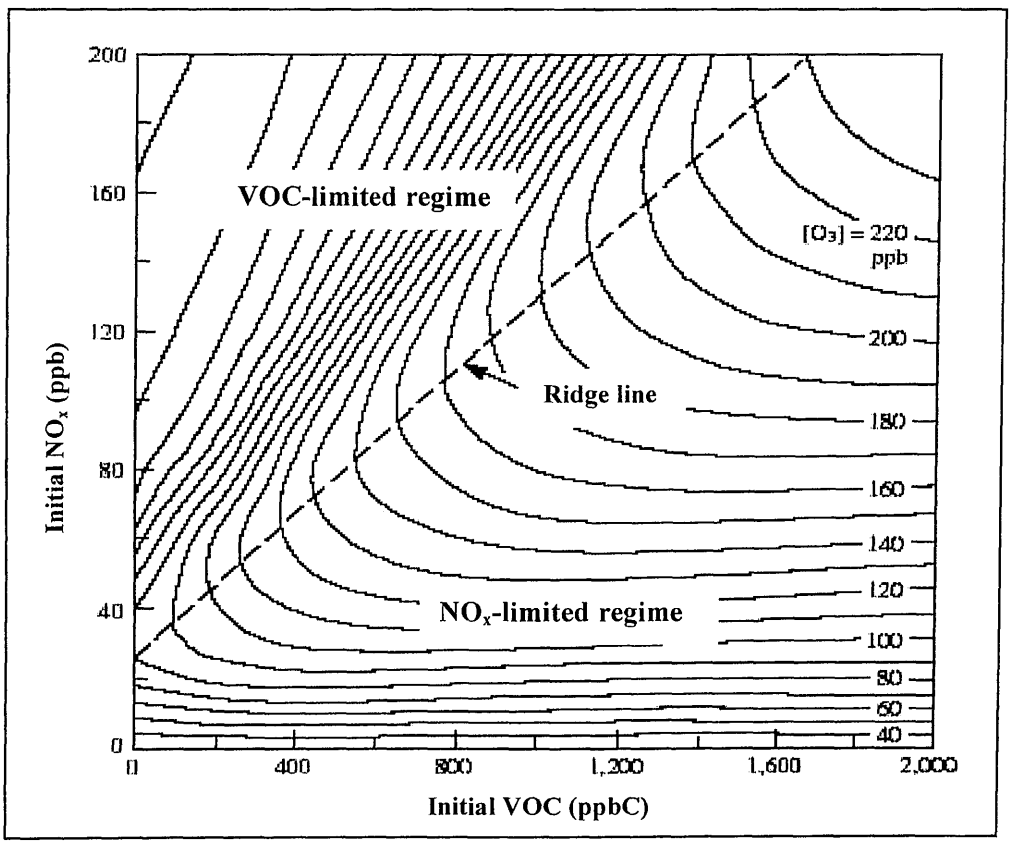

Figure 2.8: Ozone isopleths (ppb) as a function of the average emission rate for NOx and VOC during the afternoon, with a constant emission rate, at the hour corresponding to maximum O_3. The dashed line represents the transition from VOC-sensitive to NO_x-sensitive conditions (Sillman, 1999)

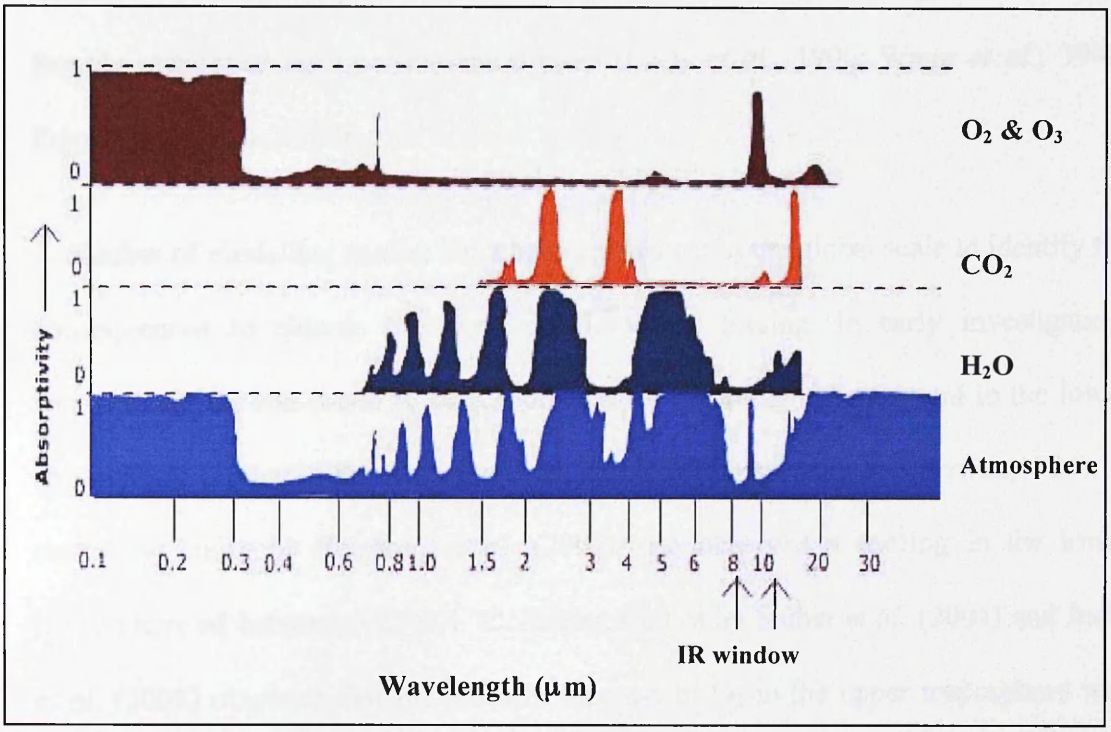

Figure 2.9: Little absorption for the atmosphere in the shortwave end of the spectrum especially in the visible light band (about 0.4-0.7 μm). The atmosphere absorbs far better in the longwave end of the electromagnetic spectrum, which is the region of maximum emission (10μm) for the Earth (*adapted from* Ritter, 2006).

Apart from being a GHG itself, O_3 is capable of modifying the lifetimes of other GHGs such as CH_4 by controlling the oxidative capacity of the atmosphere through the production of hydroxyl (OH) radicals (Naik *et al.*, 2005). The relatively short lifetime of O_3, ranging from days to a number of weeks, is shorter than the tropospheric mixing time of several months for one hemisphere. This results in a high spatial and temporal variability of O_3 distribution in the troposphere (Naik *et al.*, 2005) ranging from less than 10 ppb over remote tropical oceans up to about 100 ppb in the extratropical upper troposphere (Logan, 1999). The short lifetime of O_3 also implies that its forcing responds rapidly to changes of its precursors (Mickley, 2004). Variability in the vertical distribution of O_3 also contributes to the radiative forcing,

where changes in O_3 concentration near the tropopause result in the greatest radiative forcing efficiency on a per-molecule basis (Lacis *et al.*, 1990; Wang *et al.*, 1993; Forster and Shine, 1997).

A number of modelling studies have been carried out at the global scale to identify the consequences to climate that are specific to O_3 forcing. In early investigation, tropospheric O_3 was found to be responsible for a cooling enhancement in the lower stratosphere (about 20 km from the earth surface)(Ramaswamy and Bowen,1994). A modelling study by Berntsen *et al.* (2002) also observed a cooling in the lower stratosphere of between 0.2°–0.4 °C. Recent studies by Stuber *et al.* (2001) and Joshi *et al.* (2003) observed that the uniform increase of O_3 in the upper troposphere was responsible for a weaker temperature response than an equivalent forcing by CO_2. Meanwhile, in response to the increase of O_3 in the middle and lower troposphere, cloud feedback in a GCM was observed to be responsible for the amplification of surface temperature, O_3 emits thermal radiation and absorbs solar radiations and this alters the amount of heat added to the lower and middle troposphere (Hansen *et al.*, 1997). An increase of O_3 also allows lower troposphere the cool to space more effectively via the 9.6 um O_3 in of the Earth's infrared window. The cooling effects of O_3 in the lower troposphere could lead to increases in cloud cover in the lower troposphere but usually expect decreased stability to increase convection and so increase cloud cover (Hansen *et al.*, 1997).

Using a coupled atmosphere-ocean model, ECHAM4/OPYC3, Voss *et al.* (2002) found that the effect of a transient increase in GHG forcing contributed to an increase in global and annual mean surface temperature of 2.6 K from the present (1970–1990) to the future (2060–2089), as gauged by a time slice experiment. The warming in the

troposphere was accompanied by a 2.1% increase in global mean precipitation and evaporation. Modelling studies by Mickley *et al.* (2004) using a GCM to diagnose the specific climate response to a realistic change in tropospheric O_3 with accompanying cloud feedback from pre-industrial times to the present day have found an instantaneous radiative forcing of 0.49 W/m^2 due to the increase in O_3. The changes have resulted in an increase in global mean surface temperature of 0.28 °C. In this study, the largest increase of temperature of more than 0.8 °C was observed downwind of Europe, Asia, and North America in the summer.

2.3.1.2 Aerosols

From observational evidence and modelling studies, atmospheric aerosols can affect the climate through two basic mechanisms: directly by scattering and absorbing incoming solar radiation, and indirectly by modifying the scattering of light by clouds through variations in the concentration of cloud condensation, where aerosols are acting as CCN. The direct effect of light scattering by aerosols has its maximum effect when the size of the aerosol particles and wavelength of the scattered light are of the same order, and for this reason, aerosols from SO_2 emission and biomass burning have a comparatively stronger radiative effect than mineral dust and sea salt aerosols (Andreae, 1995). Aerosol absorption has the tendency to warm the Earth, which in turn will hinder condensation and flatten the meridional temperature gradient (MTG) (Hansen *et al.*, 1997). This phenomenon will draw less water into the atmosphere, producing in turn less cloud cover, a decrease in cloud albedo, and so will enhance further warming of the Earth system. Conversely, a cooling effect predominates the direct effects of non-absorbing aerosols, mainly through light scattering with an estimated global mean forcing of 0.4 W/m^2, but with an uncertainty

of about ±0.8 W/m^2 (Shine and Forster, 1999).

Evidence of the direct effect of aerosols can be identified through the increase in aerosol optical depth (AOD), which is the determinant of aerosol radiative forcing (Angstrom, 1964), i.e. a decrease in solar radiation penetrating through the atmosphere. Observations through satellites such as the Advanced Very High Resolution Radiometer (AVHRR) have shown an enhanced AOD, mostly in industrial regions in the northern hemisphere, areas with active biomass burning, and dust regions (Durkee *et al.*, 1991; Husar *et al.*, 1997). Satellite imagery from MODIS (Moderate resolution Imaging Spectrodiometer) and ERBE (Earth Radiation Budget Experiment) have also shown the AOD and reflectivity signals of regional plumes over continental aerosol regions (Penner *et al.*, 2002; Yu *et al.*, 2004). Apart from the observational evidence, the direct effects of aerosols have also been investigated through a number of modelling studies. Substantial modelling studies have been carried out to evaluate the direct effects of radiative forcing of sulphate aerosols, anthropogenic black carbon, and organic carbon aerosols (Haywood and Ramaswamy, 1998; Myhre *et al.*, 1998; Jacobson, 2001b).

Meanwhile, the indirect effects of aerosols through interactions between aerosols and clouds can be identified from the increase in cloud reflectivity, CCN, and cloud droplets, and a decrease in cloud effective radius (Huang, 2005). Observations of the indirect effect of aerosols through measurement of CCN concentration found a higher concentration in relatively polluted continental air, compared to clean marine air (Hudson, 1991). Brebguier *et al.* (2000) also measured cloud reflectance from ACE-2 (Second Aerosol Characterization Experiment) and found a higher reflectance in polluted air than in marine air. Satellite observations using AVHRR also found that

smoke emissions from biomass burning in the Amazon Basin and Cerrado increased the cloud reflectance and reduced the droplet size (Kaufman and Fraser, 1997).

Climate responses to the direct and indirect radiative forcing of aerosols have been investigated in numerous studies in attempts to estimate the effects. Studies by Qian and Giorgi (2000) and Zhai and Pan (2003) for example have concluded that anthropogenic aerosols have been responsible for the significant cooling trend in the Sichuan Basin and some other regions in China. Karl *et al.* (1995) also suggested that in industrial regions, the decrease in diurnal temperature range (DTR) may be partially attributed to anthropogenic aerosols. A number of modelling studies have recognised that aerosol effects combined with GHGs to produce the observed surface temperature (Santer *et al.*, 1995; Hansen *et al.*, 1995; 1997; 2001).

Precipitation, another climatic response, has a strong link with the direct and indirect effects of aerosols through their ability to modify cloud properties. Satellite observations from the Tropical Rainfall Mission (TRMM) Project have indicated that air pollution from forest fires (Rosenfeld, 1999) and industrial pollution (Rosenfeld, 2000) have suppressed rainfall in tropical regions. Based on large-eddy simulations, haze pollution is suggested to be responsible for the enhancement of cloud cover and suppression of nocturnal drizzle in stratocumulus clouds (Ackerman *et al.*, 2003). Suppression of precipitation due to direct and indirect effects of aerosols was observed in modelling studies over China (Giorgi *et al.*, 2002; 2003). Earlier studies by Menon *et al.* (2002) found two distinctive observations on the effects of anthropogenic aerosols over China and India, in which precipitation increased in southeast China, but was suppressed over northeast China. A recent study by Takemura *et al.* (2005) on the climate response to the direct and indirect effects of

aerosols concluded that the precipitation and cloud water changes are strongly affected by a variation of the dynamic hydrological cycle over the regions, where a large amount of anthropogenic aerosol and cloud water co-exist.

2.3.2 Climate Change Feedback on Atmospheric Chemistry

Climate change, on the other hand, may affect atmospheric chemistry through several mechanisms. Atmospheric chemistry feedback arises when the consequences of climate change through changes in atmospheric variables and processes (i.e. temperature, water vapour, clouds, circulation patterns, precipitation) or through changes in source and sink strengths interacting with atmospheric chemistry can lead to the alterations of concentrations and properties of the radiatively active gases and aerosols, which then produce an additional climate change (NCAR, 2003). In response to climate changes through alterations in local temperatures and precipitation, the emissions of radiatively active gases such as CH_4 from natural sources affects the lifetime of these chemical species, by modulating the abundance of oxidants such as OH radicals in the atmosphere. At high latitudes, CH_4 concentrations are expected to increase when the temperature increases (Matthews, 2000; Worthy *et al.*, 2000). In wetland areas, elevated temperatures will induce the additional release of CH_4 due to the enhancement of microbial activity (Cao *et al.*, 1998; Chapman and Thurlow, 1996; Christensen and Cox, 1995; Lashof *et al.*, 1997). The increase in temperature due to climate change is suggested to play an important role in destabilizing CH_4 clathrates in continental slope sediments and permafrost regions, resulting in the release of CH_4 (Harvey and Huang, 1995). In their modelling studies using a one-dimensional coupled atmosphere-ocean climate model, it was found that

destabilisation of clathrates led to stronger increases in both CH_4 and CO_2 concentrations. However, the uncertainty of this climate feedback is still great, partly due to the lack of knowledge of the amount of CH_4 in clathrates.

Hydroxyl radical (OH) is the primary oxidant of CH_4 and therefore the concentration of OH in the atmosphere is affected by the emission of CH_4 and also in turn, determines the lifetime of this compound. In reaction R20, the atmospheric lifetime of both reactants (OH and CH_4) are affected; and the increase of CH_4 emissions in low NO_x conditions will lead to reduced O_3 levels and thereby to a longer atmospheric lifetime and abundance of CH_4 (Eq 2.1) in the atmosphere.

$$CH_4 + OH \xrightarrow{k_{20}} CH_3 + H_2O \qquad \text{(R20)}$$

The total lifetime of atmospheric CH_4 is given by the following equation (Isaksen, 2000):

$$1/\tau_{CH_4} = 1/\tau_{OH} + 1/\tau_{additional} \qquad (2.1)$$

where, $\tau_{OH} = 1/(k_{20}[OH])$, where k_{20} is the reaction coefficient for reaction R20, which is temperature dependent (DeMore *et al*, 1997). Meanwhile, $\tau_{additional}$ denotes the methane lifetime due to the combined minor sinks such as absorption in the soil, transport to the stratosphere where it will reacts with OH, Cl and $O(^1D)$ (Isaksen, 2000). Based on this approximation (Eq 2.1), changes in atmospheric temperature will alter the rate coefficient (k_{20}) of the reaction of OH radicals with CH_4, and this will indirectly affect the lifetime and abundance of CH_4 in the atmosphere. In modelling studies by Fuglestvedt (1995), it was shown that when only the temperatures were increased, the average tropospheric annual level of OH was reduced, while the level of CH_4 was reduced at the same time. This was mainly due to the increased reaction

rate constant for the reaction between OH and CH_4 rather than the reduction of OH levels.

Changes in methane lifetime is, however, uncertain due to large uncertainties in precursor emissions (IPCC, 2001), where counteracting effects of CO and CH_4 (reduces OH through reactions R20 and R34), and NO_x and O_3 (increases OH through reactions R6 and R9) are involved. For example, Lelieveld *et al.* (1998) has calculated that a significant reduction in OH concentration in the atmosphere has lead to the increase in CH_4 lifetime from 6.2 yr (pre-industrial time) to 7.9 yr (1992). However, an earlier study by Berntsen *et al.* (1997) found the opposite result, where an increase in global OH concentration of about 6% has lead to the decrease of CH_4 lifetime. Karlsdottir and Isaksen (2000) have used 3-D model to estimate the lifetime of CH4 in related to changes in global OH distribution for period from 1980 to 1996 in nine different regions. This study shows that an increase of OH concentration of 0.43%/yr has lead to the decrease of CH_4 lifetime by 0.49%/yr. This study also suggested that the increasing anthropogenic emission in Southeast Asia, which include China, India and Japan, has been the key to the changing oxidation of CH_4. The global change of OH distribution and CH_4 lifetime due to changes in emissions of CO, NO_x and NMHC in SEA (China, India & Japan included) is shown in Figure 2.10.

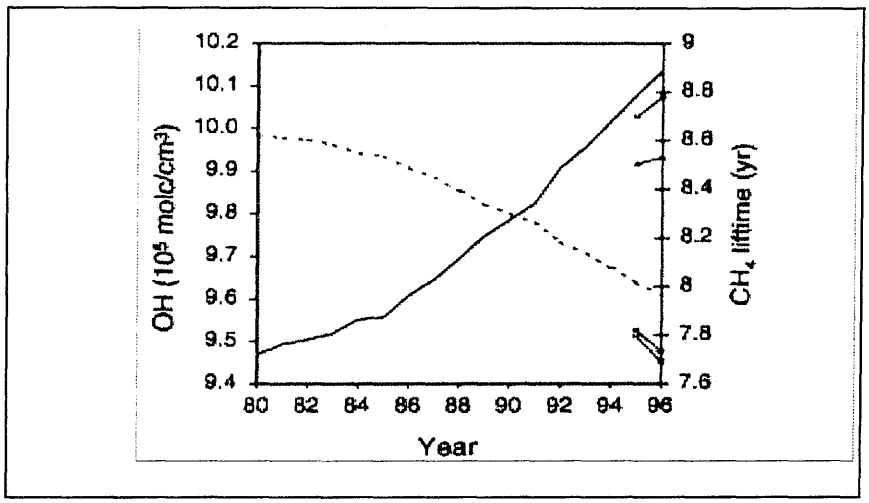

Figure 2.10: The change in global average OH concentration (—) and CH_4 lifetime, τ_{CH_4} (- - -) from 1980 to 1996 due to changes in emissions of CO, NO_x and NMHCs (adapted from Karlsdottir and Isaksen (2000))

The change in precipitation patterns also affects the hydrological cycle at the regional levels (Voss *et al.*, 2002), thus affecting soil water in wetland areas and CH_4 emissions (van den Pol-van Dasselaar *et al.*, 1999; Hilbert *et al.*, 2000). A change in humidity through changes in water vapour in the atmosphere greatly affects the production of atmospheric oxidants such as OH (NRC, 2003). In the tropics, the effect on the hydrological cycle is further aggravated due to deforestation, where the regional water balance and atmospheric water vapour content are changed significantly. The perturbation of the hydrological cycle could change the cloudiness, particularly in the tropics, and affect the radiative and chemical effects of clouds on OH radicals (Mauldin *et al.*, 1997). An increase in gas phase OH radicals could lead to a number of homogenous and heterogeneous atmospheric chemical reactions. For example, OH radicals can enhance the production of other oxidants such H_2O_2, whereby in either homogenous or heterogeneous reactions H_2O_2 can oxidise SO_2 to produce sulphates (Seinfeld and Pandis, 1998). Consequently, the production of sulphates can lead to the formation of aerosols, which play important roles in cloud

formation (see Chapter 2, Section 2.1.2). In regions with low levels of NO_x, there will be an increase in O_3 loss through reactions R5 and R6 (Fuglestvedt, 1995).

Regional differences in chemical and meteorological conditions have also been identified to significantly influence the variations of O_3 radiative forcing (Fuglestvedt *et al.*, 1999; Mickley *et al.*, 1999; Wild and Akimoto, 2001;Bernsten *et al.*, 2002). Several climate-chemistry modelling studies have indicated that the future evolution of radicals, O_3, and CH_4 are not only driven by increasing emissions, either anthropogenic or natural, but also by the changes in climate. Modelling studies on the response of tropospheric chemistry due to climate change have been carried out at global (Fuglestvedt *et al.*, 1995; Brasseur *et al.* 1998; Johnson *et al.*, 1999; Lelieveld and Dentener, 2000; Hauglustaine and Brasseur, 2001) and regional (Forkel and Knoche, 2006) scales to deepen the understanding of climate-chemistry interactions. Earlier, a 2-D modelling study by Fuglestvedt *et al.* (1995) found that tropospheric O_3 is expected to decrease by about 10% in response to a warmer and more humid climate projected for the year 2050. Another study by Brasseur *et al.* (1998) using the CCM (Climate-Chemistry Model) has projected an increase of 7% in OH abundance and a 5% decrease of tropospheric O_3 in a global mean in the year 2050. The impact occurs through the temperature dependence of key reaction rates affecting the O_3 and radical production and destruction terms. These studies have clearly shown the importance of climate-chemistry feedback.

Recent studies on climate change and its impact on the regional atmospheric chemistry in the eastern United States (Hogrefe *et al.*, 2004) and southern Germany (Forkel and Knoche, 2006) found that future climate changes have significant impacts on the concentration and distribution of tropospheric O_3. The occurrence of high

summertime concentrations of tropospheric O_3 and other photo-oxidants is strongly determined by meteorological processes (i.e. the effect of cloud cover on the amount of solar radiation) within the planetary boundary layer. Earlier modelling studies have also shown that local and regional meteorological conditions such as cloud cover, wind speed, and mixing heights (Rao *et al.*, 2003), and solar radiation and temperature (Ordonez *et al.*, 2005) have an impact on the concentration of tropospheric O_3. In addition to the extensive biomass burning, the modelling results of the increased tropospheric O_3 column (TOC) in 1997 in Southeast Asia region was found to be equally affected by the changes in meteorological conditions (Chandra *et al.*, 2002; Sudo and Takahashi, 2001).

2.4 Land Cover and Climate-Chemistry Changes Interactions

Based on a number of modelling and observation studies (see Baron *et al.*, 1998; Pielke 1998; Kanae *et al.*, 2001; Pitman *et al.*, 2004, Asner *et al.* 2004; Beltran, 2005; Adegoke *et al.*, 2007), it has become clear that changes in land cover play a significant role in local, regional, and global climate changes. Land cover changes due to deforestation and agricultural expansion, particularly in the tropics, have been of concern as these activities can induce carbon losses from soil and vegetation (Dale, 1997). In earlier estimations by Houghton and Skole (1990), land-use change has accounted for the release of 90–120 Pg C/yr. Natural wetlands are one of the most important sources of GHGs including CO and CH_4 (Harris *et al.*, 1993). The reduction of natural wetlands has reduced carbon emissions by about 28–38% due to agricultural drainage (Armentano and Menges, 1986), and on the other hand, the expansion of wetland rice production since 1951 has increased CH_4 emissions from

this source (Neue, 1993). The emissions of N_2O into the atmosphere have increased as a result of human activities such as tropical land clearing and replacement of agriculture (Luizao *et al.*, 1989), biomass burning (Crutzen and Andreae, 1990; Cofer *et al.*, 1991), increased use of fertilizers (EPA, 1990) and expansion of nitrogen-fixing leguminous plants in agriculture (Eichner, 1990).

The linkage between land cover changes and the chemistry-climate system can be seen in terms of perturbation of the CO_2 sinks (Lamptey *et al.*, 2005), changes to the emissions of reactive gases (Luizao *et al.*, 1989; Harris *et al.*, 1993; Neue, 1993) and aerosols (Bonn *et al.*, 2004), which play important roles in atmospheric chemistry, and thus climate change. Direct perturbation of BVOC emissions due to land cover changes affect their role in the production of tropospheric O_3 with sufficient NO_x (NRC, 1991; Fehsenfeld *et al.*, 1992), and formation of secondary organic aerosols (SOA) through oxidation of BVOCs by free radicals (Hoffman *et al.*, 1997; Griffin *et al.*, 1999a; 1999b).

A modelling study using GENESIS and interactive BIOME vegetation models for the years 1700–2100 found widespread results on the response of climate change to CO_2 levels (Lamptey *et al.*, 2005). Simulation of the impact of land cover changes on climate change using the IMAGE 2 model found the greatest annual warming (greater than 6°C by 2100) in the north of 60°N and south of 50°S (Alcamo *et al.* 1998). In the same scenario, during the period of June–August, the greatest warming (greater than 7 K) was observed mainly over Africa and Asia. In the same study, precipitation in far east Asia and the northern part of SEA was observed to increase up to 1.5 mm/day over most of the land area, considering the potential vegetation change from needle leaf-evergreen in the year 1700 to needle leaf-deciduous in 2100

(Lamptey *et al.*, 2005). Some notable effects of land cover changes on climate change in other parts of the world were also reported in a number of modelling studies (see Stohlgren *et al.*, 1998; Chase *et al.*, 2000; Zhao *et al.*, 2001; Diffenbaugh and Sloan, 2002, Asner *et al.*, 2004; Pitman *et al.*, 2004; Adegoke *et al.*, 2007).

Deforestation, particularly in tropical regions, is one of the important human activities that change the land-surface characteristics that may affect atmospheric circulation. A modelling study in the SEA region by Zhang *et al.* (1996) using the National Center for Atmospheric Research (NCAR) Community Climate Model (CCM1), incorporating the Biosphere-Atmosphere Transfer Scheme (BATS1e), in investigating the extent of deforestation to the local and regional climate change in Southeast Asia, generally found daily surface-temperature increases (+0.8 K). The annual precipitation in SEA was found to decrease by about 8% (-172 mm/yr). Though the climatic conditions of SEA are strongly influenced by Asian monsoons, the results of the modelling study have indicated that the modification of land cover due to deforestation has substantial effects on the surface energy budget, and thus contributes to the regional climate change. Earlier studies using GCM simulations in SEA also found that deforestation contributed small amounts to the regional climate change, in comparison with other areas such as the Amazon Basin under the same model scenarios (Henderson-Sellers *et al.*, 1993; Polchar and Laval, 1994; McGuffie *et al.*, 1995). It is also important to note that in a number of study on simulation of precipitation over SEA has found to be poorly simulated for all seasons(SW and NW monsoons), for example in the simulation using GFDL (see Fowell, 2006).

2.5 Regional Chemistry and Climate Change in SEA

In the SEA region, the first detailed climate scenario was developed by the Climate Impact Group (1992) using four general circulation models (GCMs), namely the Canadian Climate Centre model (CCCJ1), the United Kingdom Meteorological Office model (UKMO), the Geophysical Fluid Dynamics model (GFDL), and the Australian CSIRO9 model. Based on these models, the projected temperature in most of the region was projected to increase by 0.4–3.0 °C by the year 2070, which is well below the global average (Whetton, 1994). For the same projection year, the precipitation was projected to fluctuate between -5% to +15% during the northeast monsoon, and between 0 to +10% during the southwest monsoon. In further modelling studies in the region by Hulme *et al.* (1999) using the HadCM3 global model under the influence of IS92a emission scenarios, the radiative forcing was projected to increase by about 20% (1.0 W/m^2) by the year 2100. In the same studies, doubling the GHGs such as CO_2 with no aerosol forcings caused a projected global temperature and precipitation increase of 3.0 K and 3.2% respectively in the 30 year averages from the present (1961–1990) to the future (2070–2099) periods. Using the same model, Hulme *et al.* (1999) also projected that at the regional scales, Southeast Asia will experience a fairly uniform progression of warming and larger precipitation by the year 2050.

Another modelling study using the same model (HadCM3) found that the simulated 30 year averages (from 2069–2099) for temperature over Southeast Asia under the A2 and A1F1 scenarios of IPCC (1994) are 3.4 K and 4.1 K respectively, which are higher than the projected global average temperature increase of 3.2 K (Johns *et al.*, 2003), as shown in Figure 2.11. In terms of precipitation, four emission scenario experiments (B1, B2, A2, and A1F1) for the 30 year averages also found a clear and

significant signal in both monsoon seasons, where conditions are projected to be drier during the NE monsoon and wetter during the SW monsoon. Corresponding with the SW monsoon period (June–August), the mean precipitation signals were found to be higher than the global average of 0.8 mm/day, namely 0.9 mm/day (B2), 1.1 mm/day (A2), and 1.8 mm/day (A1F1) (Johns *et al.*, 2003), as shown in Figure 2.12.

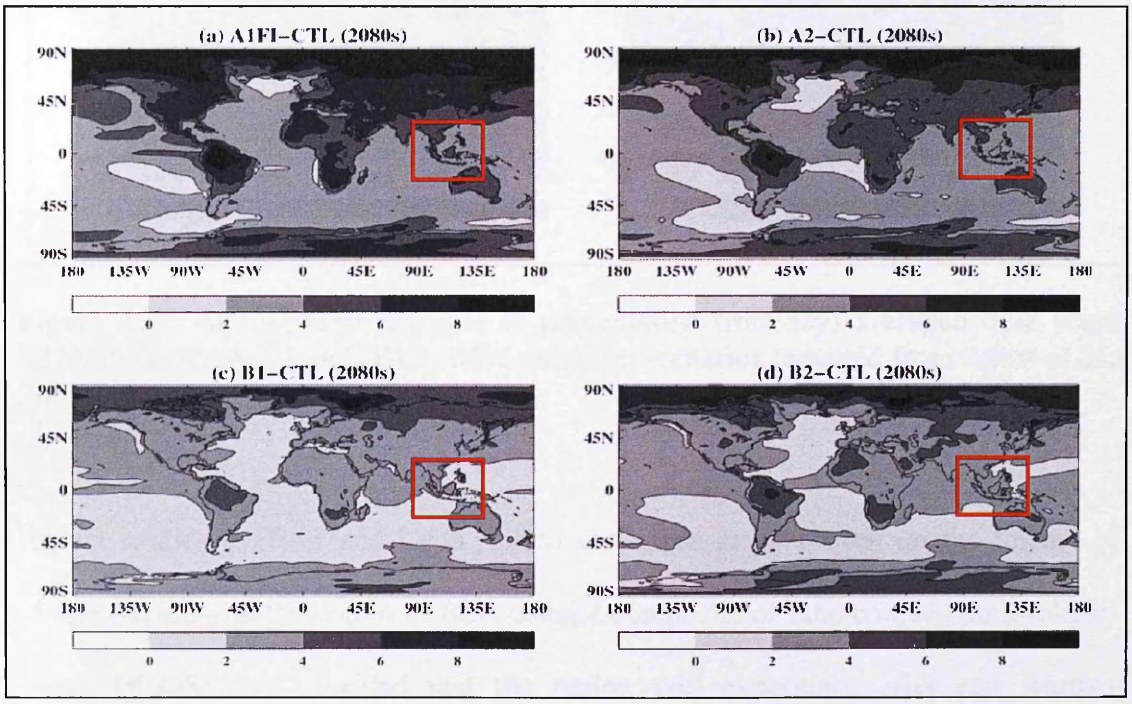

Figure 2.11: Annual mean changes in surface air temperature (K) averaged over years 2070-2099) for A1F1, A2, B1 and B2 emission scenarios (adapted from Johns *et al.*, 2003).

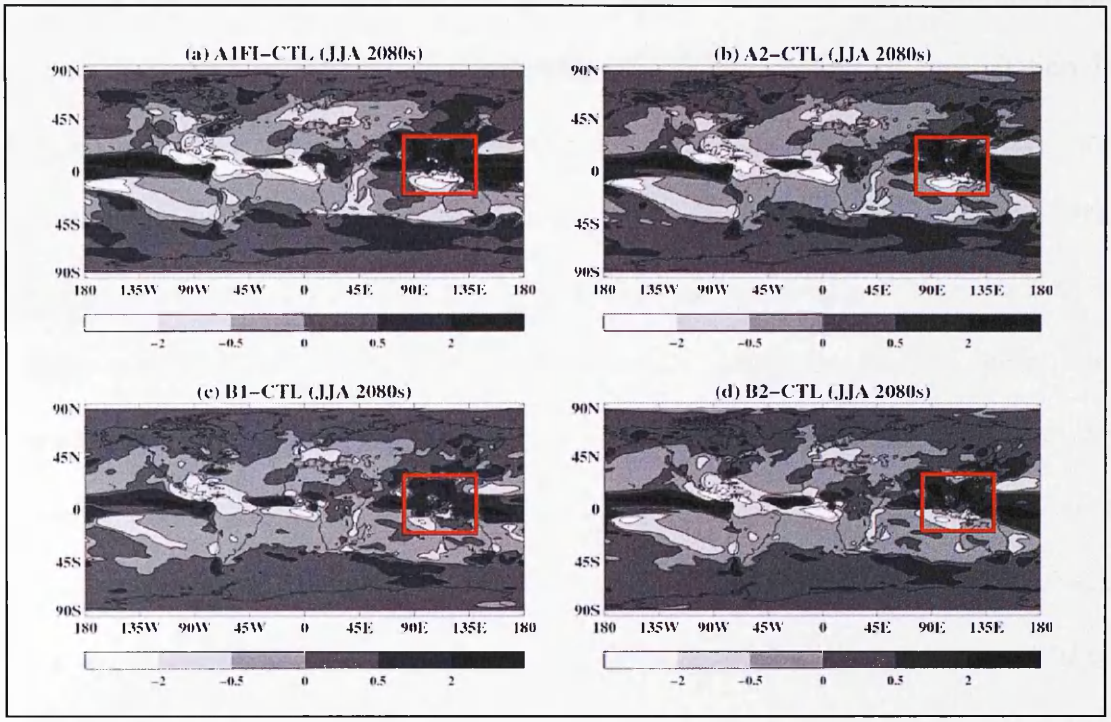

Figure 2.12: Annual mean changes in precipitation (mm/day) averaged over years 2070-2099) for A1F1, A2, B1 and B2 emission scenarios (adapted from Johns *et al.*, 2003).

Recent studies by Hori and Ueda (2006) and Ueda *et al.* (2006) on the impact of global warming in the region of SEA using a composite of nine coupled atmosphere-ocean GCMS have revealed that the region will experience drier and warmer conditions during the northeast monsoon, coinciding with the winter monsoon in East Asia that spans from December to early March for the next hundred years. The average surface temperature in SEA (90°–140° E, 30° N–5° S) during both monsoons was projected to increase between 2.2°C to 2.8°C by the year 2081–2100 (30 year averages) (*pers. communication* with Matasake E. Hori). Meanwhile, the precipitation was also projected to fluctuate between -2.4% to 6%. This climate condition in the region tends to cause drier weather than the normal weather at present conditions.

There is a general agreement from the global climate modelling results that there will be an increase in temperature and notable significant changes in precipitation in response to the increase in climatically active gases (including radiatively and chemically/photochemically active trace gases) and aerosols in the atmosphere, though there less agreement about the possible regional climate changes such as in SEA, even if the forcing and the global-mean sensitivity are the same. The disagreement has been well noted (Hulme *et al.*, 1999; Kittel *et al.*, 1998), and the fundamental differences in model designs (Hulme *et al.*, 1999), which in turn are a function of incomplete understanding of important physical processes and feedback (i.e. the treatment of the interactions between the atmosphere and the oceans and of cloud formation) have been identified as one of the attribution factors. These differences may be also attributed to different climate sensitivities and climate system unpredictability (Hulme *et al.*, 1999). Despite such limitations, certain regional responses have been shown in a number of modelling studies that have investigated the response to increasing climatically active gas and aerosol concentrations. The modelling results have also presented a strong argument that the possible future climate change scenarios are to be dominated by the response to the anthropogenic forcings (Johns *et al.*, 2003).

Chapter 3
REGIONAL CLIMATE CHANGE MODELLING

3.1 Introduction

A regional climate model (RCM) is a high resolutions model that covers a limited area of the globe. The use of the same formulation of atmospheric processes as in the global circulation model (GCM) is important to ensure that the climate projection is consistent with the GCM projection. RCMs have well-known drawbacks in terms of dependency on input from the GCM driving model, the lack of two-way nesting with its driving GCM, as well as computational cost. Nevertheless, RCMs are widely used in climate change investigations, where they provide higher spatial and temporal resolution information for a number of climatic variables while still providing better representation than the GCM for some weather extremes. RCMs are "comprehensive" physical models, which include the components of the climate system of the atmosphere and land surface, as well as the representation of the important processes within the climate system. A recently developed RCM from the Hadley Centre, UK, called PRECIS (Providing Regional Climates for Impact Studies) has been used in this study to investigate climate changes in Southeast Asia (SEA). Brief descriptions of the model parameterisations and the experimental design and setup for the climate change investigation are outlined in this chapter. The general framework of this investigation is shown in Figure 3.1. The main objective of this chapter is to assess the regional climate change due to atmospheric forcing alone.

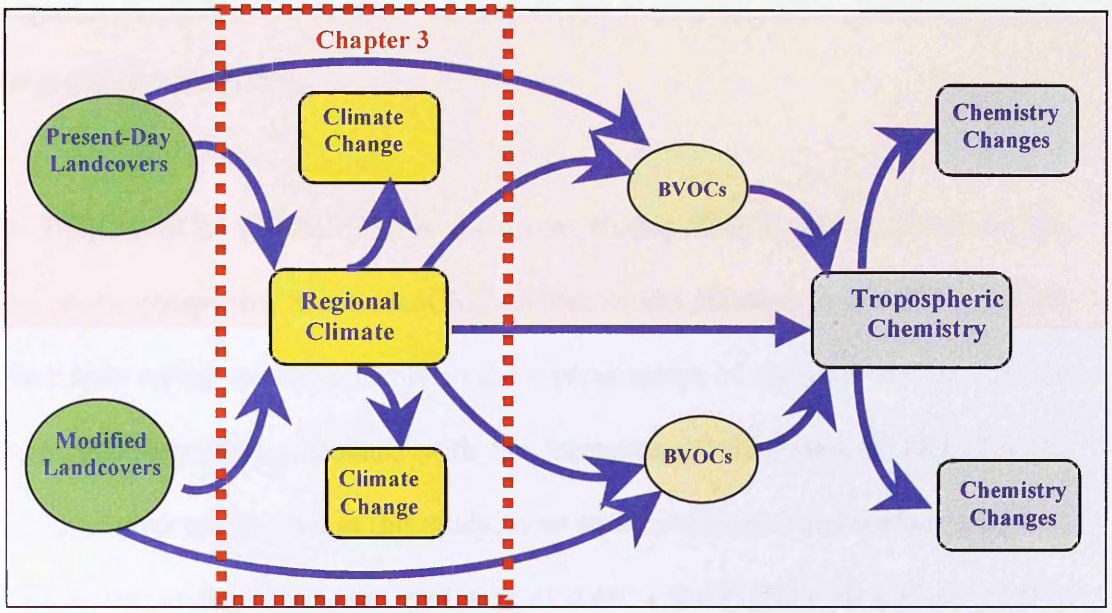

Figure 3.1: Framework for the investigation of climate changes-biogenic emissions-tropospheric chemistry interactions in Southeast Asia. The red dotted box indicates the framework for the investigation of climate changes under the present-day landcover scenario that covered in the Chapter 3.

3.2 PRECIS-Regional Climate Model

3.2.1 Model description

PRECIS is a nested regional climate model (RCM) that uses output from GCM simulations to provide boundary conditions and time-dependent lateral meteorological boundary conditions (LBC). That is, the model employs one-way nesting. The nesting ensures that the RCM results are consistent with the driving model GCM projection; the additional detail due to the increase in resolution helps interpretation of climate responses and impacts (Hudson and Jones, 2002; Arnell *et al.*, 2003; Wang *et al.*, 2004). In this approach, the GCM is used to simulate the response of the global circulation to large-scale forcing, while the RCM is used to account for sub-GCM grid-scale forcing in a physical way (orography, landcover, etc.), and to enhance the simulation of atmospheric circulation and climatic variables at fine spatial scales

(Mearns *et al.*, 2003). The approach, however, has some limitations, as highlighted by Giorgi and Mearns (1999).

The PRECIS-RCM (HadRM3P) is the latest Hadley Centre model based on the atmospheric component of the HadCM3 climate model (Gordon *et al.*, 2000), which differs from earlier versions mainly in the representation of dynamic and convective clouds, and thresholds associated with the formation of precipitation. PRECIS, the regional climate model used in this study, is an atmospheric and land surface model of a limited area with a horizontal resolution of 0.44° x 0.44° (50 x 50 km) or 0.22° x 0.22° (25 x 25 km) on its own rotated latitude-longitude grid and a timestep of 5 minutes. This model is imbedded in the atmosphere-only GCM (HadAM3P or ECHAM) with a resolution of 1.24° latitude x 1.88° longitude (~150 x 150 km) with a timestep of 15 minutes. The initial atmospheric and land surface conditions in GCM (HadAM3P) are interpolated from the output of lower-resolution (3.75° latitude x 2.5° longitude, ~300 km) coupled ocean-atmosphere model (HadCM3) (Gordon *et al.*, 2000). Both GCM (HadAM3P) and PRECIS (HadRM3P) have 19 layers in the atmosphere (from the surface to 30 km in the stratosphere) and four levels in the soil (Hudson and Jones, 2002). PRECIS-RCM also includes a representation of the sulphur cycle as sulphur aerosols play an important role in the radiation in the atmosphere.

3.2.2 Model Parameterisation

A numerical model such as the PRECIS-RCM is used to obtain an objective simulation of future climates by solving a set of equations that describe the evolution of atmospheric variables such as temperature, wind speed, humidity, and pressure. All

numerical models of the atmosphere are based upon the same set of governing equations as described in the following sections, but differ in the approximations and assumptions made in the application of these equations, how they are solved, and also in the representation of physical processes. A numerical model of the atmosphere consists of several components such as atmospheric dynamics, physical parameterisations, and sulphur cycles (Jones *et al.*, 2004; Stensrud, 2007). The following sections briefly detail the major component of PRECIS-RCM.

3.2.2.1 Atmospheric dynamics

The atmospheric component of the PRECIS-RCM is a hydrostatic version of the full primitive equations and uses a regular latitude-longitude grid, in the horizontal, and a hybrid vertical coordinate. All the governing equations of the model are solved numerically on a discrete 3-D grid spanning the area of the model domain and the depth of the atmosphere. The model simulates values at discrete and evenly spaced points in time with a 5-minute timestep to maintain numerical stability. PRECIS-RCM has 19 vertical levels, which are defined by atmospheric pressure (Cullen, 1993). The evolution of atmospheric dynamics – i.e pressure, wind, temperature, and moisture - is governed by three fundamental principles: conservation of momentum, conservation of mass, and conservation of energy.

3.2.2.2 Physical parameterisations

Physical processes in the atmosphere such as clouds and precipitation, radiation, convection and boundary layer exchanges, and gravity wave drag have been represented numerically in the PRECIS-RCM. Due to computational restraints as well

as shortcomings due to lack of understanding of the processes involved, assumptions are required for the parameterisation of these physical processes (Jones *et al.*, 2004). The following sections briefly describe the parameterisation principles of the important physical components of the atmosphere in the model.

3.2.2.2.1 Radiation

The atmosphere is driven by solar radiation, which can be divided into short-wave (incoming radiation) and long-wave (outgoing radiation) components. The amounts of short-wave (sunlight) and long-wave (terrestrial heat) radiation that are absorbed, emitted, and reflected depend on the properties of the atmosphere such as temperature, water vapour, concentration of chemically reactive gases (such as GHG, trace gases, etc.), the surface (landcover types, etc.), and the frequency of the radiation. In PRECIS-RCM, the spectrum of radiation is split into six short-wave bands and eight long-waves bands, where each band has different strengths of interaction with atmospheric constituents such as GHGs (Jones *et al.*, 2004). Short-wave fluxes depend principally on the solar zenith angle (varying according to latitude, season, and time of day), clouds, and the albedo of the surface, while long-wave fluxes depend upon the amount and temperature of the emitting medium and its emissivity (Edwards and Slingo, 1996). For full radiation calculations, both schemes require more computational expense than any other physical process, and thus longer timesteps of about three hours (Ingram *et al.*, 1997).

3.2.2.2.2 Surface exchange and sub-surface processes

Constant exchanges of heat, moisture, and momentum between the atmosphere and the underlying surface have a crucial influence on the temperature, wind, and

humidity of the atmosphere through the atmospheric boundary layer (Smith, 1990). In PRECIS, the soil and vegetation types that characterise a land grid-point are considered in the calculation of the heat, moisture, and momentum fluxes. At sea grid points, the roughness length, which is the representation of surface drag, is computed from local wind speed (see Charnock, 1955).

In PRECIS-RCM, the landcover type is used in the calculations to determine the surface albedo, surface roughness length, and hydraulic properties of the roots and the vegetated canopy. The HadAM3P component of PRECIS simulates the global atmospheric and land surface processes at a horizontal resolution of 2.5° x 3.75° using the Radiative Transfer Scheme (Edwards and Slingo, 1996) and Meteorological Office Surface Exchange Scheme (MOSES) (Cox *et al.*, 1999). Depending on the local landcover types, the parameters representing "snow-free albedo" and "maximum deep-snow albedo" in each grid box is assigned with an appropriate value. For example, the albedo parameter is assigned with a higher value for open land (e.g grassland, pasture and cropland) and lower values for woodland and forests (Cox *et al.*, 1999; Betts, 2000). Within the model, the radiative forcing due to surface albedo change can be calculated by performing additional sets of calculations of surface albedo and the shortwave radiation budget on a model timestep.

In the tropics, surface albedo change due to landcover changes may affect the climate via evapotranspiration, where the rate of evapotranspiration and the fluxes of sensible and latent heat are dependent on the parameters of rooting depth, aerodynamic roughness length, and canopy water holding capacity (Betts *et al.*, 1997). In the MOSES simulation, all these parameters are assigned with an appropriate value in

each grid box, where values are comparatively lower for open land compared to forested areas (Cox *et al.*, 1999). In the SEA region, which consists of mostly forested areas, a cooling influence is anticipated as a result of the greater flux of moisture to the atmosphere and the larger ratio of latent to sensible heat fluxes. The transpiration dependence on the resistance to water vapour loss from within plant stomata is also represented in the MOSES simulation through explicit simulation, which is aggregated to a large-scale variable of canopy conductance using leaf area index (LAI). In forested areas, LAI, which is prescribed as a further vegetation-specific parameter, has larger values than open land (Betts *et al.*, 1997). In PRECIS-RCM, the global datasets of the vegetation parameter values were derived using Wilson and Henderson-Sellers (1985) at a resolution of 1° x 1° grid. The landcover dataset specifies 53 landcover classes, which include 11 crop classes, 7 pasture/grazing classes, and 1 urban class (See Appendix 3.1). In PRECIS, the landcover dataset allows two classes of landcover for each grid, namely the primary landcover class if the coverage of the grid box is between 50-100%, and the secondary landcover class if the coverage is between 25-50%. These vegetation covers, which are represented in the HadAM3 surface parameter, are then bi-linearly interpolated to the GCM resolution.

For the soil, a 4-layer scheme is used to model the heat transport through the soil (Smith, 1996), which also includes the effects of soil water phase change and the influence of water and ice on the thermal and hydraulic properties of the soil (Jones *et al.*, 2004). In PRECIS, the soil properties dataset provided by Wilson and Henderson-Sellers (1985) was used in the parameterisation of soil scheme (see Appendix 3.2). In MOSES, the thickness of the soil layers from the top are 0.1, 0.25, 0.65, and 2.0

metres, which are specifically designed to resolve the diurnal and seasonal cycles with minimal distortion. The 4-layer scheme with appropriate values of parameters was found to provide good amplitude and phase response for periods of surface forcing between half a day and a year; which the details of the multilayer soil thermodynamics model can be found in Smith (1996).

3.2.2.2.3 Clouds and precipitation

The representation of clouds and precipitation in PRECIS-RCM is very important as clouds interact strongly with solar and infrared radiation, and of course affect the occurrence of precipitation. The release of latent heat during this process plays a critical role in the movement of air in the atmosphere. Layer cloud cover and cloud water content in each grid box of the model are calculated from a saturation variable (q_c), which is defined as the difference between total water (q_t) and the saturation of vapour pressure (see Smith, 1990). The formation of layer cloud is assumed to occur at any level of the 19 levels of the atmosphere, except at the 19^{th} level (top of the stratosphere). In PRECIS, an assumption is made that the cloud water is in liquid form above 0°C, frozen below -9°C, and a mixture in between (Smith, 1990; Smith *et al.*, 1998). The large-scale formation of precipitation is assumed to occur when the threshold values of cloud liquid water reach 1.0×10^{-3} (kg/kg) over land and 2.0×10^{-5} (kg/kg) over sea (Smith 1990). Large-scale formation of precipitation is dependent on cloud water content, with a greater efficiency of precipitation when the cloud is glaciated, and assumed to fall on 75% of the land surface within a grid box in the model regardless of layer cloud fraction (Jones *et al.*, 2004). The large-scale cloud and precipitation scheme of the model treats the water transfer between clouds and precipitation as a result of cloud physics processes, the free fall of ice and rain

downwards to the earth surface, and the calculation of fractional coverage of cloud in each grid box of the model. The cloud physics processes that are represented in the scheme are: condensation of water vapour to cloud droplets and the evaporation of these droplets, deposition of water vapour to ice crystals or aggregates and the evaporation of these particles, the riming of supercooled cloud droplets by ice particles, melting of ice particles to produce raindrops, evaporation of raindrops, accretion ("sweep-out") of cloud droplets by raindrops, the coalescence mechanism to form raindrops from cloud droplets, and the downward fall of ice particles and raindrops (Wilson and Ballard, 1999).

This model is also able to account approximately for convective precipitation (occurring on a local scale), which represents the convection of cumulus and cumulonimbus clouds. A single cloud model is used to represent a number of convective plumes within the grid box, and the convective precipitation is diagnosed within that grid box if the cloud liquid/ice content exceeds a critical amount and the cloud depth exceeds a critical value. The threshold values of cloud liquid water for convective precipitation are higher than the large-scale clouds and precipitation, being 2 g/kg over land and 0.4 g/kg over sea. The cloud depth value is set to 1.5 km over the sea and 4 km over land. However, if the cloud-top temperature is less than -10°C, the critical depth is reduced to 1 km over land or sea. Similar to large-scale precipitation, the convection scheme also allows for evaporation and melting of precipitation. In each grid box, it is assumed that the convective precipitation falls on 65% of the land surface, regardless of the convective cloud fraction (Jones *et al.*, 2004).

3.2.2.2.4 Gravity wave and orographic drag

In the free atmosphere, the gravity wave drag scheme parameterises the effect of the mountain ranges on scales between 5 km and the model grid scale, which acts as a sink for momentum. Depending on the conditions of atmospheric stability and wind shear, air passing over the mountains may create lee waves over and to the lee of the mountains (Palmer *et al.*, 1986). The fundamental elements of this scheme are the determination of surface stress, and the distribution of this stress through the atmospheric column, which is dependent on the wind speed, density, and static stability of the low-level flow, where the low-level flow is the layer of air that intersects the sub-grid scale orography (McIntyre, 1980).

Closer to the earth's surface, the orographic drag scheme parameterises the effect on the boundary layer of sub-grid scales of about 5 km or less, where the wind speed decreases due to interaction with the roughness of the earth surface. The orographic drag is determined in terms of a constant drag coefficient and linearly depends on the silhouette area of orography, which is a measure of the slopes within a grid box (Jones *et al.*, 2004). The calculation also uses an effective roughness length, which is a combination of the effects of the topography and vegetation within a grid box (see Gregory *et al.*, 1998) but does not take into account wave reflection, trapping or gravity waves generated by other means such as convective storms (Wilson and Swinbank, 1996).

3.2.2.3 Atmospheric aerosols (sulphur cycle)

The model has also taken into consideration the spatial distribution and life cycle of atmospheric sulphate (SO_4^{2-}) aerosol particles in the atmosphere, as sulphate aerosol particles tend to give a surface cooling effect through scattering of incoming solar radiation (direct effect) and increasing cloud albedo due to smaller cloud droplets (first indirect effect). The sulphur cycle scheme includes five prognostic variables to simulate the distribution of sulphate aerosols, namely sulphur dioxide (SO_2), dimethyl sulphide (DMS), and three modes of sulphate [i.e sulphate dissolved in cloud droplets, sulphate particles in Aitken mode (median radius, r_{Ait}=24 x 10^{-9}m), and sulphate particles in accumulation mode (median radius, r_{acc}=95 x 10^{-9}m)] (Jones *et al.*, 2004). These sulphur cyle tracer variables in the model are advected using trace advection scheme, mixed and dry deposited in the boundary layer, mixed convectively, and wet scavenged by large scale and convective precipitation as the model proceeds (Woodage *et al.*, 2001). This sulphur cycle can be initiated from emissions of anthropogenic sulphur dioxide, natural DMS (dimethyl sulphide), or volcanic sulphur.

The treatment of atmospheric chemistry of SO_2 in the model includes the oxidation of DMS to SO_2, and SO_2 to sulphate by radicals in gas and aqueous phases. The oxidation of DMS and SO_2 is calculated from prescribed monthly mean three-dimensional fields of OH, H_2O_2 and HO_2, which were obtained from the simulations of the Lagrangian chemistry model STOCHEM (Collins *et al.*, 1997). In dry or gas phase oxidation of SO_2, it is assumed that the rate of oxidation of SO_2 is proportional to the amount of SO_2 available (Eq. 4.1) and the integration of this equation gives an expression for the incremental change of SO_2 over timestep (Eq. 4.2).

$$\partial\{SO_2\}/\partial t = -k * \{SO_2\} \qquad (4.1)$$

$$\Delta\{SO_2\} = -[1 - \exp(-k * \Delta t)] * \{SO_2\} \quad (4.2)$$

Using the STOCHEM model (Collins *et al.*, 1997; Stevenson *et al.*, 1997) to obtain the average concentration of OH and rate constant (k), the equation for the rate of dry oxidation of SO_2 in daylight only is as in the following Eq. 4.3, where the typical values of $k_{SO2\text{-}OH}$ are of order 10^{-12} cm^3/molecule.sec and OH concentrations up to 10^6 molecules/cm^3 which gives the dry rate (k) values of around $10^{-6}s^{-1}$. The change of dry SO_2 can be obtained from Eq. 4.4.

$$k_{dry} = k_{SO2\text{-}OH} * [OH] \quad (4.3)$$

$$\Delta\{SO_2\}_{dry} = -k_{SO_2\text{-}OH} * [OH] * \{SO_2\} * \Delta t \quad (4.4)$$

For the treatment of wet or aqueous oxidation of SO_2 in the model, SO_2 in the cloud is oxidised by H_2O_2 with assumption that the number of clouds a molecule of SO_2 has to pass through before it is oxidised has a geometric distribution as shown in Eq.4.5 and Eq 4.6:

$$E(T/I) = \tau_{chem} + \tau_{clear} \exp(-\tau_{cloud}/2\tau_{chem})/p \quad (4.5)$$

$$E(T/O) = \tau_{chem} + \tau_{clear}(1/p - 0.5) \quad (4.6)$$

With the assumption that the probabilities of (O) and (I) are proportional to the number of SO_2 molecules in the clear and cloudy fractions of the grid box of the model, the value of the rate of wet oxidation can be calculated as shown in Eq 4.7, where the typical values of wet rate are in the order of $10^{-2}s^{-1}$. By considering the allowance for the depletion of H_2O_2, the change in SO_2 can be expressed as in Eq. 4.8,

where {S} is either the amount of SO_2 in the gridbox or the molar equivalent amount of H_2O_2, whichever is the smaller (Woodage *et al.*, 2001)

$$k_{wet} = 1/E(T) \tag{4.7}$$

$$\Delta\{SO_2\}_{wet} = -[1 - \exp(k_{wet} * \Delta t)] * \{S\} \tag{4.8}$$

For the treatment of DMS, in the chemistry model DMS is assumed to be oxidised by OH to produce SO_2 and MSA (methanosulfonic acid). The exponential decay rate equation for the depletion of DMS is shown in Eq 4.9, where the constant rate of 9.1 x 10^{-12} cm^3/molecule.sec and the first order approximation to the exponential term (Eq 4.9) can be made as shown in Eq 4.10.

$$\Delta\{DMS\} = -[1 - \exp(-DMSRATE * \Delta t)] * \{DMS\} \tag{4.9}$$

$$\Delta\{DMS\} = -k_{DMS-OH} * [OH] * \{DMS\} * \Delta t \tag{4.10}$$

Meanwhile, the parameterisation of three sulphate modes includes the processes of evaporation of dissolved sulphate in cloud-free grid boxes to form accumulation mode of sulphate, nucleation of accumulation mode sulphate to form dissolved SO_4^{2-}, and diffusion of Aitken mode sulphate into cloud droplets to form dissolved SO_4^{2-} In PRECIS, the sedimentation of sulphate particles (Aitken and accumulation modes) was introduced as it is an important mechanism for long transient runs for removing sulphate "trapped" in the stratosphere where other scavenging processes cannot operate (Woodage *et al.*, 2001).

3.3 Experimental Design and Setup

3.3.1 Modelling domain

For the present study, PRECIS has been configured for a domain extending from 30°N to 15°S and 90°E to 140°E in the Southeast Asian region with a horizontal resolution of 0.44° x 0.44° (Figure 3.2). The selected domain is large enough that the regional model can develop its own regional-scale circulations features with minimal "contamination" by the application of the boundary conditions, and small enough that the climate of the RCM deviates significantly from the GCM and that a simulation can be completed in a reasonable amount of time (Wanner *et al.*, 1997).

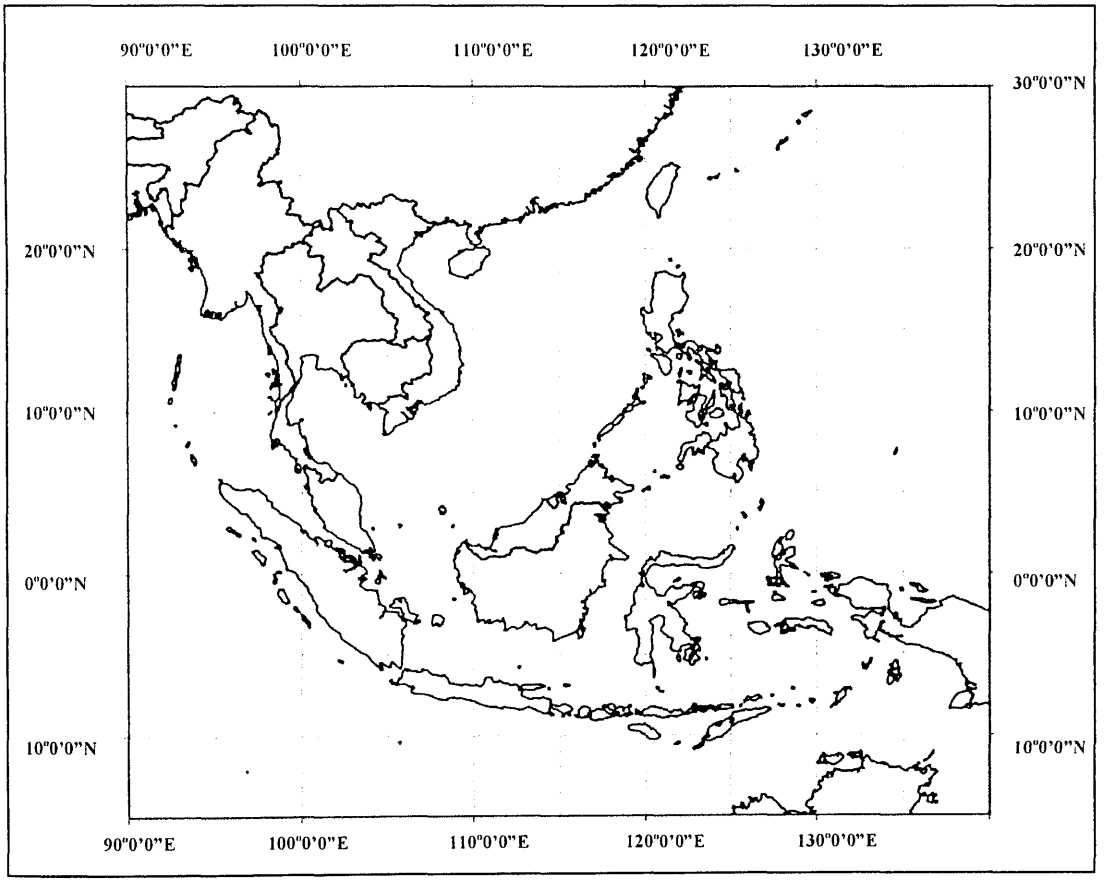

Figure 3.2: Domain for the investigation of climate changes in SEA.

3.3.2 Climatological simulation scenarios

PRECIS-RCM and the driving model (GCM-HadAM3P) use emission scenarios developed by IPCC (2000). The following section is a listing of climatological simulation scenarios used in this study, which are simulated by PRECIS-RCM and defined in terms of the source of the boundary data and the relevant emissions data.

3.3.2.1 Baseline scenario (HadAM3P: 1961-1990)

The climate of the recent past, which is assumed as belonging to the present-day climate, is used as a climatological baseline or control. Good quality climatological data is required in order to characterise the present-day climate in the SEA region for a given baseline period. The baseline period of 30 years, from 1961 to 1990, as defined by the World Meteorological Organisation (WMO) as the normal period and fulfils the criteria set by the IPCC (1994) has been used in this study as the climatological baseline. The boundary data for this scenario is derived from three 31-year (1961-1990) integration of HadAMP3P (atmosphere only GCM) with 150 km resolution (Wilson *et al.*, 2005). That is, this scenario is an ensemble of three realisations or simulations of lateral boundary conditions (*note*: in PRECIS the three realisations are labelled as [*addfa*], [*addfb*], and [*addfc*]), each spanning from 1st DJF 1960 to 1st DJF 1991, which have been integrated using different initial conditions but a common observed time series of HadISST sea-surface temperatures and sea ice for the same period (Moberg and Jones, 2004). The current climate conditions simulation is important for the evaluation of the performance of the PRECIS regional climate model and as a baseline for the climate change investigation.

3.3.2.2 ECHAM4

ECHAM4 boundary data from the atmospheric general circulation model ECHAM is also available in PRECIS-RCM for A2 and B2 scenario experiments (1960-2100). This numerical model is the fourth-generation atmospheric general circulation model developed at the Max Planck institute for Meteorology (MPI). The model is a spectral transform model with 19 atmospheric layers from the surface up to 10hPa. The prognostic variables are vorticity, divergence, logarithm of surface pressure, temperature, specific humidity and mixing ratio of total cloud water. The time-step for dynamic and physics is 24 minutes (for T42 horizontal resolution). Meanwhile the solar radiation time step is 2 hours where both seasonal and diurnal cycles in solar forcing are simulated. The transport of water vapour and cloud water in the model is calculated using a shape-preserving semi-lagrangian scheme (Williamson Rasch, 1994). Parameterisations for unresolved dynamic and physical processes were included, such as radiation, cumulus convection, stratiform clouds, gravity wave drag, vertical diffusion and surface fluxes, land surface processes and horizontal diffusion.

In ECHAM4, the parameterisation of radiation has adopted the code from the European Centre for Medium-Range Weather Forecast (ECMWF) model (Fouquart and Bomel, 1980; Morcrette *et al.*, 1986) with some modifications to the treatment of greenhouse gases, ozone and aerosols. The parameterisation of cumulus convection is based on the bulk mass flux concept by Tiedtke (1989), with the improvement suggested by Nordeng (1994) where the organized entrainment that relates to buoyancy is computed for a spectrum of clouds detraining at different heights. Meanwhile the stratiform cloud water content is calculated from the respective budget equations, including sources and sinks due to phase changes and precipitation

formation by coalescence of cloud droplets and gravitational settling of ice crystals (Roeckner, 1995). The parameterisation of gravity wave drag is based on Miller *et al.* (1989), where the simulation is using directionally dependent subgrid-scale orographic variances obtained from a high-resolution U.S Navy dataset. For the turbulent surface fluxes parameterisation, a higher order closure scheme is used to calculate the turbulent transfer of momentum, heat, moisture and cloud water. Meanwhile the eddy diffusion coefficients are calculated as a function of turbulent kinetic energy, which is obtained from the respective rate equations (Brinkop and Roeckner, 1995). Lastly, the parameterisation of land surface processes includes the soil model, which comprises the budgets of heat and water in the soil, the snow pack over land and the heat budget of land ice. Land surface parameters such as background albedo, roughness length, vegetation types, leaf area index (LAI) and soil parameters have been compiled for ECHAM4 (Claussen *et al.*, 1994) and are consistent with the definition of ecosystem complexes given by Olsen *et al.* (1983).

3.3.2.3 Assimilated ERA40 (1957-2001)

ERA40 reanalyses data are fine resolution gridded data (2.5° x 2.5°), derived from ECMWF (European Centre for Medium-Range Weather Forecasting) Re-Analyses (ERA) through data assimilation into 45 years (1957-2001) that combines observations with simulated data from a single, consistent numerical model. ERA40 is the second-generation reanalysis carried out by the ECMWF following from ERA15, with the objective of producing the best analysis with the availability of enhanced observation and computational resources (Uppala *et al.*, 2005). In comparison with ERA15, ERA40 is produced with an improved GCM where in the assimilation, sea surface temperature (SSTs), and sea ice fractions are taken from a combination of the

HadISST and NCEP observed datasets. Also, ERA40 uses the observed values of various greenhouse gases for this period to provide relevant information on atmospheric composition, compared to ERA15, which used only the average values (Jones *et al.*, 2004). Comparatively, ERA40 can provide fields with higher horizontal and vertical resolutions in the planetary boundary layer and stratosphere (Uppala *et al.*, 2005). Climate model output, using reanalysis datasets as input, is useful in describing the climatological baseline, for example in examining the relationship between reanalyses of upper air field and surface variables to produce regional climate scenarios downscaled from GCM outputs (Kaas and Frich, 1995).

3.3.2.4 Future climate scenario (HadAM3P: 2070-2100)

The Intergovernmental Panel on Climate Change (IPCC, 2000) has produced four emission scenario families with their coherent narrative storylines, namely SRES A1, SRES A2, SRES B1, and SRES B2 (Table 3.1), reflecting different possible human future activities that yield different levels of greenhouse gas emissions. These scenarios were constructed to reflect the possible future developments in environmental or economic perspectives, and reflect either global or regional development. Each storyline describes a demographic, social, economic, technological, environmental, and policy future. For future climate simulations in SEA, a time slice from 2070-2100 was selected from 240-year transient simulations (1860-2100) with HadCM3. Within this time slice, two emissions scenarios were selected, namely SRES A2 and SRES B2, which are considered the best representations for future SEA emissions. SRES A2 assumes higher population growth, slower per capita economic growth rates, and technological change, which results in higher emissions of CO_2 and larger emissions of other GHGs such as

methane, nitrous oxides, and hydrofluorocarbons (HFCs) (IPCC, 2000). The simulation study consists of an ensemble of three realisations or simulations for scenario SRES A2 (note: in PRECIS these realisations are labelled as [*addja*], [*addje*], and [*addjf*]), and one realisation for scenario SRES B2 (note: in PRECIS this realisation is labelled as [*addjd*]) running for the period 2070-2100. The running of the ensemble (particularly SRES A2) is important to address the uncertainties of the model future simulation (see also Section 3.4).

Table 3.1: Emission scenario storylines

Scenarios	Storyline Descriptions
A1	Describes a future world of very rapid economic growth, global population that peaks in mid-century and declines thereafter, and the rapid introduction of new and more efficient technologies. Major underlying themes are convergence among regions, capacity building, and increased cultural and social interactions, with a substantial reduction in regional differences in per capita income.
A2	Describes a very heterogeneous world. The underlying theme is self-reliance and preservation of local identities. Fertility patterns across regions converge very slowly, resulting in a continuously-increasing population. Economic development is primarily regionally-oriented, and per capita economic growth and technological change is more fragmented and slower than other storylines.
B1	Describes a convergent world with the same global population that peaks in mid-century and declines thereafter, as in the A1 storyline, but with rapid change in economic structures toward a service and information economy, with reductions in material intensity and the introduction of clean and resource-efficient technologies. The emphasis is on global solutions to economic, social, and environmental sustainability, including improved equity, but without additional climate initiatives.
B2	Describes a world in which the emphasis is on local solutions to economic, social, and environmental sustainability. It is a world with continuously increasing global population at a rate lower than A2, intermediate levels of economic development, and less rapid and more diverse technological change than in B1 and A1 storylines. While the scenario is also oriented towards environmental protection and social equity, it focuses on local and regional levels.

Adapted from IPCC (2000)

3.3.2.5 Observational datasets

Observational datasets used in this study were from the Climate Research Unit (CRU) (Hulme *et al.*, 1995). The CRU mean climatology from 1961 to 1990 represents an advance over existing climatologies, where it observes strict temporal fidelity and

incorporates a spatially varying dependence on elevation (Legates and Willmott, 1990; Leemans and Cramer, 1991). CRU datasets are presented in gridded global time-series of surface climate variables, which are used for the evaluation of the ability of a regional climate model (RCM) to simulate climate variability. Another observational dataset that was used in this study was the European Centre for Medium Range Weather Forecasts (ECMWF) Re-Analysis from 1957-2001 (ERA40) (Uppala, *et al.*, 2005), which was described previously in Section 3.3.2.3. But because ERA40 is not fully an observed dataset, it is not fully independent of the model used to generate it. However, this re-analysis dataset can fill gaps in the areas where observations are missing or sparse, such as in SEA. It is also important to note that climate variables such as precipitation in reanalysis datasets are model results and must not be considered as observations. Given that precipitation is among the most difficult fields simulated by today's models, the quality of re-analysis in this regard can be very poor (Moufouma-Okia, UK Meteorological Office, personal communication; Fowell, 2006).

3.3.3 Length of Simulation

For regional climate investigations in SEA, the simulation length for the current climate (1960-1990) and future climate (2070-2100) has been set for 30 years, although the minimum length requirement is at least 10 years. This length is chosen in order to provide a reasonable idea of the mean climate change and to better determine changes in higher order statistics, particularly for the analysis of climate variability (McGregor *et al.*, 1999; Kato *et al.*, 2001; Jones *et al.*, 2004). Longer periods of simulation (i.e. 30 years) were found to capture about 75% of the variance of the true climate change signals, compared to 50% for 10-year simulations (Jones *et al.*, 1997).

Another study by Huntingford *et al.* (2003) has shown that statistically significant changes in extreme precipitation can be obtained using 20-30 year simulations.

3.3.4 Boundary Conditions

Normally, RCMs are driven with either the observed boundary conditions, which are derived from Numerical Weather Prediction (NWP) analyses, or GCM boundary conditions (Gibson *et al.*, 1997; Kalnay *et al.*, 1996). For PRECIS-RCM, the boundary conditions are imposed as surface and lateral boundary conditions. Surface boundary conditions are only required over the ocean and inland water points, where time series of surface temperature and ice extent are provided and are updated daily. Meanwhile, the lateral boundary conditions provide information on atmospheric dynamics at the latitudinal and longitudinal edges of the model domain such as surface pressure, winds, temperature, humidity, and sulphur variables (if sulphur cycle is chosen) and are updated every 6 hours (Jones *et al.*, 2004).

For the simulation study, the boundary data is obtained from the four 30-year integrations of the HadAM3P (atmosphere-only GCM). For the two selected future scenarios (A2 and B2), the sea-surface boundary conditions are derived by combining changes in sea-surface temperature and sea ice simulated in integrations of HadCM3 (ocean-atmosphere GCM) with the HadISST (observed time-dependent fields of SST and sea ice), which has been detailed by Moberg and Jones (2004). Meanwhile, the evolution of greenhouse gases (GHGs) and sulphur dioxide (from anthropogenic and natural sources) concentrations prescribed in the regional model over the simulated period are the same as in the corresponding HadCM3 experiment, which were calculated offline from the SRES emission scenarios data (Jones *et al.*, 2004).

3.3.5 Initial Conditions (Spin-up)

Land, ocean, and sea ice contribute significantly to surface forcing in regional climate simulations (see Giorgi *et al.*, 1996; Pielke *et al.*, 1999; Maslanik *et al.*, 2000; Rummukainen *et al.*, 2001), and therefore, at the beginning of the RCM modelling experiment, the initialisation of surface variables, particularly soil moisture and temperature are not in equilibrium conditions. Since the atmosphere within the RCM domain takes a few model days to achieve equilibrium with its lateral boundary conditions, and while the temperature and moisture in the deep soil levels take many months to reach equilibrium, it is therefore necessary to allow the atmosphere and land surface to adjust or "spin-up" to a mutual equilibrium state prior to the commencement of climate simulation. In PRECIS, the spin-up period of 12 months is applied and during this period the RCM climate will experience some drift (Jones *et al.*, 2004). The output during this spin-up period was not analysed or used in later parts of this study.

3.3.6 Land-Sea Mask

Accurate specification of land and sea grids within the PRECIS-RCM domain is crucial, as land and sea influence the climate evolution in a very different way (Wilson *et al.*, 2005). PRECIS-RCM, used in this study, automatically creates a land-sea mask for the chosen domain, which is sourced from the global dataset at 10 minutes resolution. However, modification of the land-sea mask has been performed on the automatically created PRECIS land-sea mask by editing the grid box into a land point, if at least half of the grid box area is land in reality by using the coast outline as a guide.

3.3.7 Altitude

The altitude for each grid box within the domain is calculated as an average of topographic height of the area covered by the grid box, which is also sourced from a global dataset of mean topographic heights at 10 minutes resolution (Wilson *et al.*, 2005). For the SEA region, there was no alteration of the default altitude for a land grid point as no new land points have been inserted for a grid box, which is mainly ocean in reality. However, altitude modification has been made for inland water such as Toba Lake (904 m amsl) in Sumatra Island of Indonesia and Tonle Sap Lake (10-30 m amsl) in Cambodia (Table 3.2), where realistic heights above mean sea level were applied.

Table 3.2: Modification of grid box properties (altitude, soil and landcover) in PRECIS

Grid Box	XY Coordinate	Altitude (m)	Soil (CODE)	Landcover (STASH CODE)	
				Primary	*Secondary*
Lake Toba (Indonesia)	35,60	904	undefined	Inland water (01)	Inland water (01)
Tonle Sap (Cambodia)	47,36	20	undefined	Inland water (01)	Inland water (01)

3.3.8 Soil and Landcover

The geographical distributions of soil properties and landcover types for all land grid boxes within the domain are prescribed from the datasets created by Wilson and Henderson-Sellers (1985) on a 1° x 1° grid. Each grid box is covered with primary and secondary landcover types, which are required to be supplied in accordance to the landcover type integer codes as shown in Appendix 3.1. Primary landcover is marked by specific landcover type if the coverage of the grid box is between 50-100% and

secondary landcover if the coverage is between 25-50% (Wilson *et al.*, 2005). Meanwhile, Wilson and Henderson-Sellers (1985) have also defined 22 different soil types according to colour, texture, and drainage characteristics as shown in Appendix 3.2. The default soil and landcover can be modified if the landcover types in specific grid boxes are in question. In this case, the global landcover datasets defined by Wilson and Henderson-Sellers (1985) with 1^{o} x 1^{o} resolution for a particular latitude and longitude location can be used. As mentioned in Section 3.3.7, only two grid boxes were modified to include the two major lakes in SEA, namely the Lake Toba (Indonesia) and Lake Tonle Sap (Cambodia) (Table 3. 2).

3.3.9 Diagnostic Output

By default, over 130 outputs in total are available as PRECIS-RCM runs, which are identified with five digit numbers called STASH codes (Appendix 3.3). A STASH code is a unique positive integer, which is assigned to each different output diagnostic variable from the RCM. For the purpose of investigation in the present work, only five variables (i.e temperature, total precipitation, total cloud, solar radiation and boundary layer) were discussed as they are subsequently used as input to the BVOCEM and CiTTyCAT models for the investigation of climate changes impact on biogenic emissions (Chapter 5) and tropospheric chemistry (Chapter 6).

3.4 Uncertainties in Regional Climate Modelling

In the investigation of climate change using a RCM, there are a number of uncertainties that need to be taken into consideration when discussing the simulation results. This section discusses briefly uncertainties in climate modelling (regional or

global) arising from the development of climate scenarios or from the model itself, and how these uncertainties were addressed in PRECIS-RCM. Future emissions uncertainty is one of the most clearly identified major causes of uncertainty in future climate projection (Jones *et al.*, 2004) and has been well documented (Morita *et al.*, 2001). This is due to the inherent uncertainties in key assumptions and relationships about future population, socio-economic development, and technology changes that are the basis of the IPCC SRES Scenarios (Morita *et al.*, 2001). In PRECIS-RCM, the future emissions uncertainties have been addressed by running the Hadley Centre GCM with a range of emission scenarios (SRES A1F1, A2, B2, and B1 emissions) (Jones *et al.*, 2004).

Another important uncertainty that has been identified in RCM is the future concentration of GHG resulting from emissions, due to the lack of understanding of the processes and physics in the carbon cycle and chemical reactions in the atmosphere that affect the emissions-to-concentration relationships. So far, this uncertainty has not been yet addressed in the current PRECIS-RCM, but in the near future, this uncertainty will be reflected in climate scenarios by using atmosphere-ocean general circulation models (AOGCMs) that explicitly simulate the carbon cycle and chemistry of all relevant species (Jones *et al.*, 2004). Incomplete description of the key processes and feedbacks in the climate models has also contributed to the uncertainty in the response of climate systems (Jones *et al.* 2004). The current GCMs, which contain different representations of the climate system, project different patterns and magnitudes of climate change for the same period and same concentration scenarios (Cubasch *et al.*, 2001). In climate impact studies, this

uncertainty can be addressed by using a number of different GCMs (Jones *et al.*, 2004).

Internal variability in RCM simulations, due to linear internal dynamics not associated with the boundary forcing, has been identified as another factor of uncertainty in RCM simulations (Ji and Vernekar, 1997; Giorgi and Bi, 2000; Christensen *et al.*, 2001). Uncertainty of the model simulation is reflected by annual and decadal climate variability. This uncertainty can be quantified, and therefore can be addressed by running ensembles of climate projections. In PRECIS-RCM, an ensemble of three experiments or realisations for both Baseline (Control) Scenario and SRES A2 and one experiment for SRES B2 were provided (see Section 3.3.2), which used the same model and same emission scenarios but initiated from a different starting point (Jones *et al.*, 2004). The modelling results of the experiments will therefore address the internal variability of the model.

Uncertainties also arise from the regionalisation of climate change models from the driving GCM fields, as any errors from the GCMs are carried with them during this process. The inherent effect of systematic errors from the driving large-scale fields provided by the GCM have been observed and described in previous studies (Pan *et al.*, 2001; Mearns *et al.*, 2001; Fowell 2006). The differences in regionalisation techniques not only resulted in different projections, but even the use of the same regionalisation techniques on the same GCM projection can also give different projections. This uncertainty issue can be addressed by using other RCMs or by carrying out statistical downscaling in parallel with PRECIS (Jones *et al.*, 2004). However, quantifying these uncertainties is beyond the scope of this study.

3.5 Evaluations and Assessments of Regional Climate Model

Mearns *et al.* (2003) stressed that any regional climate model to b used for climate change studies should be capable of reproducing the present day climate of the region of interest; model errors should be also identifiable. Since the signals of GCM and RCM are often different, either at the regional or sub-regional scale, it is therefore important that the RCM simulations are validated and the performance of the simulation is verified to ensure that the model errors are identified, quantified, and understood, as these can help in the interpretation of the climate change simulations. The RCM validation is essential for a number of reasons, primarily because most of the PRECIS-RCM runs are over new areas where the model performance is untested, and also as an indicator of how much credibility the RCM results have and how the model should be used in impact studies (Wilson *et al.*, 2005). Furthermore, in assessing the model, the discrepancies between GCM, RCM, and the real observations can be addressed by identifying and quantifying the systematic model bias (errors in the model physical formulation), spatial sampling issues (differences in resolution of model and observations), and observational errors (gridding issues, instrument-dependent errors). Generally, the validation of PRECIS-RCM can be performed in three separate ways: GCM vs Observations; PRECIS-RCM driven by GCM vs GCM; or PRECIS-RCM driven by GCM vs Observations using a number of statistical analyses. In this study, the validation of the model has been carried out by statistically comparing the output data from PRECIS-RCM driven by GCM with the observed data either from CRU or ERA40 datasets and PRECIS-RCM driven by GCM with GCM.

A number of statistical measures were used in this study to evaluate the climate model results. Statistical analysis was made by means of variables such as correlation coefficient (R) (*Eq. 3.1*), fractional bias (FB) (*Eq. 3.2*), and normalised mean square error (NMSE) (*Eq. 3.3*), and a validation test (two tailed t-test). These statistical measures are widely used in meteorological and climate change investigations (see von Storch and Navarra, 1995). The correlation, or the correlation coefficient, is a normalised measure of how well the simulated and observed, or generally two series of data co-varies. The bias of a series of observations and their corresponding simulations can be interpreted as a systematic error for a given variable. If the bias is less than zero then the model is under predicting the mean, and if the bias is larger than zero then the model is overestimating the mean. The fractional bias can also be expressed in percentage. The typical difference between observations and model predictions can be estimated by using the Mean Square Error (MSE). The MSE will have the value zero for a perfect forecast. However, it is sensitive to only a few large differences between observations and predictions due to the squaring of the difference. A variant of the MSE is the Root Mean Square Error defined, which can be interpreted as the expected error of the simulations. Another variant is the Normalised Mean Square Error (NMSE) that obtains a value between 0 and 1, which can be practical when comparing the relative efficiency between observations and simulation. A two-sided student t-test can be used to measure the statistical significance of the difference between averages of two series of datasets.

$$\text{Correlation (R)} = \frac{\sum_{i=1}^{n}\left[\left(O_i-\overline{O}\right)\left(P_i-\overline{P}\right)\right]}{\left[\sum_{i=1}^{n}\left(O_i-\overline{O}\right)^2\right]^{1/2}\left[\sum_{i=1}^{n}\left(P_i-\overline{P}\right)^2\right]^{1/2}} \qquad (3.1)$$

$$\text{Fractional Bias (FB)} = \frac{\bar{O} - \bar{P}}{0.5(\bar{O} + \bar{P})} \quad (3.2)$$

$$\text{Normalised Mean Square Error} = \frac{\sum_{i=1}^{n}(O_i - P_i)^2}{\sum_{i=1}^{n}(O_i P_i)} \quad (3.3)$$

3.6 PRECIS-RCM Applications in Climate Change Studies

In the last 15 years, RCMs have been recognised as an excellent tool in a number of climate studies in smaller regions for topics such as in paleoclimate studies (Hostetler *et al.*, 1994), atmospheric chemistry studies (Stevenson *et al.*, 2005), climate impact studies (Jones *et al.*, 1997; Bhaskaran *et al.*, 1998; Hudson and Jones, 2002; Huntingford *et al.*, 2003), temperature extremes (Hennessy *et al.*, 1998; Mearns, 2004), water resources (Wang *et al.*, 1999; Stone *et al.*, 2001, 2003; Wilby *et al.*, 1997), agriculture (Mearns *et al.*, 1999a, 1999b; Erda *et al.*, 2005; Challinor *et al.*, 2006), energy demand (Lalas *et al.*, 2005), and forest fires (Wotton *et al.*, 1998). RCMs developed by the Hadley Centre, which include PRECIS-RCM, the latest version RCM (third-generation), were also used in a number of climate change impact studies worldwide, which are briefly highlighted in the following paragraphs.

3.6.1 Asia – South Asia

A recent study by Challinor *et al.* (2006) has used the meteorological output of the PRECIS-RCM to study crop responses on climate change in India. Based on

genotypic responses, this study has found that the impact of mean and extreme temperatures on mean yield were widespread, with more stress observed in some locations in India. Another study in India by Kumar *et al.* (2006) used the PRECIS-RCM to develop high-resolution climate change scenarios for the 21st century for various surface and upper air parameters. This study concluded that the PRECIS-RCM has the capability to resolve features on a higher resolution than those by GCM, particularly in projecting the spatial patterns of summer monsoon rainfall along the windward side of the Western Ghat, though notable quantitative biases (overestimate) have been identified, particularly in precipitation over some regions of the Indian sub-continents. Model simulations by PRECIS-RCM under scenarios of increasing GHG concentrations and sulphate aerosols in their study have shown marked increases in both rainfall and temperature towards the end of the 21st century.

Bhaskaran *et al.* (1998) used the earlier version of RCM developed by the Hadley Centre to study the intra-seasonal variability of the oscillation circulation and precipitation anomalies in South Asia. The study also found that the RCM model captured the intra-season variability more realistically than the driving GCM. Further investigations by Hassell and Jones (1999) for the same area concluded that a nested RCM captured observed precipitation anomalies in the active break phases of the monsoon that were not detected from the driving GCM. In Bangladesh, a study was carried out to validate the performance of PRECIS-RCM against the surface observational data of precipitation and temperature at 26 observational sites from 1961-1990 (Islam and Mannan, 2005). Results indicated that PRECIS-RCM overestimated most of the precipitation and temperature in the region, though in some locations it provides better performance.

3.6.2 Asia - Far East

In China, PRECIS-RCM was used by Erda *et al.* (2005) to investigate the future climate and to develop climate change scenarios for China. The results from this study concluded that at the end of the 21st century, depending on the level of future emissions, the average annual temperature was projected to increase between 3-4°C. Meteorological output data from PRECIS-RCM was also used to drive the regional crop models to investigate possible changes in yields of the main crops in China such as rice, maize, and wheat. The projected climate changes without carbon dioxide (CO_2) fertilization could potentially reduce the production yields by up to 37% in the next 20-80 years. Wang and Shallcross (2005) also used PRECIS-RCM to simulate Taiwan's climate, with particular interest on time-sliced between 1979-1981 of the whole modelling period. The simulation results have been compared against the observed data, reanalysis data, and other global climate models. The PRECIS simulation was found to reproduce well the spatial patterns of surface precipitation as well as the inter-annual variability of rainfall. PRECIS-RCM was also found to demonstrate good capability in simulating the spatial distribution of surface temperature over the whole selected region, particularly over Taiwan's Central Mountain Range.

3.6.3 Europe

The regional climate model, HadRM3P, which is also the model used in the regional modelling system PRECIS, was used by Moberg and Jones (2004) to evaluate the simulations of daily maximum and minimum near-surface temperatures across Europe by comparison with the observational data for the same period. The performance of

the model for surface temperature is generally good over the United Kingdom, and elsewhere between latitudes 50 and 55°N, with biases within ±0.5K. However, in other regions within the domain of study, seasonal biases were found to be higher and even biases in climatological averages were as high as ±15K. PRECIS-RCM was also used to investigate the regional climate model performance against the observed data obtained from radiosonde in Cyprus (Southeast Europe) (Hadjinicolaou *et al.*, 2006). This study also concluded that the PRECIS simulation over the selected region could satisfactorily reproduce the temporal evolution of temperature and other meteorological parameters. Lalas *et al.* (2005) also used PRECIS-RCM in Greece to evaluate the regional climate change impact on the energy system in Greece. Based on annual analysis, results have indicated that climate change in the region has caused the electric energy demand to increase approximately 5% solely due to the change in meteorological conditions.

3.6.4 North America and South America

PRECIS-RCM has also been tested over North America by Martineu (2005) to investigate climate changes in the region. In terms of performance, PRECIS-RCM has the capability to reproduce regional climates quite satisfactory, particularly over the Rocky Mountains, the Cordillera, and the Caribbean islands. The spatial patterns of precipitation and temperature of the selected domains are coherent with the observational datasets, though some biases (overestimated by 6°C) exist, particularly on seasonal datasets over the central US in the summer of 1980. Preliminary results of the PRECIS-RCM application in Brazil under SRES A2 scenario have shown a large warming in 2070-2100 for southern Amazonia (up to 6°C)(Marengo and Ambrizzi, 2006). In term of precipitation, the simulation has indicated a drier phenomenon

occurring in Eastern Amazonia and North East Brazil, and precipitation reduction in Southern Brazil and parts of Western Amazonia along the Andes. For comparison, the precipitation projection in Amazonia using the GFDL GCM was also found to show some reduction in individual locations, but the evaluation of the performance of the model in this region was rather poor (Fowell, 2006).

3.6.5 Africa

A number of studies have used PRECIS-RCM to investigate climate changes in the African continent. In one of the recent studies by Beraki (2005) over the Eritrean domain, the PRECIS-RCM simulation performed satisfactorily in terms of spatial patterns against the observed data (the correlation between the observed data was 0.88 to 0.89). Future temperature simulations over this region were found to increase in both SRES A2 and B2 scenarios at the end of this century. Meanwhile, for precipitation, mixed signals were found, though it was expected to increase in most of the Eritrean region. Earlier studies by Arnell *et al.* (2003) used the regional climate model, HadRM3H with spatial resolution of 0.44 × 0.44° with two other models (HadCM3 and HadAM3H) to investigate the macroscale river runoff in southern Africa. Jones and Hudson (2002) have also used the Hadley Centre RCM, HadRM3H, to investigate the climate change scenario over southern Africa. The results have shown that the RCM is capable of resolving features on finer scales, which includes extreme events such as tropical cyclones, though there are indications of positive biases in precipitation and negative biases in surface temperature over most of southern Africa in summer.

3.7 Results and Discussion

The results are presented in two parts: first, the evaluation of regional climate model results by comparing them with the dataset from CRU, ERA40 and the GCM; secondly, the investigation of climate changes under the present-day landcover (fixed vegetation) in the A2 and B2 climate scenarios. For the purposes of discussion, only variables that were used in the subsequent investigation of biogenic emissions (Chapter 5) and tropospheric chemistry (Chapter 6) such as surface temperature, solar radiation, boundary layer height and total cloud were discussed. In addition, precipitation was also included as it is one of the important variables in climate changes investigation. In this Chapter 3, discussion will be limited to the climate change during the northeast monsoon (NEM), which is denoted as DJF (Dec-Jan-Feb) and southwest monsoon (SEM), which is denoted as JJA (Jun-Jul-Aug). For completeness, intermediate periods appear in some tables and figures in the results but are not discussed; these are denoted as MAM (Mar-Apr-May), and SON (Sep-Oct-Nov). Other climate and hydrological variables such as latent heat, sensible heat, surface soil evaporation, canopy evaporation, total soil moisture, moisture convergence and surface pressure were also analysed and available but were not presented in this chapter.

3.7.1 Regional Climate Model Evaluation

This section evaluates the control or Baseline simulations of the PRECIS-RCM by comparison with the observed CRU data and ERA40-Reanalysis datasets for surface temperature, total precipitation, total clouds and solar radiation (ERA40 only). Evaluation of the Baseline simulation as well as the future simulation for A2 and B2

scenarios with respect to the deviations from the simulated climate of the driving GCM are also carried out. Some statistical analysis of results, including the fractional bias (FB), normalised mean square error (NMSE) and correlation, are also provided.

3.7.1.1 Comparison with the CRU datasets

Table 3.3 summarises the seasonal response statistics (for surface temperature, total precipitation and total cloud) over land points for the 0.44^{o} x 0.44^{o} resolution of CRU climatology and the PRECIS-RCM for the Baseline scenario. For the analysis, the observed CRU data were regridded to the RCM grid, and only land points were used in the interpolation. It is also important to acknowledge that the CRU datasets may subject to errors in most area of SEA due to inadequate station coverage. In addition, the uneven distribution of land in the study domain means that the CRU dataset has a different seasonality to the ERA-40 and the whole-domain PRECIS results. The 30-year seasonal mean of surface temperature over land simulated from PRECIS-RCM compared against observed CRU datasets is shown in Figure 3.3. The mean surface temperatures over the land were higher in the PRECIS-RCM compared to the CRU in all seasons with differences of about $0.82^{o}C$ (3% overestimated) during DJF and $0.95^{o}C$ (4% overestimated) during JJA. Larger differences were observed during the inter-monsoons (MAM and SON). In terms of correlation between the simulated surface temperature by PRECIS-RCM and observed (CRU), high correlations of about 0.7 were observed during DJF and JJA compared with other seasons (MAM and SON). The calculated fractional bias (FB) between the simulated (PRECIS-RCM) and observed (CRU) were less than zero except during inter-monsoon (SON) and the FB values were relatively very small. Relatively, there was less systematic error for

the simulation of surface temperature using PRECIS-RCM for SEA. The Normalised Mean Square Error (NMSE) of 0.004 during DJF and 0.003 during JJA indicated a relatively high efficiency of the PRECIS-RCM in simulating surface temperature. Generally, seasonal mean surface temperature simulated by PRECIS-RCM compared well with the observed CRU climatology in terms of the large scale spatial features.

For total precipitation, the mean differences were relatively small, from 0.42 mm/day (6% overestimated) during DJF and 0.42 mm/day (11% underestimated) during JJA (Table 3.3). The 30-year seasonal mean in total precipitation over land from the simulated PRECIS-RCM and observed CRU datasets is shown in Figure 3.4. The correlations between the simulated precipitation (PRECIS-RCM) and observed (CRU) in all seasons were relatively high, between 0.6 and 0.8. The calculated values of Fractional Bias (FB) were also small, indicating a good performance of the PRECIS-RCM in simulating precipitation over the land in SEA. The relatively small NMSE values (between 0.009 and 0.033) also indicated a high efficiency of PRECIS-RCM in the regional simulation of total precipitation. The performance of PRECIS-RCM in simulating total clouds was good, with small differences in the total cloud mean for all seasons and relatively very small values of FB and NMSE. Correlation between the simulated and observed total cloud during both DJF and JJA was high, but relatively small during other seasons (MAM and SON). The 30-year seasonal mean in total cloud over land simulated from the PRECIS-RCM and observed CRU datasets is shown in Figure 3.5.

Table 3.3: Comparison of seasonal response statistics between the Baseline scenario and CRU datasets over land grid points. The area–averaged mean and spatial standard deviation of the response are shown, together with the Fractional Bias (FB), Normalised Mean Square Error (NMSE), and Correlations between the Baseline and CRU datasets.

Variables		Baseline		CRU		Fractional Bias (FB) [%]	Normalised Mean Square Error (NMSE)	Correlation
		Mean	sd	Mean	sd			
Surface Temperature (°C)	DJF	26.88	0.24	26.06	0.24	-3.1	0.0004	0.7
	MAM	27.12	0.21	26.06	0.20	-4.0	0.003	0.4
	JJA	26.59	0.15	25.61	0.16	-3.7	0.003	0.7
	SON	25.36	0.34	24.11	0.46	0.3	0.004	0.5
Precipitation (mm/day)	DJF	7.53	1.10	7.11	1.10	-5.8	0.025	0.7
	MAM	6.97	0.93	6.97	0.90	0.1	0.009	0.8
	JJA	5.73	0.94	6.46	0.87	11.9	0.033	0.7
	SON	6.16	1.24	6.45	0.64	3.7	0.037	0.6
Total Cloud (fraction)	DJF	0.62	0.04	0.61	0.01	-0.9	0.004	0.9
	MAM	0.72	0.03	0.70	0.01	-3.3	0.003	0.4
	JJA	0.67	0.04	0.65	0.01	-2.1	0.003	0.7
	SON	0.61	0.04	0.62	0.02	0.4	0.004	0.5

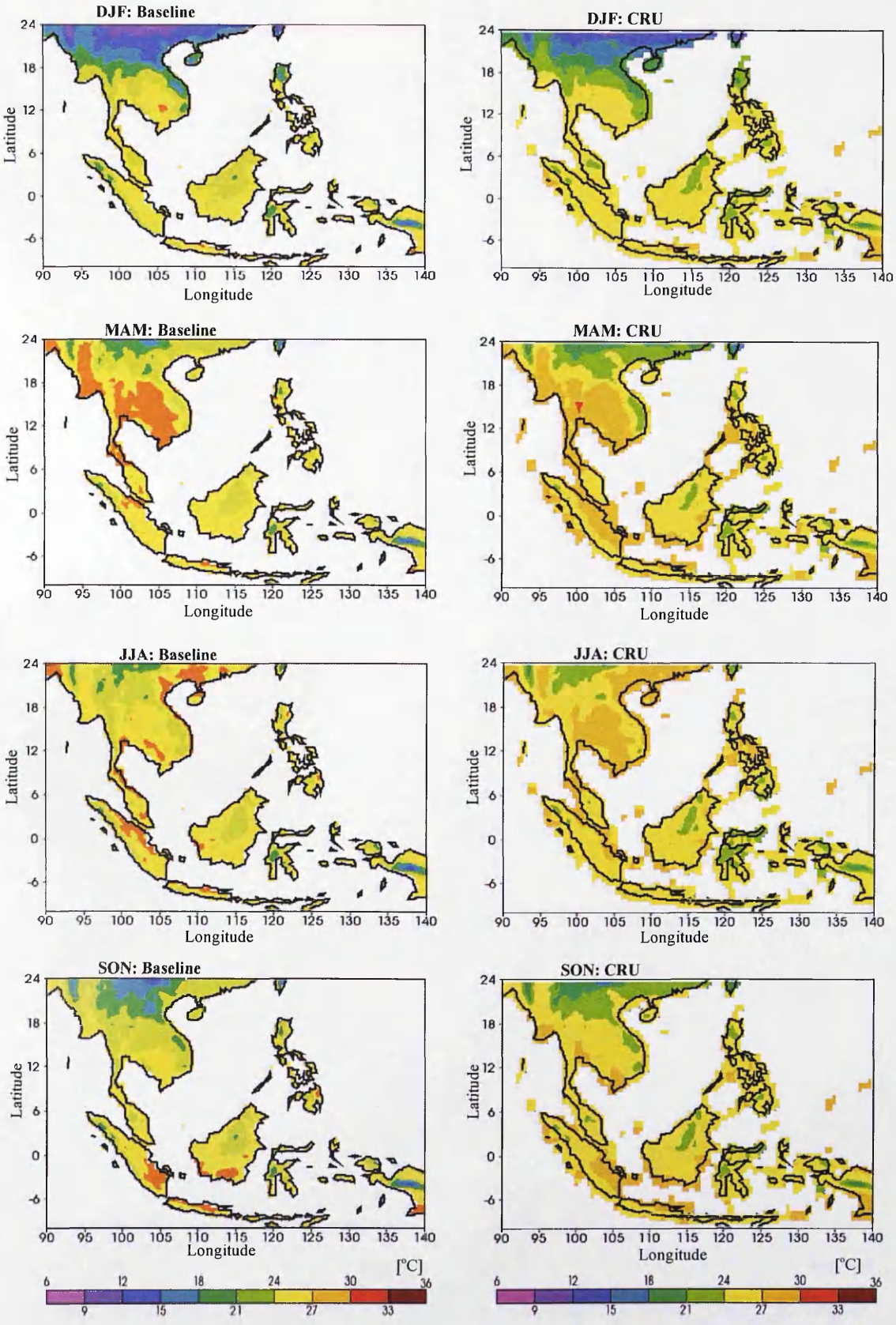

Figure 3.3: The 30-year seasonal mean in surface temperature (°C) over land from the PRECIS-RCM (*left panel*) compared against CRU (*right panel*).

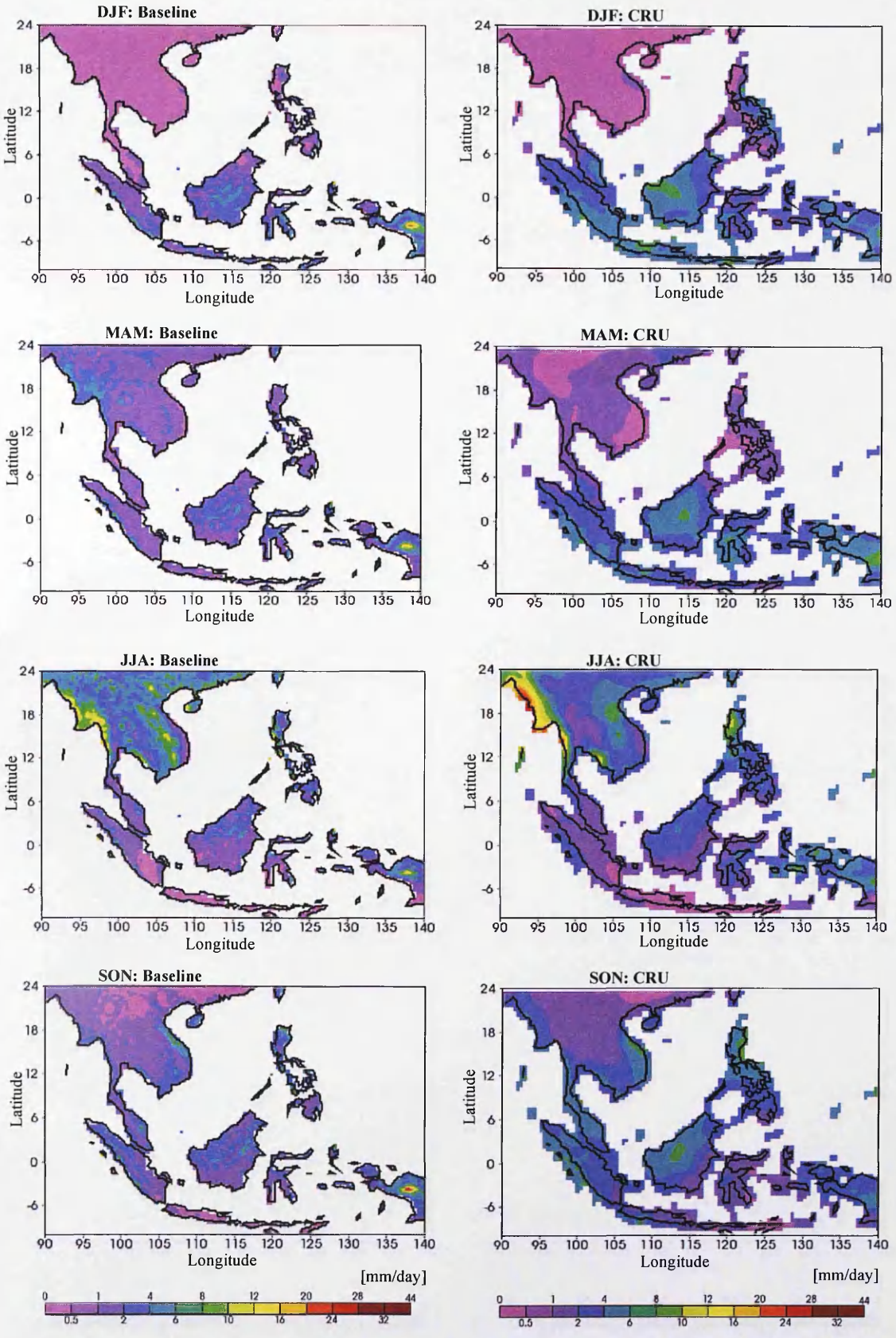

Figure 3.4: The 30-year seasonal mean in total precipitation (mm/day) over land from the PRECIS-RCM (*left panel*) compared against CRU (*right panel*).

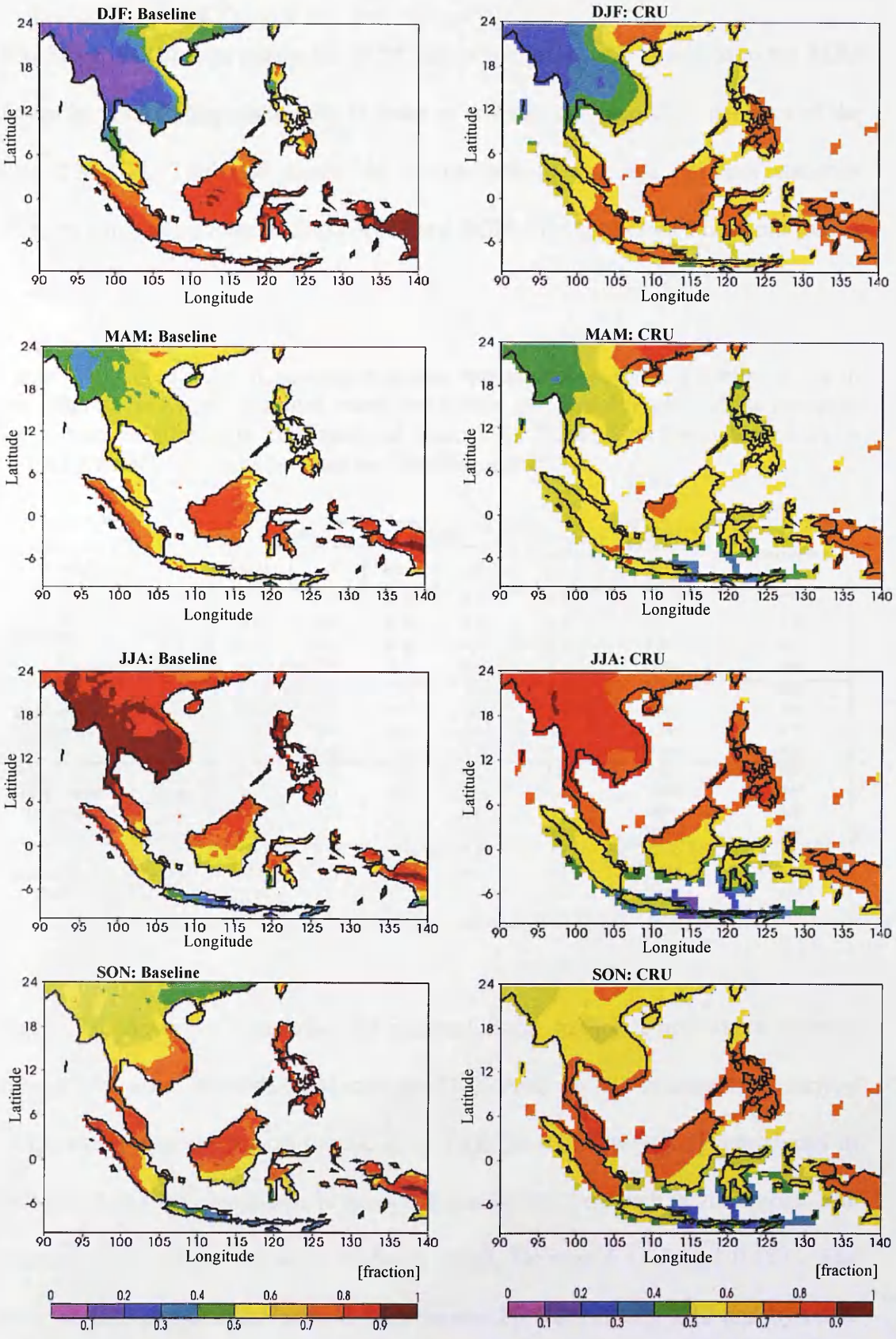

Figure 3.5: The 30-year seasonal mean in total cloud (fraction) over land from the PRECIS-RCM (*left panel*) compared against CRU (*right panel*).

3.7.1.2 Comparison with the ERA40-Reanalysis

The PRECIS-RCM, driven by the GCM lateral boundary, was compared to the RCM forced by ERA40-Reanalysis data in order to evaluate the internal model error of the PRECIS-RCM. Table 3.4 shows the comparison of seasonal response statistics between simulations from PRECIS-RCM and RCM-ERA40 for Baseline scenarios.

Table 3.4: Comparison of seasonal response statistics between the Baseline scenario and ERA40. The area –averaged mean and spatial standard deviation of the response are shown, together with the Fractional Bias (FB), Normalised Mean Square Error (NMSE), and Correlations between the Baseline and ERA40.

Variables		Baseline		ERA40		Fractional Bias (FB) (%)	Normalised Mean Square Error (NMSE)	Correlation
		Mean	sd	Mean	sd			
Surface Temperature (°C)	DJF	25.24	0.15	25.39	0.15	-0.6	0.001	0.92
	MAM	26.85	0.43	27.06	0.47	-0.8	0.001	0.90
	JJA	27.14	0.13	27.27	0.17	-0.5	0.001	0.91
	SON	26.57	0.36	26.72	0.30	-0.5	0.001	0.94
Precipitation (mm/day)	DJF	5.24	0.53	5.22	0.48	0.5	0.001	0.96
	MAM	5.46	1.29	5.33	1.08	-2.4	0.002	0.94
	JJA	8.37	0.07	8.61	0.02	-3.0	0.001	0.72
	SON	7.25	0.58	7.34	0.72	-1.3	0.001	0.89
Total Cloud (fraction)	DJF	0.61	0.03	0.60	0.01	1.2	0.001	0.96
	MAM	0.61	0.05	0.61	0.05	0.3	0.000	0.97
	JJA	0.72	0.01	0.73	0.01	-1.0	0.001	0.88
	SON	0.67	0.02	0.67	0.03	-0.8	0.001	0.97
Solar Radiation (Wm^{-2})	DJF	214.69	11.91	215.99	11.34	-0.6	0.002	0.88
	MAM	239.24	9.83	241.14	9.83	-0.8	0.002	0.87
	JJA	213.54	3.11	212.15	3.15	0.7	0.003	0.90
	SON	220.30	5.45	220.47	5.37	-0.1	0.002	0.92

Figure 3.6 shows the comparison of seasonal mean surface temperatures between simulations from PRECIS-RCM and RCM-ERA40. In all seasons, the surface temperatures over the region simulated by PRECIS-RCM were well reproduced in RCM-ERA40. The correlations between the simulations were high in all seasons. The seasonal mean differences were relatively small, between 0.13°C and 0.15°C. The mean surface temperatures were underestimated by 0.6% during DJF and by 0.5% during JJA. The differences in surface temperature in some areas over the seas in the northern part of the Philippines were found to be statistically significant during DJF

(Figure 3.7). During JJA, surface temperatures were simulated significantly (at 95% level) higher by PRECIS-RCM over Sumatra, Java and the northern part of Sulawesi compared to the RCM-ERA40 simulation.

In comparison with RCM-ERA40, most of the spatial features of the seasonal circulation of precipitation over SEA were well represented in PRECIS-RCM (Figure 3.8). The total precipitation differences between PRECIS-RCM and RCM-ERA40 were in the range of -0.02 mm/day to 0.09 mm/day. During DJF, the mean precipitation was overestimated by 0.5% but underestimated by 3% underestimated during JJA (Table 3.4). Although highly correlated, large areas over the region showed significant differences (at 95% level) in simulated seasonal mean of total precipitation between PRECIS-RCM and RCM-ERA40 (Figure 3.9). The inherited circulation bias from the driving GCM through the lateral boundaries of the PRECIS-RCM domain could be an important factor to the precipitation bias over SEA.

The simulated seasonal mean of total cloud fraction was compared to RCM-ERA40, as shown in Figure 3.10. Seasonal means across the region during the inter-monsoon periods (MAM and SON) were reproduced by PRECIS-RCM but were overestimated by 1.2% during DJF and underestimated by 1% during JJA (Table 3.4). Figure 3.11 shows that, over most of the areas where the mean cloud fraction differences were more than 0.04, mean differences were found to be statistically significant at the 95% confidence level.

Similarly with other climatic variables, the seasonal mean of solar radiation simulated by PRECIS-RCM reproduced most of the spatial features of the seasonal circulation from RCM-ERA (Figure 3.12). In all seasons, the simulated seasonal mean solar

radiation was in the range of 214 Wm^{-2} to 239 Wm^{-2} (Table 3.4). The mean solar radiation was underestimated by 0.6% during DJF and 0.1% during JJA. Statistically, mean differences were found to be significant at the 95% confidence level in some areas of the region, as shown in Figure 3.13.

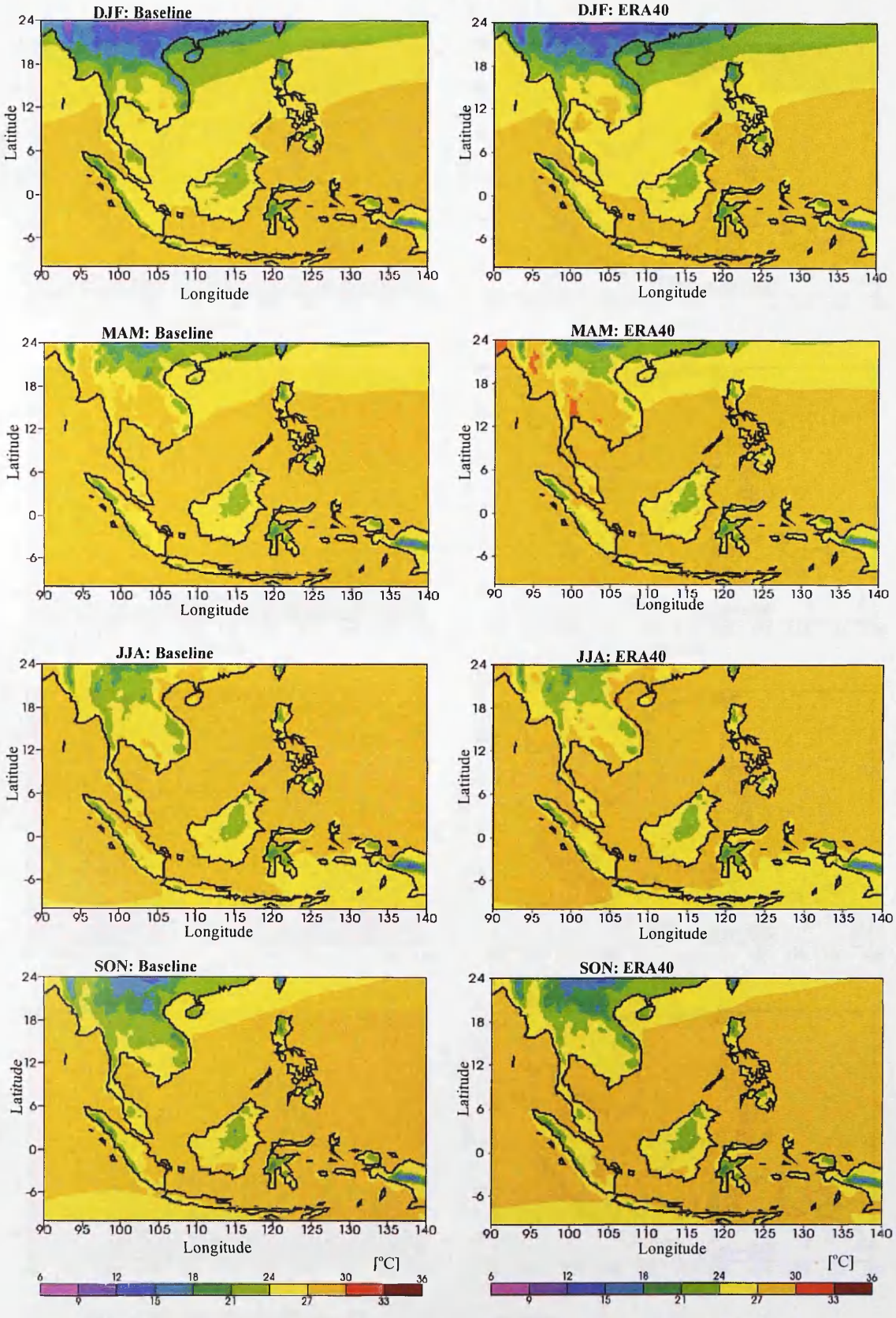

Figure 3.6: The 30-year seasonal mean in surface temperature (°C) from the PRECIS-RCM (*left panel*) compared against ERA40 (*right panel*).

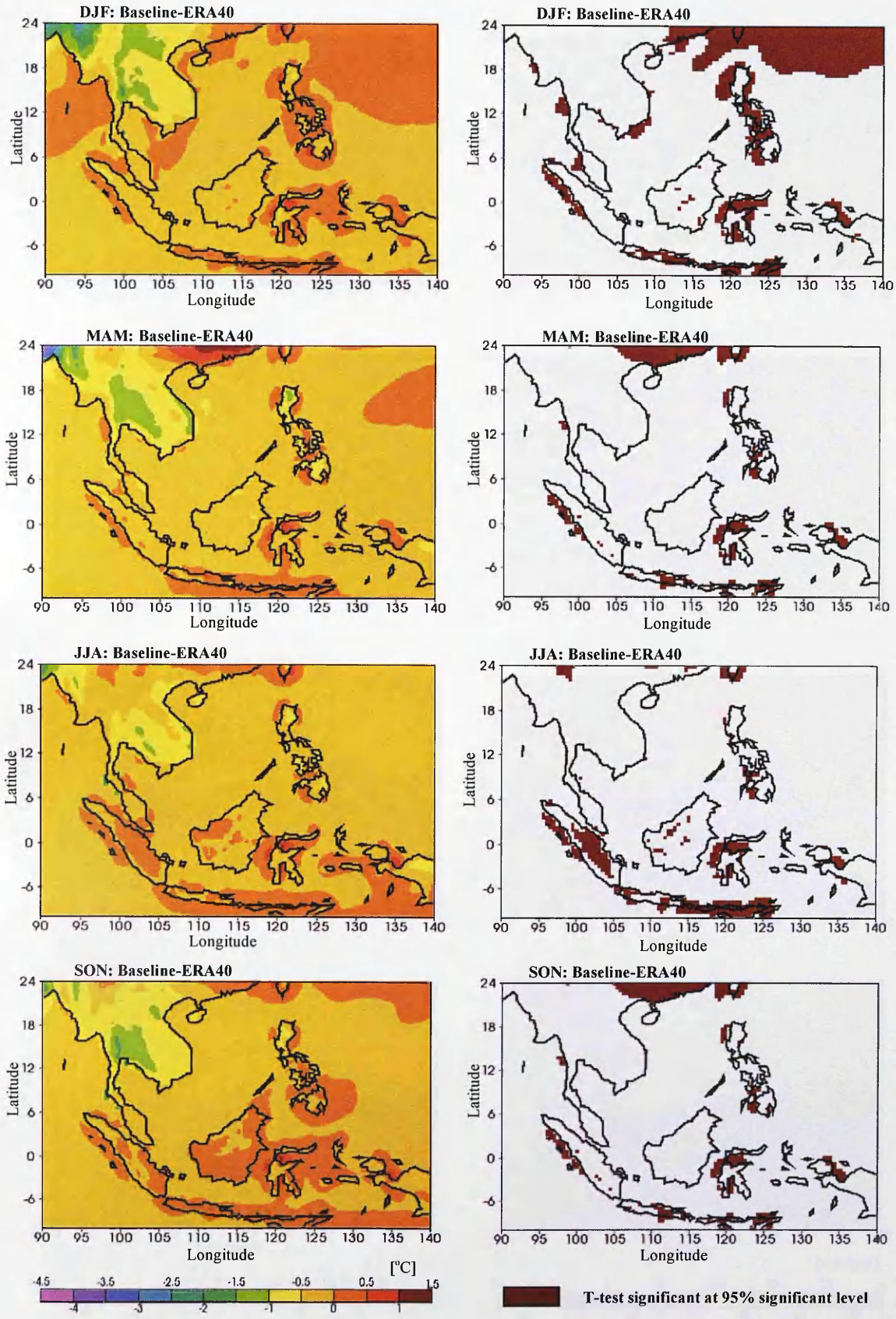

Figure 3.7: The 30-year seasonal mean differences of surface temperature (°C) between Baseline and ERA40 simulated by PRECIS-RCM (*left panel*) and the significant t-test plots (*right panel*).

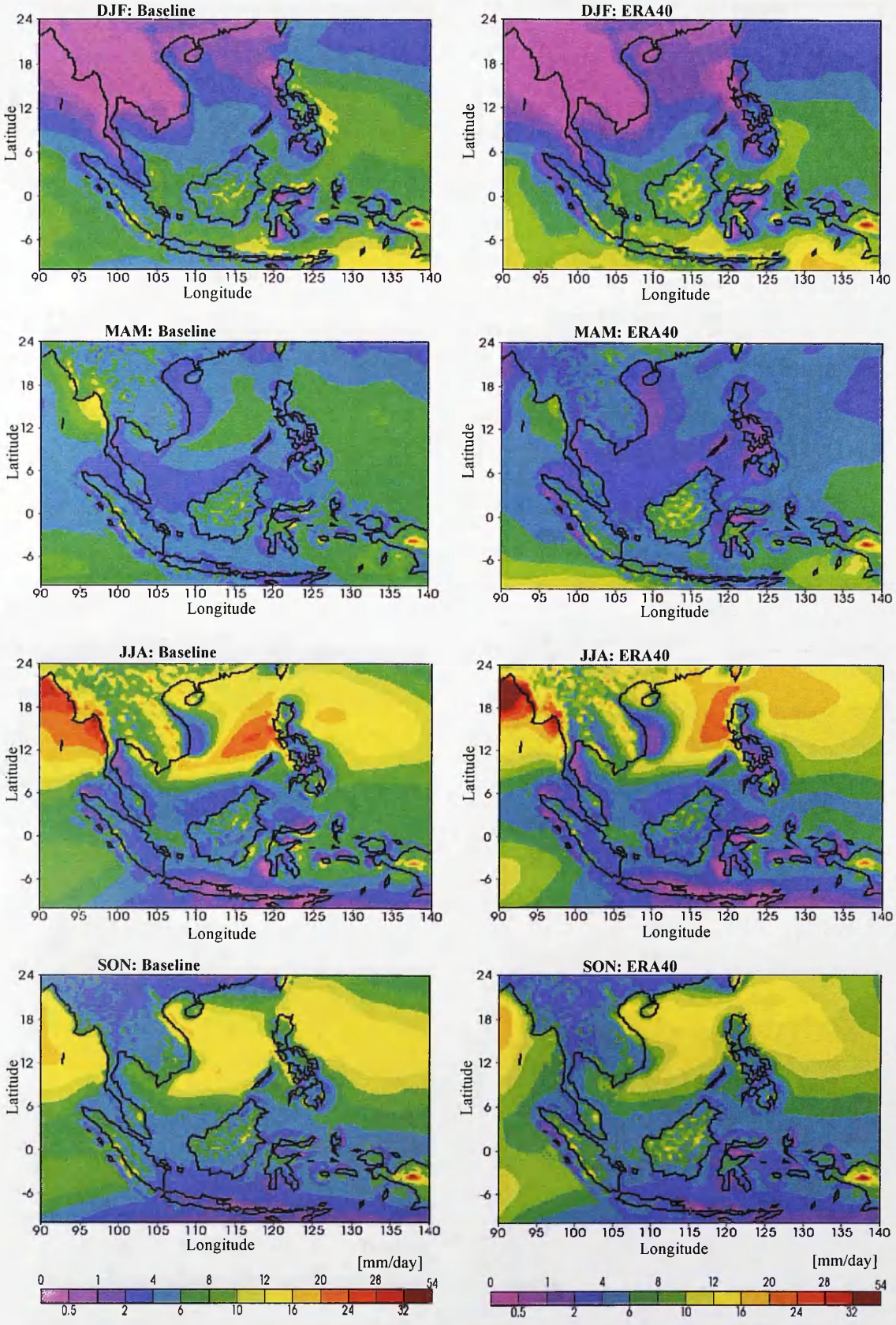

Figure 3.8: The 30-year seasonal mean in total precipitation (mm/day) from the PRECIS-RCM (*left panel*) compared against ERA40 (*right panel*).

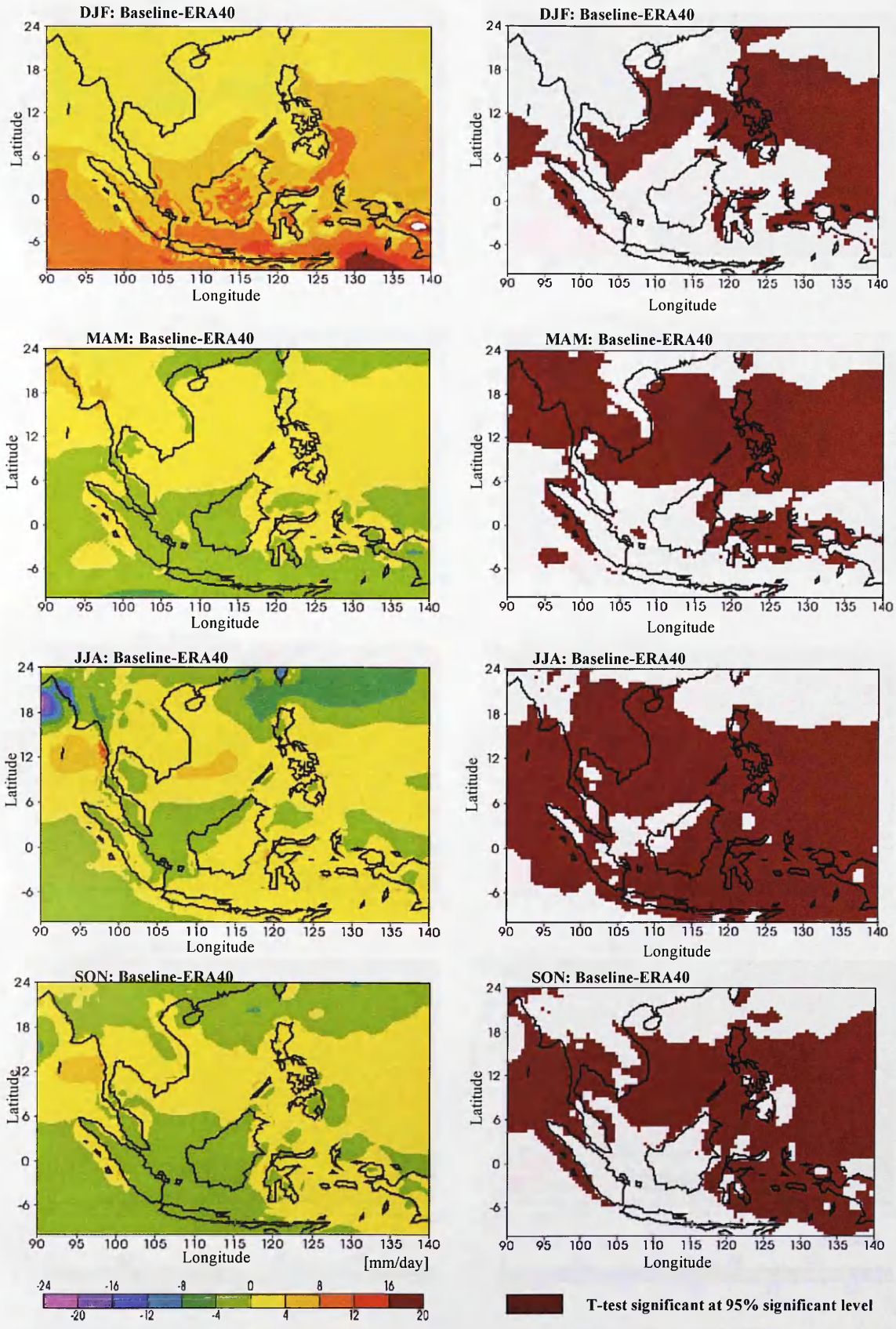

Figure 3.9: The 30-year seasonal mean differences of total precipitation (mm/day) between Baseline and ERA40 simulated by PRECIS-RCM (*left panel*) and the significant t-test plots (*right panel*).

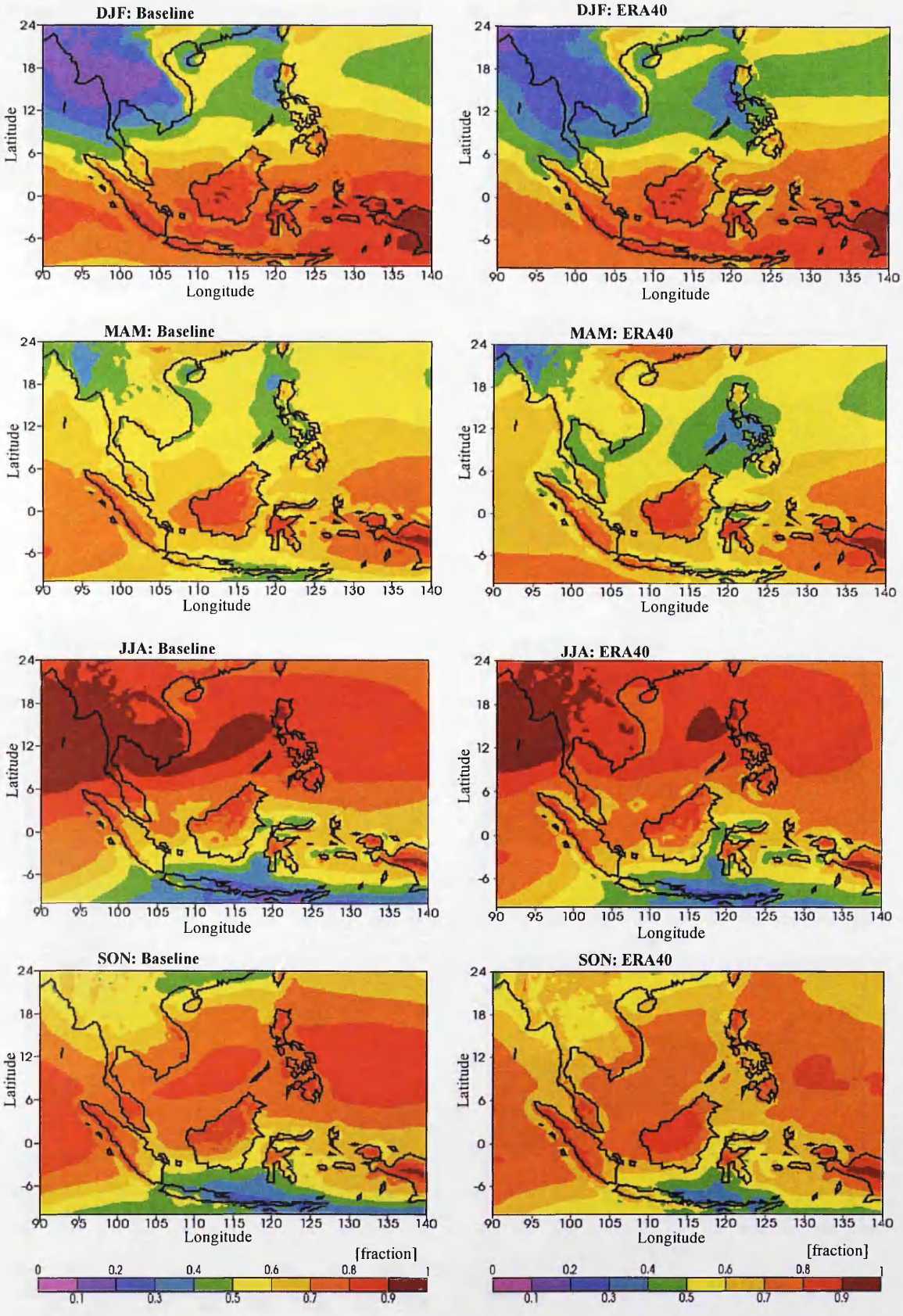

Figure 3.10: The 30-year seasonal mean in total cloud (fraction) from the PRECIS-RCM (*left panel*) compared against ERA40 (*right panel*).

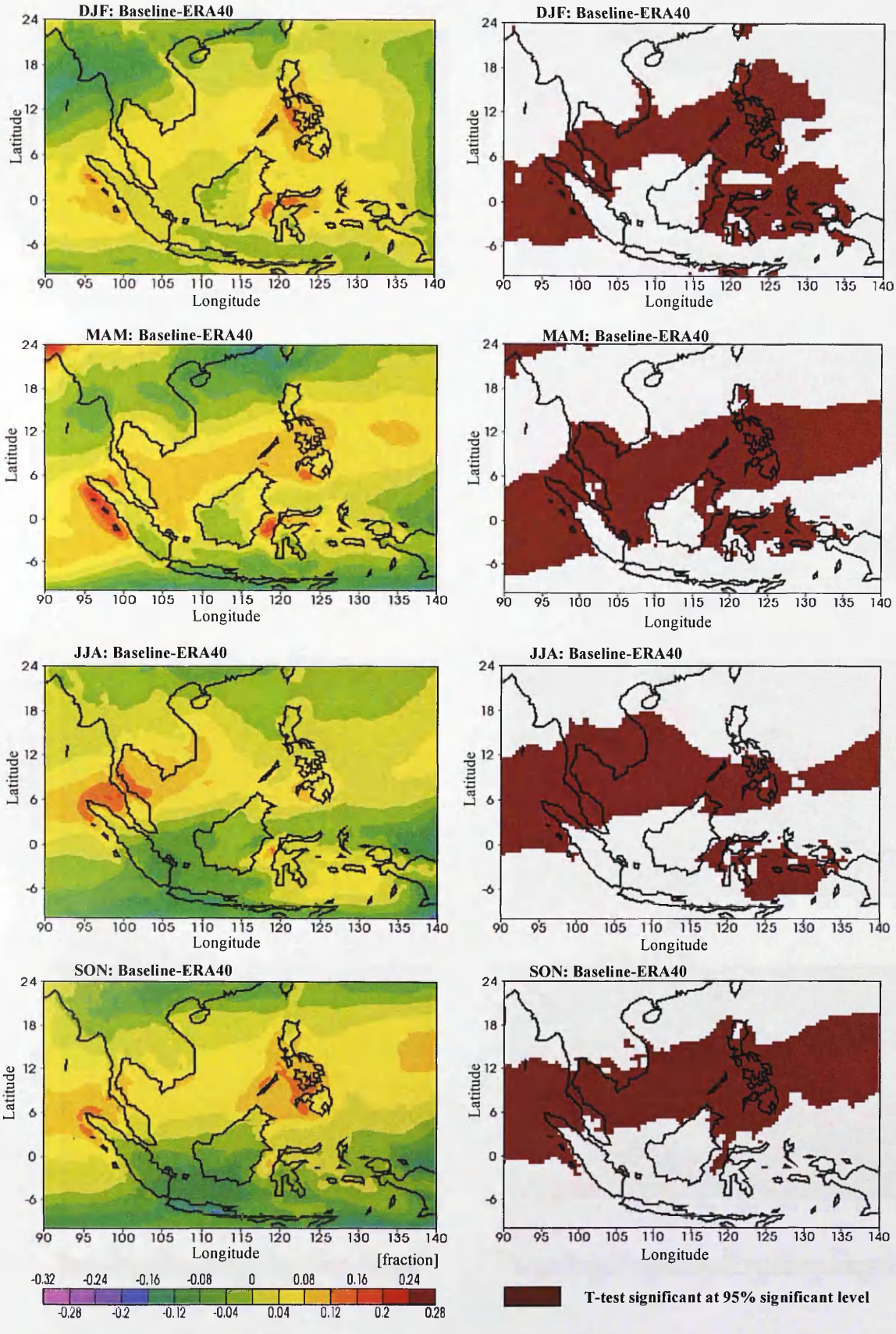

Figure 3.11: The 30-year seasonal mean differences of total cloud (fraction) between Baseline and ERA40 simulated by PRECIS-RCM (*left panel*) and the significant t-test plots (*right panel*).

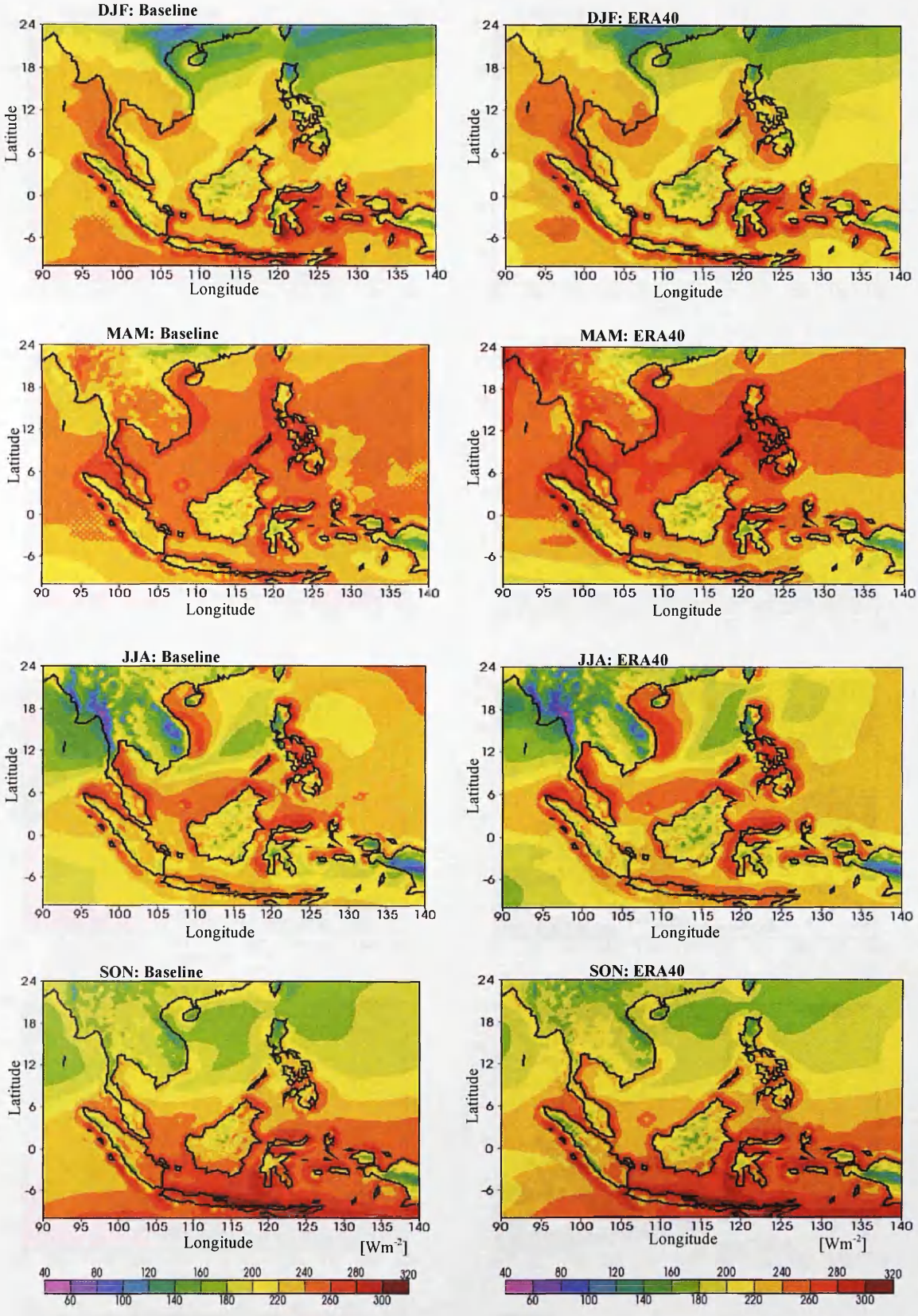

Figure 3.12: The 30-year seasonal mean in solar radiation (Wm^{-2}) from the PRECIS-RCM (*left panel*) compared against ERA40 (*right panel*).

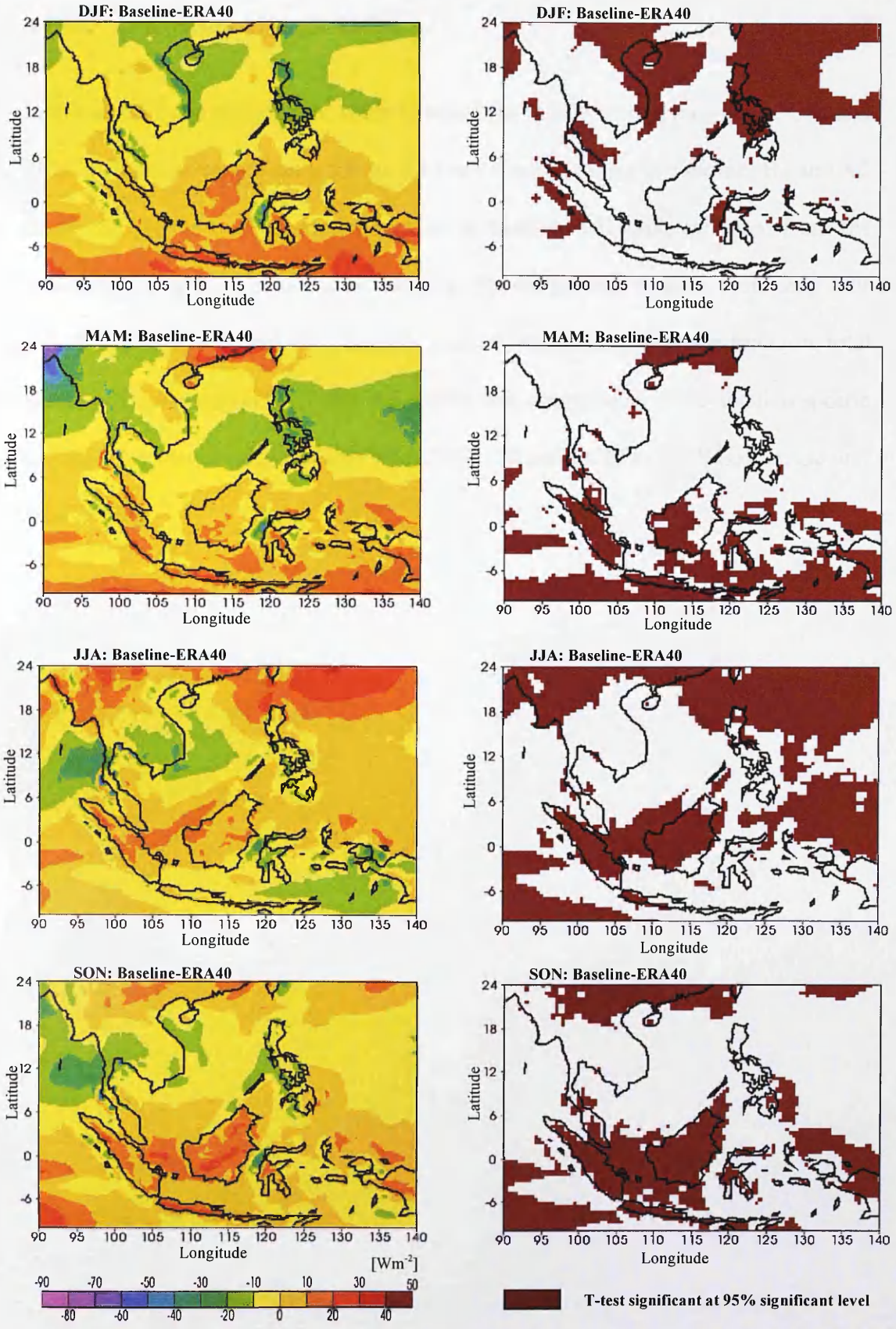

Figure 3.13: The 30-year seasonal mean differences of solar radiation (Wm^{-2}) between Baseline and ERA40 simulated by PRECIS-RCM (*left panel*) and the significant t-test plots (*right panel*).

3.7.1.3 Comparison with the GCM

In this section, comparisons are made between the responses of the driving GCM and PRECIS-RCM, averaged daily for the 30-years simulation in the Baseline, B2 and A2 scenarios over the regional-model domain, to evaluate the errors inherited from the forcing GCM through the lateral boundaries. For the purpose of discussion, only four climatic variables are dealt with, namely: surface temperature, total precipitation, total cloud, and solar radiation. Table 3.5 shows the comparison of seasonal response statistics between simulations from PRECIS-RCM and GCM in the Baseline, B2 and A2 scenarios.

Table 3.5: Comparison of the 30-year daily mean response statistics between RCM (Baseline, SRES B2 and SRES A2) and GCM. The area – averaged mean and spatial standard deviation of the response are shown, together with the Fractional Bias (FB), Normalised Mean Square Error (NMSE), and Correlation between the RCM (Baseline, SRES B2 and SRES A2) and GCM.

	Baseline		GCM		FB (%)	NMSE	Corr.	SRES B2		GCM-B2		FB	NMSE	Corr.	SRES A2		GCM		FB	NMSE	Corr
Variables	Mean	sd	Mean	sd				Mean	sd	Mean	sd				Mean	sd	Mean	sd			
Surface Temperature (°C)	26.48	0.75	26.61	0.75	-0.5	0.000	0.92	28.64	0.83	28.56	0.76	0.3	0.000	0.85	28.97	0.79	29.12	0.74	--0.52	0.000	0.99
Precipitation (mm/day)	1.72	0.11	1.35	0.26	24.5	0.125	-0.40	6.29	2.22	5.49	1.90	13.7	0.056	0.88	6.45	1.90	5.66	1.62	13.91	0.028	0.96
Total Cloud (fraction)	0.67	0.08	0.63	0.07	6.4	0.007	0.93	0.60	0.10	0.56	0.10	7.4	0.011	0.94	0.60	0.08	0.56	0.08	6.56	0.008	0.93
Solar Radiation (Wm^{-2})	221.68	13.48	228.60	12.39	3.1	0.002	0.92	227.60	15.04	233.31	14.28	-2.5	0.001	0.94	235.41	12.88	236.05	13.10	-0.27	0.000	0.99

Note: ***FB*** *= **Fractional Bias (%)***
NMSE *= **Normalised Mean Square Error***
Corr *= **Correlation***

3.7.1.3.1 Baseline

The pattern and magnitude of the 30-year daily mean comparison between the PRECIS-RCM and GCM of surface temperature, total precipitation, total cloud and solar radiation for the Baseline scenario are shown in Figure 3.14. The surface temperature over the region simulated by GCM was well reproduced by PRECIS-RCM. The simulated surface temperatures in PRECIS-RCM and GCM were highly correlated (0.92) with mean temperatures of about 26.5°C and 26.6°C respectively (Table 3.5). As expected, PRECIS-RCM was capable of simulating surface temperature with high resolution over central Borneo and some regions over Sumatra. The mean surface temperature differences between PRECIS-RCM and GCM were found to be statistically significant at 95% level in small and sporadic locations over SEA (Figure 3.15).

The main features of the total precipitation simulation in the region by GCM were well reproduced by PRECIS-RCM. PRECIS-RCM has also shown its ability to capture high precipitation over the Bay of Bengal at high resolution (Figure 3.14). However, comparing with the driving GCM, The simulated total precipitation over the region by PRECIS-RCM was about 24.5% higher than that in the GCM (Table 3.5). The simulated mean of total precipitation by PRECIS-RCM and the driving GCM were 1.72 mm/day and 1.35 mm/day with a lower correlation of about 0.4. Larger areas over the region were found to be significantly different at 95% level between the simulated PRECIS-RCM and driving GCM as shown in Figure 3.15. As a comparison, an earlier study by Fowell (2006) also found a poor simulation result (r^2=0.54) for total precipitation over SEA at the grid cell using the GFDL-GCM model. The investigation by Fowell (2006) also found that the continental region of

SEA has a large relative error, mainly due to the small observed precipitation values. Therefore, the model failed to simulate accurately during JJA in this region.

The daily means of the total cloud fraction simulated by PRECIS-RCM and GCM were 0.67 and 0.63 respectively. PRECIS-RCM was also found to simulate total cloud at better resolution over central Borneo (Figure 3.14). A higher correlation of 0.9 between the PRECIS-RCM and driving GCM was also observed. However, simulated mean cloud by PRECIS-RCM was slightly higher, by about 6%, in comparison with the driving GCM (Table 3.5). Small areas over the region were found to be significantly different at the 95% confidence level (Figure 3.15).

Similar patterns and values of solar radiation were simulated by GCM and PRECIS-RCM (Figure 3.14). The simulated daily means from PRECIS-RCM and the driving GCM was highly correlated (0.9) with means of about 221.7 Wm^{-2} and 228.6 Wm^{-2} respectively. In comparison with the driving GCM, the simulation by PRECIS-RCM was 3.1% higher. A larger area, mostly over the land, was found to be statistically different at 95% confidence level (Figure 3.15).

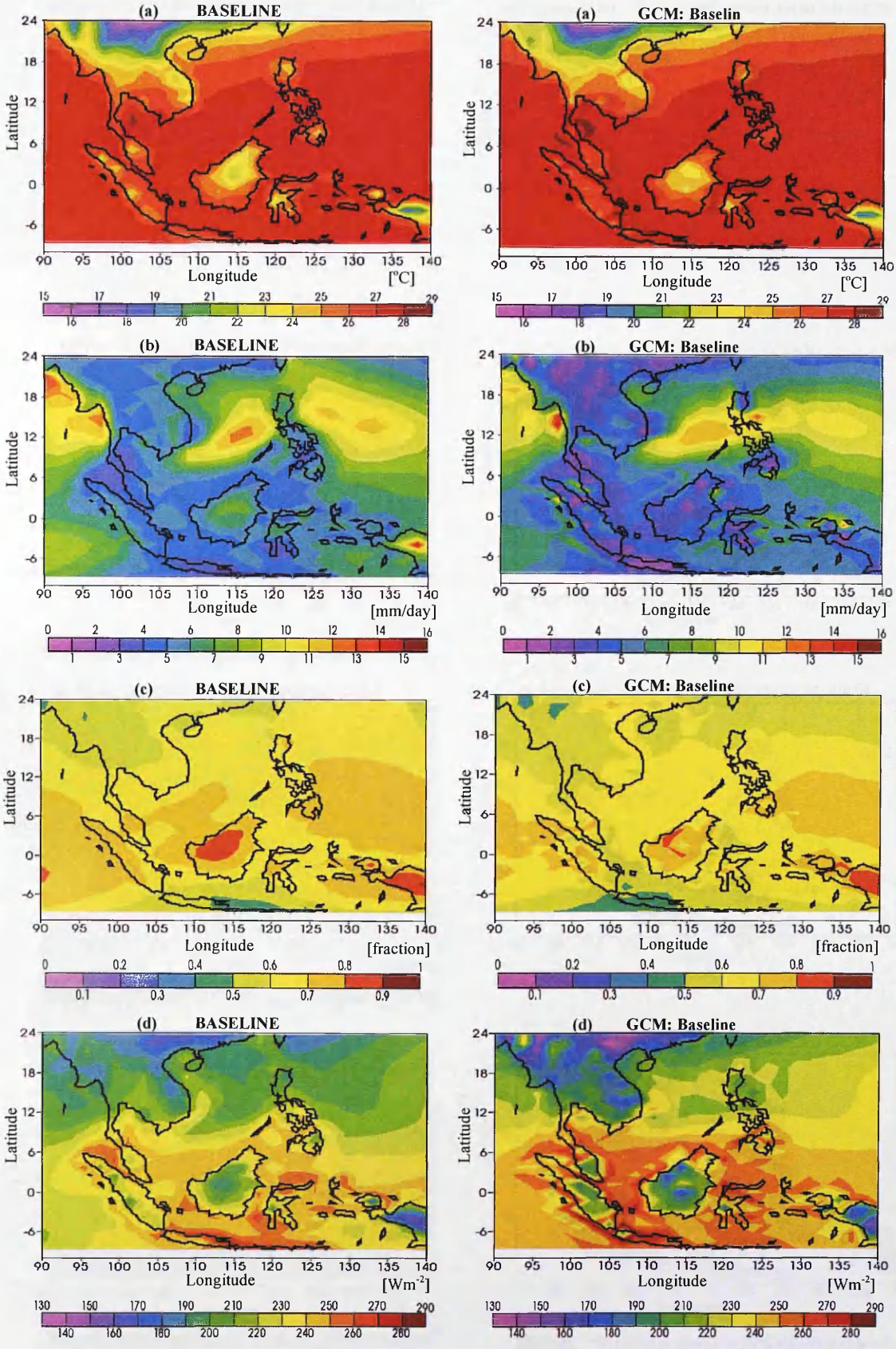

Figure 3.14: **Baseline**: Comparison of the 30-year daily mean of (a) surface temperature (°C); (b) total precipitation (mm/day); (c) total cloud (fraction); (d) solar radiation (Wm^{-2}) between the PRECIS-RCM (*left panel*) and GCM (*right panel*) simulations in the Baseline scenario.

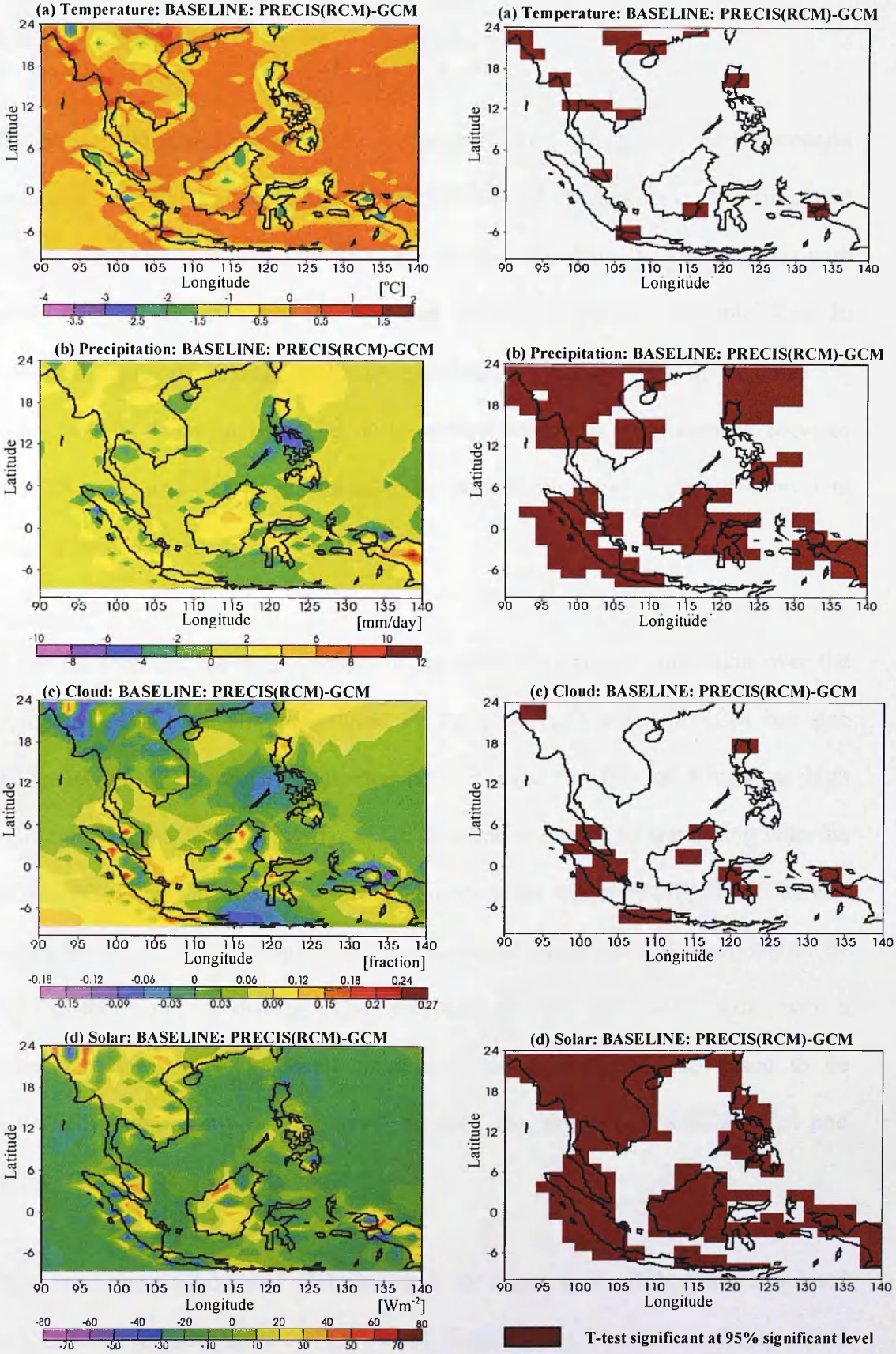

Figure 3.15: **Baseline**: The 30-year daily mean difference of (a) surface temperature (°C); (b) total precipitation (mm/day); (c) total cloud (fraction); (d) solar radiation (Wm^{-2}) between the PRECIS-RCM and GCM (*left panel*) simulations, and the significant t-test plots (*right panel*) in the Baseline scenario.

3.7.1.3.2 SRES B2

The pattern and magnitude of surface temperature over the region in the B2 scenario simulated by GCM was reproduced by PRECIS-RCM (Figure 3.16). The simulated surface temperatures by PRECIS-RCM and GCM were highly correlated (0.85) with mean temperatures of about 28.64°C and 28.56°C respectively (Table 3.5). In comparison with the driving GCM, the simulated surface temperature by PRECIS-RCM was by 0.3% higher. The mean surface temperature differences between PRECIS-RCM and GCM were found to be statistically significant at 95% level in small areas across the region (Figure 3.17).

In the B2 scenario, the main features of the total precipitation simulation over the region by GCM were also reproduced by PRECIS-RCM. PRECIS-RCM has also shown its ability to capture high precipitation over the Bay of Bengal at high resolution (Figure 3.16). Similarly, in the Baseline scenario, by comparing with the driving GCM, the simulated total precipitation over the region by PRECIS-RCM was higher by about 13.7% (Table 3.5). The simulated mean of total precipitation by PRECIS-RCM and the driving GCM were 6.29 mm/day and 5.49 mm/day with a correlation of about 0.88. Small areas over the region were also found to be statistically significantly at 95% level between the simulated PRECIS-RCM and driving GCM as shown in Figure 3.17.

The pattern and magnitude of total cloud over the region in the B2 scenario simulated by GCM was reproduced by PRECIS-RCM (Figure 3.16). The simulated total cloud fraction by PRECIS-RCM and the driving GCM were 0.60 and 0.56 respectively. In comparison with the driving GCM, simulated mean cloud by PRECIS-RCM was

7.4% higher (Table 3.5). A higher correlation of about 0.94 between the PRECIS-RCM and driving GCM was also observed. Statistically, there were small areas over the region where the total cloud simulations were significantly different, at 95% confidence level (Figure 3.17).

The solar radiation over the region simulated by GCM was also reproduced by PRECIS-RCM (Figure 3.16). The simulated daily means from PRECIS-RCM and the driving GCM was highly correlated (0.89) with means of about 513.01 Wm^{-2} and 465.86 Wm^{-2} respectively. In comparison with the driving GCM, the simulation by PRECIS-RCM was 2.5% lower. Some areas over the land were found to be statistically significant at the 95% confidence level (Figure 3.17).

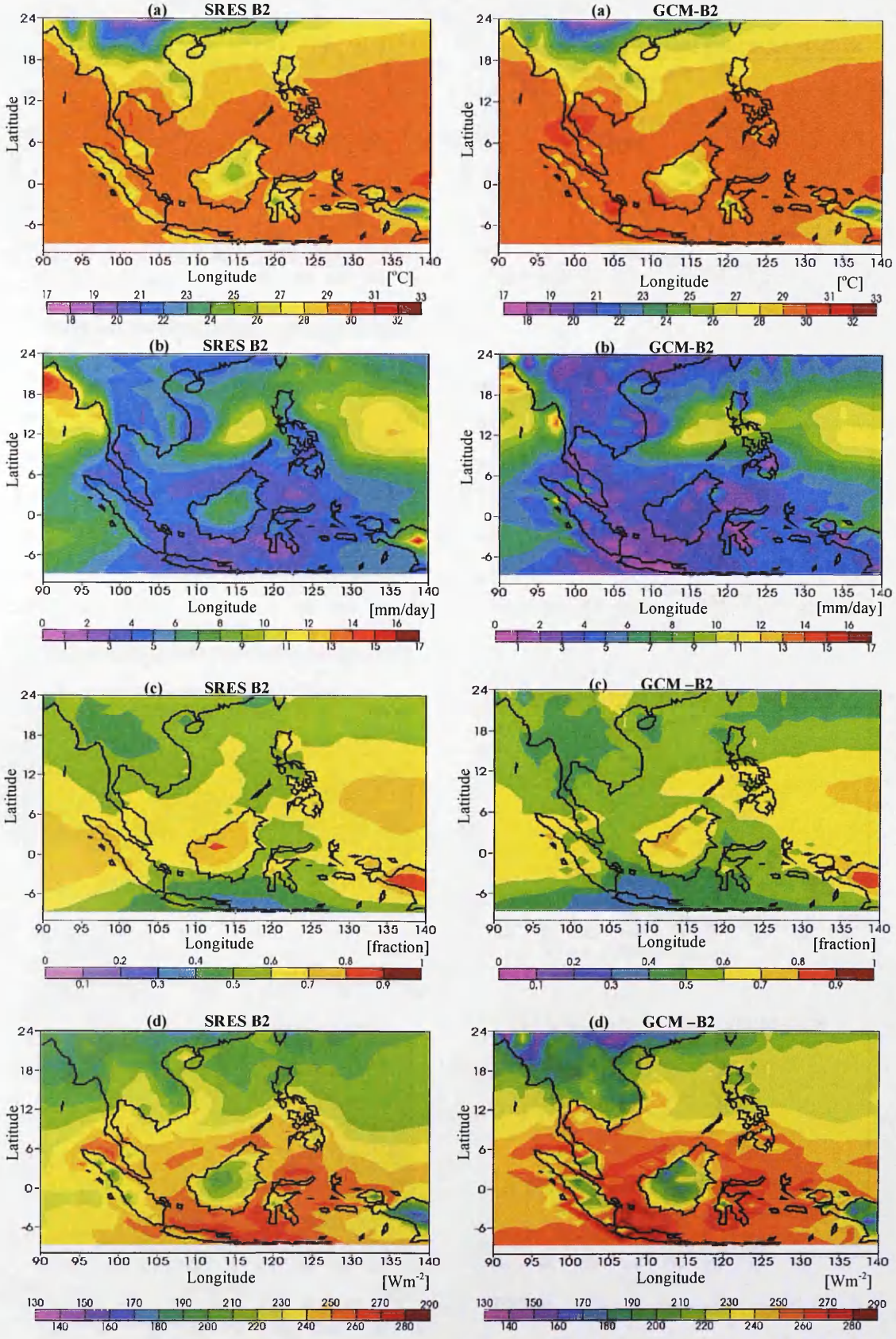

Figure 3.16: **SRES B2**: Comparison of the 30-year daily mean of (a) surface temperature (°C); (b) total precipitation (mm/day); (c) total cloud (fraction); (d) solar radiation (Wm^{-2}) between the PRECIS-RCM (*left panel*) and GCM (*right panel*) simulations in the SRES B2 scenario.

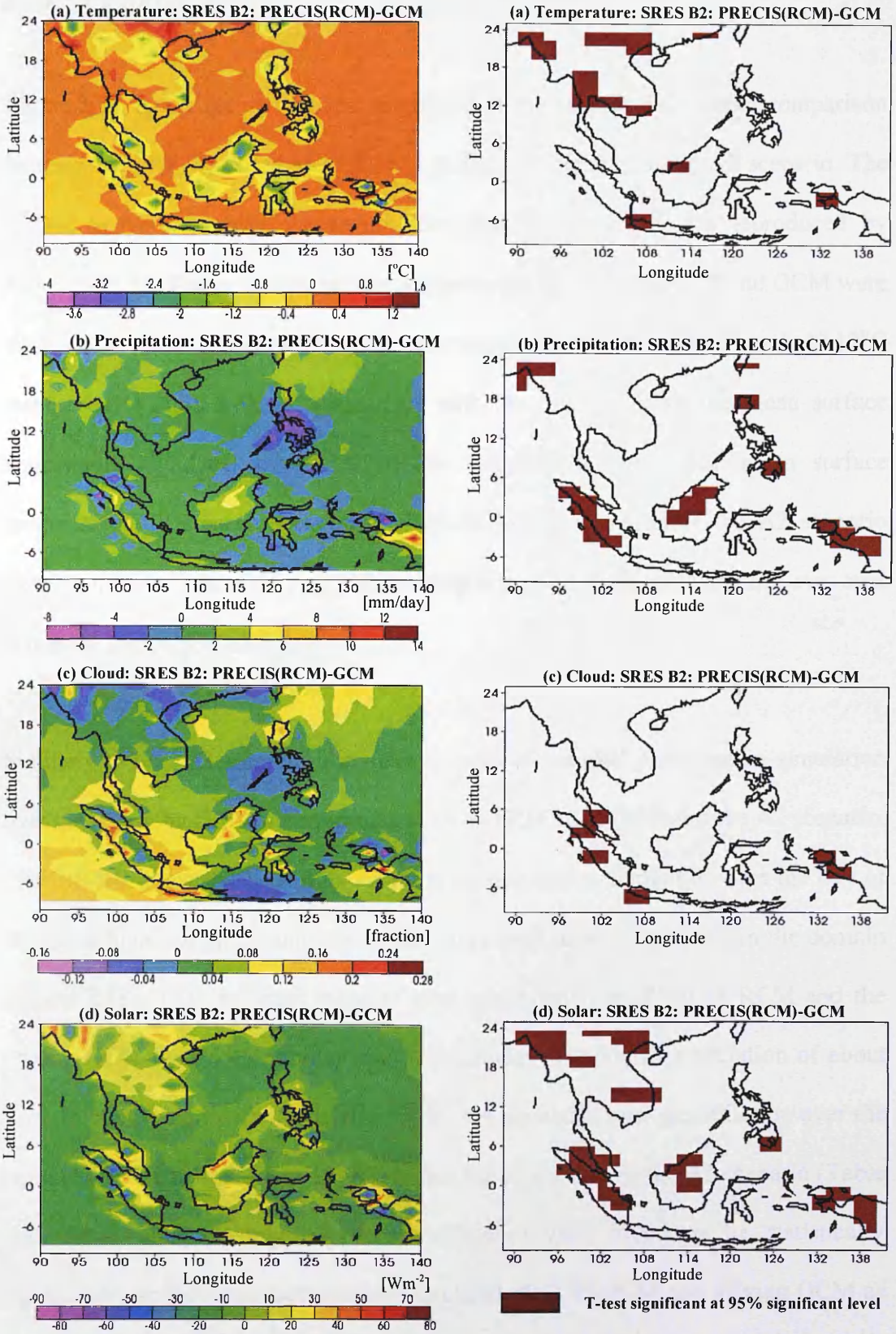

Figure 3.17: **SRES B2**: The 30-year daily mean difference of (a) surface temperature (^{o}C); (b) total precipitation (mm/day); (c) total cloud (fraction); (d) solar radiation (Wm^{-2}) between the PRECIS-RCM and GCM (*left panel*) simulations, and the significant t-test plots (*right panel*) in the SRES B2 scenario.

3.7.1.3.3 SRES A2

Figure 3.18 shows the pattern and magnitude of the 30-year daily mean comparison between the PRECIS-RCM and GCM of surface temperature under A2 scenario. The surface temperature over the region simulated by the GCM was reproduced by PRECIS-RCM. The simulated surface temperatures by PRECIS-RCM and GCM were highly correlated (0.99) with mean temperature of about 28.97°C and 29.12°C respectively (Table 3.5). In comparison with the driving GCM, the mean surface temperature simulated by PRECIS-RCM was 0.52% lower. The mean surface temperatures differences between PRECIS-RCM and GCM under the A2 scenario were found to be statistically significant at 95% level in small areas, mainly over land across the region (Figure 3.19).

Similarly to the B2 scenario, the main features of the total precipitation simulation over the region by GCM were reproduced by in PRECIS-RCM under the A2 scenario. PRECIS-RCM has also shown its ability to capture high precipitation over the Bay of Bengal at high resolution and some other areas over some islands within the domain (Figure 3.18). The simulated mean of total precipitation by PRECIS-RCM and the driving GCM were 6.45 mm/day and 5.66 mm/day with higher correlation of about 0.96. In comparison with the driving GCM, the simulated total precipitation over the region by PRECIS-RCM was 13.9% higher but lower than in the B2 scenario (Table 3.5). Some areas, mainly over the Philippines were found to be statistically significantly at 95% level between the simulated PRECIS-RCM and driving GCM as shown in Figure 3.19.

For the total cloud, the simulated daily mean fractions by PRCEIS-RCM and GCM were 0.60 and 0.56 respectively. Similarly with B2 scenario, PRECIS-RCM was also found to simulate total cloud at better resolution over central Borneo (Figure 3.18). A high correlation of 0.93 between the PRECIS-RCM and driving GCM was also observed, although the simulated cloud by PRECIS-RCM was 6.6% higher in comparison with the driving GCM (Table 3.5). Small areas over Indochina were found to be statistically significant at 95% confidence level (Figure 3.19).

As in the B2 scenario, the simulated solar radiation by GCM was reproduced by PRECIS-RCM (Figure 3.18). The simulated mean of solar radiation by PRECIS-RCM and driving GCM were 235.4 Wm^{-2} and 236.1 Wm^{-2} respectively. The simulation by PRECIS-RCM was 0.27% lower in comparison with the driving GCM simulation. Relatively larger areas and mainly over sea, were found to be statistically significant at the 95% level (Figure 3.19).

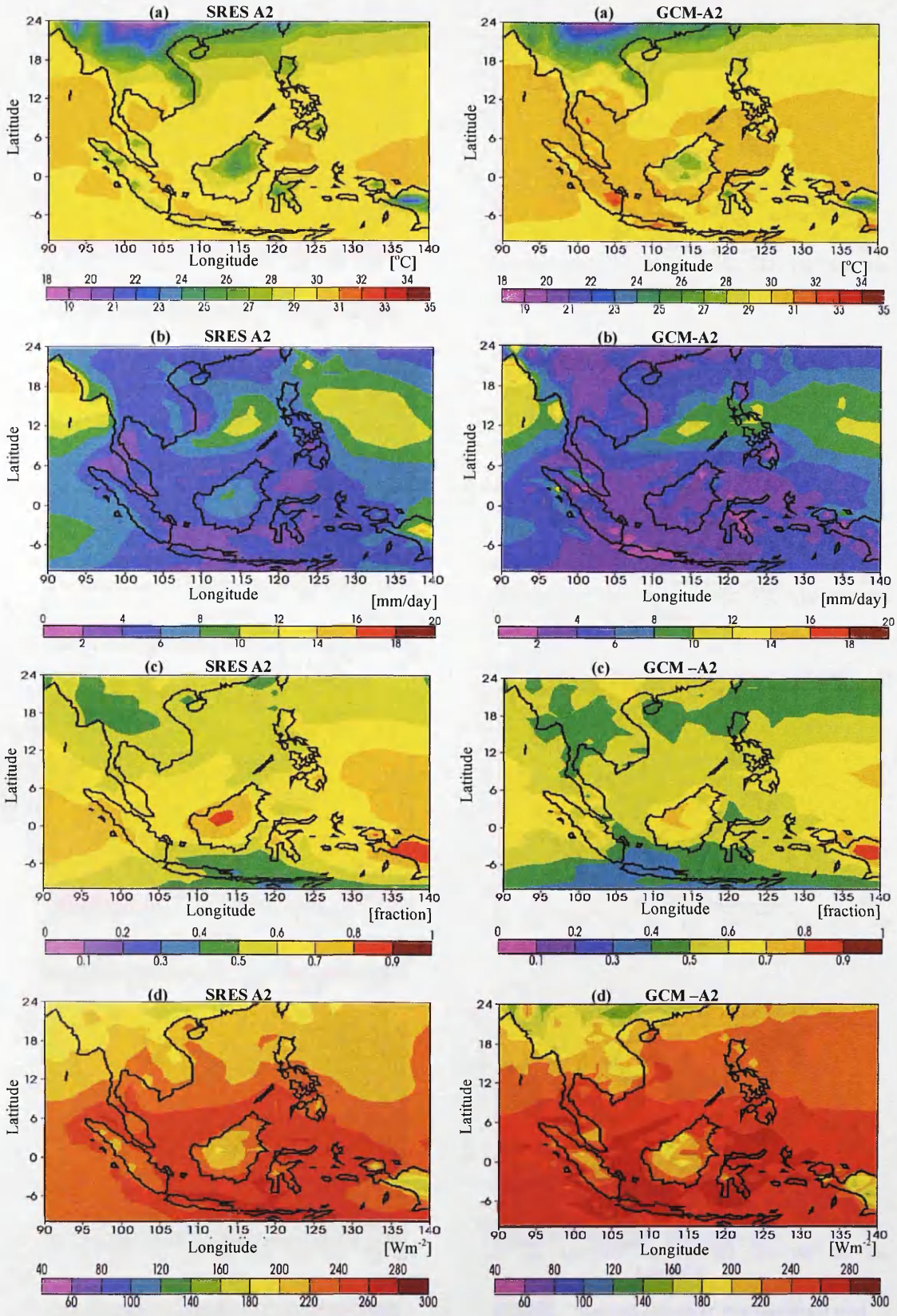

Figure 3.18: **SRES A2**: Comparison of the 30-year daily mean of (a) surface temperature (^{o}C); (b) total precipitation (mm/day); (c) total cloud (fraction); (d) solar radiation (Wm^{-2}) between the PRECIS-RCM (*left panel*) and the GCM (*right panel*) simulations in the SRES A2 scenario.

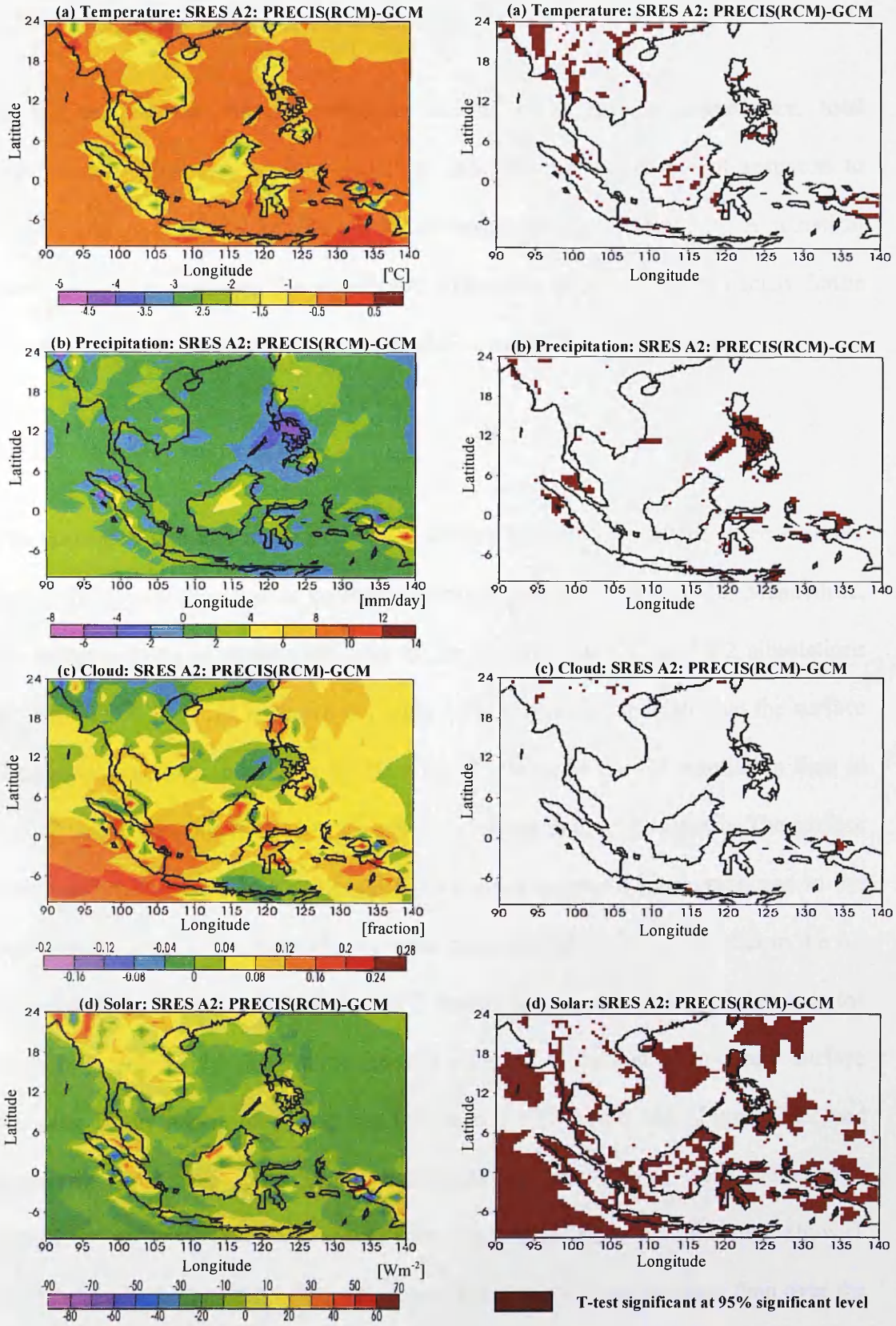

Figure 3.19: **SRES A2**: The 30-year daily mean difference of (a) surface temperature (^{o}C); (b) total precipitation (mm/day); (c) total cloud (fraction); (d) solar radiation (Wm^{-2}) between the PRECIS-RCM and GCM (*left panel*) simulations, and the significant t-test plot (*right panel*) in the SRES A2 scenario.

3.7.2 Climate Changes in Southeast Asia

In this section, the discussion focuses on the mean surface temperature, total precipitation, total clouds, solar radiation and boundary layer height response to climate change in the A2 and B2 climate scenarios during DJF and JJA. A statistical t-test is used to evaluate the significant differences between the projected future climate in A2 and B2 emission scenarios relative to the Baseline scenario.

3.7.2.1 Surface temperature

The simulated seasonal mean of average surface temperatures of the three member ensembles for the Baseline or control scenario is shown in Figure 3.20. Meanwhile, the seasonal cycle of surface temperature for the Baseline, A2 and B2 simulations from the PRECIS-RCM is shown in Figure 3.21. The results indicate that the surface temperature increase relative to the Baseline is smaller in the B2 simulation than in the A2 simulation, due to the weaker emission forcing in the B2 scenario. The surface temperatures simulated in the A2 and B2 scenarios suggest a linear response to the emission forcing. The projected future mean surface temperatures over SEA in the A2 scenario were 28.2°C during DJF and 30°C during JJA (Appendix 3.4). Relative to the Baseline scenario, the A2 future scenario over SEA showed an average surface warming in the region of 3°C during DJF, and 3.1°C during JJA (Figure 3.22 and Appendix 3.4). Surface temperature changes in all seasons were statistically significant at 95% confidence level over the whole SEA domain (not shown). Comparatively, higher temperature changes were observed over the land than over the sea in both seasons, being the highest over southern and central Myanmar during DJF and over Sumatra and Borneo during JJA.

Due to the weaker emissions forcing in the B2 scenario compared to the A2 scenario, the surface temperature increase relative to the Baseline was smaller in the B2 simulation: about 2.6°C during DJF and 2.1°C during JJA (Figure 3.23 and Appendix 3.5). The temperature changes were statistically significant at 95% level in all seasons except in some areas in the South China Sea and the Philippines Sea during DJF (not shown). Warmer temperatures were also observed over the land compared to over the sea in both seasons in the B2 scenario, with the projected future surface temperature of 27.9°C during DJF and 29.3°C during JJA. The projected future mean surface temperatures for both A2 and B2 scenarios over SEA were found to be higher than those of the previous simulation by McGregor *et al.* (1998) using DARLAM, a fine resolution (44km) regional climate model following the IS92a scenario from IPCC (1996). In recent studies by Hori and Ueda (2006) and Ueda *et al.* (2006) using a composite of nine coupled atmosphere-ocean GCMs have revealed that SEA region will experience drier and warmer conditions during the northeast monsoon (DJF) and southwest monsoon (JJA) at the end of the 21st century (2081-2100) with projected temperature to increase between 2.2°C and 2.8°C.

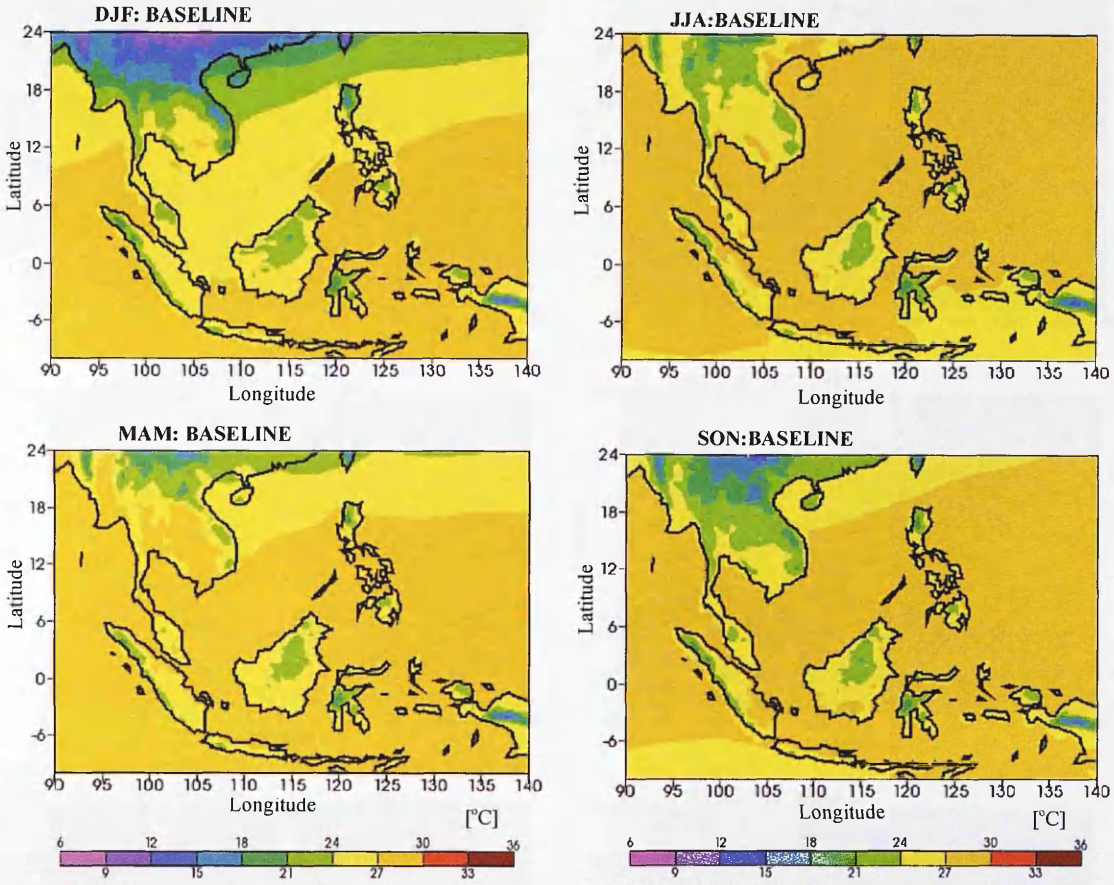

Figure 3.20: **Baseline**: Seasonal variability of surface temperature (°C) over SEA for the Baseline (1961-1990) during DJF (December to February), JJA (June to August) and inter-monsoons (March to May, MAM; September to November, SON).

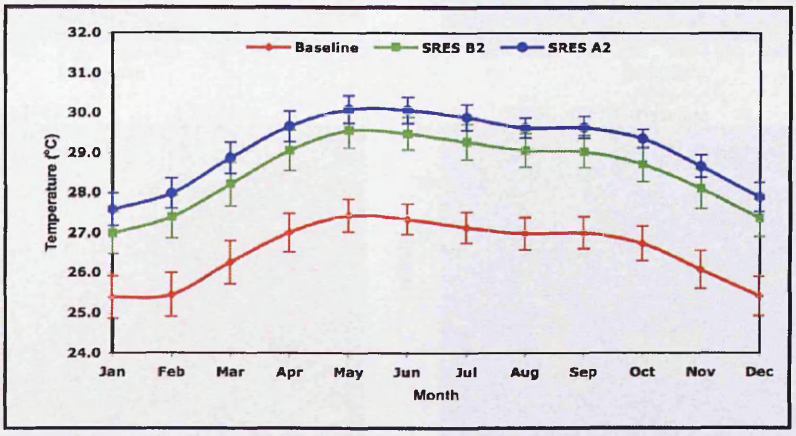

Figure 3.21: Seasonal cycle of surface temperature (°C) for the SRES B2 and SRES A2 climate scenarios compared with Baseline scenario.
(*Note: SRES- Special Report on Emissions Scenario)*

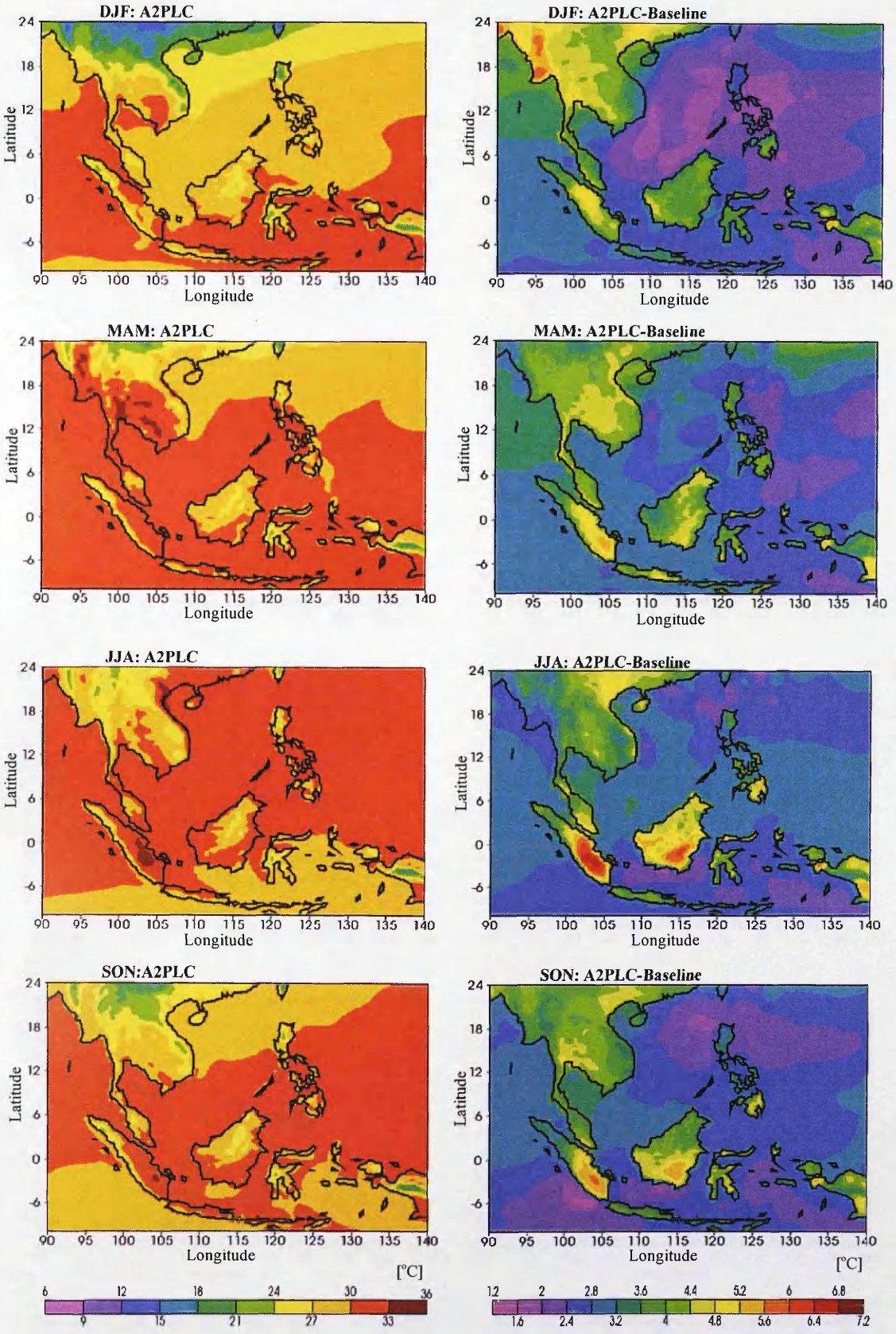

Figure 3.22: **SRES A2**: Atmospheric forcing effects on seasonal temperature (A2PLC) in the SRES A2 scenario, and the temperature difference in comparison with the Baseline scenario (A2PLC-Baseline).

(*Note: SRES A2- Special Report on Emission Scenario A2; PLC- Present-day Landcover*)

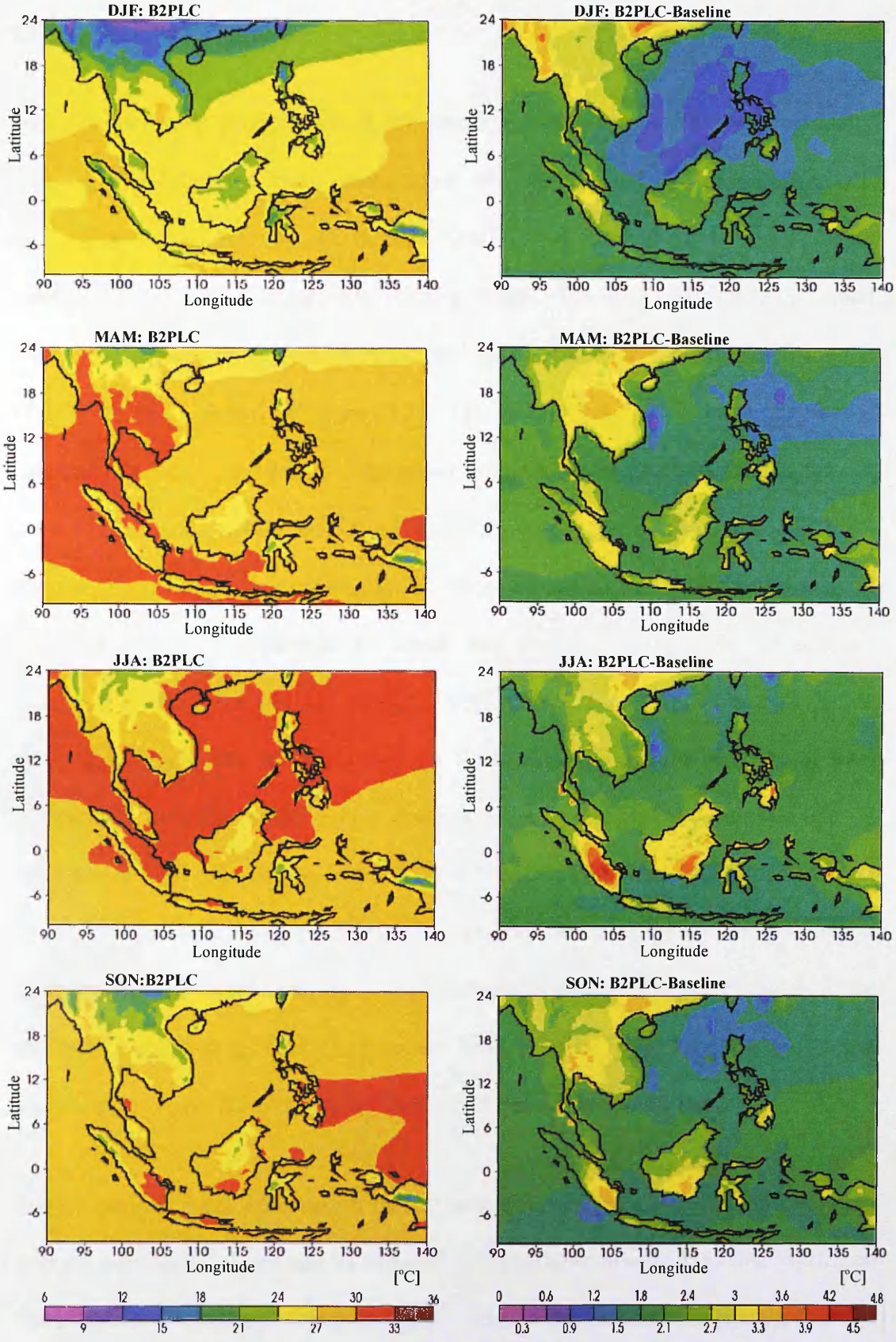

Figure 3.23: **SRES B2**: Atmospheric forcing effects on seasonal temperature (B2PLC) in the SRES B2 scenario, and the temperature difference in comparison with the Baseline scenario (B2PLC-Baseline).

(*Note: SRES B2- Special Report on Emission Scenario B2; PLC- Present-day Landcover*)

3.7.2.2 Total precipitation

The simulated total precipitation in the Baseline scenario over SEA was markedly seasonal, with relatively lower precipitation over the continental region during DJF and higher over the sea (Andaman Sea/Bay of Bengal and South China Sea/Philippines Sea) during JJA (Figure 3.24). The seasonal cycle of total precipitation over the region for the Baseline, A2 and B2 simulations from the PRECIS-RCM is shown in Figure 3.25. The results indicated a larger degree of variability between simulations. The projected future total precipitations in the A2 scenario were 4.8 mm/day during DJF and 8.6 mm/day during JJA (Appendix 3.4). Relative to the Baseline scenario, the A2 future scenario over SEA showed a small reduction in total precipitation of about -0.4 mm/day during DJF but a small increment of about 0.2 mm/day during JJA (Figure 3.26 and Appendix 3.4). These changes accounted for the 8% reduction (DJF) and 3% increment (JJA) of total precipitation over the region. Future changes in total precipitation (with less than -1 mm/day) mostly over the sea (South China Sea, Celebes Sea and Andaman Sea) during DJF and over a larger area over the sea and insular region (southern Sumatra, southern Borneo, Mindanao, Java and Sulawesi) during JJA were found to be statistically significant at 95% confidence level (Figure 3.28). The largest changes were increases over the west Pacific Ocean and Bay of Bengal during JJA.

Similar patterns were observed in the B2 scenario, where drier conditions occurred over the continental region and its adjacent seas (northern South China Sea, Andaman Sea and Gulf of Thailand) during DJF and a relative increase in precipitation over the same area during JJA (Figure 3.27). Relative to Baseline, the total precipitation decreased by -0.4 mm/day (8%) during DJF and slightly increased by 0.1 mm/day

(2%) during JJA (Appendix 3.5). Areas with roughly less than -1 mm/day in total precipitation were found to be statistically significant at 95% level in all seasons (Figure 3.28). Larger changes of precipitation were also observed over the west Pacific Ocean and Bay of Bengal during JJA. Larger changes of precipitation simulated using the regional climate model DARLAM were also observed over the west Pacific Ocean during JJA, and the South China Sea and Celebes Sea during DJF by McGregor *et al.* (1998). Studies by Hori and Ueda (2006) and Ueda et al. (2006) have also projected the precipitation to fluctuate between -2.4% and 6%, which is expected to cause drier weather than the normal weather at present conditions.

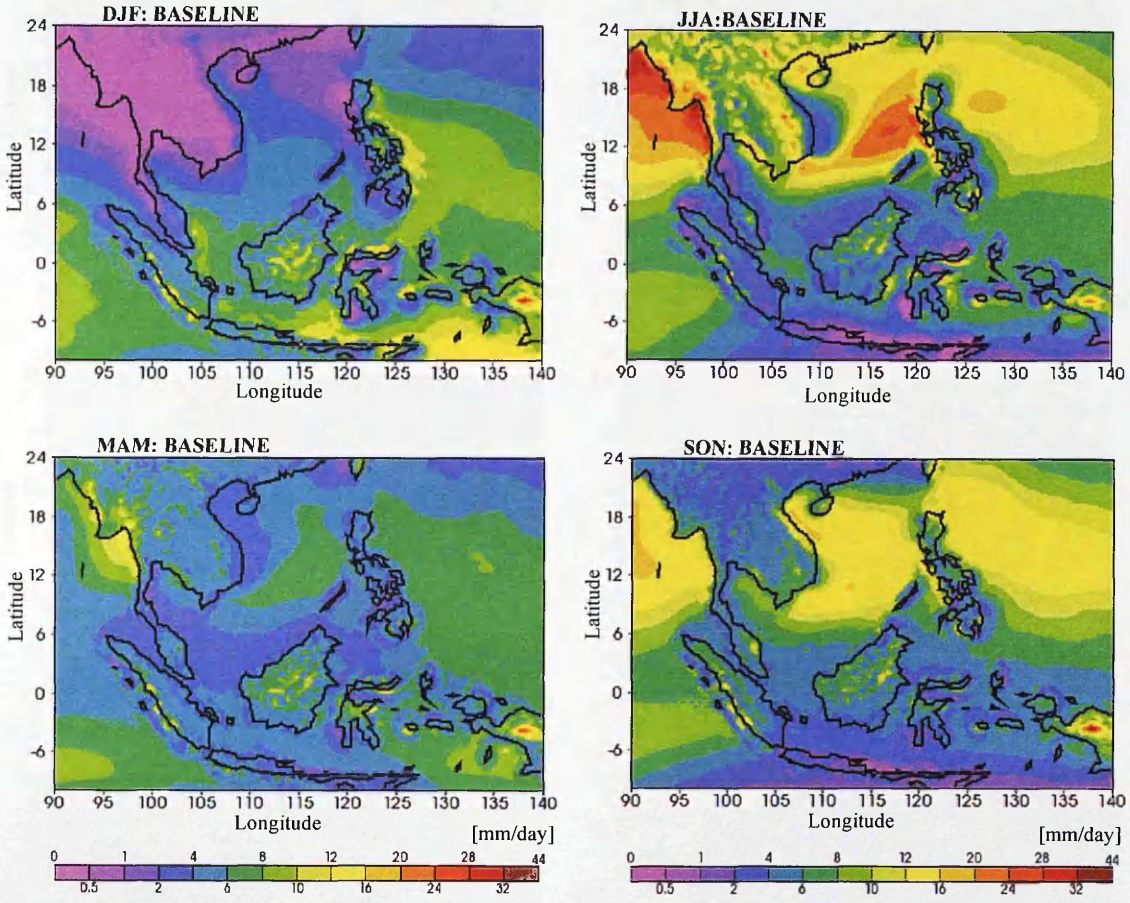

Figure 3.24 **Baseline**: Seasonal variability of total precipitation (mm/day) over SEA for the Baseline (1961-1990) during DJF (December to February), JJA (June to August) and inter-monsoons (March to May, MAM; September to November, SON).

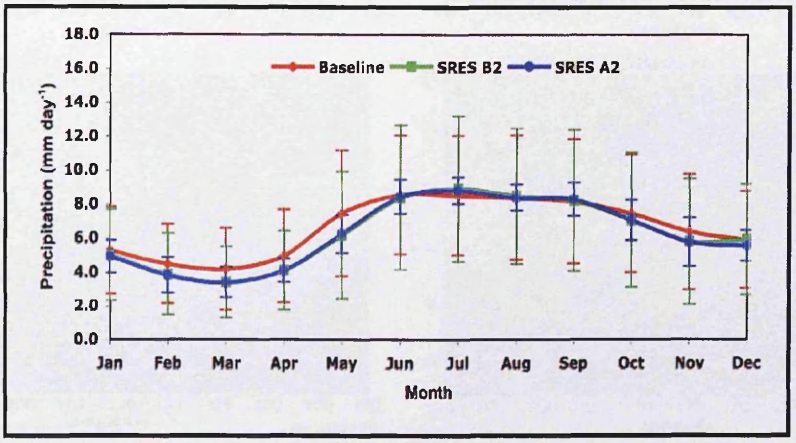

Figure 3.25: Seasonal cycle of total precipitation (mm/day) for the SRES B2 and SRES A2 climate scenarios compared with Baseline scenario.
(*Note: SRES- Special Report on Emissions Scenario)*

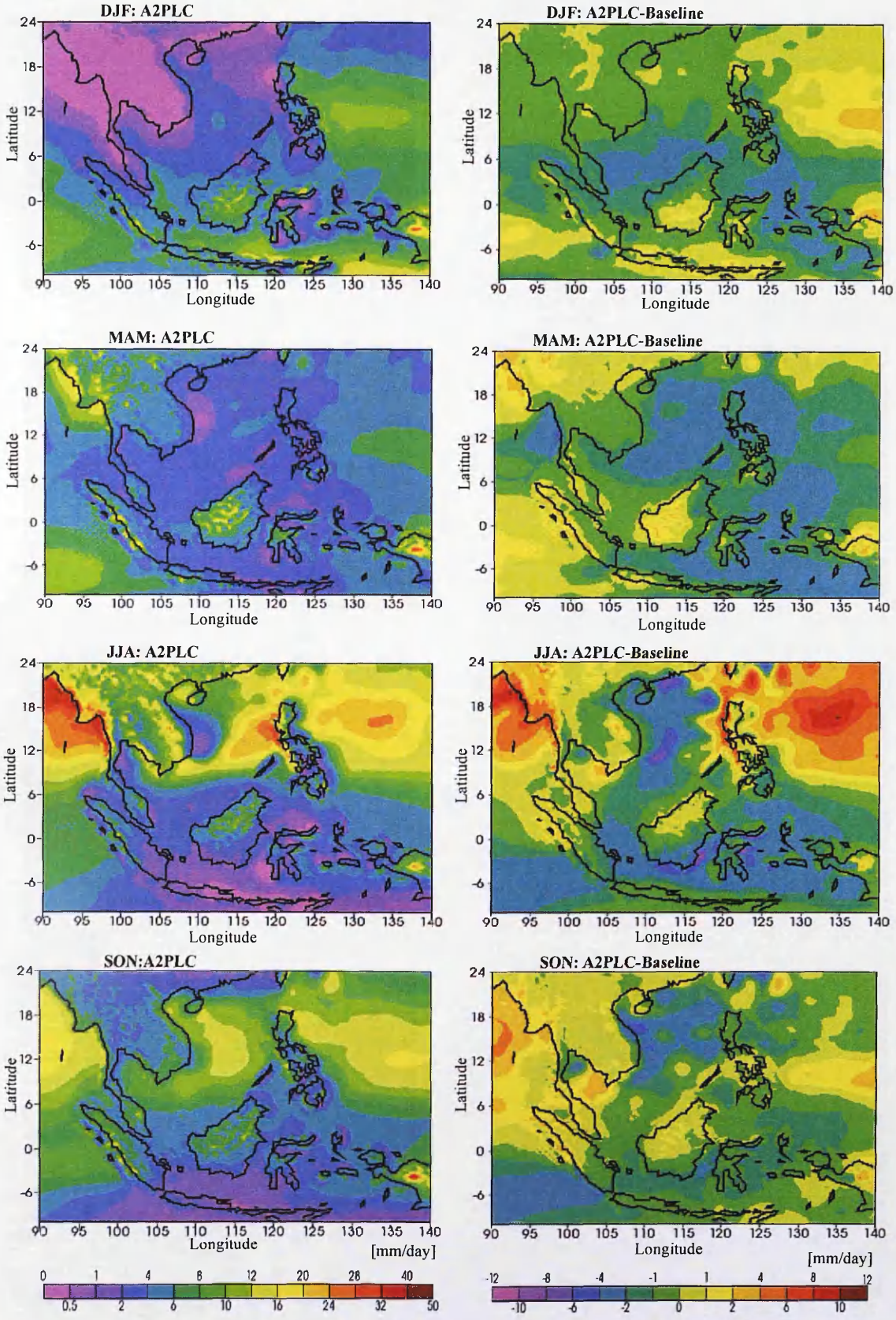

Figure 3.26: **SRES A2**: Atmospheric forcing effects on seasonal total precipitation (A2PLC) in the SRES A2 scenario, and the total precipitation difference in comparison with the Baseline scenario (A2PLC-Baseline).

(*Note: SRESA2- Special Report on Emission ScenarioA2; PLC- Present-day Landcover*)

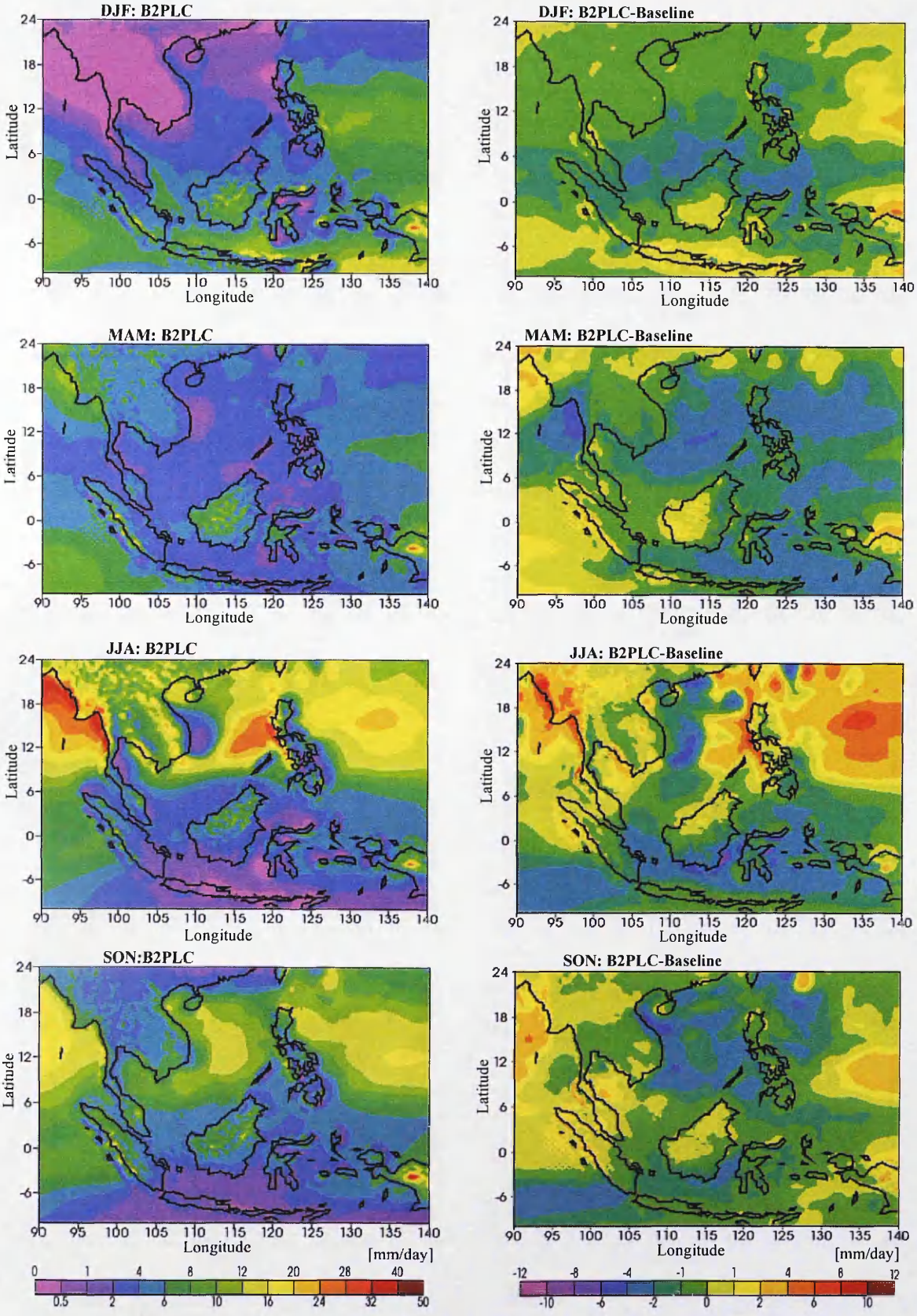

Figure 3.27: **SRES B2**: Atmospheric forcing effects on seasonal total precipitation (B2PLC) in the SRES B2 scenario, and the total precipitation difference in comparison with the Baseline scenario (B2PLC-Baseline).

(*Note: SRESB2- Special Report on Emission ScenarioB2; PLC- Present-day Landcover*)

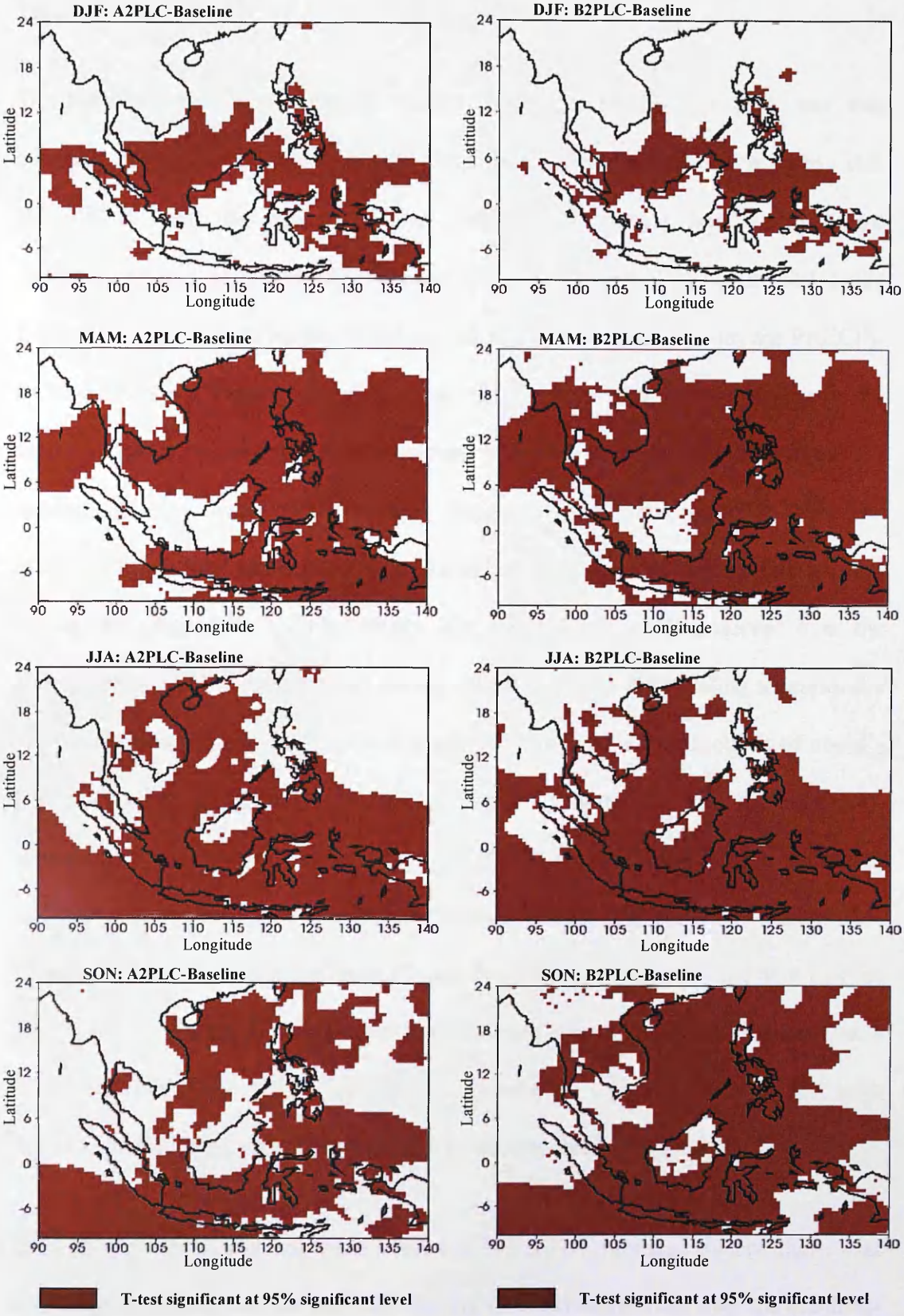

Figure 3.28: Significant t-test plots for the effect of atmospheric forcing alone on seasonal total precipitation for the A2 (A2PLC-Baseline) (*left panel*) and B2 (B2PLC-Baseline) (*right panel*) climate scenarios relative to the Baseline scenario.
(*Note: PLC-Present-day Landcover*)

3.7.2.3 Total cloud

The simulated total cloud fraction in the Baseline scenario over SEA was also markedly seasonal, with relatively less cloud over the continental region during DJF and higher over the sea (Andaman Sea/Bay of Bengal and South China Sea/Philippines Sea) during JJA (Figure 3.29). The seasonal cycle of total cloud fraction over the region for the Baseline, A2 and B2 simulations from the PRECIS-RCM is shown in Figure 3.30. Comparatively, the simulated cloud fractions in the future scenarios (A2 and B2) were observed to have less cloud than the present-day simulation, with higher cloud fraction during JJA and lower during DJF. The projected future total cloud fractions in the A2 scenario were 0.5 during DJF and 0.7 during JJA (Appendix 3.4). Relatively less cloud fraction was observed over the continent during DJF but increased during JJA. Relative to the Baseline scenario, the A2 future scenario over SEA showed a reduction in total cloud fractions of about -0.07 (12%) during DJF and -0.04 (6%) during JJA (Figure 3.31 and Appendix 3.4). Larger changes were observed over the west Pacific Ocean during DJF and extended to South China Sea and Indian Ocean between latitude 2°S and 12°N during JJA. Changes in total cloud fraction (roughly less than -0.04), mostly over the South China Sea, Indian Ocean and Celebes Sea during DJF and Indochina, the Philippines Sea, a large part of the South China Sea, and latitude between 10°S and 0° during JJA were found to be statistically significant at 95% confidence level (Figure 3.32).

Seasonally, similar patterns were observed in the B2 scenario, where there was relatively less cloud over the continent during DJF and more cloud over the continent and sea between latitude 0° and 24°N during JJA (Figure 3.31). Relative to Baseline, the changes of cloud fraction in the B2 scenario decreased to a similar magnitude as

those in the A2 scenario for both seasons (Figure 3.31 and Appendix 3.5). Future changes in total cloud fraction (roughly with less than -0.05), mostly over the same area as during DJF in the A2 scenario and mostly over the whole domain during JJA, were found to be statistically significant at 95% confidence level (Figure 3.32). Previous studies over the region by McGregor *et al.* (1998) observed a decrease in total cloud fraction of about 10% in the IS92a scenario from IPCC (1996).

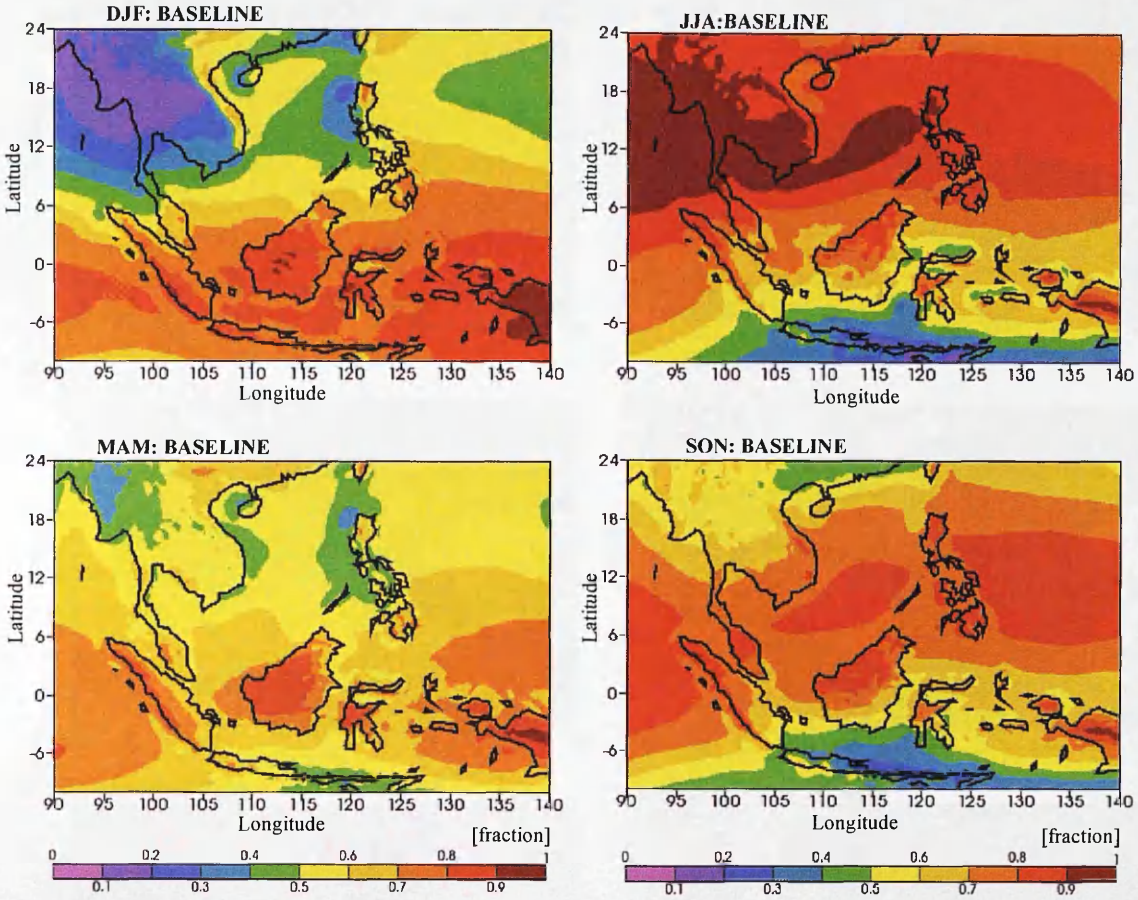

Figure 3.29: **Baseline**: Seasonal variability of total cloud fraction over SEA for the Baseline (1961-1990) during DJF (December to February), JJA (June to August) and inter-monsoons (March to May, MAM; September to November, SON).

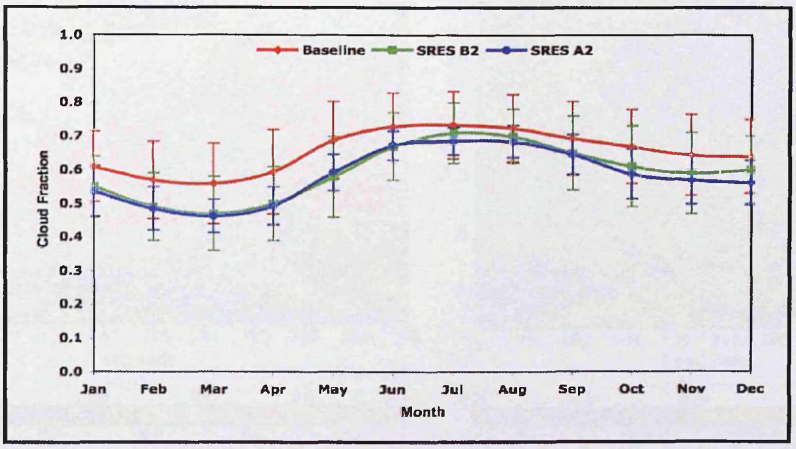

Figure 3.30: Seasonal cycle of total cloud fractions for the SRES B2 and SRES A2 climate scenarios compared with Baseline scenario.
(*Note: SRES- Special Report on Emissions Scenario)*

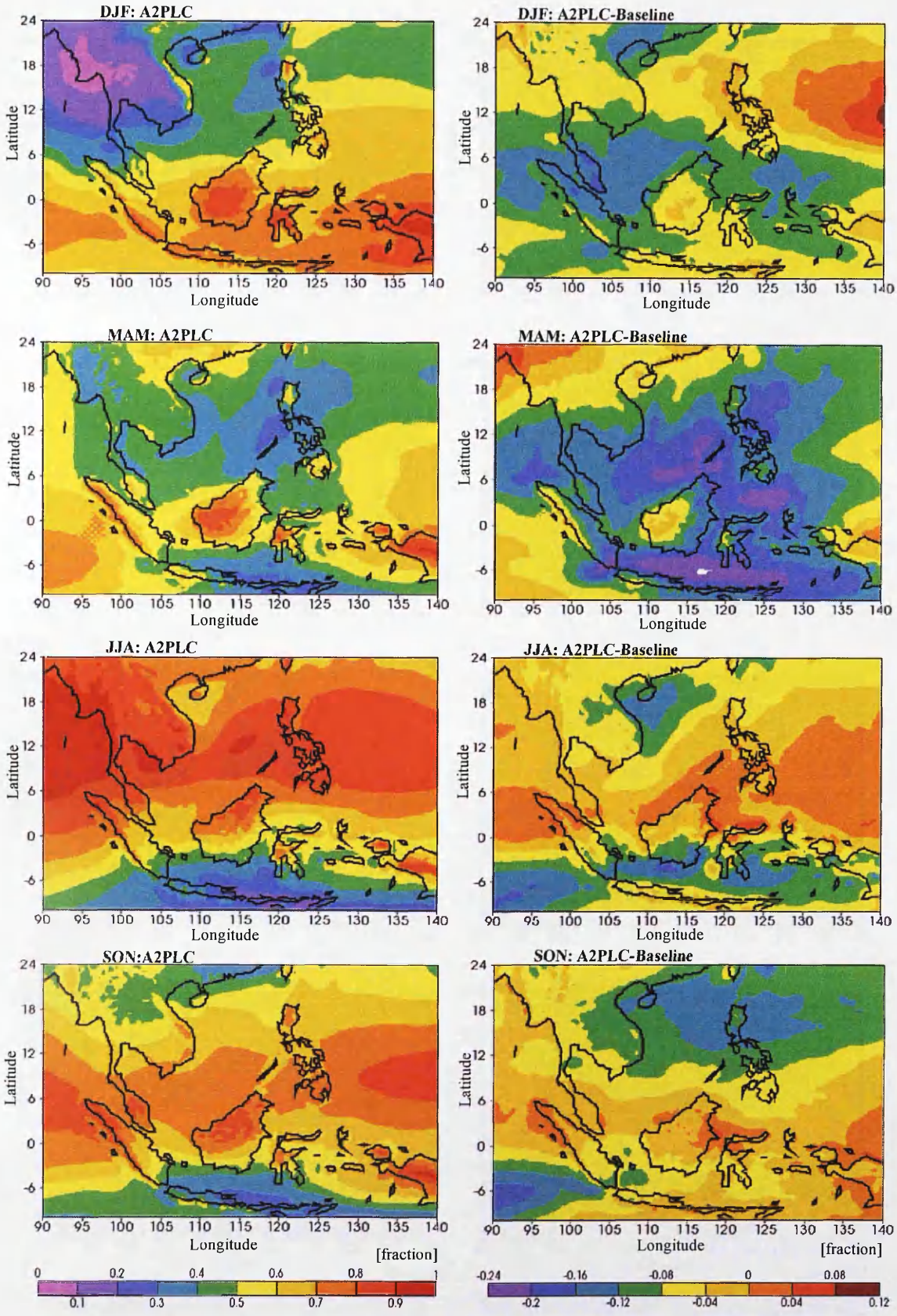

Figure 3.31: **SRES A2**: Atmospheric forcing effects on seasonal total cloud (A2PLC) in the SRES A2 scenario, and the solar radiation difference in comparison with the Baseline scenario (A2PLC-Baseline).

(*Note: SRESA2- Special Report on Emission Scenario A2; PLC- Present-day Landcover*)

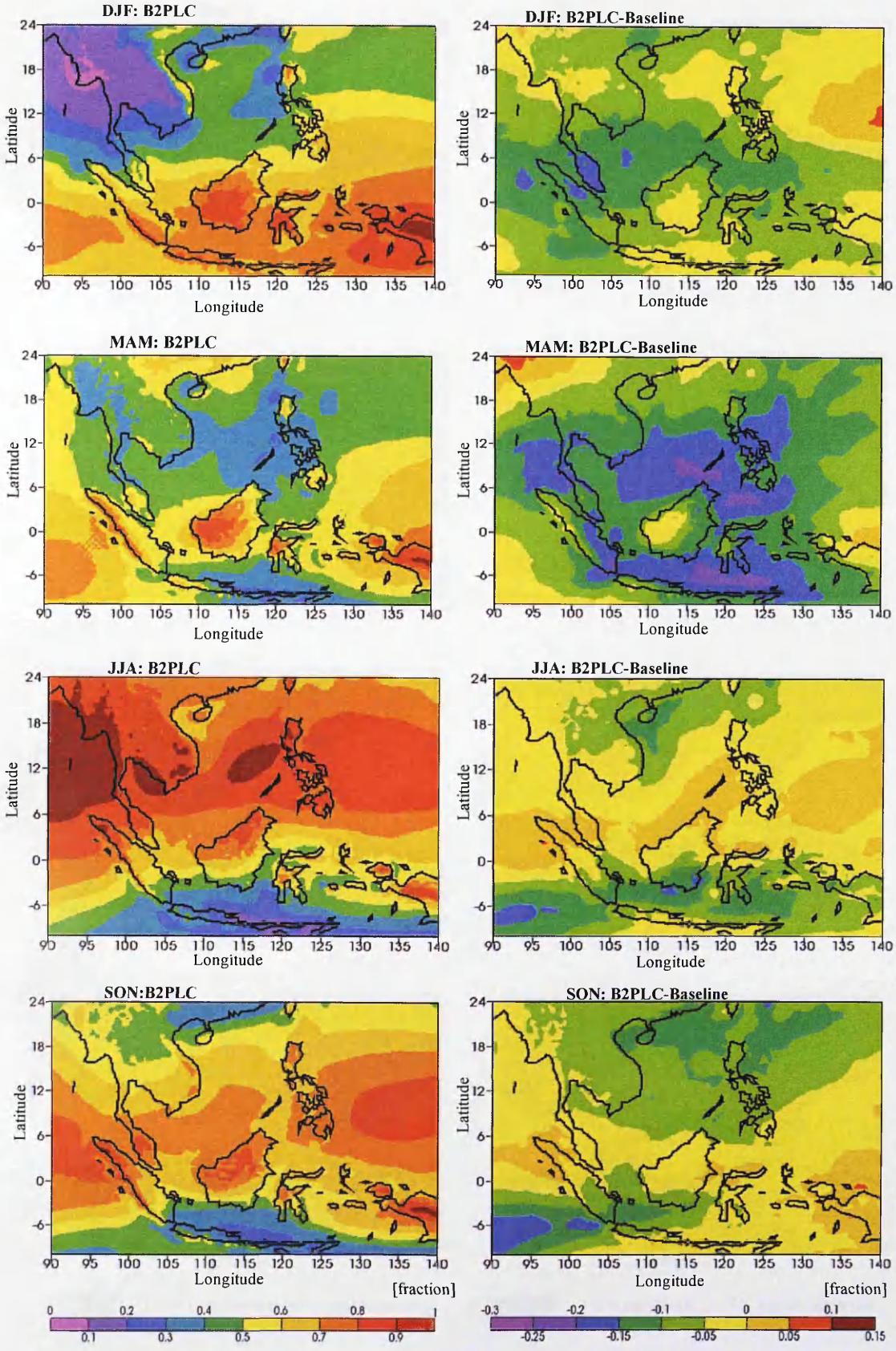

Figure 3.32: **SRES B2**: Atmospheric forcing effects on seasonal total cloud (B2PLC), in the SRES B2 scenario, and the total cloud difference in comparison with the Baseline scenario (B2PLC-Baseline) for SRES B2 scenario.

(*Note: SRESB2- Special Report on Emission ScenarioB2; PLC- Present-day Landcover*)

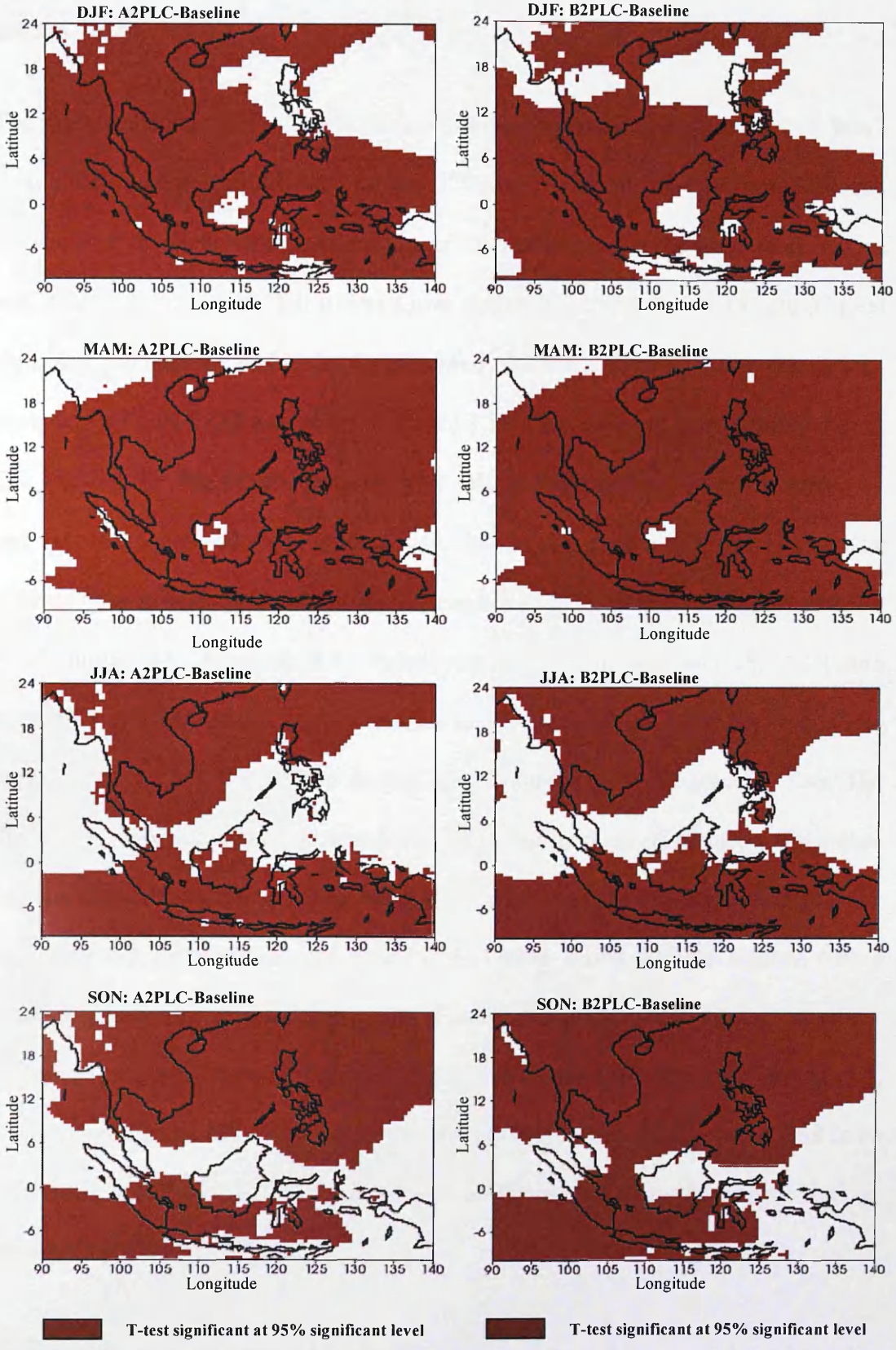

Figure 3.33: Significant t-test plots for the effect of atmospheric forcing alone on seasonal total cloud for the A2 (A2PLC-Baseline) (*left panel*) and B2 (B2PLC-Baseline) (*right panel*) climate scenarios relative the Baseline scenario.
(*Note: PLC-Present-day Landcover*)

3.7.2.4 Solar radiation

The simulated solar radiation over SEA in the Baseline scenario was about 215 Wm^{-2} during DJF and slightly higher – about 220 Wm^{-2} – during JJA (Figure 3.34 and Appendix 3.4). Higher solar radiation over the continent (i.e. the Indochina region) was observed during DJF but it was lower during JJA. The seasonal cycle of total cloud fraction over the region for the Baseline, A2 and B2 solar radiation simulations from the PRECIS-RCM are shown in Figure 3.35, each showing local minima during DJF and JJA. Comparatively, the simulated solar radiation in the future scenarios (A2 and B2) was observed to be higher than that in the present-day simulation. The projected future solar radiation in the A2 scenario was 221 Wm^{-2} during DJF and 218 Wm^{-2} during JJA (Appendix 3.4). Relative to the Baseline scenario, the A2 future scenario over SEA showed a small increase in solar radiation of about 5.6 Wm^{-2} (3%) during DJF and 4.6 Wm^{-2} (2%) during JJA (Figure 3.36 and Appendix 3.4). The increase in solar radiation was also reflected in the increase of surface temperature and decreased cloud fraction over the region in the A2 scenario. Reduction of solar radiation were observed over the west Pacific Ocean during the both seasons with a larger magnitude of changes during JJA. Future changes in solar radiation were not statistically significant in most areas of the region during DJF. However, during JJA, it was observed that areas with negative changes (less than -5 Wm^{-2}) were found to be statistically significant at 95% confidence level (Figure 3.38), mostly over the sea (i.e. the west Pacific Ocean).

Similar patterns were observed in the B2 scenario, where there was relatively higher solar radiation over the continent during DJF but lower during JJA. Higher solar radiation was also observed over coastal areas and the surrounding sea over the

insular region in both seasons. Relative to Baseline, the changes in solar radiation in the B2 scenario were smaller than those in the A2 scenario for both seasons (Figure 3.37 and Appendix 3.5). The solar radiation decreased by about 3.1 Wm^{-2} (2%) during DJF and 3.8 Wm^{-2} (2%) during JJA. A distinctive feature in solar radiation changes was the significant difference between the B2 and A2 scenarios. Much more of the region showed a statistically significant change in the B2 scenario (Figure 3.38).

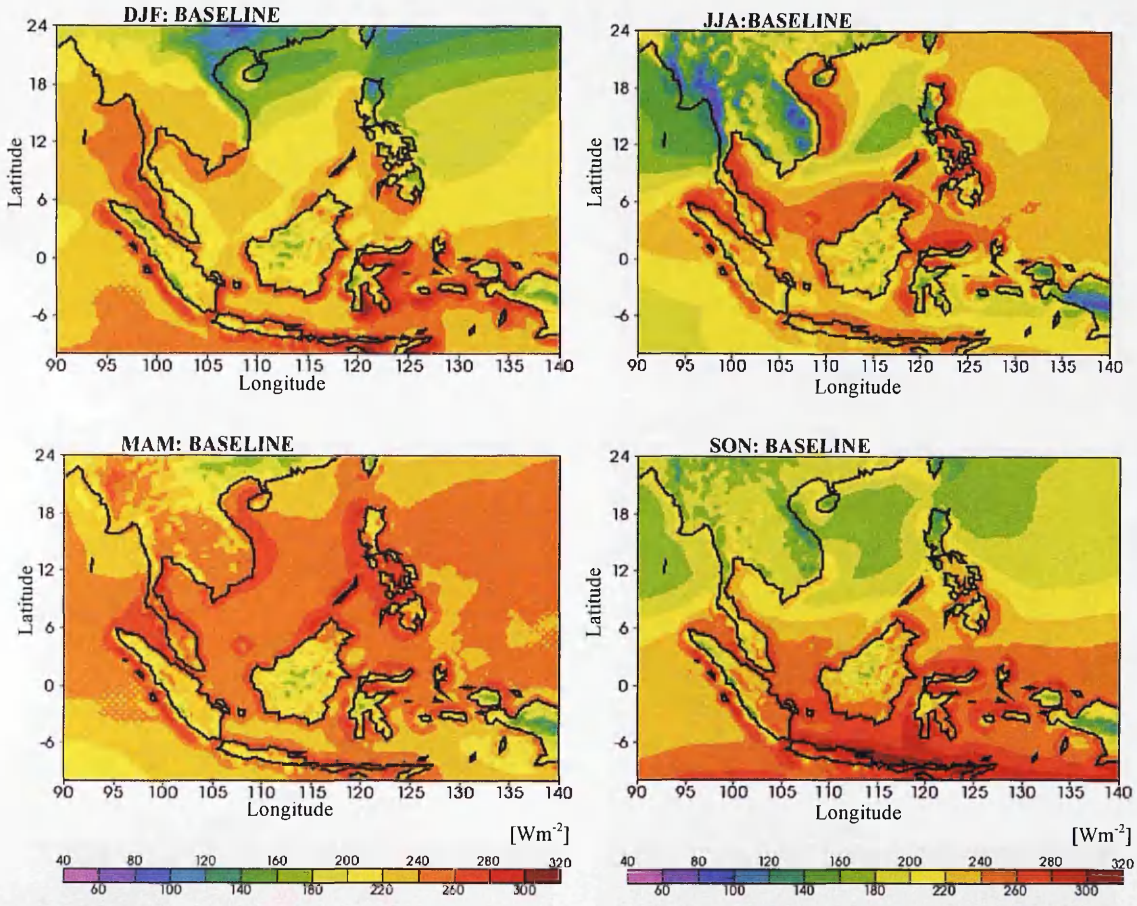

Figure 3.34: **Baseline**:Seasonal variability of solar radiation over SEA for the Baseline (1961-1990) during DJF (December to February), JJA (June to August) and inter-monsoons (March to May, MAM; September to November, SON).

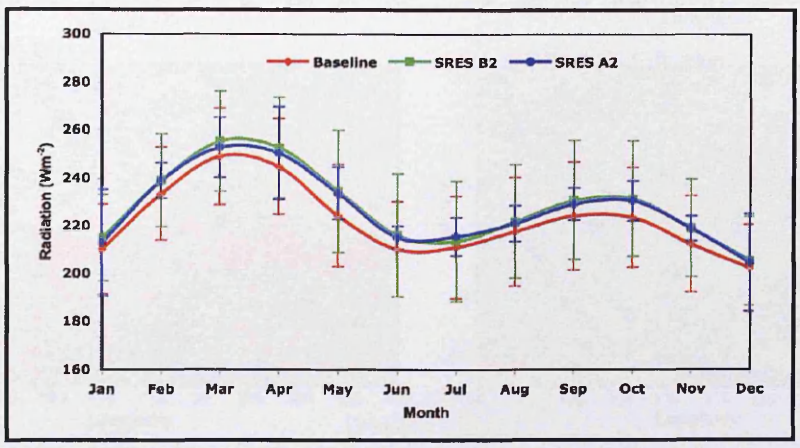

Figure 3.35: Seasonal cycle of solar radiation (Wm^{-2}) for the SRES B2 and SRES A2 climate scenarios compared with Baseline scenario.
(*Note: SRES- Special Report on Emissions Scenario)*

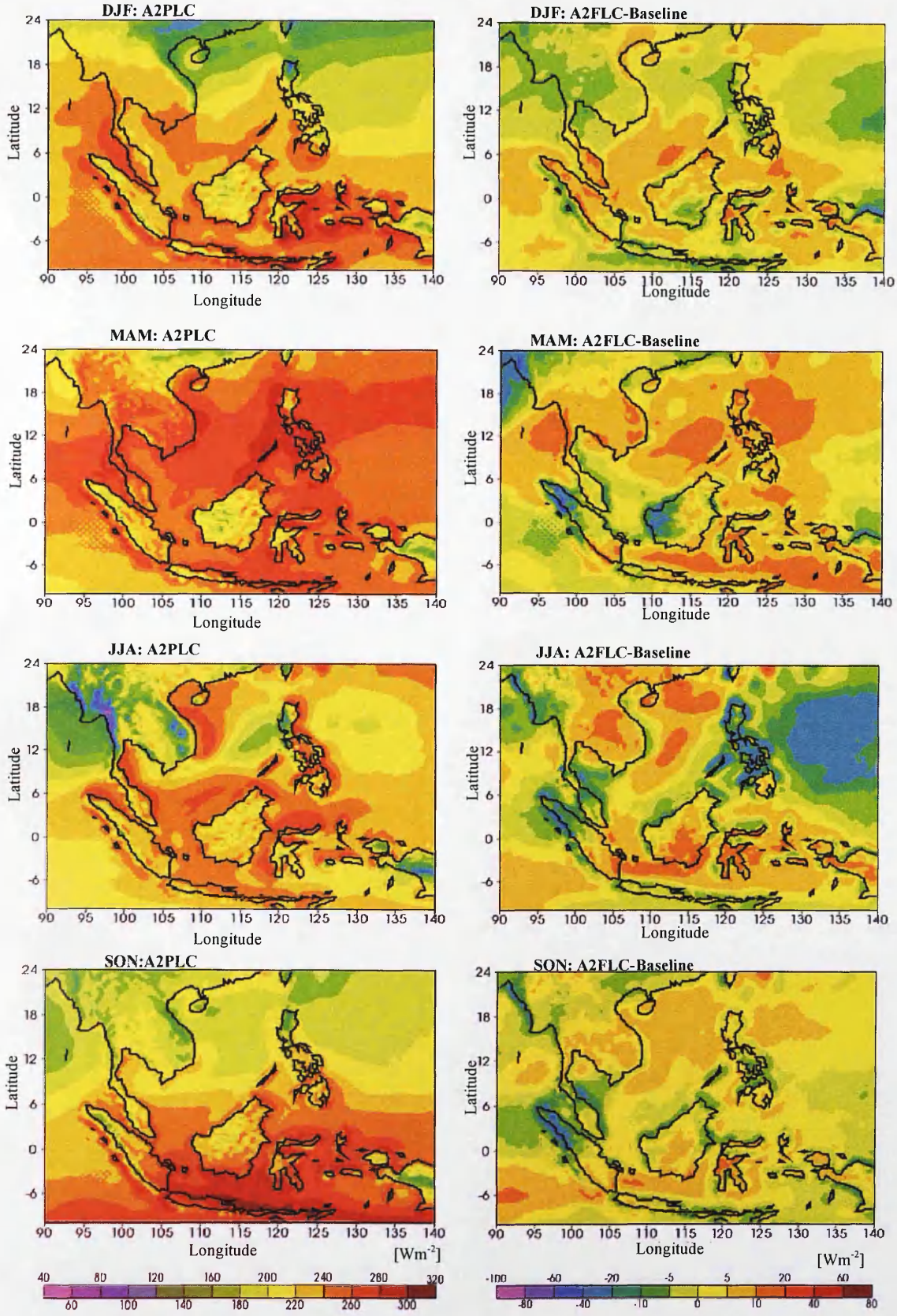

Figure 3.36: SRES A2: Atmospheric forcing effects on seasonal solar radiation (A2PLC) in the SRES A2 scenario, and the solar radiation difference in comparison with the Baseline scenario (A2PLC-Baseline).

(*Note: SRESA2- Special Report on Emission ScenarioA2; PLC- Present-day Landcover*)

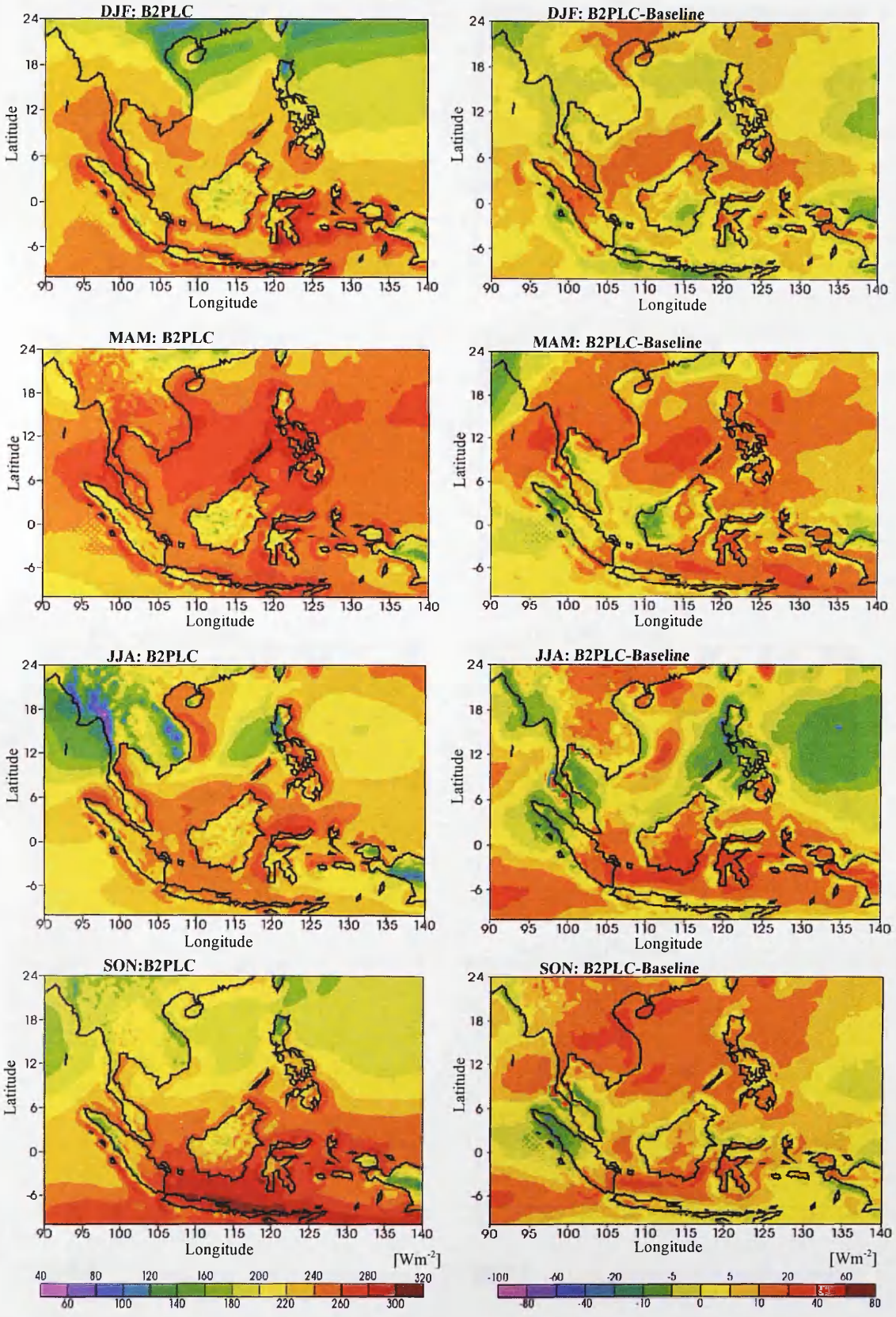

Figure 3.37: **SRES B2**: Atmospheric forcing effects on seasonal solar radiation (B2PLC) in the SRES B2, and the solar radiation difference in comparison with the Baseline scenario (B2PLC-Baseline).

(*Note: SRESB2- Special Report on Emission ScenarioB2; PLC- Present-day Landcover)*

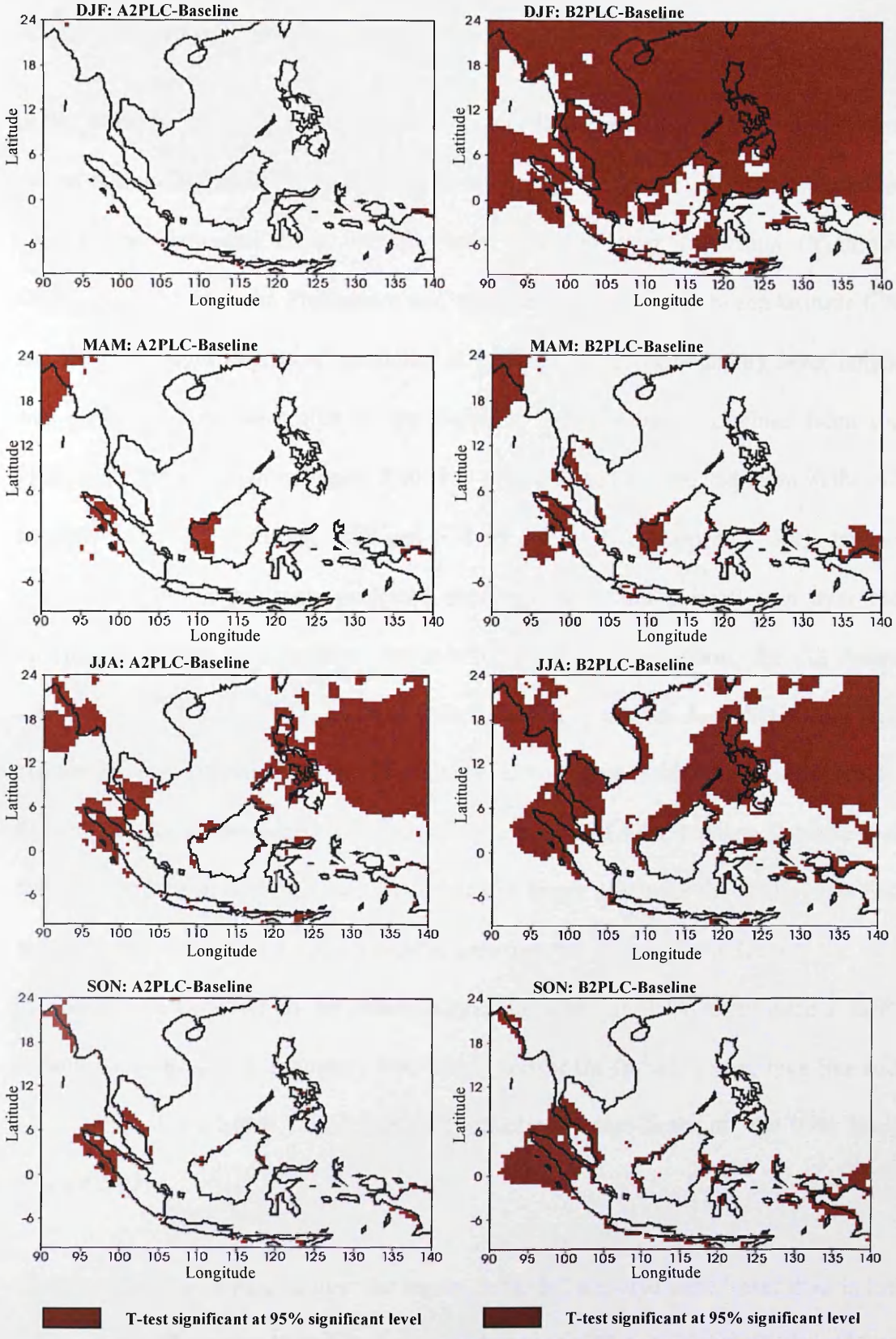

Figure 3.38: Significant t-test plots for the effect of atmospheric forcing alone on seasonal solar radiation for the A2 (A2PLC-Baseline) (*left panel*) and B2 (B2PLC-Baseline) (*right panel*) climate scenarios relative to the Baseline scenario.
(*PLC-Present-day Landcover*)

3.7.2.5 Boundary layer

In the Baseline scenario, the simulated boundary layer heights over SEA were about 545 m during DJF and slightly lower (515 m) during JJA (Figure 3.39 and Appendix 3.4). Higher boundary layer heights were observed over Indochina (Vietnam, Cambodia and Laos), the Philippines and extended over the sea between latitude 6°N and 24°N. A larger degree of variability of seasonal cycles of boundary layer height was observed over the region in the Baseline, A2 and B2 simulations from the PRECIS-RCM as shown in Figure 3.40. The projected future solar radiation in the A2 scenario was 542 m during DJF and 538 m during JJA (Appendix 3.4). Higher boundary layer heights were projected over Indochina and a small area over the Philippines during both seasons. Relative to the Baseline scenario, the A2 future scenario over SEA showed a small decrease of about -3 m (less than 1%) during DJF but an increase of about 23 m (5%) during JJA (Figure 3.41 and Appendix 3.4). Larger changes in boundary layer height were observed over western Sumatra and southern Borneo in both seasons. Statistically, a larger area over the Philippines Sea and the west Pacific Ocean, and a smaller area over the South China Sea and the Bay of Bengal were found to be statistically significant at 95% level during DJF. Meanwhile, during JJA, boundary layer changes over the Indian Ocean, Java Sea and small areas of the South China Sea were statistically significant at the 95% level (Figure 3.43).

The boundary layer heights over the region in the B2 scenario were lower than in the A2 scenario. The mean boundary layer heights were 486 m during DJF and 453 m during JJA (Appendix 3.5). Higher boundary layer heights were observed over Indochina (Vietnam, Cambodia and Laos), central Sumatra and Peninsular Malaysia

during DJF and over a larger area of Indochina during JJA (Figure 3.42 and Appendix 3.5). The boundary layer height decreased by about 5 m during DJF and 6 m during JJA. Larger areas over the sea in both seasons were found to be statistically significant at 95% level (Figure 3.43).

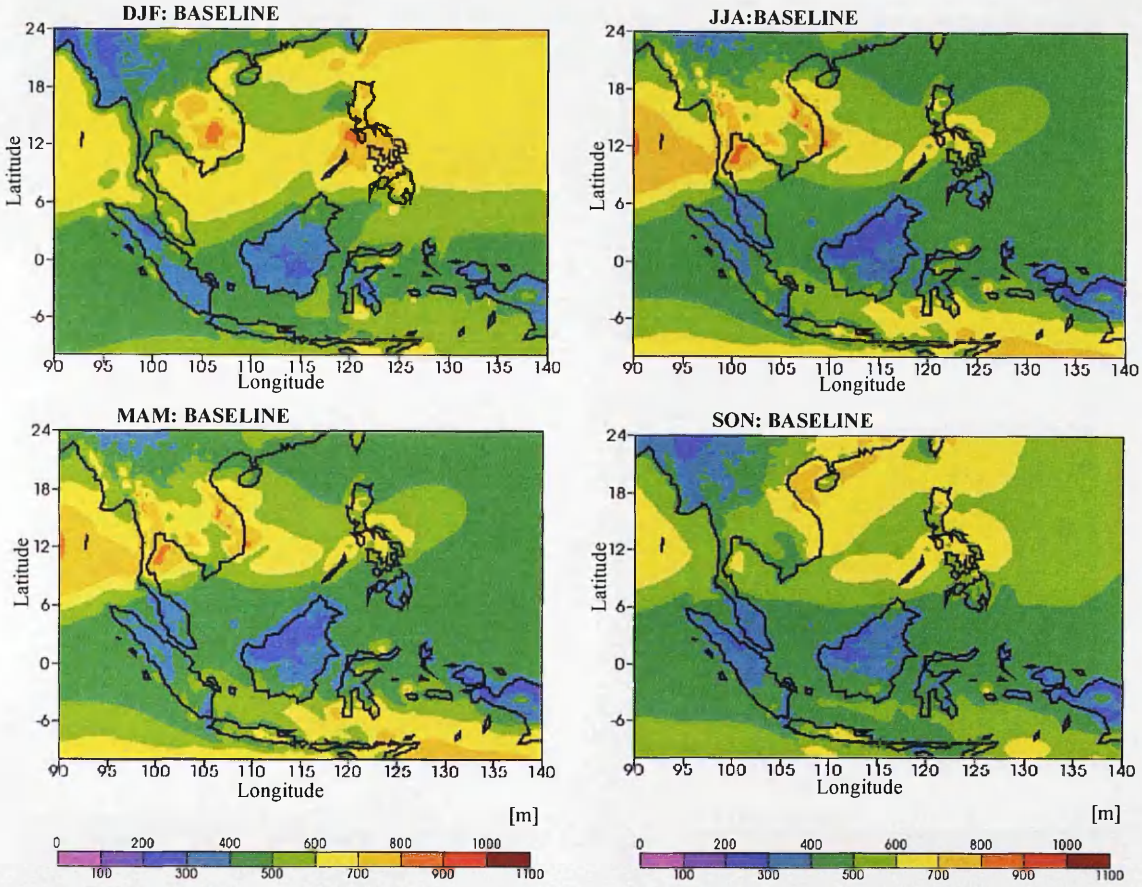

Figure 3.39: **Baseline**: Seasonal variability of boundary layer height over SEA for the Baseline (1961-1990) during DJF (December to February), JJA (June to August) and inter-monsoons (March to May, MAM; September to November, SON).

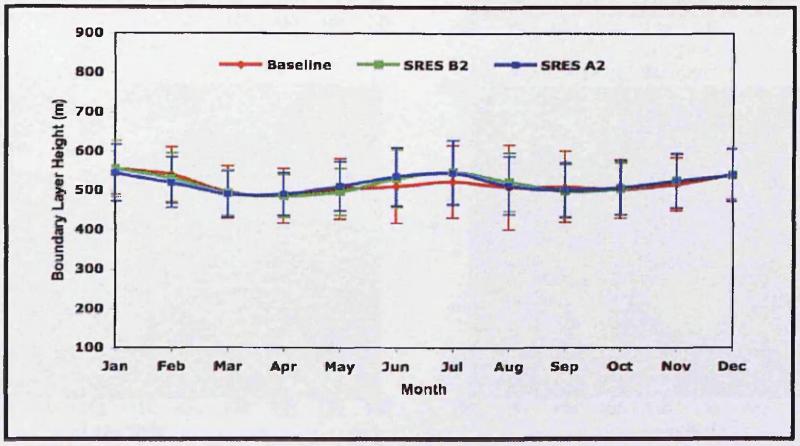

Figure 3.40: Seasonal cycle of boundary layer height (m) for the SRES B2 and SRES A2 climate scenarios compared with Baseline scenario.

(*Note: SRES- Special Report on Emissions Scenario*

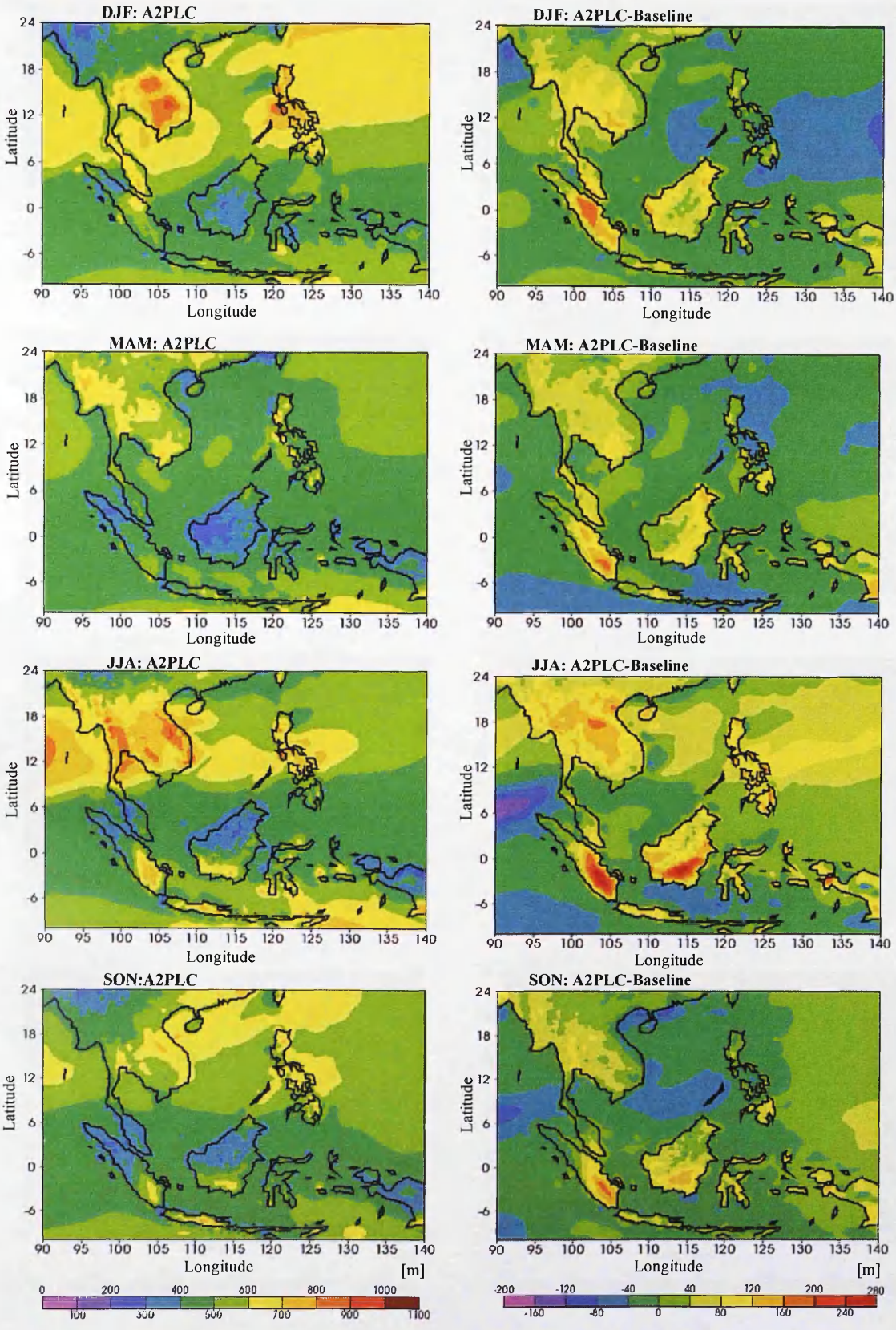

Figure 3.41: **SRES A2**: Atmospheric forcing effects on seasonal boundary layer height (A2PLC) in the SRES A2 sceanrio, and the boundary layer height difference in comparison with the Baseline scenario (A2PLC-Baseline).

(*Note: SRESA2- Special Report on Emission ScenarioA2; PLC- Present-day Landcover*)

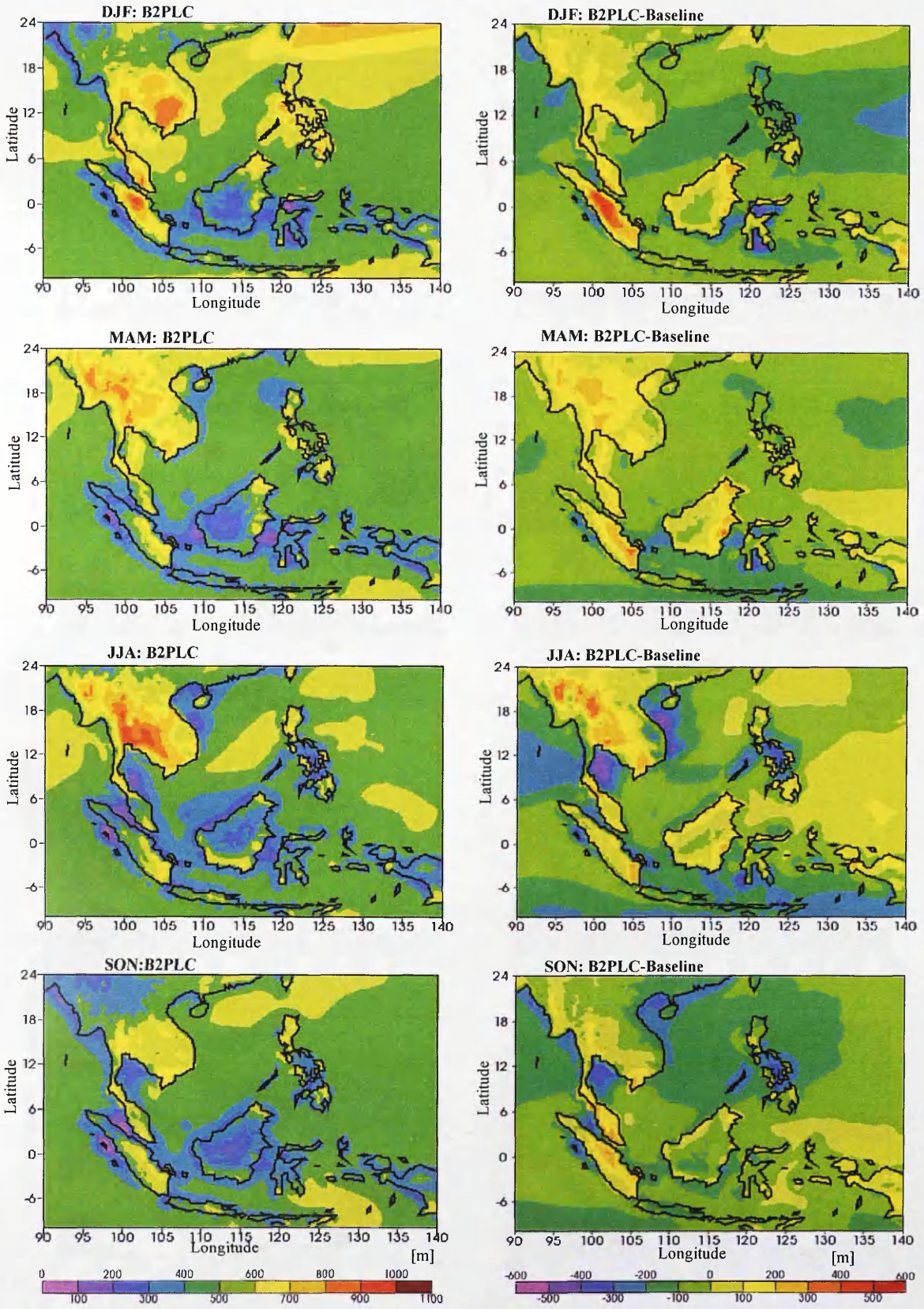

Figure 3.42: **SRES B2**: Atmospheric forcing effects on seasonal boundary layer height (B2PLC) in the SRES B2 scenario, and the boundary layer height difference in comparison with the Baseline scenario (B2PLC-Baseline).

(*Note: SRESB2- Special Report on Emission ScenarioB2; PLC- Present-day Landcover*)

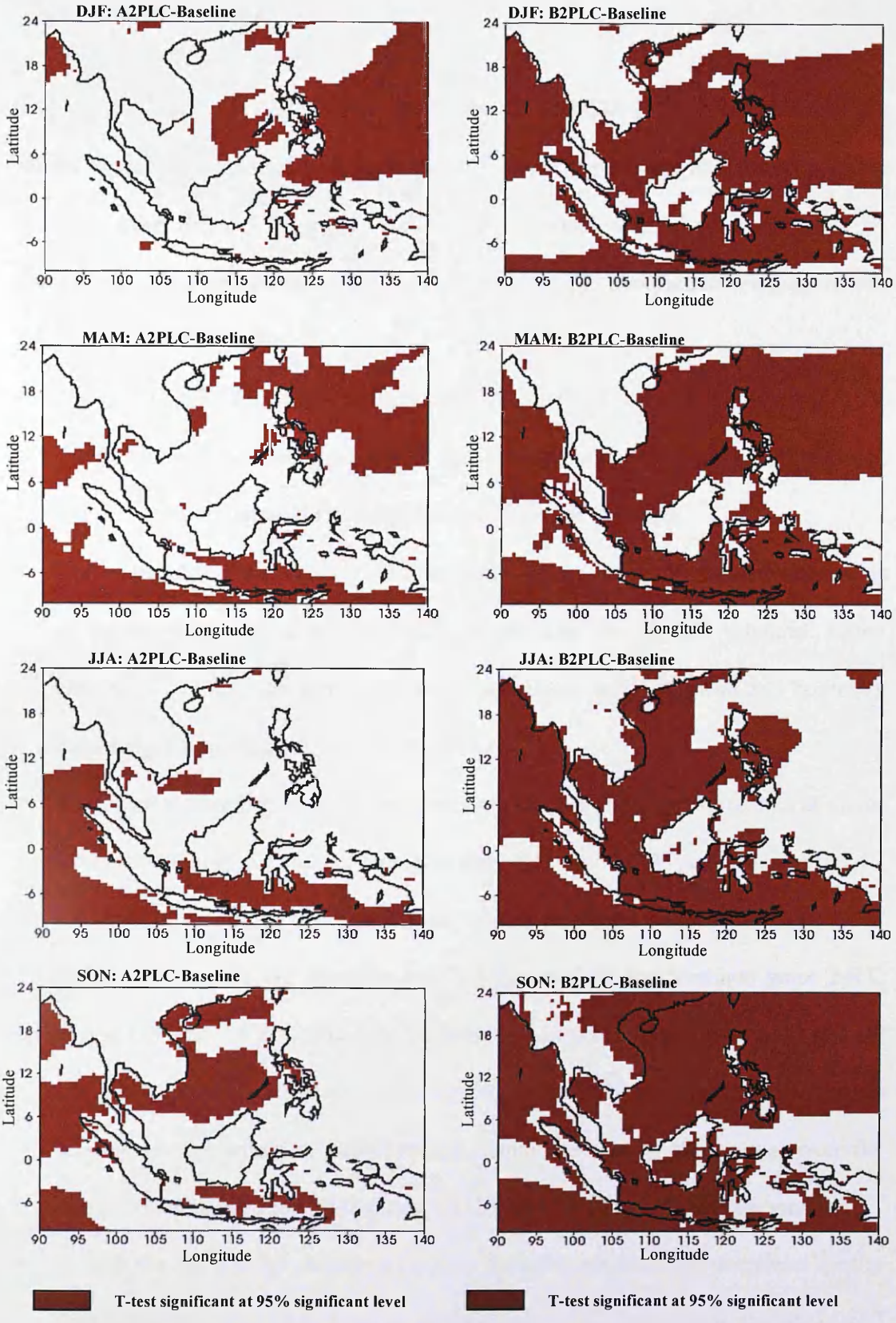

Figure 3.43: Significant t-test plots for the effect of atmospheric forcing alone on seasonal boundary layer for the A2 (A2PLC-Baseline) (*left panel*) and B2 (B2PLC-Baseline) (*right panel*) climate scenarios relative to the Baseline scenario.
(*PLC-Present-day Landcover*)

3.8 Conclusions

The present study has used a high resolution of PRECIS (5.1), a regional climate model developed by the Hadley Centre to examine present-day and future possible climates over SEA. The performance of the model was also investigated by comparing with observed data (CRU), ERA40 and GCM. Thus, some conclusions can be drawn from the results:

- The PRECIS-RCM captured the primary features of the observed data (CRU), ERA40-Reanalysis data and GCM circulations and the patterns of seasonal change, and was generally well represented for most variables.
- Due to the stronger emissions forcing in the A2 scenario, the scenario anomalies of surface temperature are generally larger than for the B2 scenario. Other climatic variables such as precipitation, total cloud, solar radiation and boundary layer height have high degrees of variability.
- There was a warming across the region, with the largest temperature increase over land areas in both A2 and B2 scenarios during DJF and JJA. According to the A2 scenario, there was an average surface warming of 3.0°C during DJF and 3.1°C during JJA. In the B2 scenario, the average surface temperatures were 2.6°C during DJF and 2.1°C during JJA. Surface temperature changes in both A2 and B2 climate scenarios were statistically significant at 95% confidence level for all seasons for the whole modelled region-domain, except in some areas over the South China Sea and the Philippines Sea during DJF in the B2 climate scenario.
- In both the A2 and B2 climate scenarios, the total precipitation decreased during DJF by about -0.4 mm/day and slightly increased during JJA by about 0.2 mm/day (A2) and 0.1 mm/day (B2) respectively. Precipitation changes of less than -1 mm/day, mostly over the sea during DJF and a larger area over the sea and

insular region during JJA were found to be statistically significant in both scenarios.

- The total cloud fraction in the A2 and B2 scenarios were projected to decrease slightly by -0.07 during DJF and -0.04 during JJA. Future changes in total cloud fraction in both seasons of roughly less than -0.04 in the A2 scenario and less than -0.05 in the B2 scenario were found to be statistically significant at 95% level.
- The projected solar radiation in the A2 climate scenario slightly increased by 5.6 Wm^{-2} during DJF and 4.6 Wm^{-2} during JJA. Similarly in the B2 scenario, the projected solar radiation increased by 3.1 Wm^{-2} during DJF and 3.8 Wm^{-2} during JJA.
- In the A2 scenario, boundary layer heights were observed to decrease slightly by -3 m during DJF and increase by 23 m during JJA. Meanhwile, in the B2 scenario, the boundary layer heights were observed to decrease in both seasons, but at a smaller magnitude.

Regional surface temperature over Southeast Asia at the end of the century was projected to increase between 3.0 and 3.1°C in the A2 and 2.1 and 2.6°C in the B2 transient climate scenarios. These increases however are relatively lower than the global best estimate (IPCC, 2007) of between 1.8 – 4.0°C. The combined impact of aerosols (sulfur cycles) and greenhouse gases (GHG) considered in the model were found to increase the future surface temperature in the region in both climate scenarios. Due to the build up of future GHGs emissions in both A2 and B2 scenarios, it has been identified that it has affected the future changes in large-scale atmospheric circulation patterns. GHGs absorb and emit infrared (heat) radiation, and because temperature decreases with height in the troposphere, increasing GHGs cause

emissions to space to arise from higher and colder levels, thus reducing radiation to space (Hansen *et al.*, 1998). This imbalance with incoming solar energy forces the Earth's surface to warm.

PRECIS-RCM projected that the increase in surface temperatures in both climate scenarios during DJF was consistent with lower precipitation during DJF, though similar trend was not observed during JJA. The slight increases in total precipitation during JJA in both climate scenarios, which is corresponding with the southwest monsoon were lower than the earlier projection for Southeast Asia (Johns *et al.*, 2003). Increasing temperatures tend to increase evaporation, which leads to more precipitation (IPCC, 2007). There is considerable uncertainty about total precipitation over the region (see also Section 3.7.1), as the PRECIS-RCM scenarios show an increase in precipitation also project warming of 3.1°C during JJA, which would generally cause evaporation to increase, and thus the model generally suggest that during JJA in the region will be drier. As suggested for future work (see Chapter 7) to investigate the climate extreme over the region, the extreme conditions could give some indication whether or not, annual or seasonal total precipitation increases, as many climate models projected that precipitation will occur in a small number of heavier storm (Titus, 2007). The changes in precipitation intensity would results both (increase or decrease) because the warmer atmosphere holds more water vapour, and because greenhouse gases considered in the model increase the radiative cooling in the upper atmosphere, which induces intense precipitation.

Relative to the land, surface temperature over the sea was relatively cooler (i.e South China Sea, west Pacific Ocean and Indian Ocean) in both the A2 and B2 climate

scenarios. Warm air rising over the land increases evaporation and plant transpiration more than by the evaporation over the sea that produces rainfall (Hansen *et al.*, 1998). This land-sea thermal gradient could be one of the key drivers of the Asian Monsoon and the meso-scale circulations over the region. These meso-circulations are very effective in transporting heat and moisture from the sea to the higher levels of the atmosphere and towards over the land. The development of the monsoon over the Indian Ocean, where the more usual northeast trade winds are replaced by Southeast Monsoon, which bring moist air and prolonged wet seasons (increase precipitation) over Southeast Asia during JJA in both climate scenarios.

Chapter 4

THE EFFECT OF LANDCOVER CHANGES ON CLIMATE CHANGES IN SOUTHEAST ASIA

4.1 Introduction

Research on landcover change on global environmental change has been emerging in the last few decades with the realisation that land surface processes influence the dynamic of the atmosphere and thus climate. Climate responses due to landcover changes and climate effects on the terrestrial ecosystem have been investigated by a number of studies (see Lamptey, 2005; Zhao *et al.*, 2001, Pielke, *et al.* 1998; Stohlgren *et al.*, 1998). There is general agreement on the complexity of the relationship between landcover and climate through feedbacks at the land-atmosphere boundary (Betts, 2000; Bonan, 2002; Doherty *et al.* 2000; Levis *et al.*, 1999). Landcover changes may alter land surface characteristics such as surface roughness, albedo, and vegetation types, all of which influence the surface energy balance fluxes and thus affect the regional climate (Lofgren, 1995). Compared to forested areas, disturbed areas generally have a higher surface albedo, and can therefore lead to increased short wave reflection, which could result in a cooling effect (Bonana *et al.*, 1992; Douville and Royer, 1997). The indirect effect of landcover change on climate through changes in atmospheric chemistry, has been less studied and is the focus of the present study.

Conversion of forested areas into cropland, pasture, or grassland will reduce the aerodynamic roughness of the landscape and decrease both the capture of precipitation on the canopy and the root extraction, which leads to less evaporation

and hence will reduce the fluxes of moisture and latent heat from the surface to the atmosphere, and therefore tend to increase the temperature (Lean and Rowntree, 1993). However the effect of landcover change in different regions to climate change has shown varying effects. A recent sensitivity study of regional climate to landcover change by Diffenbaugh (2005) over the western United States by using RegCM2.5 has observed that landcover change was responsible up to 60% of the total seasonal temperature response. However, investigation on the effect of landcover change on the regional climate over tropical West Africa, mainly due to conversion of tropical forest into agriculture, produce only a small effect (Lamptey, 2005). In the sensitivity study of Lamptey (2005), changing forest to agricultural land decreased winter (Dec-Jan-Feb) temperature by up to 1K, increased sensible heat flux (> 3 Wm^{-2}) and changed rainfall slightly (~ 0.1mm/day). Meanwhile in summertime (Jun-Jul-Aug), the temperature change was of ~ 1K and rainfall increased to 1.0 mm/day. Feddema *et al.* (2005) have also observed in their modelling study using DOE-PCM that landcover changes under A2 scenarios of the IPCC SRES contributed to significant warming of more than 2°C in the Amazon region. However, the same landcover forcing was shown to have a minor effect over Indonesia in the Southeast Asia region. Study by Defries *et al.* (2002) concluded that the future conversion (2050) of forested area into agriculture in equatorial Africa and Amazon will contribute significantly to the average temperature increases in winter (Dec-Jan-Feb) and summer (Jun-July-Aug). In an earlier study, McGuffie *et al.* (1995) observed minimal effects of landcover change to climate change over Southeast Asia compared with other tropical region such as equatorial Africa and Amazon. However, the general level of understanding of the role of landcover change on climate change in terms of albedo effects on radiative forcing is still relatively poor (IPCC, 2001).

A further investigation of the role of landcover change to climate change at the regional scale was carried out in SEA region, where anthropogenic landcover changes have been dramatically demonstrated in the last 30 years and are anticipated to continue at a higher rate in the future. So far, little regional modelling of the atmosphere-landcover feedbacks has been done specifically over SEA. Therefore, the current work is to investigate the effect of landcover change to climate change due to human-induced changes, such as the conversion of forested areas into agricultural activities (mainly to palm oil plantations), conversion of primary forest to secondary forest (including grassland), and the expansion of urban and suburban areas in line with economic and population growth in the region. The general framework of investigation of landcover change and climate change relationship is shown in Figure 4.1. The objective of this chapter is to assess the impact of landcover forcing relative to atmospheric forcing (elevated CO_2) to the climate change SEA. In achieving this objective, the investigation is guided by the three main research questions:

a) What would be the combined effect of atmospheric forcing and landcover forcing on climate changes and how significant are these changes?

b) What would be the effect of landcover forcing alone on regional climate changes and how significant are these changes?

c) What magnitude of differences do landcover forcings alone, atmospheric forcing alone and combined forcing produce in the climate in SEA?

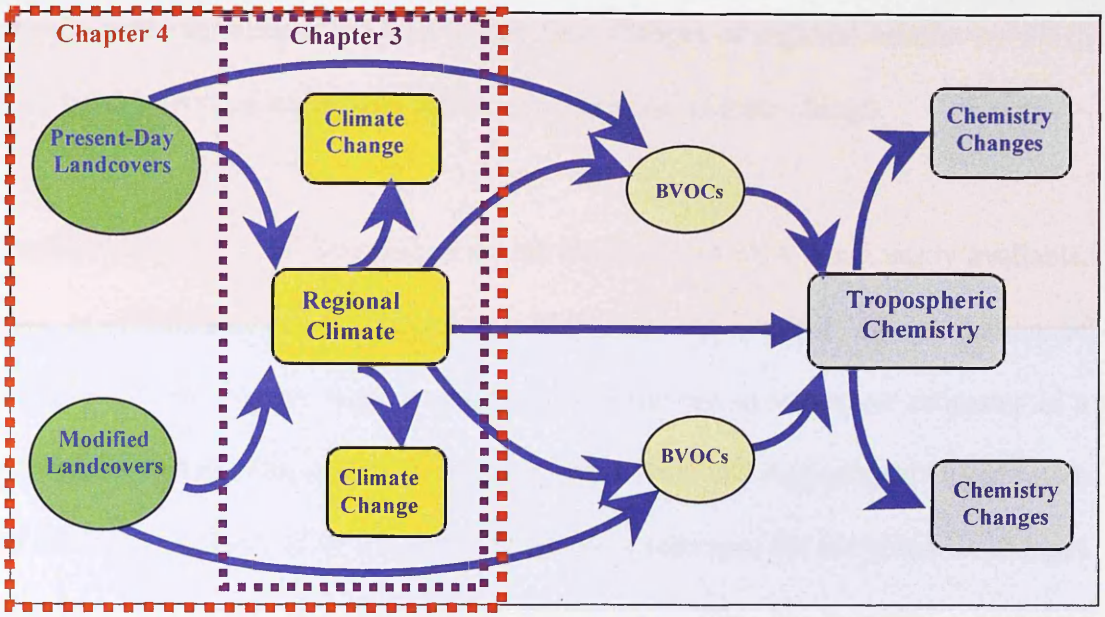

Figure 4.1 Framework for the investigation of climate changes-biogenic emissions-tropospheric chemistry interactions in Southeast Asia. The red dotted box indicates the framework for the investigation of landcover sensitivity studies to the climate changes that covered in Chapter 4.

4.2 Overview of the Present Landcover in SEA

The landcover in SEA has transformed tremendously in the last four decades and has become an ongoing feature of development, particularly in rural areas. Within this period, significant transformation patterns have been observed, such as widespread deforestation mostly due to logging activities, followed by the expansion and intensification of agricultural land uses (Kummer & Tunner, 1994; Brookfield & Byron, 1990) to meet the needs of the growing populations and changing lifestyles. Also, in the past 30 years, urban populations in SEA have increased due to rapid population growth and migration to the cities, which have contributed to the expansion of built-up areas and the size of urban and sub-urban areas (UNEP, 2000). The combination of rapid urban and industrial growth, extensive deforestation, and

unsustainable agriculture has lead to dramatic changes of regional landcover, which may be an important underlying influence on regional climate change.

Detailed and up-to-date information on the landcover of SEA is not easily available. Due to differences in procedure and techniques applied for the estimation of landcover in the region, there are substantial variations in landcover estimates in a number of studies. The statistical database of the Food and Agricultural Organisation of the United Nations (FAO, 2006) was used as a reference for the potential changes of future forest landcover estimates for SEA. FAO (2006) has provided a complete estimate of forest cover for each country in SEA, including the historical changes of forest cover in the region. In 2000, the forest cover in SEA was reduced from 53.9% to 48.6% of the land area in 1990, which is an annual reduction rate of approximately 1.0% (see Table 4.1 & Figure 4.2). Myanmar, the Philippines, Indonesia, and Malaysia were found to exceed the 1% annual reduction rate. Forest cover and historical change estimation by FAO (2006) for Indochina (which includes Cambodia, Laos, Myanmar, Thailand, and Vietnam), and for insular SEA (which includes Brunei, Indonesia, Malaysia, the Philippines, Singapore, and Timor Leste), were also compared with other studies such as Giri *et al.* (2001), Stibig & Malingreau (2003), and Gunawan & Rahmadi (2000) in order to obtain a general overview of the estimate variations.

Estimation of other types of landcover such as agriculture, grassland/shrubland/ savanna, and urban or built-up areas were gathered from various sources, though the information was not comprehensive and not available for all countries in the region. Landcover for agriculture, grassland/shrubland, and urban areas shows an annual

positive rate as shown in Table 4.2. Large areas of agricultural landcover, mainly for the cultivation of oil palm, rubber, rice, and coconuts, can be found in relatively larger countries such as Thailand, Indonesia, the Philippines, Myanmar, Cambodia, Vietnam, and Malaysia. Based on the available information, grassland/shrubland/savanna landcovers are found mostly in Vietnam, Myanmar, the Philippines, and Laos. In a preliminary regional assessment of grasslands in Asia by Garrity *et al.* (1997), the Philippines was found to have the largest proportion of grassland landcover of about 17%, followed by Vietnam (9%), Laos (4%), Indonesia (4%), Thailand (4%), Myanmar (3%), Cambodia (1%), and Malaysia (<1%). In terms of built-up area, there is clear indication of urban expansion in the region, although the proportion of urban area to land area is relatively small (< 2%). For the estimation of potential future landcover of two other dominant features in SEA, namely agriculture and grassland/shrubland, estimated figures from FAO (2004); Giri *et al.* (2001); Suprapto (2000); UNCSD (1997); Mohamad & Siew (1994) were used. Meanwhile, estimations for the urban/built-up area were taken from the database provided by Demographia (2006), though the urban areas seem to be underestimated as only the major cities are considered. Despite this, the incorporation of urban landcover is important as it is expected to make the model simulation more realistic at the regional scale.

Table 4.1: Distribution and changes of forest cover in SEA.

Country	Land Area	Forest Cover							
		FAO (2000)			Stibig & Malingreau (2003)	Gunawan & Rahmadi (2000)	Giri *et al* (2001)		
		1990	**2000**	**Change**	**2000**	**2000**	**1985/86**	**1992/93**	**Change**
	x 1000 ha	x 1000 ha (%)	x 1000 ha (%)	x 1000 ha/yr (%)	x 1000 ha (%)	x 1000 ha (%)	x 1000 ha (%)	x 1000 ha (%)	x 1000 ha/yr (%)
Brunei	527	452 (85.8)	442 (*83.9*)	-1 (*-0.2*)	465 (*88.2*)				
Cambodia	17652	9895 (56.1)	9335 (*52.9*)	-56 (*-0.6*)			11025 (*62.46*)	12932 (*73.26*)	+238 (*+2.2*)
Indonesia	181157	118106 (65.2)	104986 (*58*)	-1312 (*-1.2*)	103775* (*57.3*)	92400 (*51.0*)			
Laos	23080	13091 (56.7)	12561 (*54.4*)	-53 (*-0.4*)				16992 (*73.62*)	
Malaysia	32855	21662 (65.9)	19292 (*58.7*)	-237 (*-1.2*)	18382 (*60.0*)				
Myanmar	65755	39589 (60.2)	34419 (*52.3*)	-517 (*-1.4*)			32812 (*49.90*)	28932 (*44.00*)	-485 (*-1.5*)
Philippine	29817	6679 (22.4)	5789 (19.4)	-89 (*-1.4*)	7401 (*24.8*)				
Singapore	61	2 (*3.3*)	2 (*3.3*)	No change					
Thailand	51089	15882 (31.1)	14762 (*28.9*)	-112 (*-0.7*)			17743 (*34.73*)	15414 (*30.17*)	-291 (*-1.6*)
Timor Leste	1479	537 (36.3)	507 (*34.3*)	-3 (*-0.6*)					
Vietnam	32550	9299 (28.6)	9819 (*30.2*)	52 (*0.5*)			10123 (*31.10*)	9309 (*28.60*)	-101.8 (*-1.0*)
Total	436022	235204 (53.9)	211914 (*48.6*)	-2329 (*-1.0*)					

Table 4.2: Distribution and changes of agriculture, grassland, and urban landcovers in SEA

Country	Land Area	Agriculture			Grassland/shrubland/Savanna/Marshes			Urban/Suburban		
		Giri *et al* (2001)						Demographia (2006)		
		1985/86	**1992/93**	**Change**	**1985/86**	**1992/93**	**Change**	[year]	[year]	**Change**
	x 1000 ha	x 1000 ha (%)	x 1000 ha (%)	x 1000 ha/yr (%)	x 1000 ha (%)	x 1000 ha (%)	x 1000 ha/yr (%)	x 1000 ha (%)	x 1000 ha (%)	x 1000 ha/yr (%)
Brunei	527									
Cambodia	17652	2434 (*13.79*)	3356 (*19.01*)	+115 (*+4.7*)	948 (*5.37*)	953 (*5.40*)	+0.6 (*+0.1*)		[2005] 51.8 (0.3)	
Indonesia	181157		[1998] 66000* (*36.4*)						[2000] 291.8 (0.2)	
Laos	23080		1050 (*4.55*)			4893 (21.20)			[2005] 2.6 (<0.1)	
Malaysia	32855	4907 (*14.9*)	5769.2 (*17.6*)	+86.2 (*+1.8*)					[2002] 174.9 (1.3)	
	13158.7**							[1984]# 229.3 (0.7)	[1990] # 221.6 (1.7)	+7.8 (+4.5)
Myanmar	65755	11376 (*17.30*)	13743 (*20.90*)	+296 (*+2.6*)	19266 (*29.30*)	21831 (*33.20*)	+320 (*+0.2*)		[2004] 43.5 (0.1)	
Philippine	29817	[1990] ‡ 10002 (*33.6*)	[1996] † 10192.2 (*34.2*)	+27.2 (*+0.3*)		[1991] ‡ 9040.2 (*30.3*)		[1987]‡ 131.4 (0.4)	[2000] 158.3 (0.5)	+1.9 (+1.5)
Singapore	61								[2000] 47.9 (78.5)	
Thailand	51089	30005 (*58.73*)	32457 (*63.53*)	+306.5 (*+1.0*)					[2003] 101 (0.2%)	
Timor Leste	1479								-	
Vietnam	32550	5631 (*17.30*)	6087 (*18.70*)	+57 (*+1.0*)	15396 (*47.30*)	14322 (*44.00*)	-134 (*-1.0*)		[1999] 62.1(0.2)	
Total	436022									

Note: * including Timor Leste (Suprapto, 2000); ** Peninsular Malaysia only;
Mohamad & Siew (1994); ‡ FAO (2004); † UNCSD (1997)

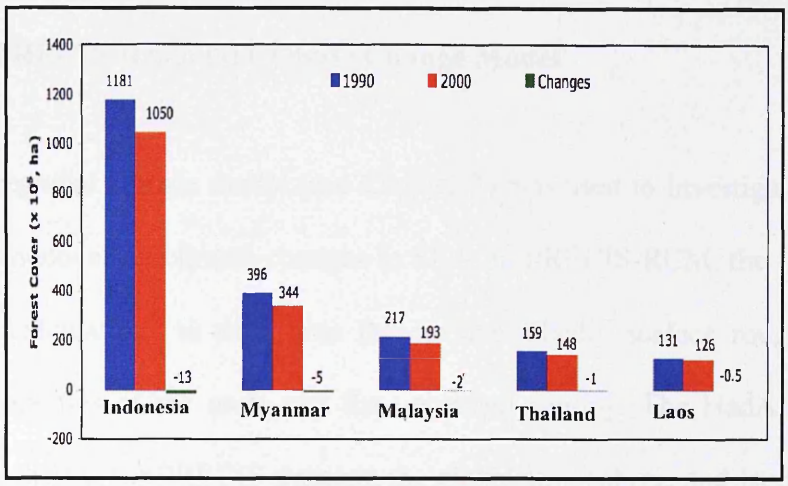

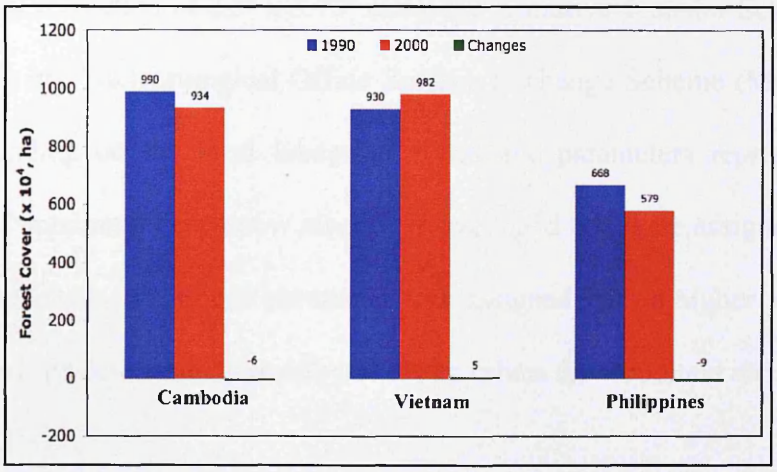

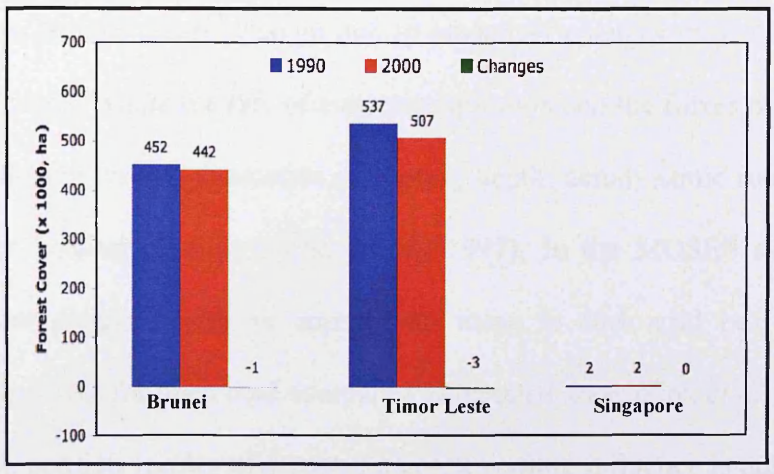

Figure 4.2: Forest cover distribution and forest cover changes from 1990 to 2000 for each country in Southeast Asia.

4.3 Model and Experimental Designs

4.3.1 PRECIS-Regional Climate Change Model

PRECIS, a regional climate model (see Chapter 3) was used to investigate on the effects of changes in landcover on climate changes in SEA. In PRECIS-RCM, the landcover type was used in the calculations to determine the surface albedo, surface roughness length, and hydraulic properties of the roots and the vegetated canopy. The HadAM3P global model boundary conditions for PRECIS simulate the global atmospheric and land surface processes at a horizontal resolution of 2.5° x 3.75° using the Radiative Transfer Scheme (Edwards and Slingo, 1996) and Meteorological Office Surface Exchange Scheme (MOSES) (Cox *et al.*, 1999). Depending on the local landcover types, the parameters representing "snow-free albedo" and "maximum deep-snow albedo" in each grid box were assigned with appropriate values. For example, the albedo parameter was assigned with a higher value for open land (e.g. grassland, pasture, and cropland) and lower values for woodland and forests (Cox *et al.*, 1999; Betts, 2000).

In the tropics, surface albedo change due to landcover changes may affect the climate via evapotranspiration, where the rate of evapotranspiration and the fluxes of sensible and latent heat are dependent on the parameters of rooting depth, aerodynamic roughness length, and canopy water holding capacity (Betts *et al.*, 1997). In the MOSES simulation, all these parameters are assigned with an appropriate value in each grid box, where values are comparatively lower for open land compared to forested areas (Cox *et al.*, 1999). In the SEA region, which consists mostly of forested areas, a cooling influence is anticipated as a result of the greater flux of moisture to the atmosphere and the larger ratio of latent to sensible heat fluxes. The transpiration dependency on the resistance to water vapour loss from within plant stomata was also represented in the MOSES simulation, which is aggregated to a large-scale

variable of canopy conductance using leaf area index (LAI). In forested areas, LAI, which is prescribed as a further vegetation-specific parameter in the model, has larger values than open land (Betts *et al.*, 2007).

In representing landcover changes in the PRECIS RCM for the sensitivity studies, the global datasets of the vegetation parameter values were derived using the Wilson and Henderson-Sellers (1985) present-day landcover dataset at a resolution of 1° x 1° grid. The present-day landcover dataset has specified 53 landcover classes, which include 11 crop classes, 7 pasture/grazing classes, and 1 urban class (See Appendix 3.1). As also mentioned in Section 3.3.8 (Chapter 3), the present-day landcover dataset allows two classes of landcover for each grid, namely the primary landcover class if the coverage of the grid box is between 50-100%, and the secondary landcover class if the coverage is between 25-50%. These vegetation covers, which are represented in the HadAM3 surface parameter, are then bi-linearly interpolated to the GCM resolution. For estimations of future landcover in SEA, certain assumptions were specified to reflect hypothetical extreme states of future vegetation for sensitivity studies as described in detail in Section 4.3.2.2 in order to derive appropriate landcover types to be assigned to each grid box in PRECIS.

4.3.2 Development of Future Landcover Scenario for SEA

4.3.2.1 Baseline landcover for SEA in PRECIS-RCM

The studied domain with 0.44° x 0.44° resolution contained 1839 landcover grid boxes with an estimated area of 459,750,000 ha. The total model landcover is higher than that given in Table 4.1 and Table 4.2 as the selected domain includes the southern part of China. For present-day conditions, the dominant primary landcover is equatorial rain forest (Code 50) with 49% of the area. The remainder of the primary cover is made up of open tropical

woodland (Code 23) (11%), tropical savannah/grassland (Code 37) (9%), open-water (Code 0) (8%), paddy rice (Code 4) (5%), dense drought deciduous forest (Code 25) (5%), arable cropland (Code 40) (4%), open drought deciduous forest (Code 26)(3%), tropical pasture (Code 33) (3%), and mangrove (Code 5), tropical broadleaf forest (Code 52) and others are accounted for 1% respectively as shown in Table 4.3. The dominant primary landcover type for the present-day scenario in the region is shown in Figure 4.3. For the secondary landcover types, equatorial rain forest and open tropical woodland dominated the landcover of the region. Meanwhile, urban or built-up area was only accounted for only 0.2% for both primary and secondary codes.

Table 4.3: Landcover types in SEA for baseline (present-day) scenario

Code	Landcover Types	Estimate Area (x 1000 ha)	Percentage
	Primary Landcover Types		***% of Primary Codes***
50	Equatorial rain forest	225,277.5	49
23	Open tropical woodland	50,572.5	11
37	Tropical savanna/grassland	41,377.5	9
0	Open water	36,780.0	8
4	Paddy rice	22,987.5	5
25	Dense drought deciduous forest	22,987.5	5
40	Arable cropland	18,390.0	4
26	Open drought deciduous forest	13,792.5	3
33	Tropical pasture	13,792.5	3
5	Mangrove	4,597.5	1
52	Tropical broadleaf forest	4,597.5	1
80	Urban	919.5	0.2
Others	Others	4,597.5	1
	Secondary Landcover Types		***% of Secondary Codes***
50	Equatorial rain forest	137,925.0	30
23	Open tropical woodland	114,937.5	25
40	Arable cropland	41,377.5	9
37	Tropical savanna/grassland	36,780.0	8
26	Open drought deciduous forest	22,987.5	5
0	Open water	22,987.5	5
33	Tropical pasture	22,987.5	5
4	Paddy rice	18,390.0	4
25	Dense drought deciduous forest	13,792.5	3
5	Mangrove	9,195.0	2
32	Tropical grassland/shrub	4,597.5	1
80	Urban	919.5	0.2
Others	Others	13,792.5	3

Note: Total land area of SEA = *436,022,000 ha*
Total grid cell (0.44° x 0.44° or 50 km x 50 km) =1839 ≈ 459,750,000 ha

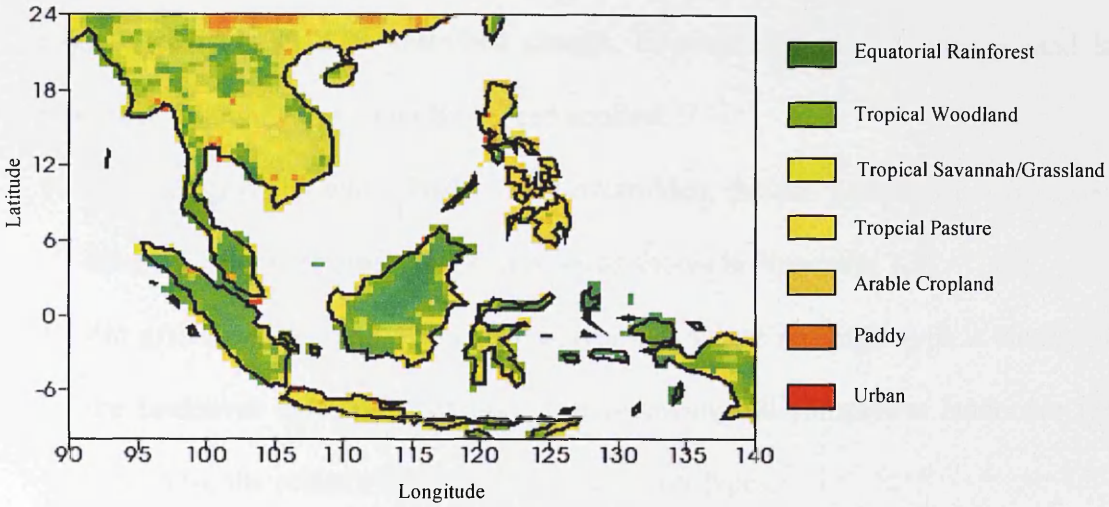

Figure 4.3: Present-day landcover scenario (primary landcover types) in Southeast Asia.

4.3.2.2 Future landcover scenario for SEA

For the sensitivity experiment, future landcover changes (2070-2100) have been developed for the SEA region. It is difficult to predict the future landcover in the region, due to the intricate interplay of social, economic, and demographic factors. Therefore, in prescribing the future landcovers for the region, assumptions were made about the reasonable reduction or increment of the present-day landcover types. Historical trends and annual rates of landcover changes as shown in Table 4.1 and Table 4.2 formed the basis of the projections used below. In this work, changes were made to only four types of landcover: tropical rainforest, agriculture, savanna/grassland, and urban/built-up areas. The first three types of landcover are the dominant landcover of the region; urban landcover was changed because urbanisation produces very large local changes to surface parameters.

The advantage of PRECIS-RCM for use in sensitivity studies is the ability to prescribe specific landcover types through alteration or by overriding the landcover types for each grid to suit the aim of the investigation. Such prescribed alterations have allowed modifications to the model formulation (e.g. boundary condition alterations) to test the sensitivity of the

model's statistics to that prescribed change. In overriding the default soil and landcover types, the following principles have been applied:

- For each grid box where landcover is overridden, the soil types must also be specified in accordance to the permissible soil types as shown in Appendix 3.2.
- For grid boxes with mixed landcover types, or where no single type is clearly dominant, the landcover types most accurately summarising all component landcover types were chosen for the primary and secondary landcover types.

In over-writing the landcover types, the soil type and both primary and secondary landcover types were specified in each grid using the appropriate integer codes. There are 22 soil types and 59 landcover types; these are listed, with their respective integer codes, in Appendix 3.1 and Appendix 3.2. As also mentioned in Section 3.3.8, in each grid box, the landcover types are coded into two types: primary and secondary types, which occupy greater and lesser extents of a grid box respectively. If no single landcover type was clearly dominant in the grid box, primary and secondary types were chosen from the most appropriate of all the component landcover types. A special treatment was applied to the landcover in coastal land grid boxes, and at over-estimated or non-resolved inland waters, where the primary and secondary landcover types of open water (code 0) and inland water (code 1) were used.

Based on average annual change rates of 0.8% for forest cover reduction in terms of land area in eight major countries (excluding Brunei, Singapore, and Timor Leste) in 2000, the primary future forest cover was assumed to reduce to 60% of the present-day coverage, mainly due to conversion to agriculture or secondary forest. In this case, present-day total grid boxes with primary code of forest landcover (69% of the total grid boxes) was reduced by 60%. Meanwhile for the secondary code of forest landcover was reduced by 30%. The major factor of forest cover reduction is expected to be from the continuous expansion and

intensification of agriculture activities, mainly oil palm and rubber plantations, in Indonesia, Malaysia, southern Thailand, and southern Philippines. In this work, the forest area that has been lost, was assumed to be converted into agriculture, savannah/grassland or urban development. It was further assumed that conversion of equatorial rain forest (natural forest) could be to either agriculture, savannah/grassland or other type of secondary forest (open tropical woodland, etc.) Other types of landcover were assumed to be the same as the present-day (baseline) condition. Future agriculture land was assumed to increase to 210% of present-day coverage. Meanwhile savannah/grassland was also assumed to increase to 197% of its present value. Built-up/urban area at the present-day condition is only 0.2% of the total grid box but it is expected that urbanisation rate will accelerate alongside with the economic and population growth in the region mostly concentrated in sub-urban and coastal areas. In this work, it was assumed the built-up/urban area would increase by 300% or about to 0.6% of the total number of grid boxes within the domain. The summary of landcover type changes between the present-day and future (2070-2100) landcover is shown in Figure 4.4 and Table 4.4.

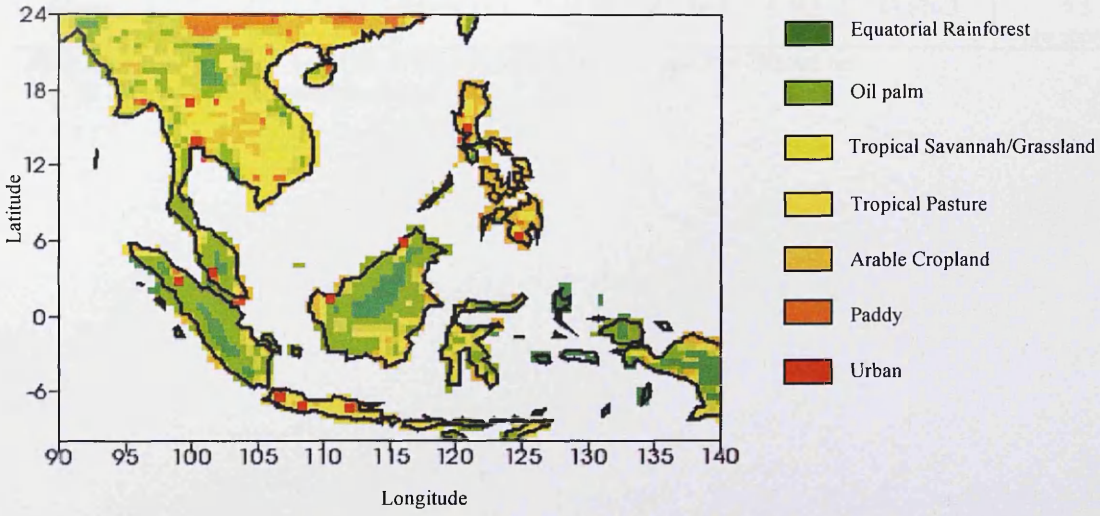

Figure 4.4: Modified future landcover scenario (primary landcover types) in Southeast Asia. Spatial distribution of landcover types can be compared with Figure 4.3 for comparison between the present-day and future landcover types distribution.

Table 4.4: Modified landcover types in SEA for future scenario

Landcover Category	Code	Landcover Types	Present-Day (Baseline)		Future (2070-2100)	
			Area (x 10^3 ha)	%	Area (x 10^3 ha)	% (Changes, %)
Primary Landcover Types						
Forest	50 23 25 26 52 5	Equatorial rain forest Open tropical woodland Dense drought deciduous forest Open drought deciduous forest Tropical broadleaf forest Mangrove	317,227.5	69.0	126,891.0	27.6 (-60)
Agriculture	4 40 33 51	Paddy rice Arable cropland Tropical pasture Tropical tree crop	51,951.8	11.3	160,452.8	34.9 (+210)
Savanna/ Tropical Grassland	37 32	Tropical savanna Tropical grassland/shrub	43,676.3	9.5	123,672.8	26.9 (+197)
Urban/ Suburban	80	Urban	919.5	0.2	2,758.5	0.6 (+300)
Others		Others	45,975.0	10.0	45,975.0	10.0 (no change)
Secondary Landcover Types						
Forest	50 23 25 26 52 5	Equatorial rain forest Open tropical woodland Dense drought deciduous forest Open drought deciduous forest Tropical broadleaf forest Mangrove	292,860.8	63.7	205,048.5	44.6 (-30)
Agriculture	4 40 33	Paddy rice Arable cropland Tropical pasture	82,295.3	17.9	132,408.0	28.8 (+61)
Savanna/ Tropical Grassland	37 32	Tropical savanna Tropical grassland/shrub	39,998.3	8.7	74,939.3	16.3 (+88)
Urban/ Suburban	80	Urban	919.5	0.2	3,678.0	0.8 (+400)
Others		Others	43,676.3	9.5	43,676.3	9.5 (no change)

Note: Total grid cell (0.44° x 0.44° or 50 km x 50 km) =1839 grid box≈ 459,750,000 ha

% - the percentage of total land area

4.4 Results and Discussion

The results are presented in two parts: first, the combined impacts of landcover forcing and atmospheric forcing on regional climate; second, the isolated impacts of landcover forcing alone on regional climate. Some results of the regional climate investigations from Chapter 3 are also used and depicted again in this chapter to facilitate the investigation of effects of landcover changes on regional climate. For the purposes of discussion, only variables that were used in the subsequent investigation of biogenic emissions (Chapter 5) and tropospheric chemistry (Chapter 6) such as surface temperature, solar radiation, boundary layer height, and total cloud – are discussed. In addition, precipitation is included as it is one of the most important variables in climate. Other climate and hydrological variables such as latent heat, sensible heat, surface soil evaporation, canopy evaporation, total soil moisture, moisture convergence, and surface pressure were analysed and available but were not presented in this chapter.

4.4.1 Combined Impacts of Atmospheric and Future Landcover Forcings on Climate Changes

A regional simulation of the combined impacts of atmospheric and future landcover forcings provides a sensitivity experiment to assess how regional forcing is manifested in SEA. The results of the combined effects produced by these forcings are presented as the difference between the all-forcings scenarios (atmospheric forcing and future landcover forcing) and the baseline scenario with present-day landcover, which are denoted as "A2FLC-Baseline" for A2 and "B2FLC-Baseline" for B2 climate scenarios. The region of SEA is noted for its monsoon climate, which is dominated by two monsoon seasons, namely the northeast monsoon (NEM) and southwest monsoon

(SEM). In this chapter, the discussion will be limited to the climate change during the northeast monsoon, which is denoted as DJF (Dec-Jan-Feb) and the southwest monsoon, which is denoted as JJA (Jun-Jul-Aug). For completeness, intermediate periods appear in some of the tables and figures in the results but are not discussed; these are denoted as MAM (Mar-Apr-May) and SON (Sept-Oct-Nov).

4.4.1.1 Surface temperature

The seasonal cycles of surface temperature for baseline and future simulations due to atmospheric forcing alone (A2PLC and B2PLC) and the combined effect of atmospheric and landcover forcings (A2FLC and B2FLC) are shown in Figure 4.5 for the A2 and B2 climate scenario simulations. The results show the temperature increase relative to the baseline was smaller in the B2 simulation compared to the A2 simulation, due to the weaker atmospheric forcing (emissions forcing) in the B2 climate scenario. In the A2 climate scenario, the surface temperatures due to the combined forcing (A2FLC) were relatively higher than due to atmospheric forcing alone (A2PLC). For the B2 climate scenario, there is no discernible difference in surface temperature due to the combined forcing (B2FLC) and atmospheric forcing alone (B2PLC). This implies that the magnitude of climate change from landcover change depends on the degree of atmospheric forcing. That is, landcover forcing and atmospheric forcing are coupled in the SEA region.

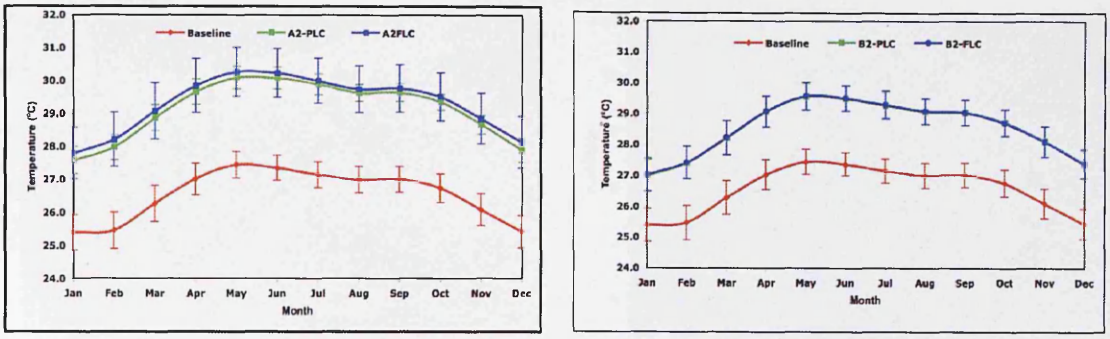

Figure 4.5: Seasonal cycle of surface temperature (°C) for the A2 (*left panel*) and B2 (*right panel*) climate scenarios in the present-day and future landcover scenarios.
(*Note: FLC- Future Landcover; PLC-Present-day Landcover*)

Figure 4.6 shows the pattern and magnitude of temperature increase for each season for the A2 climate scenario due to the effects of combined atmospheric forcing and landcover forcing. The future mean surface temperatures were 28.1°C and 30.0°C during DJF and JJA respectively (Appendix 4.1). These increased by 2.7°C during DJF and 2.8°C during JJA compared to the baseline (Figure 4.6). Higher changes in surface temperature were found to occur over land in all seasons, but were notably higher in some areas in western parts of Sumatra and the southern part of Borneo during JJA. Surface temperatures increased due to the combined forcings, and were statistically significant at the 95% confidence level in all areas of SEA (not shown). In the B2 climate scenario, the future mean surface temperatures were smaller than A2 climate scenario at 27.7°C during DJF and 28.6°C during JJA (Figure 4.7 and Appendix 4.2). These were increased by 2°C and 2.1°C during DJF and JJA, respectively compared to the baseline. Similar to the A2 climate scenario, the higher increase in surface temperature in the B2 climate scenario was observed over land, mainly in central Thailand and Myanmar during DJF and western Sumatra and southern Borneo during JJA. As with the A2 scenario, the increase in surface temperature due to the combined forcings was statistically significant at the 95% confidence level in all areas of SEA (not shown).

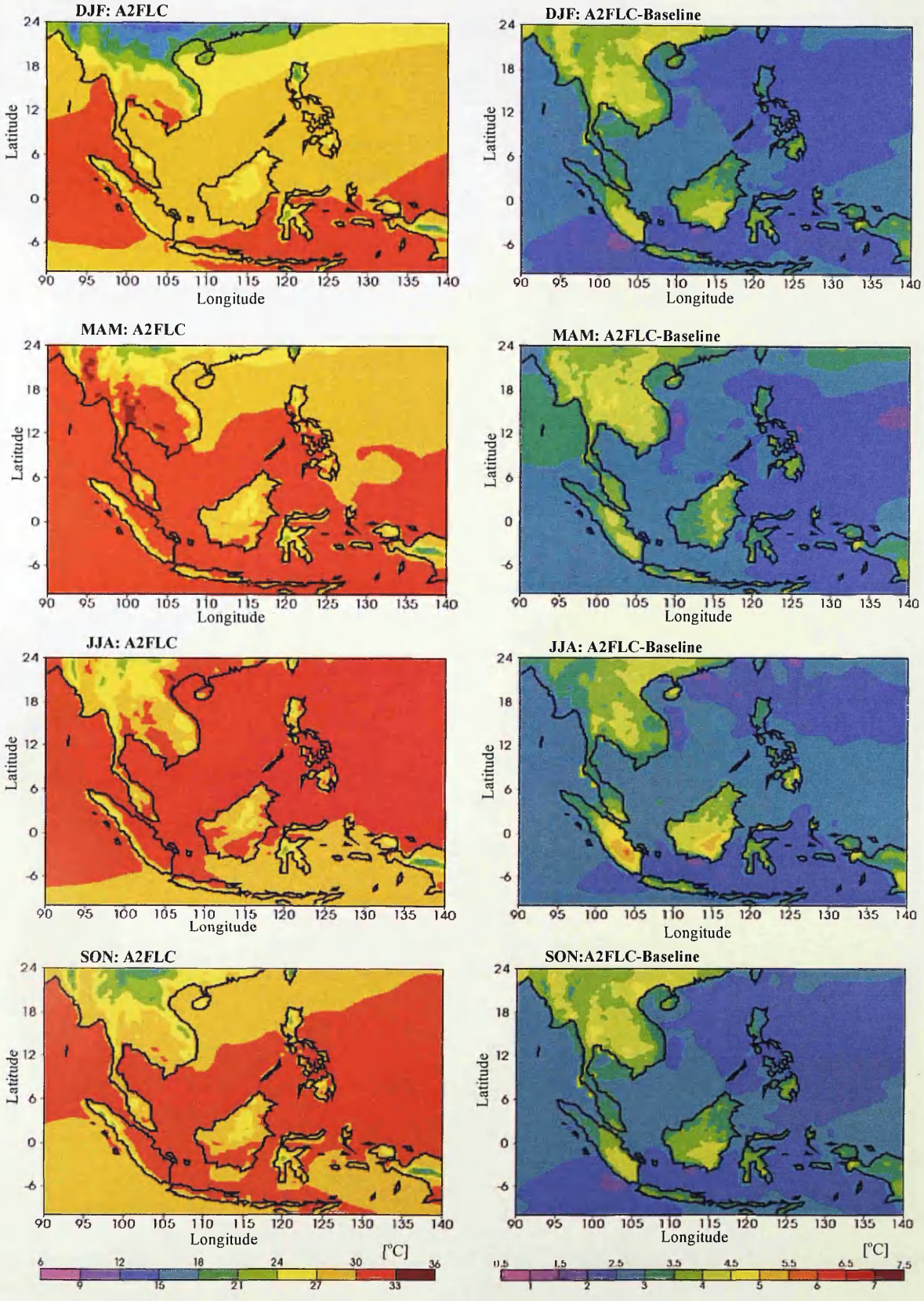

Figure 4.6: **SRES A2**: Combined effects of atmospheric and future landcover forcings on the seasonal temperature (A2FLC) in the SRES A2 scenario, and the temperature difference in comparison with the Baseline scenario (A2FLC-Baseline).
(*Note: SRES A2- Special Report on Emission Scenario A2; FLC- Future Landcover*)

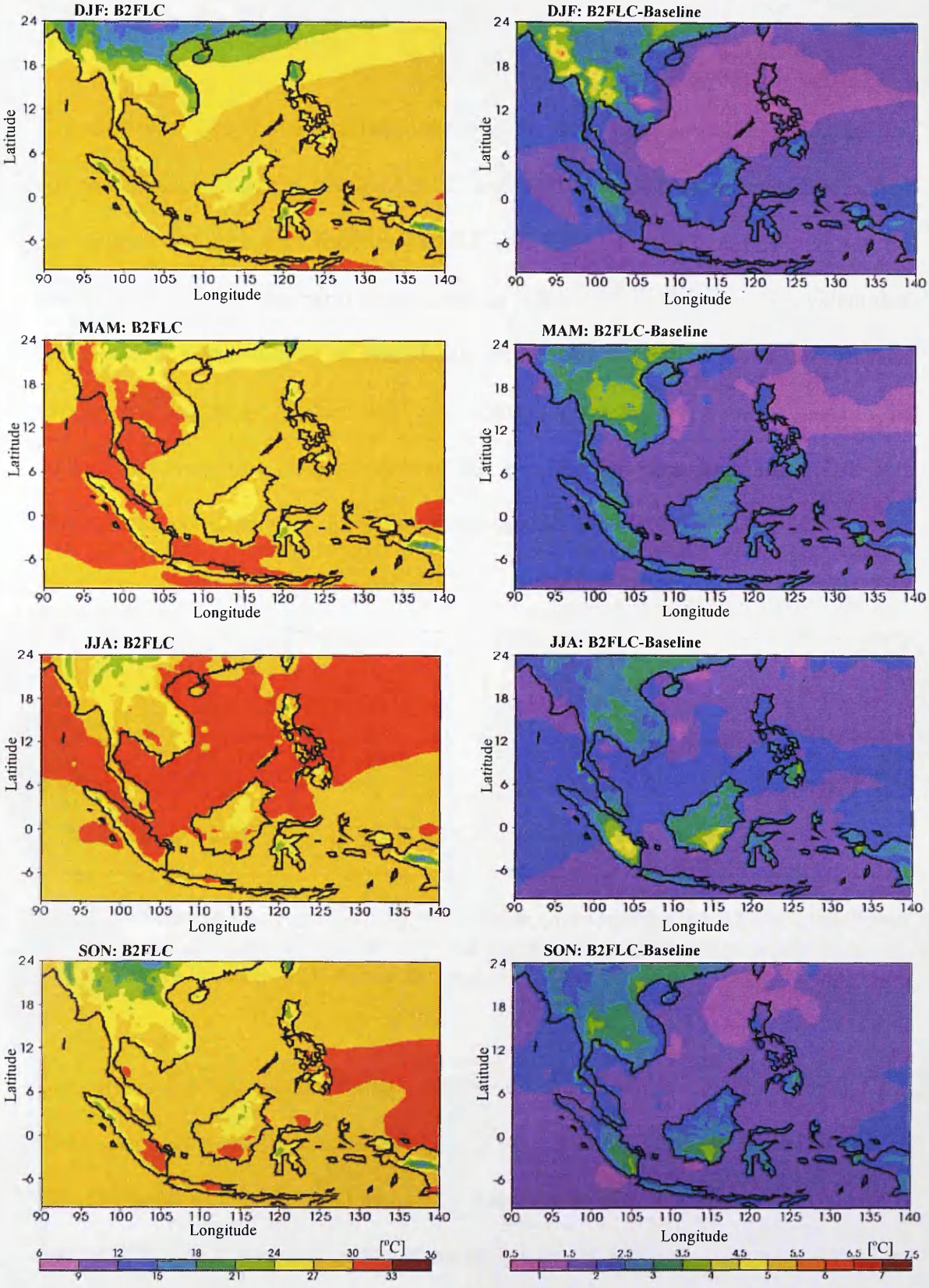

Figure 4.7: **SRES B2**: Combined effects of atmospheric and future landcover forcings on the seasonal temperature (B2FLC) in the SRES B2 sceanrio, and the temperature difference in comparison with the Baseline scenario (B2FLC-Baseline).
(*Note: SRES B2- Special Report on Emission Scenario B2; FLC- Future Landcover*)

4.4.1.2 Total precipitation

The seasonal cycles of total precipitation for the baseline and also the future simulations due to atmospheric forcing alone (A2PLC and B2PLC) with the combined forcings of atmospheric and landcover forcings (A2FLC and B2FLC) are shown in Figure 4.8 for the A2 and B2 climate scenario simulations. In both climate scenarios, it is evident that there was a larger degree of variability within simulations compared to surface temperature (Figure 4.5), which was comparatively lower than the baseline scenario. In both climate scenarios, it was observed that precipitation decreases during DJF and slightly increases during JJA for both simulations (A2 and B2).

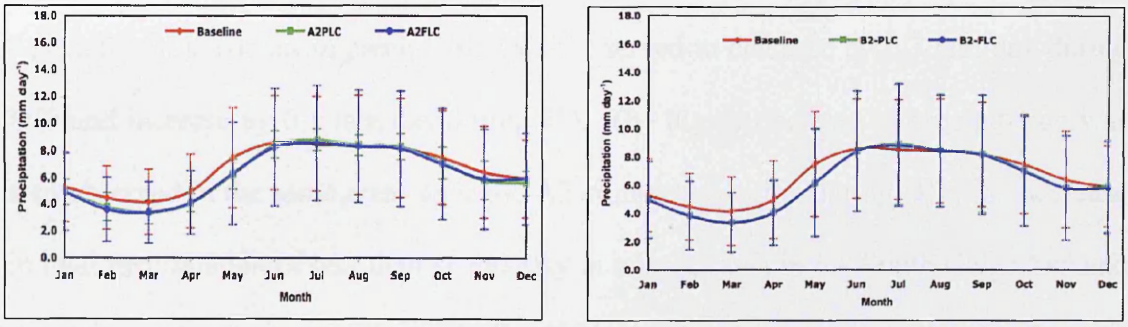

Figure 4.8: Seasonal cycle of the total precipitation (mm/day) for the A2 (*left panel*) and B2 (*right panel*) climate scenarios in the present-day and future landcover scenarios. (*Note: FLC- Future Landcover; PLC-Present-day Landcover*)

The pattern and magnitude of total precipitation changes for each season for the A2 climate scenario (combined atmospheric and landcover forcings) are shown in Figure 4.9. The impact of combined forcings on future mean precipitation was 4.8 mm/day during DJF, which was a decrease of about 0.4 mm/day (DJF) (Appendix 4.1). The lower precipitation was observed mainly in the continental region of SEA, Andaman Sea, Bay of Bengal, and the northern part of the South China Sea. During DJF, a statistically significant (95% level) increase in total precipitation is predicted in some

areas in Java, southern Borneo, the Indian Ocean, and the Pacific Ocean. During JJA, future mean precipitation increased by about 8.4 mm/day compared to during DJF. In comparison with the baseline, mean total precipitation during JJA decreased by 0.02 mm/day. A higher decrease in precipitation was observed in the surroundings of Java (northern part of Australia) and Sulawesi. A large area including the continental region, northern part of Borneo, Bay of Bengal, Andaman Sea, and Philippine Sea experienced an increase in total precipitation of more than 2 mm/day, statistically significant at the 95% level (Figure 4.11).

In the B2 climate scenario, future mean precipitation was similar to the A2 climate scenario of 4.9 mm/day during DJF and 8.5 mm/day during JJA (Figure 4.10 and Appendix 4.2). The mean precipitation was observed to decrease by 0.3 mm/day during DJF and increase by 0.1 mm/day during JJA. The higher decrease in precipitation was also observed in the same areas as in the A2 climate scenario. During DJF, the decrease in total precipitation of less than -1 mm/day in a larger area in the South China Sea and the Celebes Sea, and a small area in the Philippine Sea were statistically significant at the 95% level (Figure 4.11). Similarly during JJA, the decrease of precipitation in a larger area between latitude –10°S and 10°N and the northern part of the South China Sea, was statistically significant at the 95% level.

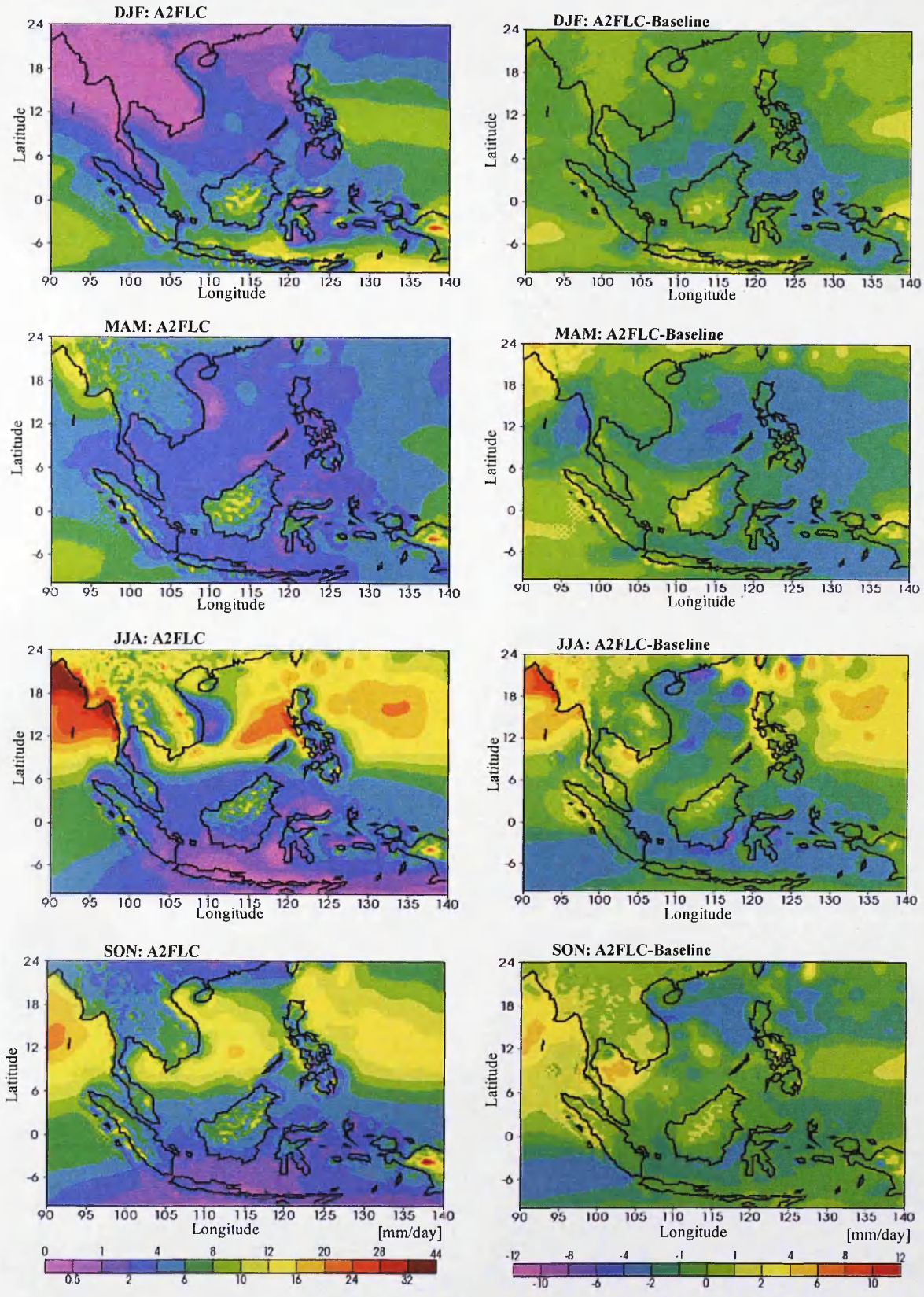

Figure 4.9: **SRES A2**: Combined effects of atmospheric and future landcover forcings on the seasonal total precipitation (A2FLC) in the SRES A2 scenario, and the precipitation difference in comparison with the Baseline scenario (A2FLC-Baseline).
(*Note: SRES A2- Special Report on Emission Scenario A2; FLC- Future Landcover*)

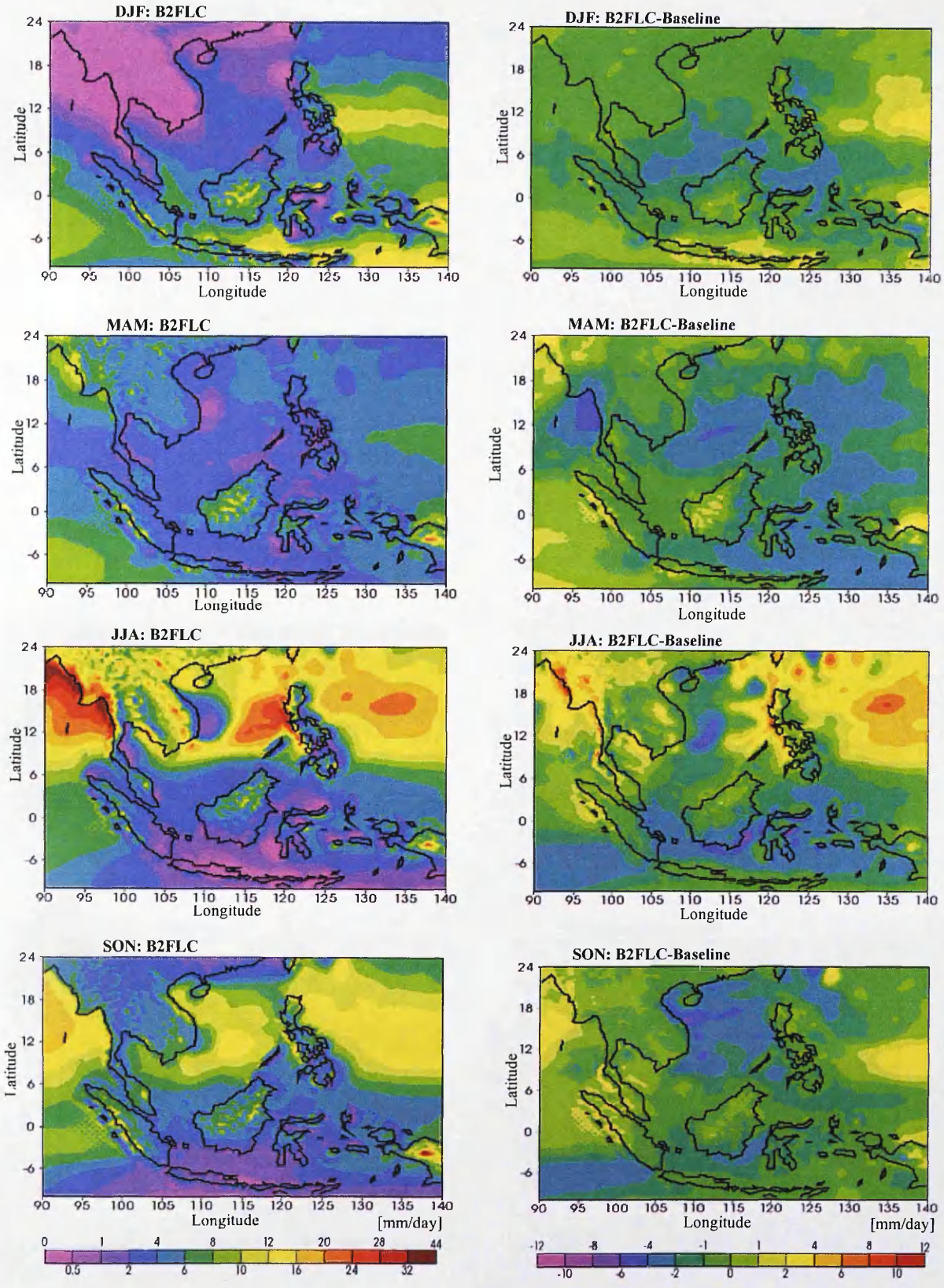

Figure 4.10: **SRES B2**: Combined effects of atmospheric and future landcover forcings on the seasonal total precipitation (B2FLC) in the SRES B2 scenario, and the precipitation difference in comparison with the Baseline scenario (B2FLC-Baseline).
(*Note: SRES B2- Special Report on Emission Scenario B2; FLC- Future Landcover*)

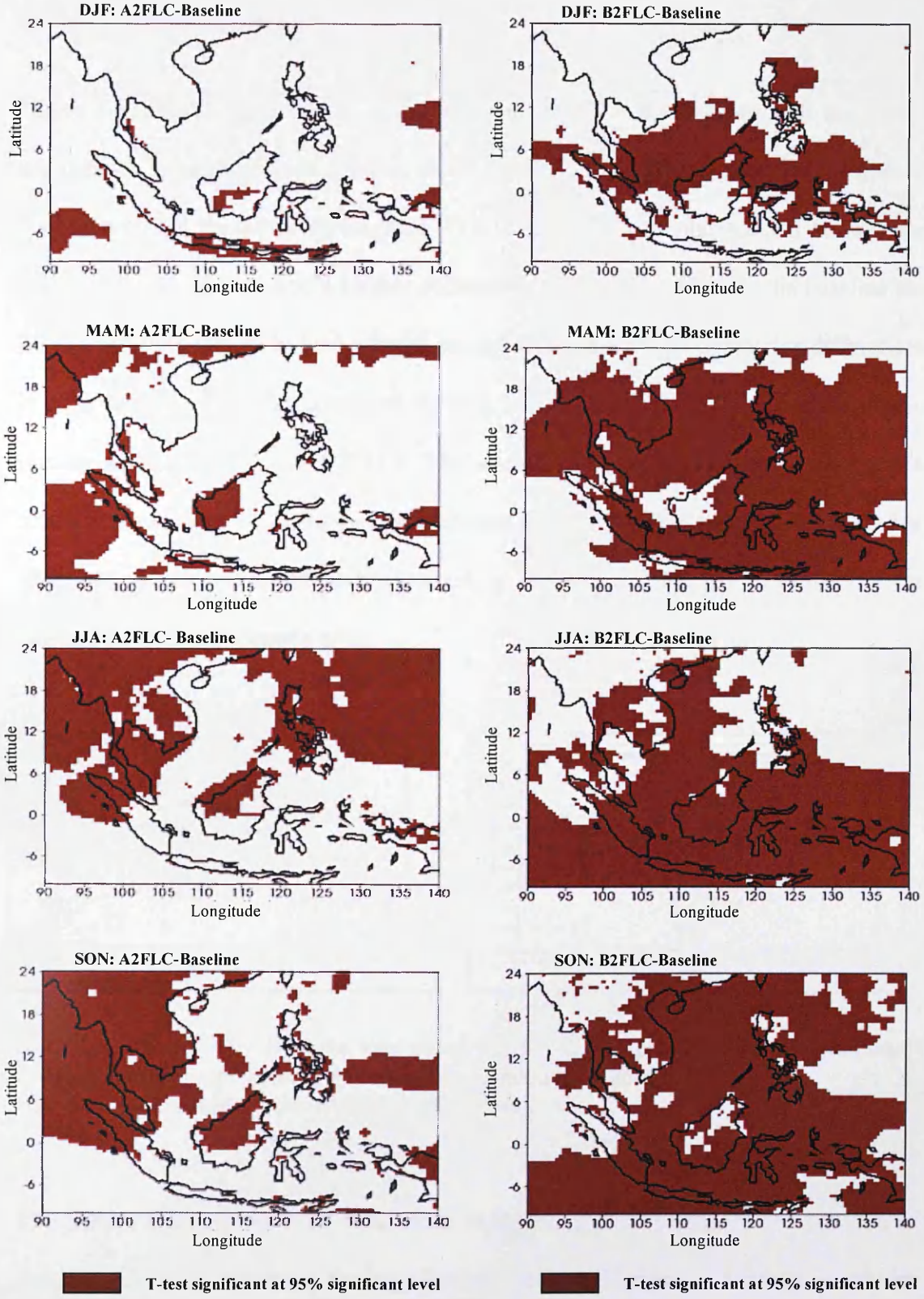

Figure 4.11: Significant t-test plots for the combined effects of atmospheric and future landcover forcing on the seasonal total precipitation for the A2 (A2FLC-Baseline) (*left panel*) and B2 (B2FLC-Baseline) (*right panel*) climate scenarios relative to the Baseline scenario.

(*Note: FLC- Future Landcover; PLC-Present-day Landcover*)

4.4.1.3 Total Cloud

Figure 4.12 shows the seasonal cycles of total cloud for the baseline and the future simulations for atmospheric forcing alone (A2PLC and B2PLC) and the combined atmospheric and landcover forcings (A2FLC and B2FLC) for the A2 and B2 climate scenario. The results showed a similar decrease in total cloud relative to the baseline for A2 and B2 simulations. In both climate scenarios, there were no distinctive differences in total cloud due to the combined forcing (A2FLC and B2FLC) and atmospheric forcing alone (A2PLC and B2PLC). The overall change in cloud cover is a much stronger signal than the change in precipitation discussed above (Section 4.4.1.2). The effect of alndcover on future total cloud is very small, and not sensitive to the atmospheric forcing scenario used.

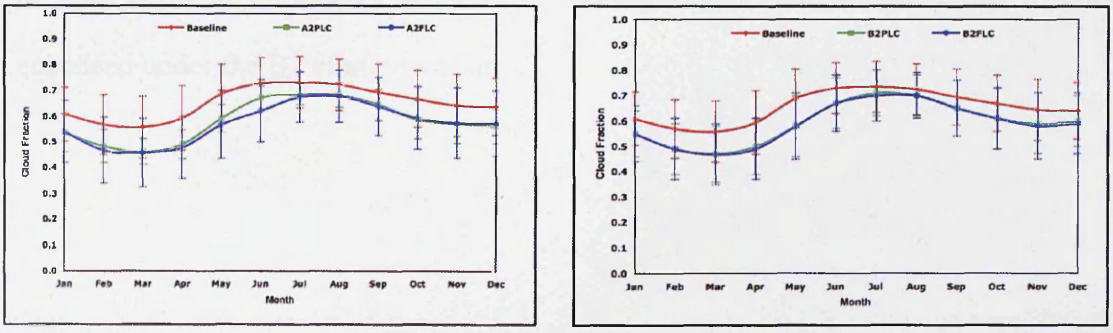

Figure 4.12: Seasonal cycle of the total cloud for the A2 (*left panel*) and B2 (*right panel*) climate scenarios in the present-day and future landcover scenarios.
(*Note: FLC- Future Landcover; PLC-Present-day Landcover*)

The pattern and magnitude of total cloud changes for each season in the A2 climate scenario due to the combined forcing of atmospheric and landcover forcings are shown in Figure 4.13. The combined forcing was observed to decrease future total cloud fraction to 0.5, a decrease of about 0.08 during DJF (Appendix 4.1). The decrease in total cloud was observed largely in the South China Sea and the Celebes Sea regions.

Statistically, the future changes in total cloud in the region during DJF showed no significant difference relative to the baseline scenario (Figure 4.15). During JJA, the future total cloud was 0.7, a decrease of about 0.06. The increase in total cloud of more than 0.02 in some areas in the Indian Ocean, South China Sea, and Pacific Ocean were observed to be statistically significant at the 95% confidence level (Figure 4.15).

In the B2 climate scenario, the future mean total clouds were similar to the A2 climate scenario of 0.6 during DJF and 0.7 during JJA (Figure 4.15 and Appendix 4.2). The changes of future mean total clouds due to combined forcing were observed to decrease by 0.07 during DJF and 0.05 during JJA. During DJF, the increase in total cloud of more than 0.02 in a small area in the west Pacific Ocean, was statistically significant at the 95% level (Figure 4.15). During JJA, significant increases (at 95% level) of total cloud in some areas in the Indian Ocean, South China Sea and Pacific Ocean were further enhanced under the B2 climate scenario.

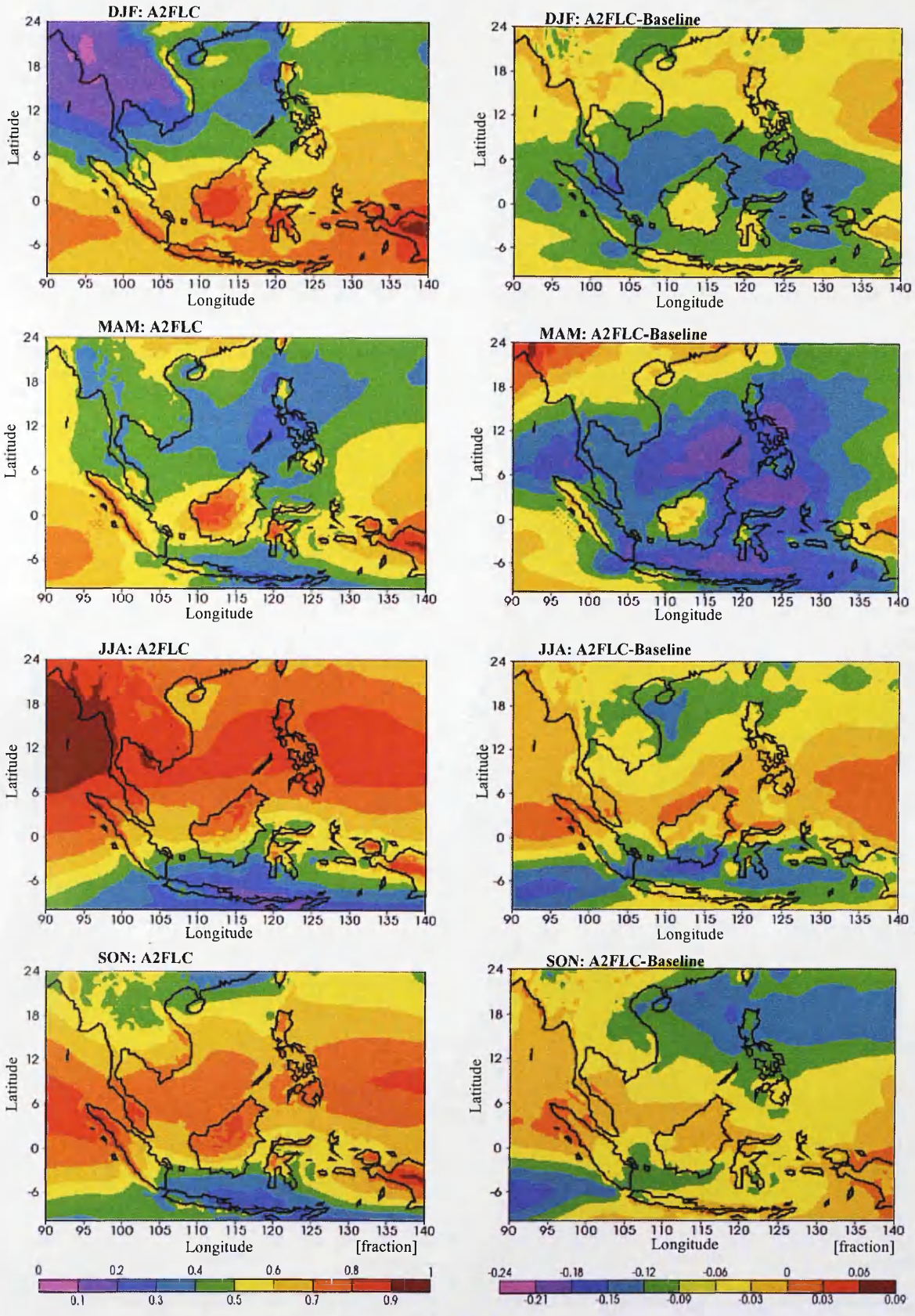

Figure 4.13: **SRES A2**: Combined effects of atmospheric and future landcover forcings on the seasonal total cloud (A2FLC) in the SRES A2 scenario, and the total cloud difference in comparison with the Baseline scenario (A2FLC-Baseline).
(*Note: SRES A2- Special Report on Emission Scenario A2; FLC- Future Landcover*)

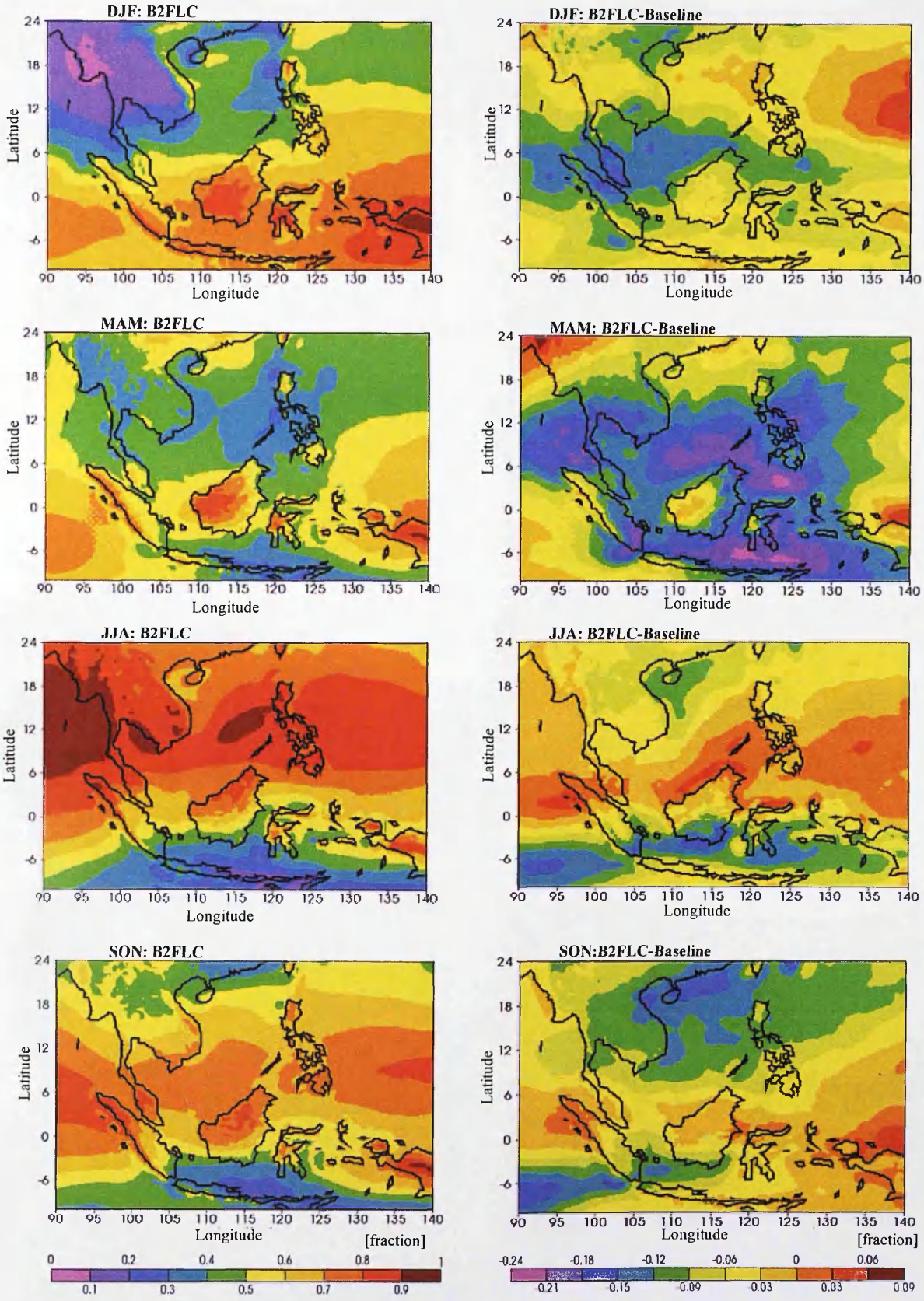

Figure 4.14: SRES B2: Combined effects of atmospheric and future landcover forcings on the seasonal total cloud (B2FLC) in the SRES B2 scenario, and the total cloud difference in comparison with the Baseline scenario (B2FLC-Baseline).

(*Note: SRES B2- Special Report on Emission Scenario B2; FLC- Future Landcover*)

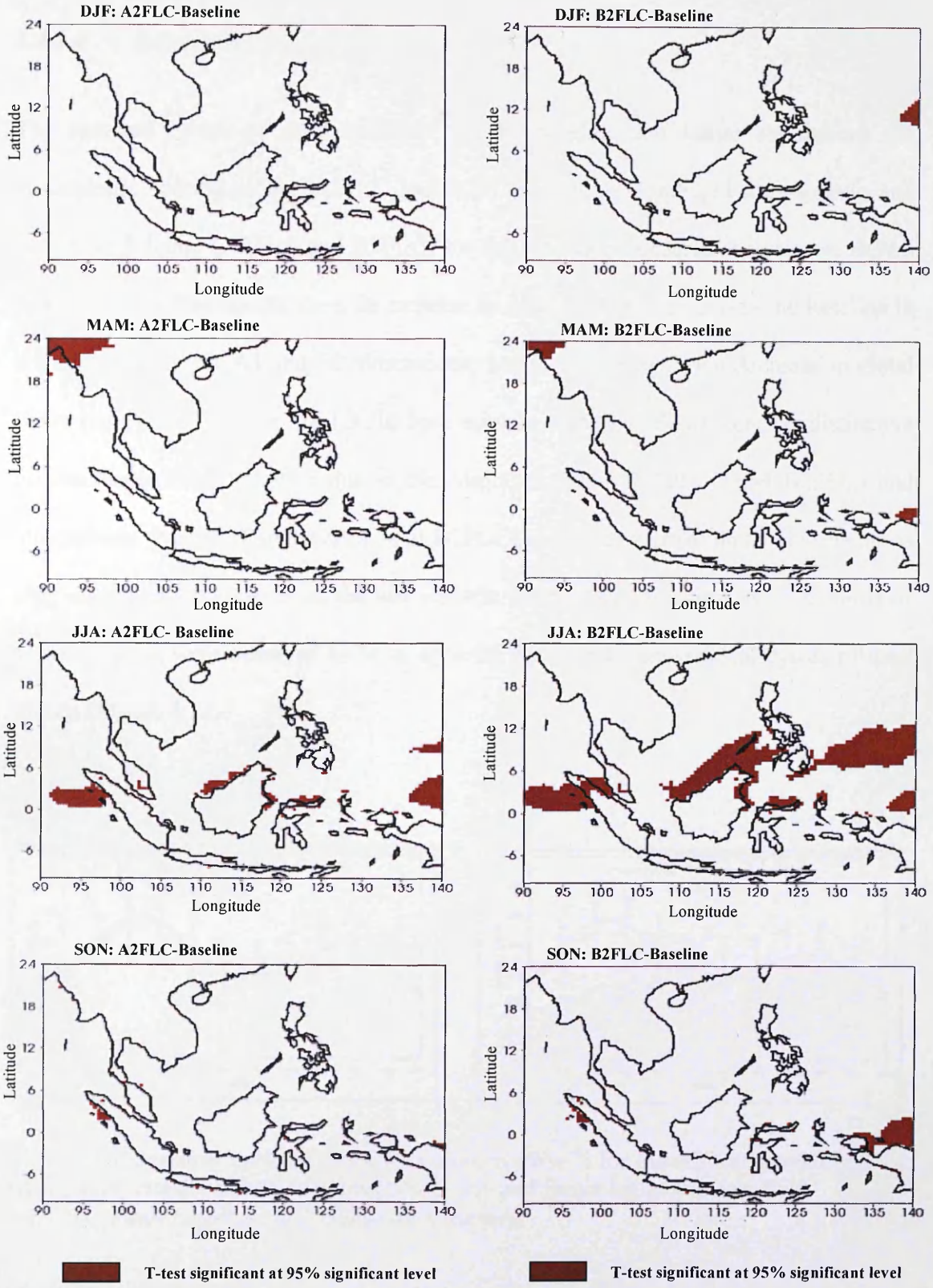

Figure 4.15: Significant t-test plots for the combined effects of atmospheric and future landcover forcings on the total cloud for the A2 (A2FLC-Baseline) (*left panel*) and B2 (B2FLC-Baseline) (*right panel*) climate scenarios relative to the Baseline scenario.
(*Note: FLC- Future Landcover; PLC-Present-day Landcover*)

4.4.1.4 Solar radiation

The seasonal cycles of solar radiation for the baseline and future simulations for atmospheric forcing alone (A2PLC and B2PLC) and the combined atmospheric and landcover forcings (A2FLC and B2FLC) for the A2 and B2 climate scenario are shown in Figure 4.16. The results show an increase in solar radiation relative to the baseline in a similar pattern for A2 and B2 simulations, and consistent with the decrease in cloud cover reported in Section 4.4.1.3. In both climate scenarios, there were no distinctive differences in solar radiation due to the combined forcing (A2FLC and B2FLC) and atmospheric forcing alone (A2PLC and B2PLC) and the effect of alndcover change is only marginally dependent on the atmospheric forcing. The seasonal cycle patterns of solar radiation were observed to be in opposite cycles with the seasonal cycles of total clouds (Figure 4.12).

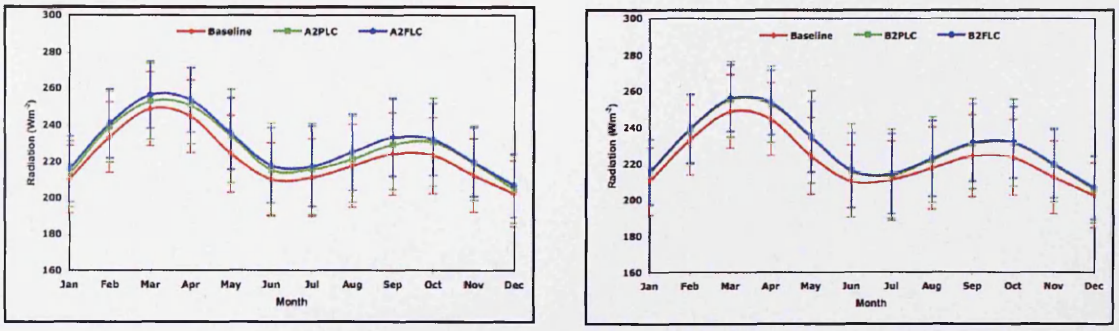

Figure 4.16: Seasonal cycle of the solar radiation (Wm^{-2}) for the A2 (*left panel*) and B2 (*right panel*) climate scenarios in the present-day and future landcover scenarios.
(*Note: FLC- Future Landcover; PLC-Present-day Landcover*)

The pattern and magnitude of solar radiation changes for each season in the A2 climate scenario due to the combined forcings are shown in Figure 4.17. The combined forcing resulted in increased solar radiation to about 221 Wm^{-2} during DJF, an increase of about

6 Wm^{-2} (Appendix 4.1). Meanwhile, during JJA, solar radiation increased to about 220 Wm^{-2}, an increase of 7 Wm^{-2} from the baseline scenario. In the B2 climate scenario, future solar radiations also increased to about 220 Wm^{-2} during DJF and 218 Wm^{-2} during JJA, an increase of 5 Wm^{-2} and 4.3 Wm^{-2} respectively (Figure 4.18 and Appendix 4.2). In both scenarios, a significant (at 95% level) decrease in solar radiation over west Pacific Ocean was observed during JJA. However, during DJF, only small areas were found to be statistically significant at the 95% confidence level (Figure 4.19).

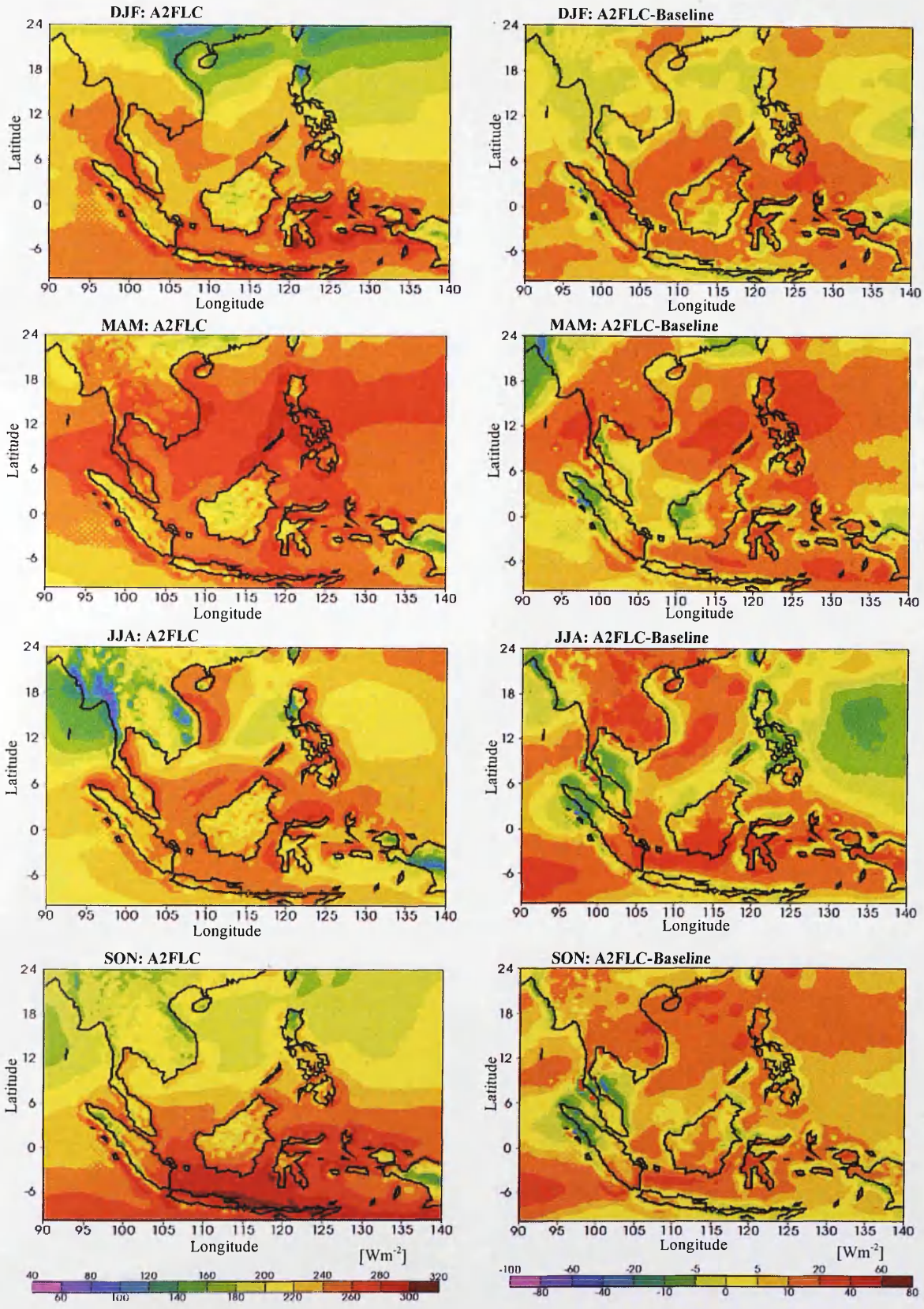

Figure 4.17: **SRES A2**: Combined effects of atmospheric and future landcover forcings on the seasonal solar radiation (A2FLC) in the SRES A2 scenario, and the solar radiation difference in comparison with the Baseline scenario (A2FLC-Baseline).
(*Note: SRES A2- Special Report on Emission Scenario A2; FLC- Future Landcover*)

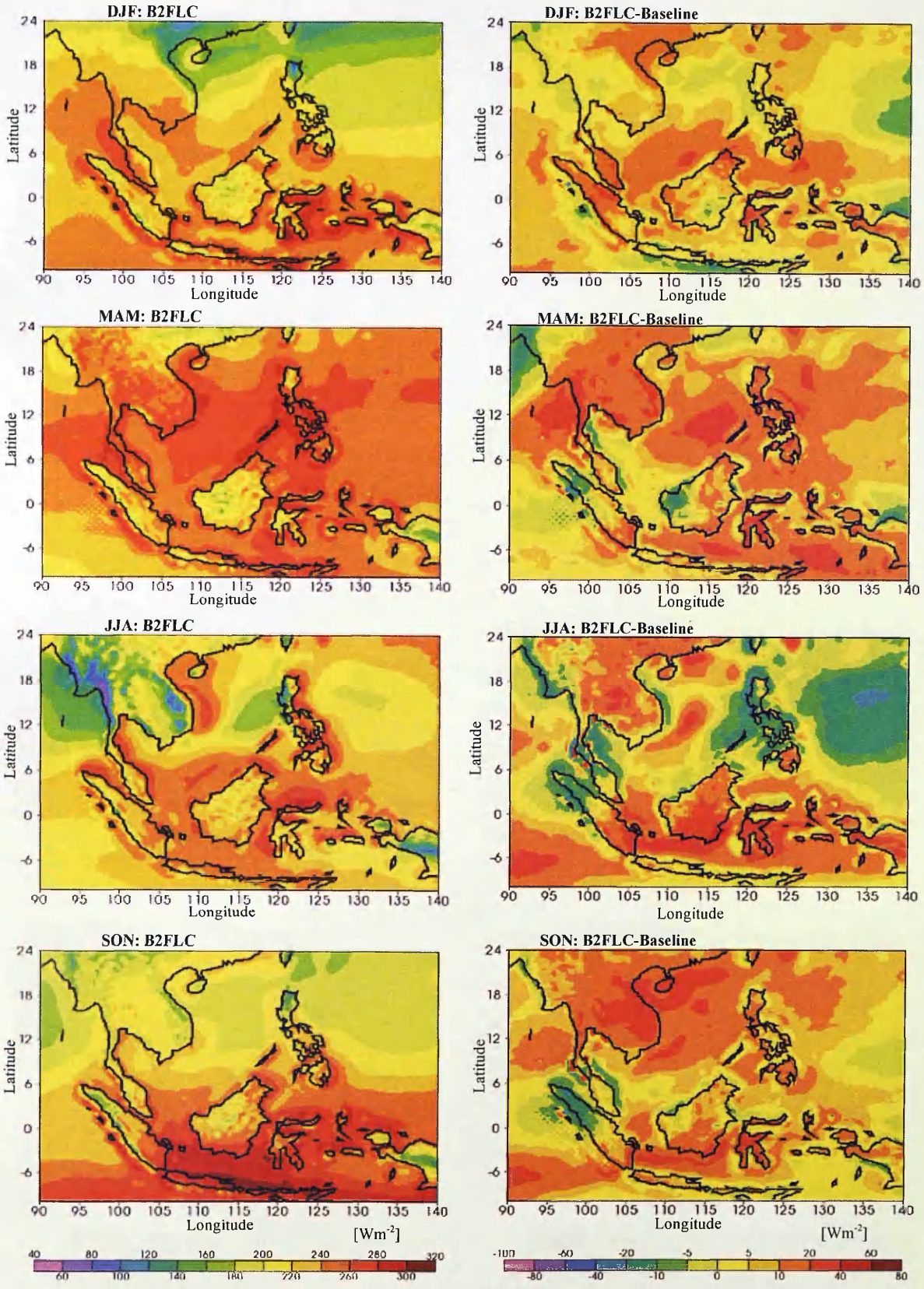

Figure 4.18: **SRES B2**: Combined effects of atmospheric and future landcover forcings on the seasonal solar radiation (B2FLC) in the SRES B2 scenario, and the solar radiation difference in comparison with the Baseline scenario (B2FLC-Baseline).
(*Note: SRES B2- Special Report on Emission Scenario B2; FLC- Future Landcover*)

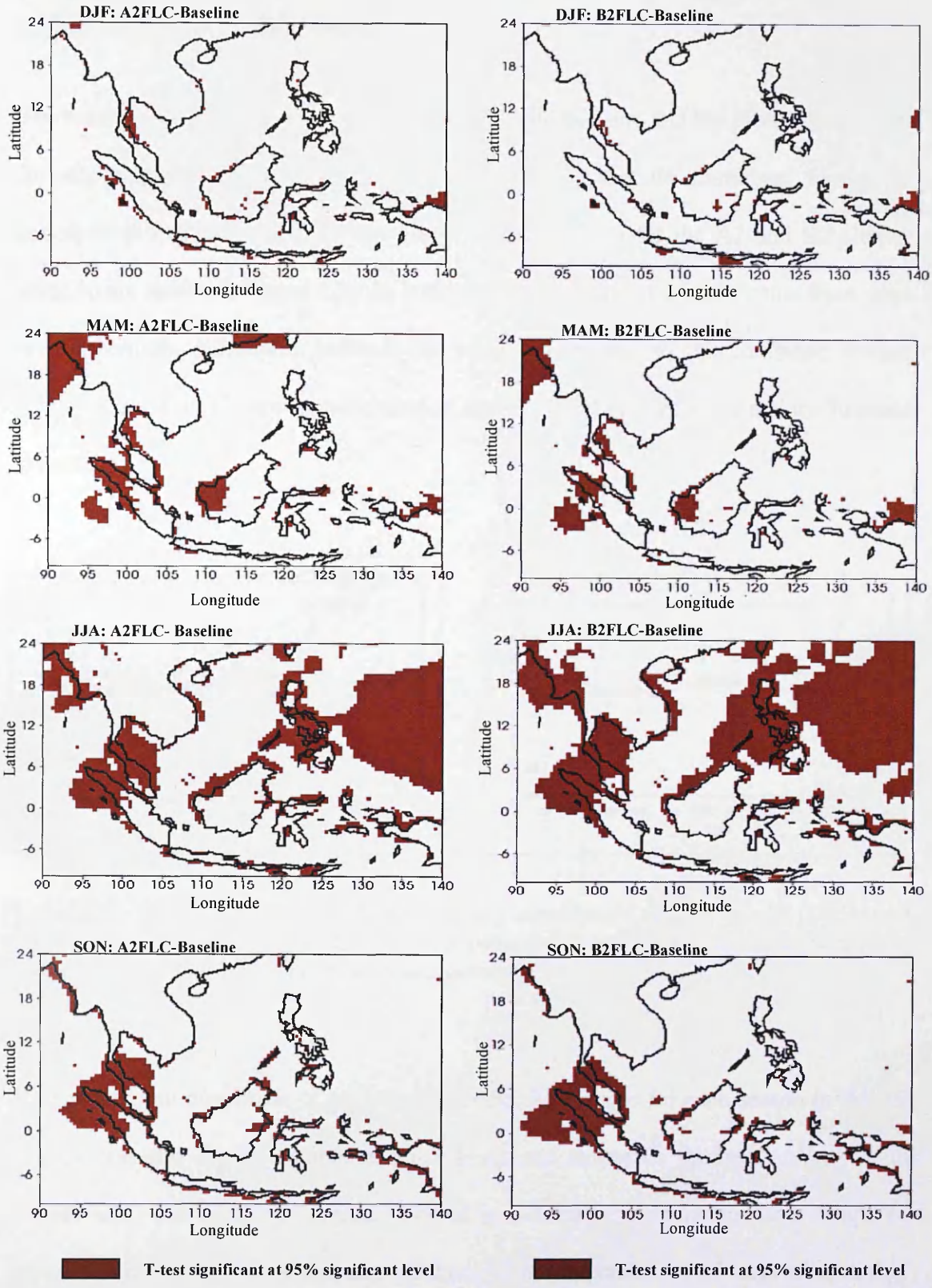

Figure 4.19: Significant t-test plots for the combined effects of atmospheric and future landcover forcings on the solar radiation for the A2 (A2FLC-Baseline) (*left panel*) and B2 (B2FLC-Baseline) (*right panel*) climate scenarios relative the Baseline scenario.
(*Note: FLC- Future Landcover; PLC-Present-day Landcover*)

4.4.1.5 Boundary layer height

The seasonal cycles of boundary layer height for the baseline and the future simulations for atmospheric forcing alone (A2PLC and B2PLC) and the combined forcing of atmospheric and landcover forcings (A2FLC and B2FLC) for the A2 and B2 climate scenario are shown in Figure 4.20. In both climate scenarios, it is evident that there were few discernible differences between the mean effects due to the combined forcing (A2FLC and B2FLC), atmospheric forcing alone (A2PLC and B2PLC) and the baseline scenario.

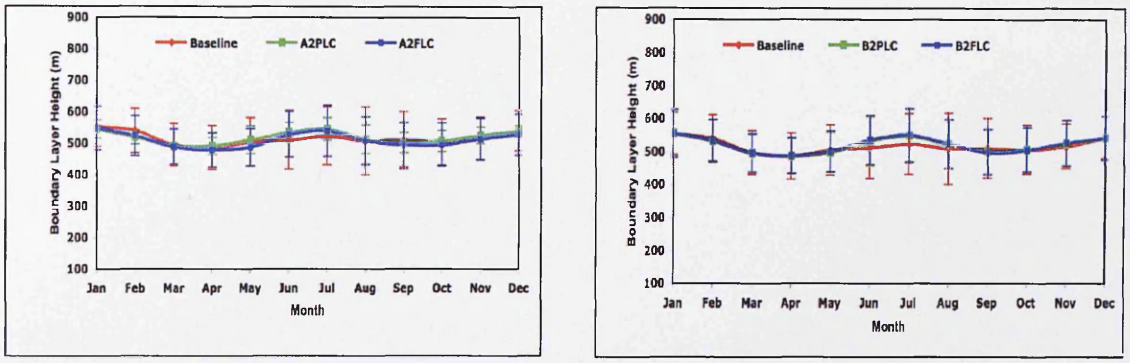

Figure 4.20: Seasonal cycle of the total boundary layer height (m) for the A2 (*left panel*) and B2 (*right panel*) climate scenarios in the present-day and future landcover scenarios. (*Note: FLC- Future Landcover; PLC-Present-day Landcover*)

The pattern and magnitude of boundary layer height changes for each season in the A2 climate scenario due to combined atmospheric and landcover forcings are shown in Figure 4.21. The combined forcing resulted in a decrease in boundary layer height to about 534 m during DJF, a decrease of about 11 m (Appendix 4.1). Meanwhile, during JJA, the boundary layer height was increased to about 526 m, an increase of 11 m from the baseline scenario. In both seasons, the increase in boundary layer height was observed over land, mainly in central Thailand and western Sumatra and southern

Borneo (Figure 4.21). Areas where changes in boundary layer height were less than -30 m in both seasons were statistically significant at the 95% level (Figure 4.23). These areas mostly occurred over the sea, suggesting that synoptic-scale changes in weather pattern, and hence boundary layer height, are more significant than local-scale changes driven directly by landcover change and surface energy balance changes.

In the B2 climate scenario, under the influence of the combined forcing, the boundary layer decreased to about 543 m during DJF and increased to about 536 m during JJA (Figure 4.22 and Appendix 4.6). In both seasons, areas where changes in boundary layer height were less than -30 m were statistically significant at the 95% level (Figure 4.23). These areas were relatively smaller in coverage than in the A2 climate scenario.

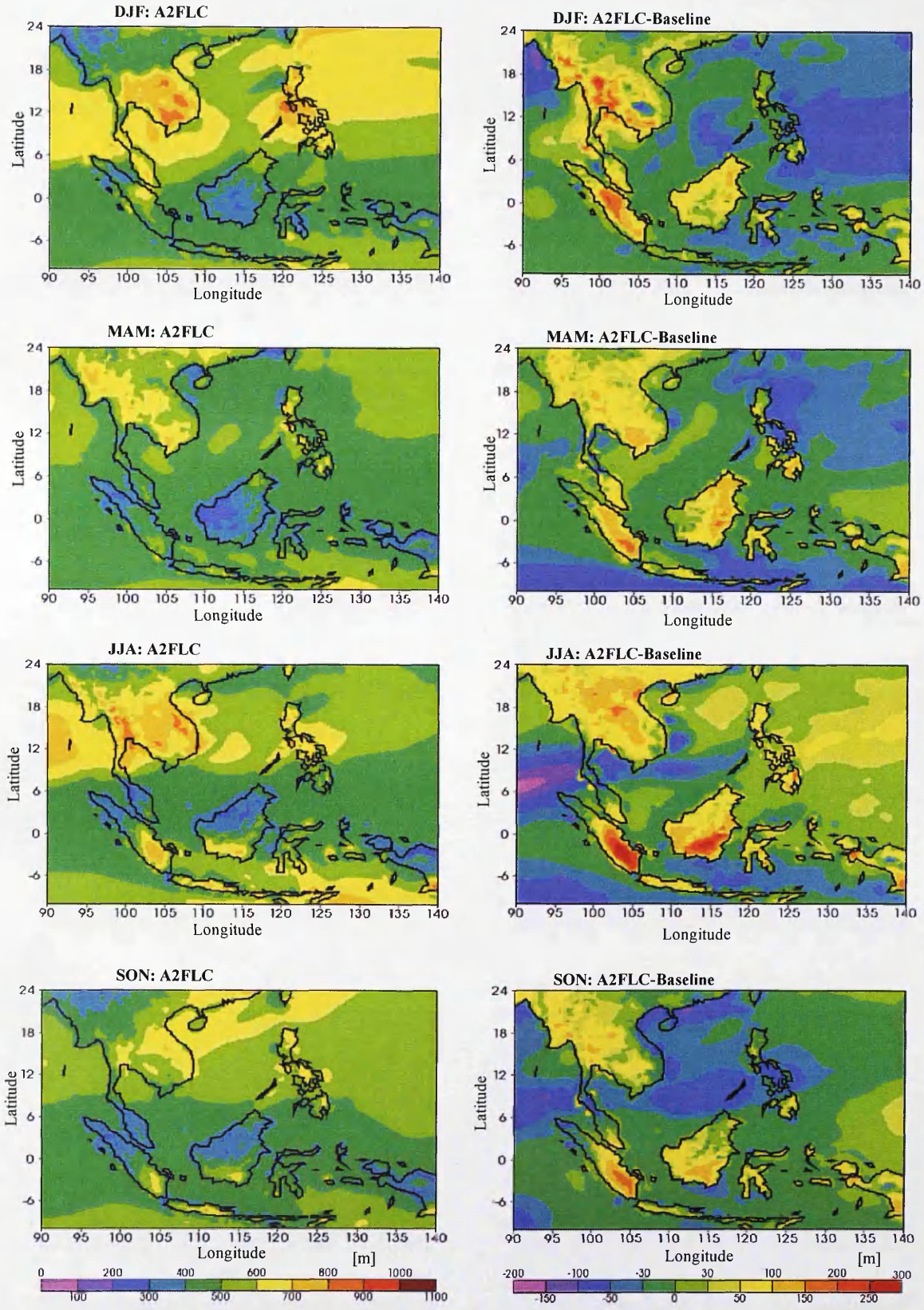

Figure 4.21: **SRES A2**: Combined effects of atmospheric and future landcover forcings on the seasonal boundary layer height (A2FLC) in the SRES A2 scenario, and the boundary layer height difference in comparison with the baseline scenario (A2FLC-Baseline).

(*Note: SRES A2- Special Report on Emission Scenario A2; FLC- Future Landcover*)

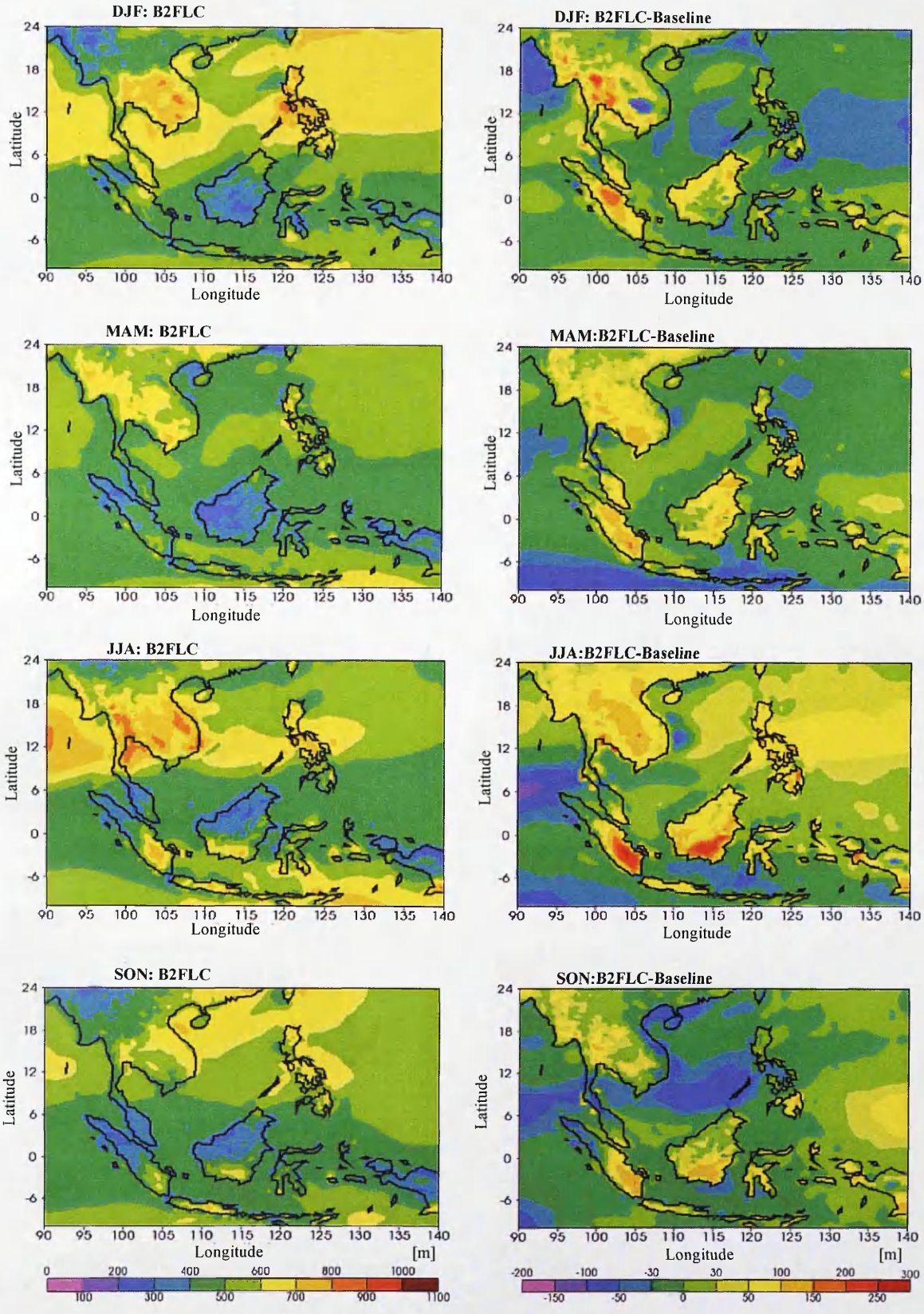

Figure 4.22: **SRES B2**: Combined effects of atmospheric and future landcover forcings on the seasonal boundary layer height (B2FLC) in the SRES B2 scenario, and the boundary layer height difference in comparison with the baseline scenario (B2FLC-Baseline).
(*Note: SRES B2- Special Report on Emission Scenario B2; FLC- Future Landcover*)

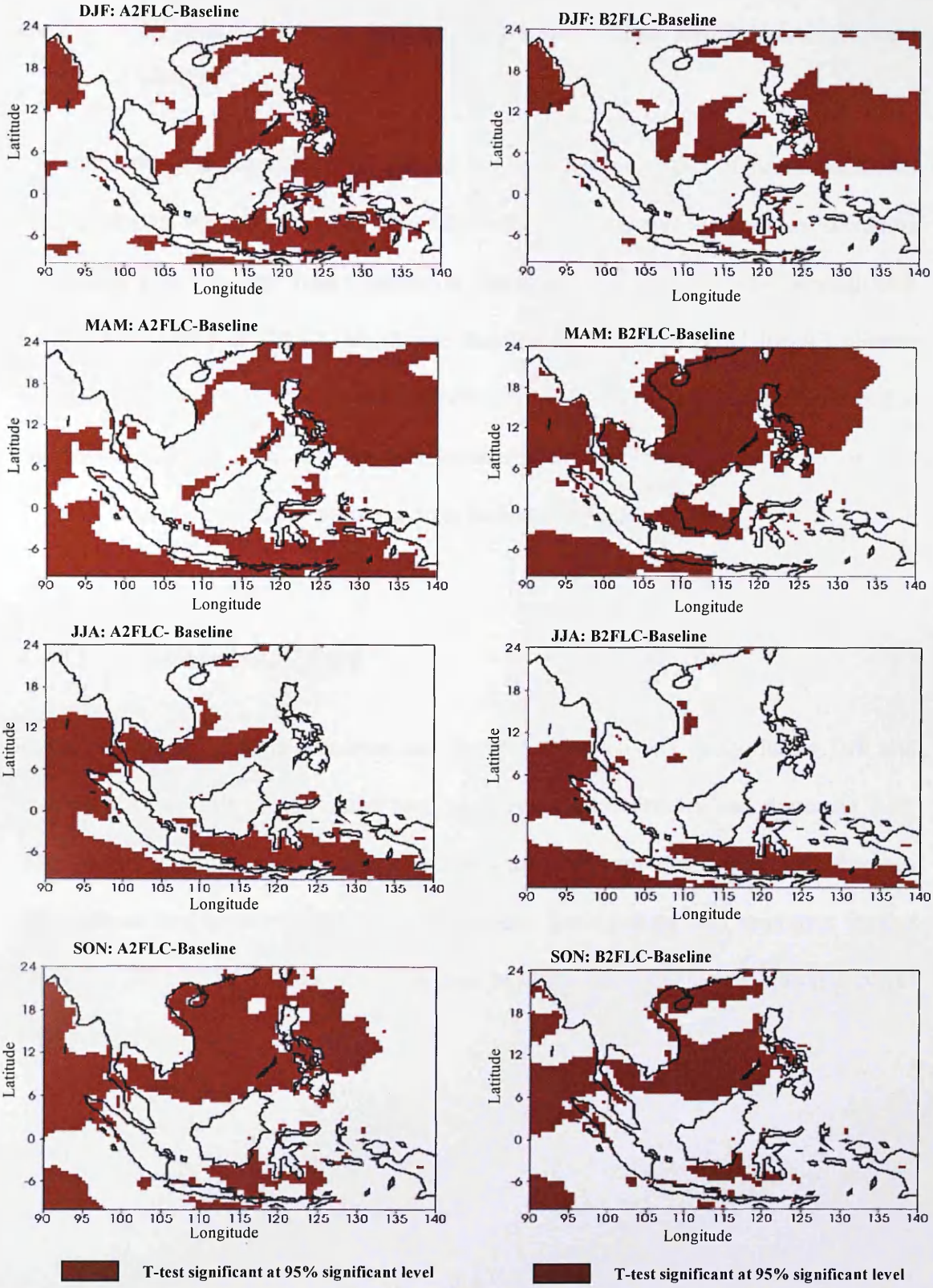

Figure 4.23: Significant t-test plots for the combined effects of atmospheric and future landcover forcings on the boundary layer height for the A2 (A2FLC-Baseline) (*left panel*) and B2 (B2FLC-Baseline) (*right panel*) climate scenarios relative to Baseline scenario.
(*Note: FLC- Future Landcover; PLC-Present-day Landcover*)

4.4.2 Impacts of Future Landcover Forcing Alone on Regional Climate Changes

To isolate the effects produced by forcing due to the modification of future landcover (FLC), results are presented as the difference between the all-forcings scenarios (atmospheric forcing and future landcover forcing) and the atmospheric forcing with present-day landcover (PLC), which are denoted as A2FLC-A2PLC for A2 climate scenario and B2FLC-B2PLC for B2 climate scenario. Since we cannot be sure that landcover effects on climate are independent of atmospheric forcing (see Section 4.4.1.1), what follows is a tentative and preliminary analysis.

4.4.2.1 Surface temperature

In the A2 and B2 climate scenarios, the impacts of landcover forcing during DJF and JJA were very small and produced cooling effects (Appendix 4.1 and Appendix 4.2). The differences in mean surface temperature between the combined forcings (atmospheric and landcover forcings), atmospheric forcing alone, and landcover forcing alone for A2 and B2 climate scenarios also becomes apparent in the seasonal cycles shown in Figure 4.24.

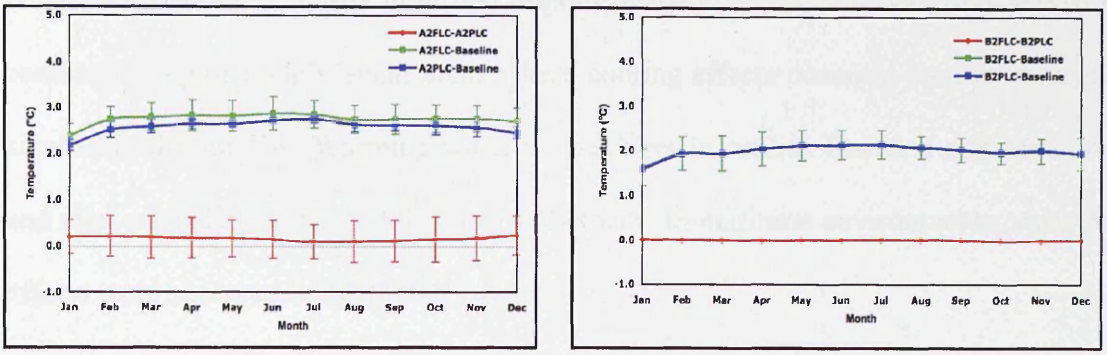

Figure 4.24: Seasonal cycle of surface temperature (°C) for the A2 (*left panel*) and B2 (*right panel*) climate scenarios due to the landcover forcing alone (A2FLC-A2PLC & B2FLC-B2PLC) and the temperature changes (A2FLC-Baseline; A2PLC-Baseline & B2FLC-Baseline; B2PLC-Baseline) in the present-day and future landcover scenarios. (*Note: FLC- Future Landcover; PLC-Present-day Landcover*)

In terms of the magnitude of surface temperature changes, the perturbation of future landcover in SEA, mainly due to conversion of forested land into agriculture under the A2 and B2 climate scenarios, is relatively small compared to changes due to atmospheric forcing alone (see Chapter 3). However, the small domain-mean figure masks larger changes in some regions. In the A2 climate scenario, the impact of landcover forcing alone resulted in surface temperature changes in the range of -1.5°C to 1.7°C during DJF and -1.8°C to 1.2°C during JJA (Figure 4.25). Based on the regional mean surface temperatures, landcover forcing alone produced a cooling effect in all seasons of -0.07°C during DJF and -0.13°C during JJA (Appendix 4.1). During DJF, the largest warming was observed in central Thailand and Myanmar, where the agricultural areas (mainly paddy) have been expanded. Warming was also observed in maritime environments, particularly in the South China Sea, presumably the results of teleconnection to continental areas for which landcover has been changed or synoptic-scale modification to circulation patterns. Areas where the mean surface temperature was less than -1°C, were statistically significant (95% level) during DJF, except areas in higher latitudes (e.g. the southern part of China) (Figure 4.25). During JJA, cooling

effects were observed mostly in insular regions, while warming effects were observed in continental regions. Only small areas where cooling effects occurred were statistically significant during JJA. Warming was still prevalent in central Thailand and Myanmar and also expanded to the middle part of Vietnam. In maritime environments, warming effects were observed in the Indian Ocean.

Under the B2 climate scenario, the impact of landcover forcing alone resulted in changes in surface temperature in the range of -1.2°C to 1.5°C during DJF and -1.5°C to 2.5°C during JJA (Figure 4.26). Similar to the A2 climate scenario, landcover forcing alone produced cooling effects in all seasons with a mean surface temperature of -0.11°C during DJF and -0.09°C during JJA. In all seasons, warming was observed in maritime environments, mostly in the South China Sea and Indian Ocean. A slightly larger total area compared to the A2 climate scenario had statistically significant surface temperature during DJF and JJA (Figure 4.26).

Relatively, the expansion of agricultural land in the future landcover scenario over SEA has resulted in cooling effects in both climate scenarios. A modelling study on global climate sensitivity due to tropical deforestation by McGuffie *et al.* (1995) also concluded that conversion of tropical forest into grassland (over a six year experiment) has decreased the surface temperature significantly by -0.7 K over Sumatra, Java, and Borneo. Modification of atmospheric circulation patterns over deforested tropical regions and disturbance of the Asian Monsoon were suggested as important factors in the decrease of surface temperature under a modified landcover scenario.

In recent studies (Polchar and Laval, 1993; Henderson-Sellers *et al.*, 1993; Feddema *et al.* 2005) in the Indonesian region, the expansion of agricultural land in the future

landcover scenario was found to have little impact on the future surface temperature in both A2 and B2 climate scenarios. Based on a multiple scale analysis, the Asian Monsoon circulation in the maritime environment (e.g. around Malaysia, Indonesia, Philippines, Brunei, Singapore, and Timor Leste) was found to be more sensitive to landcover changes than the continental environment (van der Molen, 2006). Landcover changes stimulate changes in the surface energy balance, thus developing meso-scale circulations due to the contrast in heating properties of land and sea (sea breeze circulation) or of forest and agricultural land (forest breeze circulation). These meso-scale circulations are known to be very effective in transporting heat and moisture to higher levels of the atmosphere, depending on the amount of sensible heat released at the surface. In maritime environments, the increase in moisture from a circulation change leads to an increase of evaporation, thereby compensating for decreases in latent heat flux by transpiration (Feddema *et al.*, 2005).

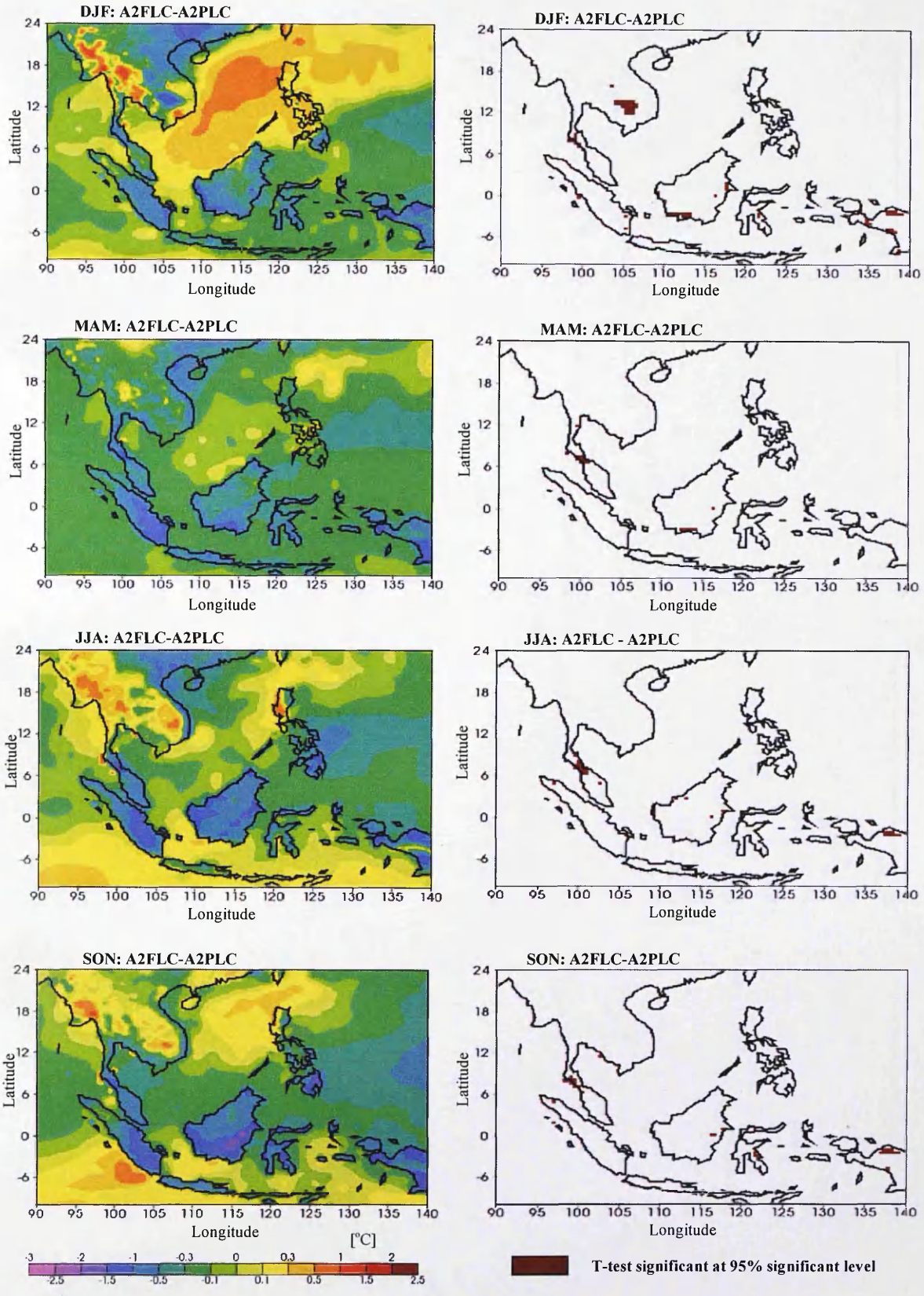

Figure 4.25: **SRES A2**: Isolated effects of the future landcover forcing alone on the seasonal surface temperature (A2FLC-A2PLC) (*left panel*) in the SRES A2 scenario, and the significant t-test plots (*right panel*).
(*Note: FLC- Future Landcover; PLC-Present-day Landcover*)

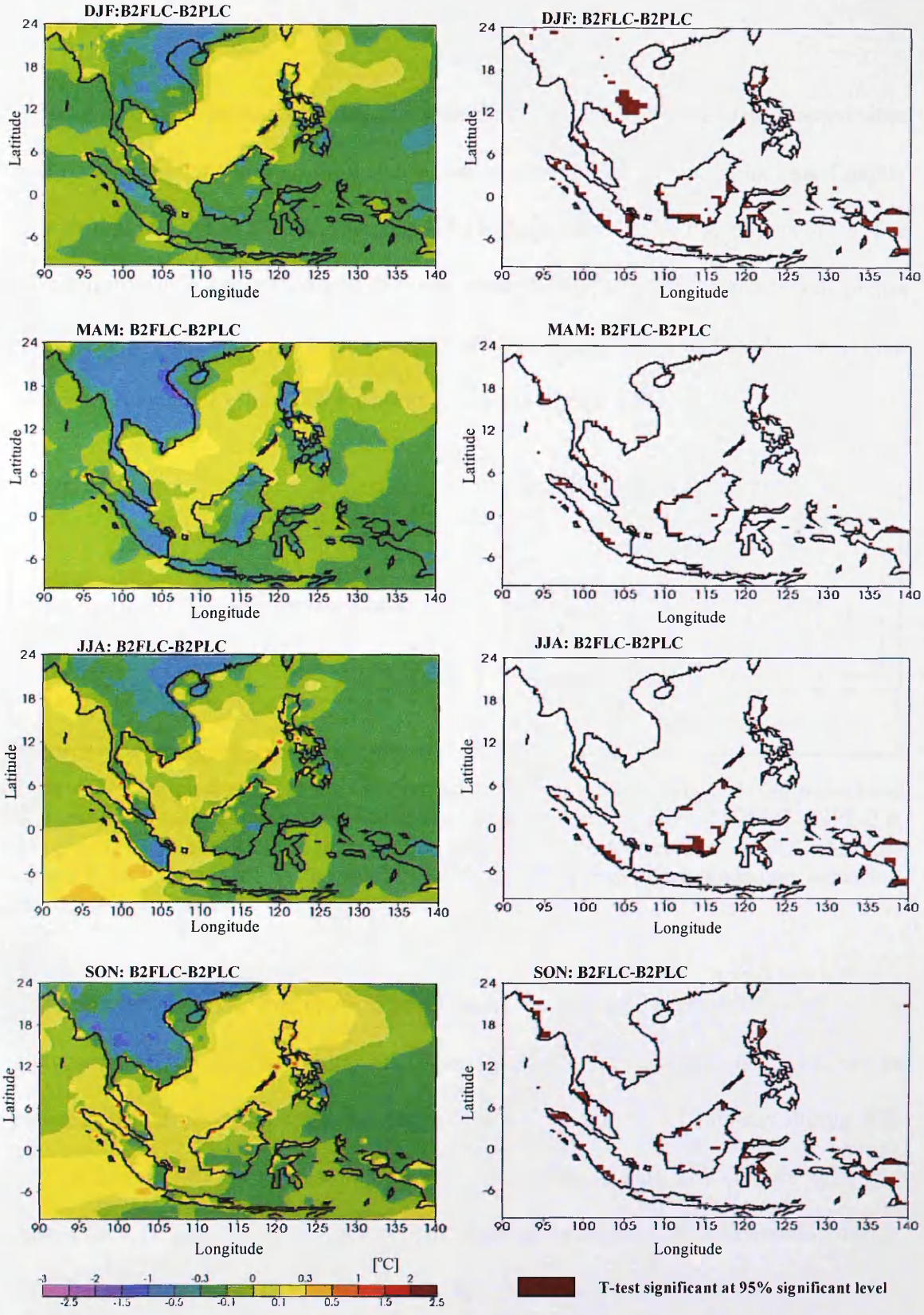

Figure 4.26: **SRES B2**: Isolated effects of future landcover forcing alone on the seasonal surface temperature (B2FLC-B2PLC) (*left panel*) in the SRES B2 scenario, and the significant t-test plot (*right panel*).
(*Note: FLC- Future Landcover; PLC-Present-day Landcover*)

4.4.2.2 Total precipitation

In the A2 and B2 climate scenarios, the impacts of landcover forcing in all seasons were relatively small compared to the impacts due to atmospheric forcing alone (see Chapter 3) and combined forcing (see Section 4.4.1) (Appendix 4.1 and Appendix 4.2). The seasonal cycles of the differences in mean precipitation between the combined forcing (atmospheric and landcover forcings), atmospheric forcing alone and landcover forcing alone for A2 and B2 climate scenarios are shown in Figure 4.27.

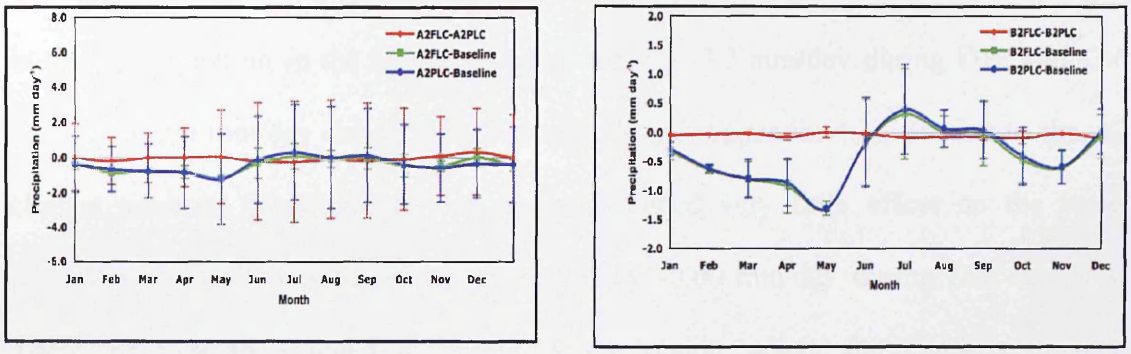

Figure 4.27: Seasonal cycle of the total precipitation (mm/day) for the A2 (*left panel*) and B2 (*right panel*) climate scenarios due to the landcover forcing alone (A2FLC-A2PLC & B2FLC-B2PLC), and the total precipitation changes (A2FLC-Baseline; A2PLC-Baseline & B2FLC-Baseline; B2PLC-Baseline) in the present-day and future landcover scenarios. (*Note: FLC- Future Landcover; PLC-Present-day Landcover*)

The impacts of future landcover forcing alone on regional precipitation due to the conversion of forested land into agriculture in A2 climate scenarios have resulted in changes in total precipitation in the range of -3.7 mm/day to 4.3 mm/day during DJF and in a large range of -16.1 mm/day to 7.5 mm/day during JJA (Figure 4.28 and Appendix 4.1). The mean precipitation was observed to increase by 0.03 mm/day during DJF and decrease by -0.29 mm/day during JJA. The total precipitation was significantly decreased (95% significant level) in regions with changes less than -2 mm/day over the Philippine Sea (the west Pacific Ocean) during DJF and over a larger area with changes

in the range of 0 mm/day to -8 mm/day during JJA (Figure 4.28). In both seasons, total precipitation increased over most converted forested land but was not statistically significant except on the southern part of Sumatra and some areas on the eastern part of Borneo during JJA. An earlier study by McGuffie *et al.* (1995) during JJA (in the month of June) observed a significant increase of total precipitation over the east of the Phillipines, but the increase of total precipitation in this study was not found to be significant.

Under the B2 climate scenario, the impact of landcover forcing alone resulted in changes in total precipitation in the range of -2.3 mm/day to 3.3 mm/day during DJF and -3.6 mm/day to 2.8 mm/day during JJA (Figure 4.29 and Appendix 4.2). Similar to the A2 climate scenario, landcover forcing alone produced very little effect on the mean precipitation in all seasons, which decreased by -0.06 mm/day during DJF and JJA. There were small isolated areas across the region where the changes in total precipitation due to landcover forcing alone were statistically significant at the 95% confidence level during DJF (Figure 4.29). Total precipitation changes over most converted forested land were not statistically significant. However, during JJA, larger areas: were found to be statistically significant at the 95% level over the land where conversion of forested land into agriculture and other types of landcover took place (Sumatra, Borneo, Sulawesi, Irian Jaya, and continental SEA) as well as Indian Ocean, Andaman Sea, South China Sea, Celebes Sea, Philippines Sea, and the west Pacific Ocean with changes more negative than -0.1 mm/day. An increase in precipitation of more than 0.5 mm/day over the northern part of the South China Sea and Philippine Sea was observed but was not statistically significant.

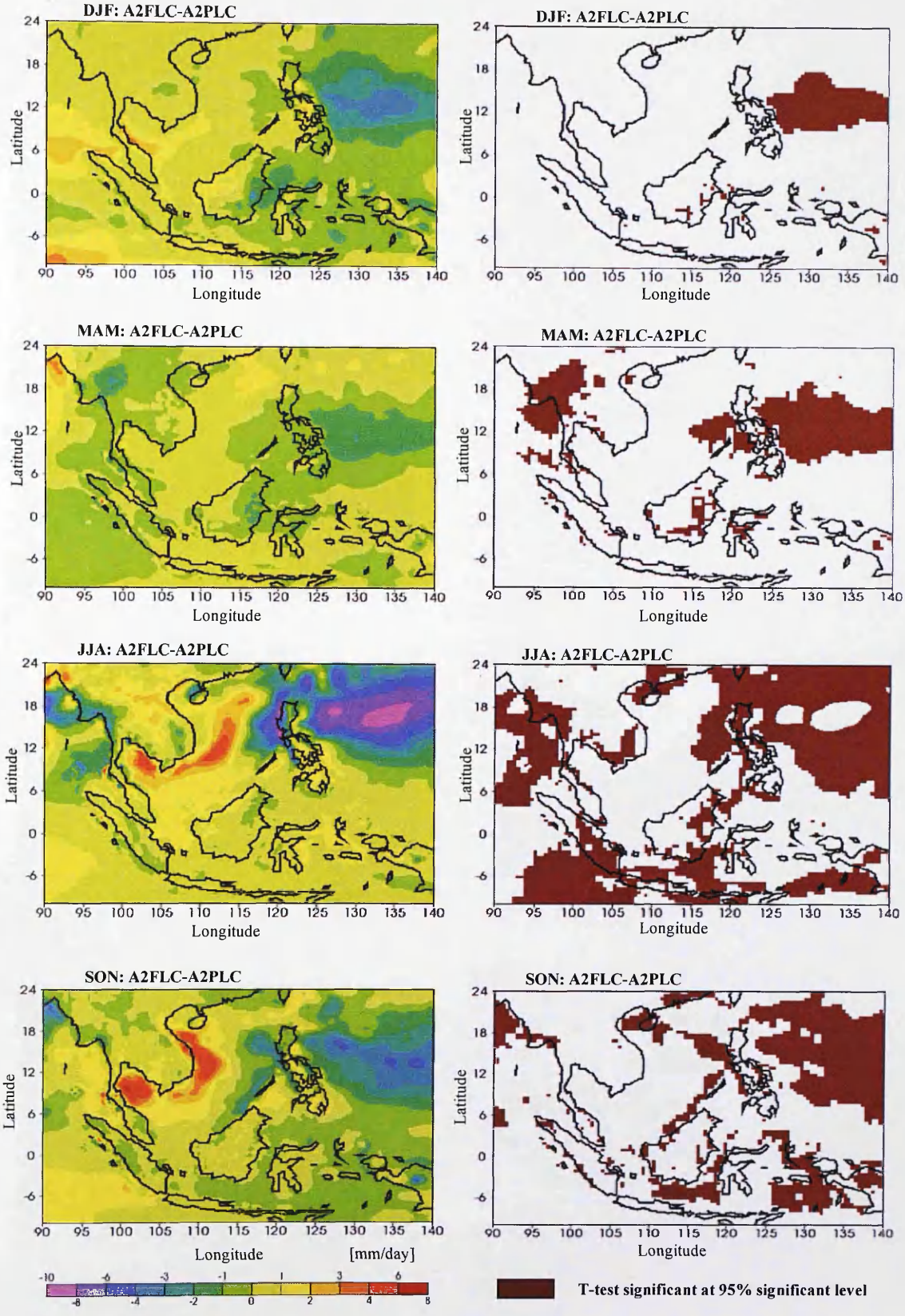

Figure 4.28: **SRES A2**: Isolated effects of the future landcover forcing alone on the seasonal total precipitation (A2FLC-A2PLC) (*left panel*) in the SRES A2 scenario, and the significant t-test plots (*right panel*).

(*Note: FLC- Future Landcover; PLC-Present-day Landcover*)

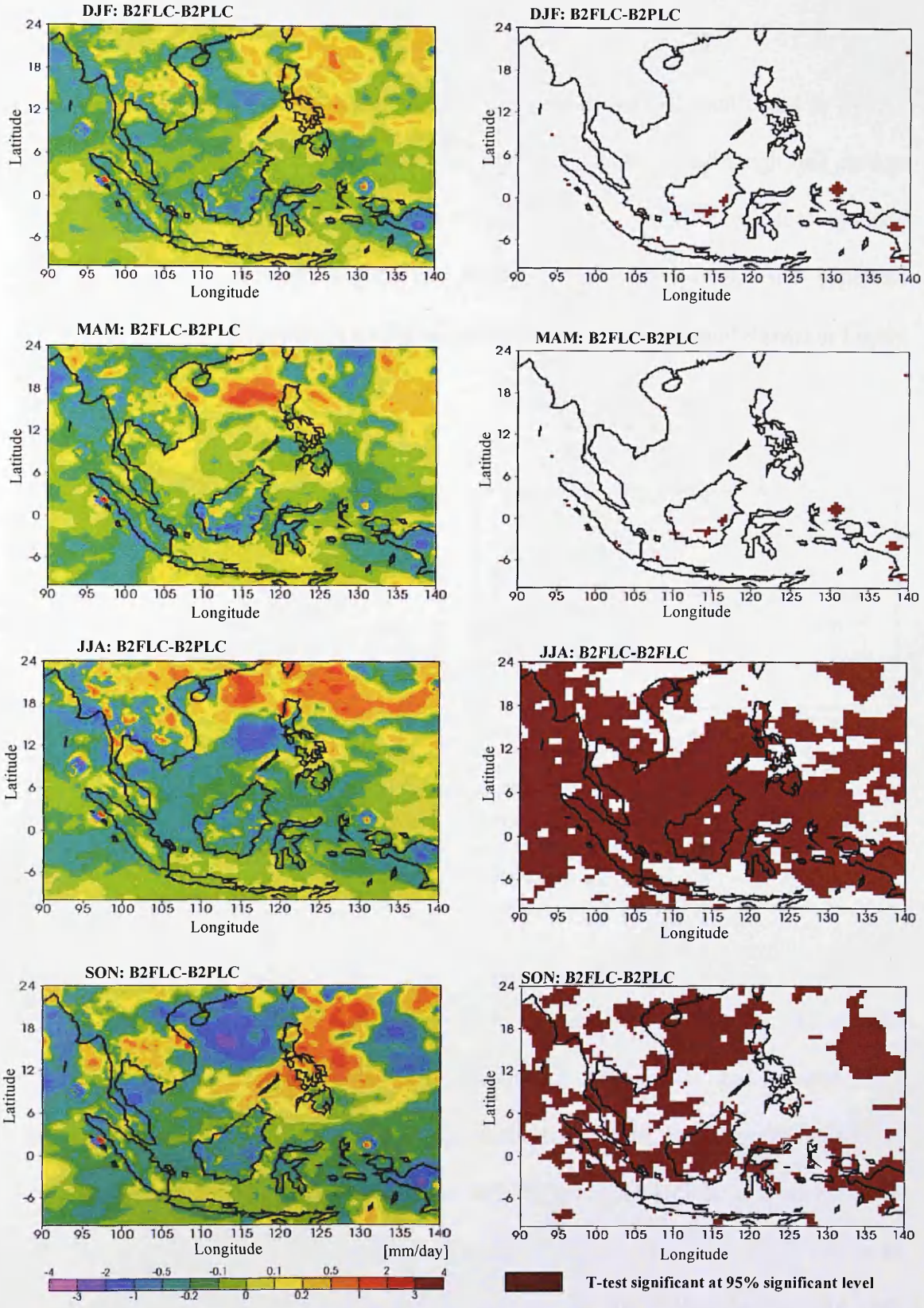

Figure 4.29: **SRES B2**: Isolated effects of the future landcover forcing alone on seasonal total precipitation (B2FLC-B2PLC) (*left panel*) in the SRES B2 scenario, and the significant t-test plots (*right panel*).

(*Note: FLC- Future Landcover; PLC-Present-day Landcover*)

4.4.2.3 Total cloud

The impacts of landcover forcing alone on the seasonal cycle of total cloud in the A2 and B2 climate scenarios was to cause a decrease in cloudiness, although this change was much smaller in magnitude compared with the impacts of atmospheric forcing alone (see Chapter 3) and combined forcing (see Section 4.4.1) (Appendix 4.1 and Appendix 4.2). The domain-mean seasonal cycles of the differences in total cloud shown in Figure 4.30.

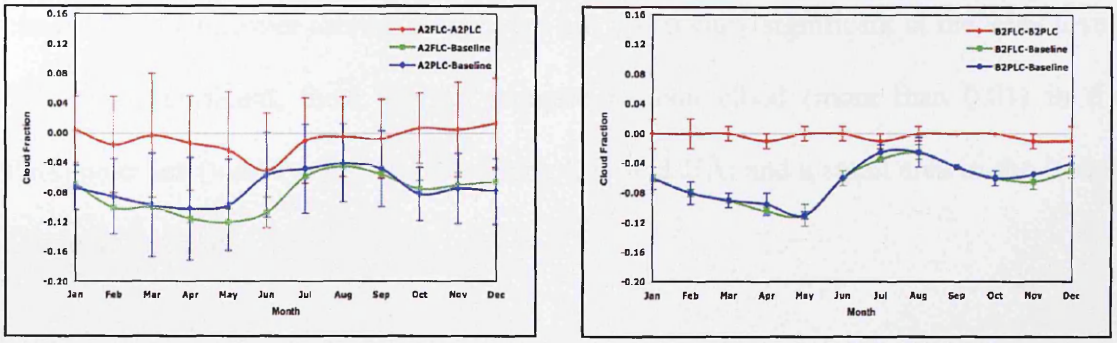

Figure 4.30: Seasonal cycle of the total cloud for the A2 (*left panel*) and B2 (*right panel*) climate scenarios due to the landcover forcing alone (A2FLC-A2PLC & B2FLC-B2PLC), and the total cloud changes (A2FLC-Baseline; A2PLC-Baseline & B2FLC-Baseline; B2PLC-Baseline) in the present-day and future landcover scenarios.
(*Note: FLC- Future Landcover; PLC-Present-day Landcover*).

The impact of future landcover forcing alone on regional total cloud in the A2 climate scenario is to change total cloud between -0.13 and 0.11 during DJF, and between -0.14 and 0.11 during JJA (Figure 4.31 and Appendix 4.1). These large spatial variations largely compensate each other over the domain; the mean total cloud was observed to decrease in both seasons by just -0.01 (DJF) and -0.001 (JJA) respectively. Total cloud was significantly decreased (95% significant level) over the Philippine Sea (the west Pacific Ocean) with less than -0.02 during DJF and over a larger area during JJA (Figure 4.31). The areas where less cloud was observed experienced less precipitation as

described in Section 4.4.2.2. Increases in total cloud were observed to develop in the southern part of China and some areas in the Andaman Sea and Indian Ocean, but were not statistically significant.

In the B2 climate scenario, the impact of landcover forcing alone resulted in relatively smaller changes in total cloud than in the A2 climate scenario. Total cloud increased slightly by 0.003 during DJF and decreased by -0.001 during JJA (Figure 3.32 and Appendix 4.2). In almost all areas in the region for both seasons, the changes in total cloud due to landcover forcing alone were not statistically significant at the 95% level. Though insignificant, there was an increase in total cloud (more than 0.01) in the Philippine Sea (west Pacific Ocean) during DJF and JJA; and a small area in the Indian Ocean during DJF.

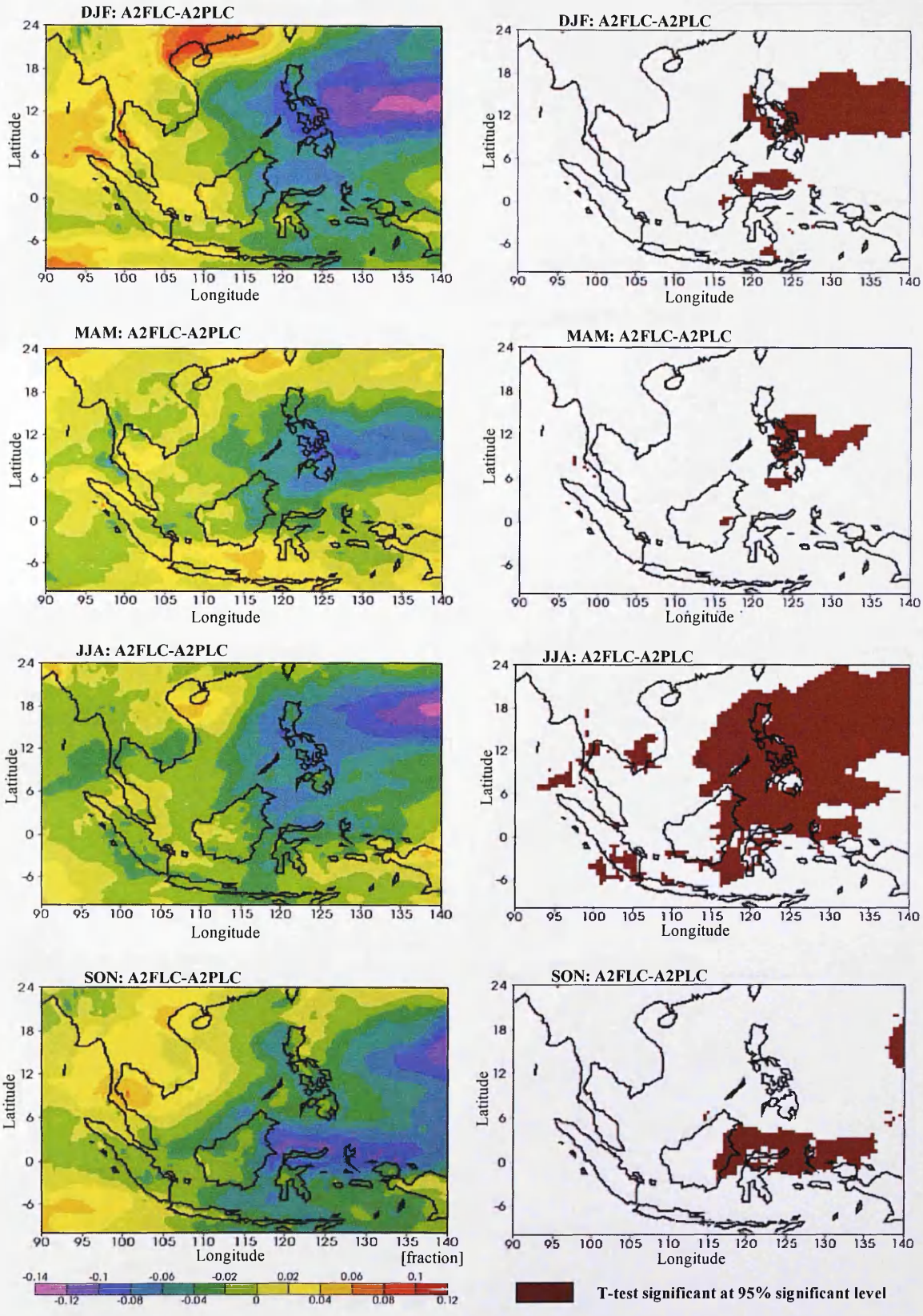

Figure 4.31: **SRES A2**: Isolated effects of the future landcover forcing alone on the seasonal total cloud (A2FLC-A2PLC) (*left panel*) in the SRES A2 scenario, and significant t-test plots (*right panel*).

(*Note: FLC- Future Landcover; PLC-Present-day Landcover*)

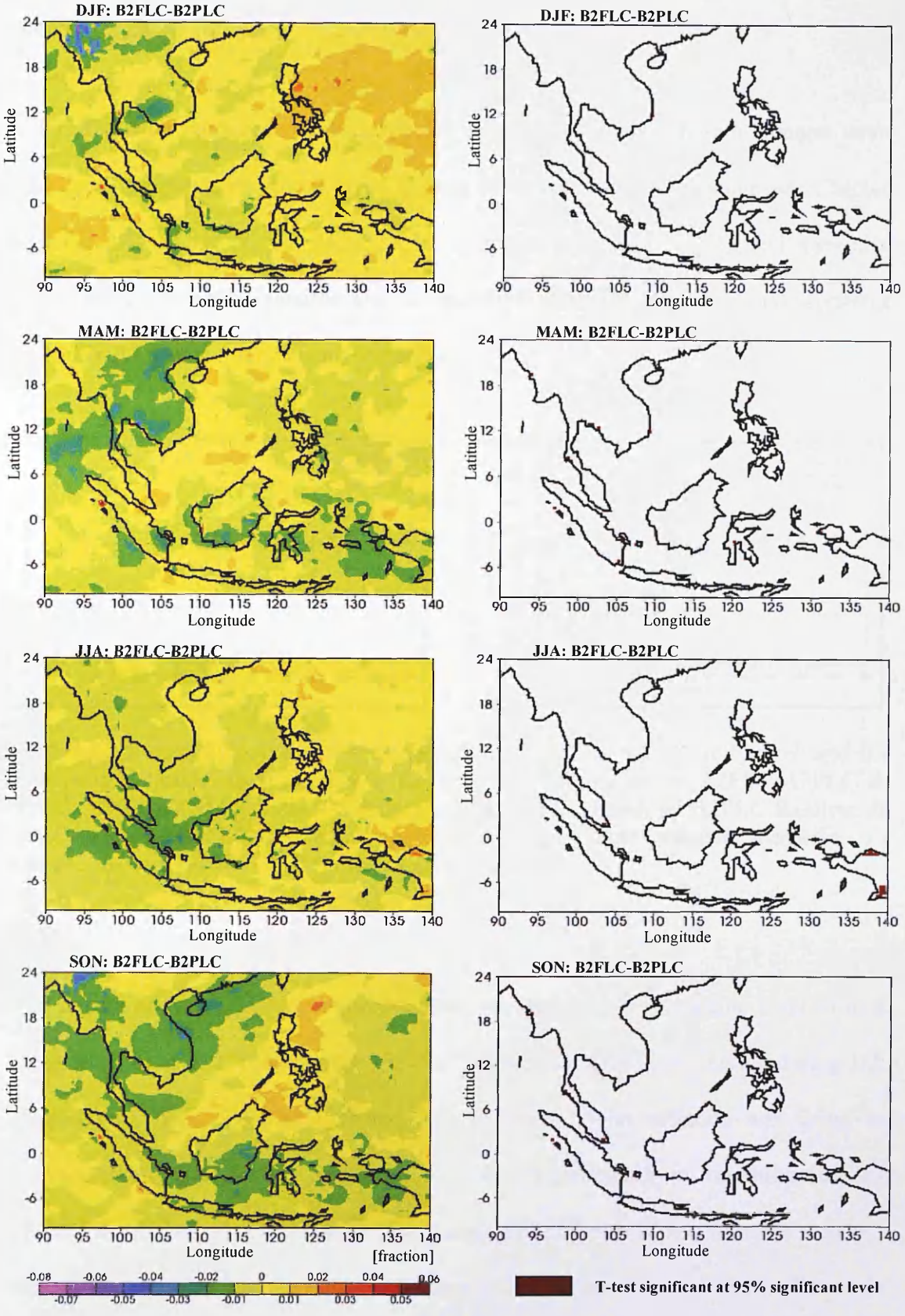

Figure 4.32: **SRES B2**: Isolated effects of the future landcover forcing alone on the seasonal total cloud (B2FLC-B2PLC) (*left panel*) in the SRES B2 scenario, and significant t-test plots (*right panel*).

(*Note: FLC- Future Landcover; PLC-Present-day Landcover*)

4.4.2.4 Solar radiation

Solar radiation increased due to landcover changes but solar radiation changes were smaller in magnitude compared to the impacts of atmospheric forcing alone (see Chapter 3) and combined forcing (see Section 4.4.1.1) (Figure 4.33; Appendix 4.1 and Appendix 4.2). Changes in solar radiation due to landcover forcing alone were more apparent under the A2 than the B2 climate scenarios.

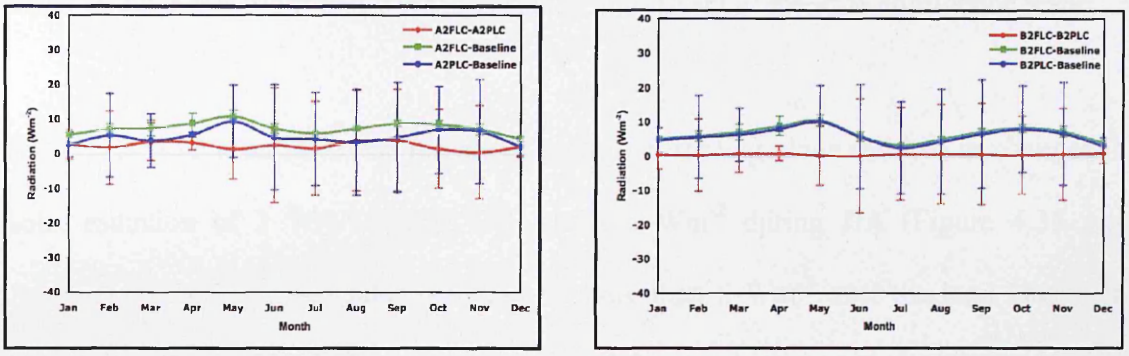

Figure 4.33: Seasonal cycle of the solar radiation (Wm^{-2}) for the A2 (*left panel*) and B2 (*right panel*) climate scenarios due to the landcover forcing alone (A2FLC-A2PLC & B2FLC-B2PLC), and the solar radiation changes (A2FLC-Baseline; A2PLC-Baseline & B2FLC-Baseline; B2PLC-Baseline) in the present-day and future landcover scenarios.
(*Note: FLC- Future Landcover; PLC-Present-day Landcover*)

The impact of future landcover forcing alone on regional solar radiation resulted in a small increase of solar radiation by 0.7 Wm^{-2} during DJF and slightly higher during JJA by about 2.1 Wm^{-2} (Figure 4.34 and Appendix 4.1). Solar radiation was found to increase mostly over the sea by more than 5 Wm^{-2}, particularly in the Philippine Sea (West Pacific Ocean) and Celebes Sea during DJF. However, the increase was not statistically significant at the 95% confidence level. The increased of solar radiation in these regions is consistent with the smaller total cloud amounts shown in Figure 4.31. A small area in the northern part of Sumatra, where the solar radiation was observed to

decrease (by less than -10 Wm^{-2}), was statistically significant at the 95% level. Similarly, during JJA, an increase by more than 10 Wm^{-2} of solar radiation in larger areas in the Philippine Sea (west Pacific Ocean) as well as in the Andaman Sea and the southern part of Myanmar were observed but found to be statistically insignificant at the 95% level. Meanwhile, solar radiation was observed to decrease in several areas including the northern part of the South China Sea, Gulf of Thailand, northern part of Sumatra, and a small area in the Bay of Bengal. These areas have changes of less than -5 Wm^{-2} in solar radiations that were statistically significant at the 95% confidence level.

In the B2 climate scenario, the impact of landcover forcing alone resulted in changes in solar radiation of 2 Wm^{-2} during DJF and 0.5 Wm^{-2} during JJA (Figure 4.35 and Appendix 4.2). Increased solar radiation of more than 6 Wm^{-2} over the land mostly in Indochina, Borneo, and the southern part of Sumatra were statistically significant. During DJF, the impact of landcover forcing on the solar radiation changes was insignificant. During JJA, solar radiation decreased largely in the Philippine Sea and west Pacific Ocean. Some of these areas (mostly over the sea to the north of the Phillipines) with the decrease by less than -2 Wm^{-2} were found to be statistically significant at 95% level. Less solar radiation in this area was also reflected in high total cloud as shown in Figure 4.32.

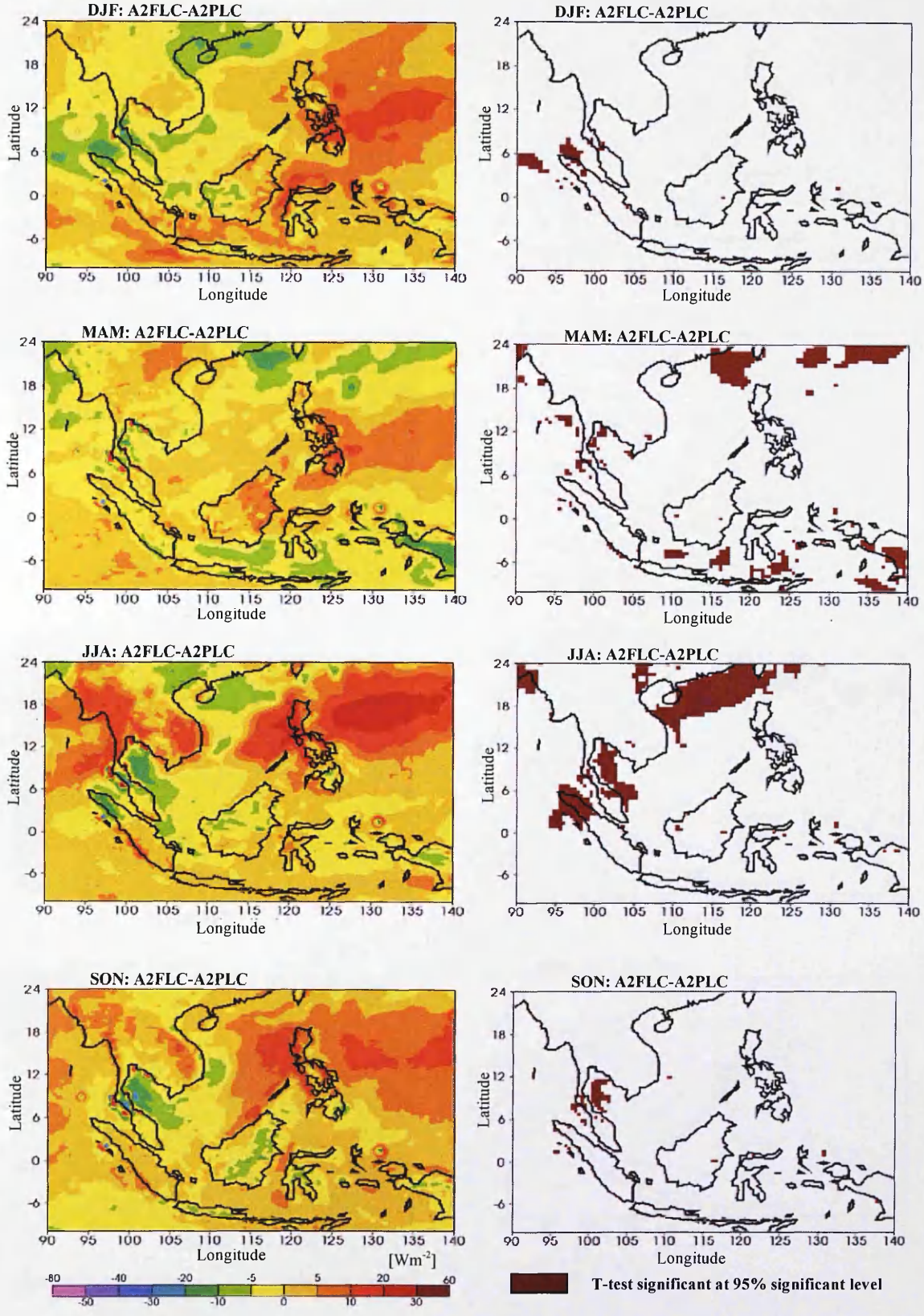

Figure 4.34: **SRES A2**: Isolated effects of the future landcover forcing alone on the seasonal solar radiation (A2FLC-A2PLC) (*left panel*) in the SRES A2 scenario, and significant t-test plots (*right panel*).

(*Note: FLC- Future Landcover; PLC-Present-day Landcover*)

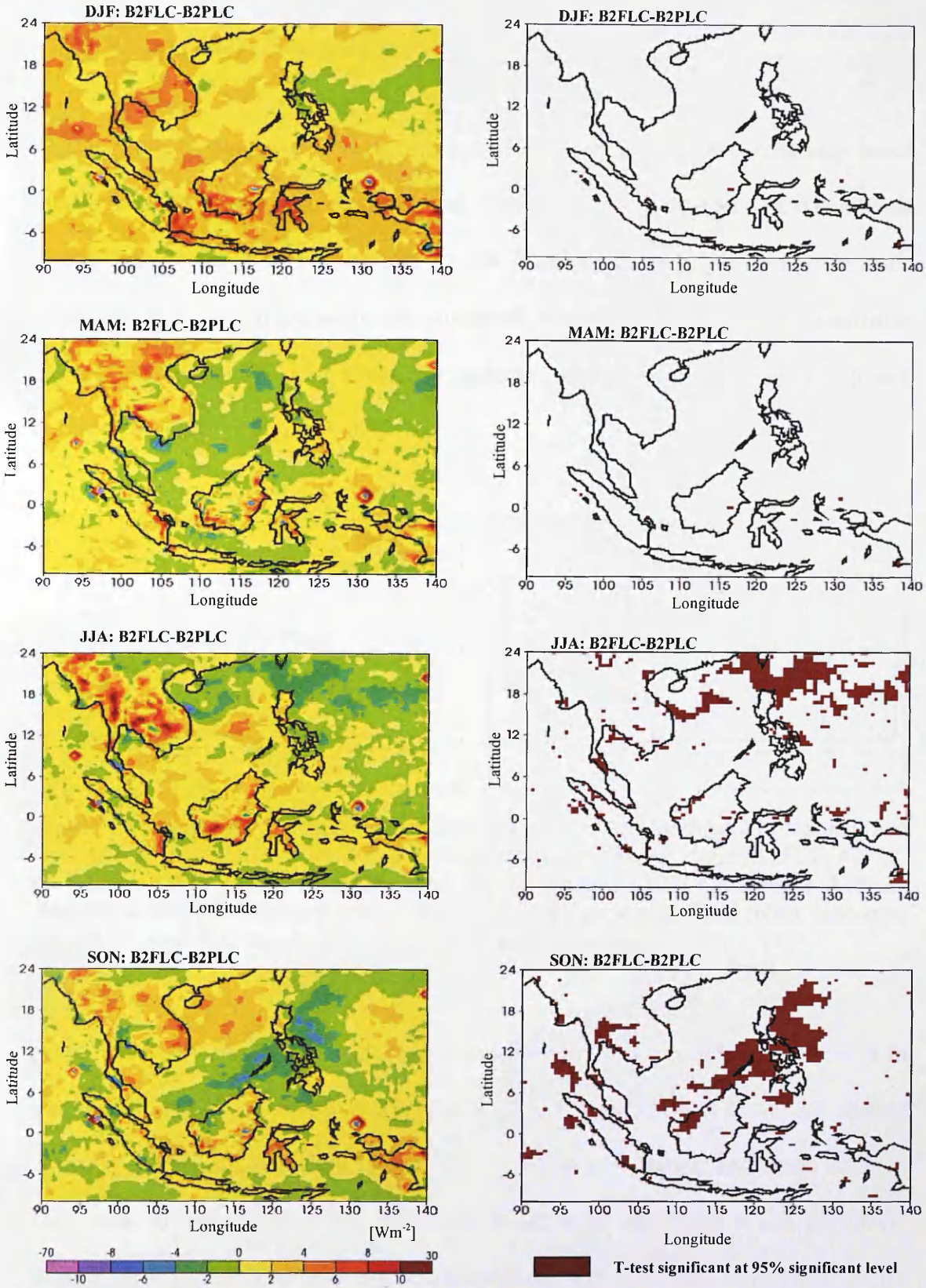

Figure 4.35: **SRES B2**: Isolated effects of the future landcover forcing alone on the seasonal solar radiation (B2FLC-B2PLC) (*left panel*) in the SRES B2 scenario, and significant t-test plot (*right panel*).
(*Note: FLC- Future Landcover; PLC-Present-day Landcover*)

4.4.2.5 Boundary layer height

The impacts of landcover forcing on boundary layer height were relatively small compared to the impacts due to atmospheric forcing alone (see Chapter 3) and combined forcing (see Section 4.4.1) (Appendix 4.1 and Appendix 4.2). The differences in mean boundary layer height between the combined forcing (atmospheric and landcover forcings), atmospheric forcing alone, and landcover forcing alone for A2 and B2 climate scenarios is shown in Figure 4.36.

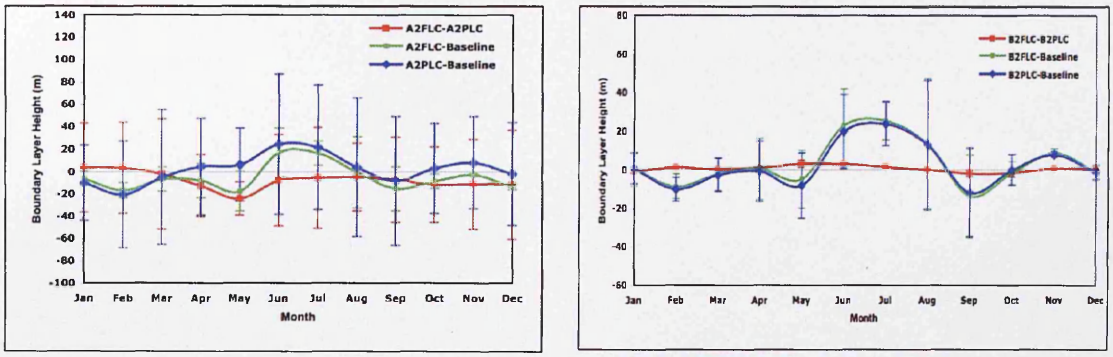

Figure 4.36: Seasonal cycle of the boundary layer height (m) for the A2 (*left panel*) and B2 (*right panel*) climate scenarios due to the landcover forcing alone (A2FLC-A2PLC & B2FLC-B2PLC), and boundary layer height changes (A2FLC-Baseline; A2PLC-Baseline & B2FLC-Baseline; B2PLC-Baseline) in the present-day and future landcover scenarios. (*Note: FLC- Future Landcover; PLC-Present-day Landcover*)

Future landcover forcing alone changes regional boundary layer height by about -8 m during DJF and -12 m during JJA (Figure 4.37 and Appendix 4.1) in the A2 climate scenario. Decreased boundary layer height in the Bay of Bengal and small areas in Indochina, southern Borneo, and Java were found to be significant at the 95% level during DJF. Meanwhile, during JJA, decreased boundary layer height of less than -30 m, which was mainly observed between latitudes of 6°N to 18°N, was statistically significant at the 95% level. Meanwhile in the B2 climate scenario, the boundary layer height changes were increased but relatively smaller than in the A2 climate scenario.

The mean boundary layer height increased to about 2 m during DJF and 4 m during JJA (Figure 4.38 and Appendix 4.2). Decreased boundary layer in areas with less than -30 m in both seasons were found to be statistically significant at the 95% confidence level (Figure 4.38). These areas were mainly found in Sumatra, Peninsular Malaysia, northern and eastern parts of Borneo, and some areas in Indochina and the Philippine Sea during DJF, and mostly in Indochina and the west Pacific Ocean to the north of Iran Jaya during JJA.

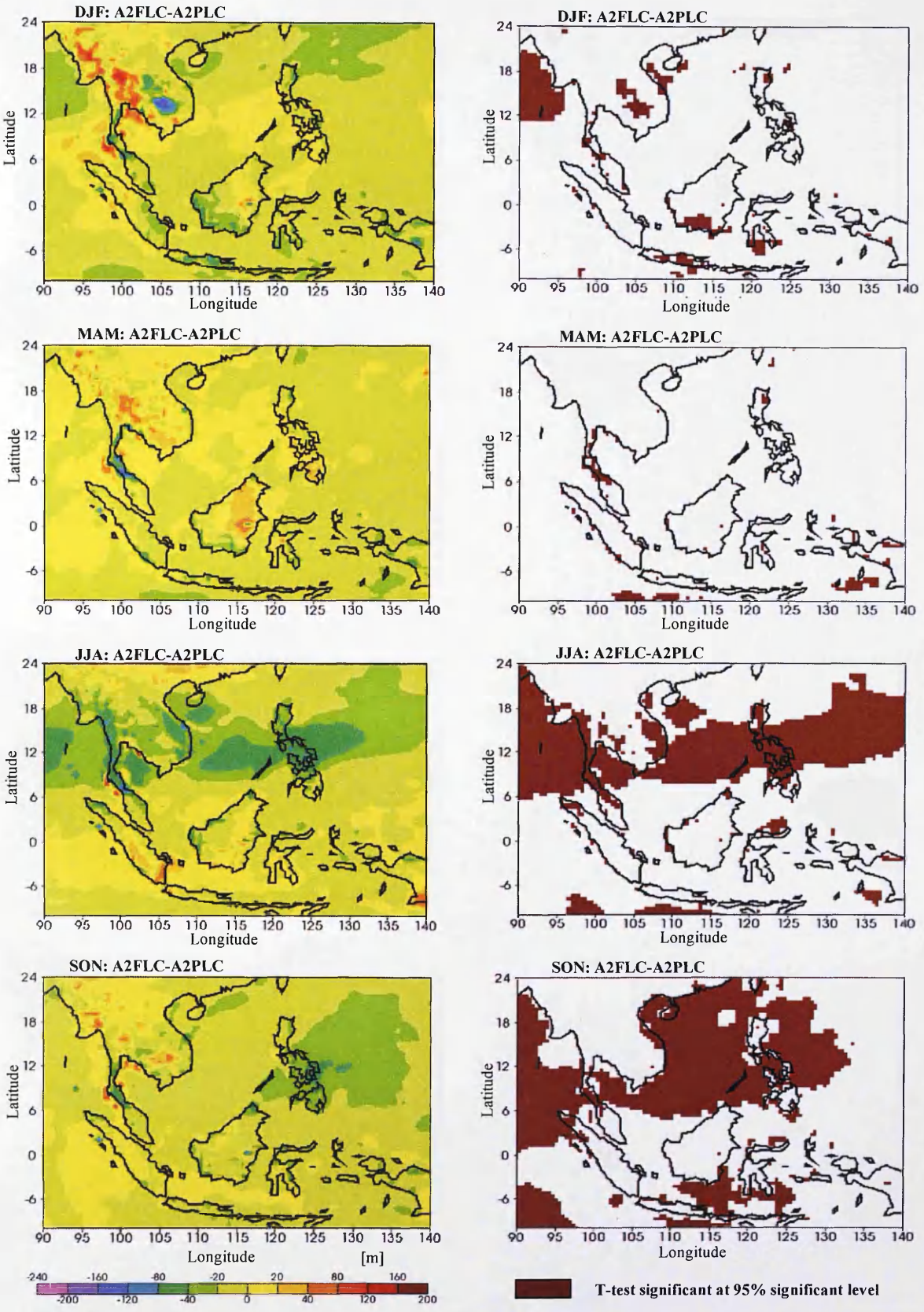

Figure 4.37: **SRES A2**: Isolated effects of the future landcover forcing alone on the seasonal boundary layer height (A2FLC-A2PLC) (*left panel*) in the SRES A2 scenario, and significant t-test plot (*right panel*).

(*Note: FLC- Future Landcover; PLC-Present-day Landcover*)

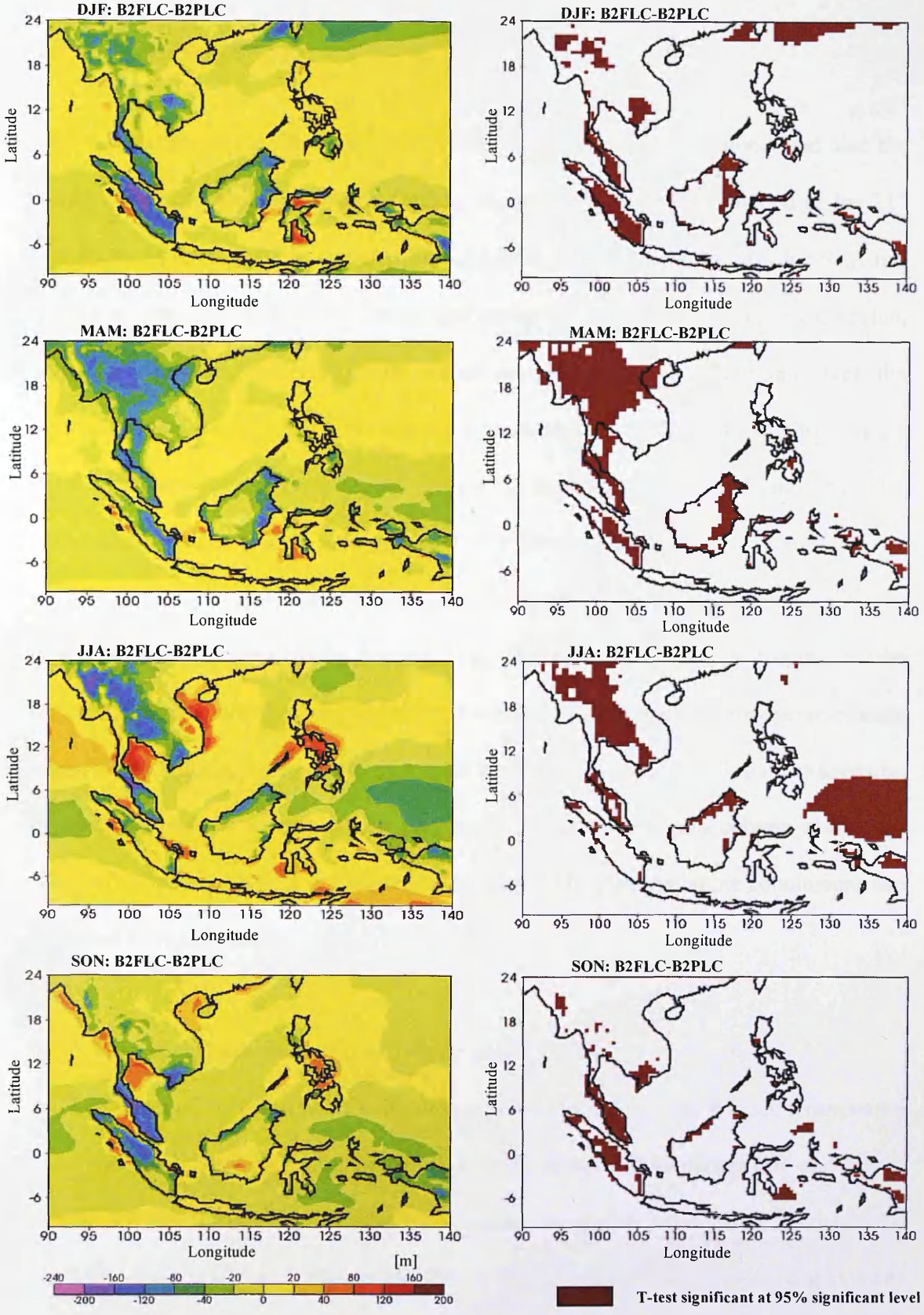

Figure 4.38: **SRES B2**: Isolated effects of the future landcover forcing alone on the seasonal boundary layer height (B2FLC-B2PLC) (*left panel*) in the SRES B2 scenario, and significant t-test plot (*right panel*).

(*Note: FLC- Future Landcover; PLC-Present-day Landcover*)

4.5 Conclusions

This study explores the effects of possible future landcover forcing alone, and also the combined effects with atmospheric forcing, on surface climate over the end of the 21st century in SEA. A possible scenario for landcover in the year 2070-2100 for SEA has been developed, which accounts for the projections of economic activity in the region, particularly in the agricultural sector. Based on this scenario of future landcover, the regional climate model (PRECIS) was used to generate future climate scenarios under A2 and B2 atmospheric forcings. By comparing the projected regional climate (2070-2100) under various climate scenarios relative to the baseline scenario (1960-1990), we are able to show the importance of landcover forcing as an isolated forcing as well as in combination with atmospheric forcing. The inclusion of landcover forcing to the regional climate model has accounted for a number of additional anthropogenic climate impacts, particularly subsequent impacts of landcover changes and climate changes on regional biogenic emissions, which play an important role in atmospheric chemistry. This is further investigated in Chapter 5 and Chapter 6. Thus far, some conclusions can be drawn from the results:

a) *The combined effects of atmospheric and future landcover forcings*

- The effect of the combined forcing was observed to increase the surface temperature significantly (at 95% confidence level) over all SEA by 2100 during DJF and JJA in the A2 and B2 scenarios. In the A2 scenario, the surface temperature increased by 2.7°C during DJF and 2.8°C during JJA. In the B2 scenario, the surface temperatures increased by 2°C during DJF and 2.1°C during JJA, but the mean surface temperatures were relatively smaller than the A2 scenario. In terms of magnitude, the combined effects in both climate scenarios were slightly lower than atmospheric

forcing alone, but the size of the landcover effect changed with the GHG scenario. Climate change from atmospheric forcing and landcover cover change are couple in the SEA, therefore.

- In both the A2 and B2 scenarios, total precipitation decreased during DJF and slightly increased during JJA. In the A2 climate scenario, regions in which precipitation increased by more than 2 mm/day during DJF, and any regions showing positive anomalies during JJA, were found to be statistically significant at the 95% level. In the B2 climate scenario, in contrast to the A2 climate scenario, region in which precipitation changes were less than -1 mm/day during DJF, and any region showing negative anomalies during JJA, were statistically significant at the 95% level.
- The combined forcing effects were observed to decrease the total cloud relative to the baseline in both A2 and B2 climate scenarios. There were few discernible differences of total cloud between the effects of combined forcing and atmospheric forcing alone. Statistically, there was no significant difference of total cloud changes during DJF in the A2 climate scenario in the region. However, small areas with an increase of total cloud fraction of roughly more than 0.02 were found to be statistically significant during JJA. In the B2 climate scenario, an increase of total cloud by more than 0.02 during DJF and JJAs were found significant at 95% level.
- In both the A2 and B2 scenarios, the solar radiation increased relative to the baseline scenario. However, there were few discernible differences with the effects due to atmospheric forcing alone. In both climate scenarios, regions showing increases in solar radiation of more than 5 Wm^{-2} during DJF, and all regions showing positive differences during JJA, were found to be statistically significant at the 95% level.

- Relatively, there were few discernible differences of boundary layer height between the effects due to the combined forcing, atmospheric forcing alone and the baseline scenarios. Areas where changes of boundary layer height were more negative than -30 m in both seasons for both climate scenarios were found to be significant at the 95% level.

b) The effects of landcover forcing alone

- The effect of future landcover forcing alone during DJF and JJA for both A2 and B2 climate scenarios were observed to be small and produced cooling temperatures compared to the effects due to the combined forcing and atmospheric forcing alone. Small and scattered areas with less than -1°C in surface temperature change due to landcover forcing alone were found to be statistically significant at the 95% confidence level during DJF and JJA for the A2 climate scenario. Similar observations were also found for the B2 climate scenario for both seasons.
- In the A2 climate scenario, the effect of landcover forcing alone was observed to cause a small increase in precipitation during DJF and a small decrease during JJA. The total precipitation was significantly decreased (95% confidence level) in areas showing changes more negative than -2 mm/day during DJF and between 0 mm/day and -8 mm/day during JJA. In the B2 climate scenario, landcover forcing alone was observed to cause a small decrease in precipitation in both seasons. Statistically, areas showing changes more negative than -0.2 mm/day in total precipitation in both seasons were found to be significant at the 95% level. These areas covered a larger area during JJA compared to DJF.
- Landcover forcing alone was observed to decrease total cloud in both seasons for the A2 climate scenario. Regions showing changes in total cloud more negative than

-0.07 during DJF, and -0.03 during JJA, were found to be statistically significantly at the 95% level in both seasons. Meanwhile, in the B2 climate scenario, total cloud increased slightly during DJF and decreased during JJA, but almost in all areas these changes were not statistically significant at 95% level.

- The impact of future landcover forcing alone on regional solar radiation resulted in a small increase in both seasons in the A2 and B2 climate scenarios, but were not statistically significant at the 95% level. In both climate scenarios, decreases in solar radiation were observed mostly over the sea (Philippine Sea/west Pacific Ocean) and some areas with changes more negative than -2 Wm^{-2} were found to be statistically significant.
- The impact of future landcover forcing alone on regional boundary height has resulted in small decreases in both seasons in the A2 climate scenario. In the B2 climate scenario, the boundary layer heights in both seasons were increased but relatively smaller in magnitude than in the A2 scenario. Decreased boundary layer heights in areas with less than -30 m in both seasons in the A2 and B2 climate scenarios were found to be statistically significant at the 95% level.

The combined of atmospheric and landcover forcings accounted for the increase of surface temperature by 2.7°C during DJF and 2.8°C during JJA for the A2, and 2°C during DJF and 2.1°C during JJA for the B2 climate scenarios. However, these increases were comparatively lower than the atmospheric forcing alone (see Section 3.7.2.1, Chapter 3). From the results, it can be concluded that atmospheric forcing and landcover forcing have an opposing effect with the landcover forcing showed more important role to the decrease in surface temperature. It was also observed that the land shows strong and rapid heating in the seasonal cycle than over the sea, which in turn has a large impact on seasonal atmospheric differential heating processes between land and sea. The

land surface processes (including changes in landcover), which modulate the seasonal heating, therefore are likely to be responsible (to some extent) for interannual variability of the monsoons (Yasunari, 2004). It was suggested that the increases in sensible heat flux and surface temperature due to landcover forcing were compensated by the increase of evaporation rates from the local precipitation and the sea as suggested by Feddema *et al.* (2005). Though the Asian Monsoon could have played important roles on local climate, large-scale landcover changes in the adjacent regions (i.e East Africa, Australia, southern and eastern Asia) could also affect the strength and timing of the large-scale Asian Monsoon circulation. Based on the numerical experiment by Yasunari *et al.* (2006), it has been suggested that in Asian monsoon region, the landcover change is essential for the formation of monsoon circulation and precipitation through strong latent heating of the atmosphere. The increase of evapo-transpiration due to landcover change plays significant role in forming thick moisture boundary layer and convection for the latent heating. It has been suggested (see Feddema *et al.*, 2005 and McGuffie *et al.* 1995) that the impacts of landcover forcing alone on the regional total precipitation were strongly influenced by the Asian monsoon circulation, though the impact was found to be depending upon the atmospheric conditions including large-scale wind field, thermal stability, etc (Yasunari, 2004). In Indochina region for example, Kanae *et al.* (2001) tried to explain the reduction of total precipitation in September by linking to the changes in albedo, surface roughness and soil moisture conditions, and when the monsoon westerly flow seasonally became weak. However, in other monsoon months, the effect of deforestation was negligible because of the effect of strong inflow and convergence of moist monsoon flow was dominated over the region. Therefore, the possible changes to the large-scale Asian Monsoon circulation could explain the climatic changes in the region due to landcover change in this investigation.

Chapter 5

THE RESPONSE OF BIOGENIC EMISSIONS TO CHANGES IN LANDCOVER AND CLIMATE IN SOUTHEAST ASIA

5.1 Biogenic Volatile Organic Compounds Emission in Relation to Landcover

Biogenic emissions such as isoprene (C_5H_8) and monoterpene ($C_{10}H_{16}$) are emitted into the atmosphere in large quantities by vegetation, particularly in the tropics. Apart from these two important compounds, plants also emit alkanes, alkenes, alcohols, esters, carbonyls and organic acids (Kirstine *et al.*, 1998; Schade and Goldstein, 2001; Villanueva-Fierro *et al.*, 2004). Changes in landcover either due to natural processes (ecological succession, fire, etc) or human activities (deforestation, agriculture, etc) affect the species composition and vegetation distribution and can significantly alter not only the micro-climate but also the biogenic emissions, and hence may also indirectly affect the regional tropospheric chemistry. In a previous study, it has been predicted that an increase in global isoprene emissions from 484 TgC/yr in the 1990s to 615 TgC/yr in the 2090s due to climate changes and vegetation distributions results in a predicted increase in ozone levels of 10-20 ppbv in some areas (Sanderson *et al.*, 2003).

As also mentioned in Section 1.3.3, conversion of forested area into agricultural land will affect biogenic emissions. In the southern part of China, conversion of about 30% of the forested area into cropland was found to reduce annual emissions of isoprene and monoterpenes by 30% and 40%, respectively (Steiner *et al.*, 2002). A study in Eastern Texas has also concluded that differences in landcover have significant impacts on the

isoprene emissions, where higher emissions were observed in areas classified as Post Oak woods, forest, and grassland than in agricultural land (Vizuete *et al.*, 2002). In the tropical region, one modelling study found that deforestation and expansion of grazing area in Amazonia reduced the maximum isoprene emission fluxes from 12 x 10^{15} to 1.2 x 10^{15} molecules m^{-2} s^{-2} (Ganzeveld and Lelieveld, 2004). A similar result was obtained from a sensitivity study investigating the impact of landcover changes through deforestation on biogenic emissions in the Amazon, Indonesia and Central Africa, where 50% of the forested areas were converted into agricultural area and 50% into tropical grasses under present-day climate conditions (Lathiere *et al.*, 2005). Results have shown that massive deforestation in the tropics has a major impact on biogenic emissions, where isoprene and other VOCs emissions decrease by 27-30%. The decreases have been found to be associated with the reduction of LAI and emission factors. Recent sensitivity studies by Weidinmyer *et al.* (2006) for the Amazon region, where 25% of the current area was replaced by oil palm (*Elaeis guineensis*) and eucalyptus (*Eucalyptus sp*) plantations, on the other hand, showed an opposite conclusion. The study concluded that the combination of landcover change and future climate contributed to an increase emission of isoprene by 37%. Therefore, the type of vegetation assigned in the sensitivity studies is crucial in determining the effects of landcover change as well as climate change on BVOC emissions in the tropics. This chapter will further investigate the sensitivity of BVOC emissions to landcover change and climate change in the SEA region.

5.2 Biogenic Volatile Organic Compounds Emissions in Relation to Climate Change

A number of studies have shown that biogenic emissions are dependent on temperature and photosynthetic photon flux density (PPFD) incident on the leaf (Guenther *et al.*, 1991;

Monson *et al.*, 1992; Guenther *et al.*, 1993; Livak *et al.*, 1996; Singsaas *et al.*, 1999; Sharkey *et al.*, 2001; Petron *et al.*, 2001). However, the dependency of isoprene emissions on these environmental conditions is not linear (Guenther *et al.*, 1996). The high temperature and the presence of light (photosynthetically active radiation) are important for the synthesis of isoprene from dimethylallyl pyrophosphate (DMPP) by isoprene synthase (Monson *et al.*, 1992; Sliver and Fall, 1995), which was linked with carbon metabolism and ATP (Adenosine Triphosphate) levels within the leaf (Sharkey and Loreto, 1993). In earlier studies by Guenther *et al.* (1991) and Monson *et al.* (1992), the dependency of isoprene emission on temperature was linked to the effect of temperature on the enzymes that are responsible for the production of isoprene. It was also found that this phenomenon was consistent across plant taxa though some variability was observed at the species level. Most plants (tropical and temperate) have shown a maximum emission of isoprene at approximately 40°C (Guenther *et al.*, 1993). Modelling studies by Vizuete *et al.* (2002), using the GLOBEIS model to investigate the effect of temperature on biogenic emissions in locations with dense hardwood and coniferous forests in Eastern Texas have also concluded that high temperature and high PAR (photosynthetically active radiation) drive large biogenic emissions in the region. Other studies have suggested that the increase in isoprene emissions from plants is part of their mechanism of their protection from rapid temperature fluctuations (Sharkey and Singsaas, 1995; Singsaas *et al.*, 1999).

Based on several recent studies (Rosenstiel *et al.*, 2003; Possell *et al.*, 2005; Wilkinson *et al.*, 2008), above ambient concentrations of atmospheric CO_2 were found to inhibit isoprene production. Heald *et al.* (2009) has observed that the perturbations of CO_2 to isoprene emissions are largely seasonal with little diurnal variability. Enhancement of

future projection of isoprene emissions induced by the increase of temperature, and at some extent where the vegetation cover is expected to increase were found to be offset by the inhibition effect of elevated CO_2 levels (Arneth *et al.*, 2007a). These observations suggest that future emissions of isoprene are largely buffered by a number of competing factors, which are certainly considered to be important in estimating the regional and global isoprene budget.

5.3 The Aims of the Study

As concluded in Chapter 3, the surface temperatures in the Southeast Asian region for both B2 and A2 emission scenarios will increase by 2.16°C and 2.49°C respectively under the present-day landcover scenarios, and this is expected to lead to high biogenic emissions of VOCs such as isoprene. Changes in landcover through conversion of forested area into agriculture and grassland, as described in details in Chapter 4, has lead to further increase in surface temperature by 2.60°C and 3.24°C for B2 and A2 transient climate scenarios, thus potentially further enhancing biogenic emissions. On the other hand, changes in landcover could also potentially lead to a decrease in isoprene, as the potential emissions from most crops and grasses are much less than for woody tree types (Guenther *et al.*, 1995). At present, the response of biogenic emissions to climate change and landcover change, particularly in the tropics is still largely unknown. In this study, the investigation has been focussed on the sensitivity of biogenic emissions at the regional scale to changes in the driving variables to gain a better understanding of their roles in the present and future biogenic emissions in the region. The aims of the work in this chapter are three fold: first, to investigate the impacts of anthropogenic landcover change on biogenic emissions. The investigation will focus on the effect of landcover forcing on biogenic emissions due to the conversion of about 60% of the forested area into other

landcover types, mainly agriculture and grassland (see Chapter 4). Second, to investigate the direct effect of the combination of climate change and landcover change to biogenic emissions. This would also determine which of these factors are more important to the biogenic emissions in the region. Finally, this study will investigate the roles of the ambient atmospheric CO_2 concentration on biogenic emissions in the region. This will focus on the impact on isoprene emissions due to the present-day concentration of CO_2 (360 ppm) and the doubled concentration of CO_2 (560 ppm) at the end of the century.

In this work, despite the uncertainties associated with future projections of landcover and climate changes in the region and the simulated effects of these changes on biogenic emissions, this sensitivity study provides a snapshot of how an interactive model can be applied at the regional scale for investigating interactions of climate, landcover (biogenic emissions), and subsequently, tropospheric chemistry. Improved knowledge of climate-landcover-tropospheric chemistry interactions-particularly in SEA, where there is a major source of biogenic emissions, is necessary for the evaluation of which processes should be built into interactive models that include chemistry, emissions, land surface and atmospheric dynamics. This work could also provide information on the significance of landcover variables (i.e type and distribution of vegetation, and LAI), and climatic conditions (i.e. ambient temperature, and PAR) for biogenic emissions particularly isoprene and monoterpenes. The schematic of the work of this chapter is illustrated in Figure 5.1.

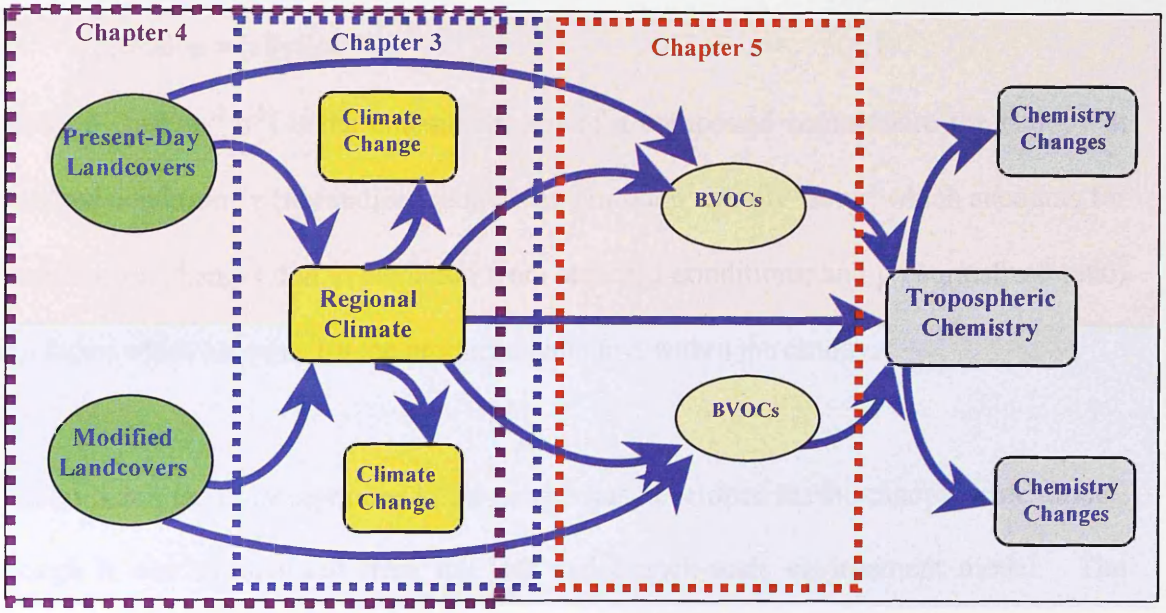

Figure 5.1: Framework for the investigation of climate changes-biogenic emissions-tropospheric chemistry ineteractions in Southeast Asia. The red dotted box indicates the framework for the investigation of biogenic emissions response to the landcover and climate changes that covered in Chapter 5.

5.4 Models and Experimental Design

5.4.1 BVOCEM to Estimate Biogenic Emissions

BVOCEM (Biogenic Volatile Organic Compounds Emission Model) was used to estimate biogenic emissions in SEA. This model (Lathiere *et al.*, in press) was developed in Sheffield University and Lancaster University, and is based on the MEGAN model as described by Guenther *et al.* (2006). In order to quantify the net emissions of biogenic emissions between the atmosphere and terrestrial ecosystem at a specific location and time, parameterisation has considered the impact of temperatures, radiation, leaf age, soil moisture and canopy loss, which is given by the following equation (Eq 5.1):

$$\text{Emission} = [\varepsilon][\gamma][\rho] \quad (5.1)$$

where ε (mg m^{-2} h^{-1}) is the emission factor of a compound emitted into the canopy at standard condition; γ (normalized ratio) is an emission activity factor, which accounts for the emission changes due to deviation from standard conditions; and ρ (normalized ratio) is a factor which accounts for the production and loss within the canopy.

The emission factor incorporated in the model was developed for the canopy-scale model, though it was extrapolated from the leaf and branch-scale environment model. The standard conditions for MEGAN canopy-scale emission factors are shown in ***Table 5.1***:

Table 5.1: Standard conditions for MEGAN emission factors at the canopy-scale.

Parameter	Standard Conditions
• Leaf Area Index (LAI)	5
• Canopy	80% mature 10% growing 10% foliage
• Solar angle	60 degrees
• Photosynthetic photon flux density transmission (PPFD)	0.6
• Air temperature	303 K
• Humidity	14 g kg^{-1}
• Wind speed	3 ms^{-1}
• Soil moisture	0.3 m^3m^{-3}
• Average canopy environmental conditions of the past 24 to 240 hr:	
- Leaf temperature	297 K
- PPFD (sun leaves)	200 μmol $m^{-2}s^{-1}$
- PPFD (shade leaves)	50 μmol $m^{-2}s^{-1}$

5.4.1.1 Emission factor at the canopy-scale (ε)

Landcover changes due to either natural or anthropogenic (such as deforestation, agricultural expansion, urbanisation, etc) activities could affect the ecosystem in terms of vegetation composition, distribution, and the canopy structure, which are important factors for biogenic emissions. Woody types of vegetation, particularly the broadleaf

trees are known to generally emit higher isoprene levels than non-woody plants. Broadleaf tree isoprene emission factors were found to be closer to the global average of 12.6 mg m^{-2} hr^{-1} in most regions whereas needle deciduous tree emission levels were lower (Guenther *et al.*, 2006). In non-woody plants, the isoprene emissions were observed to be even lower, for example grasslands in Australia (~0.004mg m^{-2} hr^{-1}) (Kirstine *et al.*, 1998) and grasslands in China (~0.004mg m^{-2} hr^{-1}) (Bai *et al.*, 2006). In some regions, crops are known to be a major source of isoprene emissions, for example the emission factors were found in the range from 3 to 28 μgC g^{-1} hr^{-1} for oil palm and from 25-130 μgC g^{-1} hr^{-1} for mango (*Mangifera indica*) (Geron *et al.*, 2006) (see Table 1.2 in Chapter 1).

In this study, a regional map of emission factors for seven Plant Functional Types (PFTs) was generated from the global map of emission factors provided by Guenther *et al.* (2006). In the MEGAN model of Guenther *et al.* (2006), PFTs are classified into a number of schemes, whose applications are dependent on the purposes of the simulation. For the global simulation, MEGAN usually uses the standard PFT-7 scheme, which includes seven PFTs namely: broadleaf evergreen trees, broadleaf deciduous trees, needle evergreen trees, needle deciduous trees, shrubs, crops, and grass plus other ground cover. Meanwhile, for the regional simulation, the PFT-REG scheme is normally used, which includes the details of the plant genera. In BVOCEM, the emission factors were assigned directly to the ecosystem types, which is similar to the PFT-7 scheme. This approach is generally accepted in the tropical region as this is considered the best option for areas in the tropical forest, which contains high species diversity (Guenther *et al.*, 1995).

5.4.1.2 Emission activity factor at the canopy-scale (γ)

The emission activity factor describes variations due to physiological and phenological processes that drive the biogenic emissions rate changes. In BVOC, the total of the emission factor due to these processes is estimated based on the product of a set of non-dimensional emission activity factors that are each equal to 1 in standard conditions, as described by Guenther *et al.* (2006) in the following Eq 5.2

$$\gamma = \gamma_{CE} \cdot \gamma_{age} \cdot \gamma_{SM} \qquad (5.2)$$

where γ_{CE} describes variation due to Leaf Area Index (LAI) and light, temperature, humidity and wind conditions within the canopy environment, γ_{age} makes adjustments for effects of leaf age, and γ_{SM} accounts for direct changes in γ due to changes in soil moisture. The calculation of each of these factors is described in the following paragraphs.

Local climatic conditions, which affect the incident PPFD and leaf temperature are known to control the biogenic emissions such as isoprene from short periods (seconds to minutes) to longer periods (hours to weeks) of time scales (Guenther *et al.*, 1993; Monson *et al.*, 1994; Sharkey *et al.*, 2000; Geron *et al.*, 2000; Petron *et al.*, 2001). At the canopy level, the influence of leaf PPFD and temperature, γ_{CE} is estimated using Eq 5.3:

$$\gamma_{CE} = \gamma_{LAI} \cdot \gamma_{P} \cdot \gamma_{T} \qquad (5.3)$$

where

γ_{LAI} accounts for variation in LAI compared to standard conditions of 5 m^2/m^2.

γ_{P} for variations in radiation

γ_{T} for variations in temperature.

The corresponding emission activity factor of LAI and temperature variations in the region are calculated using Eq. 5.4 and Eq. 5.5 respectively:

$$\gamma_{LAI} = 0.49\ LAI/[(1 + 0.2\ .\ LAI^2)^{0.5}] \quad (5.4)$$

$$\gamma_T = E_{opt}\ .\ [C_{T2}\ .\ \exp(C_{T1}\ .\ X)/(C_{T2} - C_{T1}\ .\ (1 - \exp(C_{T2}\ .\ x)))] \quad (5.5)$$

where $X = E_{opt}$ and $T_{opt} = 313+[0.6\ (T-297)]$

For the calculation of radiation effects, the following Eq. 5.6 is used:

$$\begin{cases} \text{IF} \quad a < 0 \text{ or } a > 180 \text{ THEN } \gamma_P = 0 \\ \text{ELSE } \gamma_P = \sin(a)[2.46(1+0.0005)(P_{daily}-400)(\phi) - 0.9\phi^2] \end{cases} \quad (5.6)$$

where P_{daily} is the daily average of PPFD in μmol photons $m^{-2}s^{-1}$, a is solar angle expressed in degrees and ϕ is the above canopy transmission calculated using the Eq. 5.7:

$$\phi = P_{ac}\ /(\sin(a).\ P_{toa}) \quad (5.7)$$

where P_{ac} is the above canopy PPFD, P_{toa} is the PPFD at the top of the atmosphere, which can be calculated as in Eq. 5.8:

$$Ptoa = 3000 + 99[\cos(6.28(DOY-10)/365] \quad (5.8)$$

where

DOY is the day of the year

From Eq. 5.2, the leaf age factor (γ_T) impact on isoprene emissions can be calculated based on the age of the leaf. Studies have also shown that a leaf's ability to emit isoprene is influenced by leaf phenology. The young leaves of isoprene-emitting species do not emit isoprene, while the mature leaves emit at the highest capacity and the old leaves lose their ability to photosynthesize and produce isoprene (Guenther *et al.*, 1991; 2006). To account for leaf age in the BVOC model, the parameterisation for leaf age factor as described by Guenther *et al.* (2006) was adopted and calculated using Eq. 5.9:

$$\gamma_{age} = F_{new}A_{new} + F_{grow}A_{grow} + F_{mature}A_{mature} + F_{old}A_{old} \quad (5.9)$$

where

F is foliage fraction (i.e new, grow, mature or old)

A is the relative emission rate based on the observations by Guenther *et al.* (1991), Monson *et al.* (1994), Goldstein *et al.* (1998), Petron *et al.* (2001) and Karl *et al.* (2004) (A_{new}=0.05, A_{grow}= 0.6, A_{mature}= 1.125, A_{old}= 1)

For evergreen canopies, a constant value of γ_{age} = 1 is adopted. The value for each foliage fraction is assigned for or calculated based on the change in LAI between the current time step (LAI_c) and the previous time step (LAI_p) (Guenther *et al.*, 2006) as shown in Eq 5.10 to Eq 5.17.

F_{new}=0, F_{grow}=0.1, F_{mature}=0.8, F_{old}=0.1 for $LA1_c$=LAI_p (5.10)

F_{new}=0, F_{grow}=0, F_{mature}=1-F_{old}, F_{old}=[(La_p-LAI_c)/LAI_p} for $LAI_p > LAI_c$ (Eq 5.11)

In a case where $LAI_p < LAI_c$, the values of foliage fractions are assigned or calculated as

$F_{old} = 0$ (5.12)

$F_{new} = 1 - (LAI_p/LAI_c)$ for $t \leq t_i$ (5.13)

$F_{new} = [t_i/t][1 - (LAI_p/LAI_c)]$ for $t \leq t_i$ (5.14)

$F_{mature} = (LAI_p/LAI_c)$ for $t \leq t_m$ (5.15)

$F_{mature} = (LAI_p/LAI_c) + [(t-t_m)/t][1-(LAI_p/LAI_c)]$ for $t > t_m$ (5.16)

$F_{grow} = 1 - F_{new} - F_{mature}$ (5.17)

where

t is the length of the time steps (in days between one week and one month) between LAI_c and LAI_p

t_i is the number of days between budbreak and the induction of isoprene emission

t_m is the number of days between budbreak and the initiation of peak isoprene emission rates

$t_g = t_m$ for $t > t_m$ and $t_g = t$ for $t \leq t_m$

As shown in Eq 5.2, soil moisture was also observed to play an important role in biogenic emissions through an indirect effect on stomatal conductance, which influences the leaf temperature. Studies by Pegoraro *et al.* (2004; 2005) have found that at low levels of soil moisture the isoprene emissions began to drop and eventually became negligible when plants are exposed to extended severe drought. The emission activity factor that is dependent on soil moisture has been calculated using the Eq 5.18 to Eq 5.20 (Guenther *et al.*, 2006).

$$\gamma_{SM} = 1 \qquad \theta > \theta_1 \tag{5.18}$$

$$\gamma_{SM} = (\theta - \theta_w)/\Delta\theta_1 \qquad \theta_w < \theta < \theta_1 \tag{5.19}$$

$$\gamma_{SM} = 0 \qquad \theta < \theta_w \tag{5.20}$$

where

θ is soil moisture ($m^3 m^{-3}$)

θ_w is wilting point (the soil moisture level below which plants cannot extract water from the soil, for which values range from 0.01 for sand and 0.38 m^3m^{-3} for clay soils)

$\Delta\theta_1$ is an empirical parameter ($\Delta\theta_1$= 0.06 based on Pegoraro *et al.* (2004)), and $\theta_1 = \theta_w + \Delta\theta_1$

The estimation of soil moisture from any soil depth to be used as input in the Eq 5.18 to Eq 5.20, uses the PFT dependent approach (Zeng, 2001) to determine the fraction of roots within each soil layer and applies the weighted average of emission activity factor for each soil layer (Guenther *et al.*, 2006).

Other factors such as the availability of soil nutrients, ambient carbon dioxide concentration (Possell *et al.* 2004; 2005), CO_2 (Buckley, 2001; Rosenstiel *et al.*, 2003), ozone (Velikova *et al.*, 2005), nitrogen availability (Harley *et al*, 1994), and physical stress (Alessio *et al.*, 2004) are also known to affect the biogenic emissions particularly isoprene from the plants. In the BVOC model, the impact of atmospheric CO_2 on isoprene emission was incorporated based on the function proposed by Possell *et al.* (2005). The CO_2 function is based on the normalised value of 1 for a present-day atmospheric CO_2 concentration of 366 ppmv. An atmospheric concentration of 560 ppmv for the future scenario (2100) has a CO_2 function value of 0.65.

5.4.1.3 Production and loss within canopy (ρ)

At the canopy level, the production of biogenic chemicals are emitted into the atmosphere above the canopy and at the same time there are losses through the involvement of biological, chemical and physical processes within the canopy atmosphere, vegetation surfaces and on soil. The canopy production and loss factor of these chemicals (ρ) has been taken into account in the MEGAN model as net canopy emission (Guenther *et al.*, 2006), which is important in model simulation of the impact of biogenic emissions such as isoprene on atmospheric chemistry. The net canopy emission is parameterised as a function of canopy depth, friction velocity and chemical lifetime (Eq 5.21) (e.g for isoprene), which is based on measured isoprene emission profiles and turbulence profiles in recent studies in the tropical forest (Karl *et al.*, 2004) and temperate forest (Stroud *et al.*, 2005).

$$\rho_{iso,iso} = 1 - D/[\lambda.\mu^*.\tau + D] \qquad (5.21)$$

where

D is canopy depth (m), λ is an empirically determined parameter

μ^* is friction velocity (ms^{-1})

τ is the above-canopy lifetime of isoprene (s).

The assigned values for D and λ in the model are dependent on the PFT in the PFT-schemes.

5.4.2 Monoterpenes and Other Volatile Organic Compounds

Calculations of monoterpenes and other volatile organic compounds are based on studies by Guenther *et al.* (1995), which have considered the impact of air temperature as well as emissions at the leaf-scale. In this case, only one emission factor for each PFT is used. For monoterpenes, the emission factors of 2.4 and 1.2 ugC/g dry matter/h for evergreen and deciduous needled-leaved trees and 0.2 ugC/g dry matter/h for agriculture were used. Meanwhile for other VOCs, an emission factor of 1.5 ugC/g dry matter/h for every PFT was used.

5.4.3 Developing Input Files for BVOCEM

5.4.3.1 Developing climate input fields

The climate data input for BVOCEM includes the temperature, PAR, and soil moisture content. All these climate data were obtained from PRECIS, a regional climate model, which was run over SEA with 50km x 50km resolution, as described in Chapter 3. The regional climate model was run for 10 years using ECHAM4 boundary conditions for both present-day (2000-2010) and future (2090-2100) for B2 and A2 IPCC emission

scenarios (see Chapter 3). The climate scenarios were also run under modified future landcover of the region as described in Chapter 4 for the investigation of landcover change impacts on biogenic emissions in the region. For the investigation under B2 and A2 emission scenarios, six sets of climate datasets were prepared: two climate datasets were created for the present-day climate scenarios under present-day landcover scenarios (fixed vegetation) (hereafter called BASE-B2 and BASE-A2) and another four climate datasets were created for the future climate scenarios under present-day (fixed vegetation) and modified future landcover scenarios (hereafter called FCLIM-PLC-B2, FCLIM-PLC-A2, FCLIM-FLC-B2 and FCLIM-FCL-A2) as shown in Table 5.2.

Table 5.2: Climate datasets scenarios for input in BVOCEM based on climate and landcover scenarios in B2 and A2 transient climate scenarios

Emission Scenarios	**Landcover Scenarios**	**Climate Sceanrios**
Baseline	Present-day landcover (fixed vegetation)	BASE-B2
		BASE-A2
SRES B2	Present-day landcover (fixed vegetation)	FCLIM-PLC-B2
	Future landcover (modified vegetation)	FCLIM-FLC-B2
SRES A2	Present-day landcover (fixed vegetation)	FCLIM-PLC-A2
	Future landcover (modified vegetation)	FCLIM-FLC-A2

Note:
BASE-B2 : *Baseline Climate – SRESB2*
BASE-A2 : *Baseline Climate – SRESA2*
FCLIM-PLC-B2 : *Future Climate under Present-day* Landcover – *SRESB2*
FCLIM-FLC-B2 : *Future Climate under Future* Landcover – *SRESB2*
FCLIM-PLC-A2 : *Future Climate under Present-day* Landcover – *SRESA2*
FCLIM-FLC-A2 : *Future Climate under Future* Landcover – *SRESA2*

5.4.3.2 PFT distribution and vegetation fraction

For the investigation of the impacts of landcover change on the BVOC emissions, two landcover scenarios were prepared: the present-day (baseline) and future landcover files. For the present-day landcover scenario, the plant functional type (PFT) distribution datasets for SEA were generated based on the landcover classification by Wilson and Henderson-Sellers (1985) with 50 km resolution, which is based on ecosystem type. This landcover classification was also used in regional climate change study using PRECIS (see Chapter 3 and Chapter 4). The landcover in the region was re-classified into six PFTs (i.e. tropical broadleaf trees, tropical shrubs, grassland, cropland, evergreen needle-leaf trees and deciduous needle-leaf trees) in order to fit the definition of PFT distribution used in BVOCEM. Meanwhile for the future landcover file, landcover was created based on the landcover used in the sensitivity study as described in detail in Chapter 4. The major feature of the modified future landcover was the reduction of forested area (mainly in area covered by tropical broadleaf trees) of about 60% and a significant increase of agricultural and grassland landcovers (see Table 4.5 – Chapter 4). It is recognised that the modified future landcover changes were chosen arbitrarily and may not be realistic. However, these potential changes would allow the investigation to evaluate the importance of landcover changes on BVOC emissions driven by the present-day and future climate scenarios. Based on the modified future PFTs distribution in the SEA region, the future vegetation fraction for each PFTs was generated to be used in BVOCEM to estimate future biogenic emissions in the region.

5.4.3.3 Leaf Area Index (LAI)

LAI, as projected leaf area per unit ground surface area, is an important variable of vegetation describing the structural and functional properties of plant canopy as it is directly related to the exchange of energy, CO_2, and water from vegetation canopies (Sellers *et al.*, 1986). For the investigation of the present-day biogenic emissions (year 2008) in this study, LAI values were obtained from the MODIS/TERRA satellite, which estimate LAI with almost daily global coverage. LAI values at 1 km resolutions for the SEA domain were obtained from NASA's Earth Observation System Data Information System (http://elpdl03.cr.usgs.gov/ims-bin/pub/nph-ims.cgi/u777090). The LAI datasets were aggregated to 50 km resolution in order to be compatible with other input variables of the BVOCEM. In this study, twelve datasets of LAI were obtained, representing the monthly LAI datasets for the year 2008.

As there are no future LAI datasets available, the future LAI values, which are expected to change due to conversion of the forested land into agriculture (particularly oil palm) and grasslands, were estimated from the current LAI value and vegetation fraction for each grid. As in Guenther *et al.* (2006), and also adopted by Muller *et al.* (2008), the LAI of the vegetated areas are estimated by dividing the LAI obtained from MODIS by the vegetated fraction of the grid. The LAI values assigned for each plant functional types (PFTs) used as reference for the estimation are based on Lathiere *et al.* (2005) and Loveland *et al.* (2002) as shown in Table 5.3. For tree crops like oil palm, the LAI value was based on Md Noor and Mohd Haniff (2004). Paddy rice, as it is classified in the grass family of Gramminae, and is thus assigned the same LAI value as grass.

Table 5.3: LAI values assigned for plant functional types (PFTs)

PFTs Description	LAI* (m^2/m^2)
Tropical broadleaf tree	8.5
Tropical woodland	6
Tropical tree crop (oil palm tree)	5.6**
Paddy (C3 Agriculture)	3
Arable cropland (mostly C4 Agriculture)	5
Tropical grassland (C3 grass)	3
Tropical savanna (C3 grass)	2.5
Tropical pasture (C4 grass)	1

Sources: * adapted from Lathiere *et al.* (2005); Loveland *et al.* (2002)
** adapted from Md Noor and Mohd Haniff (2004)

Based on changes to the landcover in the region mainly due to conversion of tropical forest (evergreen broadleaf trees) into agriculture (i.e oil palm and paddy) and other landcover types, the present-day (2008) LAI annual mean of 5.45 m^2/m^2 decreased to 3.44 m^2/m^2, a reduction of 2.01 m^2/m^2 (36.9 %) (Figure 5.2).

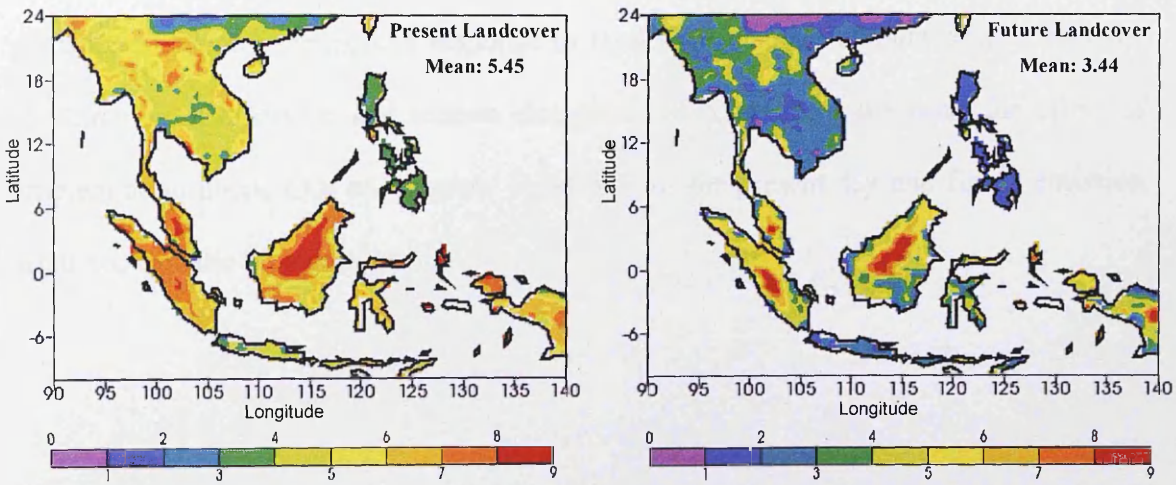

Figure 5.2: Annual mean of Leaf Area Index (LAI) for the present-day (2008) and future (2100) landcover scenarios in Southeast Asia.

5.4.4 Developing Biogenic Emission Scenarios

In order to investigate the impact of climate and landcover changes on the present and future biogenic emissions, it is necessary to estimate the biogenic emissions under the present-day (baseline) and future climate with different landcover scenarios. Atmospheric CO_2 was also considered in these scenarios, to investigate the CO_2-inhibition effect on isoprene emission. In this study, two sets of experiments were run, to reflect the impacts of regional climate and landcover changes on biogenic emissions as well as the impact of atmospheric CO_2. First, BVOCEM was run under the present-day landcover scenario and using climate datasets output from both baseline (BASE-A2 and BASE-B2) and future climate scenarios (PCLIM-PLC-B2 & PCLIM-PLC-A2) with- and without-CO_2 factor. Second, BVOCEM was run under modified future landcover scenario and using climate output datasets output from the future climate scenarios (FCLIM-FLC-B2 & FCLIM-FCL-A2) for with- and without-CO_2 factor. The investigation of biogenic emissions scenarios is shown in Table 5.4. Based on these scenarios, evaluations can be made on the response of biogenic emissions response to landcover change, climate change and the combination of landcover and climate changes in SEA. At the same time, the effect of ambient atmospheric CO_2 on biogenic emissions for the present-day and future emission scenarios can also be investigated.

Table 5.4: Experiment scenarios for the BVOC emissions investigation under the influence of different landcover and climate scenarios for both with-and without-CO_2 factors.

Emission Scenarios	Landcover Scenarios	Climate Scenarios	CO_2 Factor
Baseline	Present-day landcover (fixed vegetation)	BASE-B2	*with CO_2*
			without CO_2
		BASE-A2	*with CO_2*
			without CO_2
SRES B2	Present-day landcover (fixed vegetation)	FCLIM-PLC-B2	*with CO_2*
			without CO_2
	Future landcover (modified vegetation)	FCLIM-FLC-B2	*with CO_2*
			without CO_2
SRES A2	Present-day landcover (fixed vegetation)	FCLIM-PLC-A2	*with CO_2*
			without CO_2
	Future landcover (modified vegetation)	FCLIM-FLC-A2	*with CO_2*
			without CO_2

Note: *BASE-B2* : *Baseline Climate – SRESB2*
BASE-A2 : *Baseline Climate – SRESA2*
FCLIM-PLC-B2 : *Future Climate under Present-day* Landcover – *SRESB2*
FCLIM-FLC-B2 : *Future Climate under Future* Landcover – *SRESB2*
FCLIM-PLC-A2 : *Future Climate under Present-day* Landcover – *SRESA2*
FCLIM-FLC-A2 : *Future Climate under Future* Landcover – *SRESA2*

5.5 Results and Discussions

5.5.1 Present and Future Climate under Present-day and Modified Future Landcover Scenarios

5.5.1.1 Temperature

As concluded in Chapter 4, the regional baseline mean surface temperature for B2 and A2 emission scenarios under the present-day landcover (fixed vegetation) were 26.6°C and 27.4°C respectively (Table 5. 5). Future projections (2090-2100) of surface temperature, using fixed vegetation for both emission scenarios increased, to 29.2°C (B2) and 29.9°C (A2) respectively. Based on atmospheric forcing alone, the future surface temperature increased by about 2.5°C and 3.5°C for B2 and A2. In addition to atmospheric forcing, changes in landcover due to conversion of tropical rainforest into other landuses, mainly

agriculture (i.e oil palm), has resulted in further increases in average surface temperatures, to about 29.2°C (B2) and 30.6°C (A2). The combination of atmospheric and landcover forcings was responsible for the increase of surface temperature by 2.6°C and 3.2°C for B2 and A2 emission scenarios respectively (Table 5.6). Landcover forcing alone, has relatively little impact on the average future surface temperature (over land), which has observed only a small changes of about 0.1°C for B2 and 0.7°C for A2 emission scenarios. The projected regional surface temperatures and temperature changes for the present-day and future B2 and A2 emission scenarios and the temperature changes under fixed vegetation and modified future landcover are shown in Figure 5.3 and Figure 5.4.

Table 5.5: Temperature (°C) in the present-day (fixed vegetation) (PLC) and future (modified vegetation) (FLC) landcover scenarios. The maximum (max) and minimum (min) values are highest and lowest decadal averages for individual pixels over land in SEA.

Climate Scenario	Landcover Scenario	Temperature (°C)		
		Mean	Min	Max
Baseline B 2	Present (fixed vegetation)	26.64	13.97	31.83
Baseline A2	Present (fixed vegetation)	27.36	14.22	32.20
Future B2	Present (fixed vegetation)	29.15	16.45	34.55
Future B2	Future (modified vegetation)	29.24	16.44	34.61
Future A2	Present (fixed vegetation)	29.89	17.22	35.31
Future A2	Future (modified vegetation)	30.60	17.32	35.98

Note: Present-day – 10 years period between 2000-2010
Future – 10 years period between 2090-2100

Table 5.6 Difference in decadal-average surface temperature (°C) due to the landcover forcing alone and combination of atmospheric and landcover forcings in the present-day (PLC) and modified future landcover (FLC) scenarios.

Climate Scenario	Temperature Changes (°C)		
	Mean	Min	Max
B2PLC-BaseB 2	2.51	1.11	4.02
B2FLC-BaseB 2	2.60	1.37	4.52
B2FLC-B2PLC **	0.09	-1.18	1.54
A2PLC-BaseA2	2.53	1.06	4.10
A2FLC-BaseA2	3.24	1.72	4.91
A2FLC-A2PLC **	0.71	-1.28	2.29

Note: PLC – Present-day landcover (fixed vegetation)
FLC – Future landcover (modified vegetation)
BaseB2 – Baseline for B2 emission scenario
BaseA2 – Baseline for A2 emission scenario
B2PLC – BaseB2: atmospheric forcing alone for B2 scenario - climate change
B2FLC – BaseB2: atmospheric forcing + landcover forcing
A2PLC – BaseA2: atmospheric forcing alone for A2 sceanrio – climate change
A2FLC – BaseA2: atmospheric forcing + landcover forcing
** -Landcover forcing alone for A2 and B2 sceanrios

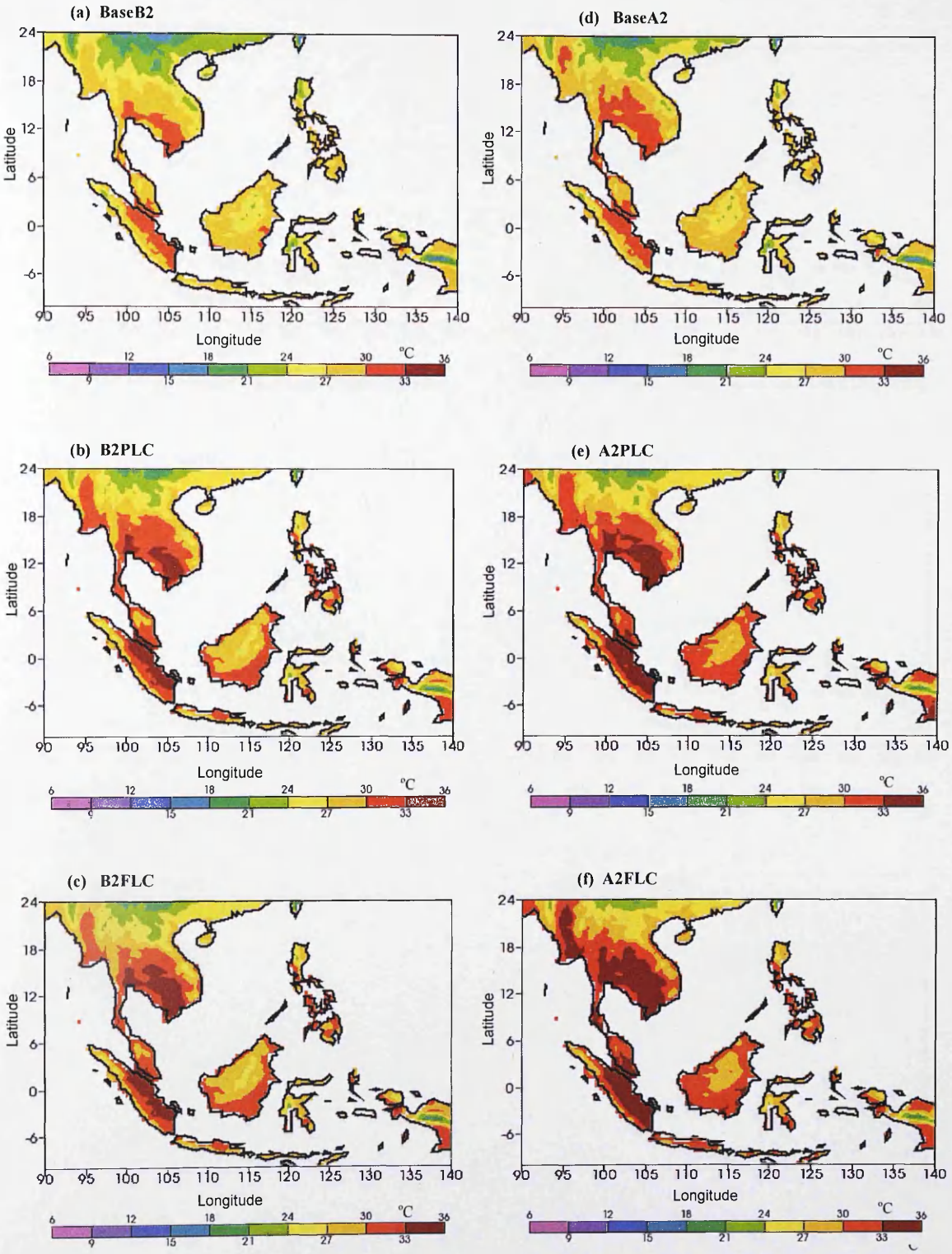

Figure 5.3: Simulated Baseline (2000-2010) and future (2090-2100) decadal-average surface temperature over SEA for the B2 (a-c) and A2 (d-f) emission scenarios in the present-day (PLC) and modified future landcover (FLC) scenarios.

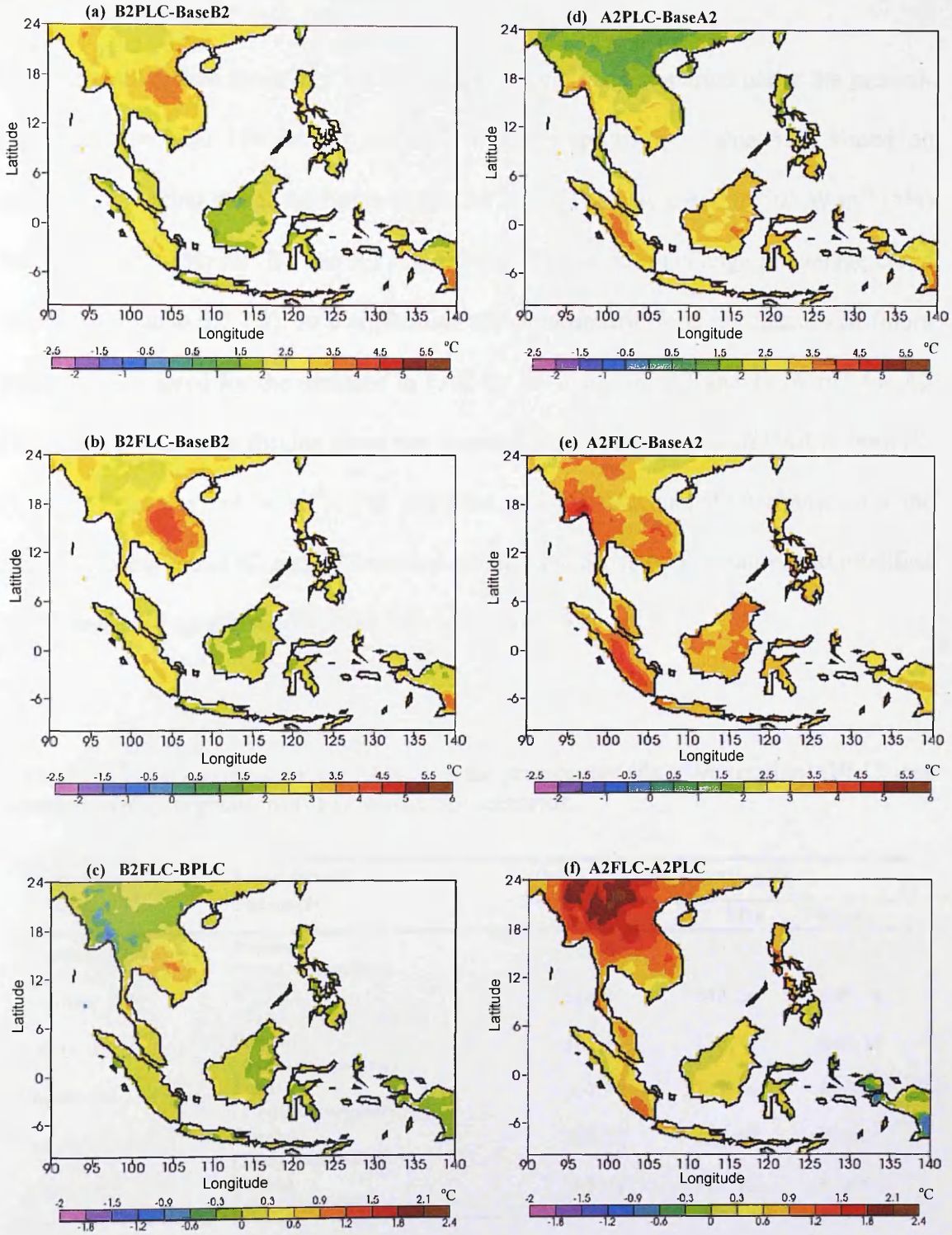

Figure 5.4: Difference in decadal-average surface temperature (°C) between **(a)** B2PLC and BaseB2, **(b)** B2FLC and BaseB2, **(c)** B2FLC and B2PLC, **(d)** A2PLC and BaseA2, **(e)** A2FLC and BaseA2, and **(f)** A2FLC and A2PLC. Note change of colour scale in panel (c) and (f).

5.5.1.2 PAR

The regional baseline mean of PAR for B2 and A2 emission scenarios under the present-day landcover were 514 W m^{-2} and 517 W m^{-2} respectively (Table 5.7). Based on atmospheric forcing alone, the future projection of PAR has increased to 505 W m^{-2} (5%) and 510 W m^{-2} (4%) for B2 and A2 respectively. This is due to change in average cloud cover (see Section 3.7.2.3). In combination with atmospheric forcing, changes in future landcover accounted for the decrease in PAR by 12 W m^{-2} for B2 and 11 W m^{-2} for A2 (Table 5.8). Landcover forcing alone was responsible for the decrease of PAR in both B2 (3 W m^{-2}) and A2 (4 W m^{-2}). The projected regional PAR and PAR changes for the present-day and future B2 and A2 emission scenarios under fixed vegetation and modified future landcover are shown in Figure 5.5 and Figure 5.6.

Table 5.7: Decadal-average PAR (Wm^{-2}) in the present-day (fixed vegetation) (PLC) and future (modified vegetation) (FLC) landcover scenarios.

Climate Scenario	Landcover Scenario	PAR (W m^{-2})		
		Mean	Min	Max
Baseline B 2	Present (fixed vegetation)	513.81	241.44	657.39
Baseline A2	Present (fixed vegetation)	516.82	244.26	649.76
Future B2	Present (fixed vegetation)	505.18	238.79	644.38
Future B2	Future (modified vegetation)	501.98	237.06	641.02
Future A2	Present (fixed vegetation)	509.72	226.63	645.65
Future A2	Future (modified vegetation)	505.99	215.78	642.97

Note: Present-day – 10 years period between 2000-2010
Future – 10 years period between 2090-2100

Table 5.8: Difference in average PAR (Wm^{-2}) due to the landcover forcing alone and combination of atmospheric and landcover forcings in the present (fixed vegetation) (PLC) and future (modified vegetation) (FLC) landcover scenarios.

Climate Scenario	PAR Changes ($W\ m^{-2}$)		
	Mean	Min	Max
B2PLC-BaseB 2	-8.63	-81.53	79.16
B2FLC-BaseB 2	-11.83	-123.00	87.15
B2FLC-B2PLC**	-3.20	-70.06	43.65
A2PLC-BaseA2	-7.10	-117.40	97.12
A2FLC-BaseA2	-10.83	-123.01	87.15
A2FLC-A2PLC**	-3.73	-35.11	24.38

Note: PLC – Present-day landcover (fixed vegetation)
FLC – Future landcover (modified vegetation)
BaseB2 – Baseline for B2 emission scenario
BaseA2 – Baseline for A2 emission scenario
B2PLC – BaseB2: atmospheric forcing alone for B2 scenario - climate change
B2FLC – BaseB2: atmospheric forcing + landcover forcing
A2PLC – BaseA2: atmospheric forcing alone for A2 sceanrio – climate change
A2FLC – BaseA2: atmospheric forcing + landcover forcing
** -Landcover forcing alone for A2 and B2 scenarios

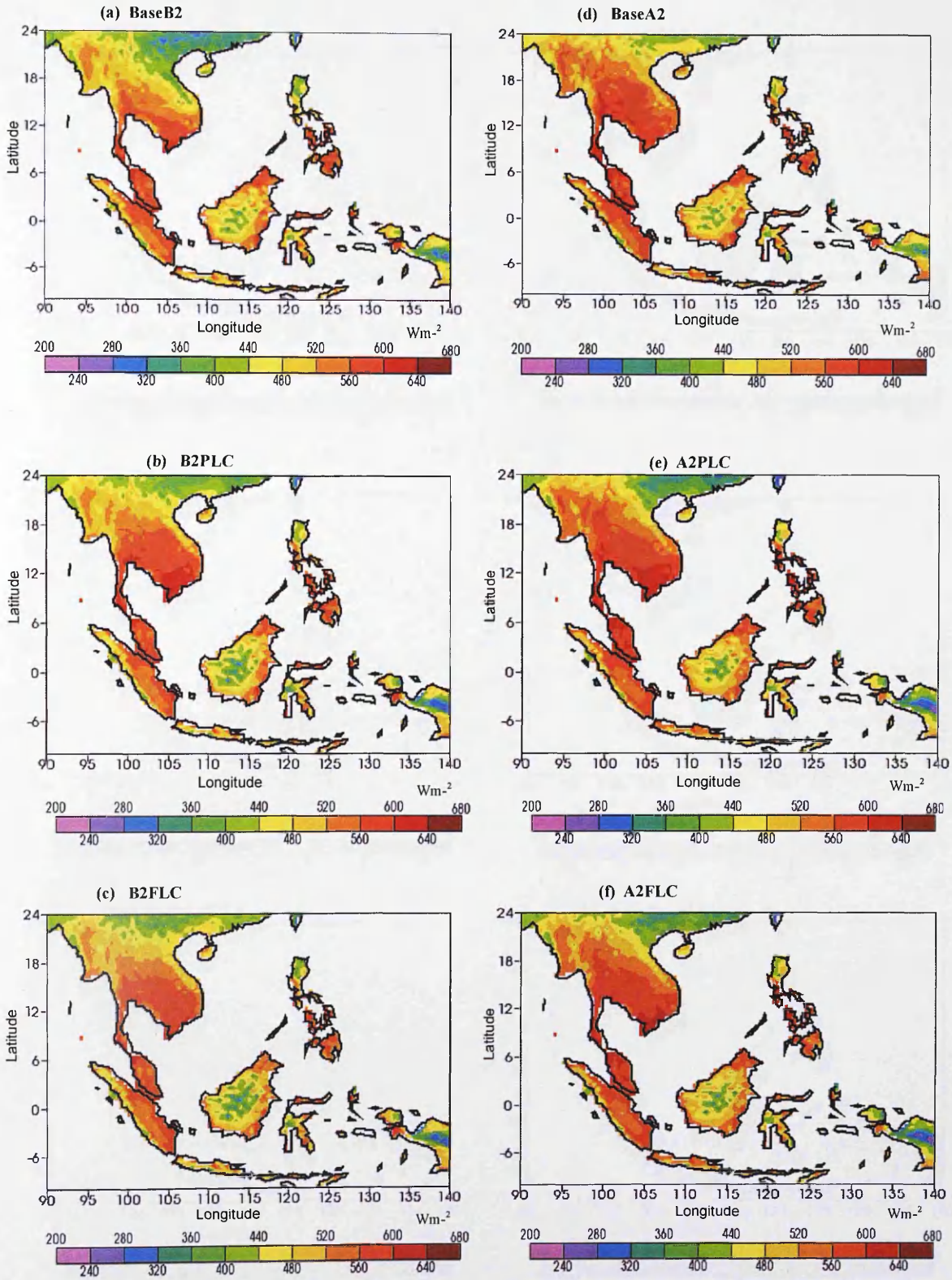

Figure 5.5: Simulated baseline (2008) and future (2100) average PAR over SEA for the B2 (a-c) and A2 (d-f) emission scenarios in the present-day (PLC) and modified future (FLC) landcovers. Compare cloud-cover model fields in Figure 3.32 (A2) and Figure 3.33 (B2).

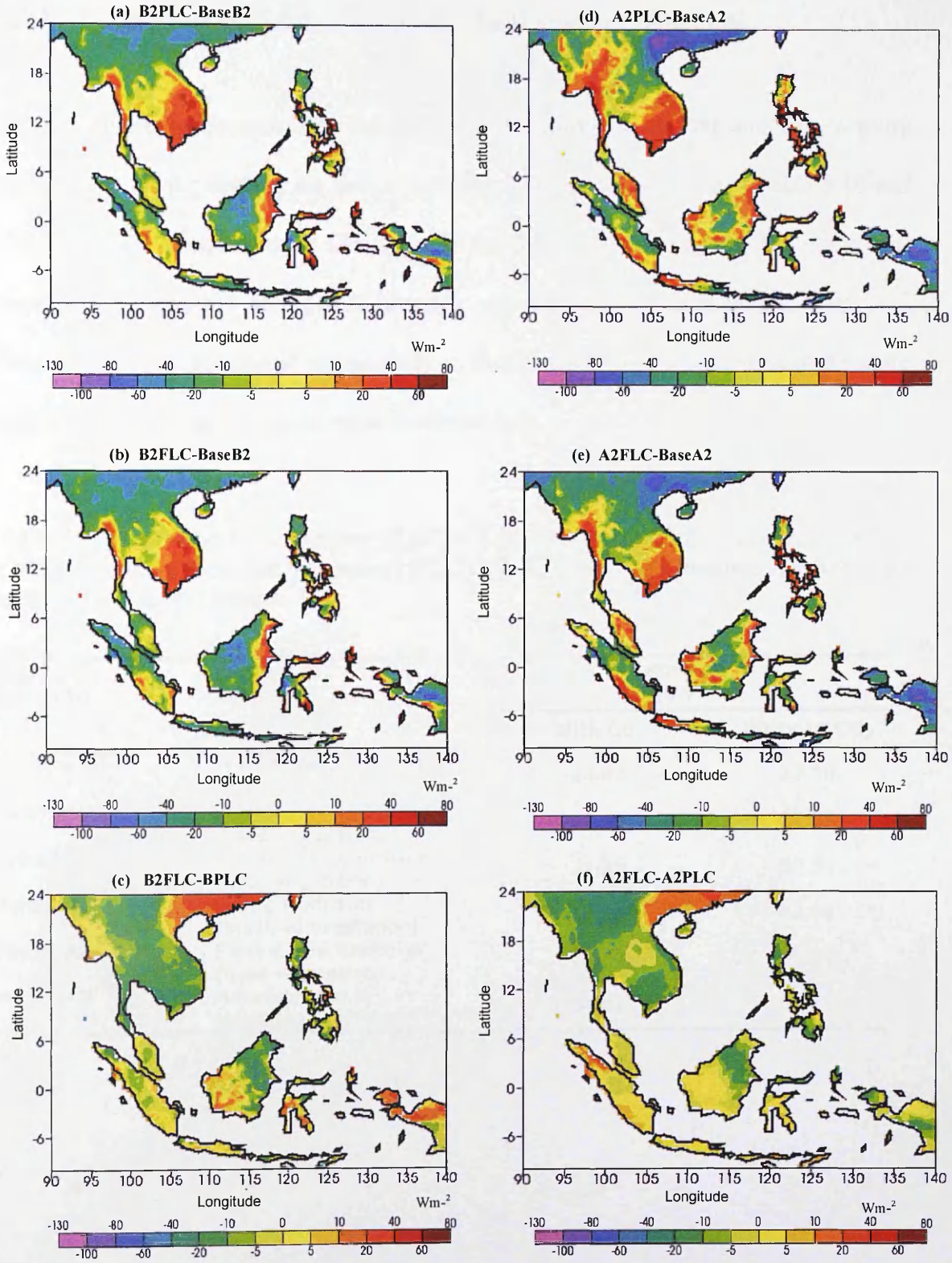

Figure 5.6: Difference in average PAR (Wm^{-2}) between **(a)** B2PLC and BaseB2, **(b)** B2FLC and BaseB2, **(c)** B2FLC and B2PLC, **(d)** A2PLC and BaseA2, **(e)** A2FLC and BaseA2, and **(f)** A2FLC and A2PLC. Note change of colour scale in panel (c) and (f).

5.5.2 Regional emissions of biogenic volatile organic compounds

The regional biogenic emissions for a number of climate, landcover and CO_2 activity factor scenarios for isoprene are shown in Table 5.9 and Table 5.11, and Table 5.10 and Table 5.12 for Monoterpene & ORVOC. In the following sections, the discussion will focus on the response of regional biogenic emissions to the isolated and combined forcings that were considered in this study to illustrate which of these forcings are more important to the biogenic emissions in Southeast Asia.

Table 5.9 Total isoprene emissions (TgC yr^{-1}) in the present (fixed vegetation) (PLC) (2008) and future (modified vegetation) (FLC) (2100) landcover scenarios, and with- and without-CO_2 activity factors.

Climate Scenario	Landcover Scenario	Isoprene (TgC yr^{-1})	
		With CO_2	Without CO_2
Baseline B2	Present-day landcover (fixed vegetation)	24.62	27.10
Baseline A2	Present-day landcover (fixed vegetation)	27.66	29.09
Future B2	Present-day landcover (fixed vegetation)	21.25	30.54
Future B2	Future landcover (modified vegetation)	19.98	32.04
Future A2	Present-day landcover (fixed vegetation)	25.39	37.04
Future A2	Future-landcover (modified vegetation)	24.21	40.22

Table 5.10 Total isoprene emissions (TgC yr^{-1}) changes in the present (fixed vegetation) (PLC) (2008) and future (modified vegetation) (FLC) (2100) landcover scenarios, and with-and without-CO_2 activity factors.

Scenario	Isoprene (TgC yr^{-1}) [%]	
	with CO_2	without CO_2
B2PLC-BaseB2	-3.37 [13.69]	3.44 [12.69]
B2FLC-BaseB2	-4.64 [18.85]	4.94 [18.23]
B2FLC-B2PLC**	-1.27 [5.98]	1.50 [4.91]
A2PLC-BaseA2	-2.27 [8.21]	5.90 [27.33]
A2FLC-BaseA2	-3.45 [12.47]	7.95 [38.26]
A2FLC-A2PLC**	-1.18 [4.65]	3.18 [8.59]

Note: PLC – Present-day landcover (fixed vegetation)
FLC – Future landcover (modified vegetation)
BaseB2 – Baseline for B2 emission scenario
BaseA2 – Baseline for A2 emission scenario
B2PLC – BaseB2: atmospheric forcing alone for B2 scenario - climate change
B2FLC – BaseB2: atmospheric forcing + landcover forcing
A2PLC – BaseA2: atmospheric forcing alone for A2 sceanrio – climate change
A2FLC – BaseA2: atmospheric forcing + landcover forcing
** -Landcover forcing alone for A2 and B2 scenarios

Table 5.11: Monoterpenes and other volatile organic compounds (ORVOC) emissions (TgC yr^{-1}) in the present-day (fixed vegetation) (PLC) (2008) and future (modified vegetation) (FLC) (2100) landcover scenarios in the B2 and A2 climate scenarios.

Climate Scenario	Landcover Scenario	Monoterpene (TgC yr^{-1})	Other VOC (TgC yr^{-1})
Baseline B2	Present-day landcover (fixed vegetation)	13.90	19.84
Baseline A2	Present-day landcover (fixed vegetation)	15.41	21.57
Future B2	Present-day landcover (fixed vegetation)	12.66	17.58
Future B2	Future landcover (modified vegetation)	11.92	16.83
Future A2	Present-day landcover (fixed vegetation)	14.29	20.36
Future A2	Future-landcover (modified vegetation)	13.49	19.32

Table 5.12: Monoterpenes and ORVOC emissions (TgC yr^{-1}) change in the present-day (fixed vegetation) (PLC) (2008) and future (modified vegetation) (FLC) (2100) landcover scenarios in the B2 and A2 climate scenarios.

Scenarios	Monoterpene ($TgCyr^{-1}$)[%]	Other VOC ($TgC\ yr^{-1}$) [%]
B2PLC-BaseB2	-1.24 [8.92]	-2.26 [11.39]
B2FLC-BaseB2	-1.98 [14.25]	-3.01 [15.17]
B2FLC-B2PLC**	-0.74 [5.85]	-0.75 [4.27]
A2PLC-BaseA2	-1.12 [7.27]	-1.21 [5.61]
A2FLC-BaseA2	-1.49 [12.46]	-2.25 [10.43]
A2FLC-A2PLC**	-1.92 [5.60]	-1.04 [5.11]

Note: PLC – Present-day landcover (fixed vegetation)
FLC – Future landcover (modified vegetation)
BaseB2 – Baseline for B2 emission scenario
BaseA2 – Baseline for A2 emission scenario
B2PLC – BaseB2: atmospheric forcing alone for B2 scenario - climate change
B2FLC – BaseB2: atmospheric forcing + landcover forcing
A2PLC – BaseA2: atmospheric forcing alone for A2 sceanrio – climate change
A2FLC – BaseA2: atmospheric forcing + landcover forcing
** -Landcover forcing alone for A2 and B2 scenarios

5.5.2.1 Impact of climate changes

The estimated present-day (baseline) total isoprene emissions for B2 and A2 emission scenario of the IPCC with present-day CO_2 activity factor of 360 ppm were 25 TgC/yr and 28 TgC/yr respectively (Figure 5.7 and Table 5.9). However, if the CO_2 activity factor is not taken into consideration, the present-day estimates for both scenarios increased by 10% (27 TgC/yr) and 5% (29 TgC/yr) respectively. The increase in future surface temperature in the region by 2.6°C (B2) and 3.5°C (A2), and without considering the CO_2 activity factor, is responsible for an increase of isoprene emissions to 31 TgC/yr (13%) for B2 and 37 TgC/yr (27%) for A2, respectively. The inclusion of future CO_2 concentration of 560 ppm at the end of this century, inhibits isoprene emissions to 21 TgC/yr (B2) and 25 TgC/yr (A2), a reduction of about 4 TgC/yr (19%) and 3 TgC/yr (8%) from the baseline estimates respectively. The inhibition effect of CO_2 on future emissions

of isoprene more than offset the effects of climate change. In terms of magnitude, the inhibitory effect of elevated CO_2 is much larger by about 10 TgC/yr (B2) and 2 TgC/yr (A2) than the effect of climate change alone of about 3 TgC/yr (B2) and 10 TgC/yr (A2) (Table 5.10 & Figure 5.8) .

The influence of an increase in temperature, as observed in this study was also observed in a number studies in the past. At the global scale, despite some differences, isoprene emissions were predicted to increase about 35% to 70% due to factors associated with increased temperature (Turner *et al.*, 1991; Sanderson *et al.*, 2003; Wiedinmyer *et al.*, 2006). In an earlier study by Guenther *et al.* (2006), an increase in temperature in the year 2100 increased the isoprene emission by a factor of 2, or even higher in some regions. In their studies, the increase of temperature alone was found to responsible for the increase of 72% of annual global isoprene emissions. Meanwhile, the increase of PAR alone accounted for an increase of 4% of annual global isoprene emissions.

The effect of climate change on isoprene emissions in the region is compensated by the increase in future atmospheric CO_2 concentration. A number of past studies have also shown an instantaneous inhibition of elevated CO_2 on isoprene emission rates, either in controlled environment or under natural field growth conditions (Rosenstiel *et al.*, 2003; Possell *et al.*, 2005). The investigation by Rosenstiel *et al.* (2003), for example, showed that the inhibition of isoprene emission rate by exposure to elevated CO_2 is linked to the increased activity of the enzyme phosphoenolpyruvate carboxylase (PEPc), which shifts the patterns of substrate use for cytosolic and chloroplastic and also limits the availability of pyruvate substrate for chloroplastic isoprene biosynthesis. Elevated CO_2 levels are also linked to an increase of mitochondrial densities in some trees species (Griffin *et al.*,

2001). The increases in mitochondrial densities are accompanied by increased expression of the PEPc gene, which is known to provide substrate to support mitochondrial respiration.

Under the present-day scenario with the incorporation of present-day CO_2 ambient concentration of 366 ppm, the emissions of monoterpene and ORVOC in Southeast Asia was 14 TgC/yr and 20 TgC/yr for B2 ; 15 TgC/yr and 22 TgC/yr for A2 scenarios (Table 5.11 & Figure 5.9) . In the future scenario, with atmospheric CO_2 concentration to double by the year 2100, accompanied with a substantial increase of regional temperature of 2.4°C (B2) and 3.6°C (A2) has shown a decrease in regional emissions of both monoterpenes and ORVOC. The decrease in both monoterpenes and ORVOC in this region could be due to the inhibitory effect of elevated CO_2. In an earlier study by Loreto *et al.* (2001) on Mediterranean evergreen oak, elevated CO_2 was found to inhibit monoterpenes (α-pinene, sabinene and β-pinene) emissions by approximately 68%. The inhibition of monoterpenes emissions was linked to the inhibition of monoterpene synthases that catalysing the formation of the three monoterpenes. Climate change impact alone has accounted for the decrease in monoterpenes emissions to 13 TgC/yr (B2) and 14 TgC/yr (A2), a decrease of 9% and 7% respectively (Table 5.12 & Figure 5.10). Similarly, ORVOC has decreased by 11% (B2) and 6% (A2) respectively.

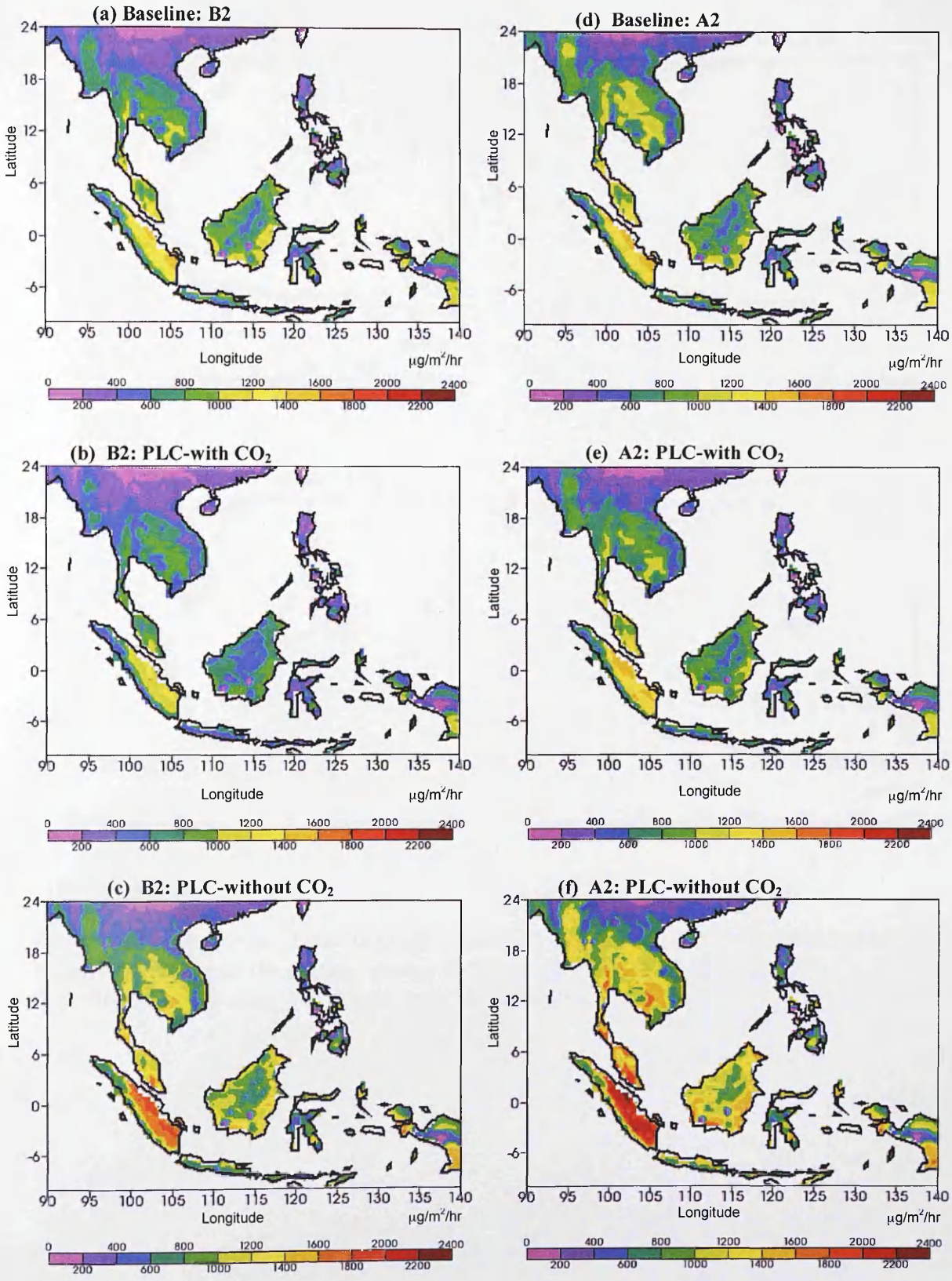

Figure 5.7: ***Isoprene***: Total isoprene emissions (µg m^{-2} hr^{-1}) with- and without-CO_2 activity factors for the Baseline (2008) and future B2 (a-c) and A2 (d-f) emissions scenarios (2100) in the present-day landcover (PLC) scenario.

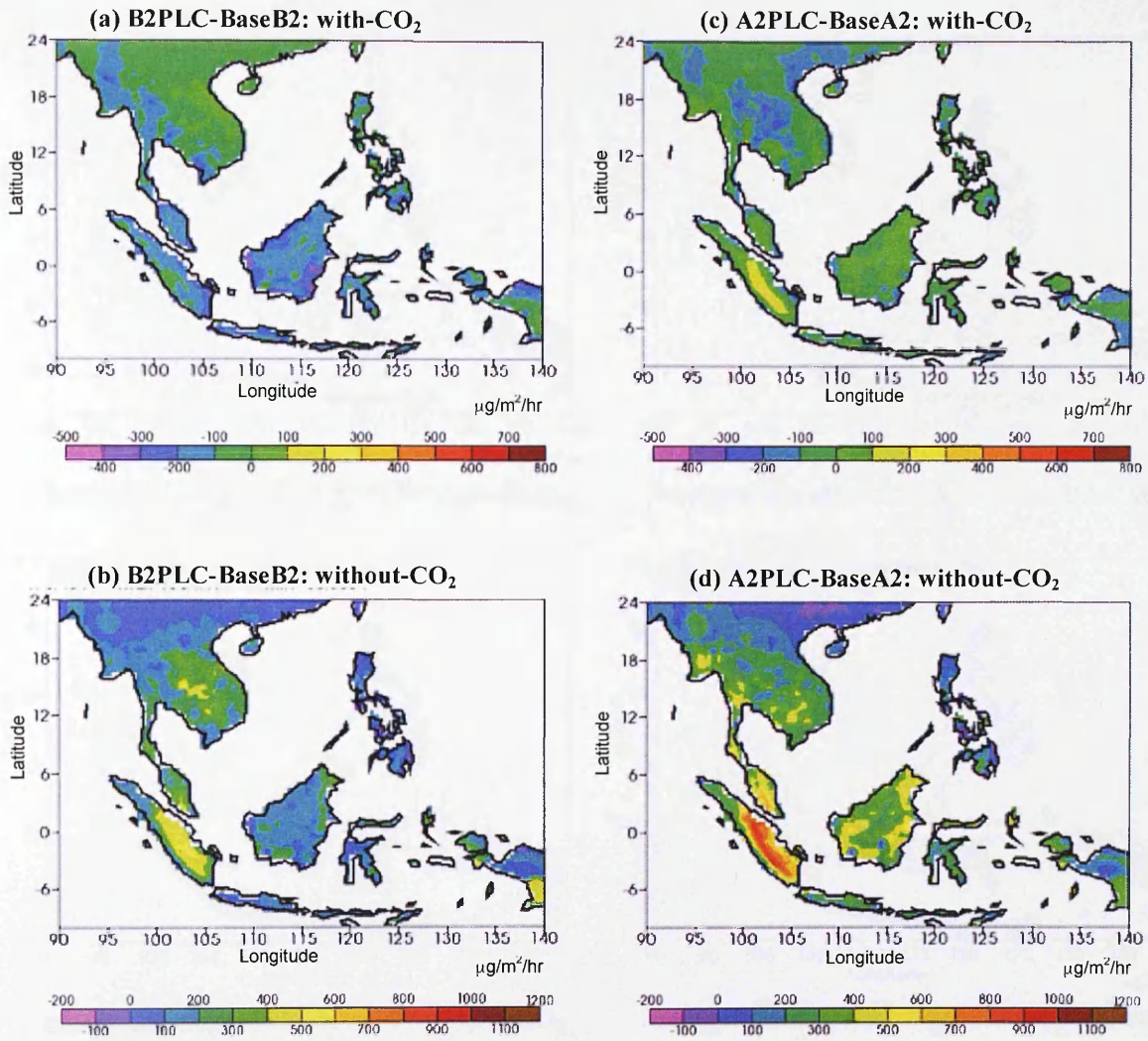

Figure 5.8: ***Isoprene***: Total isoprene emissions (µg m^{-2} hr^{-1}) with- and without-CO_2 activity factor due to the climate change forcing alone for the B2 (a & b) and A2 (c & d) scenarios. Note the change in colour scale in panels (b) and (d).

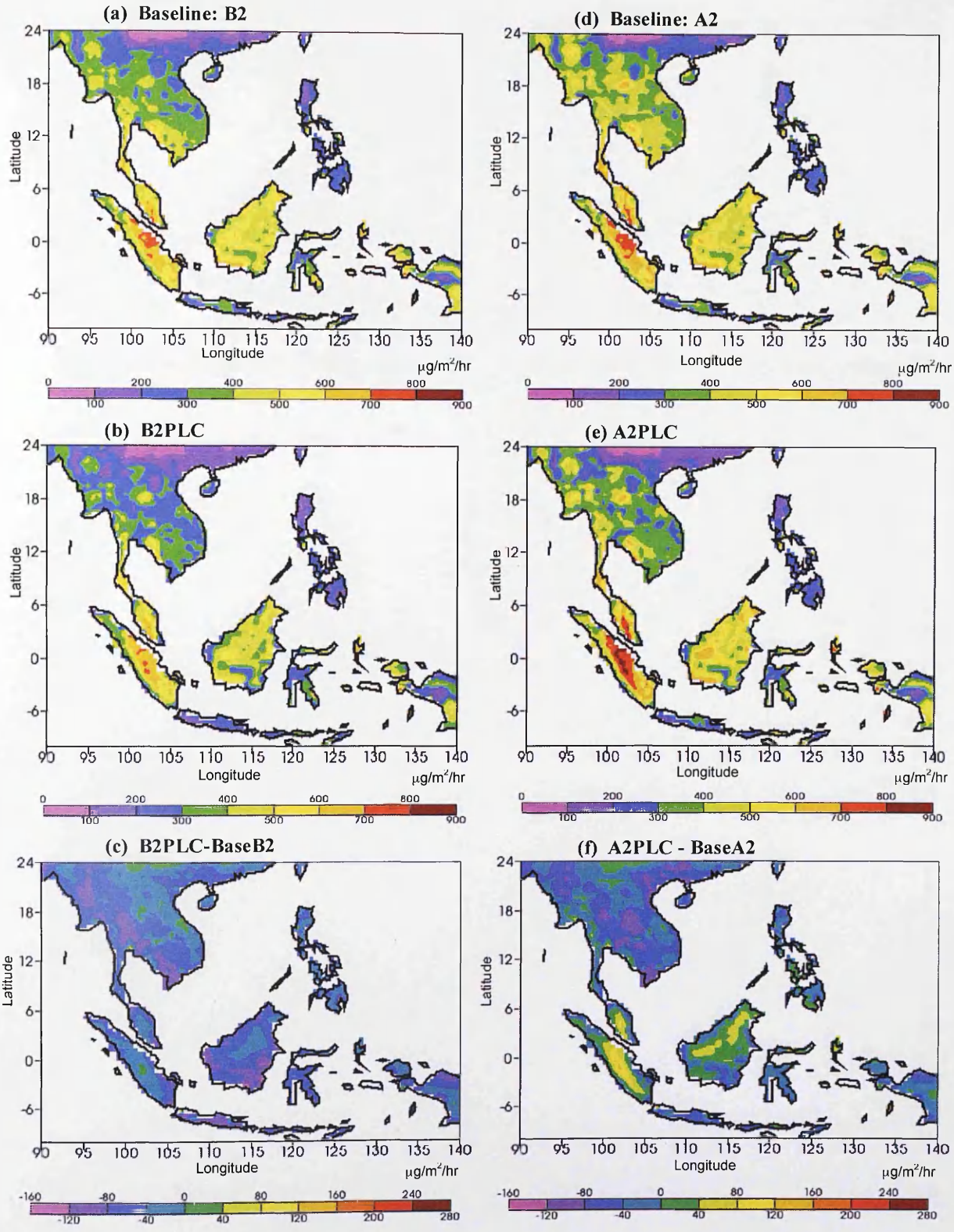

Figure 5.9: ***Monoterpenes***: Monoterpene emissions (µg m^{-2} hr^{-1}) for the Baseline (2008) (*top panel*) and future B2 (*mid panel left*) and A2 (*mid panel right*) scenarios. The impact of the climate change forcing alone on the monoterpene emissions for the both A2 and B2 scenarios are shown at the bottom panels (c & f). Note the change in colour scale for panels (c) and (f).

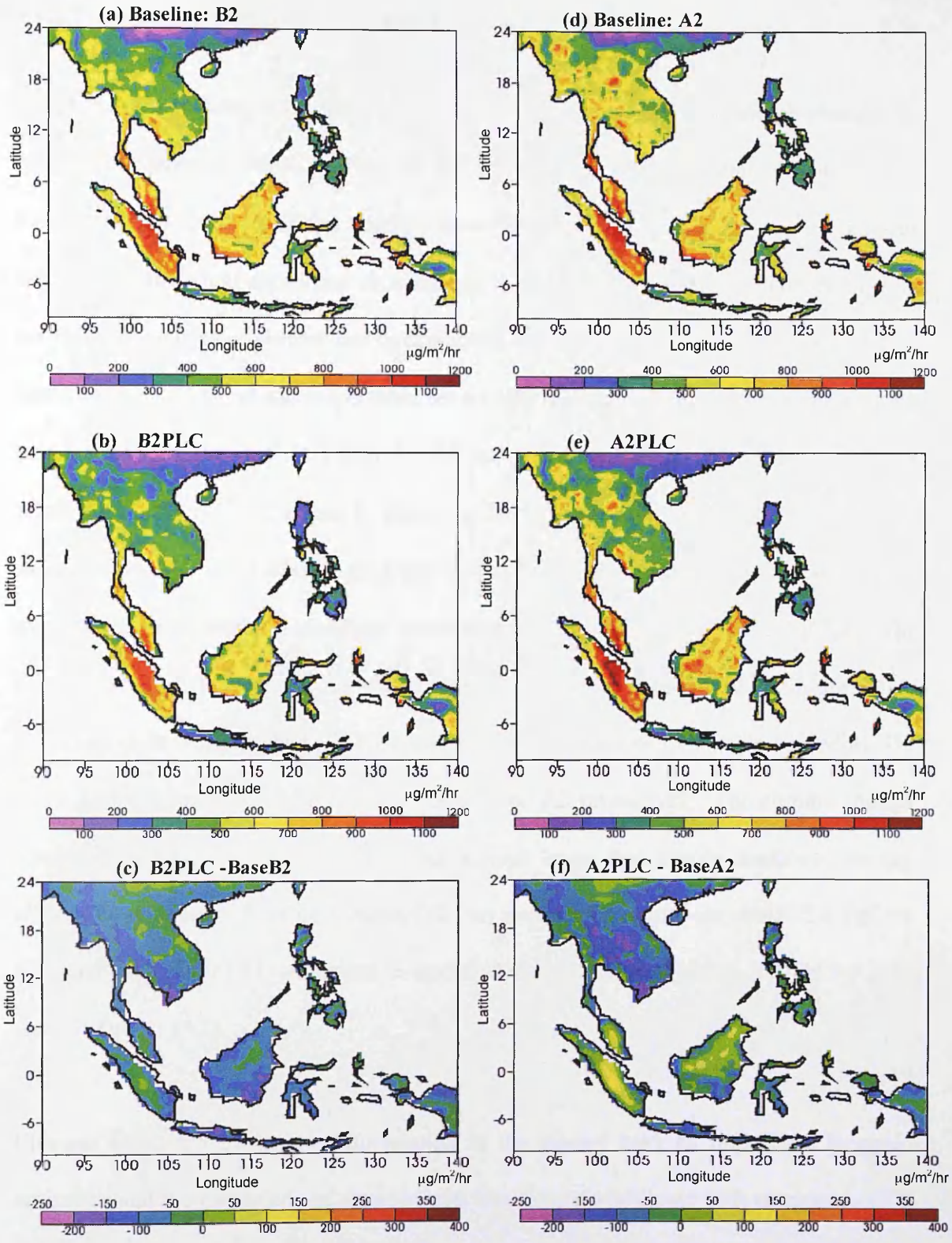

Figure 5.10 ***ORVOC***: ORVOC emissions (µg m^{-2} hr^{-1}) for the Baseline (2008) (*top panel*) and future B2 (*mid panel left*) and A2 (*mid panel right*) scenarios. The impacts of the climate change forcing alone on the ORVOC emissions for the both A2 and B2 scenarios are shown at the bottom panels (c & f). Note the change in colour scale for panels (c) and (f).

5.5.2.2 Impact of landcover changes

Direct impacts of landcover changes on biogenic emissions are seen through changes in types of vegetation, which relates to the emission factor and foliar density. The modification of future landcover considered in this study results in a regional decrease in total annual mean leaf area index as described in Section 5.4.3.3. Other indirect impacts are through changes in climate and hydrological regimes. As described in Section 5.5.1, landcover forcing alone was responsible for a slight increase in the regional mean surface temperature of about 0.1°C (1.9%) for B2 and 0.7°C (2.3%) for A2 transient climate scenarios (Table 5.6). Changes in future landcover have also resulted in a very small decrease in PAR by 3 Wm^{-2}(0.6%) and 4 Wm^{-2} (0.8%). Impacts of landcover forcing alone on regional isoprene emissions accounted for a decrease by 6% (1.3 TgC/yr) for B2 and 5% (1.2 TgC/yr) for A2 under with-CO_2 influence (Table 5.10 & Figure 5.11). However, under without the CO_2 influence, the isoprene emissions were increased by 5% (1.50 TgC/yr) and 9 % (3.18 TgC/yr) for B2 and A2 respectively. The climate change forcing impact alone on isoprene emission is much larger than that by landcover forcing alone. The inhibitory effect of elevated CO_2 on isoprene emission was about 2.8 TgC/yr (B2) and 4.4 TgC/yr (A2) compared to landcover forcing alone of about 0.2 TgC/yr (B2) and 2.0 TgC/yr (A2).

Changes in landcover due to deforestation in the tropics have an impact on biogenic emissions and the magnitude of changes was found to be associated with changes in PFT distribution. In earlier studies, at the global scale, crop expansion in the tropics was responsible for a decrease in isoprene and other volatile organic compounds by 27-30% , which has been linked to the reduction of LAI and emissions factors (Lathiere *et al.*, 2005). MEGAN simulations of global isoprene emissions using two different of PFT

databases, IMAGE with more cropland area, and MAPSS-P with less cropland area, were found to produce a decrease of 30% of isoprene emission with IMAGE and an increase of 6% with MAPSS-P (Guenther *et al.*, 2006).

In the case of monoterpenes and ORVOC, changes in future landcover in the region for B2 and A2 climate scenarios, show a decrease in emissions when the CO_2 activity factor is included. The estimated monoterpenes emissions due to landcover forcing alone were 0.74 TgC/yr (6%) for B2 and 1.92 TgC/yr (6%) for A2 (Table 5.12 & Figure 5.12). Similar trend was also observed for ORVOC, where the emissions were decrease to 0.75 TgC/yr (4%) for B2 and 1.04 TgC/yr for A2 (5%) respectively (Table 5.12 & Figure 5.13).

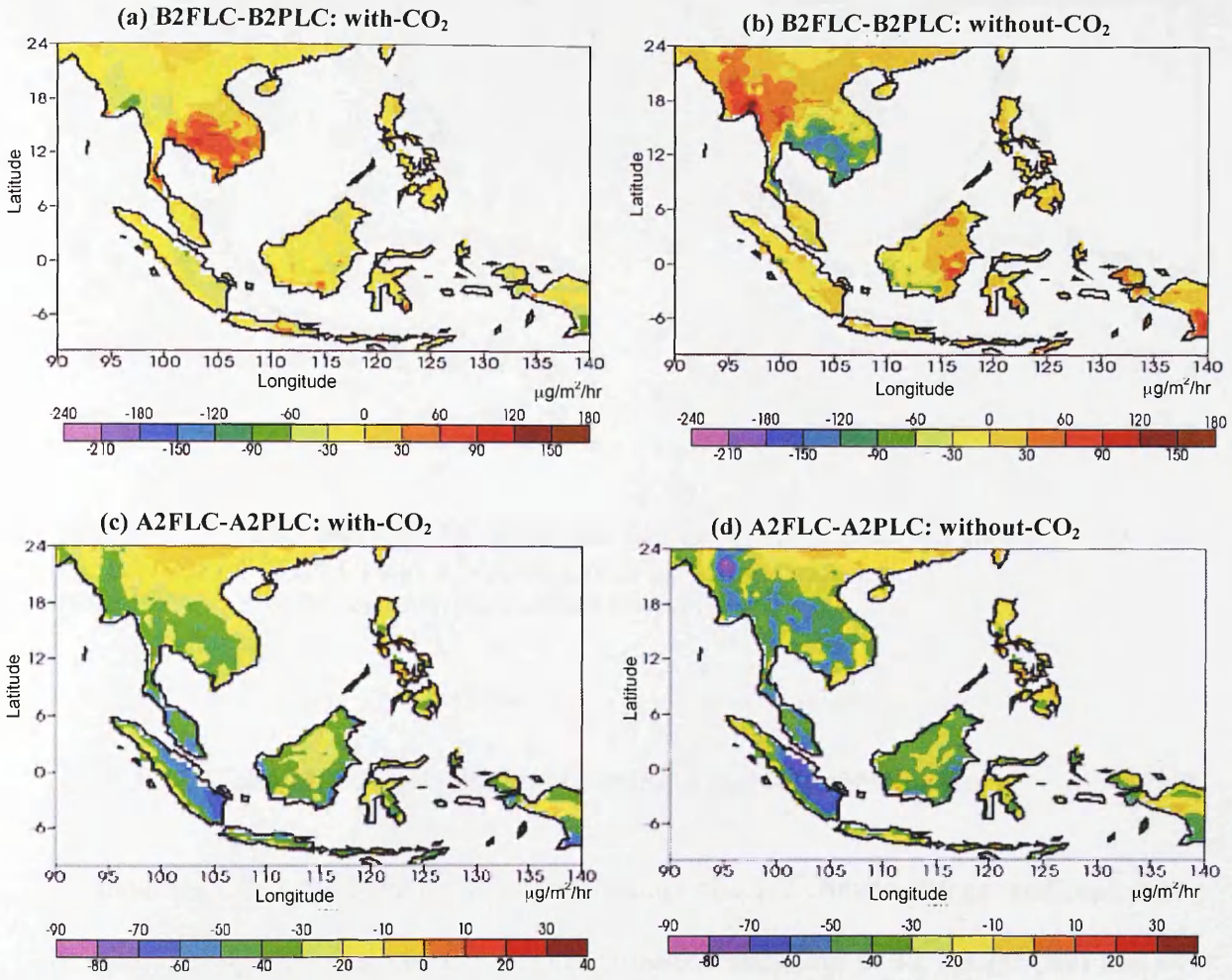

Figure 5.11 ***Isoprene***: Total isoprene emissions (µg m^{-2} hr^{-1}) with-and without-CO_2 activity factor by landcover forcing alone for the B2 (a & b) and A2 (c & d) climate scenarios. (Note: *PLC – Present-day landcover; FLC – Future landcover)*

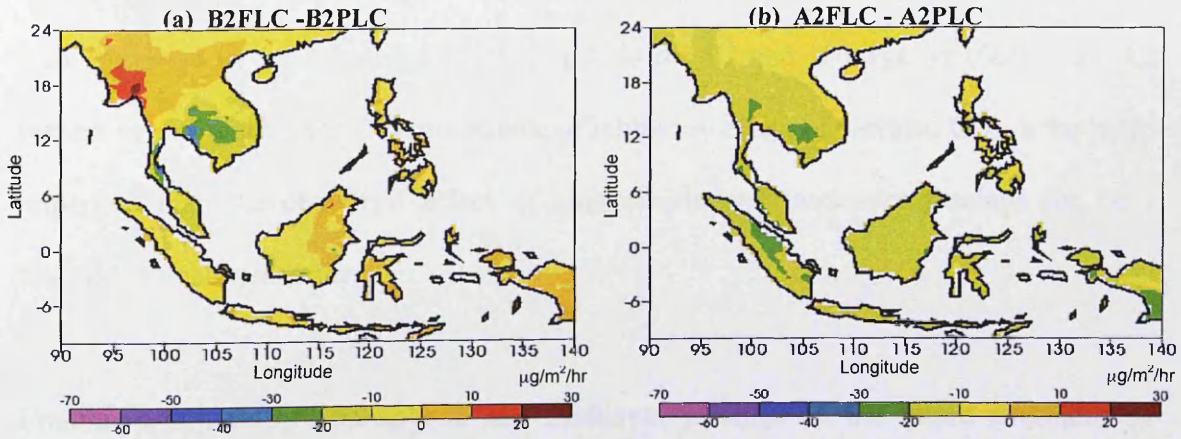

Figure 5.12 ***Monoterpene***: Monoterpene emissions (µg m^{-2} hr^{-1}) by landcover forcing alone for the B2 (B2FLC-B2PLC) and A2 (A2FLC-A2PLC) scenarios.
(Note: *PLC – Present-day landcover; FLC – Future landcover)*

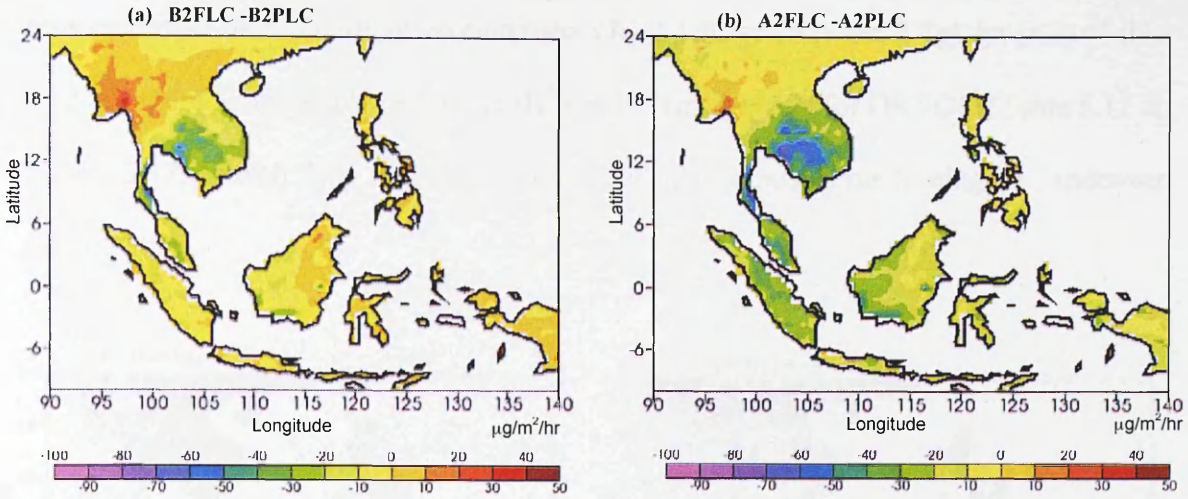

Figure 5.13: ***ORVOC***: ORVOC emissions (µg m^{-2} hr^{-1}) by landcover forcing alone for the B2 (B2FLC-B2PLC) and A2 (A2FLC-A2PLC) climate scenarios.
(Note: *PLC – Present-day landcover; FLC – Future landcover)*

5.5.2.3 Combined impact of climate changes and landcover forcings

Without the CO_2 activity factor, the combination impact of climate change and landcover forcing was found to elevate the regional isoprene emissions to 32 TgC/yr (B2) and 40 TgC/yr (A2), an increase of 5 TgC/yr (18%) and 11 TgC/yr (38%) respectively (Table 5.9, Table 5.10 & Figure 5.14). High concentration of ambient atmospheric CO_2 in the future was found to significantly inhibit the isoprene emissions. Emissions of isoprene were observed to decrease by 12 TgC/yr (60%) for B2 and 16 TgC/yr (66%) for A2 respectively (Figure 5.15). The magnitude of inhibitory effect of elevated CO_2 is far more important than the combined effect of atmospheric and landcover forcings for both transient climate scenarios.

Combined impacts of atmospheric and landcover forcings on the future emissions of monoterpenes and ORVOC was found to decrease further to 12 TgC/yr and 17 TgC/yr for B2; 14 TgC/yr and 19 TgC/yr for A2 (Table 5.11). Effects of the combined forcing were

responsible for the decrease in monoterpenes by 2 TgC/yr (B2) and 2 TgC/yr (A2) (Table 5.12 & Figure 5.16); and by 3 TgC/yr (B2) and 2 TgC/yr (A2) for ORVOC (Table 5.12 & Figure 5.17), which is a much greater impact than atmospheric forcing or landcover forcing alone.

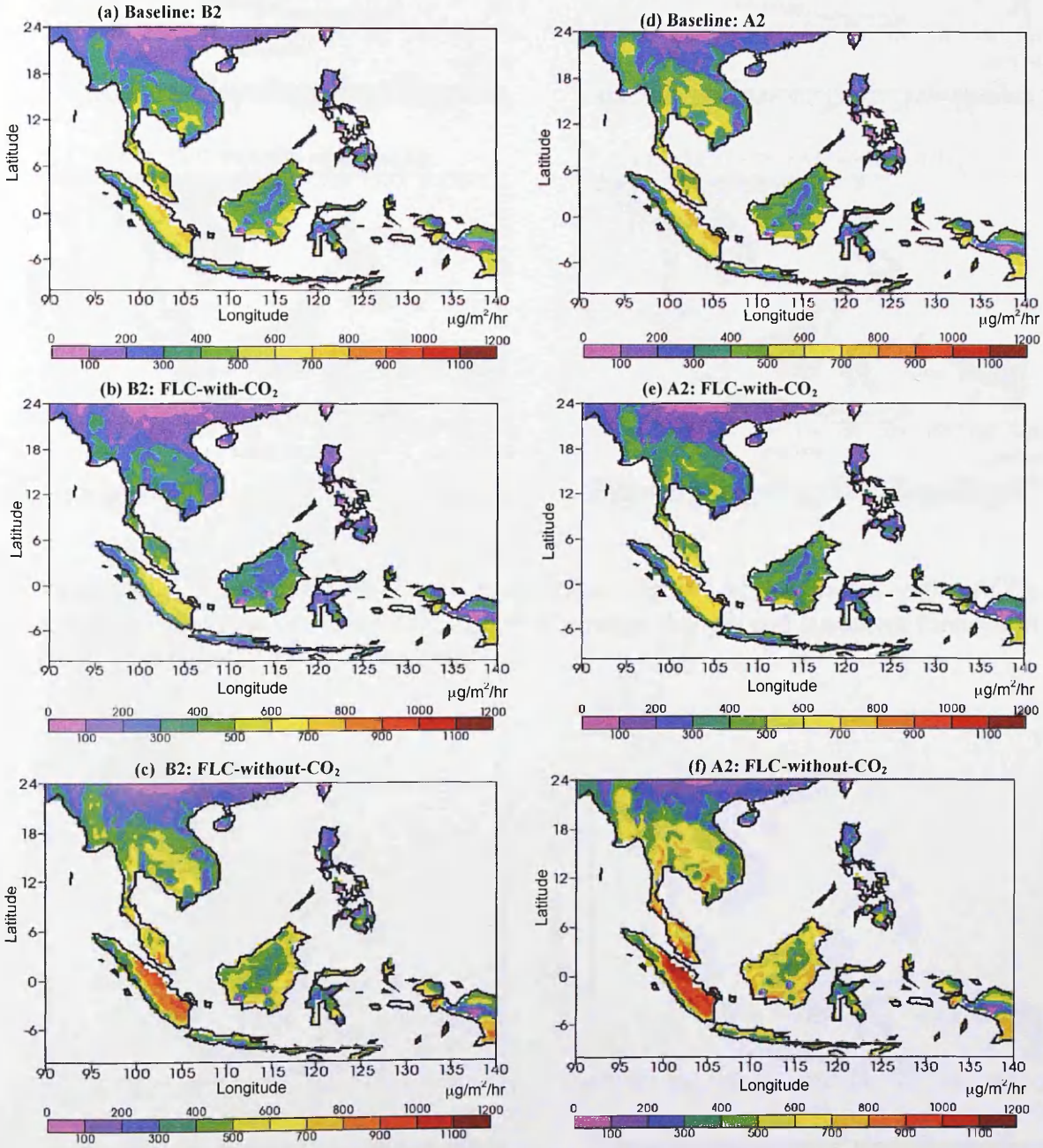

Figure 5.14: ***Isoprene***: Total isoprene emissions (µg m^{-2} hr^{-1}) with- and without-CO_2 activity factor in the Baseline (2008) and the B2 (a-c) and A2 (d-f) emissions (2100) scenarios in the future landcover (FLC) scenario.

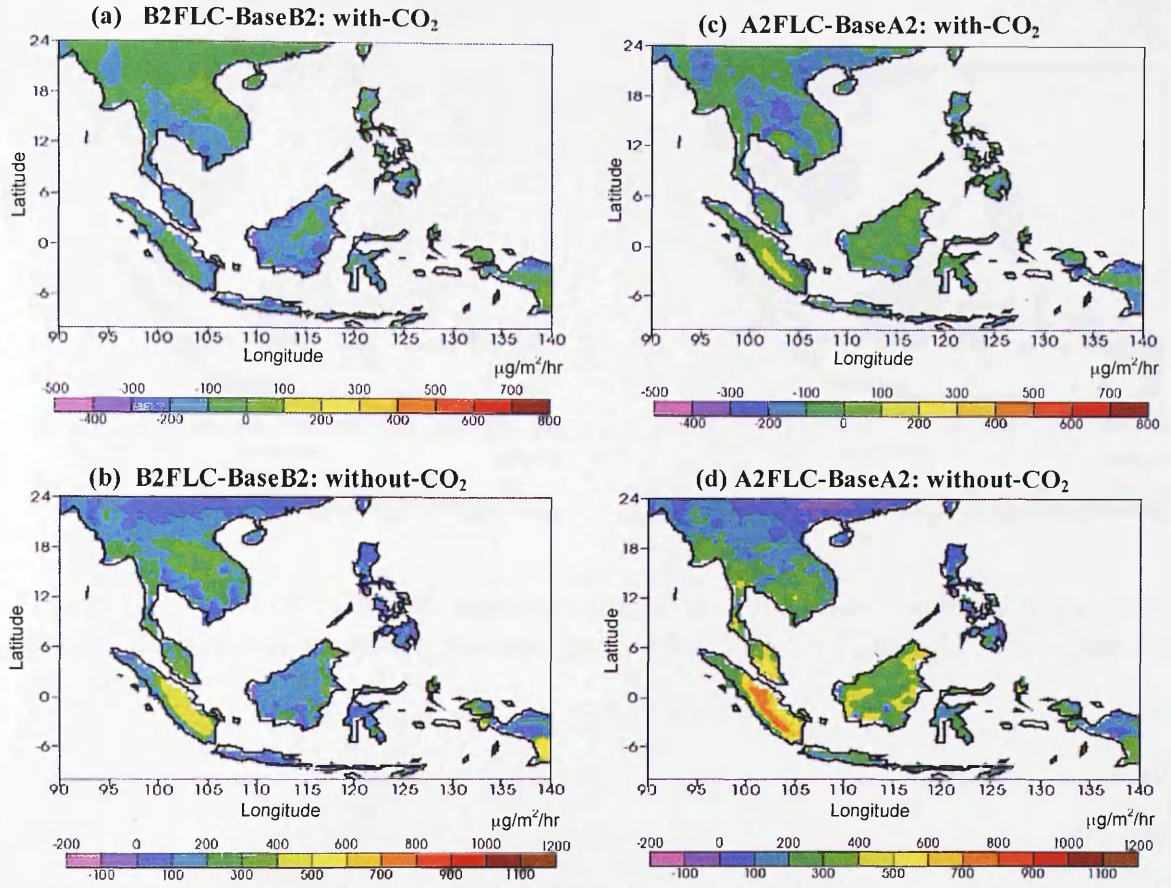

Figure 5.15: ***Isoprene***: Total isoprene emissions (µg m^{-2} hr^{-1}) with-and without-CO_2 activity factor due to the combined impacts of climate changes and landcover forcings in the B2 (a & b) and A2 (c & d) scenarios.

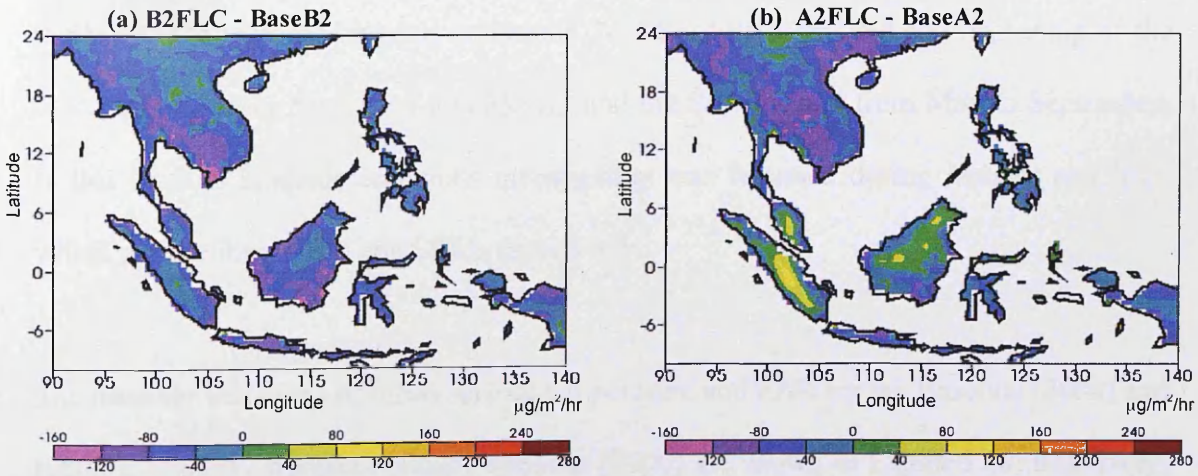

Figure 5.16: ***Monoterpene***: Monoterpene emissions (µg m^{-2} hr^{-1}) due to the combined impacts of climate changes and landcover forcings in the B2 (*left panel*) and A2 (*right panel*) scenarios.

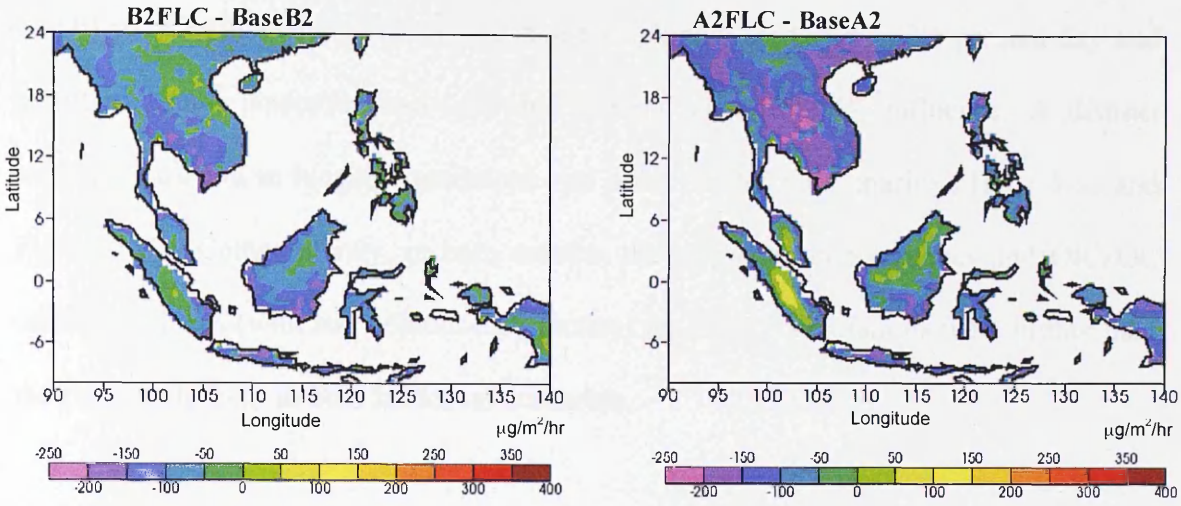

Figure 5.17 ***ORVOC***: ORVOC emissions (µg $m^{-2}hr^{-1}$) due to the combined impacts of climate changes and landcover forcings in the B2 (*left panel*) and A2 (*right panel*) scenarios.

5.5.3 Seasonal Variability of Biogenic Emissions

This study also investigates the influence of the two predominant seasonal monsoons that affecting the region, namely the northeast monsoon (NEM) and southwest monsoon (SEM) on the regional biogenic emissions. NEM occurs at the end and beginning of the year, running from November and March, and the SEM occurs from May to September. In this section, biogenic emissions investigation was focussed during January and July, which representing NEM and SEM respectively.

The monthly variations of mean surface temperature and PAR for the Baseline (2008) and future B2 and A2 transient climate scenario (2100) are shown in Figure 5.18. Relatively, the monthly means of surface temperature and PAR were higher in A2 than B2 simulations due to the weaker emissions forcing in the B2 scenario climate scenarios.

Monthly emissions fluxes of biogenic emissions for the present-day (2008) and future (2100) were estimated for B2 and A2 transient climate scenarios under present-day and modified future landcover and with and without elevated CO_2 influence. A distinct seasonal variation in biogenic emissions was observed for all scenarios (Table 5.13 and Figure 5.19). Comparatively, in both months, the isoprene, monoterpenes and ORVOC emissions fluxes (with and without-CO_2 factors) for the A2 simulations were higher than the B2 simulations, in both landcover scenarios.

Further investigation was carried out for the month of January and July, which are considered the middle of both NEM and SEM, to illustrate the seasonal pattern of biogenic emissions in the region. Generally, higher biogenic emissions were observed in July compared with biogenic emissions in January. In both months, the spatial distributions of total isoprene emissions in both the A2 and B2 climate scenario under the present-day and future landcover are shown in Figure 20 – Figure 23. Meanwhile, the spatial distributions for monoterpenes and ORVOC are also shown in Figure 24 – Figure 27 for all scenarios considered in this study. Notably, higher emission during this period is associated with relatively higher temperature and PAR conditions (Figure 5.18). In an earlier investigation on the seasonal variations in isoprene from four tropical Indian deciduous tree species by Singh *et al.* (2007) was found to be significantly high monthly variations in isoprene emissions. Higher isoprene emissions were observed during the summer and autumn months (May to November) and lower during winter and spring months (December to April). Higher temperature and PAR were responsible for the high isoprene emissions during summer and autumn.

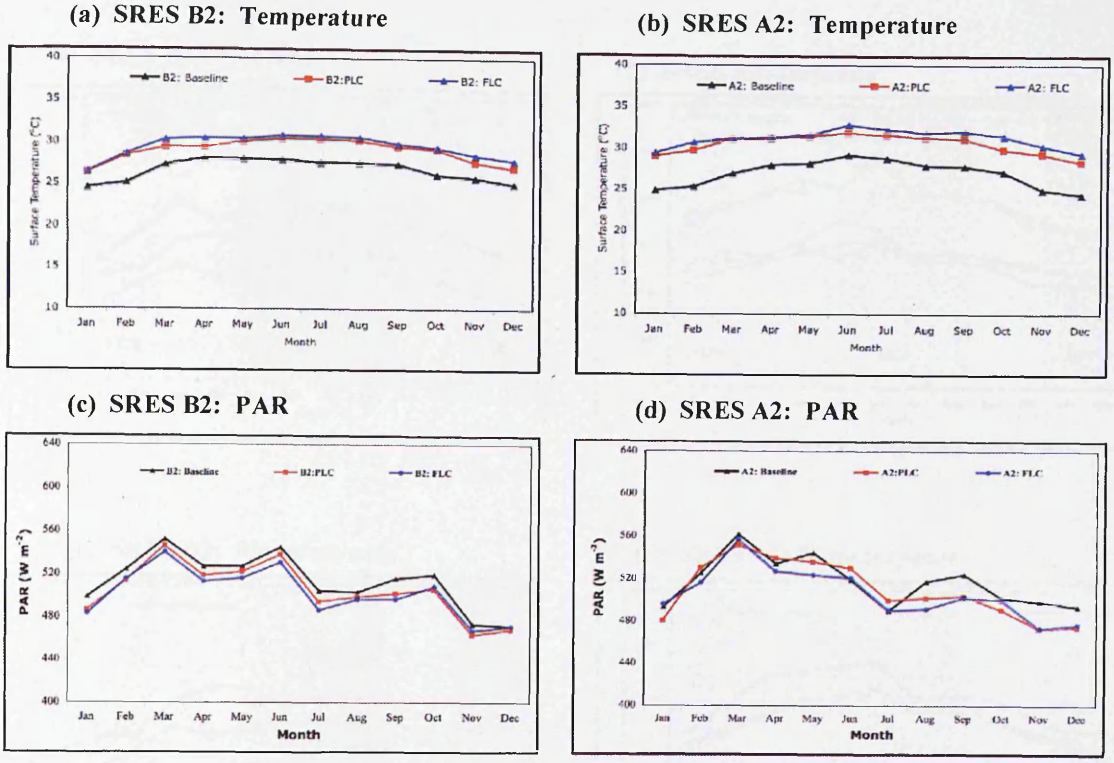

Figure 5.18: Monthly variations of mean surface temperature (°C) and PAR (Wm^{-2}) in the Baseline (2008), and the B2 and A2 scenarios (2100): (a) & (b) – Temperature; (c) & (d) – PAR.

Table 5.13 Total biogenic emissions flux ($\mu g/m^2/hr$) during January and July in the A2 and B2 climate scenarios under the present-day (PLC) and future landcover (FLC) scenarios.

			BaseB2	BaseA2	B2PLC	B2FLC	A2PLC	A2FLC
Isoprene ($\mu g/m^2/hr$)	Jan	with-CO_2	1131.43	1288.21	851.7	843.27	1124.09	1228.52
		without-CO_2	1230.97	1288.76	1306.68	1292.44	1824.57	1725.57
	July	with-CO_2	1357.14	1392.65	1196.49	1189.29	1344.13	1341.13
		without-CO_2	1524.31	1568.58	1835.65	1819.85	2057.55	2057.55
Monoterpene ($\mu g/m^2/hr$)	Jan	with-CO_2	635.84	686.69	523.16	528.18	608.05	643.36
	July	with-CO_2	797.29	808.72	696.28	700.79	753.42	763.98
ORVOC ($\mu g/m^2/hr$)	Jan	with-CO_2	897.98	988.17	738.85	741.7	908.59	909.59
	July	with-CO_2	1125.98	1142.13	983.33	989.71	1079.95	1078.95

Note: PLC – Present-day landcover
FLC – Future Landcover

(a) SRES B2: Isoprene

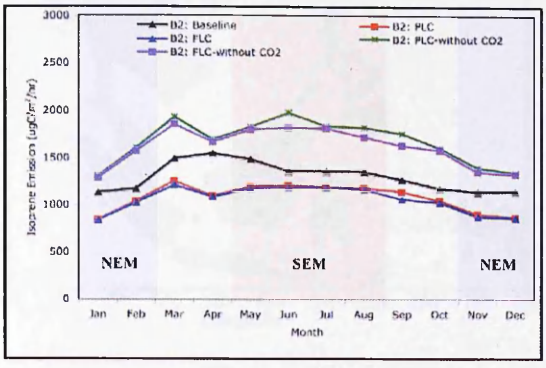

(b) SRES A2: Isoprene

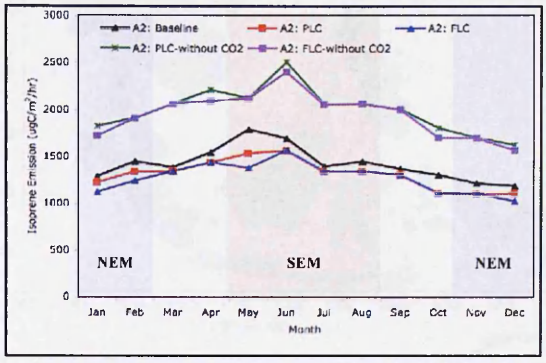

(c) SRES B2: Monoterpenes

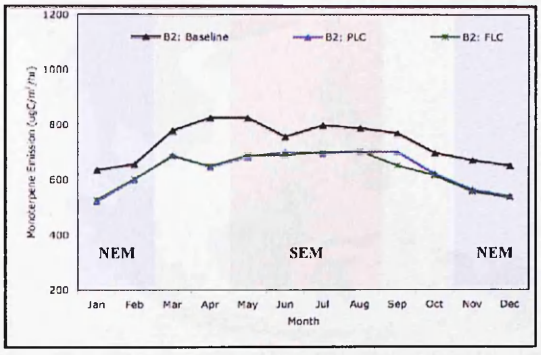

(d) SRES A2: Monoterpenes

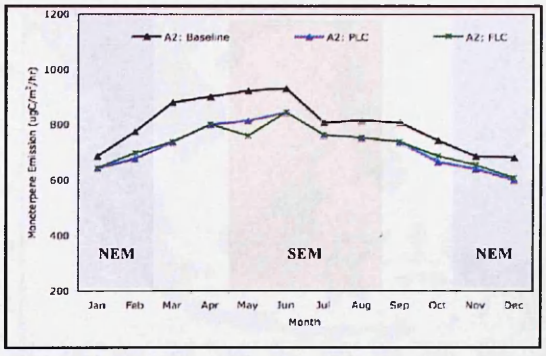

(e) SRES B2: ORVOC

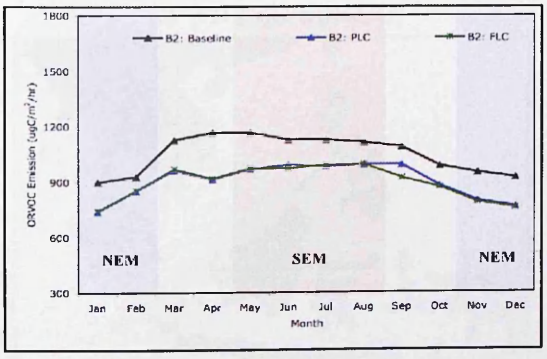

(f) SRES A2: ORVOC

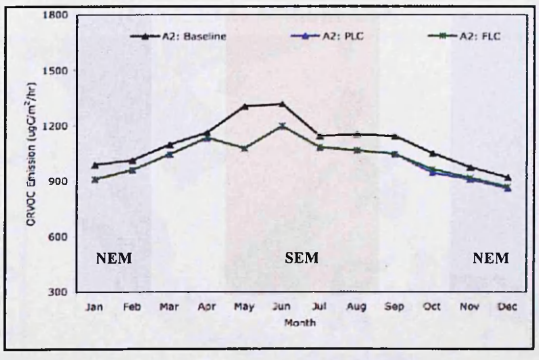

Figure 5.19: Seasonal variations (January and July) of the total biogenic emissions fluxes (ug m^{-2} hr^{-1}) in the Baseline (2008), and the B2 and A2 transient climate scenarios (2100): (a) & (b) – Isoprene; (c) & (d) – Monoterpene; (e) & (f) - ORVOC
Note: NEM – Northeast Monsoon (January)
SEM – Southeast Monsoon (July

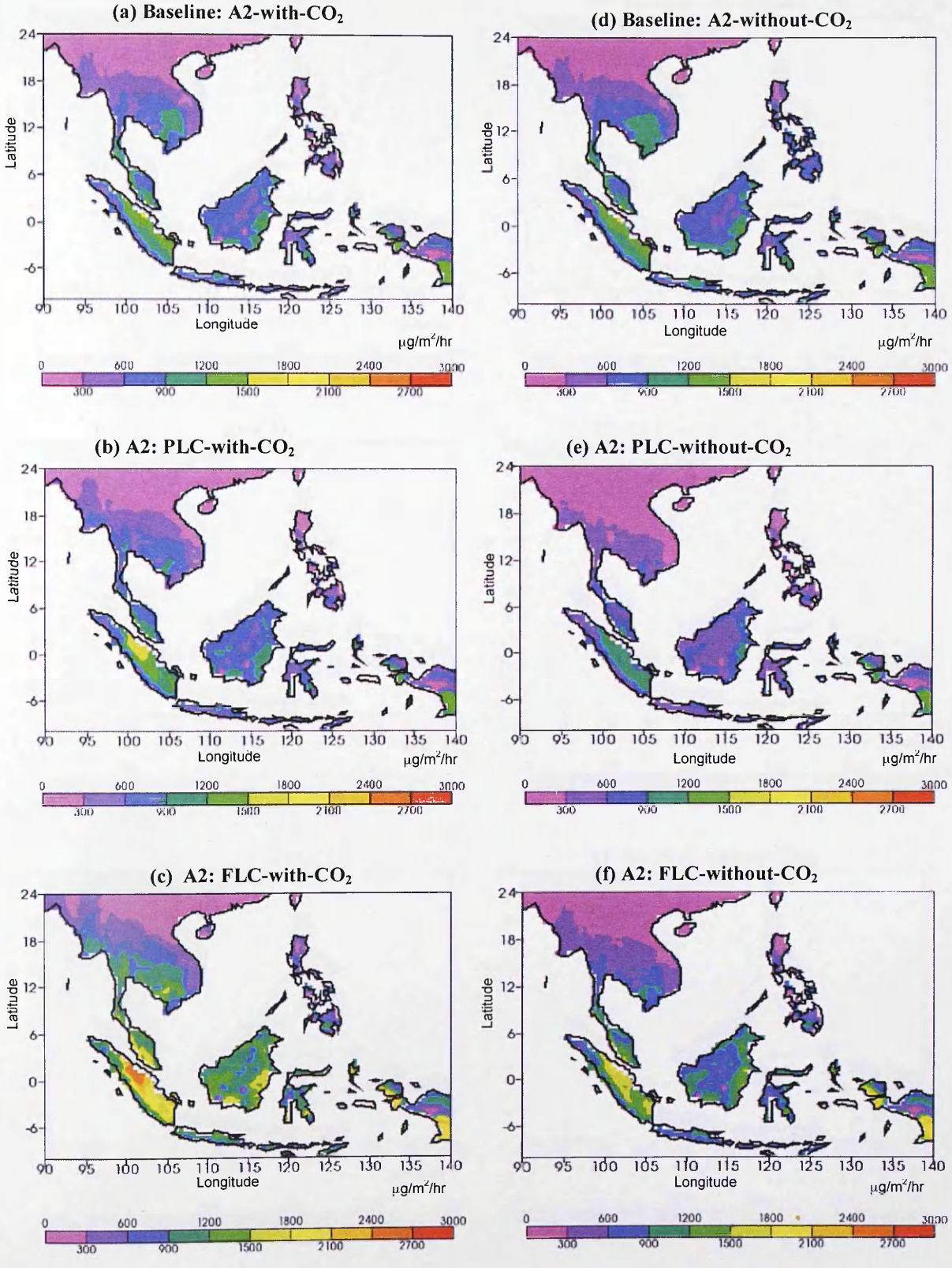

Figure 5.20: ***A2:January-Isoprene***: Isoprene emissions (µg $m^{-2}hr^{-1}$) with- and without-CO_2 activity factor in the Baseline (2008) and A2 emission scenarios in the present-day and future landcover scenarios during January.

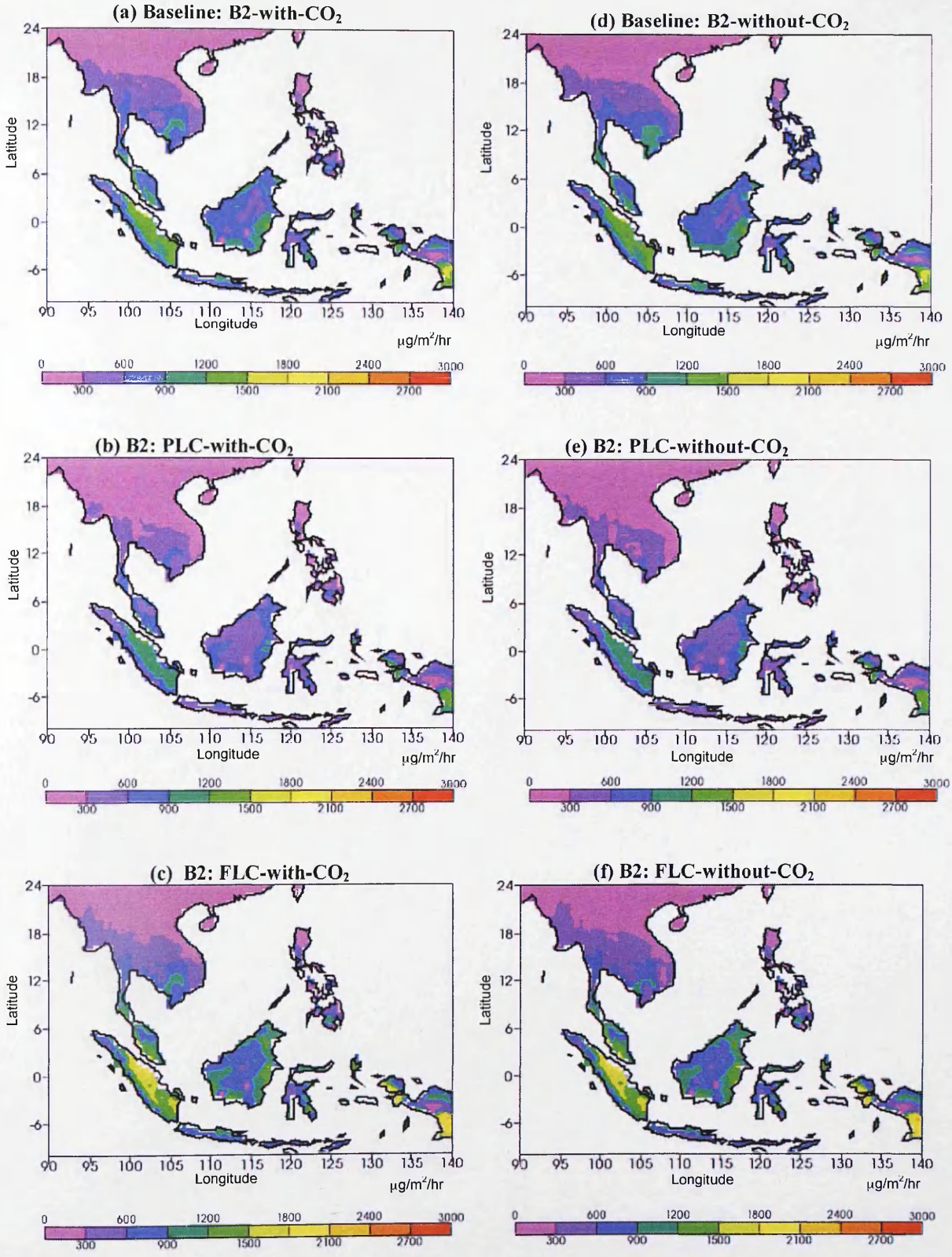

Figure 5.21: ***B2:January-Isoprene***: Isoprene emissions (µg m^{-2} hr^{-1}) with- and without-CO_2 activity factor in the Baseline (2008) and the future B2 emissions scenarios in the present-day and future landcover scenario during January.

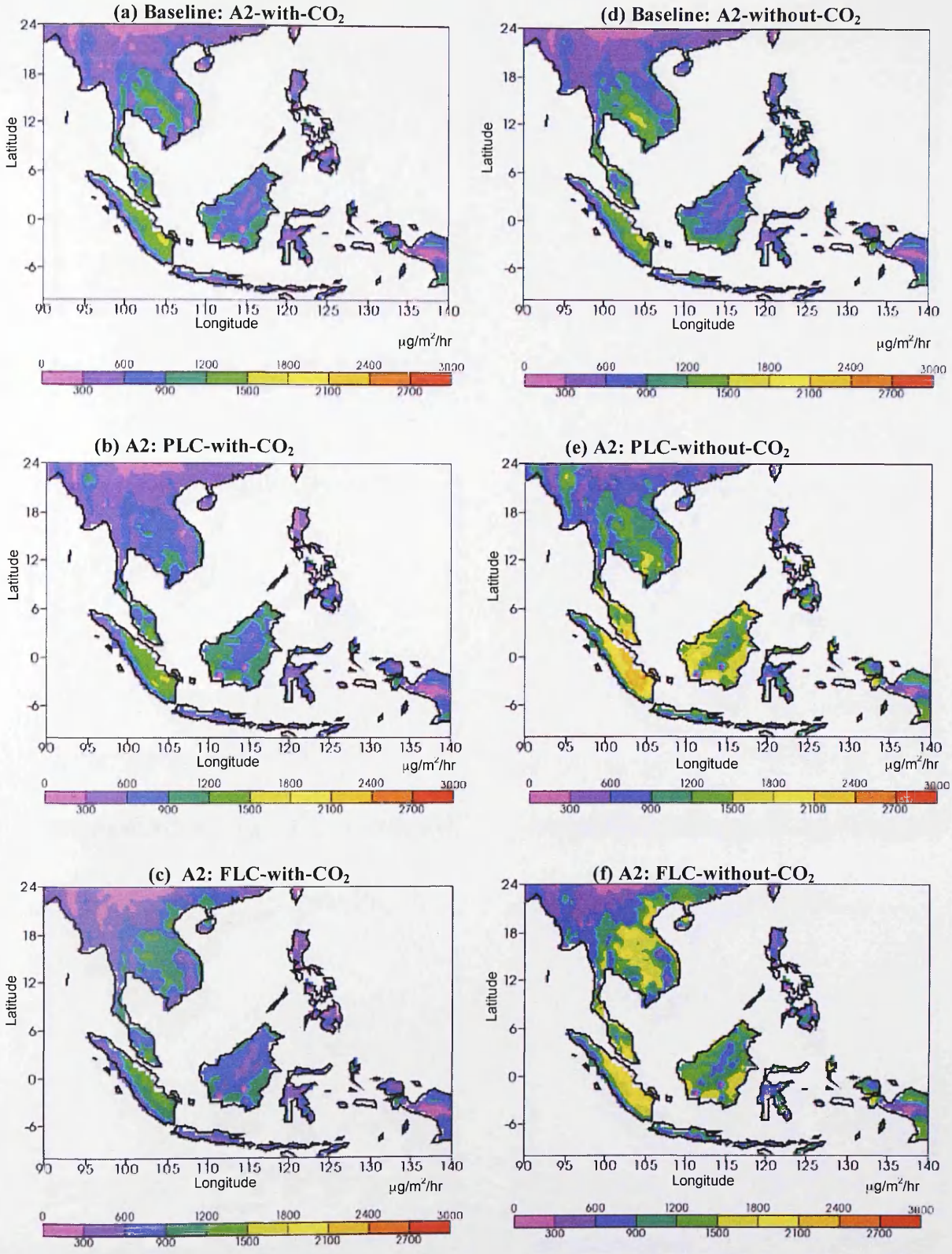

Figure 5.22: ***A2:July-Isoprene***: Isoprene emissions (µg m^{-2} hr^{-1}) with- and without-CO_2 activity factor in the Baseline (2008) and the future A2 emissions scenarios in the present-day and future landcover scenario during July.

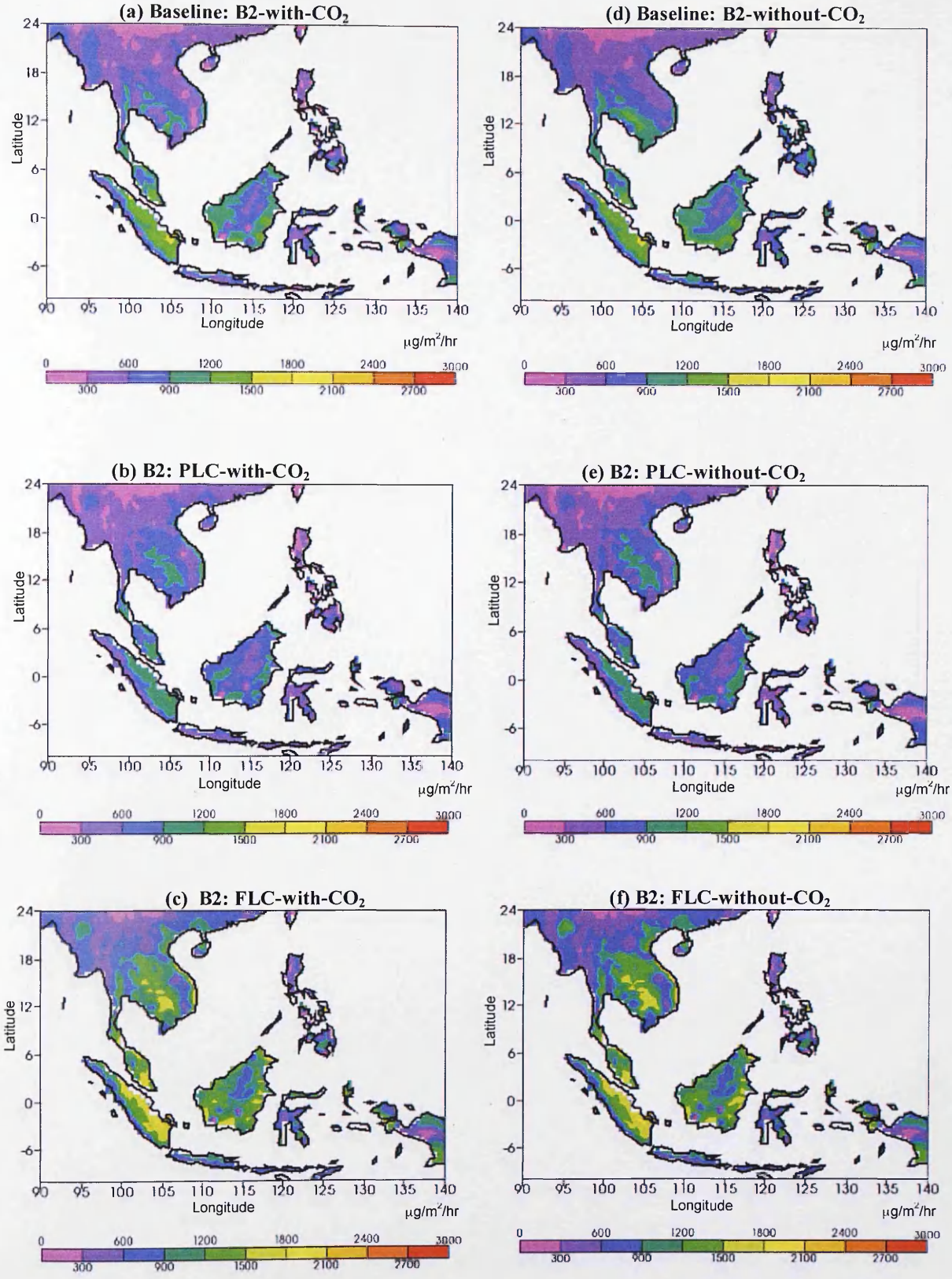

Figure 5.23: ***B2:July-Isoprene***: Isoprene emissions (µg m^{-2} hr^{-1}) with- and without-CO_2 activity factor in the Baseline (2008) and the future B2 emissions scenarios in the present-day and future landcover scenario during July.

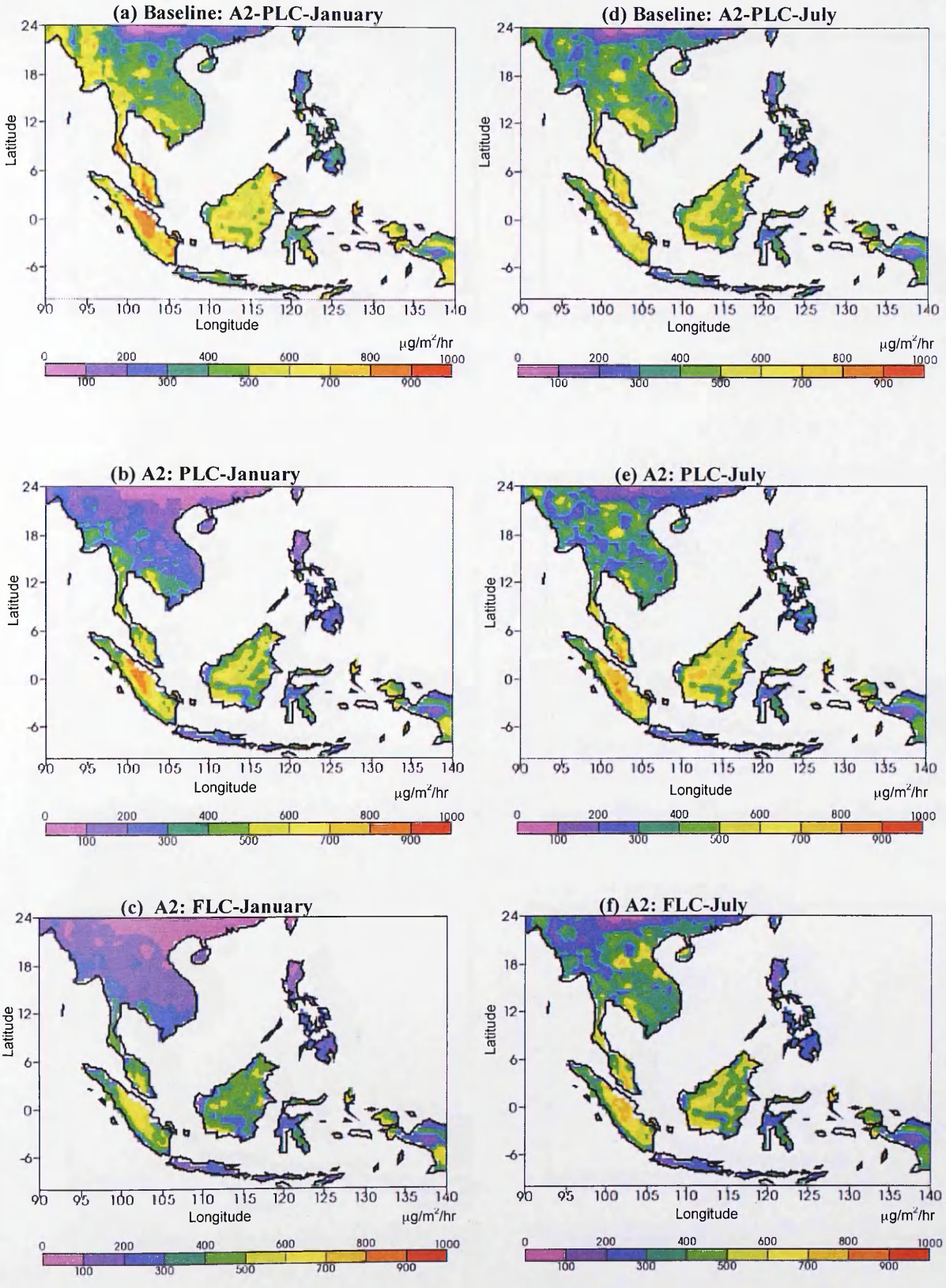

Figure 5.24: ***A2:January/July-Monoterpenes***: Monoterpenes emissions (µg m^{-2} hr^{-1}) with-CO_2 activity factor in the Baseline (2008) and the future A2 emissions scenarios in the present-day and future landcover scenario during January (*left panel*) and July (*right panel*).

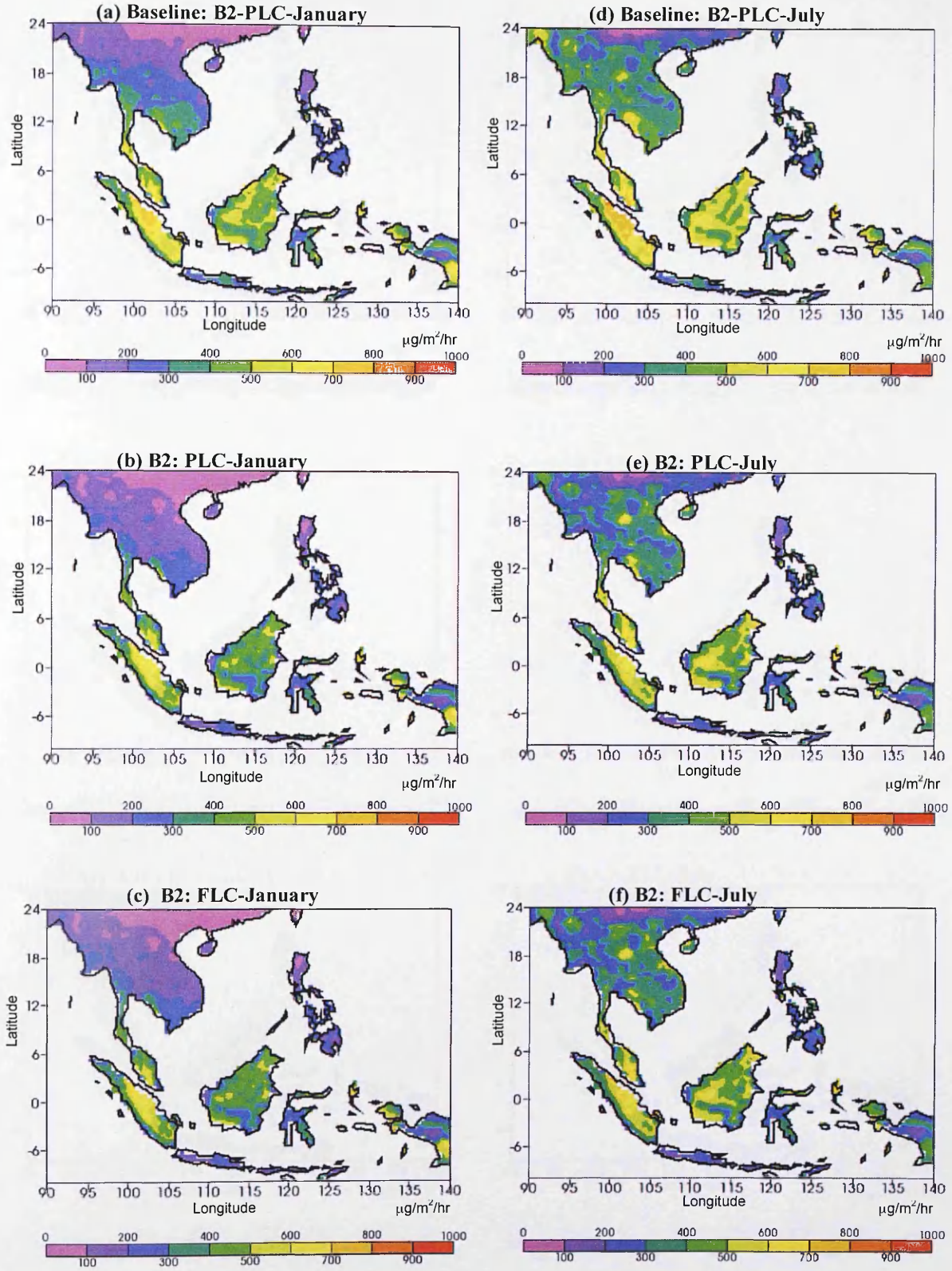

Figure 5.25: ***B2:January/July-Monoterpenes***: Monoterpenes emissions (µg m^{-2} hr^{-1}) with- and without-CO_2 activity factor in the Baseline (2008) and the future B2 emissions scenarios in the present-day and future landcover scenario during January (*left panel*) and July (*right panel*).

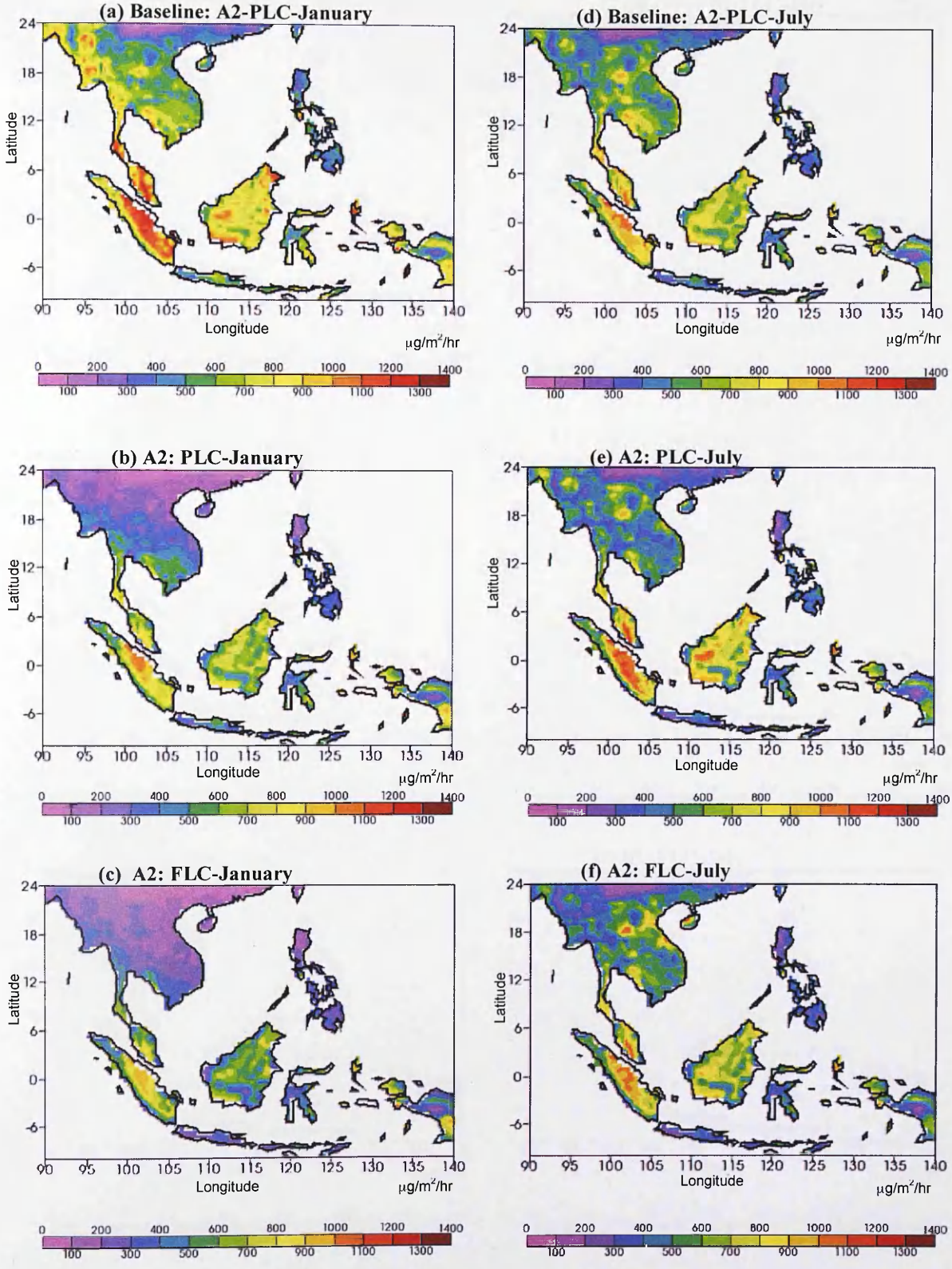

Figure 5.26: ***A2:January/July-ORVOC***: ORVOC emissions (µg m^{-2} hr^{-1}) with- and without-CO_2 activity factor in the Baseline (2008) and the future A2 emissions scenarios in the present-day and future landcover scenario during January(*left panel*) and July (*right panel*).

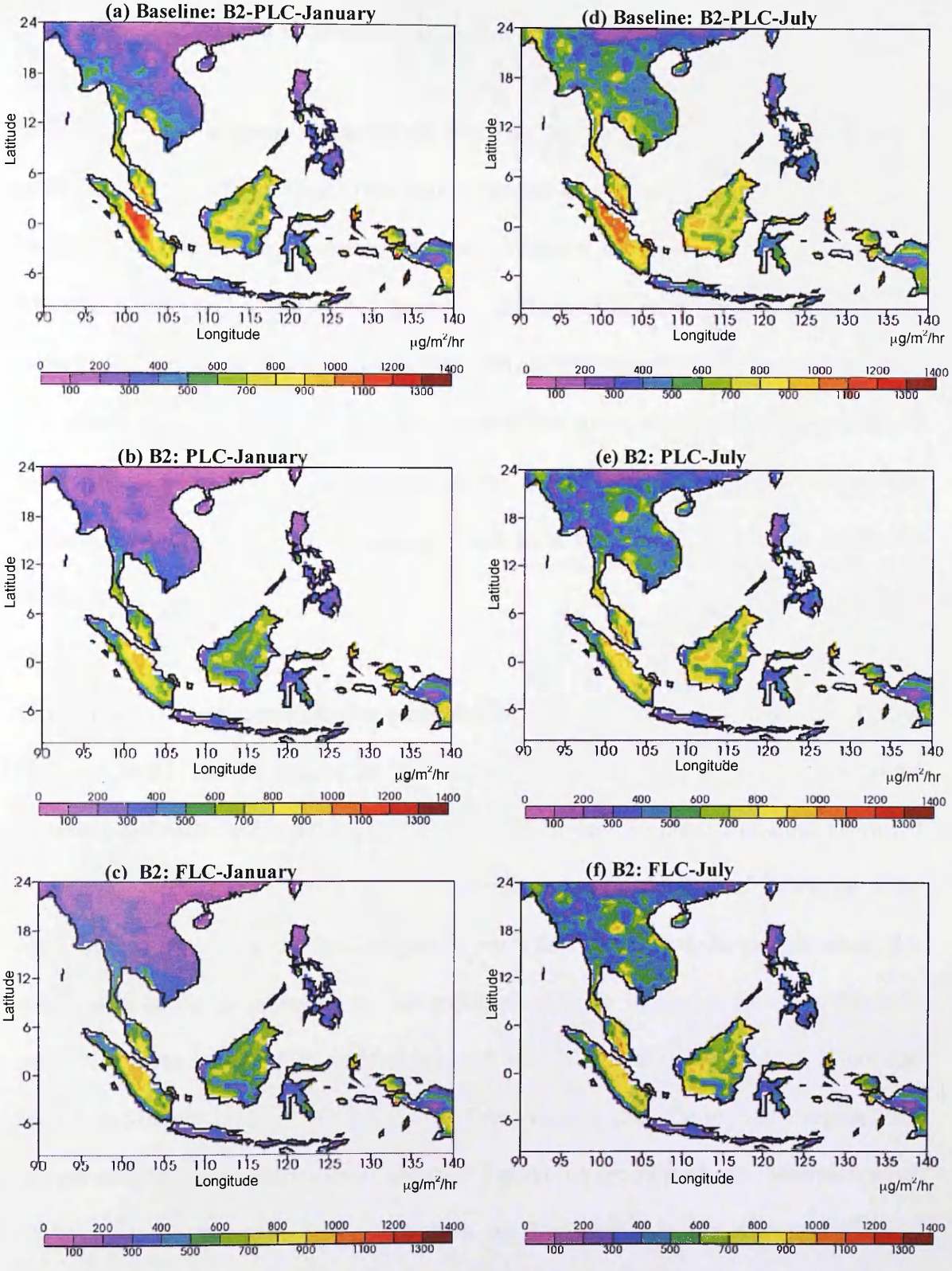

Figure 5.27: ***B2:January/July-ORVOC***: ORVOC emissions (µg m^{-2} hr^{-1}) with- and without-CO_2 activity factor in the Baseline (2008) and the future B2 emissions scenarios in the present-day and future landcover scenario during January (*left panel*) and July (*right panel*).

5.5.4 Evaluation of the Regional Biogenic Emissions

Evaluation of the biogenic emissions in Southeast Asia through comparison with other work, is extremely difficult due to the limited number of studies conducted for this region. Despite a few studies in estimating isoprene emissions in the region, there are always differences in domain of the studies, as well as differences in the methods and model used in the investigation. Despite these limitations and differences, comparing the current study with previous works provides a snapshot of isoprene emission estimates and provides a better understanding of its contribution to the global isoprene emission budget. The estimated isoprene emissions in Southeast Asia from this study and previous works are shown in Table 5.14.

In this study, the estimated baseline emissions of isoprene without-CO_2 were 27.1 TgC/yr for Baseline B2 and 29. TgC/yr for Baseline A2. These estimates are very similar to the posteriori estimates by Shim *et al.* (2005) of 29.1 TgC/year. Isoprene emissions estimated by Fu *et al.* (2007), for Indochina and Indonesia region (about 70% of Southeast Asia) using inverse modelling has found slightly lower (22 TgC/yr) than the current work; this discrepancy could be explained by the exclusion of other important source of isoprene emissions in the region, such as Malaysia and the Philippines. Fu *et al.* (2007) has also employed MEGAN model (Guenther *et al.*, 2006) in their study for the same region, and has estimated isoprene emissions of about 27 TgC/yr. A recent study by Stavrakou *et al.* (2009) using an inverse modelling technique for Southeast Asia, has estimated about 34 TgC/yr of isoprene emission, which is 14-20% higher than the estimate in the current study. Further evaluation on the isoprene emissions estimate from BVOCEM model by comparing with isoprene emissions flux measurement carried out at Danum Valley (a lowland tropical rainforest), Borneo (Malaysia) (5°N, 117.5°E) during the OP3

measurement campaign from April-July 2008. The mean isoprene emissions flux measured during the OP3 campaign was 0.49 mgm^{-2} hr^{-1}. At the same location, the model has estimated isoprene emission fluxes of 0.86 mg m^{-2} hr^{-1} for the Baseline B2 and 0.77 mg $m^{-2}hr^{-1}$ for the Baseline A2, which are higher by a factor of 1.8 (B2) and 1.6 (A2) respectively.

Table 5.14 Comparison of isoprene emissions estimate for Southeast Asia with other studies.

	Region/Domain	Model	Isoprene (TgC/yr)	
			With CO_2	Without-CO_2
This study	Southeast Asia 10°S – 24°N 90°E – 140°E	BVOCEM* (2008) Res: 0.5° x 0.5°	24.6 (Baseline B2) 27.7 (Baseline A2)	27.1 (Baseline B2) 29.1 (Baseline A2)
Stavrakou *et al* (2009)	Southeast Asia 10°S – 5°N, 95°E-150°E & 5°N – 20°N, 90°E-110°E	Inverse Modelling (2006)		31.8
		MEGAN-ECMWF* (2006) Res: 1° x 1°		40.2
Fu *et al.* (2007)	Indochina and Indonesia	Inverse Modelling/GEOS-Chem		22
		MEGAN* (2006) Res: 1° x 1°		27
Shim *et al* (2005)	Southeast Asia 4°S -30°N	Inverse Modelling/GEOS-Chem (Sep 1996 –Aug 1997)		29.1
		GEIA inventory** (1990)		38.2

Note:
* Based on MEGAN model by Guenther *et al.* (2006)
** Based on algorithm by Guenther *et al.* (1995)

5.6 Conclusions

This study has used the Biogenic Volatile Organic Compound Emissions Model (BVOCEM) to investigate biogenic emissions response to climate change and landcover forcings for B2 and A2 transient climate scenarios of the IPCC. A sensitivity study on the effect of ambient atmospheric CO_2 concentration on isoprene emissions was also carried out for a number of combinations of climate change and landcover scenarios for both B2 and A2. Some conclusions can be drawn from the results:

- The present-day estimate of regional isoprene emissions based on Baseline-B2 and Baseline-A2 climate scenarios with present-day CO_2 concentration of 366 ppm were 25 TgC/yr and 28 TgC/yr. A sensitivity study without CO_2 effects in the model emissions has found the isoprene emissions increased to 27 TgC/yr and 29 TgC/yr respectively under future climate scenario (2100).
- The present-day estimate for regional emissions of monoterpene were 14 TgC/yr (B2) and 15 TgC/yr (A2). Meanwhile ORVOC were estimated of about 20 TgC/yr and 22 TgC/yr respectively.
- The increase of future (2100) mean surface temperature in the region by 2.5°C (B2) and 3.5°C (A2) and the decrease of PAR under present-day landcover and without CO_2 activity factor, the isoprene emission increased to 31 TgC/yr (B2) and 37 TgC/yr (A2), an increase of 13% and 27% respectively. The inclusion of future CO_2 concentration of 560 ppm in the future scenarios inhibited isoprene emissions to 21 TgC/yr (B2) and 25 TgC/yr (A2), a reduction of about 19% and 8% from the baseline estimate respectively. In term of magnitude, the inhibitory effect of elevated CO_2 is much larger than the effect of climate change alone.

- The increase of temperature with double present atmospheric CO_2 concentration in the future scenarios decreases the regional emissions of both monoterpene and ORVOC, 9% (B2) and 7% (A2) for monoterpene, and 11% (B2) and 6% (A2) for ORVOC.
- Changes in future landcover alone accounted for a decrease in isoprene emissions of 6% (B2) and 5% (A2) with the CO_2 influence. Without the CO_2 influence, the isoprene emissions increased by 5% (B2) and 9% (A2) respectively. The inhibitory effect of elevated CO_2 on isoprene emissions was larger than that of landcover forcing alone. In comparison with climate change forcing, the impact of landcover forcing alone on isoprene emissions is much smaller.
- Emissions of monoterpenes and ORVOC due to landcover forcing alone were 0.7 TgC/yr and 0.8 TgC/yr for B2, and 2 TgC/yr and 1 TgC/yr for A2 respectively.
- The combined effect of climate change and landcover forcings without the CO_2 activity factor, has increased the regional isoprene emissions to 32 TgC/yr (B2) and 40 TgC/yr (A2), an increase of 18% and 38% respectively. With the inclusion of the CO_2 activity factor, the future emissions of isoprene were significantly inhibited by 60% (B2) and 66% (A2). The magnitude of CO_2 inhibitory effect is far more important than the combination effect of climate change and landcover forcings on isoprene emissions.
- The combined effect of climate change and landcover forcings, on monoterpenes and ORVOC emissions was to decrease them further, which much greater impacts than climate change forcing or landcover forcing alone.
- Biogenic emissions in the region were found to be higher during July (southwest monsoon) and lower during January (northeast monsoon), which were due to higher temperatures and PAR during July.

- Evaluation of present-day isoprene emissions by comparing with other literature found that the results in this study are similar or slightly lower . Differences in the estimates are largely attributed to differences in domain size, models, methods and to a major extent the model inputs.

The small effects of climate change, which is referred to changes in surface temperature and solar radiation in this investigation, could be linked to the enzymatic activity that producing isoprene in the plant. Changes in surface temperature and solar radiation due to climate change affects the isoprene synthase from dimethylallyl disphosphate (DMAPP) via methyl erythritoil 1-phosphate pathway (MEP pathway) that biosynthesized isoprene in plants (Schwender *et al.*, 1997; Lehning *et al.*, 1999). Investigation by Lehning et al. (1999) showed that the leaf temperature-dependent enzyme under optimal condition has been demonstrated to account for the observed leaf isoprene emissions rates. Further investigation also showed that a reduction of light intensity by 50% reduced the isoprene synthase activity by about 60% compared with full sunlight. Investigation of the effect of this leaf temperature-dependent enzyme at the gene expression level by has strongly suggested that the increase in enzymatic activity in response to temperature and radiation is regulated at the transcriptional level (Sasaki *et al.*, 2005). In the present investigation, small emissions of isoprene due to landcover forcing alone were closely linked to the reduction of emission factors, which are dependent on the PFT distribution considered in the model. The decrease of Leaf Area Index (LAI) in the region from the annual mean of 5.45 m^2/m^2 (present-day) to 3.44 m^2/m^2 (future), a reduction of 2.01 m^2/m^2 (36.9 %) mainly due to the conversion of tropical forest (evergreen broadleaf trees) into agriculture (i.e oil palm and paddy) also accounted for the small isoprene emissions.

Chapter 6

EFFECTS OF CLIMATE CHANGE AND BIOGENIC EMISSIONS ON TROPOSPHERIC CHEMISTRY IN SOUTHEAST ASIA

6.1 Introduction

A chemistry-transport model, CiTTyCAT (Cambridge Tropospheric Trajectory model of Chemistry and Transport), was used to investigate changes in tropospheric chemistry in SEA, in response to projected climate change predicted by PRECIS-RCM, and biogenic emission calculated by BVOCEM. CiTTyCAT is a zero-dimensional chemical box model, which follows a 3-D Lagrangian air parcel trajectory (Evans *et al.*, 2000). The model was developed by Wild (1995). Box models are excellent tools in the understanding of atmospheric chemistry processes, as they can take several hundred chemical species linked by a few thousand chemical reactions into account (Granier *et al.*, 1999). Box models are normally used to investigate tropospheric chemistry under specific conditions, to simplify complicated atmospheric chemistry schemes, to analyse observations of selected chemical species, and also to evaluate and parameterize sub-grid processes, such as fast chemistry occurring in the boundary layer with time scales shorter than the characteristic transport times in large scale models (Granier *et al.*, 1999).

6.2 The Aims of the Study

Potential changes and impacts of biogenic emissions must be considered for the evaluation of potential future chemistry scenarios of the atmosphere. This is important to better understand the roles of climate change and landcover changes as drivers and their impacts. At the same time, it is also important for the policy maker to design air pollution

control strategies. In Chapter 4, due to atmospheric forcing alone for the IPCC A2 and B2 climate scenarios, temperature has been observed to increase between 2.4°C and 3.6°C for the period of 2090-2100 relative to 2000-2010. The combined effects of atmospheric and landcover forcings were observed to warm the regional surface temperature between 2.9 °C to 4.3°C for the same period. Changes in landcover forcing alone, mainly through conversion of forested land into agricultural land, is projected to produce a warming of between of 0.1°C and 0.7°C for both future climate scenarios (A2 and B2) (Note: the changes of surface temperatures was the results from the simulation over land masks and not over the whole domain). Apart from contributing to the future climate change, changes in the regional land cover were also found to affect the biogenic emission such as isoprene and monoterpene (see Chapter 5), and so are subsequently expected to affect the chemistry of the troposphere in the region, particularly on surface O_3 concentrations. The schematic of the work of this Chapter 6 and its links to the previous chapter are illustrated in Figure 6.1.

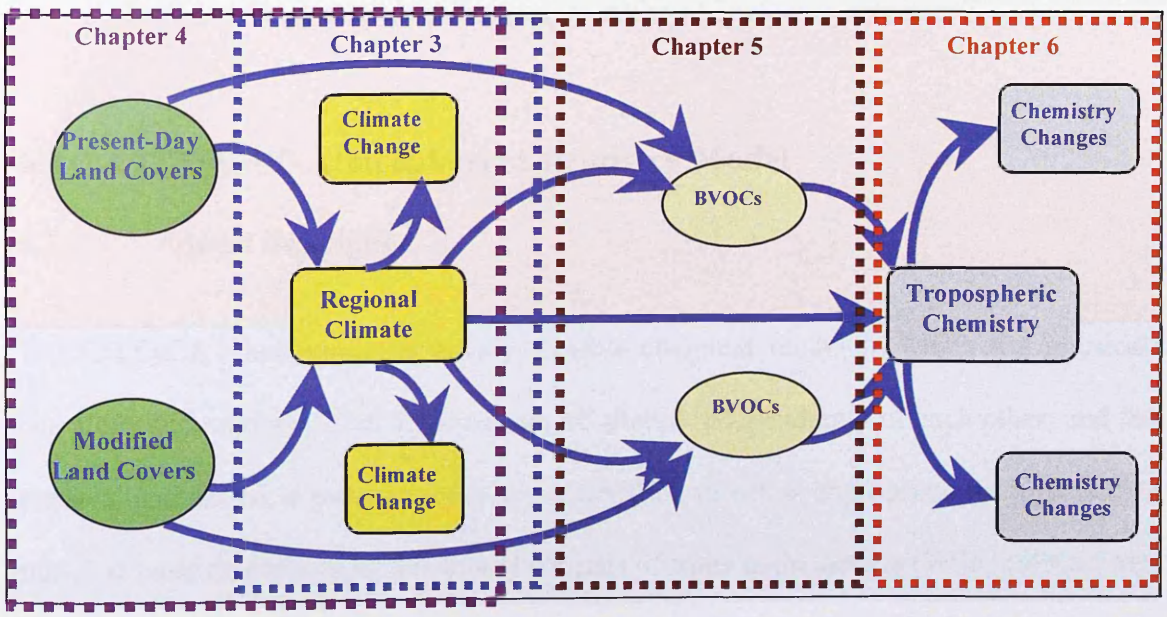

Figure 6.1: Framework for the investigation of climate change and biogenic emissions impact to the tropospheric chemistry in Southeast Asia. The red dotted box indicates the framework for the investigation that covered in Chapter 6.

The aim of this study is to better understand the effects of tropospheric chemistry compositions particularly surface O_3 concentrations that may occur as the results of changes in climate and biogenic emissions (particularly isoprene) under present-day and future landcover scenarios. This study has been performed to answer the following research questions:

a) What would be the combination effects of climate change and biogenic emissions to the present-day and future tropospheric O_3 concentrations and other trace gases and oxidants in urban and remote areas in the region under present-day landcover (PLC) and modified future landcover (FLC) scenarios?

b) How important or significant is the effect of the individual forcings on the tropospheric O_3 concentrations and other trace gases and oxidants in the urban and remote areas in the region under present-day and future landcover scenarios?

c) What would be the response of the future tropospheric O_3 concentrations and other trace gases and oxidants to the seasonal variability (January and July) of climate change and biogenic emissions under different landcover scenarios?

6.3 CiTTyCAT-Atmospheric Chemistry Model

6.3.1 Model Description

The CiTTyCAT box model is a very flexible chemical model in which the physical, chemical, and computational schemes can be altered independently of each other, and the physical and chemical processes can be switched on or off as appropriate for a particular run. The basic framework of this model consists of three main aspects (Wild, 1996). First, there is chemical scheme, which consists of the kinetic parameters for the chemical species of interest, and the production and loss terms for each of the chemical species. Second, there is the photolysis scheme, which considers the effects of solar radiation on

chemical species, mainly on the production of free radicals that play important roles in atmospheric chemistry. Thirdly, there is the physical scheme, which describes the non-chemical sources and sinks for chemical species, such as emission sources from the surface, and loss terms due to dry and wet deposition. Solving the equations in the model requires a time-stepping scheme for simultaneous ordinary differential equations, to update the condition at every time step, as shown in Figure 6.2. At each time step, the chemical composition is updated, considering photochemistry, emissions, depositions, and mixing from the free troposphere (e.g Eq. 6.1). Each process is defined by its own subroutines, which can be called from the main model programme.

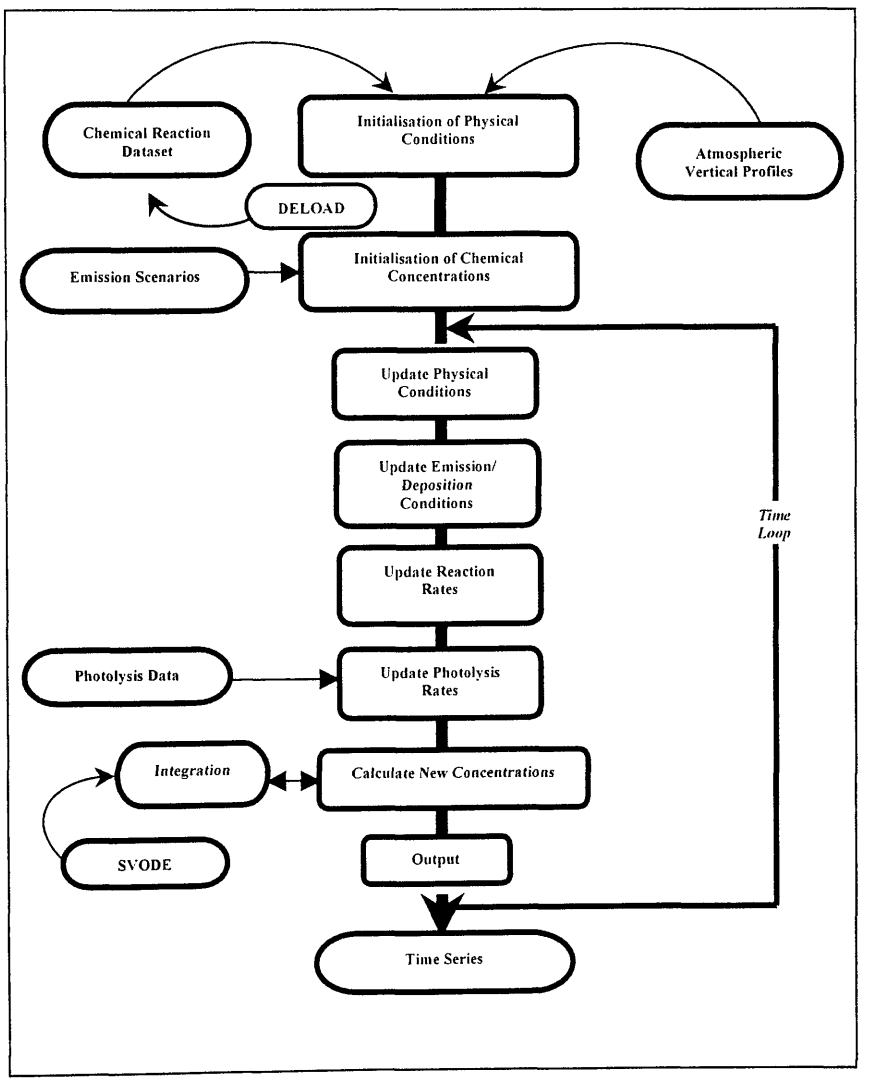

Figure 6.2: CiTTyCAT model framework flow chart (*modified from* Wild, 1996).

$$\frac{dC}{dt} = P - (L.C) + \left(\frac{E}{h}\right) - \left(\frac{VC}{h} + k_w\right) + (C' - C)\frac{1}{h}\frac{dh}{dt} \qquad (6.1)$$

where

C	is the species concentration in the boundary layer (molecules cm^{-3})
C'	is the species concentration in the free troposphere (molecules cm^{-3})
P, L	are the chemical production and loss rates (molecules cm^{-3})
$E(x,y,t)$	is the emission rate into the boundary layer (molecules cm^{-3})
$V(x,y)$	is the dry deposition velocity for the species (cm s^{-1})
k_w	is the wet deposition rate for the species (molecules cm^{-3} s^{-1})
$h(t)$	is the mixing height of the boundary layer (cm)

6.3.1.1 Chemistry scheme

A set of equations that corresponds to the production (P) and loss terms (L.C) of each chemical species is included in the model reaction set. These equations are solved simultaneously over a given time period with appropriate boundary conditions. The following equation (Eq. 6.2) given by Wild (1996) is integrated over a time step (Δt) to determine the chemical rate of change of the species over a specified period.

$$\text{P-L.C} = \frac{d[x]}{dt} = \sum_{ij} k_p [x_i][x_j] - [x]\sum_k k_l [x_k] \qquad (6.2)$$

where

k_p is the rate constant for the production terms for species x

k_l is the rate constant for the loss terms for species x

$[x_i], [x_j], [x_k]$ are the concentrations of reactants species i, j, k

As the reaction rate is dependent on temperature, any change in temperature will result in the recalculation of the reaction rate constants for bimolecular reactions at each time step

using the Arrhenius expression as shown in Eq. 6.3, with coefficients taken from DeMore *et al.* (1992) and Atkinson *et al.* (1992).

$$k_b = A(T/300)^{-n}\exp(-E/RT) \qquad (6.3)$$

where A is the pre-exponential factor displaying a temperature dependence tabulated as exponent n, and the activation temperature, E/R is required. Meanwhile, for trimolecular reactions, effective second-order rate constants are calculated using the Troë expression as shown in Eq. 6.4.

$$k_t = \left(\frac{k_o[M]}{1+k_o[M]/k_\infty}\right)F^{(1+[\log_{10}(k_o[M]/k_\infty)]^2)^{-1}} \qquad (6.4)$$

where

k_o and k_∞ are the limiting low and high pressure rate constant (both incorporate a temperature dependence, $(T/300)^{-n}$),

$[M]$ is the atmospheric density in molecules cm^{-3}

F is taken to be 0.6

The DELOAD programme (Nejad, 1986), a code-writing routine for selecting reactions and kinetics data and formatting the production and loss terms for chemical rate changes has been adapted for use with atmospheric reactions (Brown *et al.*, 1993) in order to minimise the introduction of coding errors each time an additional reaction or chemical species is introduced into the chemical reaction scheme. A central database consisting of kinetic data for bimolecular, trimolecular, and photolytic reactions has been constructed based on that of DeMore *et al.* (1992) and Atkinson *et al.* (1992), which can be altered as

rate constants are revised or new reaction rates are calculated. During the integration loop, the production and loss terms for each chemical species considered are written in a separate list, which can be picked up by the model for each run. The advantage of using the DELOAD routine is that it is separate from the model and runs offline, and therefore allows the introduction of any new chemical species into the chemical scheme to be assessed relatively simply.

6.3.1.2 Photolysis scheme

Molecules and aerosols, as well as clouds, are known to have significant influence on tropospheric chemistry through modification of solar radiation that determines photolysis frequencies. In CiTTyCAT, absorption due to O_3, O_2, and aerosols in the atmosphere is calculated at each level (Wild, 1996), with the O_3 profile taken from the US Standard Atmosphere (NOAA-NASA, 1976) and aerosols taken as average aerosols (due to wide variability in the lower troposphere), which is based on that of Braslau and Dave (1973). The photolysis scheme models the clouds as a diffusing laminar surface between model levels, which both reflects and transmits light (Wild, 1996). The albedo of a cloud layer (low, medium, or high level), which is dependent on the angle of incidence (Taylor and Stowe, 1984) and hence the zenith angle, has been parameterised using the transmission factor of three cloud types (altostratus, altocumulus, and cirrus) (Wild, 1996).

6.3.1.3 Physical scheme

6.3.1.3.1 Boundary layer

Chemical species emission from the surface, injection from the atmosphere, and physical removal through deposition processes to the surface affect the composition of

tropospheric chemical species within the model air parcel. The depth of mixing height of the planetary boundary layer, which is the lowest part of the atmosphere, is complicated by topography and meteorological conditions. In the CiTTyCAT model, the parameterisation of the average diurnal variation in mixing height is that of Derwent and Hov (1982), which assumes a nocturnal inversion layer of 300m that rises uniformly after dawn to a maximum altitude of 1300m, and remains steady at this height until the convective activity dies down at dusk and the nocturnal inversion is reformed. Convective activity at the lower layer leads to the rise of the mixing height and drives entrainment of air from the upper layer (Wild, 1996). This process leads to mixing down into the boundary layer and affects the chemical composition in the boundary layer through dilution of primary pollutants and increasing levels of chemical species, which have been depleted in the boundary layer.

6.3.1.3.2 Emissions

The emission of natural and anthropogenic pollutants is one of the major driving forces that control the chemical composition in the troposphere. For the hydrocarbon species treatment, the CiTTyCAT model has used a lumping scheme where the hydrocarbon species are lumped based on reactivity and the number of carbon species (i.e. 3, 5. and 8), after taking into consideration the grouping and variation in molecular masses (Wild, 1996). It was also assumed that the composition of hydrocarbon emissions would not vary significantly throughout the diurnal cycle. Emission treatment in the original scheme by Wild (1996) has been extended to include the emission of a number of hydrocarbon species including biogenic emissions as described in details by Evans (1999), Emmerson (2001), and Ryder (2005), which was adapted in this study but with some modifications to reflect the best emission scenario for SEA.

6.3.1.3.3 Deposition

Deposition processes, either through dry or wet deposition, have been recognised as the main physical sinks of chemical species in the atmosphere. Dry deposition occurs actively in the boundary layer through take-up by plants, soils, and the ocean. Meanwhile wet deposition actively occurs in the free troposphere through take-up of soluble species in clouds (rainout) and removal in falling water droplets (washout) . For this model, the dry deposition scheme is assumed to occur at the planetary lower boundary (Wild, 1996), Therefore information such as surface type, friction velocity, roughness length, and atmospheric stability in this particular study area is important. The deposition velocity (V_z) calculation for this model uses the method by Isaksen *et al.* (1985) as shown in Eq. 6.5. For a stationary box run, which is used in this study, friction velocity is taken from the global average value of 0.2 ms^{-1} (Wild, 1996).

$$V_z = \frac{V_1}{1 + V_1(\log(z)/ku^*)} \qquad (6.5)$$

where,

V_z is the dry deposition velocity at the box centre at 1 m,

k is the von Karman constant, and

u^* is the friction velocity at the altitude of the centre of the box z (0.2 ms^{-1} for the box run).

The roughness length is calculated from the extraction of average values from a global dataset at T15 resolution, interpolating the correct latitude and longitude, and the application of seasonal and diurnal variations, which are assumed to be sinusoidal (Wild, 1996).

For the wet deposition scheme, CiTTyCAT employs a first-order loss rate treatment, which provides an average lifetime for precipitation scavenging for soluble species (Law and Pyle, 1993). The lifetime of soluble species is taken as approximately 5 days close to the surface, and increases with altitude (Wild, 1996). HNO_3, one of the most important species considered in wet deposition, is assumed to have half of this lifetime to account for its greater solubility. In a previous study using CiTTyCAT model by Evans *et al.* (2000) the wet deposition scheme was not taken into consideration as it is assumed to be negligible for the case studies considered (see also Derwent and Jenkin, 1991; and Lindskog *et al.*, 1992).

A treatment of dispersion is also included in the model scheme, as it this has diluting effects on the chemical composition in the atmosphere. In CiTTyCAT, the dispersion scheme uses a simple expression, which is also used in plume dispersion from point sources, and has included terms for some physical processes that affect air masses as shown in Eq. 6.6. In this model, the scheme was run using the full scheme where the concentrations of all species are required at every time step (Wild, 1996).

$$\frac{dC_i}{dt} = \left(\frac{dC_i}{dt}\right)_{chem} + \frac{2(C_i' - C_i)}{\delta z(t)^2 / D} \qquad (6.6)$$

where,

C_i is the plume concentration of chemical species i,

C_i' is the background concentration of chemical species i,

t is the time since emission,

D is the diffusion coefficient (D, 3.5 $cm^{-2}s^{-1}$).

6.4 Experimental Setup

6.4.1 Study Sites

For the investigation of tropospheric chemistry in SEA, five sites were selected as shown in Table 6.1, representing urban and rural (unpolluted) areas (Figure 6.3).

Table 6.1: Study sites for the tropospheric chemistry investigations in SEA

Sites	Coordinate	Country	Description	Climatic Conditions* (Temperature & Precipitation)
Bangkok	13.75°N; 100.54°E	Thailand	Urban	26.8°C & 4.6 mm/day
Kuala Lumpur	3.10°N; 101.72°E	Malaysia	Urban	26.5°C & 3.3 mm/day
Jakarta	6.20°S; 106.82°E	Indonesia	Urban	27.9°C & 3.3 mm/day
Danum Valley	5.00 ^{0}N; 117.6 ^{0}'E	Sabah, Malaysia	Remote area	23.2°C & 12.2 mm/day
Koto Tabang	0.21°S 100.33°E	Sumatera, Indonesia	Remote area	22.2°C & 11.1 mm/day

*Note: * climatic condition simulated from PRECIS-RCM for each locations*

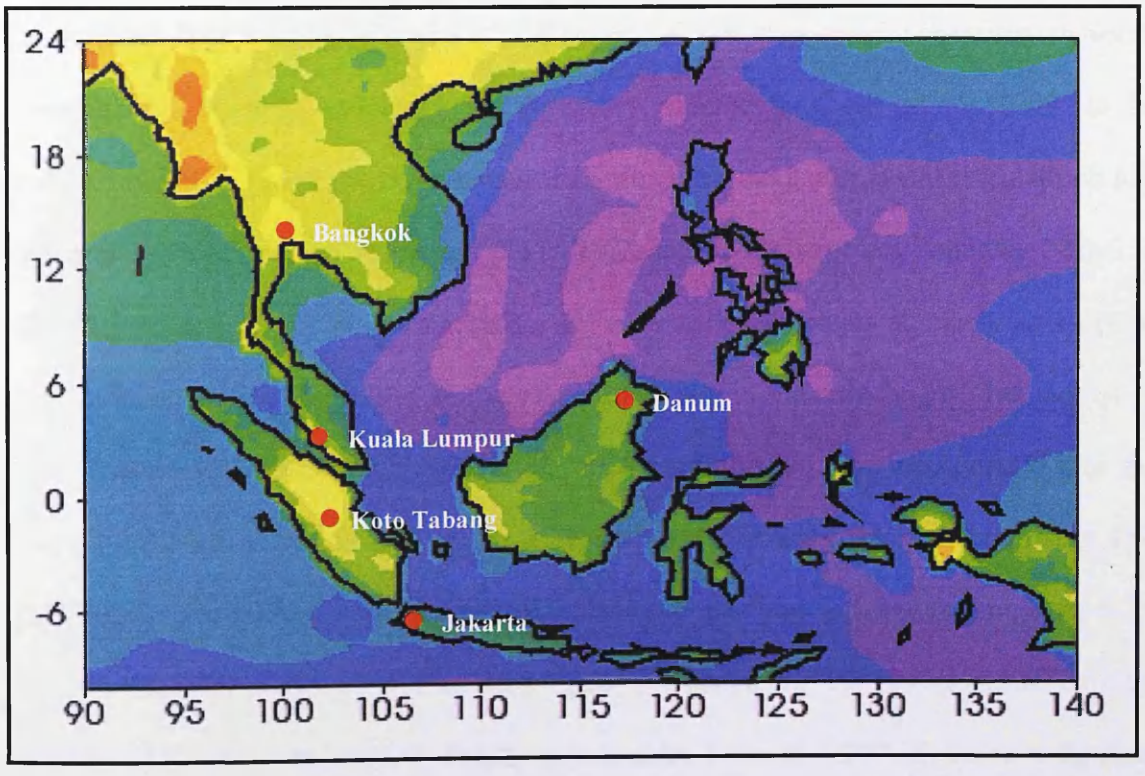

Figure 6.3: Selected sites for the tropospheric chemistry study in SEA.

6.4.2 Chemistry and Photolysis Treatments

The CiTTyCAT model is designed to allow alterations to the chemistry scheme to suit the aims of the research. In this study, the extended chemistry scheme by Evans (1999), Emmerson (2001), Ryder (2005) and the latest modification of the chemistry scheme, kinetic expressions, and the reaction rate coeficients by Pugh *et al.* (2009, to be published) was used. Emmerson (2001) has extended the chemistry scheme to include xylene (LMxyln), toluene (C_7H_8), and α-pinene (bimolecular chemical reaction No.161-202 in Appendix 6.1 and photolysis reaction No. 39-43 in Appendix 6.3) in her investigation of the potential production of secondary organic aerosols. Meanwhile Ryder (2005) has further extended the chemistry scheme of the model by incorporating new species of BVOCs such as monoterpene (d-limonene) and sesquiterpene (bimolecular chemical reaction No. 203 – 251 in Appendix 6.1 and photolysis reaction No.45 in Appendix 6.3) to investigate the roles of these BVOCs on tropospheric chemistry in South East Asia. The latest update of the chemistry scheme by Pugh *et al.* (2009, to be published) has included the amendment of the isoprene oxidation mechanism, which has included the Mainz Isoprene Mechanism (MIM2) reaction scheme developed by Pöshel *et al.* (2000). Elevated OH concentration in a pristine environment, such as tropical rainforest, appears to be due to an increased efficiency in the recycling of this radical in the oxidation of isoprene (Lelieveld *et al.*, 2008), and this has also incorporated into the latest version of CiTTyCAT. Of the fully extended chemistry scheme comprising 411 gas phase reactions (including trimolecular chemical reactions as listed in Appendix 6.2), 118 are photolysis reactions. The latest update of chemistry and photolysis scheme by Pugh *et al.* (2009, to be published) has been used by Turnock (2008) in the investigation of climate change influence on tropospheric ozone and air quality in Southeast Asia and used by Hewitt *et al.* (2009, manuscript submitted) to investigate the effect of land-use

change of rainforest to palm oil plantation on surface O_3 concentrations. In the investigation of climate change impact on tropospheric O_3 in SEA, Turnock (2008) has concluded that in urban locations, in the future climate scenarios, the surface O_3 concentrations were observed to increase with anthropogenic emissions being the most important factor than the climate change. In all locations of investigation (urban and remote locations) in SEA, climate change were generally found to exert a negative change in tropospheric O_3 concentrations whereas increases in anthropogenic emissions exerted a positive change.

6.4.3 Physical Treatment

6.4.3.1 Meteorological fields and biogenic emissions

Meteorological data are required for any atmospheric chemistry model as it controls atmospheric circulation, which controls photochemical reactions such as temperature, precipitation, wind, solar radiation, humidity, and mixing height (Sillman, 1999; Gebhart, *et al.*, 2001). The meteorological fields produced by the climate model, PRECIS-RCM (see Chapter 3) were used as input to drive the CiTTyCAT atmospheric chemistry model. Input variables from the climate model are the profile of surface temperature, clouds and mixing layer depth (boundary layer depth). Input variables datasets were prepared for each sites for the present-day (2008) and future (2100) investigations. For the investigation of tropospheric chemistry responses to seasonal variations, input variables were also prepared for the month of January (Jan) and July (Jul), which are corresponding the northeast monsoon (NEM) and southwest monsoon (SEM) in Southeast Asia. CiTTyCAT climate input variables in five locations in Southeast Asia for the baseline and future (A2 and B2) climate scenarios during January and July are summarized in Appendix 6.5 (surface temperature), Appendix 6.6 (boundary layer depth) and Appendix

6.6 (total cloud). The climate datasets were extracted for the month of January and July in the year 2008 and 2100 from the time slices of 2000-2010 and 2090-2100 respectively. Similarly, the biogenic emissions were extracted for the months of January and July for the same year.

6.4.3.1.1 Surface temperature

The summary of surface temperature changes for various climate and landcover scenarios during January and July in five locations is shown in Table 6.2. The projected surface temperature at the end of the century due to atmospheric forcing alone was found to increase in the range of 1.4°C to 4.5°C during January and 1.9°C to 5.6°C during July in the A2 climate scenario (A2PLC-BaseA2). A similar trend was observed in the B2 climate scenario (B2PLC-BaseB2), with surface temperature in the range of 1.9°C to 4.0°C during January and 1.7°C to 4.0°C during July. The combined impact of atmospheric forcing and landcover forcing in both climate scenarios (A2FLC-BaseA2; B2FLC-BaseB2) for surface temperature were found to be larger (between 1.5°C and 7.5°C for A2; and 1.9°C and 5.5°C for B2) than the isolated impacts of atmospheric forcing or landcover forcing alone.

Table 6.2: Temperature changes in several locations in Southeast Asia in various climate and landcover scenarios during January and July for present-day (2008) and future (2100) simulations.

Scenarios	Danum °C [%]		Koto Tabang °C [%]		Bangkok °C [%]		Jakarta °C [%]		Kuala Lumpur °C [%]	
	January	July	January	July	January	July	January	July	January	July
A2PLC-BaseA2	4.45 [19.2]	1.91 [6.6]	3.38 [14.5]	2.63 [9.8]	2.82 [12.2]	2.37 [7.7]	2.96 [12.3]	5.64 [20.5]	1.44 [4.8]	4.54 [15.0]
A2FLC-BaseA2	4.67 [20.8]	3.52 [12.2]	4.46 [19.1]	2.94 [10.9]	6.18 [26.6]	7.49 [24.4]	4.20 [17.5]	6.21 [22.6]	1.54 [5.1]	4.81 [15.9]
A2FLC-A2PLC	0.22 [0.8]	1.61 [5.2]	1.08 [4.0]	0.31 [1.1]	3.36 [12.9]	5.12 [15.5]	1.24 [4.6]	0.57 [1.7]	0.1 [0.3]	0.27 [0.8]
B2PLC-BaseB2	2.66 [11.6]	2.23 [7.8]	2.40 [10.5]	1.65 [6.2]	4.01 [17.6]	2.86 [9.2]	1.96 [8.1]	2.17 [8.2]	2.55 [9.8]	4.00 [14.7]
B2FLC-BaseB2	3.77 [16.5]	2.78 [9.8]	2.94 [12.9]	1.94 [7.3]	4.57 [20.1]	4.97 [16.0]	2.21 [9.2]	5.46 [20.5]	3.01 [11.5]	4.48 [16.5]
B2FLC-B2PLC	1.11 [4.3]	0.55 [1.8]	0.54 [2.1]	0.29 [1.0]	0.56 [2.1]	2.11 [6.2]	0.25 [1.0]	3.29 [11.4]	0.46 [1.6]	0.48 [1.5]

Note: *PLC-present-day landcover*
FLC-Future landcover
A2PLC-BaseA2/B2PLC-BaseB2: Temperature changes due to atmospheric forcing alone
A2FLC-BaseA2/B2FLC-BaseB2: Temperature changes due to combination of atmospheric and landcover forcings
A2FLC-A2PLC/B2FLC-B2PLC: Temperature changes due to landcover forcing alone

6.4.3.1.2 Boundary layer

The summary of boundary layer changes for various climate and landcover scenarios during January and July in five locations is shown in Table 6.3. The depth of the boundary layer varied for each scenario during January and July that were considered in this study.

Table 6.3: Boundary layer changes in several locations in Southeast Asia in various climate and landcover scenarios during the January and July for present-day (2008) and future (2100) simulations.

Scenarios	Danum (m) [%]		Koto Tabang (m) [%]		Bangkok (m) [%]		Jakarta (m) [%]		Kuala Lumpur (m) [%]	
	January	July	January	July	January	July	January	July	January	July
A2PLC-BaseA2	76 [9.2]	-118 [21.9]	159 [18.8]	7 [1.3]	-15 [1.8]	-10 [0.8]	-41 [8.4]	141 [30.0]	140 [13.6]	54 [9.2]
A2FLC-BaseA2	5 [0.6]	37 [6.8]	449 [53.2]	23 [4.6]	93 [11.2]	122 [10.6]	61 [12.8]	58 [11.8]	103 [10.0]	85 [14.4]
A2FLC-A2PLC	-71 [7.8]	155 [36.7]	290 [29]	23 [4.5]	108 [13.25]	132 [11.5]	102 [23.1]	-85 [14.0]	-37 [3.2]	30.2 [4.7]
B2PLC-BaseB2	5 [0.6]	-61 [10.2]	109 [13]	2 [0.4]	15 [1.8]	178 [16.6]	-85 [14.4]	96 [19.7]	4 [0.4]	14 [2.4]
B2FLC-BaseB2	4 [0.5]	-62 [10.2]	-100 [12.2]	-168 [35.8]	-89 [10.2]	155 [14.4]	112 [19.1]	236 [48.4]	-9 [0.9]	141 [24.2]
B2FLC-B2PLC	-0.4 [0.1]	-0.2 [0.03]	-209 [22.4]	-170 [36.1]	-104 [11.8]	-23 [1.8]	-27 [5.5]	140 [24.0]	-13 [1.3]	127 [21.3]

Note: *PLC-present-day landcover*
FLC-Future landcover
A2PLC-BaseA2/B2PLC-BaseB2: Temperature changes due to atmospheric forcing alone
A2FLC-BaseA2/B2FLC-BaseB2: Temperature changes due to combination of atmospheric and landcover forcings
A2FLC-A2PLC/B2FLC-B2PLC: Temperature changes due to landcover forcing alone

6.4.3.1.3 Total cloud

The future projection of total cloud during January and July for various climate and landcover scenarios were generally less or had no change with a few exceptions in some scenarios. The summary of total cloud fraction changes for various climate and landcover scenarios during the January and July in five locations is shown in Table 6.4.

Table 6.4: Total cloud fraction changes in several locations in Southeast Asia in various climate and landcover scenarios during January and July for present-day (2008) and future (2100) simulations.

Scenarios	Danum [%]		Koto Tabang [%]		Bangkok [%]		Jakarta [%]		Kuala Lumpur [%]	
	January	July	January	July	January	July	January	July	January	July
A2PLC-BaseA2	-0.09 [28.1]	0.05 [11.1]	-0.09 [23.1]	0.02 [41.7]	-0.02 [7.0]	-0.11 [15.7]	-0.09 [23.1]	0.02 [41.7]	-0.09 [28.1]	0.05 [11.1]
A2FLC-BaseA2	-0.09 [28.1	-0.01 [22.2]	-0.07 [18.0]	-0.06 [12.5]	-0.02 [7.0]	-0.15 [21.4]	-0.07 [18.0]	-0.06 [12.5]	-0.09 [28.1	-0.01 [22.2]
A2FLC-A2PLC	0.00 [0.0]	-0.06 [12.1]	0.02 [66.7	-0.08 [16.0]	-0.02 [7.4]	-0.04 [6.8]	0.02 [66.7	-0.08 [16.0]	0.00 [0.0]	-0.06 [12.1]
B2PLC-BaseB2	-0.37 [86.0]	-0.04 [9.3]	-0.29 [60.4]	0.01 [2.3]	-0.04 [13.3]	0.01 [1.6]	-0.29 [60.4]	0.01 [2.3]	-0.37 [86.0]	-0.04 [9.3]
B2FLC-BaseB2	-0.20 [46.5	-0.05 [11.6]	-0.14 [29.2]	0.01 [2.3]	-0.05 [16.7]	-0.07 [11.3]	-0.14 [29.2]	0.01 [2.3]	-0.20 [46.5	-0.05 [11.6]
B2FLC-B2PLC	0.17 [2.8]	-0.01 [2.6]	0.15 [78.9]	0.00 [0.0]	-0.01 [3.9]	-0.08 [12.7]	0.15 [78.9]	0.00 [0.0]	0.17 [2.8]	-0.01 [2.6]

Note: *PLC-present-day landcover*
FLC-Future landcover
A2PLC-BaseA2/B2PLC-BaseB2: Temperature changes due to atmospheric forcing alone
A2FLC-BaseA2/B2FLC-BaseB2: Temperature changes due to combination of atmospheric and landcover forcings
A2FLC-A2PLC/B2FLC-B2PLC: Temperature changes due to landcover forcing alone

6.4.3.1.4 Isoprene emissions

The isoprene emissions datasets for the present-day and future climate and landcover scenarios generated from BVOCEM (see Chapter 5) were prepared for each scenario as input to CiTTyCAT model. For the investigation of future tropospheric chemistry simulation, the generated future isoprene emissions dataset with-CO_2 was selected in order to be consistent with the emission scenario in the A2 and B2 climate scenarios. The future isoprene fluxes in remote area like Danum and Koto Tabang were found to decrease in the A2 and B2 climate scenarios except during July under the present-day landcover in the A2 scenarios. In urban area like Bangkok, the changes of future isoprene fluxes relative to baseline fluxes under present-day and future landcover scenarios in A2 and B2 scenarios were observed to increase during January but decrease during July. In other urban areas, including Kuala Lumpur, the isoprene emission fluxes were observed to decrease in all scenarios. In Jakarta, isoprene emission fluxes were observed to increase

in all scenarios except during January in the A2 scenario. The summary of isoprene emissions and changes of emissions in the present-day and future climate and landcover scenarios during January and July is shown in Table 6.5.

Table 6.5: Isoprene emissions and changes ($\mu g\ m^{-2}\ hr^{-1}$) in several locations in Southeast Asia in various climate and landcover scenarios during January and July for present-day (2008) and future (2100) simulations.

Scenarios	Danum $\mu g\ m^{-2}hr^{-1}$ [%]		Koto Tabang $\mu g\ m^{-2}hr^{-1}$ [%]		Bangkok $\mu g\ m^{-2}hr^{-1}$ [%]		Jakarta $\mu g\ m^{-2}hr^{-1}$ [%]		Kuala Lumpur $\mu g\ m^{-2}hr^{-1}$ [%]	
	January	July	January	July	January	July	January	July	January	July
BaselineA2	1222	766	960	668	320	478	921	667	1652	1155
A2PLC	724	904	942	723	600	451	875	834	1193	976
A2FLC	648	733	677	636	362	447	602	696	947	940
A2PLC-BaseA2	-498 [40.8]	138 [18.0]	-18 [1.9]	56 [8.3]	280 [87.4]	-27 [5.7]	-46 [5.0]	167 [25.0]	-459 [15.4]	-179 [11.1]
A2FLC-BaseA2	-530 [47.0]	-33 [4.3]	-283 [29.5]	-32 [4.7]	42.3 [13.2]	-249 [35.8]	-319 [34.6]	26 [3.9]	-705 [42.7]	-215 [18.6]
A2FLC-A2PLC	-76 [11.7]	-171 [23.3]	-265 [39.2]	-87 [13.7]	-237 [65.5]	-4.3 [0.96]	-273 [45.4]	-137 [19.7]	-246 [25.9]	-36 [2.5]
BaselineB2	765	858	778	775	190	618	587	651	1104	1165
B2PLC	655	757	693	568	353	455	647	670	921	783
B2FLC	648	738	677	563	284	360	602	672	947	799
B2PLC-BaseB2	-110 [14.3]	-101 [11.8]	-85 [10.9]	-207 [36.5]	162 [85.2]	-163 [26.4]	60 [10.3]	19 [2.9]	-183 [16.6]	-382 [32.8]
B2FLC-BaseB2	-116 [15.2]	-121 [14.1]	-101 [13.0]	-212 [27.4]	94 [49.4]	-258 [41.7]	15.3 [2.6]	21 [3.2]	-157 [14.2]	-366 [31.4]
B2FLC-B2PLC	-0.01 [1.0]	-20 [2.6]	-16 [2.4]	-5 [0.9]	-68 [19.4]	-95 [136]	-45 [6.9]	2 [3.0]	26.5 [2.9]	15.8 [2.0]

Note: *PLC-present-day landcover*
FLC-Future landcover
A2PLC-BaseA2/B2PLC-BaseB2: Temperature changes due to atmospheric forcing alone
A2FLC-BaseA2/B2FLC-BaseB2: Temperature changes due to combination of atmospheric and landcover forcings
A2FLC-A2PLC/B2FLC-B2PLC: Temperature changes due to landcover forcing alone

6.4.3.2 Emissions and initial conditions

The emission inventories used in this study for the present-day emission scenario were updated to include the soil NO_x component of the Global Emissions Activity (GEIA) (Yienger and Levy II, 1995), and the Regional Emissions inventory in ASia (REAS) (Ohara *et al.*, 2007) for the anthropogenic VOCS. The soil biogenic NO_x emissions, which formed the GEIA soil NO_x inventory is based on the empirical model developed by

Yienger and Levy (1995). Biogenic volatile organic compound (BVOC) emissions from tropical forests and crops such as isoprene and monoterpenes, which are important in tropical tropospheric chemistry, were taken into consideration in this study using the output from Biogenic Volatile Organic Compounds Emissions Model (BVOCEM) as described in Chapter 5. The regional monthly biogenic emissions fields on 0.5^{o} x 0.5^{o} were used to drive the CiTTyCAT. Meanwhile, the initial concentrations of chemical species such as O_3, NO_x, CH_4, CO, HCHO, H_2O_2, MeOOH, PAN, C_2H_6, and C_3H_8 were based on the latitude versus height concentration fields, which were obtained from a run of the TOMCAT chemical transport model (CTM) (Law *et al.*, 1998). All other species input to the model are initialised with zero concentration following of that Evans *et al.* (2000), Emmerson (2002) and Ryder (2005). Based on the IPCC Special Report on Emission Scenarios (SRES) for the year 2100 (IPCC, 2000), the future anthropogenic emissions (2070-2100) for A2 and B2 scenarios are expected to increase for SEA. However, for the purpose of achieving the aims of this study, all input to the CiTTyCAT model other than climate (surface temperature, boundary layer and total clouds) and biogenic emissions were kept constant.

6.4.4 Developing Tropospheric Chemistry Scenarios for SEA

In developing tropospheric chemistry scenarios for SEA, critical consideration was given to the PRECIS-RCM meteorological output datasets from a number of climate change scenarios (Chapter 3 and Chapter 4) and biogenic emission from BVOCEM (Chapter 5) to reflect the relationship between climate change, biogenic emissions and tropospheric chemistry. One of the major objectives of this study is to investigate the effect of climate

change and biogenic emissions on tropospheric O_3 concentrations in SEA. For this work, three sets of experiments for the CiTTyCAT run were set up. First, the CiTTyCAT was run using inputs of climate variables and biogenic emissions generated for the present-day and future atmospheric forcings and with present-day landcover scenarios (SET 1). Second, CiTTyCAT was run using inputs of climate variables and biogenic emissions for future atmospheric forcings and modified future landcover scenarios (SET 2). Thirdly, the CiTTyCAT runs for the first and second sets of experiments were repeated but without biogenic emissions (SET 3). The later runs were carried out to evaluate the importance of biogenic emissions to the tropospheric O_3 concentrations. Overall, the CiTTyCAT model is set up to simulate a stagnant air mass situated over the chosen locations, and for that reason the model runs are indicative of severe ozone pollution episodes from urban areas. The experimental scenarios considered in this study are summarised in Table 6.6.

Table 6.6: Tropospheric chemistry experimental scenarios under different climates and biogenic emissions scenarios.

Experiment	Landcover Scenarios	Climate Scenarios	Climate Input Scenarios	Biogenic Emissions Scenarios	Tropospheric Chemistry Scenarios
SET 1	Present-day Landcover (PLC)	Baseline-B2	Baseline-B2	BVOC-BaselineB2	TropChem-BaselineB2
		Baseline-A2	Basline-A2	BVOC-BaselineA2	TropChem-BaselineA2
		SRES-B2	B2-PLC	BVOC-B2-PLC	TropChem-A2-PLC
		SRES-A2	A2-PLC	BVOC-A2-PLC	TropoChem-B2-PLC
SET 2	Modified Future Landcover (FLC)	SRES-B2	B2-FLC	BVOC-B2-FLC	TropoChem-A2-FLC
		SRES-A2	A2-FLC	BVOC-A2-FLC	TropoChem-B2-FLC
SET 3	Repeat Set 1 & Set2			No BVOC	Same as SET 1 & SET 2

Note: *FLC= Future Landcover*
PLC= Present Landcover

6.5 Omissions and Limitations of CiTTyCAT

The chemistry scheme of the model captures the most important known processes involving the production and loss of ozone, as well as for the oxidising capacity of the troposphere. However, some reaction rates and product yields of NMVOCs are not well established. Uncertainties and introduction of errors have been found to be significant, especially in the formation yields and atmospheric lifetimes of nitrates from higher hydrocarbons (von Kuhlmann, 2001). Some groups of NMVOCs are not considered in the current scheme, such as higher alkenes (>C3), halogens, sulphur-containing organics and other compounds like higher alcohols, esters, ethers, etc. Exclusion of halogen chemistry for example, would likely affect the O_3 prediction, particularly in the marine boundary layer (Read *et al.*, 2008; Dickerson *et al.*, 1999; Sander and Crutzen, 1996). The heterogenous reaction included in this model has been limited to three reactions. Aqueous phase chemistry in cloud droplets has also been omitted in this study. Cloud droplet chemistry through aqueous phase reactions has been found to play an important role in the distribution of O_3 and other trace gases in the atmosphere (Lelieveld and Crutzen, 1990; Lelieveld and Crutzen, 1991), although other studies found it to have a moderate effect (Jonson and Isaksen, 1993; Dentener, 1993) or a lesser effect (Liang and Jacob, 1997) on global O_3.

In terms of the model design itself, Langrangian and trajectory models such as CiTTyCAT, which allow a detailed consideration of chemistry, are often used for local and regional scale studies that have been identified to have intrinsic difficulty that excludes the mixing processes, thus making their validity on longer time scales questionable (Granier *et al.*, 1999). Again, many chemical transport models, including CiTTyCAT, are off-line models, in which the meteorological field input to the models are

derived from other models, either a general circulation or a regional climate model. This technique can produce inconsistency, as the chemistry scheme in the model receives necessary meteorological information indirectly from the regional climate change model at each time step (Forkel and Knoche, 2006), and there is no opportunity for the chemistry to feedback in the meteorology. Emmerson (2001) has also identified that an assumption of instantaneous vertical mixing throughout the height of the boundary layer in CiTTyCAT does not capture concentration gradient over the boundary layer in urban areas, and this has led to an under-prediction of concentrations near to the surface and an over-prediction of concentrations higher up in the boundary layer, close to heterogenous source region (e.g particulate matter (PM) emissions from the road traffic).

6.6 Evaluation of the Output from CiTTyCAT Model

A comparison of output generated from the CiTTyCAT model against in-situ measurements in Danum during the OP3 measurement campaign in July 2008 was carried out earlier by Pugh *et al.* (2009, to be published). In their study, the CiTTyCAT model was run using the climate/meteorological datasets from the measurements at the site during the campaign, while the biogenic emissions were obtained from the run of the MEGAN model (Guenther *et al.* 2006) coupled to the CiTTyCAT model. They have concluded that certain outputs of the current version of CiTTyCAT were comparable with the measurements in Danum during the OP3 campaign during the time between 1000-1800. Good agreements were observed for O_3, NO, and NO_2. However, the modelled OH concentrations were underestimated by ~ 2 to 3 times during this period. The low OH concentrations in the model were due to the loss of about 70% at midday, which attributed to the oxidation of isoprene.

In this study, the climate variable inputs to the CiTTyCAT model were obtained from regional PRECIS-RCM, which was run for the time slices 2000-2010 (present-day) and 2090-2100 (future) over SEA (See Chapters 3 & 4). Meanwhile the biogenic emissions were obtained from BVOCEM (see Chapter 5), which was run for 2008 (present-day) and 2100 (future) over SEA using the climate variables input from the PRECIS-RCM outputs. For the purpose of evaluation, the mean-bias-error (MBE) or "bias" and root-mean-square error (RMSE) were calculated based on the definition as shown in *Eq 6.7* and *Eq 6.8*. The MBE provides information on the performance of the correlations by allowing a comparison of the actual deviation between modelled and observed values. If the bias is less than zero then the modelled value is underestimating the mean, and if the bias is larger than zero then the modelled value is overestimating the mean. The ideal value of MBE is "zero". RMSE on the other hand provides information on the expected error of the simulations.

$$\mathrm{MBE} = \frac{1}{N}\sum_{i=1}^{N}(C_{\mathrm{modelled},i} - C_{observed,i}) \qquad (6.7)$$

$$\mathrm{RMSE} = \left[\frac{1}{N}\sum_{i=1}^{N}(C_{\mathrm{modelled},i} - C_{observed,i})^2\right]^{\frac{1}{2}} \qquad (6.8)$$

To evaluate the output from CiTTyCAT model, a comparison was also made with the measurement results during the OP3 campaign. The modelled concentrations have been compared to the OP3 measurements during the first week of July 2008. The observed and modelled concentrations are plotted as both a function of time and as a scatter plot for the Danum site as shown in Figure 6.4. Generally the modelled O_3 concentrations were found to be in good agreement with the measurements, though slightly underestimated.

Similarly, modelled NO concentrations were slightly underestimated in comparison with the measured concentrations. On the other hand, the modelled NO_2 and PAN concentrations were overestimated compared with the measured concentrations. Meanwhile the modelled OH concentrations were significantly underestimated compared to the measured OH concentrations. Similar findings were found by Pugh *et al.* (2009, to be published) in their study in Danum, with the conclusion that the model fitting algorithm could possibly have overestimated the biogenic emissions fluxes, through which the main mechanism of the 70% loss of OH concentrations was isoprene oxidation.

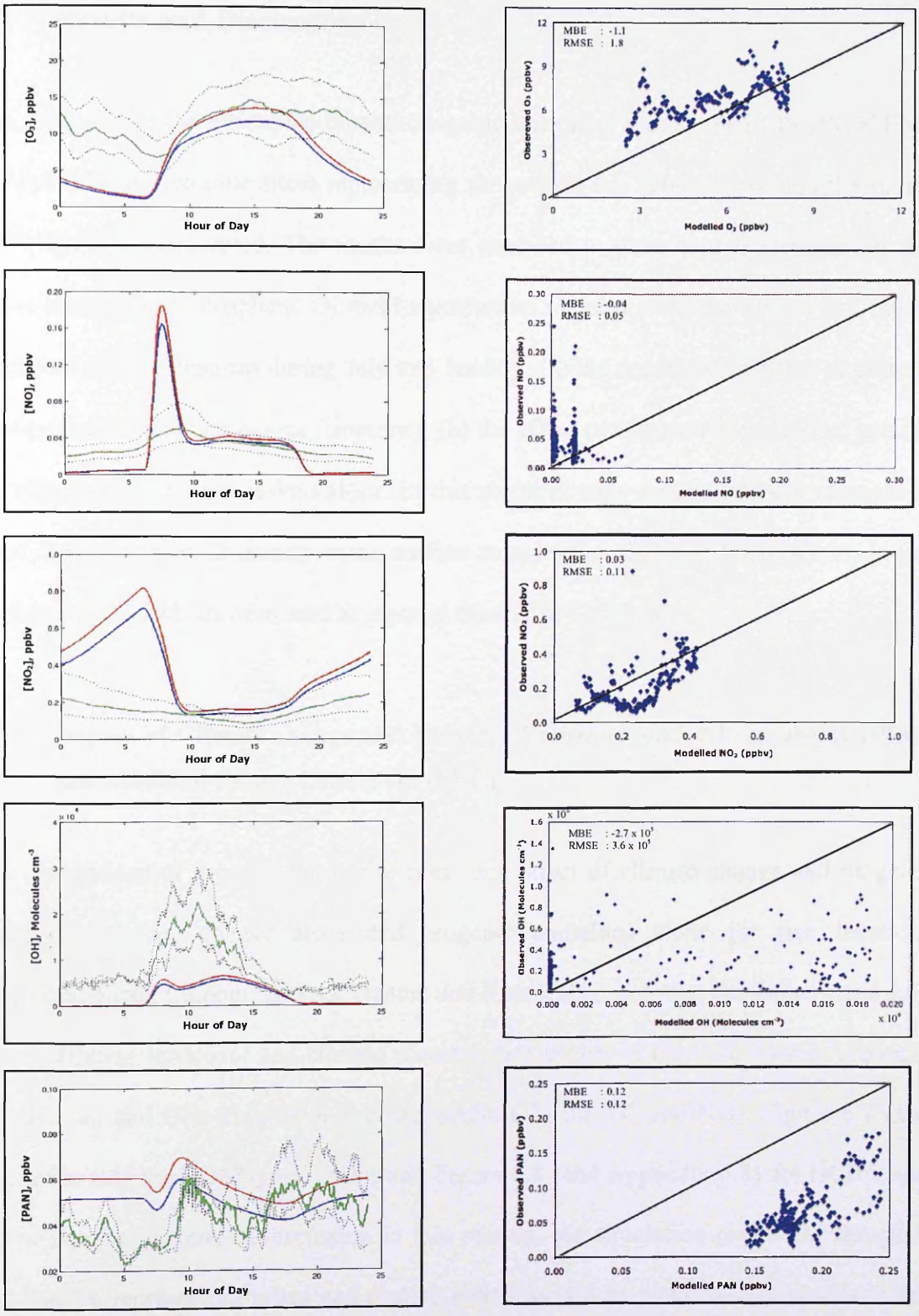

Figure 6.4: Comparison of the model output for A2 (*red line*) and B2 (*blue line*) emission scenarios with the average measurement during OP3 campaign (*green line*) at Bukit Atur (Danum). Lower and upper quartiles for the OP3 campaign measurements are indicated by black dots. The mean bias error (MBE) and RMS error (RMSE) are also given.

6.7 Results and Discussions

The results from the uncoupled climate-biogenic-chemistry model (PRECIS-BVOCEM-CiTTyCAT) for two time slices representing the present-day (2000-2010) and the future (2090-2100) are presented. The results were analysed in three terms, focusing on the future changes of tropospheric O_3 and its precursors under present-day (PLC) and future landcover (FLC) scenarios during July and January: (a) the combination effect of climate change and biogenic emissions (isoprene); (b) the effect of climate change alone; and (c) the effect of biogenic emissions alone. In this study, climate change refers to changes in three climate variables, namely mean surface temperature, depth of boundary layer and total cloudiness, which were used as input to the CiTTyCAT model.

6.7.1 Impact of Climate change and Biogenic Emissions under Present-day (PLC) and Modified Future Landcover (FLC)

The comparison of impacts due to the combined effect of climate change and biogenic emissions, climate change alone and biogenic emissions alone for five locations (Bangkok, Kuala Lumpur, Jakarta, Danum and Koto Tabang) during the January and July under different landcover and climate scenarios are shown in Figure 6.5 (and Appendix 6.7) for O_3, and OH; Figure 6.6 (and Appendix 6.7) for NO and NO_2; Figure 6.7 (and Appendix 6.8) for $HONO_2$ and PAN; and Figure 6.8 (and Appendix 6.8) for HCHO and H_2O_2. For the purpose of discussion in this section, the simulation results for Bangkok and Danum representing urban and remote locations will be elaborated in details in the following section, while for Jakarta, Kuala Lumpur and Koto Tabang, the elaboration can be found in Appendix 6.13.

(a) A2: O_3

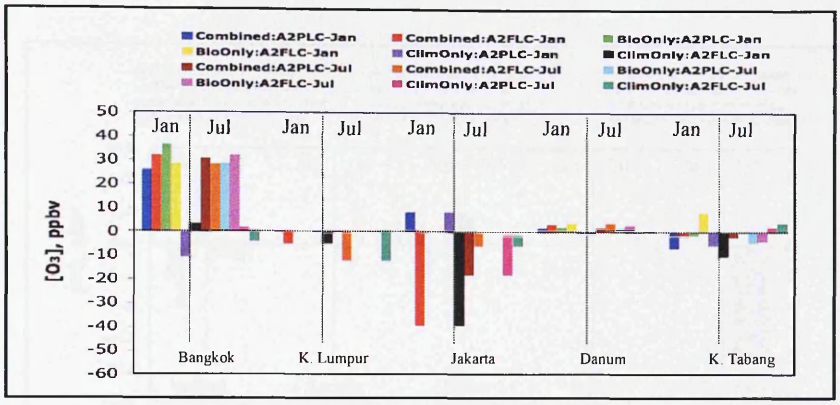

(b) B2: O_3

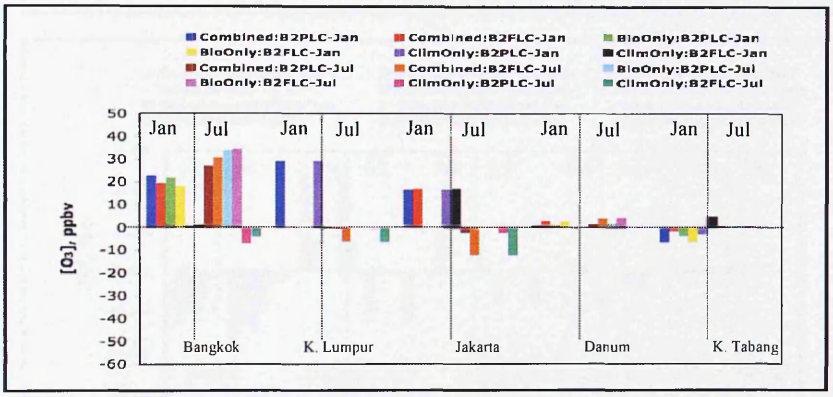

(c) A2: OH

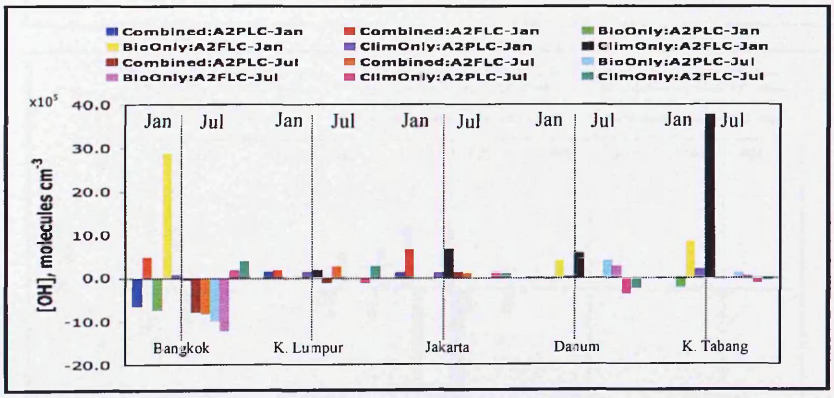

(d) B2: OH

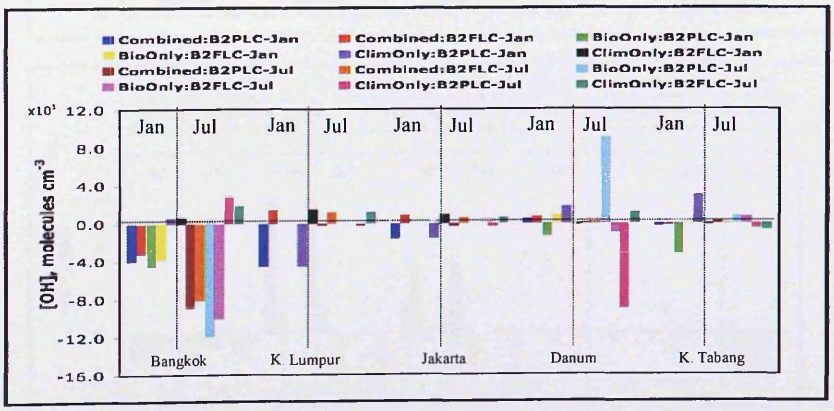

Figure 6.5: Comparison of impacts due to the combined effects of climate change and biogenic emissions, biogenic emissions alone and climate change alone during January (Jan) and July (Jul) under different landcover and climate scenarios in five locations in SEA. The A2 and B2 scenarios for a) A2: O_3; (b) B2: O_3; (c) A2: OH; (d) B2: OH

(a) A2: NO

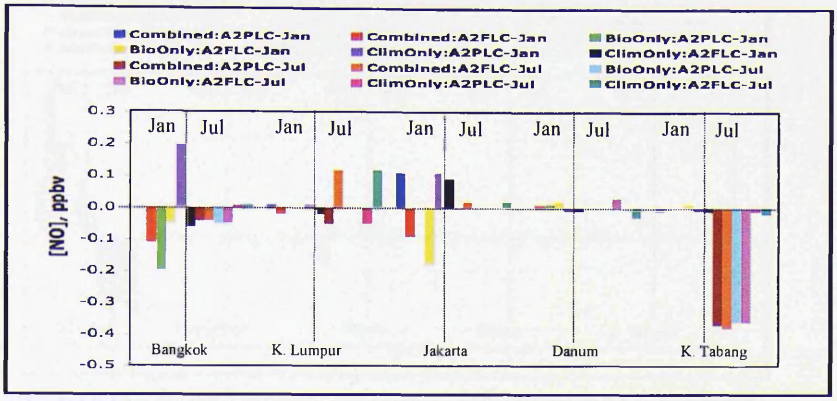

(b) B2: NO

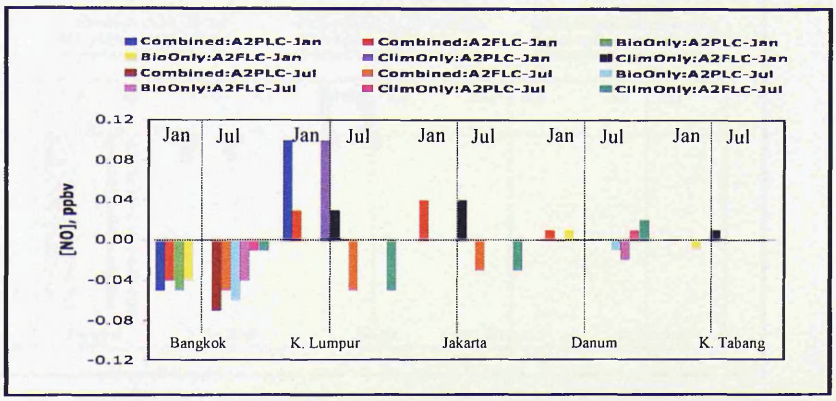

(c) A2: NO_2

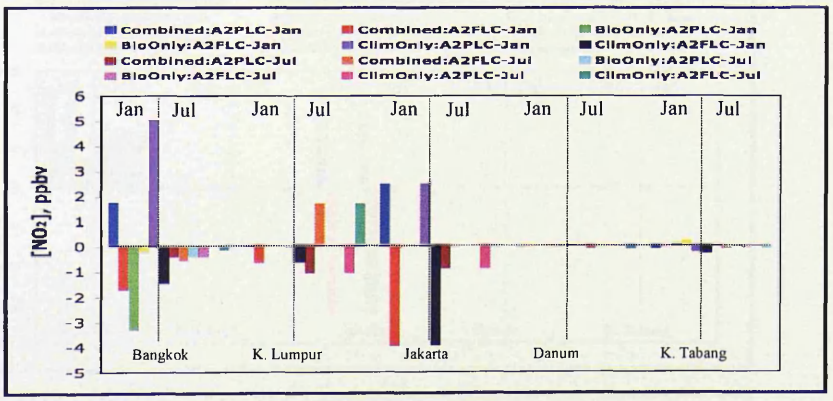

(d) B2: NO_2

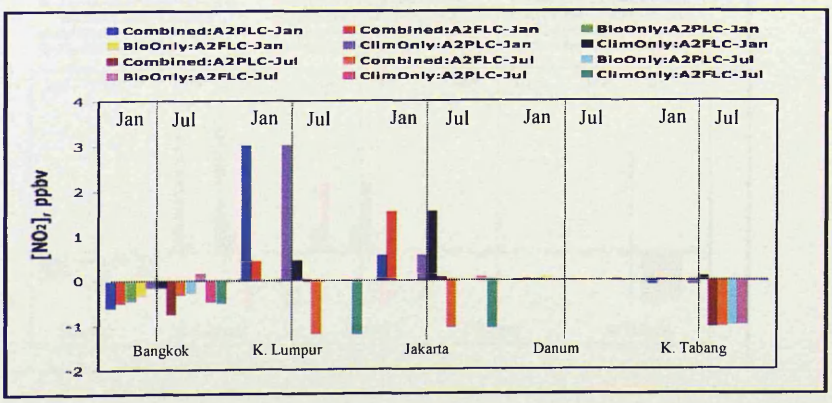

Figure 6.6: Comparison of impacts due to the combined effects of climate change and biogenic emissions, biogenic emissions alone and climate change alone during January (Jan) and July (Jul) under different landcover and climate scenarios in five locations in SEA. The A2 and B2 scenarios for a) A2: NO; (b) B2: NO; (c) A2: NO_2; (d) B2: NO_2.

(a) A2: $HONO_2$

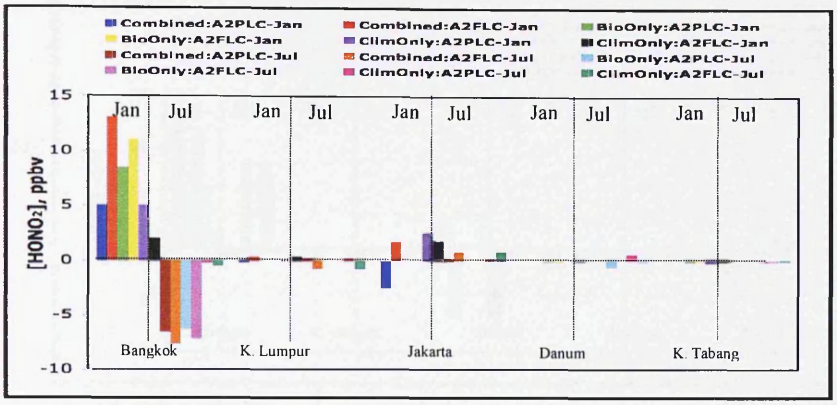

(b) B2: $HONO_2$

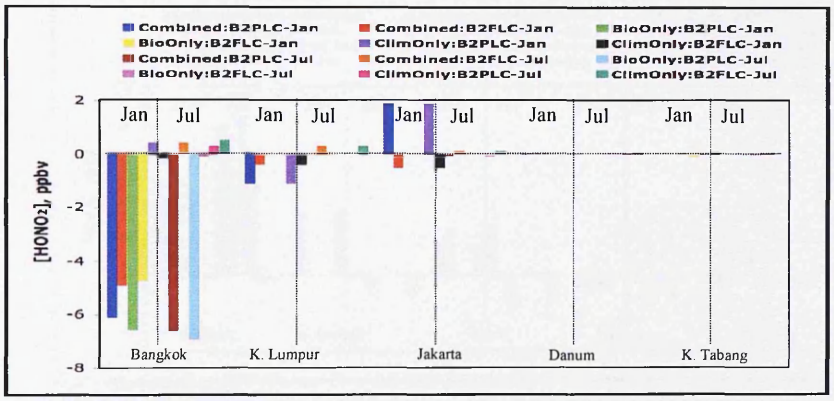

(c) A2: PAN

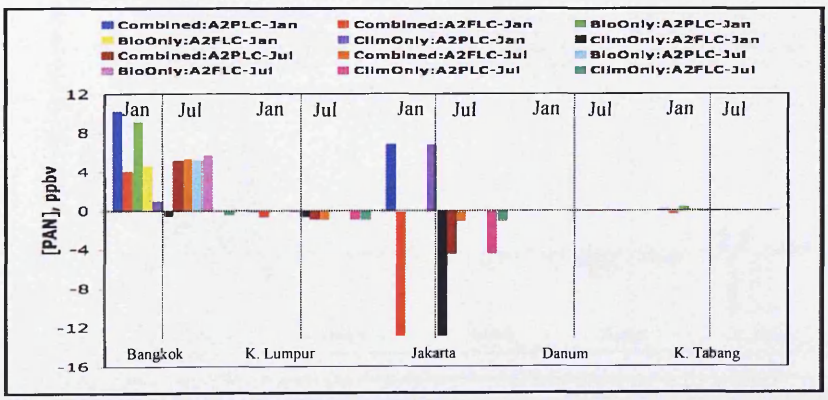

(d) B2: PAN

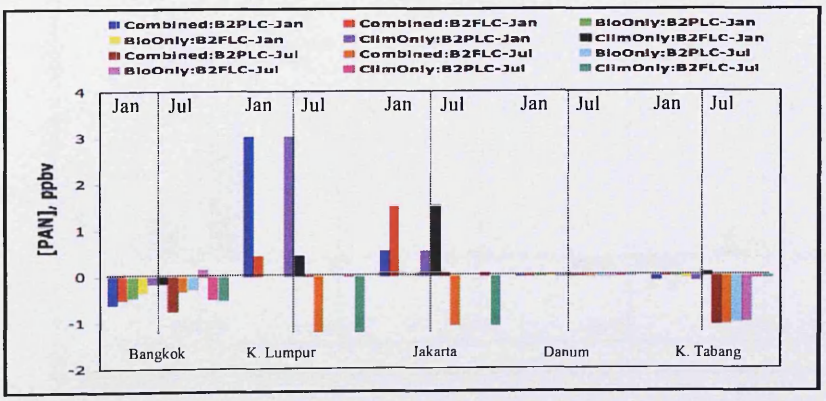

Figure 6.7: Comparison of impacts due to the combined effects of climate change and biogenic emissions, biogenic emissions alone and climate change alone during January (Jan) and July (Jul) under different landcover and climate scenarios in five locations in SEA. The A2 and B2 scenarios for a) A2: $HONO_2$; (b) B2: $HONO_2$; (c) A2: PAN; (d) B2: PAN.

(a) A2: HCHO

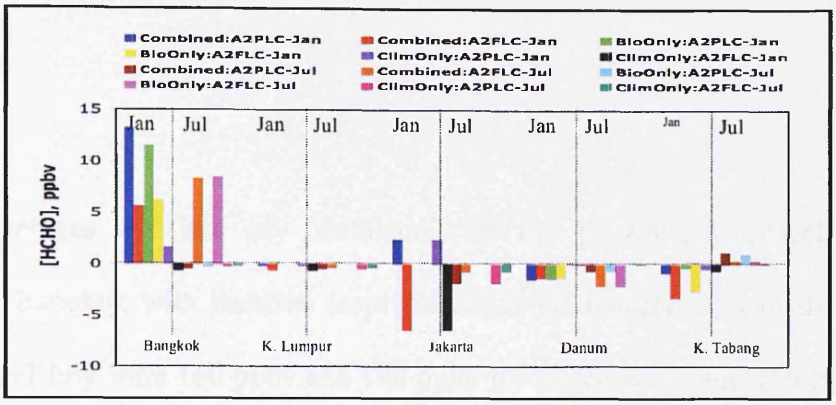

(b) B2: HCHO

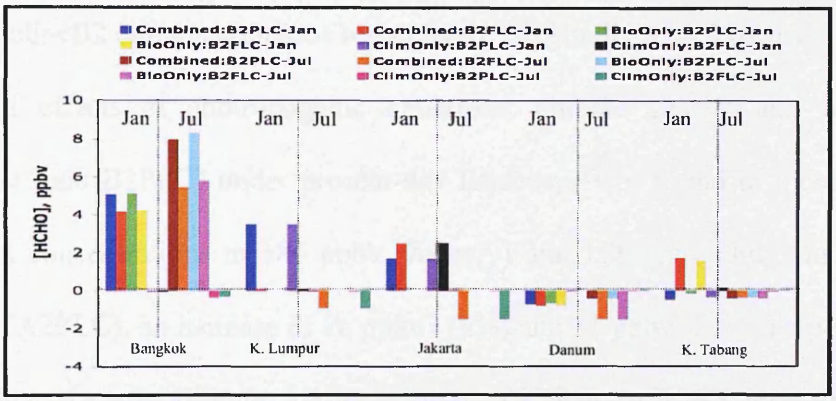

(c) A2: H_2O_2

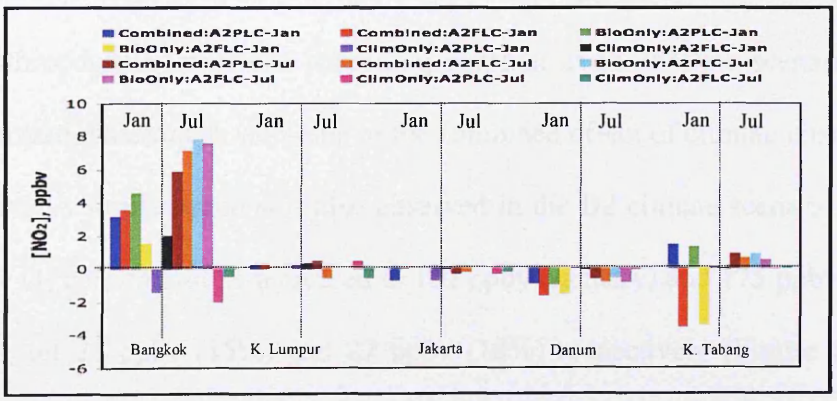

(d) B2: H_2O_2

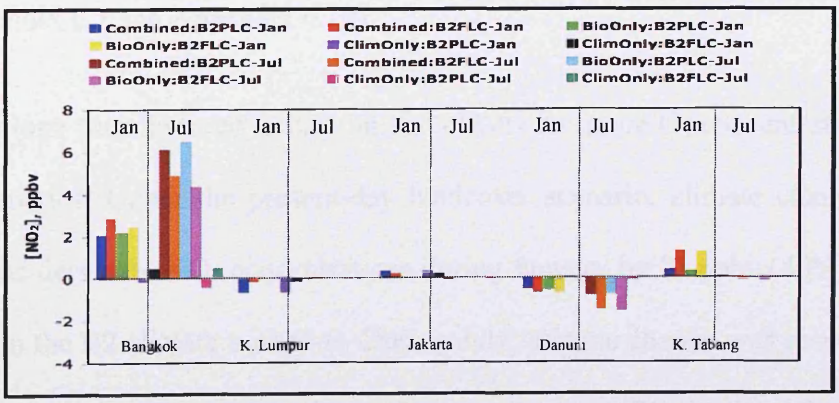

Figure 6.8: Comparison of impacts due to the combined effects of climate change and biogenic emissions, biogenic emissions alone and climate change alone during January (Jan) and July (Jul) under different landcover and climate scenarios in five locations in SEA. The A2 and B2 scenarios for a) A2: HCHO; (b) B2: HCHO; (c) A2: H_2O_2; (d) B2: H_2O_2.

6.7.1.1 Bangkok

6.7.1.1.1 O_3

The 24-hour averages for last day simulation of the present-day (baseline) O_3 concentration in Bangkok with baseline isoprene emissions incorporated in the model during January and July were 160 ppbv and 148 ppbv for BaselineA2, and 159 ppbv and 148 ppbv for BaselineB2 climate scenarios respectively (Appendix 6.9). The investigation of the combined effects of anthropogenic emissions, climate change and biogenic emissions (A2PLC and B2PLC) under present-day landcover was found to increase the future surface O_3 concentrations to 186 ppbv (January) and 178 ppbv (July) in the A2 climate scenario (A2PLC), an increase of 26 ppbv (16%) and 31 ppbv (21%) respectively, relative to baseline scenario (Figure 6.5 and Figure 6.9; Appendix 6.7 and Appendix 6.10). As the anthropogenic emissions remaining constant as in baseline scenarios, the surface O_3 concentrations changes were due to the combined effect of climate change and biogenic emissions. A similar trend was also observed in the B2 climate scenario, where the future surface O_3 concentrations increased to 182 ppbv (January) and 175 ppbv (July), an increase of about 23 ppbv (15%) and 27 ppbv (18%) respectively (Figure 6.5 and Figure 6.9; Appendix 6.7 and Appendix 6.10).

Climate change alone was observed to have mixed effects on future O_3 concentrations for both climate scenarios. Under the present-day landcover scenario, climate change was responsible for the decrease of O_3 concentrations during January by 11 ppbv (40%) in A2 and 1 ppb (5%) in the B2 climate scenarios. During July, climate change was responsible for the small increase in O_3 concentrations of about 2 ppbv (7%) in the A2 and the decrease of 7 ppbv (25%) in the B2 climate scenarios respectively. Compounding the effects of the climate change alone, the biogenic emissions alone accounted for the increase in future changes in surface O_3 concentrations of about 37 ppbv (141%) during

January and 29 ppbv (93%) during July in the A2 climate scenario relative the combined effect of climate change and biogenic emissions (Figure 6.5 and Appendix 6.7). In the B2 climate scenario, biogenic emissions alone also accounted for a higher increase in future O_3 concentrations of about 22 ppbv (95%) during January and 34 ppbv (125%) during July. The role of biogenic emissions in the increase of O_3 in a polluted environment like Bangkok could be through isoprene oxidation, which is a large source of HO_2 and RO_2 radicals, which can react with NO_x (Levy *et al.*, 1999) to produce O_3 (Trainer *et al.*, 1988). Previous studies in urban areas during summer by Watson *et al.* (2006) and Lee and Wang (2006), have also shown an increase in surface O_3 concentrations in response to high isoprene emissions, warmer temperatures and coherence with high OH diurnal cycles. Despite the anthropogenic emissions remaining constant as in baseline scenarios, the high concentration of surface O_3 in Bangkok in the future A2 and B2 climate scenarios were still largely contributed by anthropogenic NO_x and VOCs emissions. These contributed about 159 ppbv (January) and 140 ppbv (July) in the A2 climate scenario; and 158 ppbv (January) and 142 ppbv (July) in the B2 climate scenario. Anticipation of an increase in future anthropogenic emissions for both climate scenarios as projected by IPCC (2001), the future concentrations of surface O_3 are most likely to be modified due to a number of competing processes, including climate change and biogenic emissions.

The modification of future landcover in SEA has been found to modify future climate and isoprene emissions in the region. In Bangkok, the modification of future landcover has resulted in the surface temperature by 6°C during January and 8°C during July in the A2 climate scenario (Table 6.2). In the B2 climate scenario, surface temperature increased by 5°C during January and July. In the same scenarios, isoprene emissions were also affected due to climate change (Table 6.5). The combined effects of climate change and biogenic

emissions (A2FLC and B2FLC) due to the modification of future landcover have been observed to increase surface O_3 concentrations by 32 ppbv (20%) during January and 29 ppbv (19%) during July in the A2 climate scenario (Figure 6.5 and Figure 6.9; Appendix 6.7) relative to the baseline scenario. Surface O_3 concentrations were also observed to increase in the B2 climate scenario by 20 ppbv (12%) during January and 31 ppbv (21%) during July respectively. Under the future landcover scenario, climate change alone was also observed to have mixed effects on future O_3 concentrations for both climate scenarios. Climate change was responsible for the small increase of O_3 concentrations during January by 3 ppbv (10%) in A2 and 1 ppb (6%) in the B2 climate scenarios. During July, climate change was responsible for the decrease in O_3 concentrations of about 4 ppbv (13%) in the A2 and 4 ppbv (12%) in the B2 climate scenarios respectively. Considering the effects of climate change alone, the biogenic emissions alone accounted for the increase in future changes in surface O_3 concentrations of about 29 ppbv (89%) during January and 32 ppbv (113%) during July in the A2 climate scenario relative the combined effect of climate change and biogenic emissions (Figure 6.5 and Appendix 6.7). In the B2 climate scenario, biogenic emissions alone also accounted for a higher increase in future O_3 concentrations of about 19 ppbv (94%) during January and 35 ppbv (111%) during July. Climate change and biogenic emissions due to the modifications of future landcover were observed to have mixed effects on future O_3 concentrations relative to changes under present-day landcover scenario.

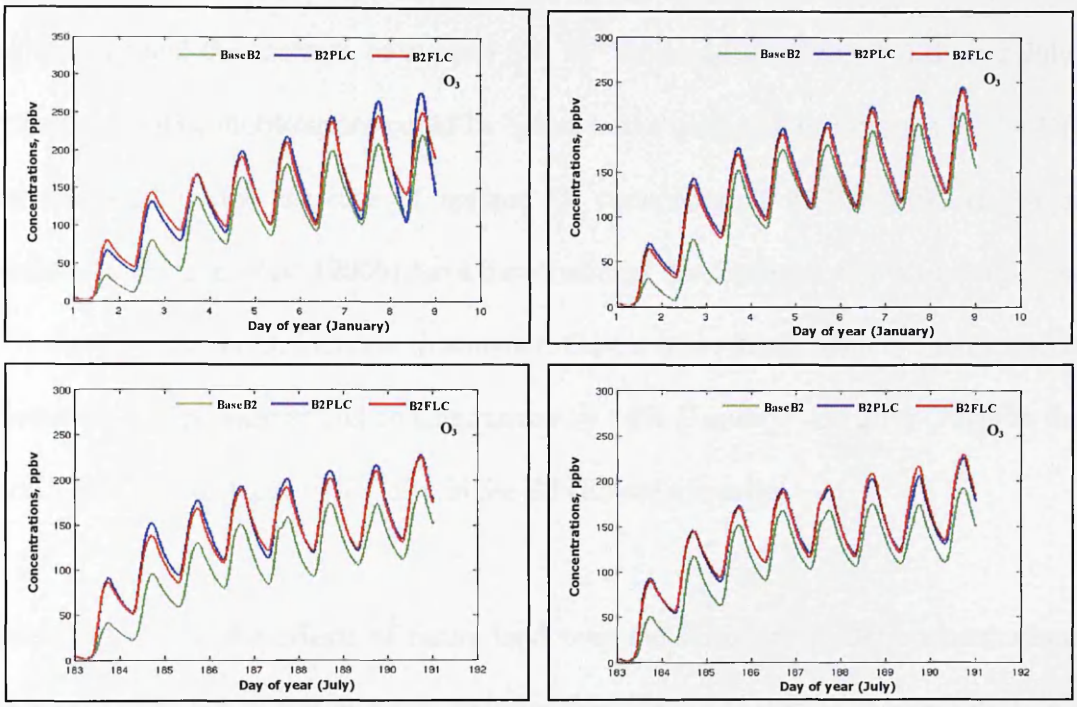

Figure 6.9: ***Bangkok***: Simulated O_3 (ppbv) during January (*top panel*) and July (*bottom panel*) in the A2 (*left panel*) and B2 (*right panel*) emission scenarios under the present-day (PLC) and modified future landcover (FLC).

6.7.1.1.2 OH

In Bangkok, the combined effects of climate change and biogenic emissions were found to decrease the future (A2PLC and B2PLC) OH concentrations by 6.4 x 10^5 molecules cm^{-3} (37%) during January and 7.8 x 10^5 molecules cm^{-3} (38%) during July in the A2 climate scenario (Figure 6.5, Figure 6.10; Appendix 6.7 and Appendix 6.10). Meanwhile, in the B2 climate scenario, a decrease of OH concentrations of about 3.9 x 10^5 molecules cm^{-3} (22%) during January and 8.9 x 10^5 molecules cm^{-3} (42%) during July was observed. The biogenic emissions impact alone accounted for a higher decrease of about 7.3 x 10^5 molecules cm^{-3} (114%) during January and 9.8 x 10^5 molecules cm^{-3} (126%) during July in the A2 climate scenario (Figure 6.5; Appendix 6.7). In the B2 climate scenario,

biogenic emissions accounted for the decrease of about 4.5 x 10^5 molecules cm^{-3} (115%) during January and the increase of about 1.1 x 10^6 molecules cm^{-3} (119%) during July. Suppression of OH concentrations could be linked to the oxidation of isoprene by the OH radical that lead to the increase of surface O_3 concentration in Bangkok. In urban environments, Watson *et al.* (2006) have demonstrated that isoprene can act to suppress the OH that leads to an O_3 increase in summer. On the other hand, climate change alone accounted for the increase in OH concentrations by 14% (January) and 26% (July) in the A2; and 15% (January) and 19% (July) in the B2 climate scenarios.

An investigation into the effects of future landcover modification on OH concentrations due to changes in climate and biogenic emissions was found to lower OH concentrations. The combination of climate change and biogenic emissions in future landcover scenarios was observed to decrease OH concentrations by 4.9 x 10^5 molecules cm^{-3} (28%) during January and 2.6 x 10^5 molecules cm^{-3} (13%) during July in the A2 climate scenario (Figure 6.5 and Figure 6.10; Appendix 6.7 and Appendix 6.10). Similarly in the B2 climate scenario, OH concentrations decreased by 3.2 x 10^5 molecules cm^{-3} (18%) during January and 5.4 x 10^5 molecules cm^{-3} (25%) during July in the B2 climate scenario. Comparatively, the combined effects of climate change and biogenic emissions under modified future landcover were observed to affect the decrease of OH concentration more than under present-day landcover, except during January in the B2 climate scenario. The additional effects on the decrease of OH concentrations were still largely contributed by biogenic emissions of about 92%.

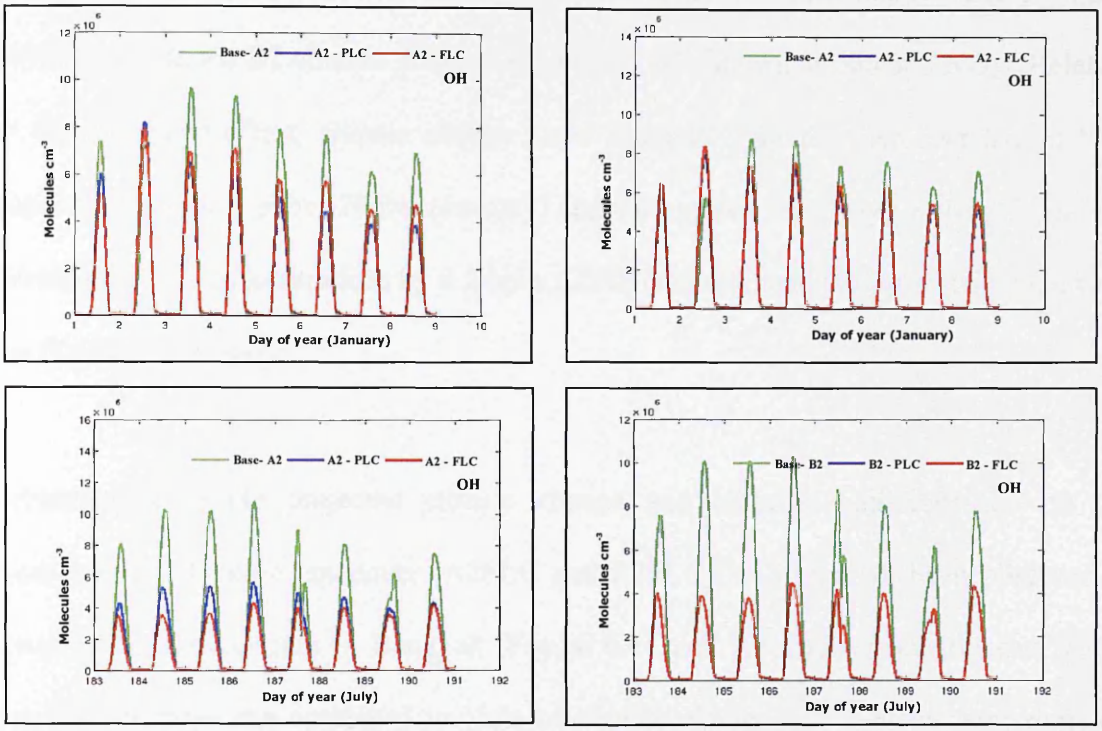

Figure 6.10: ***Bangkok***: Simulated OH (molecules cm^{-3}) during January (*top panel*) and July (*bottom panel*) in the A2 (*left panel*) and B2 (*right panel*) emission scenarios under the present-day (PLC) and modified future landcover (FLC) scenarios.

6.7.1.1.3 NO_x

The combined impact of climate change and biogenic emissions on future NO_x (NO + NO_2) under present-day landcover scenarios were also found to have mixed effects in Bangkok. Largely, the combined effects have lowered the NO_x concentrations between 8% and 15% in both months in the A2 and B2 climate scenarios, with the exception of January in the A2 climate scenario, where NO_x concentration was increased by 1.8 ppbv (20%) (Figure 6.6 and Figure 6.11; Appendix 6.7 and Appendix 6.10 – shown as NO and NO_2). Biogenic emissions alone were far more important to the decrease of NO_x in both months in the A2 and B2 climate scenarios than climate change alone. Biogenic emissions were responsible for the NO_x reduction of about 4 ppbv (194%) (January) and 0.4 ppbv

(24%) (July) in the A2 climate scenario; and 0.5 ppbv (77%) (January) and 0.3 ppbv (40%) (July) in the B2 climate scenario (Appendix 6.7- shown as NO and NO_2). Relative to the combined effect, climate change alone accounted for the high increase in NO_x concentrations by 5 ppbv (294%) (January) and 0.02 ppbv (5%) (July) in the A2; and the decrease in NO_x concentrations by 0.2 ppbv (23%) (January) and 0.5 ppbv (60%) (July) in the B2 climate scenario.

Perturbations to the projected climate change and biogenic emissions due to the modification of future landcover (A2FLC and B2FLC) in SEA have been observed to lower NO_x concentration in Bangkok (Figure 6.11 and Appendix 6.9). Relative to the baseline scenario, the combined impacts of climate change and biogenic emissions on NO_x concentrations were observed to decrease by 2 ppbv (21%) during January and 0.6 ppbv (11%) during July in the A2 scenario (Figure 6.6; Appendix 6.7 and Appendix 6.10). Meanwhile, the combined impacts of climate change and biogenic emissions in the B2 climate scenario accounted for the decrease of NO_x concentrations by 0.5 ppbv (7%) during January and 0.4 ppbv (7%) during July. Relative to the combined impacts, the biogenic emissions impact alone accounted for the decrease of NO_x concentrations of about 0.3 ppbv (17%) during January and 0.4 ppbv (79%) during July in the A2 scenario (Figure 6.6 and Appendix 6.7 –shown as NO and NO_2). In the B2 scenario, biogenic emissions accounted for the decrease of NO_x concentrations 0.4 ppbv (72%) during January and the increase of about 0.1 ppbv (34%) during July. On the other hand, in the A2 climate scenario, climate change alone accounted for the decrease of NO_x concentrations of about 2 ppbv (83%) during January and 0.1 ppbv (21%) during July. In the B2 climate scenario, climate change accounted for the decrease of about 0.2 ppbv (28%) during January and 0.5 ppbv (134%) during July (Figure 6.6 and Appendix 6.7 –

shown in NO and NO_2). In comparison with climate change, biogenic emissions impacts on NO_x concentrations were larger during July in the A2 and during January in the B2 climate scenarios.

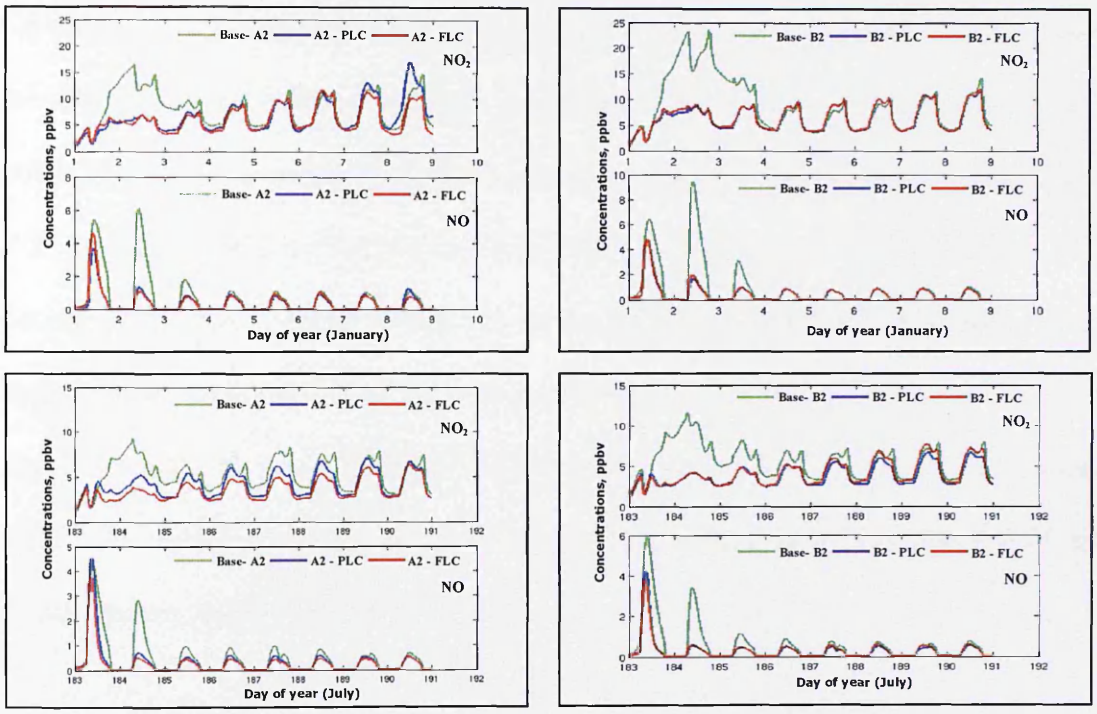

Figure 6.11: ***Bangkok***: Simulated NO & NO_2 (ppbv) during January (*top panel*) and July (*bottom panel*) in the A2 (*left panel*) and B2 (*right panel*) emission scenarios under the present-day (PLC) and modified future landcover (FLC) scenarios.

6.7.1.1.4 PAN

PAN is an important reservoir for NO_x and thus has a significant impact on O_3 production. PAN is formed in the atmosphere by reactions involving hydrocarbons and nitrogen oxides (Singh *et al.*, 1986). PAN in the atmosphere was found to be strongly impacted by isoprene, with a contribution of isoprene chemistry to the global annual PAN burden of between 22% and 32% (Pfister *et al.*, 2008). In Bangkok, the combined effects of climate change and biogenic emissions on future PAN concentration (A2PLC and

B2PLC) during both months were found to increase in Bangkok (Figure 6.12 and Appendix 6.9). Relative to the baseline scenario, the combined effects were responsible for the increase of PAN by 10 ppbv (January) and 5 ppbv (July) in the A2 climate scenario; and 4 ppbv (January) and 5 ppbv (July) in the B2 climate scenario (Figure 6.7; Appendix 6.8 and Appendix 6.10). Biogenic emissions alone were found to make a larger contribution to the increase of PAN, compared with climate change alone. Biogenic emissions alone accounted for the PAN increases of about 9 ppbv (90%) during January and 5 ppbv (100.6%) during July in the A2 climate scenario; and 4 ppbv (100%) during January and 6 ppbv (108%) during July in the B2 climate scenario. Meanwhile, climate change alone accounted for the PAN increases of about 1 ppbv (10%) during January and small decreases of about 0.03 ppbv during July. In the B2 climate scenario, climate change accounted for the small decrease of PAN concentrations of about 0.01 ppbv during January and 0.3 ppbv during July.

The combined effects of climate change and biogenic emissions under future landcover scenarios (A2FLC and B2FLC) were also observed to increase PAN concentrations in both months in the A2 and B2 climate scenarios (Figure 6.12 and Appendix 6.9). In the A2 climate scenario, PAN concentrations were increased by 4 ppbv (76%) during January and 5 ppbv (146%) during July (Figure 6.7; Appendix 6.8 and Appendix 6.10). In the B2 climate scenario, PAN concentrations were increased by 3 ppbv (58%) and 4 ppbv (116%) during January and July respectively. Biogenic emissions under future landcover scenarios were also found to be more important to the increase of PAN concentrations than the climate change alone (Figure 6.7 and Appendix 6.8). However, in terms of magnitude, these increases were relatively lower than the combined effects under present-day landcover except during January in the B2 climate scenario.

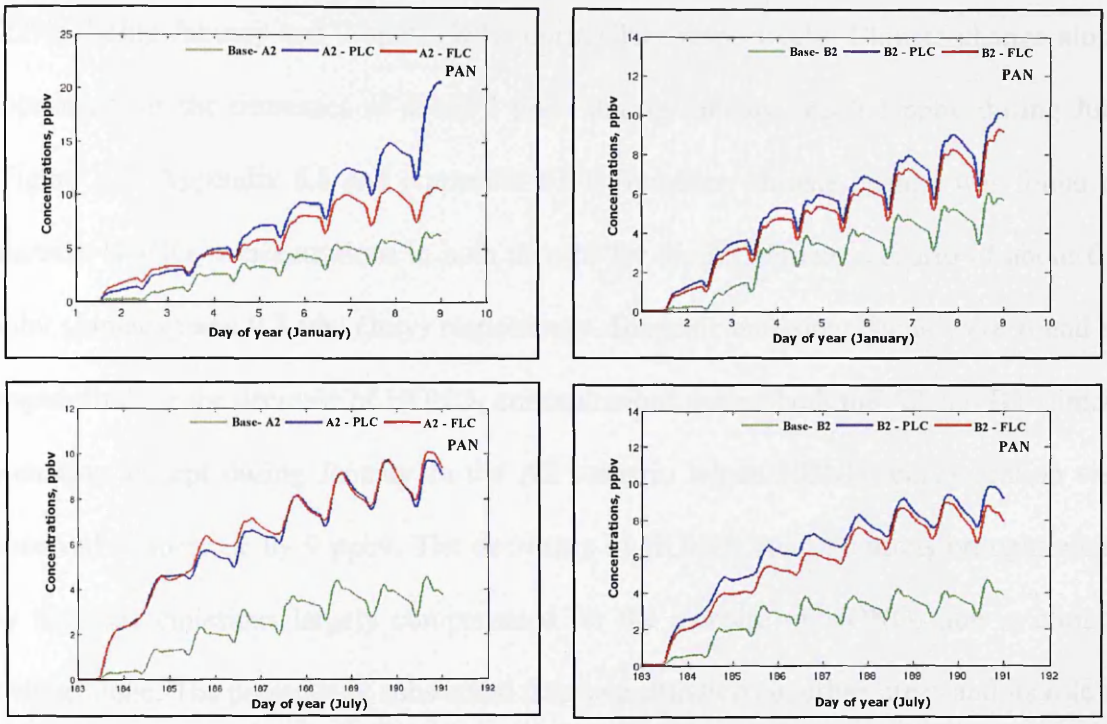

Figure 6.12: ***Bangkok***: Simulated PAN during January (*top panel*) and July (*bottom panel*) in the A2 (*left panel*) and B2 (*right panel*) emissions scenarios under the present-day landcover (PLC) and modified future landcover (FLC).

6.7.1.1.5 $HONO_2$

Another important reservoir for NO_x in the troposphere is nitric acid ($HONO_2$), which is formed through an association reaction of OH radicals with NO_2 during the day (Hanke *et al.*, 2003), and through heterogenous hydrolysis of N_2O_5 and reaction with nitrate radical (NO_3) during the night (Dentener *et al*, 1993). Relative to the baseline scenario, the simulation of future $HONO_2$ concentrations in Bangkok (A2PLC and B2PLC) with both climate change and biogenic emissions considered in the CiTTyCAT model were observed to increase by 5 ppbv (63%) during January for the A2 climate scenario, but decreased by 7 ppbv (47%) during July (Figure 6.7 and Figure 6.13; Appendix 6.8 and

Appendix 6.10). In the B2 climate scenario, $HONO_2$ decreased in both months by 6 ppbv (22%) during January and 7 ppbv (48%) during July respectively. Climate change alone accounted for the decreases of about 3 ppbv during January and 0.2 ppbv during July (Figure 6.7; Appendix 6.8 and Appendix 6.10. However, climate change was found to increase $HONO_2$ concentrations in both months for the B2 climate scenario of about 0.5 ppbv (January) and 0.3 pbv (July) respectively. Biogenic emissions alone were found to responsible for the decrease of $HONO_2$ concentrations during both the A2 and B2 climate scenarios, except during January in the A2 scenario where $HONO_2$ concentration was observed to increase by 9 ppbv. The decreases of $HONO_2$ concentrations brought about by biogenic emissions largely compensated for the increase of $HONO_2$ due to climate change alone. The presence of substantial isoprene emissions in urban areas and its role in decreasing $HONO_2$ concentrations was also demonstrated in previous work by Watson *et al.* (2006), where the increase of isoprene by a factor of 100 was found to contribute for the small decrease of maximum mixing ratios of about 0.02 ppbv (7%) during summer (July).

Relative to the baseline scenario, the combined effects of climate change and biogenic emissions under future landcover scenarios (A2FLC and B2FLC) were also observed to increase $HONO_2$ concentrations during January by 13 ppbv and decrease during July by 8 ppbv in the A2 climate scenarios (Figure 6.7 and Figure 6.13; Appendix 6.8 and Appendix 6.10). In the B2 climate scenario, $HONO_2$ concentrations were decreased by 5 ppbv during January and increased by 0.5 ppbv during July. Biogenic emissions under future landcover scenarios were also found to be more important to the increase of $HONO_2$ concentrations than the climate change alone (Figure 6.7 and Appendix 6.8). In

terms of magnitude, higher $HONO_2$ concentrations were observed under future landcover than present-day landcover scenarios in both months in the A2 and B2 climate scenarios.

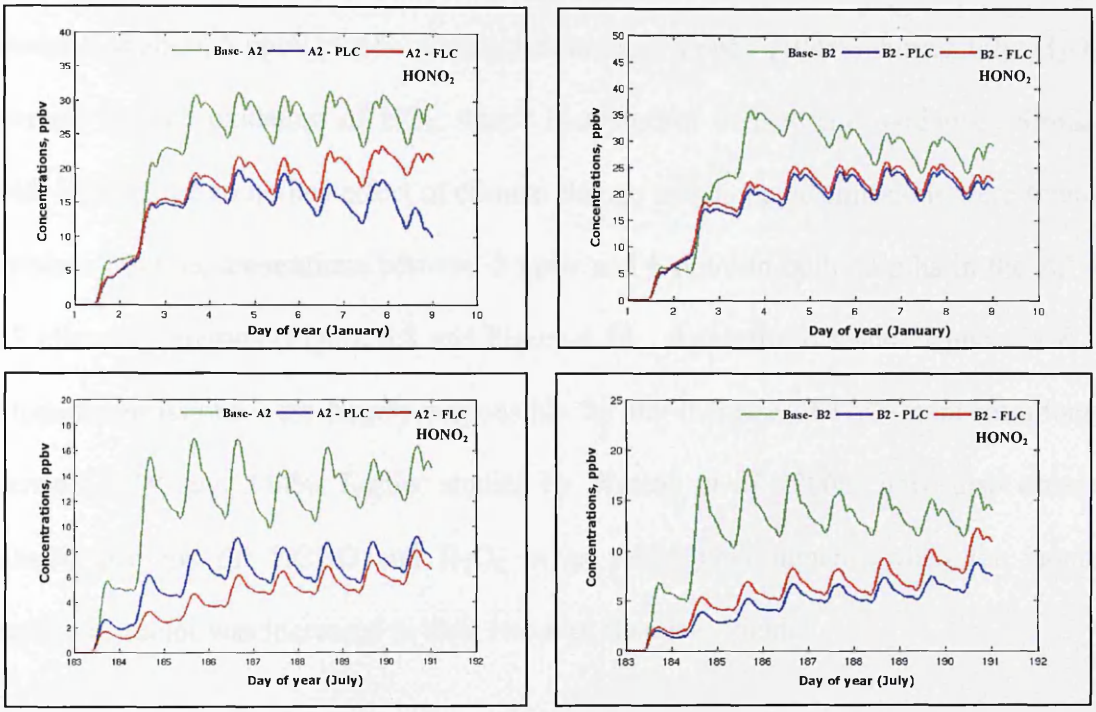

Figure 6.13: ***Bangkok***: Simulated $HONO_2$ during January (*top panel*) and July (*bottom panel*) in the A2 (*left panel*) and B2 (*right panel*) emission scenarios under the present-day landcover (PLC) and modified future landcover (FLC).

6.7.1.1.6 HCHO and H_2O_2

Formaldehyde (HCHO) is another high-yield product of isoprene oxidation. In Bangkok, the combined effects of climate change and biogenic emissions, under the present-day landcover scenario increase the HCHO concentrations by 13 ppbv during January and 7 ppbv during July in the A2 climate scenario (Figure 6.8 and Figure 6.14; Appendix 6.8 and 6.10). In the B2 climate scenario, the combined effects were observed to cause an increase of 5 ppbv and 8 ppbv during January and July respectively. Biogenic emissions alone were found to have larger effects on these changes than climate change alone. Biogenic emissions accounted for the increase of HCHO by 12 ppbv (87%) during

January and 8 ppbv (102%) during July in the A2 climate scenarios. Similarly, biogenic emissions were responsible for the increase of HCHO concentration in the B2 climate scenario of about 5 ppbv (101%) during January and 8 ppbv (104%) during July. H_2O_2 is formed through oxidation of HO_2, which is a product of isoprene oxidation. Similarly with HCHO, the combined effect of climate change and biogenic emissions were found to increase H_2O_2 concentrations between 2 ppbv and 6 ppbv in both months in the A2 and B2 climate scenarios (Figure 6.8 and Figure 6.14; Appendix 6.8 and Appendix 6.10). Biogenic emissions were largely responsible for the increase of H_2O_2 concentrations of between 92% and 144%. Earlier studies by Watson *et al.* (2006) have also observed similar patterns for HCHO and H_2O_2 in an urban environment, when the isoprene emissions factor was increased in their two-box chemistry model.

The combined effects of climate change and biogenic emissions under the modified future landcover scenarios (A2FLC and B2FLC) were also observed to increase H_2O_2 concentration by between 3 ppbv and 7 ppbv in both months in the A2 and B2 climate scenarios (Figure 6.8 and Figure 6.14; Appendix 6.8 and Appendix 6.10). Similarly to the present-day landcover scenario, biogenic emissions were more important than climate change to the increase of H_2O_2 under the future landcover scenarios. In terms of magnitude, the impacts of the combined effects of climate change and biogenic emissions in the future landcover scenarios were slightly higher than in the present-day landcover, except during July in the B2 climate scenario.

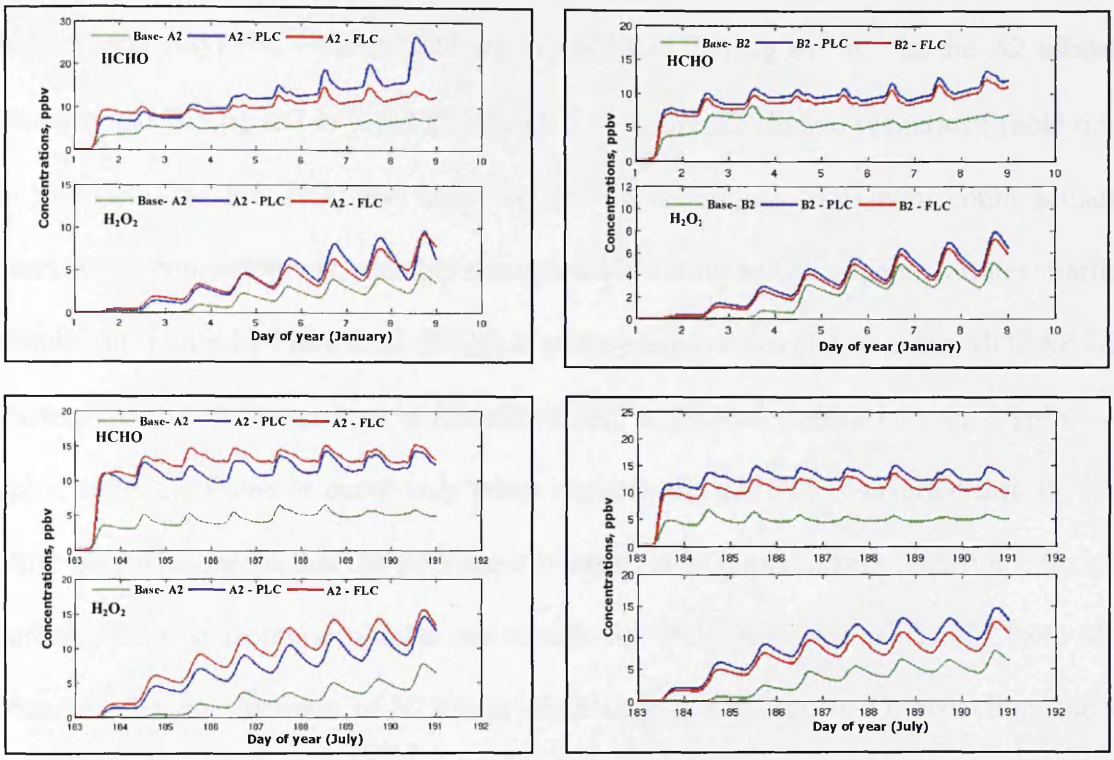

Figure 6.14: ***Bangkok***: Simulated HCHO & H_2O_2 (ppbv) during January (*top panel*) and July (*bottom panel*) in the A2 (*left panel*) and B2 (*right panel*) emission scenarios under the present-day landcover (PLC) and modified future landcover (FLC).

6.7.1.2 Danum

6.7.1.2.1 O_3

The present-day O_3 concentrations in Danum during January and July were lower of about 4 ppbv and 8 ppbv for BaselineA2, and 8 ppbv and 7 ppbv for BaselineB2 (Figure 6.15; Appendix 6.11). By removing the biogenic emissions factor, the baseline O_3 concentration for BaselineA2 increased to 15 ppbv during January and July. Almost in the same value, O_3 concentrations were also observed to increase in the BaselineB2 scenario. These increases of surface O_3 concentrations were largely due to anthropogenic NO_x and VOCs emissions that were considered as baseline anthropogenic emissions in the CiTTyCAT model input. However, the increase of surface O_3 due to anthropogenic emissions were offset by high isoprene emissions (incorporated into the model during

January and July) of about 1222 μg m^{-2} hr^{-1} and 766 μg m^{-2} hr^{-1} in the A2 climate scenario and 765 μg m^{-2} hr^{-1} and 868 μg m^{-2} hr^{-1} in the B2 climate scenarios (Table 6.6). In this case, the low NO_x and high isoprene concentrations in Danum could actually decrease O_3 concentrations, possibly through sequestering NO_x as organic nitrates. Earlier simulation studies by Fiore *et al.* (2005) in south-eastern states (USA) using MOZART-2, showed that isoprene increases in this region lead to decreased surface O_3 by 1 ppbv to 2 ppbv, and were found to occur only when isoprene nitrates were converted directly into nitric acid. This means that the isoprene ozonolysis is an important photochemical O_3 loss pathway only if isoprene nitrates are a sink for NO_2. Kang *et al.* (2003) have also observed that the increase of VOCs in some regions can lead to O_3 reduction due to increased reactions with NO_2 that produce stable organic nitrogen compounds, which result in a reduction of available NO_x. However, as identified by Fiore *et al.* (2005), uncertainty about the chemistry of isoprene-NO_x-O_3 is still an important issue, particularly concerning the fate of isoprene nitrates, and warrants further investigation. Another possible explanation for O_3 concentration decreases in the high isoprene emissions scenario is through OH titration, which enables a direct reaction of isoprene with O_3. The direct isoprene-O_3 reactions could occur in areas where NO_x is limited and there are less sensitive changes in VOCs concentrations (Zeng *et al.*, 2008; Tie *et al.*, 2005), of which Danum itself fits such a description. In tropical regions (i.e. the Amazon), where NO_x concentration are lower, von Kuhlmann *et al.* (2004) have observed that the surface concentrations of O_3 are 15% to 30% lower as a results of the lower NO_x mixing ratios.

Simulation of future O_3 concentrations due to the combined effects of climate change and biogenic emissions (A2PLC and B2PLC) under the present-day landcover scenario on surface O_3 concentrations showed an increase of 6 ppbv (January) and 10 ppbv (July), and

an increase of 2 ppbv (43%) and 2 ppbv (28%) respectively in the A2 climate scenario (Figure 6.5 and Figure 6.15; Appendix 6.7 and Appendix 6.12). Similarly, in the B2 climate scenario, future surface O_3 concentrations increased to 9 ppbv in both months, with an increase of 1 ppbv (13%) and 2 ppbv (27%) respectively. Climate change alone accounted for a decrease of 0.4 ppbv (21%) during January and an increase of 0.3 ppbv (13%) during July in the A2 climate scenario (Figure 6.5 and Appendix 6.7). In the B2 climate scenario, climate change alone accounted for the decrease of future O_3 concentrations of about 0.3 ppbv (27%) during January and 0.1 ppbv (5%) during July. Meanwhile, the impacts of biogenic emissions alone were found to be more important than climate change on the future O_3 concentrations in both climate scenarios. In terms of magnitude, biogenic emissions completely offset the negative effect of climate change on O_3 concentrations. Biogenic emissions accounted for the increase of O_3 concentrations by 2 ppbv (121%) during January and 2 ppbv (105%) during July in the A2 climate scenario (Figure 6.5 and Appendix 6.7). In the B2 climate scenario, biogenic emissions accounted for the increase of O_3 concentrations by 1 ppbv (127%) during January and 2 ppbv during July respectively.

Under future landcover scenarios, the combined effects of climate change and biogenic emissions have resulted in a further increase in O_3 concentrations in both climate scenarios. Relative to the baseline scenario, the combined effects in the A2 climate scenario were observed to increase O_3 concentrations by 3.4 ppbv (77%) during January and 4 ppbv (50%) during July (Figure 6.5 and Figure 6.15; Appendix 6.7 and Appendix 6.12). Similarly, in the B2 climate scenario, the combined effects resulted in the increase of O_3 concentrations by 3 ppbv (38%) and 4.1 ppbv (61%) during January and July respectively. Relative to the combined impact, biogenic emissions alone accounted for the

increase of O_3 concentrations by 4 ppbv (115%) during January and 3 ppbv (77%) during July in the A2 climate scenario (Figure 6.5 and Appendix 6.7). Meanwhile, in the B2 climate scenario, biogenic emissions accounted for the increase of about 3 ppbv (98%) during January and 5 ppbv (109%) during July. On the other hand, climate change alone accounted for the small decrease of O_3 of about 0.5 ppbv (15%) during January and increase of about 0.9 ppbv (23%) during July in the A2 climate scenario (Figure 6.5 and Appendix 6.7). In the B2 climate scenario, climate change alone accounted for the small increase during January (0.1 ppbv) and decrease during July (0.4 ppbv). Comparatively, biogenic emissions were more important than climate change to the changes of future O_3 concentrations under the future landcover scenario in both climate scenarios. It was also observed that the combined effects of climate change and biogenic emissions under the future landcover scenario were found to have a larger impact on surface O_3 concentrations than under the present-day landcover scenario.

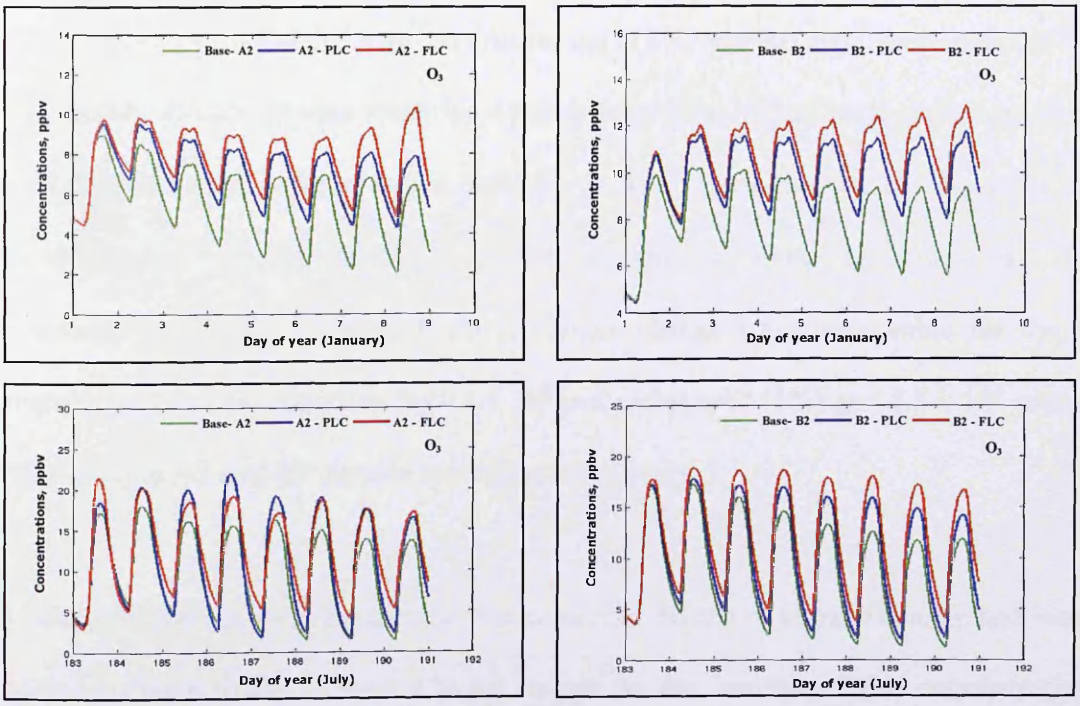

Figure 6.15: ***Danum***: Simulated O_3 (ppbv) during January (*top panel*) and July (*bottom panel*) in the A2 (*left panel*) and B2 (*right panel*) emission scenarios under the present-day landcover (PLC) and modified future landcover (FLC).

6.7.1.2.2 OH

In remote locations such as Danum, relative to the baseline scenario, the combined effects of climate change and biogenic emissions on future (A2PLC and B2PLC) OH concentrations are predicted to increase significantly by 1.5 x 10^4 molecules cm^{-3} (104%) during January and by 1.0 x 10^4 molecules cm^{-3} (42%) during July in the A2 climate scenario (Figure 6.5 and Figure 6.16; Appendix 6.7 and Appendix 6.12). In the B2 climate scenario, the combined effects were observed to increase OH concentrations by 4.8 x 10^4 molecules cm^{-3} (116%) during January and 0.7 x 10^4 molecules cm^{-3} (40%) during July. Climate change and biogenic emissions were observed to have mixed effects on these increases. Biogenic emissions alone were observed to contribute largely to the increase of OH concentrations during July in both A2 and B2 climate scenarios, which accounted for about 4.0 x 10^5 molecules cm^{-3} and 9.1 x 10^5 molecules cm^{-3} respectively (Figure 6.5 and Appendix 6.7). Meanwhile, climate change alone accounted for a small decrease in OH concentrations of about 3.9 x 10^5 molecules cm^{-3} (8%) and 9.0 x 10^5 molecules cm^{-3} (2%) during July in both climate scenarios. During January in both climate scenarios, biogenic emissions accounted for a larger decrease in OH concentrations of about 0.3 x 10^5 molecules cm^{-3} (167%) in A2 and 1.3 x 10^5 molecules cm^{-3} (275%) in B2 climate scenarios respectively. During January, climate change were responsible for the slight increase in OH concentrations by 0.4 x 10^5 molecules cm^{-3} (1%) and 1.8 x 10^5 molecules cm^{-3} (5%) in A2 and B2 climate scenarios respectively.

Under the future landcover scenario, the combined effects of climate change and biogenic emissions were found to have a larger impact on the increase of OH concentrations in Danum. In the A2 climate scenario, the combined effects were found to increase OH by 2.9 x 10^4 molecules cm^{-3} (197%) during January and 2.5 x 10^4 molecules cm^{-3} (108%)

during July (Figure 6.5 and Figure 6.16; Appendix 6.7 and Appendix 6.12). Similarly, in the B2 climate scenario, the combined effects were observed to increase OH concentrations by 5.7 x 10^4 molecules cm^{-3} (137%) and 2.1 x 10^4 molecules cm^{-3} (112%) during January and July respectively. It was also observed that climate change accounted for a larger increase of OH concentrations, despite the offsetting effect of biogenic emissions.

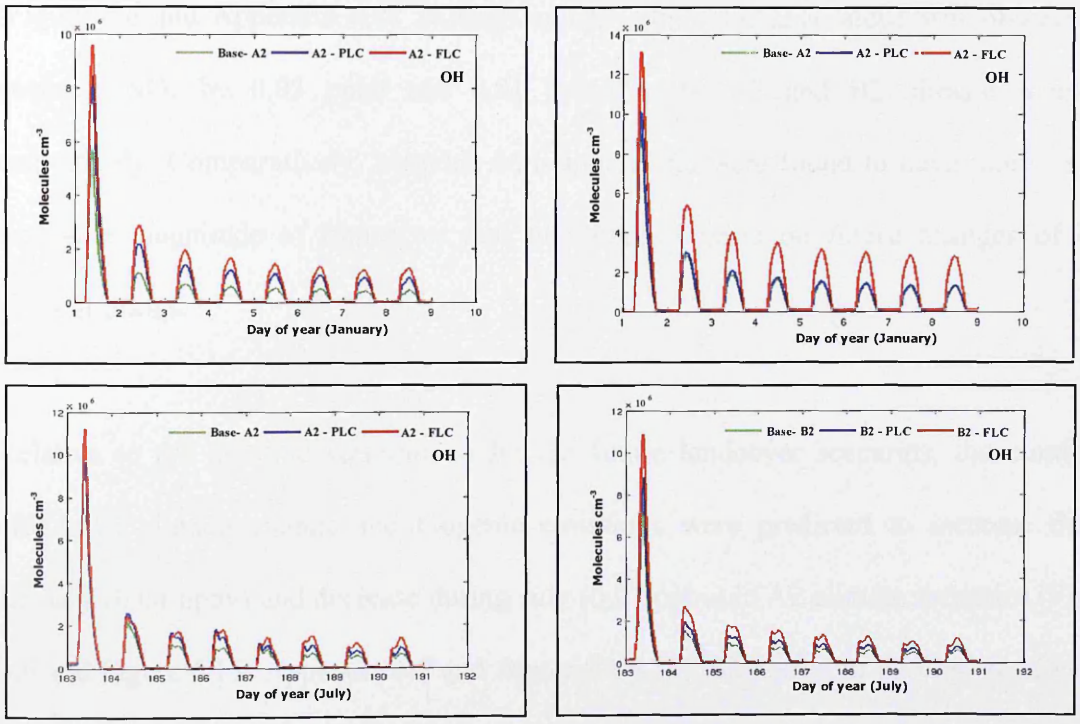

Figure 6.16: ***Danum***: Simulated OH (molecules cm^{-3}) during January (*top panel*) and July (*bottom panel*) for A2 (*left panel*) and B2 (*right panel*) emission scenarios under present-day (PLC) and modified future landcover (FLC).

6.7.1.2.3 NO_x

In Danum, the combined effects of climate change and biogenic emissions have resulted in mixed responses to the future changes of NO_x, and were largely responsible for the predicted decrease of NO_x during January and an increase during July in the A2 climate

scenario (Figure 6.6 and Figure 6.17; Appendix 6.7 and Appendix 6.12-shown as NO and NO_2). Meanwhile, in the B2 climate scenario, the combined effects were responsible for the predicted increase of NO_x during both months. Biogenic emissions were found to predict an increase in NO_x during January by 0.01 ppbv and 0.03 ppbv in A2 and B2 climate scenarios respectively. During July in both climate scenarios, biogenic emissions were observed to decrease NO_x concentration by 0.03 ppbv. Meanwhile, climate change alone was found to increase NO_x by about 0.04 ppbv during July in both climate scenarios (Figure 6.6 and Appendix 6.7). During January, climate change alone was observed to decrease NO_x by 0.03 ppbv and 0.01 ppbv in the A2 and B2 climate scenarios respectively. Comparatively, biogenic emissions alone were found to have more or less the same magnitude of impact as that of climate change on future changes of NO_x concentrations.

Relative to the baseline scenario, under the future landcover scenarios, the combined effects of climate change and biogenic emissions were predicted to increase during January (0.04 ppbv) and decrease during July (0.07 ppbv) in A2 climate scenarios (Figure 6.6 and Figure 6.17; Appendix 6.7 and Appendix 6.12). Similarly, in B2 climate scenario, the combined effects resulted in the increase of NO_x concentrations of about 0.04 ppbv during January and decrease of about 0.02 ppbv during July. In comparison, the combined effects of climate change and biogenic emissions under the future landcover scenarios have a larger impact on the increase of NO_x concentrations during January and lower during July in the A2 and B2 climate scenarios. Meanwhile, the biogenic emissions effects alone were accounted for the decrease of NO_x concentrations (0.02 ppbv) during January and increase (0.05 ppbv) during July in the A2 climate scenario (Figure 6.6 and Appendix 6.7). In the B2 climate scenario, biogenic emissions were observed to the

increase of 0.05 ppbv of NO_x concentration during January and decrease of 0.03 ppbv during July.

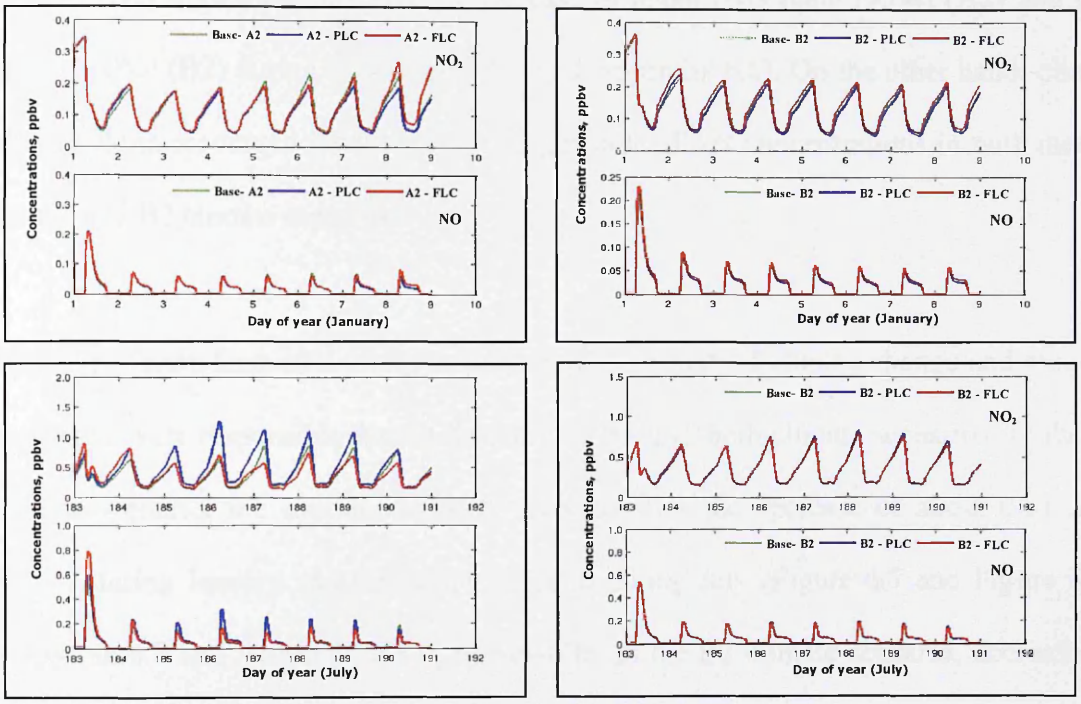

Figure 6.17: ***Danum***: Simulated NO & NO_2 (ppbv) during January (*top panel*) and July (*bottom panel*) in the A2 (*left panel*) and B2 (*right panel*) emission scenarios under the present-day (PLC) and modified future landcover (FLC).

6.7.1.2.4 PAN

Under the present-day landcover scenario, the combined effects of climate change and biogenic emissions were predicted to decrease PAN concentrations by 0.04 ppbv and 0.02 ppbv during January in the A2 and B2 climate scenarios. During July, the combined effects accounted for the increase of PAN concentrations by 0.05 ppbv and 0.04 ppbv in the A2 and B2 climate scenarios respectively (Figure 6.7; Appendix 6.8 and Appendix 6.12). Climate change and biogenic emissions were also predicted to have mixed effects on future PAN concentrations in Danum. Biogenic emissions alone were observed to have

a much larger impact on PAN concentrations than climate change alone. Biogenic emissions accounted for the decrease of about 0.04 ppbv (97.5%) (A2) and 0.02 ppbv (100%) (B2) during January and the increase of about 0.05 ppbv (75%) (A2) and 0.03 ppbv (100%) (B2) during July (Figure 6.7 and Appendix 6.8). On the other hand, climate change alone accounted for the small changes to the PAN concentrations in both months for A2 and B2 climate scenarios.

Under the future landcover scenario, the combined effects of climate change and biogenic emissions were responsible for the decrease of PAN in both climate scenarios. In the A2 climate scenario, the combined effects accounted for the decrease of about 0.01 ppbv (7.1%) during January and 0.13 ppbv (22.4%) during July (Figure 6.7 and Figure 6.18; Appendix 6.8 and Appendix 6.12). Meanwhile, in the B2 climate scenario, decreases of about 0.02 ppbv (18.2%) and 0.01 ppbv (2%) were observed during January and July respectively. In terms of magnitude, the combined impact of climate change and biogenic emissions under the present-day and future landcover were more or less the same. The effects of biogenic emission alone accounted for the small decrease of PAN concentrations for both months in the A2 and B2 climate scenario. It was also observed that the effects of biogenic emissions alone were more important than climate change alone to the changes of future concentrations of PAN.

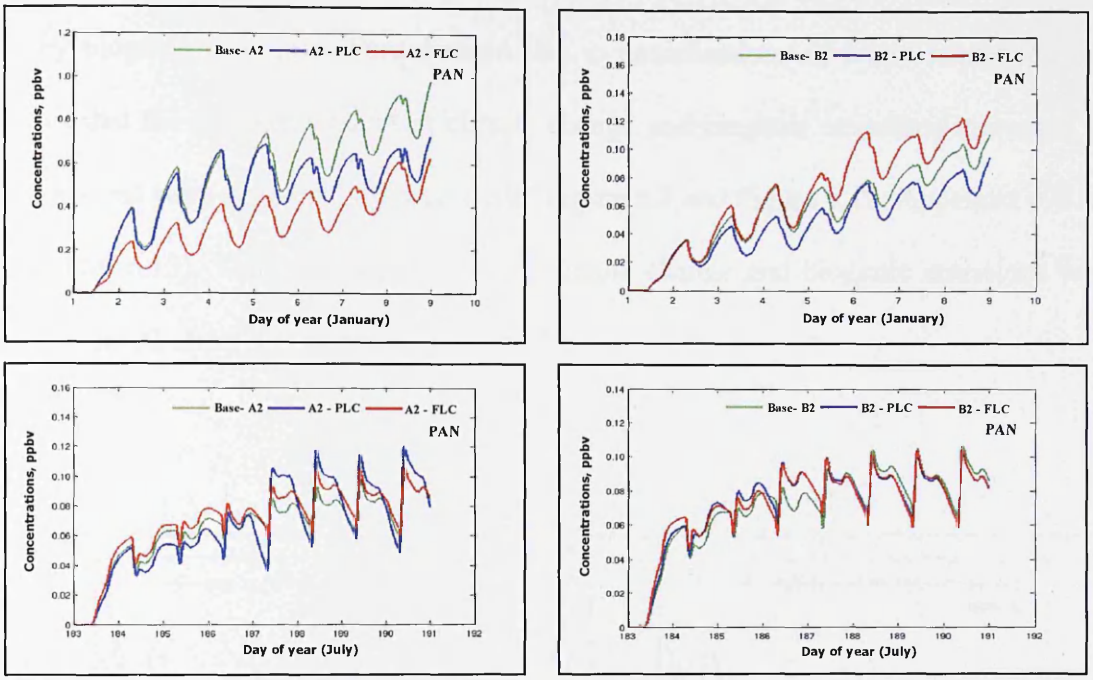

Figure 6.18: ***Danum***: Simulated PAN during January (*top panel*) and July (*bottom panel*) in the A2 (*left panel*) and B2 (*right panel*) emission scenarios under the present-day landcover (PLC) and modified future landcover (FLC).

6.7.1.2.5 $HONO_2$

Future changes to the $HONO_2$ concentrations under the present-day landcover scenario in Danum were predicted to be lower due to the balancing effects of climate change and biogenic emissions. The combined effects of climate change and biogenic emissions were less than 0.01 ppbv in both months in the A2 and B2 climate scenarios (Figure 6.7 and Figure 6.19; Appendix 6.8 and Appendix 6.12). Biogenic emissions alone accounted for the decrease of $HONO_2$ concentrations during January of 0.37 ppbv (A2) and 0.36 ppbv (B2), and the decrease during July of 0.47 ppbv (A2) and 0.43 ppbv (B2) (Figure 6.7 and Appendix 6.8). The future changes of $HONO_2$ concentrations due to climate change alone were predicted to decrease by more or less the same as biogenic emissions in both the A2 and B2 scenarios (Figure 6.7 and Appendix 6.8). The net of changes in $HONO_2$

concentrations was small, as the changes due to climate change alone were compensated for by biogenic emissions. Perturbations due to modifications of future landcover have shown that the combined effect of climate change and biogenic emissions increased the $HONO_2$, but were very small in magnitude (Figure 6.7 and Figure 6.19; Appendix 6.8 and Appendix 6.12). The balancing effects of climate change and biogenic emissions were also observed under this scenario.

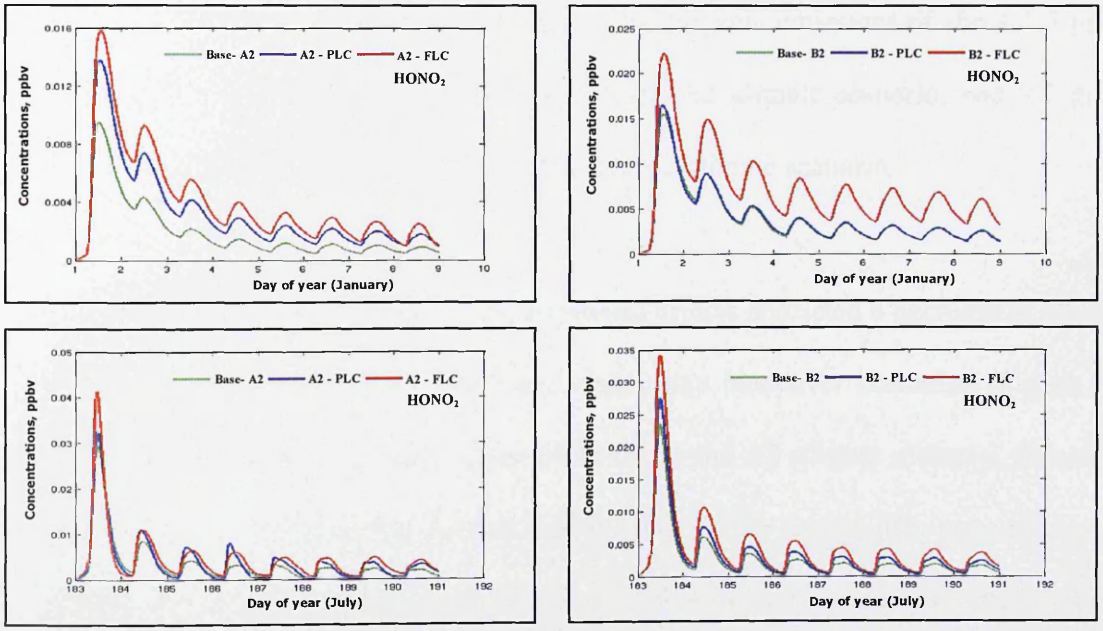

Figure 6.19: ***Danum***: Simulated $HONO_2$ during January (*top panel*) and July (*bottom panel*) in the A2 (*left panel*) and B2 (*right panel*) emission scenarios under the present-day landcover (PLC) and modified future landcover (FLC).

6.7.1.2.6 HCHO and H_2O_2

An opposite observation was found in terms of HCHO and H_2O_2 concentrations in urban areas and remote areas. The combined effects of climate change and biogenic emissions under the present-day landcover scenario were responsible for the predicted decrease of HCHO concentrations by 1.5 ppbv (29%) during January and 0.6 ppbv (6%) during July in the A2 climate scenario; and 0.7 ppbv (19%) during January and 0.4 ppbv (4%) during July in the B2 climate scenario (Figure 6.8 and Figure 6.20; Appendix 6.8 and Appendix 6.12). These changes were contributed to largely by biogenic emissions of about 1.5 ppbv (98%) (January) and 0.6 ppbv (100%) (July) in the A2 climate scenario, and 0.7 ppbv (97%) (January) and 0.4 ppbv (103%) (July) in the B2 climate scenario.

Under the future landcover scenarios, the combined effects predicted a decrease in HCHO concentrations than those shown under the present-day landcover scenarios (Figure 6.8 and Figure 6.20; Appendix 6.8 and Appendix 6.12). In the A2 climate scenario, decreases of about 1.3 ppbv (26%) during January and 2 ppbv (23%) during July were observed. Meanwhile, in the B2 climate scenario, the combined effects were responsible for a further decrease of HCHO concentrations of about 0.8 ppbv (22%) and 2 ppbv (17%) during January and July respectively. Biogenic emissions played more important role in the future changes of HCHO concentrations than the climate change.

Similarly, for H_2O_2 concentrations under the present-day landcover scenario, the combined effects of climate change and biogenic emissions were predicted to decrease by 0.9 ppbv (22%) during January and 0.6 ppbv (11%) during July in the A2 climate scenario (Figure 6.8 and Figure 6.20; Appendix 6.8 and Appendix 6.12). In the B2 climate

scenario, the combined effects accounted for a decrease of about 0.5 ppbv (18%) and 0.8 ppbv (13%) during January and July respectively.

Under the future landcover scenarios, the combined effects were predicted to decrease the H_2O_2 concentrations further – by 2 ppbv (38%) during January and 0.8 ppbv (14%) during July in the A2 climate scenario (Figure 6.8; Appendix 6.8). Similarly, in the B2 climate scenario, H_2O_2 concentrations were observed to decrease by 0.7 ppbv (22%) and 2 ppbv (24.9%) during January and July respectively. Relatively, in terms of magnitude, the combined effects of climate change and biogenic emissions to the future changes of H_2O_2 concentrations under the present-day landcover were smaller than under the future landcover scenarios. It was also predicted that the biogenic emissions were found to be largely responsible for the decrease of H_2O_2 concentrations by between 53% and 103% in both climate scenarios. The effects of climate change alone on the future changes of H_2O_2 concentrations were comparatively smaller than the biogenic emissions alone.

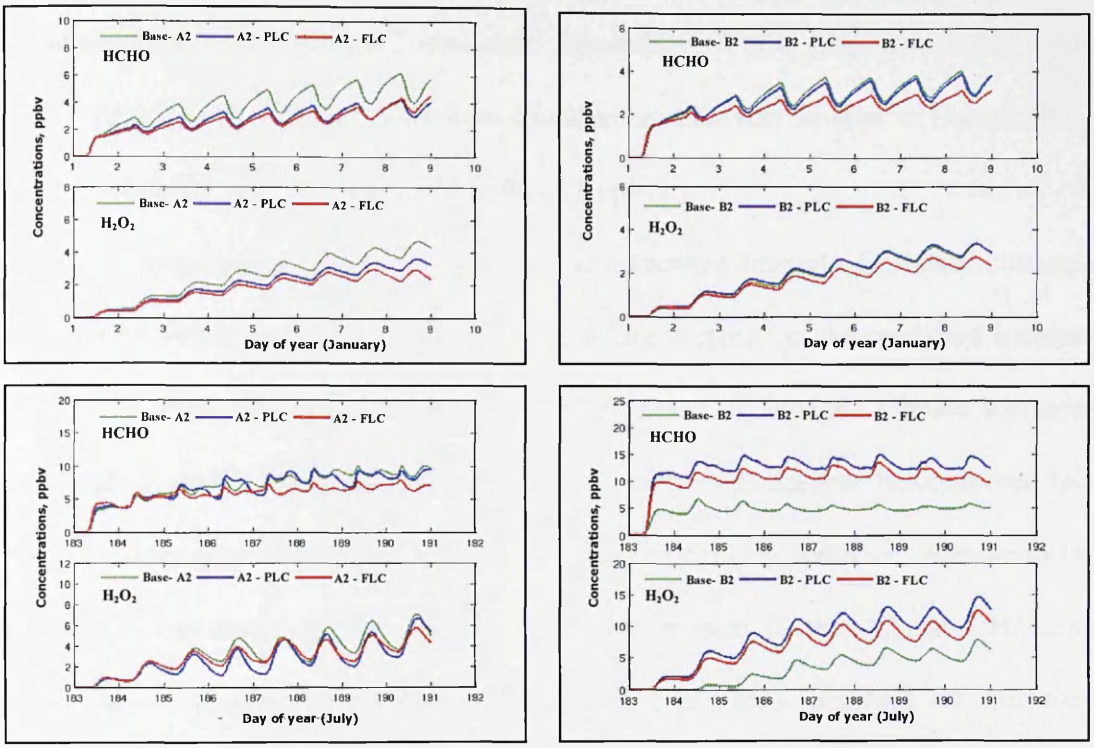

Figure 6.20: ***Danum***: Simulated HCHO & H_2O_2 (ppbv) during January (*top panel*) and July (*bottom panel*) in the A2 (*left panel*) and B2 (*right panel*) emission scenarios under the present-day landcover (PLC) and modified future landcover (FLC).

6.8 Conclusions

This study has employed the CiTTyCAT model to investigate the response of tropospheric O_3 concentrations and some trace gases and oxidants in three urban and two remote areas in Southeast Asia, to the climate change and biogenic emissions in present-day and future land cover scenarios in both BaselineA2 and BaselineB2 climate scenarios. Some conclusions can be drawn from the results:

- In urban environments, the simulations of the present-day (2008) concentrations of surface O_3 were observed to be highest in Jakarta (148 ppbv – 270 ppbv) followed by Bangkok (148 ppbv - 160 ppbv) and Kuala Lumpur (138 ppbv -144 ppbv) in both

BaselineA2 and BaselineB2 scenarios. Meanwhile, in two studied remote locations, the range of O_3 concentrations were found to be relatively smaller in Danum (4 ppbv - 8 ppbv) than in Koto Tabang (4 ppbv - 15 ppbv).

- In the present-day landcover scenario, the combined impact of climate change and biogenic emissions was observed to have a larger effect on the predicted increase of future surface O_3 concentrations for both months in A2 and B2 climate scenarios in Bangkok, and Danum. Meanwhile, in Kuala Lumpur and Jakarta the combined factors were observed to have mixed effects. In Kuala Lumpur, a predicted increase in future O_3 concentrations was also observed in both months in the A2 and B2 climate scenarios, except during July in B2, where a small decrease of surface O_3 concentration was observed. In Jakarta, the combined impact of climate change and biogenic emissions was predicted to increase surface O_3 concentrations during January but decrease them during July in both A2 and B2 climate scenarios. In Koto Tabang, the combined impact was predicted to decrease future surface O_3 in both A2 and B2 cliamte scenarios.
- In Bangkok and Danum the impact of biogenic emissions alone accounted for the larger increase in future changes of surface O_3 concentrations for both months in the A2 and B2 climate scenarios. However, in Koto Tabang, the impact of biogenic emissions alone accounted for the predicted reduction of O_3 concentrations in both months in the A2 and B2 climate scenarios, except for a small increase during July in the B2 climate scenario. On the other hand, the impact of biogenic emissions on the future changes of surface O_3 concentrations in Kuala Lumpur and Jakarta was predicted to be negligible. Comparatively, the magnitude of impacts of biogenic emissions alone on the future changes of surface O_3 concentrations in Bangkok, Danum and Koto Tabang were larger than the impact of climate change alone. The

impact of climate change alone was predicted to have a mixed effect on future changes of surface O_3 concentrations in all locations, and played a more important role in the small changes of surface O_3 concentrations in Kuala Lumpur and Jakarta.

- The combined impacts of climate change and biogenic emissions under the modified future landcover scenario also resulted in the predicted increase of surface O_3 concentrations for both months in the A2 and B2 climate scenarios in Bangkok, and Danum. In comparison with the present-day landcover scenario, the surface O_3 concentrations were predicted further increased under the modified future landcover scenario, except for a slight decrease, which was observed during July in the A2 and January in the B2 climate scenarios in Bangkok. In Kuala Lumpur, relative to surface O_3 concentration under present-day landcover scenarios, the modification of future landcover resulted in the predicted decrease of O_3 concentrations for both months in the A2 and B2 climate scenarios. Meanwhile in Jakarta, surface O3 concentrations were observed to increase during July in the A2 and during January in the B2 climate scenarios, and decrease during January in the A2 and July in the B2 climate scenarios. In Koto Tabang the combined impact was also predicted to decrease future surface O_3 concentrations during January and increase during July in both A2 and B2 climate scenarios.
- In terms of magnitude, the impact of biogenic emissions alone on the predicted increase of future surface O_3 concentrations were larger than the impact of climate change alone in Bangkok, Danum and Koto Tabang in both climate scenarios. In all locations, the impacts of climate change alone on the future changes of O_3 concentrations were mixed and small in magnitude for both months in A2 and B2 climate scenarios.

- In Bangkok, the combined impacts of climate change and biogenic emissions under present-day and future land cover scenarios were predicted to decrease OH concentrations in both months for A2 and B2 climate scenarios, and the predicted decreases were largely attributed to biogenic emissions. Suppression of OH concentrations was largely due to the oxidation of isoprene by OH radicals. The suppression of OH was much larger in the future land cover scenarios than in those for the present-day, except during January in the B2 climate scenario. However, in Danum, the combined effects under present-day and future land cover scenarios were predicted to increase OH concentrations in both months for A2 and B2 climate. The increases of OH concentrations were largely due to climate change, although suppression of OH concentrations due to biogenic emissions was also observed. In terms of magnitude, the increases of OH concentrations were predicted to be larger under future land cover than present-day land cover scenarios. In Koto Tabang, the combined impact of climate change and biogenic emissions under present-day and future land cover scenarios was found to have a mixed effect on the future changes of OH concentrations in both months in A2 and B2 climate scenarios, although large decreases of OH concentrations were widely observed. Biogenic emissions were found to be more important than climate change to the future changes of OH concentrations, in both landcover and climate scenarios. Meanwhile, in Kuala Lumpur and Jakarta, the combined impact of climate change and biogenic emissions was found to have mixed effects on the future changes of OH concentrations and these changes were mainly due to climate change.
- The combined impact of climate change and biogenic emissions under both the present-day and future landcover scenarios was observed to have a mixed effect on the future changes of NO_x, PAN, $HONO_2$, HCHO, and H_2O_2 concentrations in all

locations for both climate scenarios. In Bangkok, Danum and Koto Tabang, the impact of biogenic emissions alone was more important to changes in these parameters than climate change in both landcover and climate scenarios. Meanwhile, in Kuala Lumpur and Jakarta, the impact of climate change were more important to concentration changes, as the biogenic emissions impact was found to be negligible in both landcover and climate scenarios.

Chapter 7

CONCLUSIONS AND FUTURE WORKS

7.1 Conclusions

The Southeast Asia (SEA) region is one of the world's most populated regions, with rapid urbanisation and industrialisation, and the large expansion of agricultural activities. The forcing caused by these economic activities has drastically changed the regional landcover over the last thirty years. Rapid changes to the general landcover over the region were largely due to the deforestation and conversion into agriculture (i.e oil palm plantation). Anticipation of further changes to the regional landcover, coupled with the increase in anthropogenic emissions and naturally high levels of biogenic emissions have been the impetus of this study, which investigates the intricate relationship of climate change-landcover-biogenic emissions-tropospheric chemistry systems at the regional scale over SEA. This was achieved through the use of PRECIS, a regional climate model, which used the atmospheric forcing and landcover forcing of the present-day and future climate scenarios (SRES A2 and B2) to simulate present-day and future climate scenarios. Subsequently, simulated climate scenarios were used to drive the biogenic emissions model (BVOCEM) to estimate the biogenic emissions over the region under various climate scenarios. Finally, the simulated climate and calculated biogenic emissions under various atmospheric and landcover forcings were used to drive the Lagrangian trajectory model (CiTTyCAT) to model the present-day and future changes of tropospheric chemistry in Southeast Asia under those forcings.

The questions posed in this study are summarised into four major research questions, which will be answered in turn using the evidence provided in this study:

- What would be the pattern and magnitude of climate changes over the Southeast Asia region based on the IPCC (2001) emission scenarios?
- What would be the combined effect of atmospheric and landcover forcings, and the effect of landcover forcing alone on regional climate changes under the present-day and modified future landcover scenarios and the IPCC's (2001) emission scenarios?
- What would be the effect of climate change due to atmospheric and landcover forcings on the regional biogenic emissions under the present-day and modified future landcover scenarios and the IPCC's (2001) emissions scenarios?
- What would be the effect of climate changes and biogenic emissions changes on the regional tropospheric chemistry under the present-day and modified future landcover and the IPCC's (2001) emission scenarios?

7.1.1 What would be the pattern and magnitude of climate changes over the Southeast Asia (SEA) region based on the IPCC (2001) emission scenarios?

PRECIS-RCM was run for SEA with the aim of examining climate change scenarios for the future. The present-day simulation with the PRECIS-RCM (1961-1990) was evaluated including an identification of biases and some statistic responses in the PRECIS-RCM. The PRECIS-RCM captured the primary features of the observed data (CRU), ERA40-Reanalysis data and GCM circulations and the patterns of seasonal change are generally well represented for most variables. Due to the stronger emissions forcing in the A2 scenario, the scenario anomalies of surface temperature are generally larger than for the

B2 scenario. Other climatic variables such as precipitation, total cloud, solar radiation and boundary layer height have shown a high degree of variability.

A warming was observed across the region with largest temperature increase apparent over land areas in both the A2 and B2 scenarios during DJF and the JJA. Under the A2 scenario, there was an average surface warming of 3°C during DJF and 3.1°C during JJA. In the B2 scenario, the average surface temperatures were 2.6°C during DJF and 2.1°C during JJA. Surface temperature changes in both the A2 and B2 climate scenarios were statistically significant, at the 95% confidence levels for all seasons for the whole modelled region-domain except in some areas over the South China Sea and the Philippines Sea during DJF in the B2 climate scenario. In both A2 and B2 climate scenarios, the total precipitation decreased during DJF by about -0.4 mm/day and slightly increased during JJA by about 0.2 mm/day (A2) and 0.1 mm/day (B2) respectively. Precipitation changes with less than -1 mm/day, mostly over the sea during DJF and a larger area over the sea and insular region during JJA were found to be statistically significant (at the 95% level) in both scenarios.

The total cloud fraction in the A2 and B2 scenarios were projected to decrease slightly by -0.07 during DJF and -0.04 during JJA. Future changes in total cloud fraction in both seasons of roughly less than -0.04 in the A2 scenario and less than -0.05 in the B2 scenario were found to be statistically significant at the 95% level. Meanwhile, the projected solar radiations in the A2 climate scenario were slightly increased by 5.6 W m^{-2} during DJF and 4.6 W m^{-2} during JJA. Similarly for the B2 scenario, the projected solar radiations were increased by 3.1 W m^{-2} during DJF and 3.8 W m^{-2} during the JJA. In the A2 scenario, boundary layer heights were observed to decrease slightly by -3 m during

DJF and increase by 23 m during JJA. In the B2 scenario, the boundary layer heights were observed to decrease by about -6 m during DJF and -7 m during JJA. Changes in a larger area over the sea in both climate scenarios were found to be statistically significant at the 95% level.

7.1.2 What would be the combined effect of atmospheric and landcover forcings, and the effect of landcover forcing alone on regional climate changes under the present-day and modified future landcover scenarios and the IPCC's (2001) emission scenarios?

The combined effect of atmospheric and landcover forcings was observed to increase the surface temperature significantly (at the 95% confidence level) over the whole SEA domain during DJF and JJA in both the A2 and B2 climate scenarios. For A2, the surface temperature increased by 2.7°C during DJF and 2.8°C during JJA. For B2, the surface temperatures increased by 2°C during DJF and 2.1°C during JJA. The effects of future landcover forcing alone during DJF and JJA for both the A2 and B2 climate scenarios were observed to be small and produced cooling temperatures, compared to the effects of combined forcing and atmospheric forcing alone. Small and scattered areas with less than -1°C in surface temperature changes due to landcover forcing alone were found to be statistically significant at the 95% confidence level during DJF and JJA in both climate scenarios. In terms of magnitude, the combined effects of atmospheric and landcover forcings in both seasons for both climate scenarios were slightly higher than atmospheric forcing alone and much higher than landcover forcing alone.

In the A2 climate scenario, the combined effects have resulted in the decrease of total precipitation by about -0.39 mm/day and -0.02 mm/day during DJF and JJA respectively. The increase of total precipitation by roughly more than 2.0 mm/day during DJF, and any

increase during JJA were found to be statistically significant at the 95% level. For B2, the combined effects also resulted in a decrease of -0.35 mm/day during DJF, but were observed to increase slightly by about 0.07 mm/day during JJA. Conversely, the A2 climate scenario showed decreased precipitations of less than -1 mm/day during both seasons, which were statistically significant at the 95% level. Meanwhile, the effect of landcover forcing alone in the A2 scenario was observed to cause a small increase in precipitation during DJF (0.03 mm/day) and a small decrease during JJA (-0.29 mm/day). The change in total precipitation was statistically significant at the 95% confidence level in areas with precipitation changes of less than -2 mm/day during DJF and precipitation decreases of up to -8 mm/day during JJA. For B2, landcover forcing alone was observed to cause a small decrease in precipitation in both seasons (-0.06 mm/day). In areas with precipitation changes of less than -0.1 mm/day precipitation in both seasons were found to be statistically significant at the 95% level. In terms of magnitude, the combined effects of atmospheric and landcover forcings were more prevalent in precipitation changes in both climate scenarios.

The combined forcing effects were observed to decrease the total cloud relative to the baseline in both A2 and B2 climate scenarios. There were few discernible differences in total cloud between the effects of combined forcing and atmospheric forcing alone. The effect of landcover forcing alone was also observed to decrease total cloud in both seasons for the A2 climate scenario, while in B2 landcover forcing alone resulted in a small increase during DJF and a small decrease during JJA. The combined effect of atmospheric and landcover forcings resulted in the increase of solar radiation in both climate scenarios. The effect of landcover forcing alone was also observed to increase solar radiation in both climate scenarios, but at smaller magnitudes than that caused by

combined forcing. For the boundary layer height, the effect of the combined forcing was observed to decrease during DJF and increase during JJA in both climate scenarios. The effect of landcover forcing alone was also observed to decrease in both seasons in the A2 and slightly increase in both seasons in the B2 climate scenarios. In both forcing scenarios, changes in boundary layer height more negative than -30 m in the A2 and B2 climate scenarios were statistically significant at the 95% level.

7.1.3 What would be the effect of climate change due to atmospheric and landcover forcings on the regional biogenic emissions under the present-day and modified future landcover scenarios and the IPCC's (2001) emissions scenarios?

The present-day estimate of regional isoprene emissions based on Baseline-B2 and Baseline-A2 climate scenarios with present-day CO_2 concentration of 366 ppm were 25 TgC/yr and 28 TgC/yr. Sensitivity studies without the CO_2 activity factor in the model found that the isoprene emissions increased to 27 TgC/yr and 29 TgC/yr respectively. For the monoterpene emissions, the present-day estimates were 14 TgC/yr and 15 TgC/yr for both the B2 and A2 climate scenarios. Meanwhile ORVOC emissions were estimated at about 20 TgC/yr (B2) and 22 TgC/yr (A2) respectively. In the present-day landcover scenario without the CO_2 activity factor, the increase of future (2100) mean surface temperatures in the region by 2.4°C (B2) and 3.6°C (A2), resulted in a further increase to the regional isoprene emissions to 31 TgC/yr (B2) and 37 TgC/yr (A2), an increase of 13% and 27% respectively. The inclusion of future CO_2 concentrations of 560 ppm in the future scenarios, was found to inhibit the isoprene emissions to 21 TgC/yr (B2) and 25 TgC/yr (A2), a reduction of about 19% and 8% from the baseline estimate respectively. The inhibitory effect of elevated CO_2 on the isoprene emissions is much

larger than that of climate change alone. Meanwhile, the increase of temperature and PAR with double atmospheric CO_2 concentrations in the future scenarios decreased the regional emissions of both the monoterpene and ORVOC, accounting for 9% (B2) and 7% (A2) of monoterpene, and 11% (B2) and 6% (A2) of ORVOC.

Changes in future landcover alone were accounted for by a decrease in isoprene emissions of 6% (B2) and 5% (A2) with the inclusion of the CO_2 activity factor. However, without the CO_2 activity factor, the isoprene emissions were increased by 5% (B2) and 9% (A2) respectively. The inhibitory effect of elevated CO_2 on isoprene emissions was relatively larger in magnitude than from landcover forcing alone. In comparison with climate change forcing, the impact of landcover forcing alone on isoprene emissions is much smaller. Emissions of monoterpenes and ORVOC due to landcover forcing alone were 0.7 TgC/yr and 0.8 TgC/yr for B2, and 2 TgC/yr and 1 TgC/yr for A2 respectively.

The combined effect of climate change and landcover forcings without the CO_2 activity factor increased the regional isoprene emissions to 32 TgC/yr (B2) and 40 TgC/yr (A2), an increase of 18% and 38% respectively. With the inclusion of the CO_2 activity factor, the future emissions of isoprene were significantly inhibited by 60% (B2) and 66% (A2). The magnitude of the CO_2 inhibitory effect was more important than the combined effect of climate change and landcover change on isoprene emissions. The combined effect of climate change and landcover forcings was found to decrease monoterpenes and ORVOC emissions having a much greater impact than climate change forcing or landcover forcing alone. Biogenic emissions in the region were also found to be higher during July (southwest monsoon) and lower during January (northeast monsoon), corresponding to higher temperatures and PAR during July.

7.1.4 What would be the effect of climate changes and biogenic emissions changes on the regional tropospheric chemistry under the present-day and modified future landcover and the IPCC's (2001) emission scenarios?

In an urban area like Bangkok, the present-day (2008) ozone episode concentrations of surface O_3 were high of at about 160 ppbv (January) and 147.7 ppbv (July) in the BaselineA2 climate scenario; and 159 ppbv (January) and 148 ppbv (July) in the BaselineB2 climate scenario. In comparison with Danum, a remote site in Borneo, the present-day (2008) concentrations of surface O_3 were lower by about 4 ppbv (January) and 8 ppbv (July) in the BaselineA2 climate scenario; and 8 ppbv (January) and 8 ppbv (July) in the BaselineB2 climate scenario. In both locations, the combined impacts of climate changes and biogenic emissions was predicted to increase future (2100) surface O_3 concentrations under the present-day land cover scenario in both months in both A2 and B2 scenarios. Of the two factors considered in the model, biogenic emissions accounted for a larger effect than climate change on the predicted increase of surface O_3 concentrations in both months for A2 and B2 climate scenarios. In both locations, climate change alone was observed to have mixed effects on future surface O_3 concentrations, typically producing a decrease of O_3 concentrations, although this was completely offset by the effects of biogenic emissions. In Bangkok, under the future landcover scenario, the combined effects of climate change and biogenic emissions were observed to cause a slight increase in surface O_3 concentrations during January in the A2, and during July in the B2 scenarios; as well as a small decrease during July (A2) and January (B2) relative to the present-day landcover scenario. In Danum, the combined effects of climate changes and biogenic emissions resulted in a further increase in surface O_3 concentrations in both months for both climate scenarios. In terms of magnitude, biogenic emissions were

predicted to have larger impacts on the changes of future surface O_3 concentrations than climate changes in both climate scenarios with modified future landcover scenario.

In urban areas (Bangkok), the combined impacts of climate change and biogenic emissions under present-day and future landcover scenarios were predicted to decrease OH concentrations in both months in both A2 and B2 climate scenarios, and the predicted decreases were largely caused by biogenic emissions. Suppression of OH concentrations was largely due to the oxidation of isoprene by OH radicals. Decreasing OH concentration in these scenarios will increase the CH_4 life-time, providing an indirect positive feedback on climate. Comparatively, OH suppression was much greater under the future landcover scenario than in present-day landcover scenario, except during January in the B2 climate scenario. However, in the remote location (Danum), the combined impacts of climate change and biogenic emissions under present-day and future land cover scenarios were predicted to increase OH concentrations in both months for the A2 and B2 climate scenarios, and the increases were largely attributed by climate changes, although suppression of OH concentrations was also observed to be due to biogenic emissions through the oxidation of isoprene by OH radicals. In terms of magnitude, the increase in future OH concentrations were larger under future land cover than present-day land cover scenarios.

In the present-day landcover scenario, the combined impact of climate changes and biogenic emissions in Bangkok was observed to have a mixed effect on NO_x and $HONO_2$ concentrations in both A2 and B2 climate scenarios. Under the future landcover scenario, the combined impact was predicted to decrease NO_x concentrations and had a mixed effect on $HONO_2$ concentrations. Biogenic emissions were found to be more important to

these changes than climate changes in both climate scenarios under present-day and future landcover scenarios. In Danum, under present-day and future landcover scenarios, the combined impact of climate changes and biogenic emissions was observed to have a mixed effect on NO_x concentrations but caused a small increase in $HONO_2$ concentrations in both A2 and B2 climate scenarios. The balancing effects between biogenic emissions and climate changes on the future concentrations of NO_x and $HONO_2$ have resulted in small changes to the future concentrations in both climate scenarios.

In Bangkok, the combined impacts of climate changes and biogenic emissions under the present-day and future landcover scenarios were predicted to increase PAN concentrations in both months in the A2 and B2 climate scenarios. However, in Danum, the combined impact of climate changes and biogenic emissions under the present-day landcover scenario were predicted to decrease the PAN concentrations during January and increase during July in both climate scenarios. On the other hand, under the future landcover scenario, the combined impact was predicted to decrease PAN in both months in the A2 and B2 scenarios. In terms of magnitude, biogenic emissions were more important than climate change to the changes in PAN concentrations.

The combined impacts of climate change and biogenic emissions under present-day and future landcover scenarios in Bangkok were predicted to increase HCHO and H_2O_2 concentrations in both climate scenarios, with a large contribution from biogenic emissions. However, in Danum, the opposite was found, where the combined impacts of climate changes and biogenic emissions under present-day landcover and future landcover scenarios were observed to decrease HCHO and H_2O_2 concentrations in both climate scenarios. In both locations, biogenic emissions played a more important role in future

HCHO and H_2O_2 concentrations than climate changes in both climate and landcover scenarios.

In other urban location such as Jakarta, the present-day ozone-episode (2008) concentrations of surface O_3 were found to be higher than in Bangkok (i.e 270 ppbv (January) and 216 ppbv (July) in the A2 climate scenario; and 159 ppbv (January) and 148 ppbv (July) in the B2 climate scenario). Kuala Lumpur, another urban location, was observed to have relatively lower ozone-episode concentrations than Bangkok and Jakarta (i.e 144 ppbv (January) and 142 ppbv (July) in the BaselineA2 climate scenario; and 144 ppbv (January) and 138 ppbv (July) in the BaselineB2 climate scenario). In Jakarta and Kuala Lumpur, biogenic emissions were found to have negligible effects on future O_3 concentrations under the present-day and future landcover scenarios in both months for the A2 and B2 climate scenarios. Climate change impacts on future surface O_3 concentrations under the present-day and future landcover scenarios in both months for A2 and B2 climate scenarios were relatively small. In both cities, high surface O_3 concentrations were largely due to anthropogenic emissions. Future changes on other trace gases such as OH, NO_x, PAN, $HONO_2$, HCHO, and H_2O_2 concentrations, in present-day and future landcover scenarios in both A2 and B2 climate scenarios were largely attributable to anthropogenic emissions, as the climate changes alone have a very small impact, while the biogenic emissions impact was found to be negligible.

7.2 Summary of Contributions

The first contribution of the thesis is the generation of plausible climate change scenarios under various emission scenarios, using the first application of the latest version of a high-resolution regional climate model applied to SEA. Very few studies have been carried out for SEA, although there is a demand for fine scale (spatially and temporally) simulation within research communities as well as for policy makers. Fine-scale climate forecast is of societal benefit to stakeholders, including the scientific community and policy makers. Based on atmospheric forcing alone, this study has shown that SEA would experience a warming of temperatures in both A2 and B2 climate scenarios by the end of the century, the magnitude of which fall well in the range of global surface temperature changes. The results presented in this thesis, as well as the large number of additional parameters from the regional model output that are not presented, but which are also available, can be used in impact assessment models. The study also allows us to investigate the performance of the regional climate model in featuring a mix of continental and maritime environments.

Secondly, this study has also explored the role of landcover forcing on the regional climate change in SEA, using the available features in PRECIS-RCM that allow the prescription of specific landcover types for each grid point. The major finding in this investigation was that the combined effect of atmospheric and landcover forcing was much larger than atmospheric forcing alone. In most studies on climate change, only the atmospheric forcing was considered in the model, and landcover was assumed as fixed for the present-day and future simulations. Meanwhile, the investigation of the impacts of landcover forcing alone has lead to an observed a cooling effect, mostly over the sea/ocean. The findings in this study have also confirmed the variation of climate change response due to changes in landcover in various regions in the tropics. This study did not provide a detailed explanation of this observation, but its possible link with the Asian monsoon circulations warrant further investigation, as also mentioned in the following Section 7.3.

The third contribution of the thesis lies in the first ever attempt to estimate the regional biogenic emissions over SEA using the BVOCEM model, newly developed by Lancaster University and Sheffield University. The investigation has explored how regional climate changes and landcover changes in SEA, with- and without-CO_2 activity factors, affect the biogenic emissions. Increasing future mean surface temperatures (2100) over SEA by 2.5°C (B2) and 3.5°C (A2) and decreasing PAR in present-day landcover without the CO_2 activity factor was observed to increase isoprene emissions to 31 TgC/yr (B2) and 37 TgC/yr (A2), an increase of 13% and 27%. The inclusion of future CO_2 concentrations of 560 ppm in the future scenarios inhibited isoprene emissions to 21 TgC/yr (B2) and 25 TgC/yr (A2), a reduction of about 19% and 8% respectively. It was also found that the inhibitory effect of elevated CO_2 is much larger than the effect of climate change alone. The combined effect of climate changes and landcover forcings without the CO_2 activity factor increased the regional isoprene emissions further to 32 TgC/yr (B2) and 40 TgC/yr (A2), an increase of 18% and 38% respectively. With the inclusion of the CO_2 activity factor, the future emissions of isoprene were significantly inhibited by 60% (B2) and 66%(A2). The magnitude of the CO_2 inhibitory effect is far more important than the combined effect of climate change and lanbdcover forcings on isoprene emissions.

The final contribution of this study deals with the use of simulation results from the investigation of climate changes, landcover changes and biogenic emissions changes to investigate how climate change-landcover-biogenic emissions-tropospheric chemistry system interactions affect the tropsopheric chemistry at selected locations in urban and remote areas in SEA. Investigation in urban (Bangkok) and rural (Danum) locations have found that the combined impact of climate changes and biogenic emissions was observed to increase the future (2100) ozone-episode surface O_3 concentrations in the present-day land cover scenario during January and July in the A2 and B2 climate scenarios. Of the two factors considered in the model, biogenic emissions accounted for a larger effect on the increase of surface O_3 concentrations in both months for A2 and B2 climate scenarios.

In both locations, climate change alone was observed to have mixed effects on future surface O_3 concentrations, typically producing a decrease of O_3 concentrations, although it was completely offset by the effects of biogenic emissions. In both locations, the combined effects of climate changes and biogenic emissions in the future landcover scenario were found to have a larger impact on the increase of surface O_3 than in the present-day landcover scenario except during July in Bangkok in both climate scenarios. In terms of magnitude, biogenic emissions were observed to have a larger impact on changes in future surface O_3 concentrations than that of climate changes in both climate scenarios under the modified future landcover scenario. For OH radicals, the combined impacts of climate change and biogenic emissions under present-day and future landcover scenarios in Bangkok were found to decrease OH concentrations in both months in both A2 and B2 climate scenarios. The decreases were largely attributed by biogenic emissions. Suppression of OH concentrations was largely due to the oxidation of isoprene by OH radical. However, the opposite observation was found in Danum, where the combined impact of climate change and biogenic emissions under present-day and future land cover scenarios was observed to increase OH concentrations in both months in the A2 and B2 climate scenarios. The increases were largely attributed by climate change, although suppression of OH concentrations was observed to be largely due biogenic emissions through the oxidation of isoprene by OH radicals. The modelled decreases in OH will increase the CH_4 life time in these scenarios, providing an indirect positive feedback on climate.

7.3 Future Work

In reflecting on the research questions addressed in this thesis, a number of other related issues surfaced, which warrant further investigation and evaluation. These include:

- A high resolution regional climate model has been used to investigate the regional climate change over continental and islands in SEA, as past studies have also shown that this model has the capability to capture high climate resolution over islands. However, its also must be recognized that RCMs have deficiencies that need to be ameliorated. These include a wide range of issues that might not necessary be directly related to the findings in this study that warrant further investigation such as the sensitivity of RCM-simulated result, the resolution between nesting data and RCM, model errors or deficiencies of nesting data, and improvement of the nesting technique. Related to the scope of investigation in this thesis, it is further suggested that an assessment of the performance of the PRECIS-RCM is carried out using climate data on much finer spatial and temporal scales than is traditionally used for validating global or regional models. This includes running the model over the region at 0.22° x 0.22° resolution and to include the hourly and daily simulations. Assessing the performance of different RCMs over the same domain and comparing the results with the simulation of current climates and in their use as a dynamical downscaling tool to provide high-resolution climate change information is also suggested.

- The investigation of regional climate changes in SEA can be further expanded to include the investigation of the occurrence of extreme weather and climatic events, as these climate manifestations are of paramount importance in assessing the impact of climate change such as flooding, forest fires and localized or regional air quality deterioration episodes. Analyses of the extremes, therefore, require finer spatial and temporal resolutions.

- Landcover changes are evidently important variables in the assessment of future climate change. Ideally, landcover change should be included in transient simulations of the future climate scenarios in order to strive for realistic climate projections. In any case, additional experiments using alternative regional climate models should be used to repeat this experiment in order to ascertain the extent to which the results are dependent on the model. It can also provide insight into the importance of landcover change because these models should be capable of capturing the scale of landcover changes. Future research to represent finer spatial scales of the updated landcover map of SEA will further improve the understanding about the possible effects of landcover changes on future climates in the region.

- The analysis of regional climate change signals in response to future landcover changes in this study, and other related studies in relation to the tropics, confirms a wide variation in seasonal warming or cooling over SEA across scenarios. Meanwhile, the landcover change effects on the regional precipitation are not consistent. Findings on the cooling effect of landcover changes in the region, mainly over the sea/ocean (as observed in various other studies in the past) and a possible link to Asian monsoon circulations warrant further investigation. Further investigations of the role of landcover changes on regional climate changes should be conducted, and expanded to include other climatic and energy budget variables, as well as the hydrological variables such as specific humidity, moisture convergence, latent heat flux, sensible heat flux, albedo, total evaporation, evapotranspiration, canopy evaporation, surface runoff and soil moisture.

- The investigation of biogenic emissions over SEA can be further improved through the incorporation of improve biogenic emissions factors from various vegetation

functional types. Based on the biogenic emissions flux findings over oil palm plantation in Borneo during the OP3 Measurement Campaign in 2008, it is suggested that the existing emission factor of isoprene used in MEGAN as well as in BVOCEM models needs to be revised. Also, the improved and updated vegetation cover map over SEA is also crucial for the investigation of regional biogenic emissions. Theree is a critical need to confirm the CO_2 inhibition effect.

- To improve the understanding of the impact of climate changes and biogenic emissions on the future tropospheric chemistry, it is also suggested that future anthropogenic emissions are incorporated in the chemistry model. This will further explain the importance of anthropogenic emissions contribution to the tropospheric chemistry, and will also explore the combined impact of anthropogenic emissions, climate changes and biogenic emissions forcings on tropospheric chemistry, particularly on surface O_3 concentrations.

REFERENCES

Ackerman, A. S., O. B. Toon, D. E. Stevens, and J. A. Coakley Jr., 2003. Enhancement of cloud cover and suppression of nocturnal drizzle in stratocumulus polluted by haze. *Geophys. Res. Lett.*, **30**:1381, doi:10.1029/2002GL016634.

Adams, P., J. Seinfeld and D. Koch, 1999. Global concentrations of tropospheric sulfate, nitrate, and ammonium aerosol simulated in a general circulation model, *J. Geophys. Res.*, 104(**D11**):13791-13823.

Adegoke, J. O., Pielke, R. A. Sr., and Carleton, A. M., 2007: Observational and modeling studies of the impacts of agriculture-related land use change on climate in the central U.S.. *Agricultural and Forest Meteorology*, **132**:203-215.

Akiyama, H., and H. Tsuruta, 2003. Nitrous Oxide, Nitric Oxide, and Nitrogen Dioxide Fluxes from Soils after Manure and Urea Application. *Journal of Environmental Quality*, **32**:423-431.

Alcamo, J., E. Kreileman, M. Krol, R. Leemans, J.C. Bollen, J. van Minnen, M. Schacffer, A.M.C. Toet, and H.J.M. De Vries, 1998. Global modelling of environmental change: an overview of IMAGE 2. In *Global Change Scenarios of the 21st century. Results from the IMAGE 2.1 model* by J. Alcamo, R. leemans, and E. Kreileman (Eds). Elsevier Science, London, pp 3-94.

Alessio, G.A., M. De Lillis, M. Fanelli, P. Pinelli and F. Loreto, 2004. Direct and indirect impacts of fire on isoprenoid emissions from Mediterranean vegetation. *Functional Ecology*, **18**:357-364.

Allan, B.J., N. Carslaw, H. Coe, R.A. Burgess, and J.M.C. Plane, 1999. *Atmos. Chem.*, **33**:129-154.

Anderson, C. J., R. W. Arritt, E. S. Takle, Z. Pan, W. J. Gutowski, F. O. Otieno, R. da Silva, D. Caya, J. H. Christensen, D. Lüthi, M. Gaertner, C. Gallardo, F. Giorgi, S.-Y. Hong, C. Jones, H.-M. H. Juang, J.J. Katzfey, W. M. Lapenta, R. Laprise, J. W. Larson, G. E. Liston, J. L. McGregor, R. A. Pielke Sr., J. O. Roads, and J. A. Taylor, 2003. Hydrological processes in regional climate model simulations of the Centreal United States flood of June-July 1993. *J. Hyrometeor.*, **4**:584-598.

Andrae, M. O., 1995. Climatic effects of changing atmospheric aerosol levels. In *World Survey of Climatology, Vol. 16: Future Climates of the World*, by A. Henderson-Sellers (Ed), Elsevier, Amsterdam, pp 341-392.

Andrae, M.O. and P.J. Crutzen, 1997. Atmospheric aerosols: Biogeochemcial sources and role in atmospheric chemistry. *Science*, **276**:1052-1058

Andreae, M.O., 1993. The influence of tropical biomass burning on climate and the atmospheric environment. In *Proceedings of the 10th International Symposium on Environmental Biogeochemistry* by R.S. Oremland (Ed), 19-24 August 1991, San Francisco, Cal., 113-150.

Andreae, M.O., E.V. Browell, M. Garstang, G.L. Gregory, R.C. Harriss, G.F. Hill, D.J. Jacob, M.C. Pereira, G.W. Sachse, A.W. Setzer, P.L. Silva Dias, R.W. Talbot, A.L. Torres, and S.C. Wofsey, 1988. Biomass burning emissions and associated haze layers over amazonia. *J. Geophys. Res.*, **93**:1509-1527.

Angstrom, A.,1964. The parameters of atmospheric turbidity. *Tellus*, 16:64-65.

Armentano, T.V. and Menges, E.S. 1986. Patterns of change in the carbon balance of organic soil-wetlands of the temperate zone. *J. Ecol.* **74**: 755–774.

Arnell, N.W., Hudson, D.A., and Jones, R.G. 2003. Climate change scenarios from a regional climate model: Estimating change in runoff in southern Africa. *J. Geophys. Res.*, **108**: D164519, doi:10.1029/2002JD002782.

Arneth, A., P. A. Miller, M. Scholze, T. Hickler, G. Schurgers, B. Smith and I.C. Prentice, 2007b: CO_2 inhibition of global terrestrial isoprene emissions: Potential implications for atmospheric chemistry. *Geophys. Res. Lett.*, **34**: L18813, doi:10.1029/2007GL030615.

Arneth, A., U. Niinemets, S. Pressley, J. Bäck, P. Hari, T. Karl, S. Noe, I. Prentice, I. C., D. Serca, T. Hickler, A. Wolf and B. Smith, 2007a. Process-based estimates of terrestrial ecosystem isoprene emissions: Incorporating the effects of a direct isoprene CO_2 - isoprene interaction. *Atmos. Chem. Phys.*, **7**:31–53.

Artaxo, P., E.T. Fernandes, J. V. Martins, M.A. Yamsoe, P.V. Hobbs, W. Maenhaut, K.M. Longo and A. Castanho, 1998. Large-scale aerosol source apportionment in Amazonia. *J. Geophys. Res.*, **103**:31837-31847.

Artaxo, P., F. Gerab, M.A. Yamsoe, and J.V. Martin, 1994. Fine mode aerosol composition at three long-term atmospheric monitoring sites in the Amazon basin. *J. Geophys. Res.*, **99**:22857-22868.

Asner, G.P., A.J. Elmore, L.P. Olander, R.E. Martin, and A.T. Harris, 2004. Grazing stystems, ecosystem responses, and global change. Ann. Rev. Environ. Resources, **29**:261-299.

Atherton, C.S., 1995. *Biomass Burning Sources of Nitrogen Oxides, Carbon MoNO$_x$ide, and Non-Methane Hydrocarbons.* UCRL-ID-122583, Lawrence Livermore National Laboratory, Livermore, CA, USA, 15 pp.

Atkinson, R, Baulch D.L., Cox R.A., Hampson R.F., Kerr J.A., and Troe J., 1992. Evaluated kinetic and photochemical data for atmospheric chemistry, Supplement IV — IUPAC Subcommittee on Gas Kinetic Data Evaluation for Atmospheric Chemistry. *J. Phys. Chem. Ref. Data*, **21**:1125–1568.

Atkinson, R., 2000. Atmospheric chemistry of VOCs and NO_x. *Atmos. Environ.*, **34**:2063-2101.

Atkinson, R., D.L. Baulch, R.A. Cox, R.F. Jr. Hampson, J.A. Kerr, M.J. Rossi, and J. Troe, 1997. Evaluated kinetic and photochemical data for atmospheric chemistry: Supplement VI. *Journal of Physical and Chemical Reference Data.* **26**:1329-1499.

Atkinson, R., S.M., Aschmann, J. R. Arey, B. Shorees, 1992. Formation of OH radicals in the gas phase reactions of O3 with a series of terpenes. *J. Geophys. Res.*, **97**:6065-6073

Bakwin P. S., S. C. Wofsy, S. M. Fan, M. Keller, S. Trumbore, J. M. da Costa, 1990. Emission of nitric oxide (NO) from tropical forest soils and exchange of NO between the forest canopy and the atmospheric boundary layers. *J. Geophys. Res.*, **95**:16755-16764.

Baron, J. S., M.D. Hartman, T.G.F. Kittel, L.E. Band, D.S. Ojima, R.B. Lammers, 1998. Effects of land cover, water redistribution, and temperature on ecosytem processes in the South Platte Basin. *Ecol. Appl.*, **8**:1037-1051.

Barrette, N., and R. Laprise, 2002. Numerical modeling: A complementary tool for studying CO_2 emissions from hydroelectric reservoirs. *Global Biogeochem. Cycles*, 16(4), 1128, doi:10.1029/2002GB001976

Barrie, L.A., J.W. Bottenheim, R.C. Schnell, P.J. Crutzen, and R.A. Rasmussen, 1988. Ozone destruction and photochemical reactions at polar sunrise in the lower Arctic atmosphere. *Nature*, **334**:138-140.

Becker, K.H., J. C. Lorzer, R. Kurtenbach, P. Wiesen, T. E. Jensen, T.J. Wallington, 2000. Contribution of vehicle exhaust to the glbal N_2O budget. *Chemosphere-Global Change Science*, **2**:387-395

Bell, G. and M. Halpert, 1998. Climate assessment for 1997. *Bull. Amer. Meteor. Soc.*, 79(**5**):S1-S50.

Beltran, A. B., 2005. *Using a coupled atmospheric-biospheric modelling system (GERRAMS) to model the effects of land-use/land-cover changes on the near-surface atmosphere.* Phd Thesis, Department of Atmospheric Science, Colorado State University, 186 pp. unpublished.

Benkovitz, C.M., J. Dignon, J. Pacyna, T. Scholtz, L. Tarrasson, E. Voldner, and T.E. Graedel, 1996: Global inventories of anthropogenic emissions of SO_2 and NO_x. *J. Geophys. Res.*, **101**: 29239-29254.

Beraki, A.F., 2005. *Climate change scenario simulations over Eritrea by using a fine resolution limited area climate model: Temperature and moisture sensitivity.* Master's Dissertation, University of Pretoria, South Africa

Bergamaschi, P., R. Hein, M. Heimann, and P.J. Crutzen, 2000. Inverse modeling of the global CO cycle 1. Inversion of CO mixing ratios. *J. Geophys. Res.*, **105**:1909-1927.

Berntsen, T., Fuglestvedt, J.S., Joshi, M., Shine, K.P., Ponater, M., Sausen R., and Hauglustaine, D.A., 2002. Indirect forcing from emissions of NO_x and CO: Is the location of emission important? *Third International Symposium on non-CO_2 greenhouse gases (NCGG-3)*, Millpress, Rotterdam, pp. 363-369

Betts, R. A., 2000. Offset of the potential carbon isnk from boreal forestation by decreases in surface albedo. *Nature*, **408**:187-190

Betts, R.A., P.M. Cox, S.E. Lee, and I.F. Woodward I. F., 1997. Contrasting physiological and structural vegetation feedbacks in climate change simulations. *Nature*, **387**:796-799

Bey, I., D. J. Jacob, R. M. Yantosca, J. A. Logan, B. Field, A. M. Fiore, Q. Li, H. Liu, L. J. Mickley, and M. Schultz, 2001. Global modeling of tropospheric chemistry with assimilated meteorology: Model description and evaluation. *J. Geophys. Res.*, **106**: 23,073-23,096.

Bhaskaran, B., J.M. Murphy J.M., and R.G. Jones R.G., 1998. Intraseasonal oscillation in the Indian summer monsoon simulated by global and nested regional climate models., *Mon. Wea. Rev.*, **126**:3124-31324

Bonan, G.B., D. Pollard, and S.L. Thompson, 1992. Effects of boreal forest vegetation on global climate. *Nature*,**359**:716-718

Bonan, G.B., K.W. Oleson, M. Vertenstein, S. Levis, X. Zeng, Y. Dai, R.E. Dickinson, and Z.-L. Yang, 2002. The land surface climatology of the Community Land Model Coupled to the NCAR Community Climate Model. *American Meteorological Society*, **15**:3123-3149

Bond, D.W., S. Steiger, R. Zhang, X. Tie, and R.E. Orville, 2002. The importance of NO_x production by lightning in the tropics. *Atmos. Environ.* **36**:1509-1519.

Bonn, B., R. von Kuhlmann, and G.L. Mark, 2004. High contribution of biogenic hydroperoxides to secondary organic aerosol formation. *Geophys. Res. Lett.*, **31**:L10108, doi:10.1029/2003GL019172.

Bouchet, V. S., R. Laprise, E. Torlaschi and J. C. McConnell, 1999: Studying ozone climatology with a regional climate model. Part 1: Model description and evaluation. *J. Geophys. Res.*, **104**:30351-30372.

Bowman, F.M., C. Pilinis, and J.H. Seinfeld, 1995. Ozone and aerosol productivity of reactive organics. *Atmos. Environ.*, **29**, 579-589.

Braslau, N., and Dave J.V., E., 1973. Effect of aerosols on the transfer of solar energy through realistic model atmospheres. 1. Non-absorbing aerosols, *J. Appl. Meteorol.*, 12:601-615.

Brasseur G.P., B. Khattatov, and S. Walters, 1999. Modeling. In *Atmospheric Chemistry and Global Change* by G. Brasseur, J. Orlando, and G. Tyndall (Eds). Oxford University Press, Oxford, UK.

Brasseur, G. P., J. T. Kiehl, J.-F. Muller, T. Schneider, C. Granier, X. Tie, and D. Hauglustaine, 1998. Past and future changes in global tropospheric ozone: Impact on radiative forcing, *Geophys. Res. Lett.* **25**:3807-3810.

Brenguier, J. L., H. Pawlowska, L. Schuller, R. Preusker, J. Fischer, and Y. fouquart, 2000. Radiative properties of boundary layer clouds: Droplet effective radius versus number concentrations. *J. Atmos. Sci.*, 57(**6**):803-821.

Brinkop, S., and E. Roeckner, 1995. Sensitivity of a general circulation model to parameterizations of cloud-turbulence interactions in the atmospheric boundary layer. *Tellus*, **47A**:197-220.

Brookfield, Harold, and Yvonne Byron. 1990. Deforestation and timber extraction in Borneo and the Malay Peninsula: The record since 1965. *Global Environmental Change: Human and Policy Dimensions 1*, No. **1**: 42-56.

Brown, P. D., Carver G.D., and Wild O., 1993. *Chemistry model coding using DELOAD and the ACMSU reaction database.* UGAMP Internal Report No.31, Centre for Atmospheric Science, Cambridge.

Brown, P.N., Byrne, G.D., Hindmarsh, A.C., 1989. VODE: A variable coefficient ODE solver. *SIAM J. Sci. Stat. Comput* **10**:1038-1051

Brühl, C. H., and P.J. Crutzen, 1999. Reductions in the anthropogenic emissions of CO and their effect on CH_4,. *Chemosphere - Global Change Science* 1(**1-3**): 249-254.

Buckley, P.T., 2001. Isoprene emissions from a Florida scrub oak species grown in ambient and elevated carbon dioxide. *Atmos. Enviro.*, **35**: 631–634.

Byun, D.W. and J.K.S. Ching JKS, 1999. Science Algorithms of the EPA Models-3 Community Multiscale Air Quality (CMAQ) Modeling System. EPA-600/R-99/030. Research Triangle Park, NC:U.S. EPA Office of Research and Development, Washington

Cachier, H., 1998. Carbonaceous combustion aerosols. In Atmospheric Particles by R.M. Harrison and R. Van Grieken (Eds). JohnWiley & Sonss, Chichester, pp 295-348

Cachier, H., C. Liousse, P. Buat-Menard and G. Gaudichet, 1995. Particulate content of savanna fire emissions. *J. Atmos. Chem.*, **22**:123-148.

Cao, M.K., K. Gregson, and S. Marshall, 1998. Global methane emission from wetlands and its sensitivity to climate change. *Atmos Environ.*, **32**:3293-3299

Carslaw N., B.J. Allan, L.J. Carpenter, R.A. Burgess, K.C. Clemitshaw, S.A. Penkett and J.M.C. Plane, 1997. The simultaneous observation of nitrate and peroxy radicals in the marine boundary layer at night. *J. Geophys. Res.*, **102**:18917-18933.

Castro, L.M., C.A. Pio, Roy M. Harrison, and D.J.T. Smith, 1999. Carbonaceous aerosol in urban and rural European atmospheres: estimation of secondary organic carbon concentrations. *Atmos. Environ.* **33**:2771-2781.

Caya, D., and R. Laprise, 1999: A semi-implicit semi-Lagrangian regional climate model: The Canadian RCM. *Mon. Wea. Rev.*, 127 (**3**):341-362.

Chalita, S., Hauglustaine, D.A., Le Treut, H., Muller, J.F., 1996. Radiative forcing due to increased tropospheric ozone concentrations, *Atmos. Environ.* 30(**10/11**):1641-1646

Challinor, A.J., Wheeler T.R., Craufurd, P.Q., Ferro C.A.T., and Stephenson D.B., 2006. Adaptation of crops to climate change through genotypic responses to mean and extreme temperature. *Agriculture, Ecosystem and Environment*, 119(**1-2**):190-204

Chandra S., J. R. Ziemke, P.K. Bhartia, and R. V. Martin, 2002. Tropical tropospheric ozone: Implications for dynamic and biomass burning. *J. Geophys. Res.*, 107(**D14**), doi:10.1029/2001JD000447

Chapman, S.J., and M. Thurlow, 1996. The influence of climate on CO_2 and CH_4 emissions from organic soils. *Agricultural and Forest Meteorology*, 79:205-217

Charlson, R. J., S. E. Schwartz, J. M. Hales, R. D. Cess, J. A. Coakley Jr., J. E. Hansen, and D. J. Hoffmann, 1992. Climate forcing by anthropogenic aerosols, *Science*, **255**, 423-430.

Charlson, R.J., J. Langer, and H. Rodhe. 1990. Sulfate aerosol and climate. *Nature*, **348**:22

Charlson, R.J., J.E. Lovelock, M.O. Andreae, S.G. Warren, 1987. Oceanic phytoplankton, atmospheric sulphur, cloud albedo and climate. *Nature*, **326**:655–661.

Charnock, H., 1955. Wind stress on a water surface. *Q. J. R. Meteorol. Soc.* **81**:639-640.

Chase, T.N., R.A. Pielke, T.G.F. Kittel, R. Nemani, S.W. Running, 2000. Simulated impacts of historical land cover changes on global climate in northern winter. *Clim. Dyn.*, **16**:93-105.

Christensen, O.B., M.A. Gaertner, J.A. Prego, and J. Polcher, 2001. Internal variability of a regional climate model. *Clim. Dyn.*, **17**:875-887.

Christensen, T.R., and P. Cox, 1995. Response of methane emission from artci tundra to climatic change-Results from a model simulation. *Tellus Series B-Chemical and Physical Meteorology*, **47**:301-309

Christopher, S. A., J. Chou, R. M. Welch, D. V. Kliche, and V. S. Connors, 1998. Satellite investigations of fire, smoke, and carbon monoxide during April 1994 MAPS mission: Case studies over tropical Asia, *J. Geophys. Res.*, 103(**D15**):19327-19336.

Chung, S.H., and J.H. Seinfeld, 2002. Global distribution and climate forcing of carbonaceous aerosols. *J. Geophys. Res.*, 107(**D19**):4407, doi:1029/2001JD001397.

Claussen, M., U. Lohmann, E. Roeckner, and U. Schulzweida, 1994. *A global data set of land-surface parameters*. Max Planck Institut für Meteorologie, Report No. **135**, Hamburg, Germany, 23 pp.

Climate Impact Group, 1992. *Climate Change Scenarios for South and Southeast Asia.* Commonwealth Scientific and Industrial Research Organisation (CSIRO), Division of Atmospheric Research, Aspendale, Mordialloc, Australia, 41 pp

Cofer, W. R. III, J. S. Levine, E. L. Winstead, and B. J. Stocks, 1991. Trace gas and particulate emissions from biomass burning in temperate ecosystems. In *Global Biomass Burning: Atmospheric, Climatic, and Biospheric Implication* by J. S Levine (Ed), MIT Press, Cambridge, Mass., pp 203-208.

Collins, W. J., D. S. Stevenson, C. E. Johnson, and R. G. Derwent, 1997. Tropospheric ozone in a global-scale 3-D Lagrangian model and its response to NO*x* emission controls. *J. Atmos. Chem.*, *26*:223-274.

Collins, W. J., D. S. Stevenson, C. E. Johnson, and R. G. Derwent, 1999. Role of convection in determining the budget of odd hydrogen in the upper troposphere, J. Geophys. Res., **104**:26927-26941.

Collins, W.J., D.S. Stevenson, C.E. Johnson, R.G. Derwent, 2000. The European regional ozone distribution and its links with the global scale for the years 1992 and 2015. *Atmos. Environ.*, **34**:255-267

Connors, V. S., M. Flood, T. Jones, B. Gormsen, S. Nolf, and H. G. Reichle, Jr., 1996. Global distribution of biomass burning and carbon monoxide in the middle troposphere during early April and October 1994. In *Biomass Burning and Global Change* by J. Levine (Ed), pp. 99-106, MIT Press, Cambridge, Mass., 1996.

Cooke, W. F. and J.J. N. Wilson, 1996. A global black carbon aerosol model. *J. Geophys. Res.*, **101**:19395-19409.

Cooke, W. F., C. Liousse, H. Cachier, and J. Feichter, 1999. Construction of a 1° x 1° fossil fuel emission data set for carbonaceous aerosol and implementation and radiative impact in the ECHAM4 model, *J. Geophys. Res.*, **104**:22,137–22,162.

Cox, P.M., Betts, R.A., Bunton, C.B., Essery, R.L.H., Rowntree, P.R., and Smith J., 1999. The impact of new land surface physics on the GCM simulation of climate and climate sensitivity. *Clim. Dyn.*, **15**:183-203

Crutzen P. J., 1995. Overview of tropospheric chemistry: Developments during the past quarter century and a look ahead. *Faraday Discuss.*, **100**:1-21.

Crutzen, P. J., M. G. Lawrence and U. Poschl, 1999. On the background photochemistry of tropospheric ozone, *Tellus*, 51(**A-B**):123-146.

Crutzen, P.J., 1987. Role of the tropics in atmospheric chemistry. In: *The Geophysiology of Amazonia* , R.E. Dickinson (Ed). John Wiley, New York, pp 107-130

Crutzen, P.J., A.C. Delany, J. Greenburg, P. Haagenson, L. Heidt, R. Lueb, W. Pollack, W. Seiler, A. Wartburg, and P. Zimmerman, 1985. Observations of air composition in Brazil between the equator and 20S during the dry season, *J. Atmos. Chem.*, **2**:233-256.

Crutzen, P.J., and M. O. Andreae, 1990. Biomass burining in the tropics: Impact on atmospheric chemistry and biogeochemical cycles, *Science* **250**:1669-1678.

Cubasch, U., Meehl G.A., Boer G.J., Stouffer R. J., Dix M., Noda A. Senior C.A., Raper S., Yap K.S., Abe-Ouchi A., Brinkop S., Claussen M., Collins M., Evans J., Fischer-Bruns I., Flato G., Fyfe J.C., Ganopolski A., Gregory J.M., Hu –Z. Z., Joos F., Knutson T., Knutti R., Landsea C., Mearns L., Milly C., Mitchell J.F.B., Nozawa T., Paeth H., Räisänen J., Sausen R., Smith S., Stocker T., Timmermann A., Ulbrich U., Weaver A., Wegner J., Whetton P., Wigley T., Winton M., and Zwiers F., 2001. Projections of future climate change, Chapter 9. In *Climate Change 2001: The Scientific Basis* by J.T. Houghton et al. (eds.), Cambridge University Press, pp 525-582

Cullen, M.J.P., 1993. The unified forecast/climate model. *Meteorol. Mag.*, **122**:81-94.

Dale, V. H., 1997. The relationship between land-use change and climate change. *Ecol. Appl.*, 7(**3**):753-769.

Davies, W.E., G. Vaughan, and F.M. O'Connor, 1998. Observation of near-zero ozone concentrations in the upper troposphere at mid-latitudes. *Geophys. Res. Lett.*, ***25***:1173-1176

DeFries, R. S., L. Bounoua, and G.J. Collatz, 2002. Human modification of the alndscape and surface climate in the enxt fifty years. *Global Change Biology*, **8**:438-458

Demographia, 2006. Demographia World Urban Areas (World Agglomerations). Population and Density Estimate, Belleville, Illinois USA, http://www.demographia.com

DeMore, W. B., Sander S.P., Golden D.M., Hampson R.F., Kurylo, M.J., Howard C.J., Ravishankara A.R., Kolb C.E., and Molina M.J., 1997. *Chemical kinetics and photochemical data for use in stratospheric modeling.* JPL Publication 97-4, Jet Propulsion Lab., Pasadena.

Dentener, F. J. and Crutzen P.J., 1993. Reaction of N_2O_5 on Tropospheric Aerosols: Impact on the Global Distributions of NO_x, O_3, and OH. *J. Geophys. Res.*, **98**:7149-7163.

Dentener, F. J., 1993. *Heterogeneous chemistry in the troposphere.* Ph.D. Thesis, Universiteit Utrecht, Utrecht, Netherlands.

Dentener, F. J., G.R. Carmichael, Y. Zhang, J. Lelieveld, and P.J. Crutzen, 1996. Role of mineral aerosol as a reactive surface in the global troposphere. *J. Geophys. Res.*, **101**:22869–22889.

Derwent, R. G., and Jenkin, M.E., 1991. Hydrocarbons and the long-range transport of ozone and PAN across Europe, *Atmos. Environ.*, **25A**:1661–1678.

Derwent, R. G., and Ø. Hov, 1982. The potential for secondary pollutant formation in the atmospheric boundary layer in a high pressure situation over England. *Atmos. Environ.*, **16**:655–665

Derwent, R.G., P.G. Simmonds, S. O'Doherty, D.S. Stevenson, W.J. Collins, M.G. Sanderson, C.E. Johnson, F. Dentener, J. Cofala, R. Mechlerf M. Amann, 2006. External influences on Europe's air quality: Baseline methane, carbon monoxide and ozone from 1990 to 2030 at Mace Head, Ireland. *Atmos. Environ.*, **40**:844-855

Derwent, R.G., 1995. Volatile organic compounds in atmosphere. *Issues in Environ. Sci. and Technol.* **4**:1-15

Dickerson, R. R., Rhoads K.P., Carsey T.P., Oltmans S.J., Burrows J.P., and Crutzen P.J., 1999. Ozone in the remote marine boundary layer: A possible role for halogens. *J. Geophys. Res.*, **104**:21385-21395.

Dickerson, R. R., S. Kondragunta, G. Stenchikov, K.L. Civerolo, B.G. Doddridge, and B.N. Holben, 1997. The impact of aerosols on solar ultraviolet radiation and photochemical smog. *Science*, **278**:827-830

Dickerson, R.R., K.P. Rhoads, T.P. Carsey, S.J. Oltmans, J.P. Burrows and P.J, Crutzen, 1999. Ozone in the remote marine boundary layer: A possible role for halogens. *J. Geophys. Res.*, **104**:21385-21395.

Dickinson, R. E., R. M. Errico, F. Giorgi, and G. T. Bates, 1989. A regional climate model for the western U.S., *Climatic Change*, **15**:383-422.

Diffenbaugh, N.S., 2005. Influence of modern land cover on the climate of the United States. *Clim. Dyn.*, doi: 10.1007/s00382-009-0566-z

Diffenbaugh, N.S., and L.C. Sloan, 2002. Global climate sensitivity to land surface change: The Mid Holocene revisited. *Geophys. Res. Lett*, 29(**10**):114-1-114-4

Doherty, R., J. Kutzbach, J. Foley and D. Pollard, 2000: Fully-coupled climate/dynamical vegetation model simulations over Northern Africa during the mid-Holocene. *Clim. Dyn.*, **16**:561-573

Donovon, R.G., H.E. Stewart, S.M. Owen, A.R. MacKenzie, and C.N. Hewitt, 2005. Development and application of an urban tree air quality score for photochemical pollution episodes using the Birmingham, United Kingdom, area as a case study. *Environ. Sci. Technol.* 39(**17**):6730-6738

Dorland, van R., Dentener, F.J., and Lelieveld, J., 1997. Radiative forcing due to tropospheric ozine and sulfate aerosol, *J. Geophys. Res.*, **102**:28079-28100.

Douville, H., and J.F. Royer, 1997. Influence of the temperate and boreal forests on the Northern Hemisphere climate in the Meteo-France climate model, *Clim. Dyn.*, **13**:57-74

Durkee, P. A., F. Pfeil, E. Frost, and R. Shema, 1991. Global analysis of aerosol particle characteristics. *Atmos. Enviro.*, **25A**:2457-2471.

Durman, C.F., J.M. Gregory, D.C. Hassel, R.G. Jones, and J.M. Murphy, 2001. A comparison of extreme European daily precipitation simulated by a global and a regional climate model for present and future climates. *Q.J.R. Metreorol. Soc.*, **127**:1005-1015

Dutkiewicz. S., A. Sokolov, J. Scott and P. Stone, 2005. *A Three-Dimensional Ocean-Seaice-Carbon Cycle Model and its Coupling to a Two-Dimensional Atmospheric Model: Uses in Climate Change Studies.* Report 122, MIT Joint Program on the Science and Policy of Global Change, 49 pp. (*http://mit.edu/globalchange/www/MITJPSPGC_Rpt122.pdf*).

EC (European Commission), 2003. *Ozone-climate interactions.* Energy, Environment and Sustainable Development, Air Pollution Research Report No. 81, pp 143.

Echalar, F., P. Artaxo, J.V. Martins, M. Yamasoe, F. Gerab, W. Maenhaut, and B. Holben, 1998. Long-term monitoring of atmospheric aerosols in the Amazon Basin; source identification and apportionment. *J. Geophys. Res.*, **103**:31849-31866.

Edwards, J.M. and Slingo, A., 1996: Studies with a flexible new radiation code. 1: Choosing a configuration for a large-scale model. *Quart. J. Royal Meteorol. Soc.*, **122**:689-719.

Ehhalt, D.H., 1999. Gas phase chemistry of the troposphere. In *Global Aspects of Atmospheric Chemistry* by R. Zellner (ed), Springer, Darmstadt Steinkopff, New York, pp. 21-109.

Ehhalt, D.H., H.-P. Dorn, and D. Poppe, 1991. *The chemistry of hydroxyl radical in the troposphere.* Proceedings of the Royal Society of Edinburgh, B97, pp 17-34

Eichner, M., 1990. Nitrous oxide emissions from fertilized soils: Summary of available data. *Revista J. Envirom. Qual.*, 19(**2**):272-280.

Emberson, L.D. , J. C. I. Kuylenstierna, H.M. Cambridge, S. Cinderby, and M. R. Ashmore, 1996. Mapping relative potential sensitivity of vegetation to ozone across Europe: A preliminary analysis. Presented at workshop on Critical Levels for Ozone in Europe: Testing and Finalising the Concepts, 15-17 April 1996, Kuopio, Finland.

Emberson, L.D., M.R. Ashmore, H.M. Cambridge, D. Simpson, J.-P. Tuovinen, 2000. Modelling stomatal ozone flux across Europe. *Enviro. Pollution*, **109**:393-402

Emmerson, K.M. 2002. *Modelling the Production of Organic Atmospheric Aerosol.* PhD Thesis. University of Lancaster UK.

EPA, 2007. *Inventory of US greenhouse gas emissions and sinks: 1990-2005.* EPA 430-R-07-002. Washington

Erda L., Wei X., Hui J., Yinlong X., Yue L., Liping B., and Liyong X., 2005. Climate change impacts on crop yield and quality with CO2 fertilization in China. *Philos Trans R Soc Lond B Biol Sci.* 360(**1463**):2149-54

Evans, M.J., Shallcross, D.E., Law, K.S., Wild, J.O.F., Simmonds, P.G., Spain, T.G., Berrisford, P., Methven, J., Lewis, A.C., McQuaid, J.B., Pilling, M.J., Bandy, B.J., Penkett, S.A., Pyle, J.A., 2000. Evaluation of a Langrangian box model using field measurements from EASE (Eastern Atlantic Summer Experiment) 1996. *Atmos. Environ.* **34**:3843-3863

Fan, J. and R. Zhang, 2004. Atmospheric Oxidation Mechanism of Isoprene. *Environ. Chem.*1(**3**):140-149, doi:10.1071/EN04045

FAO, 2004. Gateway to Land and Water Information: Philippines National Report.

FAO, 2006. Specialized Country Profiles and Information System. *http://www.fao.org*

Feddema, J. J., K. W. Oleson, G. B. Bonan, L. O. Mearns, L. E. Buja, G. A. Meehl and W.M. Washington' 2005. The Importance of Land-Cover Change in Simulating Future Climates. *Science*, 310(**5754**):1474-1678, doi:10.1126/science.1118160

Fehsenfeld, F. C., and S. C. Liu, 1993. Tropospheric ozone: Distribution and sources. In *Global Atmospheric Chemical Change* by C. N. Hewitt and W. T. Sturges (Eds), Elsevier Applied Science, New York, pp. 169-231.

Fehsenfeld, F., J. Calvert, R. Fall, P. Goldan, A. B. Guenther, C.N. Hewitt, B. Lamb, S. Liu, M. Trainer, H. Westberg, and P. Zimmerman, 1992. Emissions of volatile organic compounds from vegetation and the implications for atmospheric chemistry. *Global Biogeochem. Cycles,* 6(**4**): 389-430, doi: 10.1029/92GB02125.

Felzer, B., J. Reilly, J. Melillo, D. Kicklighter, M. Sarofim, C. Wang, R. Prinn, and Q. Zhuang, 2005. Future Effects of Ozone on Carbon Sequestration and Climate Change Policy Using a Global Biogeochemical Model. *Climatic Change* 73(**3**): 345-373.

Finlayson-Pitts B.J., J.N. Pitts, 2000. Chemistry of the Upper and Lower Atmosphere - Theory, Experiments, and Applications. Academic Press, San Diego, CA.

Fiore, A. M., L. W. Horowitz, D. W. Purves, H. Levy II, M. J. Evans, Y. Wang, Q. Li. and R. M. Yantosca, 2005. Evaluating the contribution of changes in isoprene emissions to surface ozone trends over the eastern United States. *J. Geophys. Res.,* **110**:D12303, doi:10.1029/2004JD005485

Forkel, R., and R. Knoche, 2006. Regional climate change and its impact on photooxidant concentrations in southern Germany: Simulations with a coupled regional climate-chemistry model. *J. Geophys. Res.* 111, No. D12, D12302, xxxxxxx doi:10.1029/2005JD006748

Forster, P., V. Ramaswamy, P. Artaxo, T. Berntsen, R. Betts, D.W. Fahey, J. Haywood, J. Lean, D.C. Lowe, G. Myhre, J. Nganga, R. Prinn, G. Raga, M. Schulz and R. Van Dorland, 2007: Changes in Atmospheric Constituents and in Radiative Forcing. In: *Climate Change 2007: The Physical Science Basis. Contribution of Working Group I to the Fourth Assessment Report of the Intergovernmental Panel on Climate Change* [Solomon, S., D. Qin, M. Manning, Z. Chen, M. Marquis, K.B. Averyt, M.Tignor and H.L. Miller (eds.)]. Cambridge University Press, Cambridge, United Kingdom and New York, NY, USA.

Forster, P.M. de F., and Shine, K.P., 1997. Radiative forcing and temperature trends from stratospheric ozone changes. *J. Geophys. Res.*, **102**:10841-10857.

Fouquart, Y. and B. Bonnel, 1980. Computations of solar heating of the Earths atmosphere: a new parametrization. *Contrib. Phys. Atm.*, **53**:35-62.

Fowell, M., 2006. Methodologyfor evaluating GCMs at regional scales : method development and application to SE Asian hydrological variables, PhD Thesis, Lancaster University, UK.

Fowler, D., C. Flechard, J.N. Cape, R.L. Storen-West and M. Coyle, 2001. Measurementr of ozone deposition to vegetation quantifying the flux, stomatal and non-stomatal components. *Water Air Soil Pollution*, **130**:63-74

Frolking, S.E., J.L. Bubier, T.R. Moore, T. Ball, L.M. Bellisario, A. Bhardwaj, P. Carroll, P.M. Crill, P.M. Lafleur, J.H. McCaughey, N.T. Roulet, A.E. Suyker, S.B. Verma, J.M. Waddington, and G.J. Whiting, 1998. Relationship between ecosystem productivity and photosynthetically active radiation for northern peatlands. *Global Biogeochem. Cycles*, **12**:115-126.

Fu, T.M., D.J. Jacob, P.I. Palmer, K. Chance, Y.X. Wang, B. Barletta, D.R. Blake, J.C. Stanton and M.J. Pilling, 2007. Space-based formaldehyde measurements as constraints on volatile organic compound measurements in East and South Asia. Journal of Geophys. Res. Atmos., 112: D06312, doi:10.1029/2006JD007853. 8

Fuglestvedt, J. S., 1995. Model studies of indirect effects on climate through changes in the chemistry of the troposphere. PhD Thesis CICERO University of Oslo, Norway, unpublished.

Fuglestvedt, J. S., J. E. Jonson, W. C. Wang, and I. S. A Isaken, 1995. Climate change and its effect on tropospheric ozone. In: *Atmospheric Ozone as a Climate Gas*, by W. C. Wang and I. S. A. Isaken (Eds), NATO ASI Series vol. 132, Springer-Verlag, Berlin, pp 145-162.

Fuglestvedt, J.S., Bernsten, T.K., Isaksen, I.S.A, Mao, H., Liang, X.Z., Wang, W.C., 1999. Climatic forcing of nitrogen oxides through changes in tropospheric ozone and methane; global 3D model studies, *Atmos. Enviro.* **33**:961-977.

Fuhrer, J. , 1996. The critical level for effects of ozone on crops, and the transfer to mapping. Presented at workshop on Critical Levels for Ozone in Europe: Testing and Finalising the Concepts, 15-17 April 1996, Kuopio, Finland.

Fuhrer, J., L. Skärby, and M. Ashmore, 1997. Critical levelos for ozone effects on vegetation in Europe. *Enviro. Pollution*, **97**:91-106

Fujiwara, M, Y. Tomikawa, K.Kita, Y. Kondo, N. Komala, S. Saraspriya, T. Manik, A. Suripto, S. Kawakami, T. Ogawa, E. Kelana, B. Suhardi, S.W.B. Harijono, M. Kudsy, T. Sribimawati, and M.D. Yamanaka. 2003. *Atmos. Enviro.* **37**:353-362.

Fujiwara, M., Kita, K., Kawakami, S., Ogawa, T., Komala, N., Saraspriya, S., Suripto, A., 1999. Tropospheric ozone enhancements during the Indonesian forest fire events in 1994 and in 1997 as revealed by ground-based observations. *J. Geophys. Lett.*, **26**:2417–2420.

Fusco, A.C. and J. A. Logan, 2003. Analysis of 1970-1995 Trends in Tropospheric Ozone at Northern Hemisphere Midlatitudes with the GEOS-CHEM Model, *J. Geophys. Res.*, **108**:4449, doi:10.1029/2002JD002742.

Ganzeveld, L. and Lelieveld J., 1995. Dry Deposition parameterization in a chemical general circulation model and its influence on the distribution of reactive trace gases. *J. Geophys. Res.*, **100**:20999-21012

Ganzeveld, L., and J. Lelieveld, 2004. Impact of Amazonian deforestation on atmospheric chemistry. *J. Geophys. Res.*, **31**:L06105, doi:10.1029/2003GL019205

Garrity, D.P, M. Soekardi, M. van Noordwijk, R. de la Cruz, P.S Pathak, H.P. Gunasena, M.N. van So G. Huijun, N.M. Majid, 1997. The *Imperata* grasslands of tropical Asia: area, distribution and typology. *Agroforestry Systems*, **36**:3-29

Gauss, M., G. Myhre, G. Pitari, M.J. Prather, I.S.A. Isaksen, T.K. Berntsen, G.P. Brasseur, F.J. Dentener, R.G. Derwent, D.A. Hauglustaine, L.W. Horowitz, D.J. Jacob, M. Johnson, K.S. Law, L.J. Mickley, J.-F. Müller, P.-H. Plantevin, J. A. Pyle, H.L. Rogers, D.S. Stevenson, J.K. Sundet, M. van Weele, and O. Wild, 2003. Radiative forcing in the 21st century due to ozone changes in the troposphere and the lower stratosphere. J. Geophys. Res., 108(D2), 4292, doi:10.1029/2002JD002624

Gebhart, K.A., Kreidenweis S.M., Malm W.C., 2001. Back-trajectory analyses of fine particulate matter measured at Big Bend National Park in the historical database and the 1996 scoping study. *Science of the Total Environment*, **276**:185-204

Generoso, S., F.-M Breon, Y. Balkanski, O. Boucher, and M. Shultz. 2003. Improving the seasonal cycle and interannual variations of biomass burning aerosol sources. *Atmos. Chem. Phys.* **3**:1211-1222

Geron, C, A. B. Guenther, J. P. Greenberg, H. W. Loescher, D. Clark, and B. Baker, 2002. Biogenic volatile organic compound emissions from a lowland tropical wet forest in Costa Rica. *Atmos. Environ.*, **36**:3793–3802.

Geron, C., S. Owen, A. Guenther, J. Greenberg, R. Rasmussen, H. B. Jian, J. L. Qian, and B. Baker, 2006. Volatile organic compounds from vegetation in southern Yunan Province, China: Emission rates and some potential regional implications. *Atmos. Environ.* **40**:1759-1773.

Gettelman, A., J. R. Holton, and K. H. Rosenlof, 1997. Mass fluxes of O_3, CH_4, N_2O and CF_2Cl in the lower stratosphere calculated from observational data. *J. Geophys. Res.*, **102**:19149-19159.

Gibson J. K., Källberg P., Uppala S., Hernández A., Nomura A., and Serrano E., 1997, *ERA description*. ECMWF Reanalysis Project Report Series 1, ECMWF, Reading, 66 pp.

Giorgi, F. and R. Francisco, 2000. Uncertainties in regional climate change prediction: a regional analysis of ensembles simulations with the HADCM2 coupled AOGCM. *Clim. Dyn.*, **16**:169-182

Giorgi, F., Hewitson B., Christensen J., Hulme M., Von Storch H., Whetton P., Jones R., Mearns L.O., Fu C., Arritt R., Bates B., Benestad R., Boer G., Buishand A., Castro M., Chen D., Cramer W., Crane R., Crossley J.F., Dehn M., Dethloff K., Dippner J., Emori S., Francisco R., Fyfe J., Gerstengarbe F.W., Gutowski W., Gyalistras D., Hanssen-Bauer I., Hantel M., Hassell D.C., Heimann D., Jack C., Jacobeit J., Kato H., Katz R., Kauker F., Knutson T., Lal M., Landsea C., Laprise R., Leung R.L., Lynch A.H., May W., McGregor J.L., Miller N.L., Murphy J., Ribalaygua J., Rinke A., Rummukainen M., Semazzi F., Walsh K., Werner P., Widmann M., Wilby R., Wild M., and Xue Y., 2001. Regional Climate Information – Evaluation and Projections, Chapter 10. In *Climate Change 2001: The Scientific Basis* by J.T. Houghton *et al.* (eds.), Cambridge University Press, pp 583-638.

Giorgi, F., and Bi X.Q., 2000. A study of internal variability of a regional climate model. *J. Geophys. Res.*, 105(**D24**):29503-29521

Giorgi, F., and G. T. Bates, 1989. The climatological skill of a regional model over complex terrain, *Mon. Wea. Rev.*,117:2325-2347.

Giorgi, F., and Mearns L.O., 1999. Regional climate modelling revisited. An introduction to the special issue. *J. Geophys. Res.*, **104**:6335-6352.

Giorgi, F., M. R. Marinucci, and G. T. Bates, 1993. Development of a second generation regional climate model (RegCM2), Boundary-layer and radiative transfer process. *Mon. Weather Rev.*, **121**:2794-2813.

Giorgi, F., Mearns L.O., Shields C. and McDaniel L., 1998. Regional nested model simulations of present day and $^{23}CO_2$ climate over the Central Plains of the U.S. *Clim. Change*, **40**:457–493.

Giorgi, F., Mearns L.O., Shields C. and Meyer L., 1996. A regional model study of the importance of local vs. remote controls in maintaining the drought 1988 and flood 1993 conditions in the central U.S. *J. Climate*, **9**:1150–1162.

Giorgi, F., X. Bi, and Y. Qian, 2002. Direct radiative forcing and regional climate effects of anthropogenic aerosols over East Asia: a regional coupled climate-chemistry/aerosol model study, *J. Geophys. Res.*, 107(**D20**):4439, doi:10.1029/2001JD001066.

Giorgi, F., Y. Huang, K. Nishizawa, and C. Fu, 1999. A seasonal cycle simulation over eastern Asia and its sensitivity to radiative transfer and surface processes. *J. Geophys. Res.*, 104(**D6**):6403-6423.

Giorgi, G., X. Q. Bi, and Y. Qian, 2003. Indirect vs. direct effects of anthropogenic sulfate on the climate of East Asia as simulated with a regional coupled climate-chemistry/aerosol model. *Climate Change*, **58**:345-376.

Girard E. and B. Bekcic, 2005. Sensitivity of an Artic regional climate model to the horizontal resolution during winter: Implications for aerosol simulation. *Int. J. Climatol.*, **25**: doi:10.1002/joc.1205.

Giri, C., S. Shrestha, and M. Levy, 2001. Assessment and monitoring of land use/land cover change in continental Southeast Asia. Open Meeting of the Global Environmental Change Research Community, Rio de Jeaneiro, 6-8 October 2001.

Goldammer, J.G. 1999. Environmental problems arising from land use, climate variability, fire and smog in Indonesia: Development of policies and strategies for land use and fire management. In *WMO Workshop on Regional Transboundary Smoke and Haze in Southeast Asia*, Singapore, 2-5 June 1998, Vol. 2 by G.R.Carmichael (Ed), pp.13-88. World Meteorological Organization, Global Atmosphere Watch Report Ser. No. 131, WMO TD No. 948, Geneva, 346 pp.

Goldstein, A.H., M.L. Goulden, J.W. Munger, S.C. Wofsy, and C.D. Geron, 1998. Seasonal course of isoprene emissions from a midlatitude deciduous forest, J. Geophys. Res., 103(D23):31045-31056.

Gordon, C., C. Cooper, C. Senior, H. Banks, J. Gregory, T. Johns, J. Mitchell, and R.A. Wood, 2000. The simulation of SST, sea ice extents and ocean heat transports in a oupled model without flux adjustment. *Climate Dynamics*, **16**:147-168.

Graedel, T. E., and C. J. Weschler, 1981. Chemistry within aqueous atmospheric aerosols and raindrops. *Rev. Geophys. Space Phys.* **19**:505-539.

Graedel, T.E. 1978. Chemical Compounds in the Atmosphere. Academic Press, New York,

Graedel, T.E., and P. J. Crutzen, 1993. *Atmospheric Change: An Earth System Perspective*. Freeman, New York.

Granier, C., M. Kanakidou, and P. Khasiblata, F. Dentener, J. Feichter, S. Houweling, B. Khattatov, J.-F. Lamarque, M. Lawrence, S. Madronich, N. Mahowald, and S. Walters, 1999. Modelling. *In The Changing Atmosphere* by IGAC, Technical Paper, Anex I, http://medias.obs-mip.fr/igac/

Grant, K. E., C. C. Chuang, A. S. Grossman, and J. E. Penner, 1999. Modeling the spectral optical properties of ammonium sulfate and biomass burning aerosols: Parameterization of relative humidity effects and model results, *Atmos. Environ.*, **33**:2603–2620.

Greenberg, J., A.B. Guenther, G. petron, C. Wiedinmier, O. Vega, L. V. Gatti, J. Tota, and G. Fisch, 2004. Biogenic VOC emissions from forested Amazonian landscapes. *Global Change Biology*, 10(**5**):651-662

Gregory, D., Shutts G.J., and Mitchell J.R., 1998, A new gravity-wave-drag scheme incorporating anisotropic orography and low-level wave breaking: Impact upon the climate of the UK Meteorological Office Unified Model. *Quart. J. Roy. Meteor. Soc.*, **124**:463-494.

Griffin R. J., D. R. Cocker III, J. H. Seinfeld, and D. Dabdub, 1991b. Estimate of global atmospheric organic aerosol from oxidation of biogenic hydrocarbons, *Geophys. Res. Lett.* **26**:2721-2724.

Griffin R. J., D. R. Cocker III, R. C. Flagan, and J. H. Seinfeld, 1991a. Organic aerosol formation from oxidation of biogenic hydrocarbons, *J. Geophys. Res.* **104**:3555-3567.

Griffin, K.L., O.R. Anderson, M.D. Gastrich, J.D. Lewis, G. Lin, W. Schuster, J.R. Seemann, D.T. Tissue, M. Turnbull, and D. Whitehead, 2001. Plant growth in elevated CO_2 alters mitochondrial number and chloroplast fine structure. *Proceedings of the National Academy of Science of the USA*, **98**: 2473–2478.

Guenther, A., B. Baugh, G. Brasseur, J. Greenberg, P. Harley, L. Klinger, D. Serca, and L. Vierling, 1999. Isoprene emission estimates and uncertanties for the Central African EXPRESSO study domain, *J. Geophys. Res.*, **104**:30,625 – 30,639.

Guenther, A. 1997. Seasonal and spatial variations in natural volatile organic compound emissions. *Ecological Applications* 7:34-45.

Guenther, A. B., R.K., Monson and R. Fall, 1991. Isoprene and monoterpene emission rate variability: observations with eucalyptus and emission rate algorithm development. *J. Geophys. Res.* **96**:10799–10808.

Guenther, A. W. Baugh, K. Davis, P. Harley, L. Klinger, P. Zimmerman, E. Allwine, S. Dilts, B. Lamb, H. Westberg, D. Baldocchi, C. Geron, and T. Pierce. 1996. Leaf, canopy and landscape isoprene fluxes from an oak-pine-mixed deciduous forest. *J. Geophys. Res.*, **101A**:18555–18568.

Guenther, A., Hewitt C.N., Erickson D., Fall R., Geron C., Graedel T., Harley P., Klinger L., Lerdau M., McKay W.A., Pierce T., Scholes B., Steinbrecher R., Tallamraju R., Taylor J., and Zimmerman P. 1995. A global model of natural volatile organic compound emissions, *J. Geophys. Res.*, 100(**D5**), 8873-8892

Guenther, A., P.R. Zimmerman, P.C. and Harley, 1993. Isoprene and monoterpene emission rate variability: Model evaluations and sensitivity analyses. *J. Geophys. Res.* **98**:12609-12617.

Guenther, A., T. Karl, P. Harley, C. Wiedinmyer, P.I. Palmer, and C. Geron, 2006. Estimates of global terrestrial isoprene emissions using MEGAN (Model of Emissions of Gases and Aerosols from Nature). *Atmos. Chem. Phys*, **6**:3181-3210

Guicherit, R., and Roemer, M., 2000. Tropospheric ozone trend. *Chemosphere-Global Change Science*, **2**:167-183.

Gunawan, I. and A. Rahmadi, 2000. Tropical Forest Mapping and Monitoring in Indonesia. SEA Regional GOFC Planning Meeting, Bogor, pp 19-49.

Gutman, G., I. Csiszar, and P. Romanov, 2000. Using NOAA/AVHRR products to monitor El Nino impacts: Focus on Indonesia in 1997-1998. *Bull. Amer. Meteor. Soc.*, 81(**6**):1189-1205.

Hadjinicolaou, P., S. Michaelides, C. Papastavros, and A. Poyiadjis, 2006. Use of radiosonde data for validation of regional climate modelling simulations over Cyprus. COST 723 Workshop, Sofia, Bulgaria 17-19 May 2006.

Hansen, J. E., M. Sato, and R. Ruedy, 1995. Long-term changes of the diurnal temperature cycle: Implications about mechanisms of global climate change. *Atmospheric Research,* **37**:175-209.

Hansen, J. E., M. Sato, and R. Ruedy, 1997. Radiative forcing and climate response. *J. Geophys. Res.* **102**:6831-6864.

Hansen, J. E., R. Ruedy, M. Sato, M. Imhoff, W. Lawrence, D. Easterling, T. Peterson, and T. Karl, 2001. A closer look at United States and global surface temperature change. *J. Geophys. Res.*, 106: 23947-23963.

Hansen, J., M. Sato, A. Lacis, R. Ruedy, I. Tegen, and E. Matthews, 1998. Climate forcings in the industrial era. *Proc. Natl. Acad. Sci.*, **95**:12,753–12,758

Harley P., P. Vasconcellos, I. Vierling, C. C. de S. Pinheiros, J. Greenberg, A. Guenther, L. Klinger, S. S. de Almeida, D. Neill, T. baker, O. Phillups, and Y. Malhi, 2004. Variation in potential for isoprene emissions among Neotropical forest sites. *Global Change Biology*, **10**:1–21, doi: 10.1111/j.1529-8817.2003.00760.x

Harley, P.C, M.E. Litvak, T.D. Sharkey and K.R. Monson, 1994. Isoprene Emission from Velvet Bean Leaves: Interactions among Nitrogen Availability, Growth Photon Flux Density, and Leaf Development. *Plant Physiology*, 105(**1**): 279-285

Harris, R., K. Bartlett, S. Frolking, and P. Crill, 1993: Methane emissions from northern high-latitude wetlands. In *Biogeochemistry of Global Change: Radiatively Active Trace Gases* by R.S. Oremland (ed.), Chapman and Hall, New York, pp. 449-486.

Harvey, L.D.D., and Z. Huang. 1995. Evaluation of the potential impact of methane clathrate destabiliztaion on future global warming. *J. Geophys. Res.* **100**:2905-1926.

Hassel, D., and Jones R., 1999. Simulating climatic change of the soutrthern Asian monsoon using a nested regional climate model (HadRM2). Hadley Centre Technical Note, Meteorological Office UK, May 1999, 17 pp.

Hauglustaine, D.A., and G.P. Brasseur, 2001. Evolution of tropospheric ozone under anthropogenic activities and associated radiative forcing of climate, *J. Geophys. Res.*, **106**:32337-32360.

Hauglustaine, D.A., G.P. Brasseur, S. Walters, P.J. Rasch, J.F. Miller, L.K. Emmons and M.A. Caroll, 1998. MOZART, a global chemical transport model for ozone and related chemical tracers: 2. Model results and evaluation. *J. Geophys Res.* **103**:16999-17007.

Haussmann, M., and U. Platt, 1994. Spectroscopic measurement of bromine oxide and ozone in the high Arctic during Polar Sunrise Experiment 1992. *J. Geophys. Res.*, **99**:25399-25413.

Haywood, J. M. and V. Ramaswamy, 1998. Global sensitivity studies of the direct radiative forcing due to anthropogenic sulfate an black carbon aerosols, *J. Geophys. Res.*, **103**:6043-6058.

Heald, C. L., M.J. Wilkinson, R.K. Monson, C.A. Alo, G.Wang and A. Guenther, 2009. Response of isoprene emission to ambient CO_2 changes and implications for global budgets, *Glob Change Biol*, 15(**5**): 1127, doi:10.1111/j.1365-2486.2008.01802.x.

Heikes, B.G., M. Lee, D.J. Jacob, R.W. Talbot, J.D. Bradshaw, H.B. Singh, D.R. Blake, B.E. Anderson, H.E. Fuelberg, and A.M. Thompson, 1996. Ozone, hydroperoxides, oxides of nitrogen, and hydrocarbon budgets in the marine boundary layer over the South Atlantic. *J. Geophys. Res.*, **101**:24,221-24,234.

Hein, R., P.J. Crutzen and M. Heinmann, 1997. An inverse modeling approach to investigate the global atmospheric methane cycle. *Global Biogeochem. Cycles*, **11**:43-76.

Heintzenberg, J., 1989. Arctic haze: Air pollution in polar regions. *Ambio*, **18**:50-55.

Henderson-Sellers, A., R.E. Dickinson, T.B. Durbidge, P.J. Kennedy, K. McGuffie, and A.J. Pitman, 1993. Tropical deforestation: Modeling Local-to Regional-Scale Climate Change. *J. Geophys. Res.*, **98**:7289-7315.

Hennessey, K.J., Whetton, P.H., Katzfey J.J., McGregor J.L., Jones J.N., Page C.M., and Nguyen K.C., 1998. Fine resolution climate change scenarios for New South Wales. Annual Report, 1997/98, CSIRO, Australia, 48 pp.

Hilbert, D.W., N. Roulet, and T. Moore, 2000. Modelling and analysis of peatlands as dynamical systems. *J. Ecol.* **88**:230-242.

Hoffmann, T., J.R. Odum, F. Bowman, D. Collins, D. Klockow, R.C. Flagan, and J.H. Seinfeld, 1997. Formation of organic aerosols from the oxidation of biogenic hydrocarbon. *J. Atmos. Chem.*, **26**:189-222.

Hogrefe, C., B. Lynn, K. Civerolon, J.Y. Ku, J. Rosenthal, C. rosenzweig, R. Goldberg, S. Gaffin, K. Knowlton, and P.L. Kinney, 2004. Simulating changes in regional air pollution over the eastern United States due to changes in global and regional climate and emissions, *J. Geophys. Res.*, **109**:D22301, doi:10.1029/2004JD004690.

Holland, E.A., F.J. Dentener, B.H. Braswell, and J.M. Sulzman, 1999. Contemporary and pre-industrial reactive nitrogen budgets. *Biogeochemistry*, **46**:7-43.

Hori, M. E., and H. Ueda, 2006. Impact of global warming on the East Asian winter monsoon as revealed by nine coupled atmosphere-ocean GCMs, *Geophys. Res. Lett.*, **33**:L03713, doi:10.1029/2005GL024961.

Horowitz, L., S. Walters, D.L. Mauzerall, L.K. Emmons, P.J. Rasch, C. Granier, X. Tie, J-F. Lamarque, M.G. Schultz, G.S. Tyndall, J.J. Orlando, and G.P. Brasseur, 2003. A global simulation of trpospheric ozone and related tracers: Description and evaluation of MOZART, version 2. *J. Geophys. Lett.*, 108(**D24**):4784, doi:10.1029/2002JD002853.

Hostetler, S.W., F. Giorgi, G.T. Bates, and P.J. Bartlein, 1994. Lake-atmosphere feedbacks associated with paleolakes Bonneville and Lahontan, *Science*, **263**: 665-668

Hough, A. M., 1988. The calculation of photolysis rates for use in global tropospheric modelling studies, AERE Report R-13259, H. M. Stationery Office, London

Hough, A. M., 1991. Development of a two-dimensional global tropospheric model: Model chemistry, *J. Geophys. Res.*, **96**:7325–7362.

Houghton, J.T., L.G. Meira Filho, B.A. Callander, N. Harris, A. Kattenberg, and K. Maskell (eds.), 1996: *Climate Change 1995. The Science of Climate Change.* Contribution of Working Group I to the Second Assessment Report of the Intergovernmental Panel on Climate Change, Cambridge University Press, Cambridge.

Houghton, R.A., and D.L. Skole, 1990. Carbon. In *The Earth Transformed by Human Action* by B.L. Turner (Ed), Cambridge University Press, Cambridge, pp 393-408.

Houweling, S., F. Dentener, and J. Lelieveld, 1998. The impact of non-methane hydrocarbon compounds on tropospheric photochemistry. *J. Geophys. Res.*, **103**:10673-10696. http://www.fao.org/ag/agl/swlwpnr/reports/y_ta/z_ph/ph.htm

Huang, Y., 2005. Assessments of the direct and indirect effects of anthropogenic aerosols on regional precipitation over East Asia using a coupled regional climate-chemistry-aerosol model. PhD dissertation, Georgia Institute of Technology, Atlanta, GA.

Hudson, D.A and Jones, R.G. 2002. *Simulations of present-day and future climate over Southern Africa using HadAM3H.* Hadley Centre Technical Note 38, Met. Office, UK.

Hudson, J. G., 1991. Observation of anthropogenic cloud condensation nuclei. *Atmos. Enviro.*, **25A**:2449-2455.

Hulme, M., Conway D., Jones P.D., Jiang T., Barrow E.M., and Turney C., 1995. Construction of a 1961-1990 European climatology for climate change modelling and impact applications. *Int. J. Climatology* **15**:1333-1363.

Hulme, M., G. Jenkins, X. Lu, J. Turnpenny, T. Mitchell, R. Jones, J. Lowe, J. Murphy, D. Hassell, P. Boorman, R. Macdonald, and S. Hill, 2002. *Climate-Change Scenarios for the United Kingdom: The UKCIP02 Scientific Report.* Tyndall Centre for Climate Change Research.

Hulme, M., J. Mittchell, W. Ingram, J. Lowe, T. Johns, M. New, and D. Viner, 1999. Climate change scenarios for global impact studies, *Global Environmental Change* **9**:S3-S9.

Huntingford, C., Jones R.G., Prudhomme, C., Lamb R., Gash J.H.C., and Jones, D.A., 2003. Regional climate m odel predictions of extreme rainfall for a changing climate. *Q. J. R. Meteorol. Soc.*, **129**:1607-1621

Husar, R. B., J. M. Prospero, and L. L. Stowe, 1997. Characterization of tropspheric aerosols over the oceans with the NOAA advanced very high resolution radiometer optical thickness operational product. *J. Geophys. Res.*, 102(**D14**):16,889-16909.

IES (Institute for Environmental and Sustainability), 2006. Global Landcover 2000. European Commission. Joint Research Centre. *http://www-gvm.jrc.it/glc2000/*

IMF (International Monetary Fund), 2006. World Economic and Financial Survey. World Economic Outlook Database Surveys. September 2006 Edition. http://www.imf.org/external/pubs/ft/weo/2006/02/data/index.asp

Impey, G.A., C.M. Mihele, K.G. Anlauf, L.A. Barrie, D.R. Hastie and P.B. Shepson, 1999. Measurements of photolyzable halogen compounds and bromine radicals during the Polar Sunrise Experiment 1997. *J. Atmos. Chem.*, **34**:21-37.

Ingram, W.J., Woodward, S., and Edwards, J., 1997. Radiation. Unified Model Documentation Paper No. 23. Version 3. Climate Research, Meteorological Office, Bracknell, Berkshire, UK , pg 1-33

Intergovernmental Panel on Climate Change (IPCC) 1994. *Radiative forcing of climate change.* The 1994 Report of the scientific Assessment Working Group of IPCC. Summary for Policymakers.

Intergovernmental Panel on Climate Change (IPCC) 2000. *Emissions Scenarios.* (Eds. N. Nakicenovic *et al.*), Cambridge University Press, Cambridge, UK.

Intergovernmental Panel on Climate Change (IPCC) 2001. Climate Change 2001: The Scientific Basis. (Eds J.T. Houghton *et al.*), Cambridge University Press, Cambridge, UK.

Intergovernmental Panel on Climate Change (IPCC), 1995. Climate change 1994: Radiative forcing of climate cahneg and an evaluation of the IPCC IS92 emission scenarios, by J. T. Houghton et al. (Eds), Cambridge University Press, New York, 339 pp.

Iskasen, I.S.A., 2000. The atmospheric sink of methane. IGACtivities Newsletter, No.21, September 2000. http://www.igac.noaa.gov/newsletter/igac21/methane_sink.html

Isaksen, I. S. A., Ø. Hov, S. A. Penkett, and A. Semb, 1985. Model analysis of the measured concentration of organic gases in the Norwegian Arctic, *J. Atmos. Chem.*, **3**:3–27

Islam, M.N. and Mannan A., 2005. Validation of PRECIS regional climate model in Bangladesh. PRECIS Working Group in Bangladesh, Climate Change Cell-DFID-Department of Environment-UNDP, 47 pp.
J., 2002. *Carbon emissions from tropical deforestation and regrowth based on satellite observations for the 1980's and 1990's*, Proceedings of the National Academy of Sciences, ***99***:14256-14261.

Jacob D.J., and S.C. Wofsy, 1990. Budgets of reactive nitrogen, hydrocarbons and ozone over the Amazon forest during the wet season, *J. Geophys. Res*, **95**:16737-16754.

Jacob, D. J., W. F. Fitzerald, J. Hansen, J. T. Kiehl, J. A. Logan, L. J. Mickley, J. E. Penner, R. G. Prinn, V. Ramanathan, S. T. rao, S. E. Schwartz, and J. H. Seinfeld, 2005. *Interactions of Climate Change and Air Quality: Research Priorities and New Directions*. Electric Power Research Institute (EPRI) Report, Palo Alto, 22 pp.

Jacob, D.J., 2000. Heterogeneous chemistry and tropospheric ozone. *Atmos. Environ.*, **34**:1235-2159

Jacobson, M. Z., 2001a. Global direct radiative forcing due to multicomponent anthropogenic and natural aerosols, *J. Geophys. Res.*, **106**:1551-1568.

Jacobson, M. Z., 2001b. Strong radiative heating due to the mixing state of black carbon in atmospheric aerosols. *Nature*, **409**:695-697.

Jaegle, L., L. Steinberger, R.V. Martin and K. Chance, 2005. Global partitioning of NO_x sources using satellite obser vations: Relative roles of fossil fuel combustion, biomass burning and soil emissions, Faraday Discuss., **130**:407–423.

Janowiak J., Mo K. C., Ropelewski C., Wang J., Leetmaa A., Reynolds R., Jenne R. and Joseph D., 1996. The NCEP/NCAR 40-Year Reanalysis Project. *Bull. Am. Met. Soc.*, **77**: 437–471.

Jenkin, M. E., and Clemitshaw K.C., 2000. Ozone and other secondary photochemical pollutants: chemical processes governing their formation in the planetary boundary layer. *Atmos. Environ.*, **34**:2499-2527.

Ji, Y., and A. D. Verneker, 1997. Simulation of the Asian summer monsoon of 1987 and 1988 with a regional model nested in a global GCM. *J. Climate*, **10**:1965-1979

Johns, T.C., J.M. Gregory, W.J. Ingram, C.E. Johnson, A. Jones, J. A. Lowe, J.F.B. Mitchell, D.L. Roberts, D.M.H. Sexton, D.S. Stevenson, S.F.B. Tett, and M.J. Woodge, 2003. Anthropoegnic climate change for 1860 to 2100 simulated with the HadCM3 model under updated emissions scenarios, *Clim. Dyn.* **20**:583-612, doi 10:1007/s00382-002-0296-y.

Johnson, C.E., W.J. Collins, D.S. Stevenson, and R.G. Derwent, 1999. Relative roles of climate and emissions changes on future tropospheric oxidant concentrations, *J. Geophys. Res.*, 104(**18**):631-645.

Jones, R.G., Hassel D. and Ward K., 1999. First results from the Hadley Centre's new regional climate model including effects of enhanced resolution. DETR report, March 1999, Hadley Centre for Climate Prediction and Research, London Road, Bracknell, UK.

Jones, R.G., Murphy J.M., Noguer M., and Kean A. B., 1997. Simulation of climate change over Europe using a nested regional-climate model. II: Comparison of driving and regional model responses to a doubling of carbon dioxide, *Q. J.R. Meteorol. Soc.*, **123**:265-292

Jones, R.G., Noguer, M., Hassel, D.C., Hudson, D., Wilson, S.S., Jenkins, G.J., Mitchell, J.F.B., 2004. *Generating high resolution climate change scenarios using PRECIS.* Met. Office Hadley Centre. Exeter.

Jonson, J. E. and Isaksen I.S.A., 1993. Tropospheric Ozone Chemistry. The Impact of Cloud Chemistry. *J. Atmos. Chem.*, **16**:99-122.

Kaas, E., and Frich, P., 1995. Diurnal temperature range and cloud cover in the Nordic countries: Observed trends and estimates for the future. *Atmos. Res.*, **37**:211-228.

Kalnay, E., Kanamitsu M., Kistler R., Collins W., Deaven D., Gandin L., Iredell M., Saha S., White G., Woollen J., Zhu Y. Chelliah M., Ebisuzaki W., Higgins W., Janowiak J., Mo K. C., Ropelewski C., Wang J., Leetmaa A., Reynolds R., Jenne R. and Joseph D., 1996. The NCEP/NCAR 40-Year Reanalysis Project. *Bull. Am. Met. Soc.*, **77**: 437–471.

Kanae, S., T. Oki, and K. Musiake, 2001. Impact of deforestation on regional precipitation over the Indochina Peninsula., *J. Hydrometeor.*, **2**:51-70

Kanakidou, M., K. Tsigaridis, F. Dentener, and P.J. Crutzen, 2000. Human-activitry-enhacned formation of organic aerosols by biogenic hydrocarbon oxidation. *J. Geophys. Res.*, **105**:9243-9254.

Kang, D., Aneja V.P., Mathur R., and Ray J.D. 2003, Nonmethane hydrocarbons and ozone in three rural southeast United States national parks: A model sensitivity analysis and comparison to measurements, *J. Geophys. Res.*, 108 (**D19**), 4604, doi: 10.1029/2002JD003054.

Kang. D., V. P. Aneja, R. Mathur and J.D. Ray, 2004. Observed and modeled VOC chemistry under high VOC/NOx conditions in the Southeast United States national parks. *Atmos. Environ., 38(**29**): 4969-4974.*

Karl, T. R., R. W. Knight, G. Kukla, and G. Gavin, 1995. Evidence for the radiative effects of anthropogenic sulfate in the observed climatic record. In *Aerosol Forcing of Climate*, by R. Charlson and J. heintzenberg (Eds), John Wiley, New York, 382 pp.

Karl, T. R, M. Potosnak, A. Guenther, D. Clark, J. Walker, J.D. Herrick, and C. Geron, 2004. Exchange processes of volatile organic compounds above a tropical rain forest: Implications for modeling tropospheric chemistry above dense vegetation, *J. Geophys. Res.*, 109(**D18**): D18306, doi:10.1029/2004JD004738

Karlsdottir, S. and I. S.A. Isaksen, 2000. Changing methane lifetime: Possible cause for reduced growth. *Geophysical Research Letters* 27(1): doi: 10.1029/1999GL010860.

Kato, H., Nishizawa, K., Hirakuchi H., Kadokura S., Oshima N., and Giorgi F., 2001. Performance of the RegCM2.5/NCAR-CSM nested system for the simulation of climate change in East Asia caused by global warming. *J. Met. Soc. Japan,* **79**:99-121

Kaufman, Y. J. and R. S. Fraser, 1997. The effect of smoke particles on clouds and climate forcing. *Science,* **277**:1636-1639.

Kaufman, Y.J., D. Tanre, and O. Boucher, 2002. A satellite view of aerosols in the climate system. *Nature*, **419**:215-223

Kaufman, Y.J., O. Boucher, D. Tanre, M. Chin, L.A. remer, and T. Takemura, 2005. Aerosol anthropogenic component estimated from satellite data. *Geophys. Res. Lett.,* **32**:L17804, doi:10.1029/2005GL023125

Keene, W. C., R. Sander, A. A. P. Pszenny, R. Vogt, P. J. Crutzen, and J. N. Galloway, 1998. Aerosol pH in the marine boundary layer: A review and model evaluation. *J. Aerosol Sci.*, **29**:339-356.

Keppler K., J. T. G. Hamilton, M. Bra and T. Röckmann. 2006. Methane emissions from terrestrial plants under aerobic conditions. *Nature* **439**:187-191

Kiehl, J. T. and B. P. Breigleb, 1993. The relative roles of sulfate aerosols and greenhouse gases in climate forcing. *Science*, **260**:311-314.

Kiehl, J. T., T. L. Schneider, P. J. Rasch, M. C. Barth and J. Wong, 2000. Radiative forcing due to sulfate aerosols from simulations with the NCAR community model (CCM3), *J. Geophys. Res.*, **105**:1441-1458.

Kirchoff, V.W.J.H. and R. A. Rasmussen, 1990. Time variations of CO and O_3 concentrations in a region subject to biomass burning. *J. Geophys. Res.*, 95(**D6**): 7521-7532.

Kirstine W., I. Galbally, Y. Ye and M. Hooper, 1998. Emissions of volatile organic compounds (primarily oxygenated species) from pasture, *Journal of Geophysical Research,* **103**(D9):10605–10619.

Kittel, T. G. F., F. Giorgi, and G. A. Meehl, 1998. Intercomparison of regional biases and doubled CO2-sensitivity of coupled atmosphere-oceana general circulation model experiments. *Clim. Dyn.*, **14**:1-15

Kleindienst, T.E., D. F. Smith, W. Li, E. O. Edney, D. J. Driscoll, R. E. Speer, and W. S. Weathers, 1999. Secondary organic aerosol formation from the oxidation of aromatic hydrocarbons in the presence of dry submicron ammonium sulfate aerosol. *Atmos. Environ.*, 33(**22**): 3669-3681.

Klinger, L.B,. Q-.S. Li, A.B. Guenther, J.P. Greenberg, B. Baker, and J.-H. Bai, 2002. Assessment of volatile organic carbon emissions from ecosystems of China. *J. Geophys. Res.*, 107(**D21**):4603, doi 10.1029/2001JD001076.

Klinger, L., J. Greenberg, A. Guenther, G. Tyndall, P. Zimmerman, M. Bangui, J-M. Moutsamboté, and D. Kenfack, 1998. Patterns in volatile organic compound emissions along a savanna-rainforest gradient in central Africa. *J. Geophys. Res.*, **103**:1443-1454.

Klonecki, A., P. Hess, L. Emmons, L. Smith, J. Orlando and D. Blake, 2003. Seasonal changes in the transport of pollutants into the Arctic troposphere-model study. *J. Geophys. Res.*, 108(**D4**):8367, doi:10.1029/2002JD002199.

Koch, D., 2001. Transport and direct radiative forcing of carbonaceous and sulfate aerosols in the GISS GCM. *J. Geophys. Res.*, 106(**D17**):20311-20332.

Koe, L. C. C., A. F. Arellano Jr., and J. L. McGregor, 2001. Investigating the haze transport from 1997 biomass burning in Southeast Asia: Its impact upon Singapore. *Atmos. Enviro.* **35**:2723-2734.

Kondragunta, S. 1997. The impact of aerosols on urban photochemical smog production. PhD Thesis, University of Maryland USA.

Kumar, K.R., Sahai, A.K., Kumar, K.K., Patwardhan, S.K., Mishra, P.K., Revadekar J.V., Kamala K., and Pant G.B., 2006. High resolution climate change scenarios for India for the 21st century. *Current Science* 90(**3**):334-345

Kummer, D.M., and B.L. Turner, 1994. The human causes of deforestation in southeast Asia. *BioScience*, **44**:323-328.

Kunhikrishnan, T., M.G. Lawrence, R. von Kuhlmann, A. Richter, A. Ladstatter-Weißenmayer, and J.P. Burrows, 2004. Analysis of tropospheric NOx over Asia using the model of atmospheric transport and chemistry (MATCH-MPIC) and GOME-satellite observations, *Atmos Environ.*, 38(**4**):581–596.

Lacis, A.A., Wuebbles, D.J. and Logan, J.A. 1990. Radiative forcing of climate by changes in the vertical distribution of ozone. *J. Geophys. Res.* **95**:9971-9981

Lalas, D, Kotroni, V., Lagouvardos K., Mirasgentis S., Georgopoulou E., and Sarafidis, Y., 2005. Regional climate forecasts in Eastern Mediterranean: results for the period 2071-2100. National Observatory of Athens.

Lammel, G., and J.N. Cape, 1996. Nitrous acid and nitrite in the atmosphere. *Chemical Society Review*, 361-369.

Lamptey, B.L., E.J. Barron, and D. Pollard, 2005. Simulation of the relative impact of land cover and carbon dioxide to climate change from 1700 to 2100. *J. Geophys. Res.*, 110(**D20**): D20103, doi 10.1029/2005JD0005916.

Laprise, R., D. Caya, A. Frigon, and D. Paquin, 2003: Current and perturbed climate as simulated by the second-generation Canadian Regional Climate Model (CRCM-II) over north-western North America. *Clim. Dyn.*, **21**: 405-421

Laprise, R., D. Caya, G. Bergeron and M. Giguère, 1997: The formulation of André Robert MC2 (Mesoscale Compressible Community) model. *Atmos.-Ocean*, 35(**1**):195-220.

Lashof, D.A., B.J. DeAngelo, S.R. Saleska, and J. Harte, 1997. Terrestrial ecosystem feedbacks to global climate change. *Annu. Rev. Energy Environ.* **22**:75-118

Lathiere, J., Hauglustaine, D.A., Friend, A., De Noblet-Ducoudre, N., Viovy, N., and Folberth, G., 2005. Impact of climate variability and land use changes on global biogenic volatile organic compound emissions. *Atmos. Chem. Phys. Discuss.* **5**:10613-10656

Lathiere, J., Hewitt C.N. and Beerling D.J., 2009. Sensitivity of isoprene emissions from the terrestrial biosphere to 20th century changes in CO_2, climate and land use. *Global Biogeochemical Cycles*, in press.

Law, K. S., and Pyle, J.A., 1993. Modeling trace gas budgets in the troposphere. 1. Ozone and odd nitrogen. *J. Geophys. Res.*, 98:18,377-18,400.

Law, K.S., Nisbet, E.G., 1996. Sensitivity of the CH_4 growth-rate to changes in CH_4 emissions from natural gas and coal. *J. Geophys. Res.*, **101**:14387-14377

Law, K.S., P.-H. Plantevin, D.E. Shallcross, H.L. Rogers, J.A. Pyle, C. Grouhel, V. Thouret and A. Marenco, 1998. Evaluation of modeled O_3 using Measurements of Ozone by Airbus In-Service Aircraft (MOZAIC) data, *J. Geophys. Res.*, **103**: 25,721-25,737

Lean, J. & Rowntree, P. R. 1993. A GCM simulation of the impact of Amazonian deforestation on climate using an improved canopy represenatation. *Q. J. R. Meteorol. Soc.* **119**:509–530.

Lebel, L and W. Steffen, 1998. Global Environmental Change and Sustainable Development in Southeast Asia: Science Plan for a SARCS Integrated Study. SARCS: Thailand

Lee, B.-S., and J.-L. Wang, 2006. Concentration variation of isoprene and its implications for peak ozone concentration. *Atmos. Environ.*, **40**:5486-5495 doi:10.1016/j.atmosenv.2006.03.035.

Lee, D.S., I. Köhler, E. Grobler, F. Rohrer, R. Sauen, L. Gallardo-Klenner, J.J.G. Olivier, F.J. Dentener and A.F. Bouwman, 1997. Estimates of global NO_x emissions and their uncertainties. *Atmos. Environ.*, **31**:1735-1749.

Leemans, R. & Cramer, W. 1991. The IIASA database for mean monthly values of temperature, precipitation and cloudiness of a global terrestrial grid. International Institute for Applied Systems Analysis (IIASA). RR-91-18.

Lefer, B.L., R. E. Shetter, S.R. Hall, J. H. Crawford, and J.R. Olson, 2003. Impact of clouds and aerosols on photolysis frequencies and photochemistry during TRACE-P:1. Analysis using radiative transfer and photochemical box models, *J. Geophys. Res.*, **108**, doi:10.1029/2002JD003171

Legates, D. R., and Willmott C. J., 1990. Mean seasonal and spatial variability in global surface air temperature. *Theor. Appl. Climatol.*, **41**: 11-21.

Lehning, A., I. Zimmer, R. Steinbrecher, N. Broggemann, and J.-P. Schnitzler, 1999. Isoprene synthase activity and its relation to isoprene emissions in *Quercus robur* L. leaves. *Plant, Cell and Environment*, **22**:495-504

Lelieveld, J., and Crutzen P.J., 1990. Influences of cloud photochemical processes on tropospheric ozone. *Nature*, **343**:227–233.

Lelieveld, J., and Crutzen P.J., 1991. The role of clouds in tropospheric photochemistry. *J. Atmos. Chem.*, **12**:229–267, 1991.

Lelieveld, J., and F. Dentener, 2000. What controls troposheric ozone, *J. Geophys. Res.*, **105**:3531-3551

Lelieveld, J., P. Crutzen, and F.J. Dentener, 1998. Changing concentration, lifetime and climate forcing of atmospheric methane. *Tellus*, **50B**:128-150

Lelieveld, J., P. J. Crutzen, V. Ramanathan, M. O. Andreae, C. A. M. Brenninkmeijer, T. Campos, G. R. Cass, R. R. Dickerson, H. Fischer,1 J. A. de Gouw, A. Hansel, A. Jefferson, D. Kley, A. T. J. de Laat, S. Lal, M. G. Lawrence, J. M. Lobert, O. L. Mayol-Bracero, A. P. Mitra, T. Novakov, S. J. Oltmans, K. A. Prather, T. Reiner, H. Rodhe, H. A. Scheeren, D. Sikka, and J. Williams, 2002. The Indian Ocean Experiment: Widespread Air Pollution from South and Southeast Asia. *Science*, **291**:1031-1036

Lerdau, M., A. Guenther, and R. Monson, 1997, Plant production and emission of volatile organic compounds. *Bioscience*, **47**:373-383.

Lerdau, M., and H. Throop, 2000. Sources of variability in isoprene emission and photosynthesis in two species of tropical wet forest trees. *Biotropica*. **32**:670-676.

Lerdau, M.T., and M. Keller, 1997. Isoprene emission from trees in a sub-tropical dry forest. *Plant, Cell, and Environment*, **20**:569-578.

Leung, R., L. Mearns, F. Giorgi, and R. Wilby, 2003. *Regional Climate Research*, BAMS, 89-95.

Levin, Z., E. Ganor, and V. Gladstein, 1996, The effects of desert particles coated with sulfate on rain formation in the eastern Mediterranean. *J. Appl. Meteor.*, **35**:1511-1523.

Levis, S., J.A. Foley and D. Pollard, 1999: Climate-vegetation feedbacks at the Last Glacial Maximum. *J. Geophys. Res.*, **104**:31191-31198

Levy H., II, W. J. Moxim, A. A. Klonecki, and P. S. Kasibhatla, 1999. Simulated tropospheric NO_x: Its evaluation, global distribution and individual source contributions, *J. Geophys. Res.*, **104**:26,279-26,306.

Levy II, H., 1971. Normal atmosphere: Large radical and formaldehyde concentrations predicted. *Science*, **173**, 141-143.

Liang, J., and Jacob D.J., 1997. Effect of aqueous phase cloud chemistry on tropospheric ozone. *J. Geophys. Res.*, 102:5993-6001.

Li-Jones, X. and J.M. Prospero, 1998. Variations in the size distribution of non-sea-salt sulphate aerosol in the marine boundary layer at Barbados: Impact of African dust. *J. Geophys. Res.*, **103**:16073-16084.

Lindskog, A., Y. Anderssonskold, P. Grennfelt, and J. Mowrer, 1992. Concentration profiles of hydrocarbons during episodes in relation to emission pattern, model-calculations and oxidants, *J. Atmos. Chem.*, 14:425–438

Litvak M. E., F. Loreto, P.C. Harley, T.D. Sharkey and R.K. Monson, 1996. The response of isoprene emission rate and photosynthetic rate to photon flux and nitrogen supply in aspen and white oak trees. *Plant Cell Environ.*,**19**:549–559.

Liu H., J.H. Crawford, R. B. Pierce, P. Norris, S. E Platnick, G. Chen, J.A. Logan, R. M. Yantosca, M. J. Evans, C. Kittaka, Y. Feng, and X. Tie, 2006. Radiative effect of clouds on tropospheric chemistry in a global three dimensional chemical transport model. *J. Geophys. Res.* **111**: D20303, doi:10.1029/2005JD006403

Liu, H., D. J. Jacob, J. E. Dibb, A. M. Fiore, and R. M. Yantosca, 2004. Constraints on the sources of tropospheric ozone from ^{210}Pb-^{7}Be-O_3 correlations. *J. Geophys. Res.* **109**:D07306, doi:10.1029/2003JD003988, 2004

Liu, H., D.J. Jacob, I. Bey, and R. M. Yantosca, 2001. Constraints from ^{210}Pb and ^{7}Be on wet deposition and transport in a global three-dimensional chemical tracer model driven by assimilated meteorological fields. *J. Geophys. Res.*, **106**:12109-12128

Lobert, J. M., and J.M. Harris, 2002. Trace gases and air mass origin at Kaashidhoo, Indian Ocean. *J. Geophys. Res.*, 107(**D19**):8013, doi:10.1029/2001JD000731.

Lofgren, B.M., 1995. Sensitivity of land-ocean circulations, precipitation, and soil moisture to perturbed land surface albedo. *J. Clim.*, **8**:2521-2542

Logan, J.A., 1999. An analysis of ozonesonde data for the troposphere: recommendations for testing 3-D models and development of a gridded climatology for tropospheric ozone. *J. Geophys. Res.*, **104**, 16115-16149.

Loveland, T.R., B.C. Reed, J.F. Brown, D.O. Ohlen, Z. Zhu, L. Yang and J.W. Merchant, 2002. Development of a global landcover characteristics database and IGBP DISCover from 1 km AVHRR data. *Intern. J. Rem. Sens.*, 21(**6-7**):1303-1330

Luizao, F., P. A. Matson, G. Livingston, R. Luizao, and P. M. Vitousek, 1989. Nitrous oxide flux following tropical land clearing, *Global Biogeochem. Cycles*, **1**:163-170, 1989.

Lüthi, D., A. Cress, H.C. Davies, C. Frei, and C. Schär, 1996. Interannual Variability and Regional Climate Simulations. *Theor. Appl. Climatol.*, **53**:185-209 .

Manes F., M. Vitale, A. M. Fabi, F. De Santis and D. Zona, 2007. Estimates of potential ozone stomatal uptake in mature trees of *Quercus ilex* in a Mediterranean climate. *Environmental and Experimental Botany*, **59**:235-241

Marengo J.A., and Ambrizzi T., 2006. Use of regional climate models in impacts assessment and adaptations studies from continental to regional and local studies. *Proceeding of 8 ICSHMO*, Foz do Iguacu, Brazil, April 24-28, INPE, pp 291-296

Martineu, P. 2005. An assessment of the PRECIS Regional Climate Modelling System-Simulations over North America Using PRECIS. In *Research Activities in Atmospheric and Oceanic Modelling WMO/TD* by J. Cote (ed.), Report No. 35, pp 7-21

Maslanik, J.A., Lynch A.H. and Serreze M., 2000. A case study simulation of Arctic regional climate in a coupled model. *J. Climate.* **13**:383-401.

Matson, P. A., W. H. McDowell, A. R. Townsend, and P.M. Vitousek, 1999. The globalization of N deposition: ecosystem consequences in tropical environments. *Biogeochemistry*, **46**:67-83

Matsueda, H., and H. Y. Inoue, 1996. Measurements of atmospheric CO2 and CH4 using a commercial airliner from 1993 to 1994. *Atmos. Environ.* 30(**10/11**):1647-1655.

Matsueda, H., H. Y. Inoue, Y. Sawa, Y. Tsutsumi, and M. Ishi, 1998. Carbon monoxide in the upper troposphere over the western Pacific between 1993 and 1996. *J. Geophys. Res.* 103(**D15**):19093-19110.

Matsueda, H., H. Y. Inoue, M. Ishi, and Y. Tsutsumi, 1999. Large injection of carbon monoxide into the upper troposphere due to intense biomass burning in 1997. J. *Geophys. Res.* 104(**D21**):26867-26879.

Matsueda, H., S. Taguchi, H. Y. Inoue, and M. Ishi, 2002. A large impact of tropical biomass burning on CO and CO_2 in the upper troposphere. *Science in China*, **45**:116-125.

Matthew, E., 2000. Wetlands. In *Atmospheric Methane: Its Role in the Global Environment,* by Khalil, M. (Ed). Springer Verlag, New York, pp 202-233

Mauldin, R.L., S. Madronich III , S., S.J. Flocke, F.L. Eisele, G.J. Frost, and A.S.H. Prevot, 1997. New insights on OH: Measurements around and in clouds. *Geophys. Res. Lett.*, **24**:3033-3036.

McGregor, J.L., J.J. Katzfey and K.C. Nguyen, 1998. Fine resolution simulations of climate change for southeast Asia. Final report for a Research Project commissioned by Southeast Asian Regional Committee for START (SARCS), Aspendale, Vic.: CSIRO Atmospheric Research. VI, 15, 35pp.

McGregor, J.L., Katzfey J.J and Nguyen K.C., 1999. Recent regional climate modelling experiments at CSIRO. In Research Activities in Atmospheric anc Oceanic Modelling by H. Ritchie (ed.). CAS/JSC Working Group on Numerical Experimentation Report 28:WMO/TD No. 942, Geneva- WMO pg 7.37-7.38

McGuffie, K., A. Henderson-Sellers, H. Zhang, T. B. Durbridge, and A. J. Pitman, 1995. Global Climate Sensitivity to Tropical deforestation, *Global and Planetary Change,* **10**:97-128.

McIntyre, M., 1980. An introduction to the generalised Lagrangian-mean description of wave mean-flow interaction. *Pure Appl. Geophys.*, **118**:152-176

McLinden, C., S. Olsen, B. Hannegan, O. Wild, M. Prather, and J. Sundet, 2000. Stratospheric ozone in 3-D models: a simple chemistry and the cross-tropopause flux. *J. Geophys. Res.*, **105**:14653-14665.

Mearns, L. O., 2004. NARCCAP North American Regional Climate Change Assessment program A Multiple AOGCM and RCM Climate Scenario Project over North America. 12/17/2004. AGU Fall Meeting, San Francisco, USA.

Mearns, L. O., M. Hulme, T.R. Carter, R. Leemans, M. Lal, P. Whetton, L. Hay, R.N. Jones, R. Katz, T. Kittel, J. Smith, and R. Wilby, 2001. Climate scenario development, Chapter 13. In *Climate Change 2001: The Scientific Basis* by J.T. Houghton et al. (eds.), Cambridge University Press, pp 739-768

Mearns, L.O., Easterling W., Hays C., and Marx D., 1999a. Comparison of agricultural impacts of climate change calculated from high and low resolution climate model scenarios: Part 1. The uncertainty due to spatial scale. *Climatic Change*, **51**:131-172

Mearns, L.O., F. Giorgi, P. Whetton, D. Pabon, M. Hulme, and M. Lal, 2003. *Guidelines for Use of Climate Scenarios Developed from Regional Climate Model Experiments.* Final Version. DDC of IPCC TGCIA, 36 pp.

Mearns, L.O., Mavromatis T., Tsvetsinskaya E., Hays C., and Easterling W., 1999b. Comparative responses of EPIC and CERES crop models to high and low resolution climate change scenarios. *J. Geophys. Res.*, 104(**D6**):6623-6646

Menon, S., J. Hansen, L. Nazarenko and Y. Luo, 2002. Climate effects of black carbon aerosols in China and India. *Science*, **297**:2250-2253.

Mentel, T.F., D. Bleilebens, and A. Wahner, 1996. A study of nighttime nitrogen oxide oxidation in a large reaction chamber-fate of NO2, N2O5, HNO_3, and O_3 at different humidties. *Atmos. Environ.*, **30**:4007-4020.

Methven, J., M. Evans, P. Simmonds, and G. Spain, 2001. Estimating relationships between air mass origin and chemical composition, *J. Geophys. Res.*, **106**:5005–5019.

Mickley, L. J., D. J. Jacob, and D. Rind, 2002. Climatic implications of changes in tropospheric ozone. Air Pollution as a Climate Forcing Workshop, Honolulu, April 29-May 3, 2002.

Mickley, L. J., Murti, P.P., Jacob, D.J., Logan, J.A., Rind, and Koch, D., 1999. Radiative forcing from tropospheric ozone calculated with a unified chemistry-climate model, *J. Geophys. Res.*, **104**:30153-30172

Mickley, L.J., D.J. Jacob, B.D. Field, and D. Rind, 2004. Climate response to the increase in tropospheric ozone since preindustrial times: A comparison between ozone and equivalent CO_2 forcings. *J. Geophys. Res.*, **109**: D05106, doi:10.1029/2003JD003653.

Middleton, P., 1995. Sources of Air Pollution. In *Composition, Chemistry, and Climate of the Atmosphere* by H.B. Singh (Ed),. Van Nostrand Reinhold, New York, pp 88-119.

Mikkelsen, T.N., H. Ro-Poulsen, K. Pilegaard, M.F. Hovmand, N.O. Jensen, and P. Hummeshoej, 2000. Ozone uptake by an evergreen forest canopy: temporal variation and possible mechanisms. *Enviro. Pollution*, 109(**3**):423-429.

Miller, M.J., T.N. Palmer, and R. Swinbank, 1989. Parameterization and influence of sub-grid scale orography in general circulation and numerical weather prediction models. *Meteorol. Atmos. Phys.*, **40**:84-109.

Moberg, A, and Jones P.D., 2004. Regional climate model simulations of dialy maximum and minimum near-surface temperatures across Europe compared with observed station data 1961-1990. *Climate Dynamics*, **23**:695-715.

Mohamad, S. and Siew, K.Y., 1994. Land resources and landuse planning in Peninsular Malaysia. In proceedings of the workshop on soil science in Malaysia towards the year 2020 1994, (Aminuddin,B.Y, Zulkefli,M and Ghazalli, M.Z., Eds.).pp: 1-13

Monson R. K., P.C. Harley, M.E. Litvak, M. Wildermuth, A. Guenther, P.R Zimmermann and R. Fall, 1994. Environmental and developmental controls over the seasonal pattern of isoprene emission from aspen leaves. *Oecologia*, **9**: 260–270.

Monson, R.K, C.H. Jaeger, W.W. Adams, E.M. Driggers, G.M. Silver, and R. Fall, 1992. Relationships among isoprene emission rate, photosynthesis, and isoprene synthase activity as influenced by temperature. *Plant Physiol.*, **98**:1175–1180.

Monson, R.K., and E. Holland, 2001. Biospheric trace gas fluxes and their control over tropospheric chemistry. *Annual Review of Ecology and Systematics* **32**: 547-576.

Morcrette, J.J., 1991. Radiation and cloud radiative properties in the European Center for Medium Range Forecasts forecasting system. *J. Geophys. Res.*, **96**:9121-9132.

Morita T., Robinson J., Adegbulugbe A., Alcamo J., Herbert D., Lebre La Rovere E., Nakicenovic N., Pitcher H., Raskin P., Riahi K., Sankovski A., Sokolov V., de Vries B., Zhou D., Jiang K., Manders T., Matsuoka Y., Mori S., Rana A., Roehrl R. A., Rosendahl K. E., Yamaji K., 2001. Greenhouse Gas Emission Mitigation Scenarios and Implications, Chapter 2. In *Climate Change 2001: Mitigation.* Contribution of Working Group II to the Third Assessment Report of the Intergovernmnetal Panel on Climate Change by Metz B., O. Davidson, R. Swart and J.Pan (Eds.), Geneva, Switzerland. Pg 115-167

Murphy, D.M., and D.W. Fahey, 1994. An estimate of the flux of stratospheric reactive nitrogen and ozone into the troposphere. *J. Geophys. Res.*, **99**:5325-5332.

Myhre, G., F. Stordal, K. Restad, and I. S. A. Isaken, 1998. Estimation of the direct radiative forcing due to the sulfate and soot aerosols. *Tellus*, **50B**:463-477.

Naik, V., Mauzerall, D., Horowitz, L., Schwarkopf, D., Ramasamy, V., and Oppenheimer, M. 2005. Attribution of regional radiative forcing due to tropospheric ozone: A step towards climate credit from reductions in emissions of ozone precursors, *J. Geophys. Res. 110,* doi:10.1029/2005JD005908

NEAA (Netherlands Environmental Agency), 2005. Emission Database for Global Atmospheric Research (EDGAR) (*http://www.mnp.nl/edgar*)

Nejad, L. A. M., 1986. Ph.D. Thesis, University of Manchester, Manchester, UK, 1986.

Nemitz, E., P. Misztal, B. Langford, D. Oram, G. Phillips, C. di Marco, B. Davison, C.N. Hewitt and N. Cape, 2008. Fluxes and In-Canopy Gradients of Biogenic Volatile Organic Compounds Above Contrasting South East Asian Land Uses. *American Geophysical Union*, Fall Meeting 2008, abstract #A14C-07

Neue, H. 1993. Methane emission from rice fields: Wetland rice fields may make a major contribution to global warming. *BioScience* 43 (7): 466-73.

New, M.G., M. Hulme, and P.D. Jones. 1999. Representing twentieth-century space time climate variability. Part I: development of 1961-1990 mean monthly terrestrial climatology. *J. Clim* **12**:829-856

Newell, R.E., and M. J. Evans, 2000. Seasonal changes in pollutant transport to the North Pacific: the relative importance of Asian and European sources. *J. Geophys. Res. Lett.*, **27**:2509-2512

NOAA-NASA (National Oceanic and Atmospheric Administration, National Aeronautics and Space Administration), 1976. *U.S. Standard Atmosphere.* U.S. Air Force, U.S. Govt. Printing Office Washington, D.C., October.

Noguer M., Jones R.G. and Murphy J.M., 1998. Sources of systematic errors in the climatology of a nested regional climate model (RCM) over Europe. *Clim. Dyn.*, **14**:691–712.

Nordeng, T.E., 1994. *Extended versions of the convective parameterization scheme at ECMWF and their impact on the mean and transient activity of the model in the tropics*. ECMWF, Technical Memo n. 206, Reading, England, 41 pp.

Novelli, P.C., K.A. Masarie, and P.M. Lang, 1998. Distributions and recent changes in atmospheric carbon monoxide. *J. Geophys. Res.*, 103:19,015-19,033.

NRC (National Research Council), 1991. *Rethinking the O_3 Problem in Urban and Regional Air Pollution*, National Academy of Science Press, Washington, 500 pp.

NRC (National Research Council), 2003. *Understanding Climate Change Feedbacks*. The National Academy of Science Press, Washington, 152 pp.

O'Brien, K.L. 2000. Upscaling tropical deforestation: implication for climate change. *Climatic Change* **44**:311-329

Odum, J.R., T. Hoffman, F. Bowman, D. Collins, and R.C. Flagan, 1996. Gas particle partitioning and secondary organic aerosol yields. *Environ. Sci. Technol.*, **30**:2580-2585.

Ohara, T., H. Akimoto, J. Kurokawa, J., N. Horii, K. Yamaji, X. Yan and T. Hayasaka, 2007. An Asian emission inventory of anthropogenic emission sources for the period 1980–2020, *Atmos. Chem. Phys.*, 7:4419-4444.

Olivier, J.G.J., A.F. Bouwman, K.W. van der Hoek, and J.J.M. Berdowski, 1998. Global Air Emission Inventories for Anthropogenic Sources of NO_x, NH_3 and N_2O in 1990. *Environ. Poll.*, **102**:135-148.

Olson, J.S., J.A. Watts, and L.J. Allison, 1983. *Carbon in live vegetation of major world ecosystems*. ORNL-5862, Oak Ridge National Laboratory, Oak Ridge, TN.

Ordonez, C., H. Methis, M. Furger, S. henne, C. Huglin, J. Staehelin, and A. S. H. Prevot, 2005. Changes of daily surface ozone maxima in Switzerland in all seasons from 1992 to 2002 and discussion of summer 2003. *Atmos. Chem. Phys.*, 5:1187-1203

Oum, K.W., M.J. Lakin and B.J. Finlayson-Pitts, 1998. Bromine activation in the troposphere by the dark reaction of O-3 with seawater ice. *Geophys. Res. Lett.*, **25**:3923-3926.

Palmer, T.N., Shutts G.J., and Swinbank R., 1986. Alleviation of a systematic westerly bias in general circulation and numerical weather prediction models through an orographic gravity wave drag parameterisation. *Quart. J. Roy. Met. Soc.*, **112**:1001-1031.

Pan, Z., Christensen J.H., Aritt R.W., Gutwski Jr. W.J., Takle, E.S., and Otieno F., 2001. Evaluation of uncertainties in regional climate change simulations. *J. Geophys. Res.* 106(**D16**):17735-17751.

Park, J.H., M.K.W. Ko, C.H. Jackman, R.A. Plumb, J.A. Kaye and K.H. Sage, 1999. *M&M-2, NASA: Models and Measurements Intercomparison II. TM_1999_209554*, September 1999, 502 pp.

Park, R.J, J. J. Daniel, N. Kumar, and R. M. Yantosca, 2006. Regional visibility statistics in the United States: Natural and transboundary pollution influences, and implications for the Regional Haze Rule. *Atmos. Environ.* XX(xx):xxx-xxx.

Parton, W.J., D.S. Ojima, and D.S. Schimel, 1994. Environmental change in grasslands: assessment using models (review). *Climatic Change*, **28**:111-141.

Pegoraro E., A. Rey, G. Barron-Gafford, R. Monson, Y. Malhi, and R. Murthy, 2005. The interacting effects of elevated atmospheric [CO_2], drought and leaf-to-air vapour pressure deficit on ecosystem isoprene fluxes. *Oecologia,* **146**: 120–129.

Pegoraro E., A. Rey, E.G. Bobich, G. Barron-Gafford, K.A. Grieve, Y. Malhi, R. Murthy, 2004. Effect of CO2 concentration and vapour pressure deficit on isoprene emission from leaves of Populus deltoides during drought. *Functional Plant Biology* 31: 1–11.

Penner, J. E., C. C. Chuang, and K. Grant, 1998. Climate forcing by carbonaceous and sulfate aerosols, *Clim. Dyn.*, **14**:839-851.

Penner, J. E., S. Y. Zhang, M. Chin, C. C. Chuang, J. Feichter, Y. Feng, I. V. Geogdzhayev, P. Ginoux, M. Herzog, A. Higurashi, D. Koch, C. Land, U. Lohmann, M. Mishchenko, T. Nakajima, G. Pitari, B. Soden, I. Tegen, L. Stowe, 2002. A comparison of model- and satellite-derive aerosol optical depth and reflectivity. *J. Atmos. Sci.*, 59(**3**):441-460.

Penner, J.E. M. Andreae, H. Annegarn, L. Barrie, J. Feichter, D.A. Hegg, R. Leaitch, D. Murphy, J. Nganga, and G.Pitari, 2001. Aerosols, their direct and indirect effects. In Climate Change 2001: The Scientific Basis, Contribution of Working Group I to the Third Assessment Report of the Intergovernmental Panel on Climate Change (IPCC), edited by J.T. Houghton, et al. Chapter 5, pp289-348, Cambridge University Press, New York.

Penner, J.E., D.H. Lister, D.J. Griggs, D.J. Dokken and M. McFarland, 1999. *Aviation and the Global Atmosphere.* A Special Report of IPCC Working Groups I and III, Cambridge University Press, Cambridge, UK, 373 pp.

Penner, J.E., H. Eddleman, and T. Novakov, 1993. Towards the development of a global inventory of black carbon emissions, *Atmos. Environ.*, **27A**:1277-1295.

Petron, G., P. Harley, J. Greenberg, and A. Guenther, 2001. Seasonal temperature variations influence isoprene emission. *Geophys. Res. Lett.* 28(**9**):1707-1710.

Pfister, G. G., L. K. Emmons, P. G. Hess, J.-F. Lamarque, J. J. Orlando, S. Walters, A. Guenther, P. I. Palmer, and P. J. Lawrence, 2008. Contribution of isoprene to chemical budgets: A model tracer study with the NCAR CTM MOZART-4, *J. Geophys. Res.*, *113*, D05308, doi:10.1029/2007JD008948

Phadnis, M. J., H. Levy II, and W. J. Moxim, 2002. On the evolution of pollution from South and Southeast Asia during the winter-spring monsoon, *J. Geophys. Res.* 107(**D24**):4700, doi:101029/2002JD002190.

Pickering, K. E., Y. Wang, W. K. Tao, C. Price, and J.F. Mueller, 1998. Vertical distributions of lightning NO_x for use in regional and global chemical transport models, *J. Geophys. Res.*, **103,** 31,203-31,216,

Pielke, R.A. Sr., G. Marland, R.A. Betts, T.N. Chase, J. Eastman, J.O. Niles, D. Niyogi, and S. Running., 2002. The influence of land-use change and landscape dynamics on the climate system- relevance to climate change policy beyond the radiative effect of greenhouse gases. *Phil. Trans. A. Special Theme Issue,* **360,** 1705-1719

Pielke, R.A. Sr., R. Avissar, M. Rauapch, A.J. Dolman, X. Zeng and A.S.Denning, 1998. Interactions between the atmosphere and terrestrial ecosytems: influence on weather and climate. *Global Change Biology*, **4**:461-475

Pielke, R.A., Sr. Walko R.L., Steyaert L., Vidale P.L., Liston G.E. and Lyons W.A., 1999. The influence of anthropogenic landscape changes on weather in south Florida. *Mon. Wea. Rev.*, **127**: 1663-1673.

Pitman, A.J., Pitman, A.J., G.T. Narisma, R.A. Sr. Pielke, and N.J., Holbrook, 2004. The impact of land cover change on the climate of southwest Western Australia. *J. Geophys. Res.* **109**:D18109, doi:10.1029/2003JD004347

Platt, U. and G.K. Moortgat, 1999. Heterogeneous and homogeneous chemistry of reactive halogen compounds in the lower troposphere - XXIII General Assembly of the EGS. *J. Atmos. Chem.*, **34**:1-8.

Pochanart, P., J. Kreasuwun, P. Sukasem, W. Geeratithadaniyam, M.S. Tabulanon, J. Hirokawa, Y. Kajii, and H. Akimoto, 2001. Tropical tropospheric ozone observed in Thailand. *Atmos. Environ.*, **35**:2657-2668

Pochanart, P., O. Wild, and H. Akimoto, 2004a. Air Pollution Import to and Export from East Asia. In *Intercontinental Transport of Air Pollution* by A. Stohl (Ed), TheHandbook of Environmental Chemistry, Springer. Berlin. Heidelberg. New York. Hong Kong. London. Milan. Paris. Tokyo. Pp. 99-130

Pochanart, P., S. Kato, T. Katsuno, and H. Akimoto, 2004b. Eurasian continental background and regionally polluted levels of ozone and CO observed in northeast Asia, *Atmos. Environ.*, **38**:1325 – 1336.

Pocharnart P., H. Akimoto, Y. Kajii, and P. Sukasem, 2003. Carbon monoxide, regional-scale transport, and biomass burning in tropical continental Southeast Asia: Observations in rural Thailand. *J. Geophys. Res.* 108:D17, 4552 doi:10.1029/2002JD003360

Poisson, N., M. Kanakidou, P.J. Crutzen, 2000. Impact of non-methane hydrocarbons on tropospheric chemistry and the oxidizing power of the global troposphere: 3-dimensional modelling results. *Atmos. Chem.* **36**:157–230.

Polcher, J. and K. Laval, 1994. A statistical study of the regional impact of deforestation on climate in the LMD-GCM. *Climate Dynamics* **10**:205-219.

Portmann, R. W., S. Solomon, J. Fishman, J. R. Olson, J. T. Kiehl, and B. Briegleb, 1997. Radiative forcing of the Earth's climate system due to tropical tropospheric ozone production, *J. Geophys. Res.*, **102**:9409-9417.

Pöschl, U., R. von Kuhlmann, N. Poisson, and P. J. Crutzen. 2000. Development and Intercomparison of Condensed Isoprene Oxidation Mechanisms for Global Atmospheric Modeling. *J. Atmos. Chem.*, 37(**1**):29-52, doi:10.1023/A:1006391009798.

Possell M., C.N. Hewitt, and D.J. Beerling, 2005. The effects of glacial atmospheric CO2 concentrations and climate on isoprene emissions by vascular plants. *Global Change Biology*, **11**:60–69

Possell, M., J. Heath, C.N. Hewitt, E. Ayres and G. Kerstiens, 2004. Interactive effects of elevated CO2 and soil fertility on isoprene emissions from *Quercus robur*. *Glob. Change Biol.* **10**:1835–1843.

Prados, A.I., R.R. Dickerson, B.G. Doddridge, P.A. Milne, J.L. Moody and J.T. Merrill, 1999: Transport of ozone and pollutants from North America to the North Atlantic Ocean during the 1996 Atmosphere/Ocean Chemistry Experiment (AEROCE) intensive. *J. Geophys. Res.*, **104**:26219-26233.

Prather, M., and D. Jacob, 1997. A persistent imbalance in HO_x and NO_x photochemistry of the upper troposphere driven by deep tropical convection. *Geophys. Res. Lett.*, **24**:3189-3192

Prather, M., D. Enhalt, F. Deterner, R. Derwent, E. Dlugokencky, E. Holland, I. Isaksen, J. Katima, V. Kirchhoff, P. Matson, P. Midgley, and M. Wang, 2001. Atmospheric chemistry and greenhouse gases. *Chapter 4 of Climate Change 2000: The Scientific Basis* by J.T. Houghton, Y. Ding, D.J. Griggs, M. Noguer, P.J. van der Linden, X. Dai, K. Maskell and C.A. Johnson. Cambridge University Press, UK.

PRB (Population Reference Bureau), 2006. 2006 World Population Datasheet. http://www.prb.org/Publications/Datasheets/2006/2006WorldPopulationDataSheet

Prinn, R., H. Jacoby, A. Sokolov, C. Wang, X. Xiao, Z. Yang, R. Eckhaus, P. Stone, D. Ellerman, J. Melillo, J. Fitzmaurice, D. Kicklighter, G. Holian, and Y. Liu, 1999, Integrated global system model for climate policy assessment: feedbacks and sensitivity studies. *Climatic Change,* **41**:469-546.

Prinn, R.G. and R. Zander, 1999. *Long-lived Ozone Related Compounds. In Scientific Assessment of Ozone Depletion: 1998.* Global Ozone Research and Monitoring Project. Report No. 44, World Meteorological Organization, Geneva, Switzerland, pp 1.1-54.

Pugh, T.A.M, A.R. MacKenzie, C.N. Hewitt, B. Langford, P. Misztal, J. Lee, S. Moller, 2009. Atmospheric composition over a South-East Asian tropical rainforest: Goodness-of–fit of an optimized model. *Submitted*

Purves, D.W., Caspersen J.P., Moorcroft P.R., Hurtt G.C., and Pacala S.W. 2004. Human-induced changes in U.S. Biogenic VOC emissions: evidence from long-term forest inventory data. *Global Change Biology*, **10**:1-19

Qian, Y., and F. Giorgi, 2000. Regional climatic effects of anthropogenic aerosols? The case of Southwestern China. *Geo. Res. Lett.*, **27**:3521-3524

Querol, X., J.L. Fernandez-Turiel, and A. Lopez-Soler, 1995. Trace element in coal and their behaviour during combustion in large power station. *Fuel*, **74**:331-343

Ramanathan, V., P. J. Crutzen, J. T. Kiehl, and D. Rosenfeld, 2001. Aerosols, climate, and the hydrological cycle. *Science*, **294**:2119-2124.

Ramaswamy V., O. Boucher, J. Haigh, D. Hauglustaine, J. Haywood, G. Myhre, T. Nakajima, G.Y. Shi, S. Solomon, R. Betts, R. Charlson, C. Chuang, J. S. Daniel, A. Del Genio, R. van Dorland, J. Feichter, J. Fuglestvedt, P. M. de F. Forster, S.J. Chan, A. Jones, J.T. Kiehl, D. Koch, C. Land, J. lean, U. Lohmann, K. Minschwaner, S.E Schwartz, M. D. Schwarzkopf, K. P. Shine, S. Smith, D. S. Stevenson, F. Stordal, I. Tegen, and Y. Zhang, 2001. Radiative forcing of climate change. In *Climate Change 2001: The Scientific Basis*, IPCC Report, J. T. Houghton, Y. Ding, D. J. griggs, m. Noguer, P. J. van Linden, X. dai, K. Maskell, and C. A. Johnson (Eds), Cambridge University Press, Cambridge, pp 351-416

Rao, S.T., J. Y. Ku, S, Berman, D. Zhang, and H. Mao, 2003. Summertime characteristics of the atmospheric boundary layer and relationships to ozone levels over the eastern United States. *Pure Appl. Geophys.*, **160**:21-55.

Rappenglucka, B., R. Schmitza, M. Bauerfeinda, F. Cereceda-Balicb, D. von Baerc, H. Jorquerad, Y. Silvae, and P. Oyolaf, 2005. An urban photochemistry study in Santiago de Chile. *Atmos. Environ.* **39**: 2913–2931.

Ravishankara, A.R. and S. Liu, 2003. Highlight from the Joint SPARC-IGAC Workshop on Climate-Chemistry Interaction. SPARC Newsletter 21, July 2003.

Read K.A, A. S. Mahajan, L. J. Carpenter, M.J. Evans, B.V.E. Faria, D.E. Heard, J.R. Hopkins, J.D. Lee, S. J. Moller, A.C. Lewis, L. Mendes, J. B. McQuaid, H. Oetjen, A. Saiz-Lopez, M. J. Pilling, and J. M. C. Plane, 2008. Extensive halogen-mediated ozone destruction over the tropical Atlantic Ocean, *Nature,* **453**:1232-1235

Reichardt, J., A. Ansmann, M. Serwazi, C. Weitkamp, and W. Michaelis, 1996. Unexpectedly low ozone concentration in mid latitude tropospheric ice clouds: A case study. *Geophys. Res. Lett.* **23**:1929-1932

Ritter, M. E., 2006. The Physical Environment: An Introduction to Physical Geography. http://www.uwsp.edu/geo/faculty/ritter/geog101/textbook/title_page.html

Rodhe, H. 1999. Modeling. In *Atmospheric Chemistry and Global Change* by G. P. Brasseur et al. (Eds.), Oxford University Press, New York, Oxford, pp 423-463.

Roeckner, E., 1995. *Parameterization of cloud radiative properties in the ECHAM4 model.* In Proceedings of the WCRP Workshop: cloud microphysics parameterizations in global circulation models, WCRP Report n. 93, WMO/TD-no **713**:105-116.

Roelofs, G. J. and J. S. Lelieveld, 1997. Model study of cross-tropopause O_3 transport on tropospheric O_3 level, *Tellus*, **49B**:38-55

Rosenfeld, D., 1999. TRMM observed first direct evidence of smoke from forest fires inhibiting rainfall. *Geophys. Res. Lett.*, 26:3105-3108

Rosenfeld, D., 2000. Suppression of rain and snow by urban and industrial air pollution. *Science*, **287**:1793-1796

Rosenstiel T.N., M.J. Potosnak, K.L. Griffin, R. Fall, and R.K. Monson, 2003. Increased CO2 uncouples growth from isoprene emission in an agriforest ecosystem. *Nature*, **421**:256–259

Rummukainen M., Räisänen J., Bringfelt B., Ullerstig A., Omstedt. A, Willén U., and Hansson U., 2001. A regional climate model for northern Europe—model description and results from the downscaling of two GCM control simulations. *Clim. Dyn*, **17**:339–359.

Russell, A., 1997. Regional photochemical air quality modeling: Model formulations, history, and state of the science, *Annu. Rev. Energy Environ.* **22**: 537-588

Ryder, J. 2005. Modelling Tropospheric Chemistry in South-east Asia. MSc Thesis. University of Lancaster, UK.

Sadanaga, Y., J. Matsumoto, and Y. Kajii, 2003. Photochemical reactions in the rban air: Recent understandings of radical chemistry. *Journal Photochemistry and Photobiology*, **4**:85-104.

Sander, R., and P. J. Crutzen, 1996. Model study indicating halogen activation and ozone destruction in polluted air masses transported to the sea. *J. Geophys. Res.*, **101**:9121 – 9138.

Sanderson, M. G., C.D. Jones, W.J. Collins, C.E. Johnson and R.G. Derwent, 2003. Effect of climate change on isoprene emissions and surface ozone levels. *Geophys. Res. Lett.* **30**, 18. doi:10.1029/2003GL017642

Sanhueza, E., L. Donoso, M. Santana, E. Fernández, J. Romero, 1999. Atmospheric chemistry over the Auyantepuy (5° 46' N; 62° 30' W; 2100 meters a.s.l.). *Interciencia,* **24**: 372-380.

Santer, B. D., T. M. L., Wigley, J. E. Penner, P. D. Jones, and U. Cubash, 1995. Towards the detection and attribution of an anthropogenic effect on climate. *Climate Dynamics*, **12**:77-100

Sasaki, K, K. Ohara, and K. Yazaki, 2005. Gene expression and characterization of isoprene synthase from *Populus alba*. FEBS Letter, 579(**11**):2514-2518.

Saunders, S. M., M. E. Jenkin, R. G. Derwent, and M. J. Pilling, 1997. World Wide Web site of a Master Chemical Mechanism (MCM) for use in tropospheric chemistry models. *Atmos. Environ.*, **31**:1249.

Schade G. W., and A. H. Goldstein, 2001: Fluxes of oxygenated volatile organic compounds from a ponderosa pine plantation. *J. Geophys. Res*, **106**:3111–3123.

Scholes, M. and M.O. Andreae, 2000. Biogenic and pyrogenic emissions from Africa and their impact on the global atmosphere. *Ambio*, **29**:23-29

Schumann, U. and H. Huntrieser, 2007. The global lightning-induced nitrogen oxides source. *Atmos. Chem. and Phys.*, 7:3823 – 3907

Schwender J., J. Zeidler, R. Gröner, C. Müller, M. Focke, S. Braun, F.W. Lichtenthaler, and H.K. Lichtenthaler, 1997. Incorporation of 1-deoxy-D-xylulose into isoprene and phytol by higher plants and algae. *FEBS Letters*, **414**:129-134.

Seinfeld, J.H., and J.F. Pankow, 2003. Organic atmospheric particulate material. *Annu. Rev. Phys. Chem.*, **54**:121-140.

Seinfeld, J.H., and S.N. Pandis, 1998. Atmospheric chemistry and physics: From air pollution to climate change. John Wiley, New York, 1326 pp

Sharkey T. D. and F. Loreto, 1993. Water stress, temperature, and light effects on the capacity for isoprene emissions and photosynthesis of kudzu leaves. *Oecologia*, **95**:328–333.

Sharkey, T. D., X. Chen and S. Yeh, 2001. Isoprene Increases Thermotolerance of Fosmidomycin-Fed Leaves, *Plant Physiol.*, **125**:2001-2006

Sharkey, T.D. and E.L. Singsaas, 1995. Why plants emit isoprene. *Nature,* **374**: 769

Shim, C., Y. Wang, Y. Choi, P.I. Palmer, D. S. Abbot, and K. Chance, 2005. Constraining global isoprene emissions with Global Ozone Monitoring Experiment (GOME) formaldehyde column measurements. *J. Geophys. Res.*, 110: D24301, doi:10.1029/2004JD005629.

Shine, K.P. and P.M. de F. Forster, 1999: The effects of human activity on radiative forcing of climate change: a review of recent developments. *Global and Planetary Change*, **20**:205-225.

Siegert, F., Ruecker, G., Hinrichs, A. & Hoffmann, A.A., 2001. Increased damage from fires in logged forest during droughts caused by El Niño. *Nature*, **414**:437–440.

Sillman, S. 1999. The relation between ozone, NOx, and hydrocarbons in urban and polluted rural environments. *Atmos. Enviro.*, 33(**12**):1821-1846

Silver, G.M, and R. Fall, 1995. Characterization of aspen isoprene synthase, an enzyme responsible for leaf isoprene emission to the atmosphere. *J. Biol. Chem.*, **270**:13010–13016.

Singh A.P., C.K. Varshney and U.K. Singh, 2007. Seasonal Variations in Isoprene Emission from Tropical Deciduos Tree Species. *Environ. Mont. Assess.*, **131**:231-235

Singh, A., S.M. Sarin, P. Shanmugan, and N. Sharma. 1997. Ozone distribution in the urban environment of Delhi during winter months. *Atmos. Environ.*, 31(**20**):3421-3427

Singh, H., 1999. Carbon-Containing Compounds. In *Atmospheric Chemistry and Global Change* by G. P. Brasseur et al. (Eds). Oxford University Press, New York Oxford, pp 325-347.

Singsaas, E.L, M.M. Laporte, J-Z. Shi, R.K. Monson, D.R. Bowling, K. Johnson, M. Lerdau, A. Jasentuliyana and T.D. Sharkey, 1999. Leaf temperature fluctuation affects isoprene emission from red oak (Quercus rubra) leaves. *Tree Physiol.*, **19**:917–924.

Smith R.N.B., 1996. Subsurface, surface and boundary layer processes. Unified Model Documentation Paper No. 24. Version 2. Climate Research, Meteorological Office, Bracknell, Berkshire, UK , pg 1-54

Smith, R. N. B., Gregory, D., Mitchell, F. F. B., Bushell A. C. B., and Wilson, D.R., 1998. Large-Scale Precipitation. Unified Model Documentation Paper No. 26. Version 5. Climate Research, Meteorological Office, Bracknell, Berkshire, UK , pg 1-13

Smith, R.N.B., 1990. A scheme for predicting layer clouds and their water content in a general circulation model. *Q. J. R. Meteorol. Soc.* **116**:435-460

Sokolov, A.P., C.A. Schlosser, S. Dutkiewicz, S. Paltsev, D.W. Kicklighter, H.D. Jacoby, R.G. Prinn, C.E. Forest, J. Reilly, C. Wang, B. Felzer, M.C. Sarofim, J. Scott, P.H. Stone, J.M. Melillo, and J. Cohen, 2005. *The MIT Integrated Global System Model (IGSM) Version 2: Model Description and Baseline Evaluation.* Report 124, MIT Joint Program on the Science and Policy of Global Change, 40 pp. (*http://mit.edu/globalchange/www/MITJPSPGC_Rpt122.pdf*).

Staudt, A. C., D. J. Jacob, J. A. Logan, D. Bachiochi, T. N. Krishnamurti, and G. W. Sachse, 2001. Continental sources, transoceanic transport, and interhemispheric exchange of carbon monoxide over the Pacific, *J. Geophys. Res.*, **106**: 32,571-32,589.

Stavrakou T., J.F. Müller, I. De Smedt, M. Van Roozendael, G. R. van der Werf, L. Giglio and A. Guenther, 2009. Evaluating the performance of pyrogenic and biogenic emission inventories against one decade of space-based formaldehyde columns. *Atmos. Chem. Phys.*, 9:1037–1060.

Steiner, A., C. Luo, Y. Huang, and W.L. Chameides, 2002. Past and present day biogenic volatile organic compound emissions in East Asia. *Atmos. Environ.*, 36(**31**):4895–4905

Stensrud, D.J., 2007. *Parameterization schemes : keys to understanding numerical weather prediction models.* Cambridge University Press, 459 pp.

Stevenson, D. S., C. E. Johnson, W. J. Collins, and R. G. Derwent, 1997. The impact of aircraft nitrogen oxide emissions on tropospheric ozone studied with a 3D Lagrangian model including fully diurnal chemistry. *Atmos. Environ.*, **31**:1837-1850

Stevenson, D. S., C. E. Johnson, W. J. Collins, R. G. Derwent, and J. M. Edwards, 2000. Future tropospheric ozone radiative forcing and methane turnover—The impact of climate change. *Geophys. Res. Lett.*, **27**: 2073 – 2076.

Stevenson, D., Doherty R., Sanderson M., Johnson C., Collins B., and Derwent D., 2005. Impacts of climate change and variability on tropospheric ozone and its precursors. *Faraday Discuss.*, **130**:1-17

Stewart, D.J., C. M. Taylor, C. E. Reeves, and J. B. McQuaid, 2007.Biogenic emissions of NO_x from recently wetted soils over West Africa observed during the AMMA 2006 campaign. *Atmos. Chem. Phys. Discuss.*, **7**:16253–16282

Stibig, H.-J., and J.P. Malingreau, 2003. Forest cover of insular southeast Asia mapped from recent satellite images of coarse spatial resolution. *Ambio*, 32(**7**):469-475

Stockwell, W.R., 1995. On the HO_2-HO_2 reaction-its misapplication in atmospheric chemistry models. *J. Geophys. Res.*, **100**:11695-11698

Stohlgren, T.J., T.N. Chase, R.A. Sr. Pielke, T.G.F. Kittel, and J.S. Baron, 1998. Evidence that local land use practices influence regional climate, vegetation, and stream flow patterns in adjacent natural areas. *Global Change Biology*, **4**:495-504.

Stone, M.C., Hotchkiss R.H., and Mearns L.O., 2003. Water yield responses to hih and low spatial resolution climate change scenarios in the Missouri River Basin Water Yield. *Geophys. Res. Lett.*, **30**:1186-1189.

Stone, M.C., Hotchkiss R.H., Hubbard C.M., Fontaine T.A., Mearns L.O., Arnold J.G., 2001. Impacts of climate change on Missouri River Basin Water Yield. *J. of American Water Resources Association*, 37(**5**):1119-1130

Streets, D. G., T. C. Bond, G. R. Carmichael, S. D. Fernandes, Q. Fu, D. He, Z. Klimont, S. M. Nelson, N. Y. Tsai, M. Q. Wang, J-H. Woo, and K. F. Yarber, 2003a. An inventory of gaseous and primary aerosol emissions in Asia in the year 2000, *J. Geophys. Res.*,108(**D21**):8809, doi:10.1029/2002JD003093.

Streets, D. G., and S.T. Waldhoff, 1999. Greenhouse-gas emissions from biofuel combustion in Asia, *Energy*, **24**:841-855

Streets, D. G., G. R. Carmicheal, M. Amann, R. l. Amdt, 1999. Energy consumption and acid deposition in Asia, *Ambio*, **28**:135-143.

Streets, D.G., K.F. Yaber, J.-H. Woo, and G.R. Carmicheal, 2003b. Biomass burning in Asia: Annual and seasonal estimates and atmospheric emissions. *Global Biogeochem. Cycles*., 17(**4**):1099, doi: 10.1029/2003GB002040.

Stroud, C., P.A. Makar, T. Karl, A. Guenther, C. Geron, A.A. Turnipseed, E. Nemitz, B. Baker, M. Potosnak, J.D. Fuentes, H. McCarthy and R. Oren, 2005. Role of Canopy-Scale Photochemistry in Modifying Biogenic-Atmosphere Exchange of Reactive Terpene Species: Results from the CELTIC Field Study, *J. Geophys. Res.-Atmos.*, **110**: D17303, doi:10.1029/2005JD005775.

Sudo, K., M. Takahashi, 2001. Simulation of tropospheric ozone changes during 1997-1998 El Nino: Meteorological impact on tropospheric photochemistry, *Geophys. Res. Lett.* 28(**21**):4091-4094, 10.1029/2001GL013335.

Suprapto, A., 2002. Land and water resources development in Indonesia. In *Investment in land and water* by FAO, RAP Publication 2002/09, FAO, Bangkok, pp 233-242.

Takemura, T., T. Nozawa, S. Emori, T. Y. Nakajima, and T. Nakajima, 2005. Simulation of climate response to aerosol direct and indirect effects with aerosol transport-radiation model *J. Geophys. Res.*, **110**:5D02202, doi:10.1029/2004JD005029.

Tan, Q., Y. Huang, W. L. Chameides, 2002. The Budget and Export of Anthropogenic SOx From East Asia During Continental Outflow Conditions, *J. Geophys. Res.*, 107(**D13**): 4167, doi 10.1029/2001JD000769.

Tang, Y., G. R. Carmicheal, I. Uno, J. H. Woo, G. Kurata, B. Lefer, R. Shetter, H. Huang, B. E. Anderson, M. A. Avery, A. D. Clarke, and D. R. Blake, 2003. Impacts of aerosols and clouds on photolysis frequencies and photochemistry during TRACE-P:2. Three-dimensional study using a regional chemical transport model. *J. Geophys. Res.*, **108**: 8822, doi:10.1029/2002JD003100

Taylor, V. R., and Stowe L.L., 1984. Reflectance characteristics of uniform Earth and cloud surfaces derived from Nimbus-7 ERB, *J. Geophys. Res.*, **89**:4987–4996

Thompson A.M., K. E. Pickering, D. P. McNamara, M. R. Schoeberl, R. D. Hudson, J. H. Kim, E. V. Browell, V. W. J. H. Kirchhoff, and D. Nganga D, 1996. Where did tropospheric ozone over southern Africa and the tropical Atlantic come from in October 1992? Insights from TOMS, GTE TRACE-A and SAFARI 1992, *J. Geophys. Res.*, **101**:24,251-24,278

Thompson, A. M., 1992. The oxidizing capacity of the Earth's atmosphere. Probable past and future changes. *Science*, **256**:1157-1165

Thompson, A. M., J. C. Witte, R. D. Hudson, H. Guo, J. R. Herman, and M. Fujiwara, 2001. Tropical tropopsheric ozone and biomass burning, *Science*, **291**: 2128-2132.

Tie, X., S. Chandra, J. R. Ziemke, C. Granier, and G. P. Brasseur, 2006. Satellite measurements of tropospheric column O3 and NO2 in eastern and southeastern Asia: Comparison with a global model (MOZART-2), *J. Atmos. Chem.*, doi:10.1007/S10874-006-9045-7.

Tiedke, M., 1989. A comprehensive mass flux scheme for cumulus parameterization in large-scale models. *Mon. Wea. Rev.*, **117**:1779-1800.

Titus, J.G., 2005. Greenhouse gas and global Warming. In: *Encyclopedia of Coastal Science* by M. L. Schwartz (Ed.), Springer. pg 493-502

Trainer, M., E. Y. Hsie, S. A. McKeen, R. Tallamraju, D. D. Parrish, F. C. Fehsenfeld, and S. C. Liu, 1987. Impact of natural hydrocarbons on hydroxyl and peroxy-radicals at a remote site, *J. Geophys. Res.*, **92**:11,879–11,894.

Tuovinen, J.-P, 2000. Assessing vegetation exposure to ozone: properties of the AOT40 index and modifications by deposition modeling. *Enviro. Pollution*, **109**:361-372.

Turco, R.P., 1999. Aerosols and Clouds. In *Atmospheric Chemistry and Global Change* by G. P. Brasseur et al. (Eds). Oxford University Press, New York Oxford, pp 117-157.

Turner, D.P., J.V. Baglio, A.G. Wones, D. Pross, R. Vong, B.D. McVeety and D.L. Phillips, 1991. Climate change and isoprene emissions from vegetation, *Chemosphere*, 23 (**1**):37-56.

Turnock, S., 2008. The Influence of Climate Change on Tropospheric Ozone and Air Quality in Southeast Asia. Master Thesis. Lancaster University, 54 pp.

Ueda, H., A. Iwai, K. Kuwako, and M.E. Hori, 2006. Impact of anthropogenic forcing on the Asian summer monsoon as simulated by 8 GCMs. *Geophys. Res. Lett*, **33**: L06703, doi:10.1029/2005GL025336.

UNCSD (United Nations Commission on Sustainable Development), 1997. National Implementation of Agenda21: Review of progesss made since the United Nations conference on environment and development 1992. Malaysia Country Profile. http://www.un.org/esa/earthsummits/malay_cp.htm#chap10

UNDP, 1995. Environment and natural resource management. Strategy and action plan for UNDP Vietnam. 2nd edition.

UNEP (United Nations Environemntal Programme), 2000. Global Environmental Outlook 2000 (GEO2000). http://www.unep.org/geo2000/english/ index .htm

Uppala, S.M., Kållberg, P.W., Simmons, A.J., Andrae, U., da Costa Bechtold, V., Fiorino, M., Gibson, J.K., Haseler, J., Hernandez, A., Kelly, G.A., Li, X., Onogi, K., Saarinen, S., Sokka, N., Allan, R.P., Andersson, E., Arpe, K., Balmaseda, M.A., Beljaars, A.C.M., van de Berg, L., Bidlot, J., Bormann, N., Caires, S., Chevallier, F., Dethof, A., Dragosavac, M., Fisher, M., Fuentes, M., Hagemann, S., Hólm, E., Hoskins, B.J., Isaksen, L., Janssen, P.A.E.M., Jenne, R., McNally, A.P., Mahfouf, J.-F., Morcrette, J.-J., Rayner, N.A., Saunders, R.W., Simon, P., Sterl, A., Trenberth, K.E., Untch, A., Vasiljevic, D., Viterbo, P., and Woollen, J. 2005: The ERA-40 re-analysis. *Quart. J. R. Meteorol. Soc.*, **131**:2961-3012, doi:10.1256/qj.04.176

USEPA, 2002. Greenhouse Gases and Global Warming Potential Values. Excerpt from the inventory of US Greenhouse Emissions and Sinks:1990-2000. pp 16

van Aardenne, J. A. , G. R. Carmichael, H. Levy II, D. Streets, and L. Hordijk, 1999. Anthropogenic NOx emissions in Asia in the period 1990 – 2020. *Atmos. Environ.*, **33**:633-646.

van den Pol van Dasselaar, A., M. L. Van Beusichem, and O. Oenema, 1999. Methane emissions from wet grasslands on peat soil in a nature preserve. *Biogeochemistry*, **49**:205-220.

van der Molen, M.K. A.J. Dolman, M.J. Waterloo, L.A. Bruijnzeel, 2006. Climate is affected more by maritime than by continental land use change: A multiple scale analysis. *Global and Planetary Change*, **54**:128-149.

van Dorland, R., F.J. Dentener, and J. Lelieveld, 1997: Radiative forcing due to tropospheric ozone and sulfate aerosols. *J. Geophys. Res.*, **102**:28079-28100.

Velikova V, P. Pinelli, S. Pasqualini, L. Reale, F. Ferranti, and F. Loreto, 2005. Isoprene decreases the concentration of nitric oxide in leaves exposed to elevated ozone. *New Phytol* **166**: 419–426.

Vidale, P.L., D. Lüthi, C. Frei, S. Seneviratne, and C. Schär, 2003. Predictability and uncertainty in a regional climate model. *J. Geophys. Res.*, 108**(D18)**:4586, doi: 10.1029/2002JD002810.

Villanueva-Fierro, I., C.J. Popp and R.S. Martin, 2001. Biogenic emissions and ambient concentrations of hydrocarbons, carbonyl compounds and organic acids from ponderosa pine and cottonwood trees at rural and forested sites in Central New Mexico. *Atmos. Environ.*, 2:249-260.

Vizuete, W., V. Junquera, E. McDonald-Buller, G. McGaughey, G. Yarwood and D. Allen, 2002. Effects of temperature and land use on predictions of biogenic emissions in Eastern Texas, USA, *Atmos. Environ.* **36**:3321–3337.

Vogt, R., R. Sander, R. von Glasow, and P.J. Crutzen, 1999. Iodine chemistry and its role in halogen activation and ozone loss in the marine boundary layer: A model study. *J. Atmos. Chem.* **32:** 375–395.

Volk, C.M., J.W. Elkins, D.W. Fahey, G.S. Dutton, J.M. Gilligan, M. Lowenstein, J.R. Podolske, K.R. Chan, and M.R. Gunson, 1997. Evaluation of source gas lifetimes from stratospheric observations. *J. Geophys. Res.*, **102**:25543-25564.

von Kuhlmann R., Lawrence M.G., Poschl U., and Crutzen P.J. 2004. Sensitivitoes in global scale modelling of isoprene. *Atmos Chem. Phys.*, **4**:1-17.

von Kuhlmann, R. 2001. Tropospheric Photochemistry of Ozone, its Precursors and the Hydroxyl Radical: A 3D-Modeling Study Considering Non-Methane Hydrocarbons. PhD Dissertation, University of Johannes Gutenberg, Mainz, Germany (unpublished).

von Storch, H. and A. Navarra. *Analysis of Climate Variability.Applications of statistical techniques*. Springer, Berlin Heildelberg New York Barcelona Budapest Hong Kong London Milan Paris Tokyo , pp 334.

Voss, R., W. May, and E. Roeckner, 2002. Enhanced resolution modelling study on anthropogenic climate change: changes in exteremes of the hydrological cycle. *Int. J. Climatology,* **22**:755-777.

Wang, C., and R.G. Prinn, 1999. Impact of emissions, chemistry and climate on atmospheric carbon monoxide: 100-year predictions from a global chemistry-climate model. *Chemosphere-Global Change Sci.*, 1(**1–3**):73–81.

Wang, K.Y. and Shallcross, D.E., 2005. Simulation of the Taiwan climate using the Hadley Centre PRECIS regional climate modelling system: The 1979-1981 results. *Terr. Atmos. Ocean. Sciences*,16(**5**):1017-1043.

Wang, Q.J., Nathan R.J., Moran R.J., and James B., 1999. Impact of Climate Changes on the Security of the Water Supply of the Campaspe System. Proceedings of the 25th Hydrology and Water Resources Symposium, Vol. 1, 6-8 July, Brisbane, Institution of Engineers, Australia, Water99 Joint Congress, pp 135-140.

Wang, W.C., Pinto, J.P. and Yung, Y.L. 1980. Climatic effects due to halogenated compounds in the Earth's atmosphere. *J. Atmos. Sci.* **37**;333-338.

Wang, W.C., Zhuang, Y.C., and Bojkov, R.D., 1993. Climate implicatios of observed changes in O_3 vertical distributions at middle and high latitudes of the Northern Hemisphere. *Geophys. Res. Letter.*, **20**:1567-1570

Wang, Y., D. J. Jacob, and J. A. Logan, 1998. Global simulation of tropospheric O_3 - NO_x-hydrocarbon chemistry, 1. Model formulation. *J. Geophys. Res.*, 103(**10**):10727-10755.

Wang, Y.X., McElroy, M.B., Jacob, D.J., and Yantosca, R.M., 2004. A nested grid formulation for chemical transport over Asia: Application to CO, *J. Geophys. Res.*, **109**:D22307 doi:10.1029/2004JD005237

Wanner, H., Rickli R., Salvisberg E., Schmutz C. and Schepp M. , 1997. Global climate change and variability and its influence on Alpine climate – concepts and observations. *Theor. Appl. Climatol.*, **58**:221–243.

Watson, L. A., K-Y. Wang, H. Paul and D. Shallcross, 2006. The potential impact of biogenic emissions of isoprene on urban chemistry in the United Kingdom. *Atmospheric Science Letters*, 7(**4**):96-100.

Wayne R.P., I. Barnes, P. Biggs, J. P. Burrows, C. E. Canosa-Mas, J. Hjorth, G. Le Brasshort, G. K. Moortgat, D. Perner, G. Pouletshort, G. Restelli and H. Sidebottom, 1991. The nitrate radical: physics, chemistry, and the atmosphere. *Atmos. Enviro. Part A (General Topics)*, 25A(**1**):1-203.

Wayne, R.P., 2000. *Chemistry of Atmosphere. An introduction to the chemistry of the atmosphere of Earth, the planets and their satellites.* Oxford University Press. 3rd Edition. pp 775.

Wesley, M.L., and B.B. Hicks, 2000. Review of the current status of knowledge on dry deposition. *Atmos. Environ.*, **34**:2261-2281.

Whetton, P., 1994: Constructing climate scenarios: the practice. In: *Climate Impact Assessment Methods for Asia and the Pacific* by Jakeman, A.J. and A.B. Pittock (eds.). Proceedings of a regional symposium, organised by ANUTECH Pty. Ltd. on behalf of the Australian International Development Assistance Bureau 10-12 March 1993, Canberra, Australia, pp. 21-27.

Wiedinmyer, C., A. Guenther, P. Harley, N. Hewitt, C. Geron, P. Artaxo, R. Steinbrecher, and R. Rasmussen, 2004. Global organic emissions from vegetation. In *Emissions of Atmospheric Trace Compounds* by C. Granier et al. (Eds). Kluwer Academic Publishers, Dodrecht/Boston/London, pp115-170.

Wiedinmyer, C., X. Tie, A. Guenther, R. Neilson and C. Granier, 2006. Future changes in biogenic isoprene emissions: How might they affect regional and global atmospheric chemistry?, *Earth Interactions*, **10**:1–19.

Wilby, R.L., and Wigley T.M.L., 1997. Downscaling general circulation model output: a review of methods and limitations. *Prog. Phys. Geography*, **21**:530-540.

Wild, J. O. F., 1995. *Some problems in the numerical modelling of tropospheric chemistry*, Ph.D. Thesis, University of Cambridge, Cambridge, UK.

Wild, J. O. F., 1996. *Cambridge Tropospheric Trajectory Model.* University of Cambridge, Cambridge, UK, 66 pp.

Wild, O. and M. J. Prather, 2000. Excitation of the primary tropospheric chemical mode in a global CTM, *J. Geophys. Res.* **105**:24647-24660.

Wild, O. Law, K.S., McKenna, D.S., Bandy, B.J., Penkett, S.A, Pyle, J.A., 1996. Photochemical trajectory modelling studies of the North Atlanctic region August 1993. *J. Geophys. Res.*,**101**: 29269-29288.

Wild, O., and Akimoto, H., 2001. Intercontinental transport of ozone and its precursors in a three-dimensional global CTM, *J. Geophys. Res.*, **106**:27729-27744.

Williamson, D. L. and P. J. Rasch, 1994. Water vapour transport in the NCAR CCM2. *Tellus* **46A**:34-51.

Wilson, C. A. and Swinbank, R., 1996. Gravity Wave Drag. Unified Model Documentation Paper No. 22. Version 2.3. Numerical Weather Prediction Research, Meteorological Office, Bracknell, Berkshire, UK , pg 1-5.

Wilson, D.R. and Ballard, S.P., 1999: A microphysically based precipitation scheme for the Meteorological Office Unified Model. *Quart. J. Royal Meteorol. Soc.*, **125**: 1607-1636.

Wilson, M.F. and A. Henderson-Sellers, 1985. A global archive of land cover and soils data for use in general circulation climate models. *J. of Climatol.*, **5**:119-143.

Wilson, S., Hassell, D., Hein, D., Jones, R., and Taylor, R. 2005. *Installing and using Hadley Centre regional climate modelling system*, PRECIS. Ver 1.3.

WMO (World Meteorological Organisation), 1985. *Atmospheric Ozone 1985: Assessment of our understanding of the processes controlling its present distribution and change.* Global Ozone Research and Monitoring Project, Report 16.

WMO (World Meteorological Organisation), 2006. The state of greenhouse gases in atmosphere using Global Observations through 2005. No.2 , 1 November 2006.

Woodage, M., L. Robinson, and D.L. T. Roberts, 2001. Aerosol processes –sulphur cycle and soot aerosol scheme, Version 1, Model Version 4.5. UMDP No. 20. Climate Research Meteorological Office, UK. Pp 20.

Worthy, D., I. Levin, F. Hopper, M. Ernst, and N. Trevett, 2000. Evidence for a link between climate and northern wetland methane emissions. *J. Geophys. Res.* **105**:4031-4038.

Wotton, B.M., Stocks B.J., Flannigan M.D., Laprise R., and Blanchet J.P., 1998. Estimating future 2 x CO_2 fire climates in the boreal forest of Canada using a regional climate model. In: *Proceeding of Third International Conference on Forest Fire Research and the 14th Conference in Fire and Forest Meteorology.* University of Coimbra Portugal, pp 1207-1221.

WRI (World Resources Institute), 1994. World Resources 1994-1995: *A guide to the global environment.* Oxford University Press.

Wu, J., W. Jiang, C. Fu, B. Su, H. Liu, and J. Tang, 2004. Simulation of the radiative effect of black carbon aerosols and the regional climate response over China. *Adv. Atmos. Sci.*, **21**:637 – 649.

Wuebbles, D. J. and K. Hayhoe, 2002. Atmospheric methane and global change. *Earth-Science Reviews*, **57**:177-210.
www.climate.noa.gr/Miscellaneous/pdf/precis_brochure_eng.pdf

Yasunari, T. 2007. Role of land-atmosphere interaction on Asian Monsoon climate. *Journal of the Meteorological Society of Japan*, **85B**:55-75.

Yasunari, T, K. Saito, and K. Takata, 2006. Relative roles of large-scale orography and land surface processes on global hydro-climate. Part I. Impacts on monsoon systems and tropics. *J. Hydrometeor.* **7**:626-641.

Yienger, J.J. and H. Levy II, 1995: Empirical model of global soil-biogenic NO_x emissions. *J. Geophys. Res.*, **100**:11447-11464.

Yonemura, S., H. Tsuruta, S. Kawashima, S. Sudo, L.C. Peng, L.S. Fook, Z. Johar, and M. Hayashi. 2002a. Tropospheric ozone climatology over Peninsula Malaysia from 1992 to 1999. *J. Geophy. Res.* **107**, 10.1029/2001JD000993.

Yonemura, S., H. Tsuruta, T. Maeda, S. Kawashima, S. Sudo, and M. Hayashi. 2002b. Tropospheric ozone variability over Singapore from august 1996 to December 1999. *Atmos. Enviro.* **36**:2061-2070.

Young, P. J.., A. Arneth, G. Schurgers, G. Zeng and J. A. Pyle, 2009. The CO2 inhibition of terrestrial isoprene emission significantly affects future ozone projections. *Atmos. Chem. Phys.*, **9**: 2793–2803.

Yu J-.Y. and C.R. Mechoso, 1999. A discussion on the errors in the surface heat fluxes simulated by a coupled GCM. *J. Climate*, **12**:416-426.

Yu, H., R. E. Dickinson, M. Chin, Y.J. Kaufman, M. Zhou, L. Zhou, Y. Tian, O. Dubovik, and B. N. Holben, 2004. The direct radiative effect of aerosols as determined from a combination of MODIS retrievals and GOCART simulations. *J. Geophys. Res.*, **109**:D03206, doi:10.1029/2003JD003914.

Yu, J.-Y, 2004. Identification and applications of coupled climate models. In *Environmental Systems by Achim Sydow* (Ed.), *in Encyclopedia of the Life Support Systems (EOLSS)*, Developed under the Auspices of the UNESCO, Eolss Publisers, Oxford. UK

Zeng, X., 2001. Global vegetation root distribution for land modeling. *J. Hydrometeor.*, **2**:525–530.

Zhai, P. M., and X. H. Pan, 2003. Trends in temperature extremes during 1951-1999 in China. *Geophys. Res. Lett.*, 30(**17**):1913, doi:10.1029/2003/GL018004.

Zhang, D., and R. Zhang, 2002. Mechanism of OH formation from ozonolysis of isoprene: A Quantum-chemical study. J. Am. Chem. Soc., 124(11):2692-2703, doi:10.1021/ja0115181.

Zhang, D., W. Lei, and R. Zhang, 2002. Mechanism of OH formation from ozonolysis of isoprene: Kinetics and product yields. *Chem. Phys. Lett.*, 358(**3-4**):171-179, doi:10.1016/S0009-2614(02)00260-9.

Zhang, H, K. McGuffie, and A.Henderson-Sellers A, 1996. Impacts of tropical deforestation. Part II: The role of large-scale dynamics. *J. Clim.* **9**:2498-2521.

Zhang, L., Brook, J. R, and Vet, R., 2003. A revised parameterization for gaseous dry deposition in air-quality models, *Atmos. Chem. Discuss.*, **3**:1777-1804

Zhang, L., Moran, M. D., Makar, P.A., Brook, J.R. and Gong, S., 2002. Modelling gaseous dry deposition in AURAMS: a unified regional air-quality modelling system, *Atmos. Enviro.*, **36**:537-560.

Zhao, M., A.J. Pitman, and T. Chase, 2001. The impact of land cover change on the atmospheric circulation. *Clim. Dyn.* **17**:467-477.

WHS land cover classes

Code	Land Cover Description
00	• open water
01	• inland water
02	• bog or marsh
03	• ice
04	• paddy rice
05	• mangrove (tree swamp)
10	• dense needleleaf evergreen forest
11	• open needleleaf evergreen forest
12	• dense mixed evergreen + deciduous forest
13	• open mixed evergreen + deciduous woodland
14	• evergreen broadleaf woodland
15	• evergreen broadleaf cropland
16	• evergreen broadleaf shrub
17	• open deciduous needleleaf woodland
18	• dense deciduous needleleaf forest
19	• dense evergreen broadleaf forest
20	• dense deciduous broadleaf forest
21	• open deciduous broadleaf woodland
22	• deciduous tree crops (temperate)
23	• open tropical woodland
24	• woodland + shrub
25	• dense drought deciduous forest
26	• open drought deciduous woodland
27	• deciduous shrub
28	• thorn shrub
30	• temperate meadow + permanent pasture
31	• temperate rough grazing
32	• tropical grassland + shrub
33	• tropical pasture
34	• rough grazing + shrub
35	• pasture + tree
36	• semi arid rough grazing
37	• tropical savanna (grassland + tree)
39	• pasture + shrub
40	• arable cropland
41	• dry farm arable
42	• nursery + market gardening
43	• cane sugar
44	• maize
45	• cotton
46	• coffee
47	• vineyard
48	• irrigated cropland
49	• tea
50	• equatorial rain forest
51	• equatorial tree crop
52	• tropical broadleaf forest (slight seasonality)
61	• tundra
62	• dwarf shrub (tundra transition + high altitude wasteland)
70	• sand desert + barren land
71	• shrub desert + semi desert
73	• semi desert + scattered trees
80	• urban

WHS Soil codes and their properties

Code	Colour	Texture	Drainage
11	light	coarse	free
12	light	intermediate	free
13	light	fine	free
14	light	coarse	impeded
15	light	intermediate	impeded
16	light	fine	impeded
17	medium	coarse	free
18	medium	intermediate	free
19	medium	fine	free
20	medium	coarse	impeded
21	medium	intermediate	impeded
22	medium	fine	impeded
23	dark	coarse	free
24	dark	intermediate	free
25	dark	fine	free
26	dark	coarse	impeded
27	dark	intermediate	impeded
28	dark	fine	impeded
29	light	—	poor
30	medium	—	poor
31	dark	—	poor
34	ice	—	—

Standard Diagnostics: Climate Means

STASH CODE	DESCRIPTION	UNITS	TIME	DOMAIN
1	SURFACE PRESSURE	P_a	Mean	Single
2	WIND U-COMPONENT (=U) (WIND GRID)	ms^{-1}	Mean	MLC 19
3	WIND V-COMPONENT (=V) (WIND GRID)	ms^{-1}	Mean	MLC 19
4	POTENTIAL TEMPERATURE (THETA)	K	Mean	MLC 19
10	SPECIFIC HUMIDITY	kg kg^{-1}	Mean	MLC 19
10	SPECIFIC HUMIDITY	kg kg^{-1}	Mean	Col. mean
24	SURFACE TEMPERATURE	K	Mean	Single
24	SURFACE TEMPERATURE	K	MDmax	Single
25	**BOUNDARY LAYER (=BL) DEPTH**	**m**	**Mean**	**Single**
31	SEA ICE FRACTION ($0 \leq x \leq 1$)	—	Mean	Single
58	SULPHUR DIOXIDE EMISSIONS	kg m^{-2} s^{-1}	Mean	Single
59	DIMETHYL SULPHIDE EMISSIONS	kg m^{-2} s^{-1}	Mean	Single
101	SO2 MASS MIXING RATIO	kg kg^{-1}	Mean	MLC 19
102	DIMETHYL SULPHIDE MIX RAT	kg kg^{-1}	Mean	MLC 19
103	SO4 AITKEN MODE AEROSOL	kg kg^{-1}	Mean	MLC 19
104	SO4 ACCUM. MODE AEROSOL	kg kg^{-1}	Mean	MLC 19
105	SO4 DISSOLVED AEROSOL	kg kg^{-1}	Mean	MLC 19
106	H2 O2 MASS MIXING RATIO	kg kg^{-1}	Mean	MLC 19
121	NATURAL SO2 EMISSIONS	kg m^{-2} s^{-1}	Mean	MLC 19
122	OH CONCENTRATIONS	molecules cm^{-3}	Mean	MLC 19
123	HO2 CONCENTRATIONS	molecules cm^{-3}	Mean	MLC 19
124	H2 O2 CONCENTRATIONS	kg kg^{-1}	Mean	MLC 19
125	OZONE FOR SULPHUR CYCLE	kg kg^{-1}	Mean	MLC 19
126	HIGH LEVEL SO2 EMISSIONS	kg m^{-2} s^{-1}	Mean	Single
1201	NET DOWN SURFACE SW FLUX	W m^{-2}	Mean	Single
1203	NET DOWN SW RAD FLUX: OPEN SEA	W m^{-2}	Mean	Single
1204	NET DOWN SURFACE SW FLUX BELOW 690NM	W m^{-2}	Mean	Single
1207	INCOMING SW FLUX AT TOA	W m^{-2}	Mean	Single
1208	OUTGOING SW FLUX AT TOA	W m^{-2}	Mean	Single
1209	CLEAR-SKY UPWARD SW FLUX AT TOA	W m^{-2}	Mean	Single
1210	CLEAR-SKY DOWN SURFACE SW FLUX	W m^{-2}	Mean	Single
1211	CLEAR-SKY UP SURFACE SW FLUX	W m^{-2}	Mean	Single
1221	LAYER CLD LIQ RE × LAYER CLD AMOUNT		Mean	MLC 18
1223	LAYER CLD AMT IN SWRAD (MICROPHYSICS)	—	Mean	MLC 18
1235	**TOTAL DOWNWARD SURFACE SW FLUX**	**W m^{-2}**	**Mean**	**Single**
1241	DROPLET NUMBER CONC × CLOUD AMOUNT		Mean	MLC 18
1242	LAYER CLOUD LWC × CLOUD AMOUNT		Mean	MLC 18
1243	SO4 CCN MASS CONC × COND SAMP WEIGHT		Mean	MLC 18
1244	CONDITIONAL SAMPLING WEIGHT	—	Mean	MLC 18
1245	2-D EFFECTIVE RADIUS × 2-D RE WEIGHT		Mean	Single
1246	WEIGHT FOR 2-D EFFECTIVE RADIUS	—	Mean	Single
1262	WEIGHTED SW LAYER CLOUD EXTINCTION	—	Mean	MLC 18
1263	WEIGHTS FOR LAYER CLD SW EXTINCTION	—	Mean	MLC 18
1264	WEIGHTED SW CONV. CLOUD EXTINCTION	—	Mean	MLC 18
1265	WEIGHTS FOR CONV.CLD SW EXTINCTION	—	Mean	Single
2201	NET DOWN SURFACE LW FLUX	W m^{-2}	Mean	Single
2203	NET DOWN LW FLUX: OPEN SEA	W m^{-2}	Mean	Single
2204	**TOTAL CLOUD FRACTION ($0 \leq x \leq 1$)**	—	**Mean**	**Single**
2205	OUTGOING LW FLUX AT TOA	W m^{-2}	Mean	Single
2206	CLEAR-SKY UPWARD LW FLUX AT TOA	W m^{-2}	Mean	Single
2207	TOTAL DOWNWARD SURFACE LW FLUX	W m^{-2}	Mean	Single
2208	CLEAR-SKY DOWN SURFACE LW FLUX	W m^{-2}	Mean	MLC 18
2262	WEIGHTED LAYER CLOUD ABSORPTIVITY	—	Mean	MLC 18
2263	WEIGHTS FOR LAYER CLOUD ABSORPTIVITY	—	Mean	MLC 18
2264	WEIGHTED CONV. CLOUD ABSORPTIVITY	—	Mean	MLC 18
2265	WEIGHTS FOR CONV. CLOUD ABSORPTIVITY	—	Mean	Single
2269	ISCCP CLOUD WEIGHTS		Mean	MLC 7
2270	ISCCP CLOUD $0.1 \leq \tau$		Mean	MLC 7
2271	ISCCP CLOUD $\tau < 0.1$		Mean	MLC 7
2272	ISCCP CLOUD $0.1 \leq \tau < 1.3$		Mean	MLC 7
2273	ISCCP CLOUD $1.3 \leq \tau < 3.6$		Mean	MLC 7
2274	ISCCP CLOUD $3.6 \leq \tau < 9.4$		Mean	MLC 7

Continued on next page

STASH CODE	DESCRIPTION	UNITS	TIME	DOMAIN
2275	ISCCP CLOUD $9.4 \leq \tau < 23.0$		Mean	MLC 7
2276	ISCCP CLOUD $23.0 \leq \tau < 60.0$		Mean	MLC 7
2277	ISCCP CLOUD $60.0 \leq \tau$		Mean	MLC 19
2278	OZONE CONCENTRATION	kg kg $^{-1}$	Mean	Single
3026	ROUGHNESS LENGTH m	m	Mean	Single
3201	HEAT FLUX THROUGH SEA ICE	W m^{-2}	Mean	Single
3202	HEAT FLUX FROM SURF TO DEEP SOIL LEV	W m^{-2}	Mean	MLB 5
3217	SURFACE & BL HEAT FLUXES W m−2	Wm^{-2}	Mean	MLB 5
3223	SURFACE & BL MOISTURE FLUXES	kg m^{-2} s^{-1}	Mean	Single
3224	WIND MIXING ENERGY FLUX INTO SEA	W m^{-2}	Mean	Single
3225	WIND U-COMPONENT AT 10 METRES (WIND GRID)	ms^{-1}	Mean	Single
3226	WIND V-COMPONENT AT 10 METRES (WIND GRID)	ms^{-1}	Mean	Single
3228	SURFACE SENSIBLE HEAT FLUX FROM SEA	W m^{-2}	Mean	Single
3232	EVAPORATION FROM SEA	kg m^{-2} s^{-1}	Mean	Single
3234	SURFACE LATENT HEAT FLUX	W m^{-2}	Mean	Single
3236	**TEMPERATURE AT 1.5 METRES**	**K**	**Mean**	**Single**
3236	TEMPERATURE AT 1.5 METRES	K	MDmin	Single
3236	TEMPERATURE AT 1.5 METRES	K	MDmax	Single
3237	SPECIFIC HUMIDITY AT 1.5 METRES	**kg kg $^{-1}$**	Mean	**Single**
3245	RELATIVE HUMIDITY AT 1.5 METRES	%	Mean	Single
3249	WIND SPEED AT 10 METRES (WIND GRID)	**ms^{-1}**	Mean	**Single**
3249	WIND SPEED AT 10 METRES (WIND GRID)	**ms^{-1}**	MDmax	**Single**
3254	THETAL AT 1.5 METRES	K	Mean	Single
3255	QT AT 1.5 METRES	kg kg^{-1}	Mean	Single
3259	CANOPY CONDUCTANCE		Mean	Single
3270	SO2 SURFACE DRY DEP FLUX	kg m^{-2} s^{-1}	Mean	Single
3271	SO4 AIT SURF DRY DEP FLUX	kg m^{-2} s^{-1}	Mean	Single
3272	SO4 ACC SURF DRY DEP FLUX	kg m^{-2} s^{-1}	Mean	Single
3273	SO4 DIS SURF DRY DEP FLUX	kg m^{-2} s^{-1}	Mean	Single
3296	EVAPORATION FROM SOIL SURFACE	kg m^{-2} s^{-1}	Mean	Single
3297	EVAPORATION FROM CANOPY RATE	kg m^{-2} s^{-1}	Mean	Single
3298	SUBLIMATION FROM SURFACE RATE	kg m^{-2} s^{-1}	Mean	Single
3299	TRANSPIRATION RATE	kg m^{-2} s^{-1}	Mean	Single
3312	POTENTIAL EVAPORATION RATE	kg m^{-2} s^{-1}	Mean	Single
3313	SOIL MOISTURE AVAILABILITY FACTOR		Mean	Single
4203	LARGE SCALE RAINFALL RATE	kg m^{-2} s^{-1}	Mean	Single
4204	LARGE SCALE SNOWFALL RATE	kg m^{-2} s^{-1}	Mean	Single
4205	CLOUD LIQUID WATER CONTENT		Mean	MLC 19
4206	CLOUD ICE CONTENT		Mean	MLC 19
4216	SO2 SCAVENGED BY LS PPN	kg m^{-2} s^{-1}	Mean	Single
4217	SO4 AITKEN SCAVNGD BY LS PPN	kg m^{-2} s^{-1}	Mean	Single
4218	SO4 ACCUMULATION SCAVNGD BY LS PPN	kg m^{-2} s^{-1}	Mean	Single
4219	SO4 DISSOLVED SCAVNGD BY LS PPN	kg m^{-2} s^{-1}	Mean	Single
5205	CONVECTIVE RAINFALL RATE	kg m^{-2} s^{-1}	Mean	Single
5206	CONVECTIVE SNOWFALL RATE	kg m^{-2} s^{-1}	Mean	Single
5209	TEMPERATURE (AFTER CONVECTION)	K	Mean	Single
5209	TEMPERATURE (AFTER CONVECTION)	K	Mean	Single
5212	CONVECTIVE CLOUD AMOUNT ($0 \leq x \leq 1$)	-	Mean	Single
5216	**TOTAL PRECIPITATION RATE**	**kg m^{-2} s^{-1}**	**Mean**	**Single**
5234	GRIDBOX MEAN CONV. CLOUD WATER PATH	kg m^{-2} s^{-1}	Mean	Single
5238	SO2 SCAVENGED BY CONV PPN	kg m^{-2} s^{-1}	Mean	Single
5239	SO4 AIT SCAVENGED BY CONV PPN	kg m^{-2} s^{-1}	Mean	Single
5240	SO4 ACC SCAVENGED BY CONV PPN	kg m^{-2} s^{-1}	Mean	Single
5241	SO4 DIS SCAVENGED BY CONV PPN	kg m^{-2} s^{-1}	Mean	Single
8023	SNOW MASS	kg m^{-2}	Mean	Single
8208	SOIL MOISTURE CONTENT IN ROOT ZONE1	kg m^{-2}	Mean	Single
8209	CANOPY WATER CONTENT	kg m^{-2}	Mean	Single
8223	SOIL MOISTURE CONTENT IN A LAYER	kg m^{-2}	Mean	SL 4
8225	DEEP SOIL TEMPERATURE	K	Mean	SL 4
8229	UNFROZEN SOIL MOISTURE FRACTION ($0 \leq x \leq 1$)	-	Mean	SL 4
8230	FROZEN SOIL MOISTURE FRACTION ($0 \leq x \leq 1$)	-	Mean	SL 4
8231	SNOW MELT RATE (LAND)	kg m^{-2} s^{-1}	Mean	Single
8233	CANOPY THROUGHFALL RATE	kg m^{-2} s^{-1}	Mean	Single
8234	SURFACE RUNOFF RATE	kg m^{-2} s^{-1}	Mean	Single
8235	SUB-SURFACE RUNOFF RATE	kg m^{-2} s^{-1}	Mean	Single
9201	LAYER CLOUD AMOUNT ($0 \leq x \leq 1$)	-	Mean	MLC 19
9206	CLOUD LIQUID WATER CONTENT	kg kg $^{-1}$	Mean	MLC 19
9207	CLOUD ICE CONTENT	kg kg $^{-1}$	Mean	MLC 19
9282	CRITICAL RELATIVE HUMIDITY ($0 \leq x \leq 1$)	-	Mean	MLC 19

STASH CODE	DESCRIPTION	UNITS	TIME	DOMAIN
12201	WIND W-COMPONENT (=W) (WIND GRID)	ms^{-1}	Mean	MLC 19
15201	WIND U-COMPONENT (=U) (WIND GRID)	ms^{-1}	Mean6	PL 17+
15202	WIND V-COMPONENT (=V) (WIND GRID)	ms^{-1}	Mean6	PL 17+
15214	ERTEL POTENTIAL VORTICITY	$K\ kg^{-1}\ m^2\ s^{-1}$	Mean6	TL 5
15215	U xV (WIND GRID)	$m^2\ s^{-2}$	Mean6	PL 17+
15216	TEMPERATURE (=T) (WIND GRID)	K	Mean6	PL 17+
15217	U xT (WIND GRID)	$ms^{-1}\ K$	Mean6	PL 17+
15218	VxT (WIND GRID)	$ms^{-1}\ K$	Mean6	PL 17+
15219	T2 (WIND GRID)	K 2	Mean6	PL 17+
15220	U2 (WIND GRID)	$m2\ s^{-2}$	Mean6	PL 17+
15221	V2 (WIND GRID)	$m2\ s^{-2}$	Mean6	PL 17+
15222	WIND W-COMPONENT (=W) (WIND GRID)	ms^{-1}	Mean6	PL 17+
15223	W xT ON (WIND GRID)	$ms^{-1}\ K$	Mean6	PL 17+
15224	W xU ON (WIND GRID)	$m^2\ s^{-2}$	Mean6	PL 17+
15225	W xV ON (WIND GRID)	$m^2\ s^{-2}$	Mean6	PL 17+
15226	SPECIFIC HUMIDITY (=Q) (WIND GRID)	$kg\ kg^{-1}$	Mean6	PL 17+
15227	Q xU (WIND GRID)	$kg\ kg^{-1}\ ms^{-1}$	Mean6	PL 17+
15228	Q xV (WIND GRID)	$kg\ kg^{-1}\ ms^{-1}$	Mean6	PL 17+
15235	Q xW (WIND GRID)	$kg\ kg^{-1}\ ms^{-1}$	Mean6	PL 17+
15238	GEOPOTENTIAL HEIGHT (=Z) (WIND GRID)	m	Mean6	PL 17+
15239	U xZx106 (WIND GRID)	$m^2\ s^{-1}$	Mean6	PL 17+
15240	V xZx10 6 (WIND GRID)	$m^2\ s^{-1}$	Mean6	PL 17+
15242	W2 (WIND GRID)	$m^2\ s^{-2}$	Mean6	PL 17+
16202	GEOPOTENTIAL HEIGHT (=Z)	m	Mean6	PL 17+
16203	TEMPERATURE (=T)	K	Mean6	PL 17+
16204	RELATIVE HUMIDITY	%	Mean6	PL 17+
16222	PRESSURE AT MEAN SEA LEVEL	P_a	Mean6	Single
16224	Z2	m^2	Mean6	PL 17+
17203	MSA	$kg\ kg^{-1}$	Mean	MLC 19

Appendix 3.4

Characteristic of climatic variables taken from the 30-year (2070-2100) seasonal mean field over Southeast Asia for the A2 scenario under the present-day land cover (PLC) during DJF (Dec-Jan-Feb), JJA (Jun-Jul-Aug) as well as during the two inter-monsoon periods (MAM and SON). The minimum and maximum values thus represent spatial over the seasonal mean fields.

Climatic Variables		SRES A2								
		BASELINE			A2PLC			A2PLC-BASELINE		
		Mean	Min	Max	Mean	Min	Max	Mean	Min	Max
Surface Temperature (°C)	DJF	25.28	6.73	28.82	28.23	10.81	31.65	2.95	1.78	6.03
	MAM	26.88	13.64	32.78	30.00	17.27	35.69	3.12	2.08	5.54
	JJA	27.14	13.20	29.97	30.23	16.78	34.23	3.09	1.83	6.82
	SON	26.59	12.74	29.22	29.54	16.45	33.16	2.95	1.17	5.71
Total Precipitation (mm/day)	DJF	5.24	0.04	31.29	4.83	0.02	33.94	-0.40	-5.19	8.69
	MAM	5.47	28.42	0.31	4.64	0.16	32.62	-0.83	-5.55	6.21
	JJA	8.42	48.66	0.01	8.63	0.01	56.06	0.21	-11.24	12.51
	SON	7.27	0.18	37.42	7.10	0.11	42.74	-0.17	-6.04	5.86
Total Cloud Fraction	DJF	0.61	0.11	0.98	0.54	0.07	0.97	-0.07	-0.19	0.12
	MAM	0.61	0.22	0.95	0.51	0.22	0.93	-0.11	-0.25	0.07
	JJA	0.73	0.12	0.99	0.69	0.12	0.98	-0.04	-0.18	0.09
	SON	0.67	0.14	0.95	0.61	0.94	0.17	-0.06	-0.19	0.09
Solar Radiation (Wm^{-2})	DJF	215.00	81.56	317.91	220.64	81.08	313.96	5.64	-25.24	38.58
	MAM	239.44	114.38	300.98	248.68	109.08	303.86	9.24	-35.98	42.41
	JJA	213.50	57.70	300.09	218.08	53.89	284.61	4.60	-25.06	49.42
	SON	220.27	92.80	317.49	225.70	104.39	313.45	5.43	-28.65	35.69
Boundary Layer Height (m)	DJF	545.22	184.98	902.04	542.15	189.76	929.00	-3.06	-105.35	200.76
	MAM	495.47	173.01	765.18	488.45	152.97	787.05	-7.02	-87.87	175.30
	JJA	514.82	165.78	920.72	538.06	176.14	1000.55	23.24	-163.93	278.44
	SON	510.74	178.33	808.97	510.70	158.40	854.99	-0.04	-98.51	173.80

Appendix 3.5

Characteristic of climatic variables taken from the 30-year (2070-2100) seasonal mean field over Southeast Asia for the B2 scenario under the present-day land cover (PLC) during DJF (Dec-Jan-Feb), JJA (Jun-Jul-Aug) as well as during the two inter-monsoon periods (MAM and SON). The minimum and maximum values thus represent spatial over the seasonal mean fields.

Climatic Variables		SRES B2								
		BASELINE			B2PLC			B2PLC-BASELINE		
		Mean	Min	Max	Mean	Min	Max	Mean	Min	Max
Surface Temperature (°C)	DJF	25.28	6.73	28.82	27.92	7.57	28.28	2.64	0.84	3.94
	MAM	26.88	13.64	32.78	28.93	16.04	34.68	2.05	0.79	3.85
	JJA	27.14	13.20	29.97	29.27	15.66	32.66	2.12	0.91	4.53
	SON	26.59	12.74	29.22	28.60	15.18	31.74	2.00	0.89	4.52
Total Precipitation (mm/day)	DJF	5.24	0.04	31.29	4.87	-0.01	32.21	-0..36	-5.15	6.99
	MAM	5.47	28.42	0.31	4.55	0.16	31.87	-0.92	-5.77	5.21
	JJA	8.42	48.66	0.01	8.55	0.01	50.44	0.14	-10.19	10.22
	SON	7.27	0.18	37.42	6.97	0.13	42.98	-0.30	-6.27	6.84
Total Cloud Fraction	DJF	0.61	0.11	0.98	0.54	0.96	0.09	-0.07	-0.19	0.07
	MAM	0.61	0.22	0.95	0.51	0.21	0.94	-0.10	-0.23	0.08
	JJA	0.73	0.12	0.99	0.69	0.12	0.98	-0.04	-0.18	0.08
	SON	0.67	0.14	0.95	0.61	0.94	0.17	-0.06	-0.19	0.05
Solar Radiation (Wm^{-2})	DJF	215.00	81.56	317.91	218.15	80.47	312.59	3.14	-25.71	32.28
	MAM	239.44	114.38	300.98	247.32	115.65	301.24	7.88	-35.97	56.57
	JJA	213.50	57.7	300.09	217.32	52.13	287.31	3.82	-58.83	73.36
	SON	220.27	92.80	317.49	227.27	104.57	315.90	7.00	-30.78	63.78
Boundary Layer Height (m)	DJF	545.22	184.98	902.04	486.33	89.96	924.48	-5.89	-475.81	506.24
	MAM	495.47	173.01	765.18	452.57	96.52	895.03	-4.90	-345.13	337.53
	JJA	514.82	165.78	920.72	453.10	71.69	988.43	-6.72	-510.98	354.07
	SON	510.74	178.33	808.97	437.69	67.66	772.15	-7.04	-385.90	344.15

Appendix 4.1

Characteristic of climatic variables taken from the 30-year (2070-2100) seasonal mean field over Southeast Asia for the three A2 scenario experiments under the modified future land cover (FLC) during DJF (Dec-Jan-Feb), JJA (Jun-Jul-Aug) as well as during the two inter-monsoon periods (MAM and SON). The standard deviation, minimum and maximum values thus represent spatial over the seasonal mean fields.

Climatic Variables		SRES A2								
		A2FLC			A2FLC-BASELINE			A2FLC-A2PLC		
		Mean	Min	Max	Mean	Min	Max	Mean	Min	Max
Surface Temperature (°C)	DJF	28.07	10.94	31.22	2.78	1.49	5.34	-0.07	-1.54	1.70
	MAM	29.75	16.88	35.76	2.84	1.73	4.72	-0.25	-1.53	0.76
	JJA	30.00	16.51	33.62	2.84	1.46	5.58	-0.13	-1.86	1.15
	SON	29.39	16.49	32.58	2.76	1.49	5.34	-0.16	-2.33	1.38
Total Precipitation (mm/day)	DJF	4.83	0.03	32.61	-0.39	-6.33	7.56	0.03	-3.67	4.33
	MAM	4.62	0.16	31.69	-0.85	-6.28	5.97	0.06	2.63	5.19
	JJA	8.39	0.001	51.16	-0.02	-10.71	12.01	-0.29	-16.08	7.47
	SON	7.01	0.10	39.80	-0.20	-5.70	6.39	-0.02	-5.08	7.48
Total Cloud Fraction	DJF	0.53	0.07	0.97	-0.08	-0.19	0.06	-0.01	-0.13	0.11
	MAM	0.50	0.23	0.94	-0.11	-0.25	0.10	-0.001	-0.10	0.07
	JJA	0.67	0.11	0.97	-0.06	-0.21	0.06	-0.02	-0.14	0.11
	SON	0.60	0.16	0.94	-0.06	-0.20	0.08	-0.02	-0.15	0.07
Solar Radiation (Wm^{-2})	DJF	221.36	80.81	314.74	6.36	-60.17	41.46	0.72	-58.18	18.49
	MAM	248.65	110.81	303.34	9.21	-74.40	57.31	-0.03	-71.01	41.80
	JJA	220.2	58.56	285.51	6.70	-72.98	77.73	2.12	-64.60	59.06
	SON	228.40	103.78	314.38	8.13	-75.50	54.92	2.70	-68.80	40.40
Boundary Layer Height (m)	DJF	534.04	196.50	907.28	-11.18	-129.48	240.05	-8.11	-214.3	198.3
	MAM	485.04	156.88	797.07	-10.43	-165.09	184.25	-3.41	-184.45	106.57
	JJA	526.06	926.33	172.82	11.24	-188.40	295.14	-12.00	-159.40	168.60
	SON	501.81	158.99	849.34	-8.93	-181.90	168.76	-8.89	-160.58	153.05

Note: BASELINE and A2PLC values can be seen in Appendix 3.4

Appendix 4.2

Characteristic of climatic variables taken from the 30-year (2070-2100) seasonal mean field over Southeast Asia for the B2 scenario experiment under the modified future land cover (FLC) during DJF (Dec-Jan-Feb), JJA (Jun-Jul-Aug) as well as during the two inter-monsoon periods (MAM and SON). The standard deviation, minimum and maximum values thus represent spatial over the seasonal mean fields.

Climatic Variables		SRES B2								
		B2FLC			B2FLC-BASELINE			B2FLC-B2PLC		
		Mean	Min	Max	Mean	Min	Max	Mean	Min	Max
Surface Temperature (°C)	DJF	27.23	9.72	30.62	1.95	0.65	5.69	-0.12	-1.19	1.52
	MAM	28.95	15.97	34.74	2.79	0.82	3.96	-0.15	-2.95	1.41
	JJA	29.29	15.64	32.54	2.14	0.87	4.77	-0.09	-1.47	2.47
	SON	28.59	15.18	31.74	2.00	0.62	4.52	-0.06	1.64	2.46
Total Precipitation (mm/day)	DJF	4.88	0.01	29.88	-0.35	-5.17	6.41	-0.06	-2.32	3.27
	MAM	4.49	0.16	30.22	-0.99	-6.15	5.46	-0.07	-2.31	4.65
	JJA	8.49	0.02	49.76	0.07	-10.77	10.57	-0.06	-3.55	2.82
	SON	6.83	0.12	40.51	-0.44	-6.96	6.85	-0.15	-2.90	4.06
Total Cloud Fraction	DJF	0.55	0.07	0.97	-0.06	-0.19	0.09	0.003	-0.07	0.04
	MAM	0.55	0.21	0.96	-0.10	-0.24	0.09	-0.003	-0.09	0.07
	JJA	0.69	0.12	0.98	-0.04	-0.19	0.08	-0.001	-0.03	0.07
	SON	0.61	0.14	0.95	-0.06	-0.19	0.06	-0.004	-0.05	0.05
Solar Radiation (Wm^{-2})	DJF	220.11	82.42	314.58	5.14	-55.05	34.87	1.96	-51.20	19.99
	MAM	247.95	115.72	301.44	8.51	-73.66	57.38	0.63	-68.70	23.50
	JJA	217.82	53.94	285.34	4.32	-72.92	74.12	0.50	-58.50	22.0
	SON	227.80	103.64	316.23	7.52	-72.95	63.17	0.53	-66.80	28.70
Boundary Layer Height (m)	DJF	542.70	195.41	914.25	-2.52	-137.02	230.30	1.82	-165.90	184.02
	MAM	493.35	162.62	799.46	-2.12	-163.38	153.71	2.35	-99.22	143.85
	JJA	535.53	168.03	968.74	20.72	-194.17	259.15	4.01	-153.69	197.67
	SON	508.51	156.60	850.60	-2.12	-187.10	169.84	-4.30	-174.73	143.02

Note: BASELINE and B2PLC values can be seen in Appendix 3.5

Bimolecular chemical equations and rate constants, k ($cm^{-3}molecule^{-1}s^{-1}$)

No	Bimolecular Reactions				Rate Constant, k
1	CH_3	$+ O_2$	→	$HCHO + OH$	$3x10^{-16}$
2	CH_3	$+ O_3$	→	?	$5.1x10^{-12}exp(-210/T)$
3	EtOO	+ EtOO	→	$EtOH + MeCHO + O_2$	$3.27x10^{-14}exp(-110/T)$
4	EtOO	+ EtOO	→	$EtO + EtO + O_2$	$3.27x10^{-14}exp(-110/T)$
5	EtOO	+ EtOO	→	$EtOOEt + O_2$	$3.26x10^{-14}$ exp(-110/T)
6	H	$+ HO_2$	→	$H_2 + O_2$	$5.60x10^{-12}$
7	H	$+ HO_2$	→	$OH + OH$	$7.20x10^{-11}$
8	H	$+ HO_2$	→	$H_2O + O$	$2.40x10^{-12}$
9	H	$+ NO_2$	→	$OH + NO$	$4.00x10^{-10}exp(-340/T)$
10	H	$+ O_3$	→	$OH + O_2$	$1.40x10^{-10}$ exp(-480/T
11	HCO	$+ O_2$	→	$CO + HO_2$	$5.50x10^{-12}$
12	HO_2	+ HCHO	→	?	$6.7x10^{-15}exp(600/T)$
13	HO_2	$+ HO_2$	→	$H_2O_2 + O_2$	$2.20x10^{-13}exp(600/T)$
14	HO_2	+ MeOO	→	$O_2 + MeOOH$	$3.80x10^{-13}exp(780/T)$
15	HO_2	+ NO	→	$OH + NO_2$	$3.70x10^{-12}exp(240/T)$
16	HO_2	$+ NO_3$	→	$O_2 + HNO_3$	$2.15x10^{-12}$
17	HO_2	$+ NO_3$	→	$OH + NO_2 + O_2$	$2.15x10^{-12}$
18	HO_2	$+ O_3$	→	$OH + O_2 + O_2$	$1.40x10^{-14}$ exp(-600/T)
19	$HOCH_2CH_2OO$	$+ HOCH_2CH_2OO$	→	$HOCH_2CH_2OH + HOCH_2CHO + O_2$	$1.50x10^{-12}$
20	$HOCH_2CH_2OO$	$+ HOCH_2CH_2OO$	→	$HOCH_2CH_2O + HOCH_2CH_2O + O_2$	$8.30x10^{-13}$
21	MeO	+ NO	→	HCHO + HNO	$4.00x10^{-12}$ (T/300)$^{-0.7}$
22	MeO	$+ O_2$	→	$HCHO + HO_2$	$7.20x10^{-14}$ exp(-1080/T)
23	MeOO	+ MeOO	→	$MeOH + HCHO + O_2$	$3.67x10^{-14}exp(365/T)$
24	MeOO	+ MeOO	→	$MeO + MeO + O_2$	$3.67x10^{-14}exp(365/T)$
25	MeOO	+ MeOO	→	$MeOOMe + O_2$	$3.66x10^{-14}exp(365/T)$
26	MeOO	+ NO	→	$MeO + NO_2$	$4.20x10^{-12}exp(180/T)$
27	MeOO	$+ O_3$	→	?	$3.00x10^{-17}$
28	N_2O_5	$+ H_2O$	→	$HNO_3 + HNO_3$	$2.00x10^{-21}$
29	NO	$+ NO_3$	→	$NO_2 + NO_2$	$1.80x10^{-11}exp(110/T)$
30	NO	$+ O_3$	→	$NO_2 + O_2$	$1.80x10^{-12}exp(-1370/T)$
31	NO_2	$+ NO_3$	→	$NO + NO_2 + O_2$	$4.50x10^{-14}$ exp(-1260/T)
32	NO_2	$+ O_3$	→	$NO_3 + O_2$	$1.20x10^{-13}exp(-2450/T)$
33	NO_3	$+ C^2H^2$	→	?	$1.00x10^{-16}$
34	NO_3	$+ C^2H^4$	→	?	$3.3x10^{-12}exp(-2880/T)$
35	NO_3	$+ C^3H^6$	→	?	$9.4x10^{-15}$
36	NO_3	+ CO	→	$NO_2 + CO_2$	$4.00x10^{-19}$
37	NO_3	+ HCHO	→	$HNO_3 + HCO$	$5.80x10^{-16}$
38	O	$+ C_2H_2$	→	$C_2HO + H$	$1.50x10^{-11}exp(-1600/T)$
39	O	$+ C_2H_2$	→	$CH_2 + CO$	$1.50x10^{-11}exp(-1600/T)$
40	O	$+ CH_3$	→	HCHO + H	$1.40x10^{-10}$
41	O	$+ H_2O_2$	→	$OH + HO_2$	$1.40x10^{-12}exp(-2000/T)$
42	O	+ HCHO	→	OH + HCO	$3.40x10^{-11}exp(-1600/T)$
43	O	$+ HO_2$	→	$OH + O_2$	$2.70x10^{-11}exp(224/T)$
44	O	$+ HO_2NO_2$	→	?	$7.8x10^{-11}exp(-3400/T)$
45	O	$+ HONO_2$	→	$OH + NO_3$	$3.00x10^{-17}$
46	O	+ MeCHO	→	MeCO + OH	$1.80x10^{-11}$ exp(-1100/T)
47	O	$+ N_2O_5$	→	?	$3x10^{-16}$
48	O	$+ NO_2$	→	$O_2 + NO$	$6.5x10^{-12}exp(120/T)$
49	O	$+ NO_3$	→	$O^2 + NO_2$	$1.7x10^{-11}$
50	O	$+ O_3$	→	$O_2 + O_2$	$8x10^{-12}exp(-2060/T)$
51	O	+ OH	→	$O_2 + H$	$2.3x10^{-11}exp(110/T)$
52	O(1D)	$+ CH_4$	→	$OH + CH_3$	$1.35x10^{-10}$
53	O(1D)	$+ CH_4$	→	$HCHO + H_2$	$1.5x10^{-11}$
54	O(1D)	$+ H_2O$	→	OH + OH	$2.2x10^{-10}$
55	O(1D)	$+ N_2$	→	$O + N_2$	$1.8x10^{-11}exp(107/T)$
56	O(1D)	$+ O_2$	→	$O + O_2$	$3.2x10^{-11}exp(67/T)$

Continue to the next page

No	Bimolecular Reactions			Rate Constant, k
57	O(1 D)	+ O_3	→ O_2 + O + O	$1.20x10^{-10}$
58	O(1 D)	+ O_3	→ O_2 + O_2	$1.20x10^{-10}$
59	OH	+ CH_4	→ H_2O + CH_3	$3.90x10^{-12}exp(-1885/T)$
60	OH	+ CO	→ H + CO_2	$1.50x10^{-13}$
61	OH	+ H_2O_2	→ H_2O + HO_2	$2.90x10^{-12}exp(-160/T)$
62	OH	+ HCHO	→ H_2O + HCO	$8.80x10exp^{-12}(25/T)$
63	OH	+ HO_2	→ H_2O + O_2	$4.80x10exp^{-11}(250/T)$
64	OH	+ HNO_3	→ H_2O + NO_3	$1.50x10^{-13}$
65	OH	+ MeOOH	→ H_2O + CH_2	$1.00x10exp^{-12}(190/T)$
66	OH	+ MeOOH	→ H_2O + MeOO	$1.90x10exp^{-12}(190/T)$
67	OH	+ NO_3	→ HO_2 + NO_2	$2.30x10^{-11}$
68	OH	+ O_3	→ HO_2 + O_2	$1.90x10exp^{-12}(-1000/T)$
69	OH	+ OH	→ H_2O + O	$4.2010exp^{-12}(-240/T)$
70	OH	+ HONO	→ H_2O + NO_2	$1.80x10^{-11}$
71	O_3	+ HONO	→ O_2 + HNO_3	$5.00x10^{-19}$
72	C_2H_6	+ OH	→ EtOO	$1.23x10^{-12}exp(-444/T)$
73	C_3H_8	+ OH	→ 0.33EtOO + 0.585BuOO	$1.14x10^{-12}exp(14/T)$
74	C_4H_{10}	+ OH	→ 0.28EtOO + 0.59BuOO + 0.18HxOO	$1.55x10exp^{-11}(-540/T)$
75	C_5H_{12}	+ OH	→ 0.25EtOO + 0.663BuOO + 0.308HxOO	$3.90x10^{-12}$
76	C_6H_{14}	+ OH	→ 0.24EtOO + 0.705BuOO + 0.45HxOO	$5.60x10^{-12}$
77	EtOO	+ NO	→ 0.985MeCHO + 0.985HO2 + 0.985NO_2	$4.87x10exp^{-12}(180/T)$
78	MeCHO	+ OH	→ $MeCO_3$	$5.60x10exp^{-12}(310/T)$
79	MeCHO	+ NO_3	→ $MeCO_3$ + HNO_3	$1.40x10exp^{-12}(-1860/T)$
80	$MeCOO_2NO_2$ (PAN)	+ OH	→ HCHO + NO_2	$1.20x10exp^{-12}(-650/T)$
81	$MeCO_3$	+ NO	→ MeOO + NO_2	$7.77x10exp^{-12}(180/T)$
82	BuOO	+ NO	→ 0.91EtCOMe + 0.91HO_2 + 0.91NO_2	$4.87x10exp^{-12}(180/T)$
83	EtCOMe	+ OH	→ MeCOOHCOMe	$1.80x10exp^{-11}(-890/T)$
84	MeCOOHCOMe	+ NO	→ 0.92 MeCHO + 0.92 MeCO3 + 0.92 NO2	$4.20x10exp^{-12}(180/T)$
85	HxOO	+ NO	→ 0.96EtCOMe + 0.96EtOO + 0.96NO_2	$4.87x10exp^{-12}(180/T)$
86	$HOCH_2CH_2OO$	+ NO	→ *fa*HCHO + *fb*MeCHO + HO_2 + NO_2	$4.20x10exp^{-12}(180/T)$
87	C_2H_4	+ O_3	→ HCHO + 0.42CO + 0.12HO2 + 0.12H_2	$1.20x10exp^{-14}(-2633/T)$
88	$CH3CH(OO)CH_2OH$	+ NO	→ HCHO + MeCHO + HO_2 + NO_2	$4.20x10exp^{-12}(180/T)$
89	C_3H_6	+ O_3	→ 0.525HCHO + 0.50MeCHO + 0.33CO +	$1.30x10exp^{-14}(-2105/T)$
90			0.23HO_2 + 0.215MeOO + 0.095OH +	
91			0.06CH_4 + 0.06H_2	
92	C_6H_6	+ OH	→ 0.64ArOO	$7.57x10exp^{-12}(-529/T)$
93	C_7H_8	+ OH	→ 0.76ArOO	$2.10x10exp^{-12}(322/T)$
94	ArOO	+ NO	→ MeCOCHO + HCOCHCHCHO+HO_2+NO_2	$4.20x10exp^{-12}(180/T)$
95	HCOCHCHCHO	+ OH	→ $HCOCHCHCO_3$	$3.00x10^{-11}$
96	$HCOCHCHCO_3$	+ NO	→ HCOCHO+CO+HO_2+3.0NO_2 - 2.0NO	$4.20x10exp^{-12}(180/T)$
97	HCOCHO	+ OH	→ 2.00CO + HO_2	$1.15x10^{-11}$
98	MeCOCHO	+ OH	→ $MeCO_3$ + CO	$1.70x10^{-11}$
99	EtOO	+ HO_2	→ EtOOH	$6.50x10exp^{-13}(650/T)$
100	BuOO	+ HO_2	→ BuOOH	$6.50x10exp^{-13}(650/T)$
101	HxOO	+ HO_2	→ HxOOH	$6.50x10exp^{-13}(650/T)$
102	$MeCO_3$	+ HO_2	→ $MeCO_3H$	$6.50x10exp^{-13}(650/T)$
103	MeCOOHCOMe	+ HO_2	→ MeCHO + $MeCO_3$ + OH	$6.50x10exp^{-13}(650/T)$
104	$HOCH_2CH_2OO$	+ HO_2	→ *fa*HCHO + *fb*MeCHO + HO_2 + OH	$6.50x10exp^{-13}(650/T)$
105	$CH_3CH(OO)CH_2OH$	+ HO_2	→ HCHO + MeCHO + HO_2 + OH	$6.50x10exp^{-13}(650/T)$
106	ArOO	+ HO_2	→ ?	$6.50x10^{-13}exp(650/T)$
107	$HCOCHCHCO_3$	+ HO_2	→ ?	$6.50x10^{-13}exp(650/T)$
108	MeOO	+ $MeCO_3$	→ HCHO + 0.50 MeOO + 0.50 HO2	$2.20x10^{-12}exp(490/T)$
109	$MeCO_3$	+ $MeCO_3$	→ 2.00 MeOO	$2.80x10^{-12}exp(530/T)$
110	EtOOH	+ OH	→ 0.75MeCHO + 0.75OH + 0.25EtOO	$2.00x10^{-11}$
111	BuOOH	+ OH	→ EtCOMe + OH	$2.00x10^{-11}$
112	HxOOH	+ OH	→ HxOO	$3.00x10^{-12}$
113	MeCO3H	+ OH	→ $MeCO_3$	$5.00x10^{-12}$
114	MVK	+ OH	→ MVKOO	$3.00x10^{-12}$ exp(500/T)
115	MVKOO	+ NO	→ 0.60$MeCO_3$ + 0.60MeCHO + 0.30HCHO	$4.20x10^{-12}exp(180/T)$
			+ 0.30MeCOCHO + 0.30HO_2 + 0.90NO_2	
116	MVKOO	+ HO_2	→ 1.80CO + 0.60H_2	$6.50x10^{-13}exp(650/T)$
117	MVK	+ O_3	→ 0.50MeCOCHO + 0.50HCHO + 0.15$MeCO_3$	$4.00x10^{-15}exp(-2000/T)$
			+ 0.15MeCHO+0.21HO_2 + 0.20CO + 0.06H_2	

Continue to the next page

No	Bimolecular Reactions				Rate Constant, k
118	MACR	+ OH	→	MACROO	$3.86\times10^{-12}\exp(500/T)$
119	MACROO	+ NO	→	0.90MeCOCHO + 0.90HCHO + 0.90HO_2 + 0.90NO_2	$4.20\times10^{-12}\exp(180/T)$
120	MACROO	+ HO_2	→	2.20CO + 0.60H_2	$6.50\times10^{-13}\exp(650/T)$
121	MACR	+ O_3	→	0.50MeCOCHO + 0.65HCHO + 0.36HO_2 + 0.35CO + 0.36H_2 + 0.15NO_2 - 0.15NO	$4.40\times10^{-15}\exp(-2500/T)$
122	ISOPRENE	+ OH	→	ISOPROO	$1.50\times10^{-11}\exp(500/T)$
123	ISOPROO	+ NO	→	0.90HCHO + 0.90HO_2+ 0.90NO_2 +0.45MVK + 0.45MACR	$4.20\times10^{-12}\exp(180/T)$
124	ISOPROO	+ HO_2	→	2.75CO + 0.90H2	$6.50\times10^{-13}\exp(650/T)$
125	ISOPRENE	+ O_3	→	0.50HCHO + 0.30MACR + 0.20MVK + 0.20CO + 0.06HO_2 + 0.06H_2	$7.00\times10^{-15}\exp(-1900/T)$
126	$HOSO_2$	+ O_2	→	HO_2 + SO_3	$1.3\times10^{-12}\exp(-330/T))$
127	MeOO	+ SO_2	→	MeO + SO_3	5×10^{-17}
128	SO	+ NO_2	→	SO_2 + NO	1.4×10^{-11}
129	SO	+ O_2	→	SO_2 + O	$1.4\times10^{-13}\exp(-2280/T)$
130	SO	+ O_3	→	SO_2 + O_2	$4.5\times10^{-12}\exp(-1170/T)$
131	SO	+ OH	→	SO_2 + H	8.6×10^{-11}
132	SO_2	+ H_2O	→	OH + SO_3	1×10^{-18}
133	SO_2	+ HONO	→	SO_3 + O_2	$3\times10^{-12}\exp(-7000/T)$
134	SO_3	+ HONO	→	H_2SO_4	6.5×10^{-15}
135	O_3	+ DMS	→	O_2 + $HONO_2$	5×10^{-19}
136	OH	+ DMS	→	H_2O + NO_2	$1.8\times10^{-11}\exp(-390/T)$
137	OH	+ NO	→	$MeSCH_2OO$	$9.6\times10^{-12}\exp(-234/T)$
138	NO_3	+ HO_2	→	$MeSCH_2OO$ + $HONO_2$	$1.9\times10^{-13}\exp(520/T)$
139	$MeSCH_2OO$	+ MeOO	→	MeS + HCHO + NO_2	$4.2\times10^{-12}\exp(180/T)$
140	$MeSCH_2OO$	+ $MeSCH_2OOH$	→	$MeSCH_2OOH$	$1.5\times10^{-13}\exp(1250/T)$
141	MeSCHOO	+ NO3	→	MeS + HCHO + MeO	3×10^{-13}
142	OH	+ O3	→	$MeSCH_2OO$	1.5×10^{-11}
143	$MeSCH_2OO$	+ NO2	→	$MeSCH_2OO$ + HCHO + NO_2	1×10^{-12}
144	MeS	+ O_3	→	MeSO + O_2	$2\times10^{-12}\exp(290/T)$
145	MeS	+ NO_2	→	MeSO + NO	$2.1\times10^{-11}\exp(320/T)$
146	MeSO	+ O_3	→	$MeSO_2$	6×10^{-13}
147	MeSO	+ NO_2	→	$MeSO_2$ + NO	8×10^{-12}
148	$MeSO_2$	+ O_3	→	$MeSO_3$	3×10^{-13}
149	$MeSO_2$	+ NO_2	→	$MeSO_3$ + NO	4×10^{-12}
150	$MeSO_3$	+ HO_2	→	MSA	5×10^{-11}
151	$MeSO_3$	+ HCHO	→	MSA + CO + HO_2	1.6×10^{-15}
152	MeOO	+ NO_3	→	MeO + NO_2 + O_2	1×10^{-12}
153	$MeCO_3$	+ NO_3	→	MeOO + CO_2 + NO_2	5×10^{-12}
154	EtOH	+ OH	→	MeCHO + HO_2	$4.99\times10^{-13}\exp(532/T)$
155	EtOH	+ OH	→	$HOCH_2CH_2OO$	$3.18\times10^{-14}\exp(532/T)$
156	CH_2ClO_2	+ NO	→	CH_2ClO + NO_2	1.87×10^{-11}
157	CH_2ClO_2	+ HO_2	→	CH_2ClOOH + O_2	$3.26\times10^{-13}\exp(822/T)$
158	CH_2ClO	+ O_2	→	HCOCl + HO_2	3×10^{-14}
159	HCOCl	+ OH	→	H_2O + CO + Cl	$3.67\times10^{-11}\exp(1419/T)$
160	CH_2ClOOH	+ OH	→	CH_2CLO_2 + H_2O	$1.9\times10^{-12}\exp(190/T)$
161	LMXYLN	+ OH	→	0.8HCOCHCHCHO + 0.8MeCOCHO + 0.2XYLX + HO_2	1.37×10^{-11}
162	LMXYLN	+ NO_3	→	0.8HCOCHCHCH + 0.8MeCOCHO + HO_2 + $HONO_2$ + 0.2XYLX	3.8×10^{-16}
163	XYLX	+ OH	→	0.9HCOCHCHCHO + 0.9MeCOCHO + 0.9HO_2 + 0.1XYLX1	4.6×10^{-11}
164	XYLX	+ NO_3	→	0.9HCOCHCHCHO + 0.9MeCOCHO + 0.9HO_2 + 0.9$HONO_2$ + 0.1LMXYLY	2.0×10^{-13} 1.0×10^{-11}
165	XYLX1	+ NO_2	→	LMXYLY	1.0×10^{-11}
166	XYLX1	+ HO_2	→	XYLX	2.7×10^{-12}
167	LMXYLY	+ OH	→	HCOCHCHCHO + MeCOCHO + NO_2	7.0×10^{-14}
168	LMXYLY	+ NO_3	→	HCOCHCHCHO + MeCOCHO + $_2NO_2$	$1.6\times10^{-12}\exp(335/T)$ +
169	C_7H_8	+ OH	→	0.8HCOCHCHCHO + 0.8HCOCHO + 0.2TOLX + HO_2	$7.58\times10^{-18}T^2\exp(11/T)$
170	TOLX	+ OH	→	0.9HCOCHCHCHO + 0.9HCOCHO + 0.9HO2 + 0.1TOLX1	3.4×10^{-11}

Continue to the next page

No	Bimolecular Reactions			Rate Constant, k
171	TOLX	+ NO_3	→ 0.9HCOCHCHCHO + 0.9HCOCHO + 0.9HONO$_2$ + 0.1TOLY	2.0x10^{-13}
172	TOLX1	+ NO_2	→ TOLY	1.0x10^{-11}
173	TOLX1	+ HO_2	→ TOLX	1.0x10^{-11}
174	TOLY	+ OH	→ HCOCHCHCHO + HCOCHO + NO_2	1.4x10^{-12}
175	TOLY	+ NO_3	→ HCOCHCHCHO + HCOCHO + 2NO_2	7.0x10^{-14}
176	ALPHAP	+ OH	→ APINO$_2$	1.2x10^{-11}exp(444/T)
177	APINO$_2$	+ NO	→ PINAL + HO_2 + NO_2	8.9x10^{-13}exp(180/T)
178	APINO$_2$	+ HO_2	→ APINOOH	2.9x10^{-13}exp(1250/T)
179	APINO$_2$	+ m	→ 0.7PINAL + 0.7HO_2 + 0.3APINOH	2.8x10^{-13} xRO_2
180	APINOH	+ OH	→ PINAL + HO_2	2.4x110^{-11}
181	APINOOH	+ OH	→ PINAL + OH	2.8x10^{-11}
182	PINAL	+ NO_3	→ PINALO$_2$ + $HONO_2$	3.8x10^{-14}
183	PINAL	+ OH	→ PINALO$_2$	8.9x10^{-11}
184	PINALO$_2$	+ NO	→ $CO_{23}C_4CHO$ + $MeCOCH_3$ + HCHO + CO_2 + HO_2 + NO_2 + 4O_3	1.1x10^{-11}exp(180/T)
185	PINALO$_2$	+ HO_2	→ 0.29O_3 + PINONIC	4.3x10^{-13}exp(1040/T)
186	PINALO$_2$	+ m	→ 0.7$CO_{23}C_4CHON$ + 0.7$MeCOCH_3$ + 0.7HCHO + 0.7CO_2 + 0.7HO_2 + 2.84O_3 + 0.3PINONIC	5.0x10^{-12}xRO_2
187	PINONIC	+ OH	→ PINALO$_2$	6.2x10^{-12}
188	$CO_{23}C_4CHO$	+ OH	→ $CO_{23}C_4CO_3$	2.1x10^{-11}
189	$CO_{23}C_4CHO$	+ NO_3	→ $CO_{23}C_4CO_3$ + $HONO_2$	1.4x10^{-12}exp(-1860/T)
190	$CO_{23}C_4CO_3$	+ NO	→ $MeCO_3$ + HCHO + CO	1.1x10^{-11}exp(180/T)
191	$CO_{23}C_4CO_3$	+ m	→ CH_3CO_3 + HCHO + CO CO_2 + O_3	5.0x10^{-12} x RO_2
192	ALPHAP	+ O_3	→ 0.85$CO_{23}C_4CHO$ + 0.85$MeCOCH_3$ + 0.85HCHO + 0.85OH+ 0.85CO + 0.15APINOO + 3.4O_3	1.0x10^{-15}exp(-732/T)
193	APINOO	+ H_2O	→ 0.38PINAL + 0.38H_2O_2 + 0.62PINONIC	1.6x10^{-17}
194	APINOO	+ SO_2	→ PINAL + SO_3	7.0x10^{-14}
195	ALPHAP	+ NO_3	→ NAPINO$_2$	1.2x10^{-12}exp(490/T)
196	NAPINO$_2$	+ NO	→ PINAL + NO_2 + NO_2	8.9x10^{-13}exp(180/T)
197	NAPINO$_2$	+ m	→ PINAL + NO_2	2.8x10^{-14} x RO_2
198	$MeCOCH_3$	+ OH	→ $MeCOCH_2O_2$	5.34x10^{-18}exp(-230/T)
199	$MeCOCH_2O_2$	+ NO	→ $MeCO_3$ + HCHO + NO_2	2.9x10^{-12}exp(8180/T)
200	$MeCOCH_2O_2$	+ HO_2	→ CO_2C_3OOH	1.36x10^{-13}exp(1250/T)
201	$MeCOCH_2O_2$	+ m	→ 0.6$MeCO_3$ + 0.6HCHO + 0.4MeCOCHO	2.0x10^{-12} x RO_2
202	CO_2C_3OOH	+ OH	→ MeCOCHO + OH	1.2 x 10^{-11}
203	LIM	+ OH	→ LIMP	1.71x10^{-10}
204	LIM	+ NO_3	→ 0.13OLNN + 0.87OLND	1.22x10^{-11}
205	LIM	+ O_3	→ 0.04HCHO + 0.46OLT + 0.14CO + 0.16EtOO + 0.42$MeCOCH_2O_2$ + 0.85OH + 0.10HO_2 + 0.02H_2O_2 + 0.79MACR + 0.01ORA1 + 0.07ORA2	2.00x10^{-16}
206	LIMP	+ NO	→ 0.65HO_2 + 0.4MACR + 0.25OLI + 0.25HCHO + 0.35ONIT + 0.65NO	4.00x10^{-12}
207	LMP	+ HO_2	→ OP2	1.50x10^{-11}
208	LIMP	+ MeOO	→ 1.4HCHO + 0.6MACR + 0.4OLI + 2HO_2	3.83x10^{-13}
209	LIMP	+ $MeCO_3$	→ 0.60MACR + 0.40OLI + 0.40HCHO + HO_2 + MeOO	9.63x10^{-12}
210	LIMP	+ NO_3	→ 0.60MACR + 0.40OLI + 0.40HCHO + HO_2 + NO_2	1.20x10^{-12}
211	OLNN	+ NO	→ HO_2 + ONIT +NO_2	4.00x10^{-12}
212	OLNN	+ NO_3	→ ONIT + HO_2 + NO_2	1.20x10^{-12}
213	OLNN	+ HO_2	→ ONIT	1.30x10^{-11}
214	OLNN	+ OLNN	→ 2ONIT + HO_2	2.00x10^{-12}
215	OLNN	+ OLND	→ 0.202HCHO + 0.64MeCHO + 0.50HO_2 + 0.149$MeCOCH_3$ + 1.50ONIT + 0.50NO_2	1.22x10^{-12}
216	OLNN	+ MeOO	→ 0.75HCHO + HO_2 + ONIT	1.72x10^{-12}
217	OLNN	+ $MeCO_3$	→ ONIT + 0.5ORA2 + 0.5MeOO + 0.5HO_2	1.15x10^{-11}
218	OLND	+ NO	→ 0.287HCHO + 1.24MeCHO + 0.464$MeCOCH_3$ + 2NO_2	4.00x10^{-12}
219	OLND	+ NO_3	→ 0.28HCHO + 1.24MeCHO + $MeCOCH_3$ + 2NO_2	1.20x10^{-12}

Continue to the next page

No	Bimolecular Reactions			Rate Constant, k
220	OLND	+ HO_2	→ ONIT	$1.30x10^{-11}$
221	OLND	+ OLND	→ 0.504HCHO + 1.21MeCHO + 0.285$MeCOCH_3$ + ONIT	$8.50x10^{-13}$
222	OLND	+ MeOO	→ 0.96HCHO + 0.5HO_2 + 0.64MeCHO + 0.149$MeCOCH_3$ + 0.5NO_2 + 0.5ONIT	$1.04x10^{-12}$
223	OLND	+ $MeCO_3$	→ 0.207HCHO + 0.65MeCHO + 0.167MeCOCH3 + 0.484ORA2 + 0.484ONIT + 0.516NO_2 + 0.516MeOO	$7.00x10^{-12}$
224	OLT	+ OH	→ OLTP	$3.06x10^{-11}$
225	OLT	+ NO_3	→ 0.43OLNN + 0.57OLND	$3.95x10^{-14}$
226	OLT	+ O_3	→ 0.64HCHO + 0.044MeCHO + 0.37CO + 0.14ORA1 + 0.10ORA2 + 0.25HO_2 + 0.40OH + 0.03$COCH_3$ + 0.03$MeCOCH_2O_2$ + 0.06CH_4 + 0.05H_2 + 0.006H_2O_2 + 0.03C_2H_6 + 0.19Me00 + 0.10EtOO	$1.03x10^{-17}$
227	OLTP	+ NO	→ 0.94MeCHO + HCHO + HO_2 + NO_2 + 0.06$MeCOCH_3$	$4.00x10^{-12}$
228	OLTP	+ HO_2	→ OP_2	$1.30x10^{-11}$
229	OLTP	+ MeOO	→ 1.25HCHO + HO_2 + 0.699MeCHO + 0.081$MeCOCH_3$	$1.57x10^{-12}$
230	OLTP	+ $MeCO_3$	→ 0.859MeCHO + 0.501HCHO + 0.501HO_2 + 0.501MeOO + 0.499ORA2 + 0.141$MeCOCH_3$	$1.06x10^{-11}$
231	OLTP	+ NO_3	→ HCHO + 0.94MeCHO + 0.06$MeCOCH_3$ + HO_2 + NO_2	$1.20x10^{-12}$
232	OLI	+ OH	→ OLIP	$7.12x10^{-11}$
233	OLI	+ NO_3	→ 0.11OLNN + 0.89OLND	$3.91x10^{-12}$
234	OLI	+ O_3	→ 0.02HCHO + 0.99MeCHO + 0.16$MeCOCH_3$ + 0.30CO + 0.011H_2O_2 + 0.14ORA2 + 0.074CH_4 + 0.22HO_2 + 0.63OH + 0.23MeOO + 0.12$MeCOCH_2O_2$ + 0.06C_2H_6 + 0.18EtOO	$2.58x10^{-16}$
235	OLIP	+ NO	→ HO_2 + 1.71MeCHO + 0.29$MeCOCH_3$ + NO_2	$4.00x10^{-12}$
236	OLIP	+ HO_2	→ OP2	$1.30x10^{-11}$
237	OLIP	+ MeOO	→ 0.755HCHO + HO_2 + 0.932MeCHO + 0.313$MeCOCH_3$	$9.87x10^{-13}$
238	OLIP	+ $MeCO_3$	→ 0.941MeCHO + 0.29$MeCHOCH_3$ + 0.51HO_2 + 0.51MeOO + 0.49ORA2	$6.63x10^{-12}$
239	OLIP	+ NO_3	→ 1.71MeCHO + 0.29$MeCOCH_3$ + HO_2 + NO_2	$1.20x10^{-12}$
240	OP2	+ OH	→ 0.44HC3P + 0.08MeCHO + 0.41$MeCOCH_3$ + 0.49OH + 0.07XO2	$6.43x10^{-12}$
241	XO2	+ HO_2	→ OP2	$1.30x10^{-10}$
242	XO2	+ MeOO	→ HCHO + HO_2	$9.50x10^{-13}$
243	XO2	+ $MeCO_3$	→ MeOO	$6.38x10^{-12}$
244	XO2	+ XO_2	→ ?	$1.42x10^{-12}$
245	XO2	+ NO	→ NO_2	$4.00x10^{-12}$
246	XO2	+ NO_3	→ NO_2	$1.2x10^{-12}$
247	ONIT	+ OH	→ HC3P + NO_2 + H_2O	$2.22x10^{-22}$
248	$C_{15}H_{24}$	+ OH	→ PM10	$1.97x10^{-12}$
249	$C_{15}H_{24}$	+ NO_3	→ PM10	$1.92x10^{-11}$
250	$C_{15}H_{24}$	+ O_3	→ PM10	$1.20x10^{-14}$
251	$C_{15}H_{24}$	+ NO_2	→ PM10	$5.00x10^{-19}$

Trimolecular chemical equations and rate constants, k ($cm^{-3}molecule^{-1}s^{-1}$)

No	Trimolecular Reactions			Rate Constant, k_o	Rate Constant, k_∞
1	CH_3	$+ O_2 + m$	$\rightarrow MeOO + m$	$4.5x10^{-31}(T/300)^{-3}$	$1.8x10^{-12}(T/300)^{-1.7}$
2	EtOO	$+ NO_2 + m$	$\rightarrow EtONO_2 + m$	0.00	$1.3x10^{-13}$
3	EtOO	$+ NO_2 + m$	$\rightarrow EtO_2NO_2 + m$	$1.01x10^{-29}(T/300)^{-6.2}$	$8.8x10^{-12}$
4	H	$+ O_2 + m$	$\rightarrow HO_2 + m$	$4.84x10^{-32}(T/300)^{-1.6}$	$7.5x10^{-11}$
5	HO_2	$+ HCHO + m$	$\rightarrow HOCH_2OO + m$	0.00	$9.7x10^{-15}$
6	HO_2	$+ HO_2 + m$	$\rightarrow H_2O_2 + O_2 + m$	$1.70x10^{-33}exp(980/T)$	
7	HO_2	$+ NO_2 + m$	$\rightarrow HO_2NO_2 + m$	$1.4x10^{-31}(T/300)^{3.2}$	$4.7x10^{-12}$
8	HO_2NO_2	$+ m$	$\rightarrow HO_2 + NO_2 + m$	$3.90x10^{-6}exp(980/T)$	$2.6x10^{15}exp(-10900/T)$
9	MeO	$+ NO + m$	$\rightarrow MeONO + m$	$1.4x10^{-29}(T/300)^{-3.8}$	$3.6x10^{-11}(T/300)^{-0.6}$
10	MeO	$+ NO_2 + m$	$\rightarrow MeONO_2 + m$	$1.1x10^{-28}(T/300)^{-4}$	$1.6x10^{-11}(T/300)^{-1}$
11	N_2O_5	$+ m$	$\rightarrow NO_2 + NO_3 + m$	$1.72x10^{-3}exp(-11080/T)(T/300)^{-4}$	$9.7x10^{-14}(T/300)^{0.1}exp(11080/T)$
12	NO	$+ NO + m$	$\rightarrow NO_2 + NO_2 + m$	$6.93x10^{-40}exp(530/T)$	
13	NO_2	$+ NO_3 + m$	$\rightarrow N_2O_5 + m$	$2.11x10^{-30}(T/300)^{-3.4}$	$2x10^{-12}(T/300)^{0.2}$
14	O	$+ NO + m$	$\rightarrow NO_2 + m$	$7.8x10^{-32}(T/30)^{-2}$	$3x10^{-11}(T/300)^{0.3}$
15	O	$+ NO_2 + m$	$\rightarrow NO_3 + m$	$7.02x10^{-32}(T/300)^{-2}$	$2x10^{-11}$
16	O	$+ O_2 + m$	$\rightarrow O_3 + m$	$6x10^{-34}(T/300)^{-2.3}$	
17	O(1D)	$+ N_2 + m$	$\rightarrow N_2O + m$	$3.5x10^{-37}(T/300)_{-0.6}$	
18	OH	$+ NO + m$	$\rightarrow HONO + m$	$7x10^{-31}(T/300)^{-2.6}$	$3.6x10^{-11}(T/300)^{-0.1}$
19	OH	$+ NO_2 + m$	$\rightarrow HONO_2 + m$	$2.5x10^{-30}(T/300)^{-4.4}$	$1.6x10^{-11}(T/300)^{-1.7}$
20	OH	$+ OH + m$	$\rightarrow H_2O_2 + m$	$6.24X10^{-31}(T/300)^{-0.8}$	$3x10^{-11}$
21	$MeCO_3$	$+ NO_2 + m$	$\rightarrow PAN + m$	$9.7X10^{-29}(T/300)^{-5.6}$	$9.3x10^{-12}(T/300)^{-1.5}$
22	PAN	$+ m$	$\rightarrow MeCO_3 + NO_2 + m$	$9.9X10^{-3}exp(12100/T)$	$3.7x10^{16}exp(-13600/T)$
23	C_2H_4	$+ OH + m$	$\rightarrow HOCH_2CH_2OO + m$	$1.5x10^{-28}(T/300)^{-3.5}$	$8x10^{-12}$
24	C_3H_6	$+ OH + m$	$\rightarrow HOPriOO + m$	$8x10^{-27}(T/300)^{-3.5}$	$3x10^{-11}$
25	C_2H_2	$+ OH + m$	$\rightarrow HCOCHO + OH + m$	$5.5x10^{-30}$	$8.3x10^{-13}(T/300)^{2}$
26	MeO_2NO_2	$+ m$	$\rightarrow MeOO + NO_2 + m$	$9x10^{-5}exp(9690/T)$	$1.1x10^{16}exp(-10560/T)$
27	MeOO	$+ NO_2 + m$	$\rightarrow MeO_2NO_2 + m$	$2.3x10^{-30}(T/300)^{-4}$	$8x10^{-12}$
28	O	$+ SO_2 + m$	$\rightarrow SO_3 + m$	$3.12x10^{-32}exp(100/T)$	
29	OH	$+ SO_2 + m$	$\rightarrow HOSO_2 + m$	$3.12x10^{-31}(T/300)^{-3.3}$	$2x10^{-12}$
30	$MeSO_2$	$+ m$	$\rightarrow MeOO + SO_2 + m$		
31	$MeSO_3$	$+ m$	$\rightarrow MeOO + SO_3 + m$		

Photolysis chemical equations and

No	Photolysis Reactions			
1	CH_4	+ hν	→	?
2	CO	+ hν	→	C + O
3	H_2O	+ hν	→	OH + H
4	H_2O_2	+ hν	→	OH + OH
5	HO_2	+ hν	→	OH + O
6	HO_2NO_2	+ hν	→	OH + NO_3
7	HO_2NO_2	+ hν	→	HO_2 + NO_2
8	$HONO_2$	+ hν	→	OH + NO_2
9	MeOOH	+ hν	→	MeO + OH
10	MeOOH	+ hν	→	MeO + O + H
11	N_2O_5	+ hν	→	NO_3 + NO_2
12	N_2O_5	+ hν	→	NO_3 + NO + O
13	NO	+ hν	→	N + O
14	NO_2	+ hν	→	NO + O
15	NO_3	+ hν	→	NO + O_2
16	NO_3	+ hν	→	NO_2 + O
17	O_2	+ hν	→	O + O
18	O_3	+ hν	→	O_2 + O
19	O_3	+ hν	→	O_2 + O(1D)
20	HCHO	+ hν	→	CO + HO_2 + HO_2
21	HCHO	+ hν	→	CO + H_2
22	MeCHO	+ hν	→	MeOO + HO_2 + CO
23	MeCHO	+ hν	→	CH_4 + CO
24	EtCOMe	+ hν	→	EtOO + $MeCO_3$
25	HCOCHO	+ hν	→	?
26	MeCOCHO	+ hν	→	$MeCO_3$ + HO_2 + CO
27	EtOOH	+ hν	→	MeCHO + HO_2 + OH
28	BuOOH	+ hν	→	EtCOMe + HO_2 + OH
29	HxOOH	+ hν	→	EtCOMe + EtOO + OH
30	$MeCO_3H$	+ hν	→	MeOO + OH
31	PAN	+ hν	→	MeCOO + NO_2
32	HCOCHCHCHO	+ hν	→	$HCOCHCHCO_3$ + HO_2
33	MeO_2NO_2	+ hν	→	MeOO + NO_2
34	SO_2	+ hν	→	SO + O
35	HONO	+ hν	→	OH + NO
36	CH_2ICl	+ hν	→	CH_2ClO_2
37	HCOCl	+ hν	→	HO_2 + CO + Cll
38	APINOOH	+ hν	→	PINAL + HO_2 + OH
39	PINONIC	+ hν	→	$CO_{23}C_4CHO$ + $MeCOCH_3$ + HCHO + CO_2 + HO_2 + OH + $4O_3$
40	PINAL	+ hν	→	$CO_{23}C_4CHO$ + $MeCOCH_3$ + HCHO + CO + $2HO_2$ + $4O_3$
41	$CO_{23}C_4CHO$	+ hν	→	$MeCO_3$ + HCHO + 2CO + CO_2 + O_3
42	CO_2C_3OOH	+ hν	→	$MeCO_3$ + HCHO + OH
43	$MeCOCH_3$	+ hν	→	$MeCO_3$ + MeO_2
44	OP2	+ hν	→	MeCHO + HO_2 + OH

Surface temperature for a number of climate and landcover scenarios during January and July, generated from the PRECIS-RCM (ECHAM4)

Locations	Scenarios	January (wet season)			July (dry season)		
		Mean	Max	Min	Mean	Max	Min
Danum	BaseA2	22.45	5.62	18.86	28.93	32.11	26.00
	A2PLC	26.90	30.28	23.67	30.84	34.65	28.04
	A2FLC	27.12	30.83	23.43	32.45	36.525	30.43
	BaseB2	22.89	25.82	19.72	28.47	31.27	26.77
	B2PLC	25.55	29.20	21.69	30.70	33.97	28.97
	B2FLC	26.66	30.34	22.62	31.25	34.26	29.02
Koto Tabang	BaseA2	23.38	26.46	19.85	26.91	31.11	24.91
	A2PLC	26.76	31.15	22.88	29.54	32.76	27.36
	A2FLC	27.84	31.53	23.24	29.85	33.31	27.12
	BaseB2	22.88	26.01	19.79	26.49	29.28	24.73
	B2PLC	25.28	28.86	21.24	28.14	30.98	26.54
	B2FLC	25.82	28.31	21.12	28.43	31.43	26.79
Bangkok	BaseA2	23.20	27.45	19.41	30.75	34.93	26.00
	A2PLC	26.02	31.84	19.16	33.12	36.06	31.62
	A2FLC	29.38	34.35	24.56	38.24	41.68	34.81
	BaseB2	22.77	26.82	17.99	31.16	34.07	29.53
	B2PLC	26.78	31.92	21.99	34.02	36.92	32.17
	B2FLC	27.34	31.65	23.10	36.13	39.33	33.67
Jakarta	BaseA2	24.05	27.38	20.66	27.52	32.36	23.89
	A2PLC	27.01	30.92	23.04	33.16	36.23	31.16
	A2FLC	28.25	32.36	23.88	33.73	36.51	31.95
	BaseB2	24.12	27.49	20.30	26.58	28.65	25.20
	B2PLC	26.08	29.23	22.56	28.75	31.43	26.81
	B2FLC	26.33	29.85	22.55	32.04	34.06	30.72
Kuala Lumpur	BaseA2	30.72	33.77	27.03	30.24	32.78	28.06
	A2PLC	30.18	33.53	26.43	34.78	38.22	32.88
	A2FLC	30.62	33.96	26.92	35.05	37.82	33.32
	BaseB2	26.15	29.25	22.82	27.18	29.83	25.46
	B2PLC	28.70	31.63	25.51	31.18	33.83	29.46
	B2FLC	29.16	32.57	25.74	31.66	34.84	30.07

Note: BaseA2 – Baseline for A2
BaseB2-Baseline for B2
PLC – Present-day landcover
FLC- Modified future landcover

APPENDIX 6.5

Boundary layer depth (m) for a number of climate and landcover scenarios during January and July, generated from the PRECIS-RCM (ECHAM4)

Locations	Scenarios	January (wet season)			July (dry season)		
		Mean	Max	Min	Mean	Max	Min
Danum	BaseA2	826.39	1331.63	562.91	540.91	936.38	310.06
	A2PLC	902.19	1490.68	648.41	422.70	878.57	195.12
	A2FLC	831.53	1475.81	384.91	577.91	1228.71	265.58
	BaseB2	806.10	1334.27	521.25	825.52	1394.02	491.90
	B2PLC	810.80	1380.18	519.30	539.83	994.79	393.41
	B2FLC	810.40	1427.15	375.26	539.83	994.79	393.41
Koto Tabang	BaseA2	843.28	1387.19	602.11	499.07	924.22	342.79
	A2PLC	1001.97	1965.85	630.12	505.71	1089.86	224.84
	A2FLC	1292.20	2256.94	704.82	528.48	802.14	178.30
	BaseB2	825.52	1394.02	491.90	469.77	1052.88	323.82
	B2PLC	934.11	1618.03	51143	471.80	1028.63	300.16
	B2FLC	725.17	1461.96	344.17	301.58	304.29	299.86
Bangkok	BaseA2	830.92	1461.12	549.10	1156.19	2123.48	725.83
	A2PLC	815.70	1948.00	309.30	1146.63	1924.68	878.03
	A2FLC	923.82	1969.68	508.16	1278.51	2071.62	975.48
	BaseB2	866.84	1694.84	477.31	1071.33	2092.36	740.93
	B2PLC	882.01	1547.60	575.80	1248.89	2163.79	1006.94
	B2FLC	778.14	1413.92	466.94	1225.93	1876.30	882.75
Jakarta	BaseA2	479.36	876.08	318.05	470.54	909.98	301.28
	A2PLC	438.89	1038.14	249.72	611.61	951.00	428.43
	A2FLC	540.46	983.07	385.63	526.24	735.26	346.21
	BaseB2	585.49	1017.33	378.20	488.42	933.02	349.23
	B2PLC	501.01	853.80	279.38	488.82	933.02	349.23
	B2FLC	473.59	972.38	354.72	526.24	735.26	346.21
Kuala Lumpur	BaseA2	1028.51	1684.95	710.36	587.80	1028.70	463.76
	A2PLC	1168.02	2029.91	794.53	642.05	1347.15	441.29
	A2FLC	1130.87	1820.30	791.60	672.29	1127.24	349.25
	BaseB2	1035.59	1704.97	700.22	584.40	956.30	428.69
	B2PLC	1039.39	1732.62	752.08	598.34	975.32	434.76
	B2FLC	1026.24	1690.55	709.12	725.68	1204.61	524.10

Note: BaseA2 – Baseline for A2
BaseB2-Baseline for B2
PLC - Present-day landcover
FLC - Modified future landcover

Total cloud for a number of climate and landcover scenarios during January and July, generated from the PRECIS-RCM (ECHAM4)

Locations	Scenarios	January (wet season)			July (dry season)		
		Mean	Max	Min	Mean	Max	Min
Danum	BaseA2	0.32	0.87	0.00	0.45	0.97	0.00
	A2PLC	0.23	0.80	0.00	0.50	1.00	0.00
	A2FLC	0.23	0.72	0.00	0.44	0.90	0.00
	BaseB2	0.43	0.95	0.00	0.43	0.95	0.00
	B2PLC	0.06	0.21	0.00	0.39	1.00	0,.00
	B2FLC	0.23	0.68	0.00	0.38	1.00	0.00
Koto Tabang	BaseA2	0.39	1.00	0.00	0.48	1.00	0.00
	A2PLC	0.30	0.95	0.00	0.50	1.00	0.00
	A2FLC	0.32	1.00	0.00	0.42	0.79	0.00
	BaseB2	0.48	1.00	0.00	0.43	0.84	0.00
	B2PLC	0.19	0.51	0.00	0.44	0.92	0.00
	B2FLC	0.34	0.93	0.00	0.44	0.96	0.00
Bangkok	BaseA2	0.29	0.80	0.00	0.70	1.00	0.00
	A2PLC	0.27	0.84	0.00	0.59	1.00	0.00
	A2FLC	0.25	0.70	0.00	0.55	1.00	0.00
	BaseB2	0.30	0.78	0.00	0.62	0.98	0.00
	B2PLC	0.26	0.89	0.00	0.63	1.00	0.00
	B2FLC	0.25	0.70	0.00	0.55	1.00	0.00
Jakarta	BaseA2	0.39	1.00	0.00	0.48	1.00	0.00
	A2PLC	0.30	0.95	0.00	0.50	1.00	0.00
	A2FLC	0.32	1.00	0.00	0.42	0.79	0.00
	BaseB2	0.48	1.00	0.00	0.43	0.84	0.00
	B2PLC	0.19	0.51	0.00	0.44	0.92	0.00
	B2FLC	0.34	0.93	0.00	0.44	0.96	0.00
Kuala Lumpur	BaseA2	0.32	0.87	0.00	0.45	0.97	0.00
	A2PLC	0.23	0.80	0.00	0.50	1.00	0.00
	A2FLC	0.23	0.72	0.00	0.44	0.90	0.00
	BaseB2	0.43	0.95	0.00	0.43	0.95	0.00
	B2PLC	0.06	0.21	0.00	0.39	1.00	0,.00
	B2FLC	0.23	0.68	0.00	0.38	1.00	0.00

Note: BaseA2 – Baseline for A2
BaseB2-Baseline for B2
PLC – Present-day landcover
FLC- Modified future landcover

Summary of comparison of impacts due to the combined effects of climate changes and biogenic emissions, biogenic emissions alone and climate change alone during January and July under different landcover and climate scenarios in five locations in SEA for: (a) O_3; (b) OH; (c) NO; (d) NO_2.

Scenarios	Season	Bangkok				Kuala Lumpur				Jakarta				Danum				Koto Tabang			
		O_3	OH x10^5	NO	NO_2	O_3	OH x10^5	NO	NO_2	O_3	OH x10^5	NO	NO_2	O_3	OH x10^5	NO	NO_2	O_3	OH x10^5	NO	NO_2
Combined:A2PLC	Wet season (January)	26.2	-6.4	0.00	1.8	0.3	1.5	0.01	0.04	8.6	1.3	0.11	2.54	1.9	0.2	0.00	-0.02	-6.7	-0.2	-0.01	-0.08
Combined:A2FLC		32.2	4.9	-0.11	-1.7	-4.9	1.9	-0.02	-0.62	-39.3	6.7	-0.09	-3.94	3.4	0.3	0.01	0.03	-1.9	0.0	0.00	-0.03
BioOnly:A2PLC		36.8	-7.3	-0.20	-3.30	0.0	0.0	0.00	0.00	0.0	0.0	0.00	0.00	2.3	-0.3	0.01	0.00	-1.3	-2.3	0.00	0.12
BioOnly:A2FLC		28.8	5.3	-0.05	-0.25	0.0	0.0	0.00	0.00	0.0	0.0	-0.18	0.00	3.9	-5.5	0.02	-0.04	8.2	-37.8	0.01	0.23
ClimOnly:A2PLC		-10.6	0.9	0.20	5.1	0.3	1.5	0.01	0.04	8.6	1.3	0.11	2.54	-0.4	0.4	-0.01	-0.02	-5.4	2.1	-0.01	-0.2
ClimOnly:A2FLC		3.4	-0.4	-0.06	-1.45	-4.9	1.9	-0.02	-0.62	-39.3	6.7	0.09	-3.94	-0.5	5.8	-0.01	0.07	-10.1	37.8	-0.01	-0.26
Combined:A2PLC	Dry season (July)	31.0	-7.8	-0.04	-0.38	0.1	-1.1	-0.05	-1.03	-17.9	1.4	0.00	-0.85	2.1	0.1	0.00	0.01	-2.0	-0.1	-0.37	0.07
Combined:A2FLC		28.6	-8.2	-0.04	-0.52	-12.0	2.9	0.12	1.72	-5.7	1.2	0.02	-0.01	3.9	0.3	0.00	-0.07	0.1	0.0	-0.38	-0.1
BioOnly:A2PLC		28.9	-9.8	-0.05	-0.39	0.0	0.0	0.00	0.00	0.0	0.0	0.00	0.00	1.8	4.0	0.00	-0.03	-4.3	1.1	-0.36	0.03
BioOnly:A2FLC		32.4	-12.2	-0.05	-0.39	0.0	0.0	0.00	0.00	0.0	0.0	0.00	0.00	3.0	2.8	0.03	0.02	-3.7	0.5	-0.36	-0.04
ClimOnly:A2PLC		2.1	2.0	0.01	0.01	0.1	-1.1	-0.05	-1.03	-17.9	1.4	0.00	-0.85	0.3	-3.9	0.00	0.04	2.3	-1.2	-0.01	0.04
ClimOnly:A2FLC		-3.8	4.0	0.01	-0.13	-12.0	2.9	0.12	1.72	-5.7	1.2	0.02	-0.01	0.9	-2.5	-0.03	-0.09	3.8	-0.5	-0.02	-0.06
Combined:B2PLC	Wet season (January)	23.1	-3.9	-0.05	-0.6	29.4	-4.5	0.10	3.03	16.8	-1.6	0.00	0.56	0.97	0.5	0.00	0.02	-6.27	-0.3	0.00	-0.09
Combined:B2FLC		19.6	-3.2	-0.04	-0.5	0.5	1.5	0.03	0.44	17.2	0.9	0.04	1.54	2.9	0.7	0.01	0.03	-1.4	-0.1	0.00	0.03
BioOnly:B2PLC		22.0	-4.5	-0.05	-0.45	0.0	0.0	0.00	0.00	0.0	0.0	0.00	0.00	1.23	-1.3	0.00	0.03	-3.5	-3.3	0.00	0.01
BioOnly:B2FLC		18.5	-3.8	-0.04	-0.35	0.0	0.0	0.00	0.00	0.0	0.0	0.00	0.00	2.84	0.8	0.01	0.04	-6.39	0.0	-0.01	-0.05
ClimOnly:B2PLC		1.1	0.6	0.00	-0.15	29.4	-4.5	0.10	3.03	16.8	-1.6	0.00	0.56	-0.26	1.8	0.00	-0.01	-2.77	3.0	0.00	-0.1
ClimOnly:B2FL		1.1	0.6	0.00	-0.15	0.5	1.5	0.03	0.44	17.2	0.9	0.04	1.54	0.06	-0.1	0.00	-0.01	4.99	-0.1	0.01	0.08
Combined:B2PLC	Dry season (July)	27.1	-8.9	-0.07	-0.75	-0.5	-0.2	0.00	0.02	-2.2	-0.3	0.00	0.07	1.8	0.1	0.00	0.01	0.7	0.2	0.00	-1.05
Combined:B2FLC		31.2	-8.1	-0.05	-0.33	-6.1	1.2	-0.05	-1.21	-12	0.6	-0.03	-1.07	4.1	0.2	0.00	-0.02	0.51	0.0	0.00	-1.04
BioOnly:B2PLC		33.8	-11.9	-0.06	-0.27	0.0	0.0	0.00	0.00	0.0	0.0	0.00	0.00	1.89	9.1	-0.01	-0.02	1.07	0.7	0.00	-1.01
BioOnly:B2FLC		34.8	-10.0	-0.04	0.17	0.0	0.0	0.00	0.00	0.0	0.0	0.00	0.00	4.45	-1.0	-0.02	-0.01	0.92	0.7	0.00	-1.00
ClimOnly:B2PLC		-6.7	3.0	-0.01	3.0	-0.5	-0.2	0.00	-0.2	-2.2	-0.3	0.00	0.07	-0.09	-9.0	0.01	0.03	-0.37	-0.5	0.00	-0.04
ClimOnly:B2FLC		-3.6	1.9	-0.01	1.9	-6.1	1.2	-0.05	1.2	-12	0.6	-0.03	-1.07	-0.35	1.2	0.02	-0.01	-0.41	-0.7	0.00	-0.04

*All units are in ppbv except OH in molecules cm^{-3}

Note: *A2- SRES A2 climate scenario*
B2 – SRES B2 climate scenario
PLC – Present-day landcover scenario
FLC – Future landcover scenario
Combined – Combined effect of climate changes and biogenic emissions
BioOnly - The effect of biogenic emissions only
ClimOnly- The effect of climate change only

Summary of comparison of impacts due to the combined effects of climate changes and biogenic emissions, biogenic emissions alone and climate change alone during January and July under different landcover and climate scenarios in five locations in SEA for: (a) $HONO_2$; (b) PAN; (c) HCHO; (d) H_2O_2.

Scenarios	Season	Bangkok				Kuala Lumpur				Jakarta				Danum				Koto Tabang			
		$HONO_2$	PAN	HCHO	H_2O_2	$HONO_2$	PAN	HCHO	H_2O_2	$HONO_2$	PAN	HCHO	H_2O_2	$HONO_2$	PAN	HCHO	H_2O_2	$HONO_2$	PAN	HCHO	H_2O_2
Combined:A2PLC	Wet season (January)	5.1	10.30	13.30	3.2	-0.1	-0.08	-0.12	0.29	-2.5	6.90	2.50	-0.7	0.0	-0.04	-1.50	-0.9	0.00	0.23	-0.82	1.46
Combined:A2FLC		13.1	4.10	5.70	3.6	0.4	-0.66	-0.57	0.32	1.8	-12.90	-6.40	0.1	0.0	-0.01	-1.30	-1.6	0.00	-0.31	-3.23	-3.52
BioOnly:A2PLC		8.5	9.25	11.60	4.60	0.0	0.00	0.00	0.00	0.0	0.00	0.00	0.00	0.0	-0.04	-1.47	-0.97	-0.37	0.36	-0.39	1.32
BioOnly:A2FLC		11.1	4.63	6.27	1.58	0.0	0.00	0.00	0.00	0.0	0.00	0.00	0.00	0.1	-0.01	-1.35	-1.55	-0.33	-0.12	-2.66	-3.45
ClimOnly:A2PLC		-3.4	1.05	1.70	-1.4	-0.1	-0.08	-0.12	0.29	-2.5	6.90	2.50	-0.7	0.0	0.00	-0.03	0.07	-0.37	-0.13	-0.43	0.14
ClimOnly:A2FLC		2.0	-0.53	-0.57	2.02	0.4	-0.66	-0.57	0.32	1.8	-12.90	-6.40	0.1	-0.1	0.00	0.05	-0.05	-0.33	-0.19	-0.57	-0.07
Combined:A2PLC	Dry season (July)	-6.5	5.20	-0.41	5.9	0.2	-0.87	-0.41	0.49	0.2	-4.40	-1.80	-0.3	0.0	0.05	-0.60	-0.6	0.00	0.04	1.20	0.91
Combined:A2FLC		-7.6	5.40	8.40	7.2	-0.7	-0.88	-0.35	-0.55	0.8	-1.10	-0.70	-0.2	0.0	-0.13	-2.10	-0.8	0.00	0.02	0.39	0.65
BioOnly:A2PLC		-6.3	5.23	-0.27	7.88	0.0	0.00	0.00	0.00	0.0	0.00	0.00	0.00	-0.6	0.05	-0.63	-0.56	-0.47	-0.03	1.01	0.89
BioOnly:A2FLC		-7.2	5.78	8.53	7.65	0.0	0.00	0.00	0.00	0.0	0.00	0.00	0.00	0.0	-0.13	-2.09	-0.82	-0.43	-0.02	0.37	0.56
ClimOnly:A2PLC		-0.2	-0.03	-0.14	-1.98	0.2	-0.87	-0.41	0.49	0.2	-4.40	-1.80	-0.3	0.6	0.00	0.03	-0.04	-0.47	0.07	0.19	0.02
ClimOnly:A2FLC		-0.5	-0.38	-0.13	-0.45	-0.7	-0.88	-0.35	-0.55	0.8	-1.10	-0.70	-0.2	0.0	0.00	-0.01	0.02	-0.43	0.04	0.02	0.09
Combined:B2PLC	Wet season (January)	-6.1	3.60	5.1	2.1	-1.1	4.90	3.5	-0.64	1.9	4.50	1.7	0.56	0.0	-0.02	-0.7	-0.5	0.00	-0.18	-0.48	0.42
Combined:B2FLC		-4.9	2.90	4.2	2.9	-0.4	0.14	0.09	-0.14	-0.5	6.20	2.5	1.54	0.0	-0.02	-0.8	-0.7	0.00	0.16	1.74	1.29
BioOnly:B2PLC		-6.6	3.61	5.14	2.23	0.0	0.00	0.00	0.00	0.0	0.00	0.00	0.00	0.0	-0.02	-0.68	-0.56	-0.36	-0.08	-0.16	0.34
BioOnly:B2FLC		-4.8	2.91	4.24	2.44	0.0	0.00	0.00	0.00	0.0	0.00	0.00	0.00	0.0	-0.02	-0.80	-0.72	-0.37	0.06	1.58	1.20
ClimOnly:B2PLC		0.5	-0.01	-0.04	-0.13	-1.1	4.90	3.5	-0.64	1.9	4.50	1.7	0.56	0.0	0.00	-0.02	0.06	-0.36	-0.10	-0.32	0.08
ClimOnly:B2FL		-0.2	-0.01	-0.04	0.46	-0.4	0.14	0.09	-0.14	-0.5	6.20	2.5	1.54	0.0	0.00	0.00	0.02	-0.37	0.10	0.16	0.09
Combined:B2PLC	Dry season (July)	-6.6	5.10	8	6.1	0.0	-0.05	-0.02	-0.02	-0.1	-0.20	0.04	0.07	0.0	0.04	-0.4	-0.8	0.00	-0.01	-0.4	0.03
Combined:B2FLC		0.5	4.30	5.5	4.9	0.3	-1.60	-0.91	0.1	0.1	-3.70	-1.5	-1.07	0.0	-0.01	-1.5	-1.5	0.00	-0.01	-0.37	-0.09
BioOnly:B2PLC		-6.9	5.53	8.32	6.49	0.0	0.00	0.00	0.00	0.0	0.00	0.00	0.00	0.0	0.03	-0.41	-0.75	-0.43	0.01	-0.36	-0.03
BioOnly:B2FLC		-0.1	4.62	5.80	4.36	0.0	0.00	0.00	0.00	0.0	0.00	0.00	0.00	0.0	-0.02	-1.53	-1.55	-0.46	0.01	-0.40	-0.15
ClimOnly:B2PLC		0.3	-0.43	-0.32	-0.39	0.0	-0.05	-0.02	-0.02	-0.1	-0.20	-0.05	0.07	0.0	0.01	0.01	-0.05	-0.43	-0.02	-0.04	0.06
ClimOnly:B2FLC		0.5	-0.32	-0.30	0.54	0.3	-1.60	-0.91	0.1	0.1	-3.70	0.00	-1.07	0.1	0.01	0.03	0.05	-0.46	-0.02	0.03	0.06

*All units are in ppbv except OH in molecules cm^{-3}

Note: *A2- SRES A2 climate scenario*
B2 – SRES B2 climate scenario
PLC – Present-day landcover scenario
FLC – Future landcover scenario
Combined – Combined effect of climate changes and biogenic emissions
BioOnly - The effect of biogenic emissions only
ClimOnly- The effect of climate change only

APPENDIX 6.9

BANGKOK: Tropospheric chemistry composition under various climate, landcover, biogenic emissions during January and July.

Bangkok (Thailand)		With BVOC						Without BVOC					
		January (wet season) (ppbv)			July (dry season) (ppbv)			January (wet season) (ppbv)			July (dry season) (ppbv)		
		Mean	Min	Max	Mean	Min	Max	Mean	Min	Max	Mean	Min	Max
O_3	BaseA2	160.20	109.4	221.1	147.70	112.10	188.6	158.6	108.30	219	140.10	106	179.5
	BaseB2	159	112.10	215.1	147.9	109.4	192	158.4	111.7	214	141.9	104.8	184.6
	B2PLC	182.1	128.3	244.6	175	130	225	159.5	112.7	215.1	135.2	101.5	173.5
	B2FLC	178.6	125.8	240.1	179.1	134.3	229.1	159.5	112.7	215.7	138.30	104.20	176.80
	A2PLC	186.4	105.5	277.4	178.7	133.8	227.6	148	83.58	226.2	142.2	107.3	181.5
	A2FLC	192.4	142.10	250.9	176.3	131.1	225.4	162	120	212.10	136.3	102.7	173.6
OH	BaseA2	1.74E6	2.35E4	6.98E6	2.06E6	2.57E4	1.7E6	1.78E06	2.34E04	7.16E0	2.27E06	2.14E04	8.41E16
	BaseB2	1.75E6	2.14E4	7.06E6	2.14E6	2.55E4	7.79E6	1.77E6	2.39E4	7.14E6	2.31E6	2.40E4	8.54E6
	B2PLC	1.36E6	2.62E4	5.13E6	1.25E6	2.87E4	4.31E6	1.83E6	2.54E4	7.38E6	248E6	2.52E4	9.16E6
	B2FLC	1.43E6	2.61E4	5.46E6	1.60E6	2.99E4	5.61E6	1.83E6	2.45E4	7.38E6	2.50E6	2.55E4	9.20E6
	A2PLC	1.1E6	2.16E4	3.9E6	1.28E6	2.95E4	4.37E6	1.87E6	2.03E4	7.35E6	2.47E6	2.55E4	9.06E6
	A2FLC	1.25E6	2.67E4	4.77E6	1.34E6	2.95E4	4.18E6	1.74E6	2.43E4	7.06E6	2.67E6	2.67E4	9.79E6
NO	BaseA2	0.33	0.001	1.09	0.22	7.7E-4	0.69	0.33	1.01E-3	1.11	0.23	7.26	0.71
	BaseB2	0.31	1.18-3	1.02	0.25	8.80-4	0.74	0.31	1.16E-3	1.02	0.25	8.24E-4	0.77
	B2PLC	0.26	1.41-3	0.87	0.18	1.12-3	0.54	0.31	1.13E-3	1.01	0.24	7.71E-4	0.72
	B2FLC	0.27	1.36-3	0.90	0.20	8.60-4	0.61	0.31	1.13E-3	1.01	0.24	7.24E-4	0.71
	A2PLC	0.33	2.16-3	1.25	0.18	1.16-3	0.55	0.57	1.85E-4	1.92	0.24	7.63E-4	0.72
	A2FLC	0.22	1.18-3	0.76	0.18	1.25-3	0.52	0.27	9.43E-4	0.88	0.24	8.23E-4	0.73
NO_2	BaseA2	8.14	4.30	14.90	4.84	3.06	7.46	8.16	4.32	15.02	4.80	3.13	7.41
	BaseB2	7.63	4.01	14.1	5.18	3.17	7.94	7.64	4.02	14.15	5.16	3.24	8
	B2PLC	7.05	3.75	11.66	4.43	2.66	6.63	7.49	4.05	13.72	4.68	3.17	7.03
	B2FLC	7.16	3.80	12.12	4.85	2.82	7.25	7.49	4.05	13.72	4.66	3.06	6.94
	A2PLC	9.91	4.32	17.02	4.46	2.67	6.75	13.26	5.18	24.16	4.81	3.18	7.29
	A2FLC	6.44	3.39	10.72	4.32	2.66	6.40	6.71	3.67	12.37	4.67	3.15	6.93
$HONO_2$	BaseA2	8.14	4.30	14.90	14.06	12.01	16.35	27.88	23.89	30.66	15.17	12.98	17.65
	BaseB2	27.55	23.91	30.27	13.61	11.35	16.15	27.76	24.08	30.49	14.56	12.17	17.26
	B2PLC	21.49	19.11	23.65	7.03	5.78	8.74	28.22	24.55	30.64	14.88	12.57	17.62
	B2FLC	22.68	20.07	24.9	9.66	7.68	12.15	28.22	24.55	30.22	15.10	12.75	18.0
	A2PLC	13.24	10.15	17.54	7.52	6.32	9.17	24.49	17.87	30.93	14.98	12.62	17.81
	A2FLC	21.25	19.08	22.53	6.50	5.37	8.07	29.90	26.77	31.65	14.72	12.22	17.69
PAN	BaseA2	5.47	3.78	6.52	3.69	2.71	4.53	5.25	3.604	6.32	2.93	2.04	3.18
	BaseB2	4.98	3.43	6.02	3.70	2.67	4.67	4.90	3.36	5.95	3.05	2.09	4.06
	B2PLC	8.57	6.38	10.12	8.82	7.63	9.81	4.89	3.37	5.90	2.62	1.81	3.49
	B2FLC	7.85	5.78	9.27	7.99	6.73	8.79	4.89	3.37	5.90	2.73	1.91	3.57
	A2PLC	15.77	11.4	20.59	8.85	7.63	9.70	6.3	4.09	7.94	2.9	2.61	3.81
	A2FLC	9.61	7.49	10.77	9.07	7.93	10.06	4.72	3.30	5.55	2.55	1.74	3.45
HCHO	BaseA2	7.05	6.56	7.54	5.24	4.93	5.82	6.70	6.28	7.09	4.02	3.75	4.42
	BaseB2	6.48	6.01	6.84	5.13	4.79	5.78	6.33	5.90	6.65	4.09	3.85	4.63
	B2PLC	11.60	10.2	13.22	13.10	12.23	14.54	6.29	5.93	6.57	3.77	3.53	4.25
	B2FLC	10.65	9.42	12.02	10.66	9.77	11.67	6.29	5.93	6.57	3.79	3.52	4.26
	A2PLC	20.32	15.39	26.63	12.79	11.66	14.34	8.42	6.85	9.97	3.88	3.63	4.36
	A2FLC	12.71	11.86	13.92	13.65	12.62	15.22	6.13	5.74	6.57	3.61	3.34	4.17
H_2O_2	BaseA2	3.38	2.36	4.74	5.48	3.92	7.68	3.27	2.28	4.61	3.41	7.08	4.91
	BaseB2	12.07	11.07	13.25	5.77	4.34	7.81	3.75	2.78	5.0	5.28	3.19	7.30
	B2PLC	5.91	4.27	7.87	11.84	9.64	14.59	3.62	2.58	5.00	4.89	3.52	6.89
	B2FLC	5.41	3.91	7.22	9.79	7.77	12.39	3.62	2.58	5.00	4.97	3.46	7.19
	A2PLC	6.55	3.96	9.64	11.42	8.98	14.52	1.59	1.36	2.53	5.39	3.89	7.60
	A2FLC	6.97	5.07	9.26	12.70	1043	15.5	3.79	2.56	5.45	5.29	3.99	7.22

Note: BaseA2 – Baseline for A2
BaseB2-Baseline for B2
PLC – Present-day landcover
FLC- Modified future landcover

BANGKOK: Tropospheric chemistry composition changes under various climate, biogenic emissions and landcover scenarios January and July.

Season	Scenarios	O_3 ppbv [%]	NO ppbv [%]	NO_2 ppbv [%]	OH Molecules cm^{-3} [%]	$HONO_2$ ppbv [%]	PAN ppbv [%]	HCHO ppbv [%]	H_2O_2 ppbv [%]
Wet Season (January)	A2PLC-BaseA2	26.2 [16.4]	0.0 [0.0]	1.8 [21.7]	-6.4E5 [36.8]	-5.1 [62.7]	10.3 [188.2]	13.3 [188.2]	3.2 [93.8]
	A2FLC-BaseA2	32.2 [20.1]	-0.11 [33.3]	-1.7 [21.4]	-4.9E5 [28.2]	13.11 [161.1]	4.1 [75.7]	5.7 [80.3]	3.6 [106.2]
	A2FLC-A2PLC	6.0 [3.2]	-0.11 [33.3]	-3.5 [35.0]	4.3E6 [76.6]	8.01 [60.5]	-6.2 [39.1]	-7.6 [37.5]	0.2 [2.9]
	XA2PLC-XBaseA2	-10.6 [6.7]	0.2 [72.7]	5.1 [62.5]	9.0E4 [5.1]	-3.4 [12.2]	1.05 [20.0]	1.7 [25.7]	-1.4 [42.2]
	B2PLC-BaseB2	23.1 [14.5]	-0.05 [16.1]	-0.6 [7.6]	-3.9E5 [22.3]	-6.1 [21.9]	3.6 [72.1]	5.1 [79.0]	2.1 [55.6]
	B2FLC-BaseB2	19.6 [12.3]	-0.04 [12.9]	-0.5 [6.4]	-3.2E5 [18.3]	-4.9 [17.7]	2.9 [57.6]	4.2 [64.4]	2.9 [112.2]
	B2FLC-B2PLC	-3.5 [1.9]	0.01 [3.9]	0.11 [1.6]	7.0E4 [5.2]	1.2 [5.5]	-0.7 [8.4]	-1.0 [8.2]	0.5 [8.5]
	XB2PLC-XBaseB2	1.1 [0.7]	0.0 [0.0]	-0.15 [2.0]	6.0E4 [3.4]	0.46 [1.7]	-0.01 [2.0]	-0.04 [0.6]	-0.13 [3.5]
Dry Season (July)	A2PLC-BaseA2	31.0 [21.0]	-0.04 [18.2]	-0.38 [7.9]	-7.8E5 [37.9]	-6.5 [46.5]	5.2 [139.8]	7.6 [144.1]	5.9 [108.4]
	A2FLC-BaseA2	28.6 [19.4]	-0.04 [18.2]	-0.52 [11.3]	-2.6E5 [12.6]	-7.6 [53.8]	5.4 [145.8]	8.4 [160.5]	7.2 [131.8]
	A2FLC-A2PLC	-2.4 [1.3]	0.0 [0.0]	-0.14 [3.1]	6.0E4 [4.7]	-1.02 [13.6]	0.2 [2.5]	0.9 [6.7]	1.3 [11.2]
	XA2PLC-XBaseA2	2.1 [1.5]	0.01 [4.4]	0.01 [0.2]	2.0E5 [8.8]	-0.2 [1.3]	-0.03 [1.02]	-0.14 [3.5]	1.98 [58.1]
	B2PLC-BaseB2	27.1 [18.3]	-0.07 [28.0]	-0.75 [46.0]	-8.9E5 [41.6]	-6.6 [48.4]	5.1 [138.4]	8.0 [155.4]	6.1 [105.2]
	B2FLC-BaseB2	31.2 [21.1]	-0.05 [20.0]	-0.33 [5.2]	-5.4E5 [25.2]	-4.0 [29.0]	4.3 [116.0]	5.5 [107.8]	4.0 [69.7]
	B2FLC-B2PLC	4.1 [2.3]	0.02 [11.1]	0.42 [9.5]	8.0E4 [9.0]	2.6 [37.4]	-0.8 [9.4]	-2.4 [18.6]	-2.1 [17.3]
	XB2PLC-XBaseB2	-6.7 [4.7]	-0.01 [4.0]	-0.48 [9.3]	3.0E5 [15.2]	0.32 [2.2]	-0.43 [14.1]	-0.32 [7.8]	-0.39 [7.4]

Note: *PLC-present-day landcover*
FLC-Future landcover
A2PLC-BaseA2/B2PLC-BaseB2: Changes due to climate changes and biogenic emissions under present-day landcover
A2FLC-BaseA2/B2FLC-BaseB2: Changes due to climate changes and biogenic emissions under future-day landcover
A2FLC-A2PLC/B2FLC-B2PLC: Changes between present-day landcover and future landcover sceanrios

DANUM: Tropospheric chemistry composition in various climate, biogenic emissions and landcover scenarios during January and July.

Danum, Borneo (Malaysia)		With BVOC						Without BVOC					
		January (wet season) (ppbv)			July (dry season) (ppbv)			January (wet season) (ppbv)			July (dry season) (ppbv)		
		Mean	Min	Max	Mean	Min	Max	Mean	Min	Max	Mean	Min	Max
O_3	BaseA2	4.40	2.03	6.48	7.72	1.37	13.66	15.10	13.40	16.64	14.53	9.65	19.89
	BaseB2	7.62	5.56	9.35	6.68	1.19	11.82	14.97	13.32	16.47	15.04	11.02	19.32
	B2PLC	8.59	6.55	10.30	8.45	2.16	14.16	14.71	13.03	16.23	14.95	10.38	19.68
	B2FLC	10.53	8.00	11.77	10.75	4.08	16.69	15.03	13.40	16.46	14.69	9.39	20.09
	A2PLC	6.31	4.34	7.94	9.84	2.38	16.55	14.70	13.18	16.04	14.80	8.84	20.88
	A2FLC	7.80	4.86	10.34	11.58	5.26	17.23	14.60	12.11	17.07	15.41	11.36	19.62
OH	BaseA2	1.45E4	533.60	4.52E4	2.27E4	536.6	6.44E4	3.43E6	2.37	1.31E07	5.23E6	3.13E3	2.04E07
	BaseB2	4.17E4	2.63E3	1.31E05	1.90E4	442.2	5.64E4	3.50E6	2.411	1.32E7	5.06E6	2.99E3	1.93E7
	B2PLC	8.97E4	2.43E3	1.32E5	2.66E4	0.85E3	7.70E4	3.68E6	2.43E3	1.36E7	4.97E6	3.01E-3	1.92E7
	B2FLC	9.88E4	6.06E3	3.67E5	4.02E4	1.86E3	1.18E5	3.49E6	2.30E3	1.31E7	4.94E6	2.90E3	1.95E7
	A2PLC	2.96E4	1.69E3	9.25E4	3.23E4	1.03E3	9.36E4	3.47E6	2.27E3	1.30E7	4.84E6	2.80E3	1.92E7
	A2FLC	4.30E4	2.16E3	1.28E3	4.72E4	2.54E3	1.40E5	4.01E6	2.89E3	1.51E7	4.98E6	3.01E3	1.88E7
NO	BaseA2	0.01	593.4	0.06	0.03	1.24E-3	0.19	0.05	3.19E-4	0.15	0.14	1.94E-4	0.59
	BaseB2	0.01	6.11E-4	0.06	0.03	1.16E-3	0.17	0.05	3.69E-4	0.14	0.11	1.71	0.45
	B2PLC	0.02	6.12E-4	0.06	0.03	9.83E-4	0.15	0.05	3.78E-4	0.15	0.12	1.46E-3	0.50
	B2FLC	0.02	5.33E-4	0.06	0.03	9.6E-4	0.13	0.05	3.08E-4	0.14	0.13	1.26E7	0.57
	A2PLC	0.01	6.24E-4	0.05	0.03	8.12E-4	0.16	0.04	3.31E-4	0.14	0.14	1.16E-3	0.63
	A2FLC	0.02	8.27E-4	0.08	0.03	9.92E-4	0.12	0.06	5.35E-4	0.20	0.11	1.51E-3	0.44
NO_2	BaseA2	0.13	0.05	0.23	0.38	0.15	0.82	0.25	0.14	0.38	0.59	0.24	1.08
	BaseB2	0.12	0.06	0.21	0.33	0.13	0.71	0.25	0.14	0.37	0.51	0.21	0.91
	B2PLC	0.12	0.05	0.20	0.34	0.15	0.70	0.24	0.13	0.36	0.54	0.22	0.98
	B2FLC	0.15	0.07	0.23	0.33	0.15	0.64	0.24	0.13	0.36	0.58	0.23	1.09
	A2PLC	0.11	0.05	0.19	0.39	0.17	0.80	0.23	0.13	0.34	0.63	0.24	1.17
	A2FLC	0.16	0.07	0.27	0.31	0.15	0.58	0.32	0.17	0.48	0.50	0.21	0.90
$HONO_2$	BaseA2	6.82E-4	4.62E-4	9.02E-4	1.16E-3	2.66E-4	1.97E-3	0.38	0.25	0.54	0.41	0.07	0.41
	BaseB2	1.93E-3	1.41E-3	2.59E-3	9.98E-4	3.09E-4	1.61E-3	0.36	0.25	0.52	0.41	0.11	0.83
	B2PLC	1.86E-3	1.32E-3	2.46E-3	1.44E-3	4.21E-4	2.39E-3	0.36	0.24	0.51	0.43	0.10	0.89
	B2FLC	6.0E-3	4.0E-3	8.0E-3	2.2E-3	7.0E-4	3.7E-3	0.38	0.26	0.54	0.46	0.09	0.97
	A2PLC	1.37E-3	1.00E-3	1.77E-7	1.92E-3	4.21E-4	3.33E -3	0.37	0.26	0.52	0.47	6.08	1.020
	A2FLC	1.66E-3	9.37E-4	0.49E-3	2.5E-3	9.95E4	4.12E-3	0.33	0.17	0.55	0.43	0.13	0.84
PAN	BaseA2	0.14	0.10	0.19	0.58	0.49	0.70	0.01	7.03E-3	0.03	0.02	0.01	0.04
	BaseB2	0.11	0.07	0.14	0.50	0.42	0.60	0.01	6.68E-3	0.03	0.01	6.50	0.03
	B2PLC	0.10	6.07	0.13	0.54	0.42	0.65	0.01	0.005	0.02	0.02	0.01	0.04
	B2FLC	0.09	0.06	0.10	0.49	0.37	0.60	0.01	0.07	0.02	0.02	0.01	0.04
	A2PLC	0.10	0.06	0.14	0.63	0.49	0.77	0.009	0.006	0.02	0.02	0.01	0.05
	A2FLC	0.13	0.09	0.17	0.45	0.34	0.56	0.01	6.66E-3	0.03	0.02	7.71E-3	0.03
HCHO	BaseA2	5.21	4.02	6.18	9.14	8.39	10.03	0.76	0.73	0.86	0.72	0.52	1.05
	BaseB2	3.52	2.95	4.03	8.95	7.98	9.87	0.75	0.71	0.86	0.70	0.54	0.99
	B2PLC	3.40	2.87	3.88	8.57	7.65	9.49	0.73	0.68	0.85	0.71	0.54	1.01
	B2FLC	2.73	2.50	2.96	7.45	6.74	8.33	0.75	0.71	0.85	0.73	0.54	1.05
	A2PLC	3.68	2.99	4.28	8.57	7.95	9.56	0.73	0.69	0.83	0.75	0.54	1.09
	A2FLC	3.88	3.35	4.47	7.05	6.28	8.00	0.81	0.72	0.96	0.71	0.56	0.99
H_2O_2	BaseA2	4.21	3.70	4.73	5.23	3.63	7.06	0.77	0.63	0.93	0.77	0.63	0.93
	BaseB2	3.02	2.70	3.35	5.98	4.57	7.56	0.81	0.69	0.96	0.40	0.26	0.60
	B2PLC	3.06	2.74	3.38	5.22	3.73	6.88	0.87	0.75	1.00	0.35	0.19	0.58
	B2FLC	2.35	2.10	2.62	4.49	3.25	5.90	0.83	0.69	0.99	0.29	0.12	0.54
	A2PLC	3.28	2.93	3.64	4.68	2.88	6.66	0.84	0.72	0.99	0.31	0.52	0.17
	A2FLC	2.63	2.29	2.98	4.48	3.41	5.71	0.67	0.56	0.79	0.39	0.23	0.63

Note: BaseA2 – Baseline for A2
BaseB2-Baseline for B2
PLC – Present-day landcover
FLC- Modified future landcover

DANUM: Tropospheric chemistry composition changes in various climate changes, biogenic emissions and landcover scenarios during January and July.

Season	Scenarios	O_3 ppbv [%]	NO ppbv [%]	NO_2 ppbv [%]	OH Molecules cm^{-3} [%]	$HONO_2$ ppbv [%]	PAN ppbv [%]	HCHO ppbv [%]	H_2O_2 ppbv [%]
Wet Season (January)	A2PLC-BaseA2	1.9 [43.4]	<0.001 [<0.01]	-0.02 [15.4]	1.5E4 [104.1]	6.9E-4 [100.9]	-0.04 [28.6]	-1.5 [29.4]	-0.9 [22.1]
	A2FLC-BaseA2	3.4 [77.3]	0.01 [100.0]	0.03 [23.1]	2.9E4 [196.6]	9.8E-4 [143.4]	-0.01 [7.1]	-1.3 [25.5]	-1.6 [37.5]
	A2FLC-A2PLC	1.5 [23.6]	0.01 [100.0]	0.05 [45.5]	1.3E4 [45.3]	2.9E-4 [21.2]	0.03 [30.0]	0.2 [5.4]	-0.7 [20.3]
	XA2PLC-XBaseA2	-0.4 [2.6]	-0.01 [20.0]	-0.02 [8.0]	4.0E4 [1.2]	-0.01 [2.6]	-0.001 [10.0]	-0.03 [4.0]	0.07 [9.1]
	B2PLC-BaseB2	0.97 [12.7]	0.01 [100.0]	0.02 [16.7]	4.8E3 [115.8]	2.6E-3 [132.7]	-0.02 [18.2]	-0.7 [19.3]	-0.5 [17.9]
	B2FLC-BaseB2	2.9 [38.2]	0.01 [100.0]	0.03 [25.0]	5.7E4 [136.9]	4.0E-3 [206.1]	-0.02 [18.2]	-0.8 [22.4]	-0.7 [22.2]
	B2FLC-B2PLC	0.5 [4.8]	0.01 [100.0]	0.01 [7.1]	9.1E3 [10.1]	1.4E-3 [31.6]	-0.001 [1.1]	-0.11 [3.9]	-0.13 [5.2]
	XB2PLC-XBaseB2	-0.3 [1.7]	<0.001 [0.00]	-0.01 [4.0]	1.8E5 [5.1]	<0.001 [<0.01]	<0.001 [<0.01]	-0.02 [2.7]	0.06 [7.4]
Dry Season (July)	A2PLC-BaseA2	2.1 [27.5]	<0.001 [0.0]	0.01 [2.6]	9.6E3 [42.3]	7.6E-4 [66.5]	0.05 [8.6]	-0.6 [6.2]	-0.6 [10.5]
	A2FLC-BaseA2	3.9 [50.0]	<0.001 [<0.01]	-0.07 [18.4]	2.5E4 [107.9]	1.3E-3 [115.5]	-0.13 [22.4]	-2.1 [22.9]	-0.8 [14.3]
	A2FLC-A2PLC	1.7 [17.7]	<0.001 [<0.01]	-0.08 [20.5]	1.5E4 [46.1]	6.1E-4 [31.8]	-0.18 [28.6]	-1.5 [17.7]	-0.2 [4.3]
	XA2PLC-XBaseA2	0.3 [1.9]	<0.001 [0.00]	0.04 [6.8]	-3.9E5 [7.5]	0.06 [12.8]	<0.001 [0.00]	0.03 [4.2]	-0.04 [12.9]
	B2PLC-BaseB2	1.8 [26.5]	<0.001 [<0.01]	0.01 [3.0]	7.6E3 [40.0]	4.4E-4 [44.3]	0.04 [8.0]	-0.4 [4.2]	-0.8 [12.7]
	B2FLC-BaseB2	4.1 [60.9]	<0.001 [<0.01]	-0.02 [6.1]	2.1E4 [111.6]	1.2E-3 [118.4]	-0.01 [2.0]	-1.5 [16.8]	-1.5 [24.9]
	B2FLC-B2PLC	2.3 [27.2]	<0.001 [<0.01]	-0.01 [2.9]	1.4E4 [51.0]	7.4E-4 [51.4]	-0.05 [9.3]	-1.12 [13.1]	-0.7 [14.0]
	XB2PLC-XBaseB2	-0.1 [0.6]	0.01 [9.1]	0.03 [5.9]	-9.0E5 [98.2]	0.02 [4.9]	0.01 [100.0]	0.01 [1.4]	-0.05 [12.5]

Note: *PLC-present-day landcover*
FLC-Future landcover
A2PLC-BaseA2/B2PLC-BaseB2: Changes due to climate changes and biogenic emissions under present-day landcover
A2FLC-BaseA2/B2FLC-BaseB2: Changes due to climate changes and biogenic emissions under future-day landcover
A2FLC-A2PLC/B2FLC-B2PLC: Changes between present-day landcover and future landcover scenarios
XA2PLC-XBaseA2/XB2PLC-XBaseb2: Changes due to climate changes alone (without biogenic emissions)

KUALA LUMPUR, JAKARTA & KOTO TABANG :Impact of Climate Changes and Biogenic Emissions under Present-day and Modified Future Landcover (PLC)

A6.13.1.1 Kuala Lumpur

A6.13.1.1.1 O_3

The present-day O_3 concentrations during January and July in Kuala Lumpur were relatively lower than in Jakarta and Bangkok by about 143.8 ppbv and 141.5 ppbv for BaselineA2, and 143.6 ppbv and 137.8 ppbv for BaselineB2 climate scenarios (Appendix 6.14). The combined effects of climate change and biogenic emissions (A2PLC and B2PLC) were observed to have very little impact on the increase of future O_3 concentrations, only about 0.3 ppbv (0.2%) during January and 0.1 ppbv (0.1%) during July in the A2 climate scenario (Figure 6.5 and Figure A6.13.1; Appendix 6.7 and Appendix 6.15). In the B2 climate scenario, future surface O_3 concentrations were increased by 29.4 ppbv (20.5%) during January but decreased by 0.5 ppbv (0.4%) during July. Similar to those observed in Bangkok and Jakarta, future surface O_3 concentrations in Kuala Lumpur were also found to be higher during January than July in both the A2 and B2 climate scenarios.

To investigate the isoprene emissions effects on future O_3 concentrations, the biogenic factor was removed from the CiTTyCAT model and compared with the run that had the biogenic emissions factor. Results were similar to those observed in Jakarta, where biogenic emissions have been shown to have no impact on surface O_3 concentrations, despite relatively high biogenic emissions. As the anthropogenic emissions were kept constant in the future climate scenario simulations, the changes in surface O_3 concentrations were due to climate changes alone. Similar to other major cities in SEA, Kuala Lumpur is an urban area with a projection of high anthropogenic emissions. As the impact of biogenic emissions on future surface O_3 were negligible and the effect of climate change was relatively minimal, anthropogenic emissions of NO_x and VOCs could have played important roles in the increase of O_3 in Kuala Lumpur, despite the fact that anthropogenic emissions were kept constant in the future simulations. If future anthropogenic emissions are taken into consideration, expected to be higher than the present scenario (IPCC, 2000), the current simulation of future O_3 concentrations will certainly be further modified due to several competing processes. Based on present-day inventory for anthropogenic emissions, NO_x and VOCs accounted for a larger portion of the future O_3 production. Production of O_3 through direct photolysis of NO_2 and

subsequent reactions involving NO_x and photochemical oxidation of anthropogenic VOCs are the most possible pathway in an urban environment like Kuala Lumpur.

Modification of future landcover in SEA has also shown no impact by biogenic emissions on the surface O_3 concentrations. Climate changes alone were observed to decrease surface O_3 by 4.9 ppbv (3.4%) and 12 ppbv (8.5%) during January and July respectively in A2 the climate scenario (Figure 6.5 and Figure A6.13.1; Appendix 6.7 and Appendix 6.15). In the B2 climate scenario, climate change was responsible for the small increase of O_3 during January of about 0.5 ppbv (0.4%). Comparatively, climate change impact on future O_3 concentrations was much larger in the present-day landcover scenario.

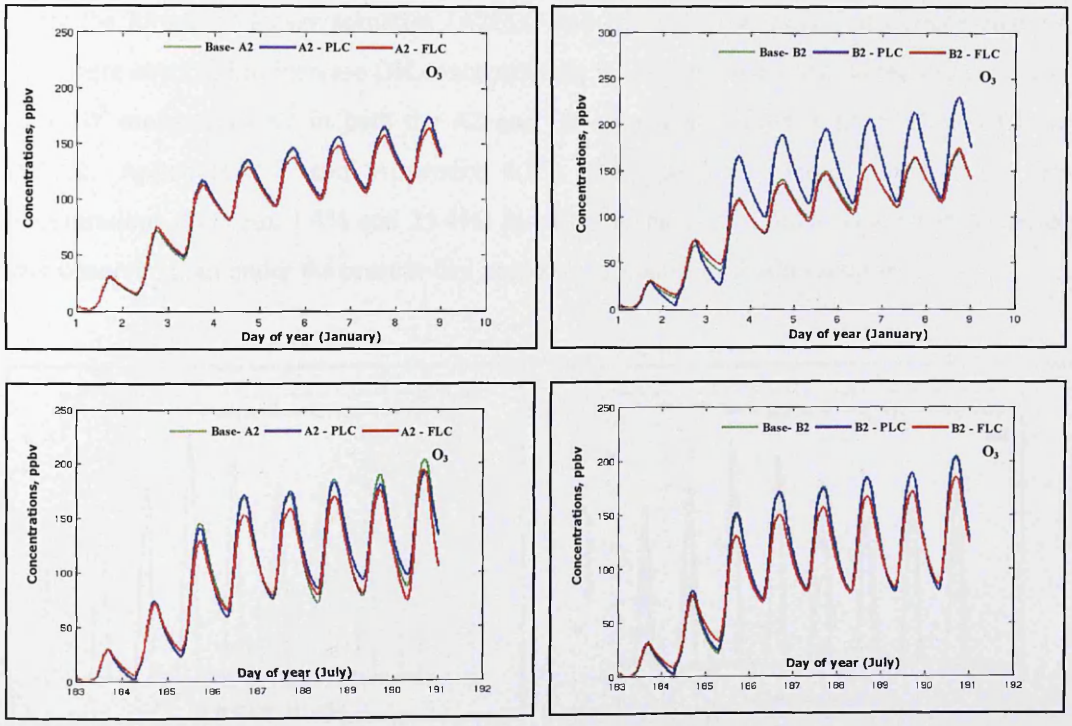

Figure A6.13.1: ***Kuala Lumpur***: Simulated O_3 (ppbv) during January and July for the A2 (*left panel*) and B2 (*right panel*) emission scenarios under present-day (PLC) and modified future landcover (FLC).

A6.13.1.1.2 OH

Under the present-day landcover scenarios (A2PLC and B2PLC), climate changes played a much larger role in the future changes of OH concentrations in Kuala Lumpur, while biogenic emissions were observed to have no impact on them (Appendix 6.14). Climate changes alone were responsible for the increase of OH concentrations by 1.5 x 10^5 molecules cm^{-3} (5.4%) during January and a decrease by 1.1 x 10^5 molecules cm^{-3} (4.5%) during July in A2 (Figure 6.5 and Figure A6.13.2; Appendix 6.7 and Appendix 6.15). In the B2 climate scenario, climate changes accounted for the decrease of about 4.5 x 10^5 molecules cm^{-3} (16%) and 2.0 x 10^5 molecules cm^{-3} (0.8%) during January and July respectively.

Under the future landcover scenarios (A2FLC and B2FLC), the impact of climate changes alone were observed to increase OH concentrations by between 0.4 x 10^5 molecules cm^{-3} and 2.9 x 10^5 molecules cm^{-3} in both the A2 and B2 climate scenarios (Figure 6.5 and Figure A6.13.2; Appendix 6.7 and Appendix 6.15). Comparatively, larger impacts on OH concentrations (between 1.4% and 25.4%) by climate changes in future landcover scenarios were observed than under the present-day landcover scenario in Kuala Lumpur.

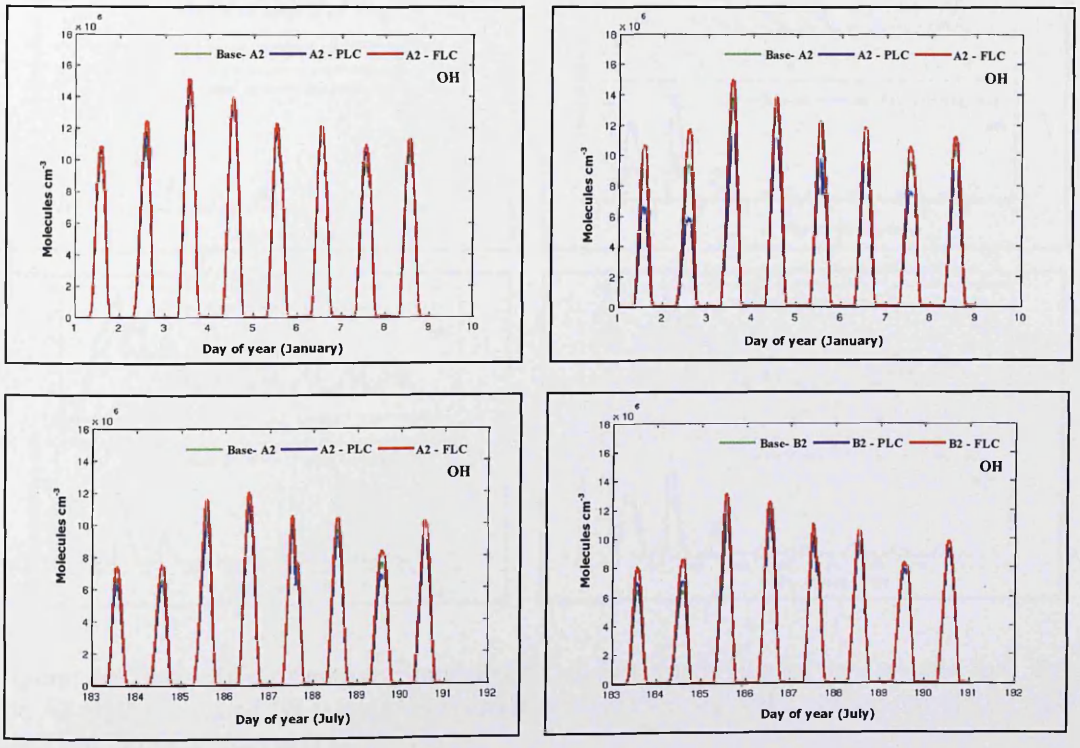

Figure A6.13.2: ***Kuala Lumpur***: Simulated OH (molecules cm^{-3}) during January and July for the A2 (*left panel*) and B2 (*right panel*) emission scenarios under the present-day (PLC) and modified future landcover (FLC).

A6.13.1.1.3 NO_x

Biogenic emissions effects on future NO_x concentrations in the present-day landcover scenarios (A2PLC and B2PLC) were also found to be negligible in Kuala Lumpur (Appendix 6.14). Climate changes alone accounted for the increase of NO_x in both months for the A2 and B2 climate scenarios, with the exception of July in the A2 climate scenario (Figure 6.6 and Figure A6.13.3; Appendix 6.7 and Appendix 6.15). However, the impact of climate changes were relatively small – between 0.3% and 1.1%, except during January in the B2 climate scenario, where there was an increase of about 3.1 ppbv (66%). Climate changes impact on NO_x concentrations in the future landcover scenarios (A2FLC and B2FLC) have been observed to decrease by 0.6 ppbv during January and increase by 0.4 ppbv during July in the A2 climate scenario. In the B2 climate scenario, climate changes accounted for the increase of 1.7 ppbv during January and the decrease of 1.2 ppbv during July (Figure 6.6 and Figure A6.13.3; Appendix 6.7 and Appendix 6.15).

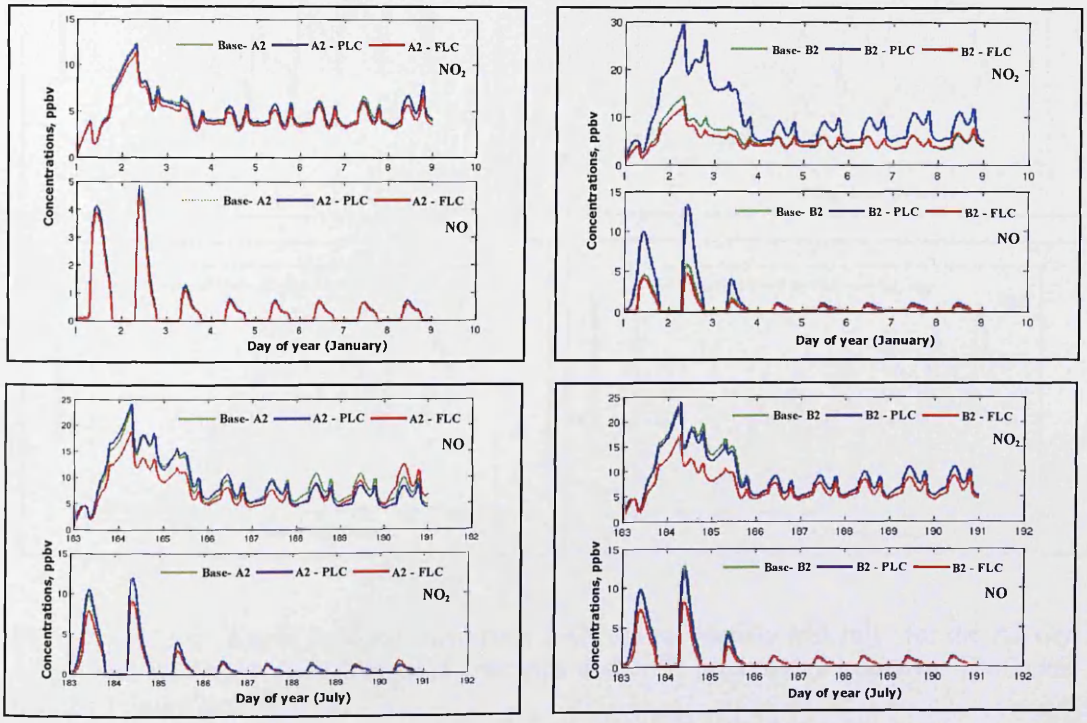

Figure A6.13.3: ***Kuala Lumpur***: Simulated NO & NO_2 (ppbv) during January and July for the A2 (*left panel*) and B2 (*right panel*) emission scenarios under the present-day (PLC) and modified future landcover (FLC).

A6.13.1.1.4 PAN

Biogenic emissions were also found to have no impact on future PAN concentrations in Kuala Lumpur (Appendix 6.14). Therefore, the future changes in PAN concentrations under present–day landcover scenarios (A2PLC and B2PLC) were largely due to climate changes. Climate changes showed a mixture of effects on future PAN concentrations. Climate changes were responsible for the small decrease of between 0.7% and 12.1% of PAN concentrations in both months in the A2 and B2 climate scenarios, except during January in B2, where climate changes were observed to increase significantly by 4.9 ppbv (113.5%) (Figure 6.7 and Figure A6.13.4; Appendix 6.8 and Appendix 6.15). A similar trend was observed in future landcover scenarios but the impact of climate change was much larger under present-day landcover scenarios.

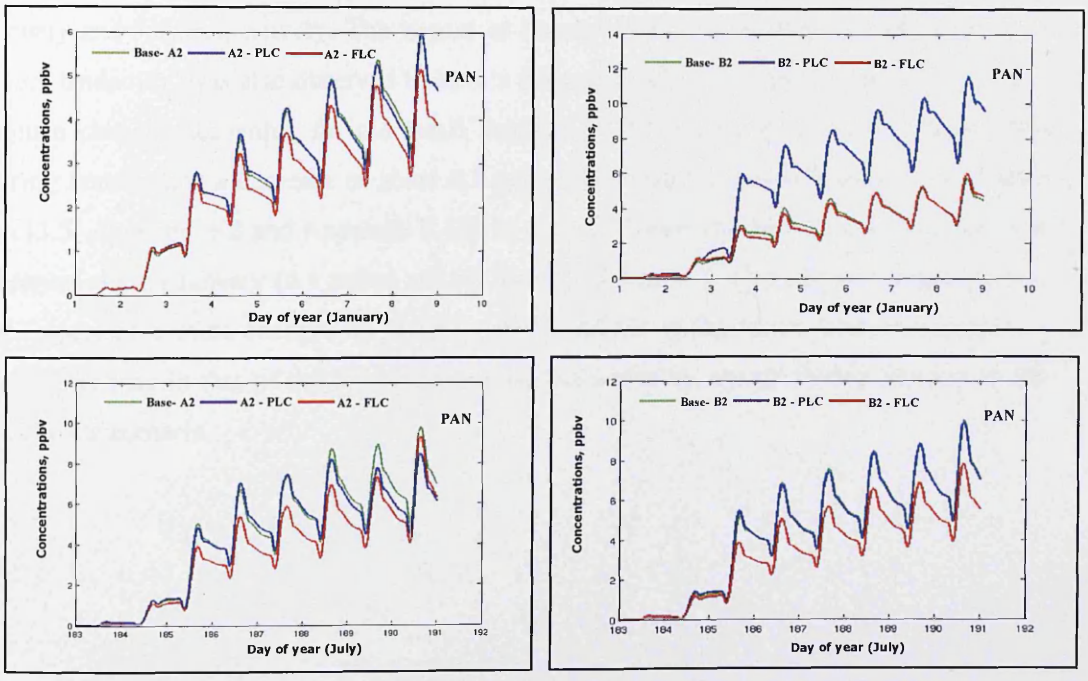

Figure A6.13.4: ***Kuala Lumpur***: Simulated PAN during January and July for the A2 (*left panel*) and B2 (*right panel*) emission scenarios under the present-day landcover (PLC) and modified future landcover (FLC).

A6.13.1.1.5 $HONO_2$

The effects of climate changes in present-day landcover scenarios (A2PLC and B2PLC) on future changes of $HONO_2$ concentrations were found to be smaller in Kuala Lumpur than Bangkok or Jakarta in both months in the A2 and B2 climate scenarios (Appendix 6.14). Biogenic emissions impacts on $HONO_2$ were found to be negligible. In this case, climate changes were solely responsible for the future changes of $HONO_2$ concentrations. However, the impact of climate changes alone only accounted for a small decrease in $HONO_2$ concentrations of about 0.1 ppbv (1%) during January and an increase by 0.2ppbv (2.9%) during July in the A2 climate scenario (Figure 6.7 and Figure A6.13.5; Appendix 6.8 and Appendix 6.15).

In the B2 climate scenario, the impact of climate change alone was responsible for the small decrease in $HONO_2$ concentrations of about 1.1 ppbv (5.6%) and 0.01 ppbv (0.1%) during the January and July respectively. The impact of climate change alone, due to perturbations of future landcover, was also observed to have a mixture of effects. In the A2 climate scenario, climate changes accounted for the small increase of $HONO_2$ of about by 0.4 ppbv (2%) during January and a decrease of about 0.7 ppbv (8.9%) during July (Figure 6.7 and Figure A6.13.5; Appendix 6.8 and Appendix 6.15). In the B2 climate scenario, a small decrease was observed during January (0.4 ppbv) and an increase during July (0.3 ppbv). Comparatively, the impact of climate changes on $HONO_2$ concentrations in the future landcover scenarios was larger than in that of the present-day landcover scenarios, except during January in the B2 climate scenario.

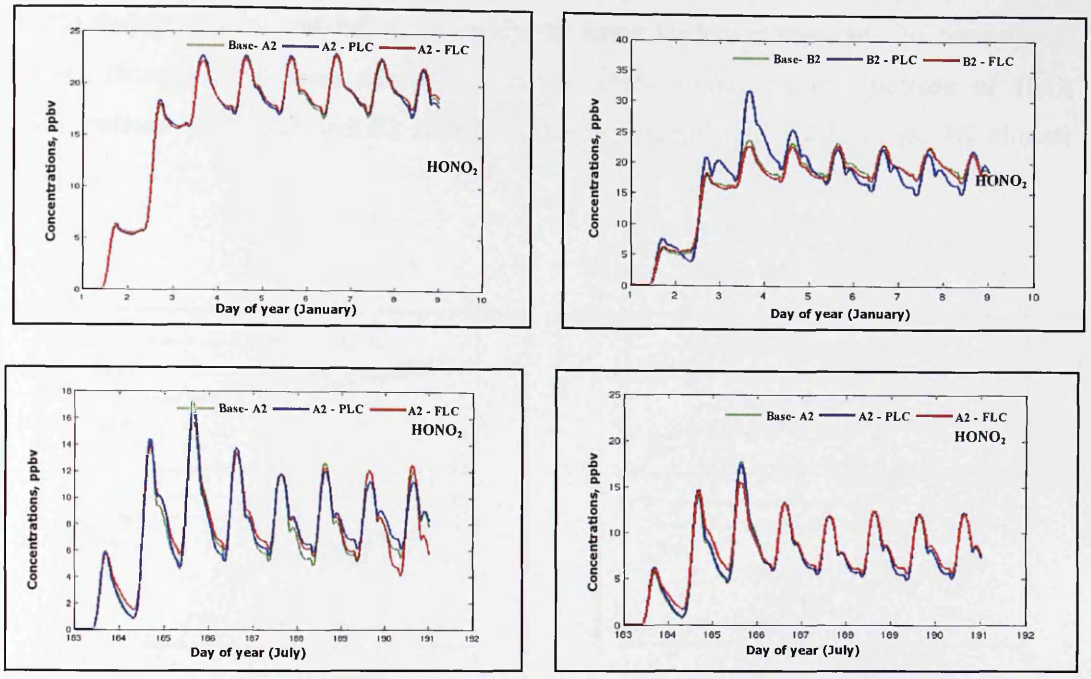

Figure A6.13.5: ***Kuala Lumpur***: Simulated $HONO_2$ during January and July for the A2 (*left panel*) and B2 (*right panel*) emission scenarios under the present-day landcover (PLC) and modified future landcover (FLC).

A6.13.1.1.6 HCHO and H_2O_2

Climate changes in the present-day landcover scenarios (A2PLC and B2PLC) also played the major role in the changes in future HCHO and H_2O_2 concentrations in Kuala Lumpur (Appendix 6.14). Climate changes were responsible for the small decrease (between 0.02 ppbv and 0.4 ppbv) of HCHO in the A2 and B2 climate scenarios, except for an increase of about 3.5 ppbv (61.3%) during January in the B2 climate scenario (Figure 6.8 and Figure A6.13.6; Appendix 6.8 and Appendix 6.15). Under future landcover scenarios, climate changes accounted for the small decrease of HCHO concentrations in both climate scenarios, except during January in the B2 climate scenario. Relatively, the impact of climate changes in present-day landcover scenarios was much larger than that in future landcover scenarios, except during January in the B2 climate scenario.

In the present-day landcover scenarios (A2PLC and B2PLC), the climate change impacts have mixed effects on H_2O_2 concentrations in the A2 and B2 climate scenarios. In the A2 climate scenario, climate changes were found to increase H_2O_2 concentrations by 0.3ppbv (7.4%) and 0.5 ppbv (19%) during January and July respectively (Figure 6.8 and Figure A6.13.6; Appendix 6.8 and Appendix 6.15). Meanwhile, in the B2 climate scenario, climate

changes accounted for the decrease of H_2O_2 concentration by 0.6 ppbv (14.7%) and 0.02 ppbv (0.9%) during January and July respectively. In future landcover scenarios, in comparison, climate changes have been shown to have a larger impact on the increase of H_2O_2 concentrations in the A2 and B2 climate scenarios, except during July in the B2 climate scenario.

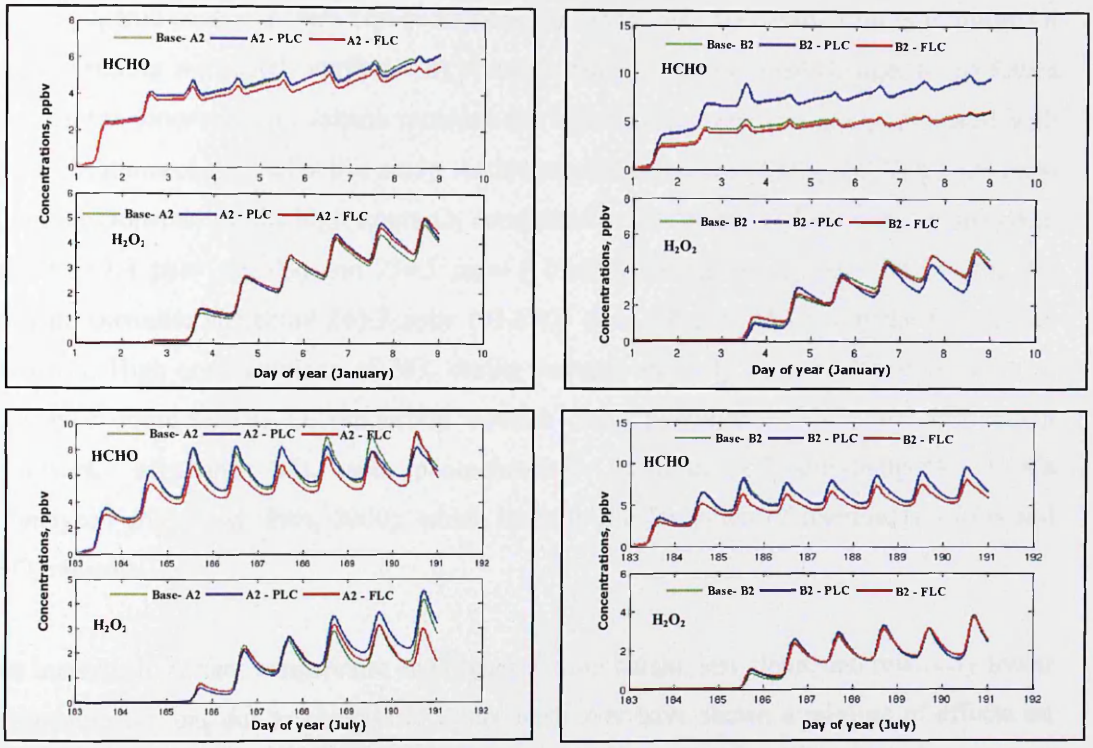

Figure A6.13.6: ***Kuala Lumpur***: Simulated HCHO & H_2O_2 (ppbv) during January and July for the A2 (*left panel*) and B2 (*right panel*) emission scenarios under the present-day landcover (PLC) and modified future landcover (FLC).

A6.13.1.2 Jakarta

A6.13.1.2.1 O_3

The present-day O_3 concentrations during both the January and July in Jakarta were found to be higher than in Bangkok by about 270 ppbv and 216 ppbv for BaselineA2, and 244 ppbv and 219.0 ppbv for BaselineB2 (Appendix 6.16). The combined effects of climate change and biogenic emissions were observed to have mixed effects on the future simulation of surface O_3 concentration, and relatively little impact, which was less than 10%. Future surface O_3

concentrations were found to increase by 8.6 ppbv (3.2%) and 16.8 ppbv (6.9%) during January in both the A2 and B2 climate scenarios respectively. Meanwhile, during July in both scenarios, the simulated O_3 concentrations were decreased by 17.9 ppbv (8.3%) and 2.2 ppbv (1.0%) respectively (Figure 6.5 and Figure A6.13.7; Appendix 6.7 and Appendix 6.17). Based on the sensitivity runs of the model with- and without-biogenic emissions, a distinctive difference between Bangkok and Jakarta was observed, where biogenic emissions in Jakarta were found to have negligible effects on the future changes of surface O_3. As the anthropogenic emissions were kept constant in the model runs, the small changes in future O_3 concentrations were solely attributed by climate changes. Despite small changes to the future surface O_3 concentrations, Jakarta recorded the highest concentrations of O_3 compared with other locations considered in this study. Anthropogenic emissions of NO_x and VOCs are most likely responsible for the high future O_3 concentrations in Jakarta, which were estimated at about 269.3 ppbv (96.9%) and 234.5 ppbv (109.0%) during January and July in the A2 climate scenario; and about 243.7 ppbv (93.6%) and 219 ppbv (101%) in the B2 climate scenario. High concentrations of NO_x during January and July in the A2 and B2 climate scenarios could lead to O_3 production through direct photolysis of NO_2 and subsequent reactions, involving NO_x and photochemical oxidation of anthropogenic VOCs (Finlayson_Piyys and Pitts, 2000), which leads to the formation of intermediate RO_2 and HO_2 radicals.

An increase in surface temperature and higher mixing height, less cloud, and relatively lower isoprene emissions due to changes in future landcover have shown a mixture of effects on future surface O_3 concentrations. Similarly in present-day landcover scenarios, the removal of biogenic emissions in the model runs for the sensitivity studies was found to have no effects on future surface O_3 concentrations in future landcover scenarios. Therefore, as the anthropogenic emissions were kept constant in the simulations, any future changes in surface O3 concentrations were due to climate change alone. In this case, climate changes alone accounted for a decrease in O_3 concentrations by about 39.3 ppbv (14.6%) during January and an increase of about 17.2 ppbv (7.1%) during July in the A2 climate scenario (Figure 6.5 and Figure A6.13.7; Appendix 6.7 and Appendix 6.17). In the B2 climate scenarios, climate changes accounted for the small decrease of O_3 concentrations of about 5.7 ppbv (2.6%) and 12 ppbv (5.5%) during January and July respectively.

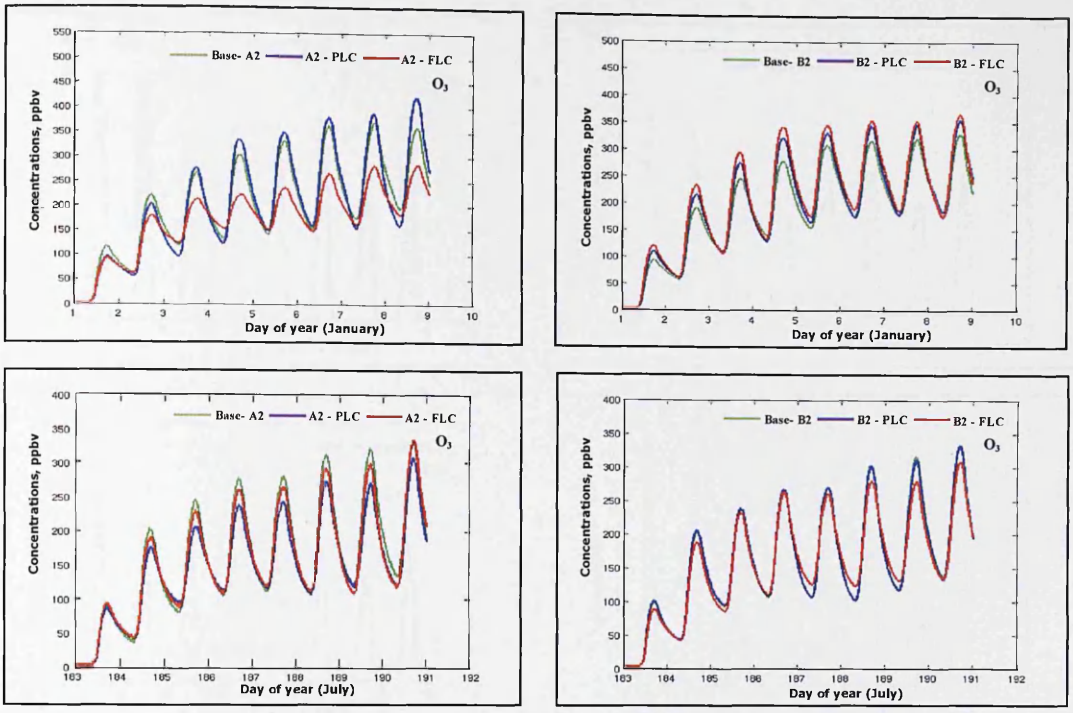

Figure A6.13.1.7: ***Jakarta***: Simulated O_3 (ppbv) during January and July for the A2 (*left panel*) and B2 (*right panel*) emission scenarios under the present-day (PLC) and modified future landcover (FLC).

A6.13.1.2.2 OH

In Jakarta, climate changes played a much larger role in the future changes of OH concentrations than the biogenic emissions. Climate changes were responsible for the increase of future OH concentrations by 1.3 x 10^5 molecules cm^{-3} (January) and 1.4 x 10^5 molecules cm^{-3} (July) in the A2 climate scenario (Figure 6.5 and Figure A6.13.8; Appendix 6.7 and Appendix 6.17). Meanwhile, climate changes accounted for the decrease of about 1.6 x 10^5 molecules cm^{-3} (January) and 3 x 10^5 molecules cm^{-3} (July) in the B2 climate scenario. Future changes in landcover have found to have no effect on biogenic emissions. On the other hand, climate changes accounted for the increase of OH concentrations by 6.7 x 10^5 molecules cm^{-3} (29%) during January and 1.2 x 10^5 molecules cm^{-3} (6.7%) during July in the A2 climate scenario (Figure 6.5 and Figure A6.13.8; Appendix 6.7 and Appendix 6.17). In the B2 climate scenario, climate changes alone accounted for the decrease of OH concentration of about 0.7 x 10^5 molecules cm^{-3} (2.8%) during January and the increase of about 0.6 x 10^5 molecules cm^{-3} (3.3%) during July. Comparatively, in the future landcover scenarios, climate changes were found to have a larger impact on the increase of OH concentrations than in present-day landcover scenarios except during January in the B2 climate scenario.

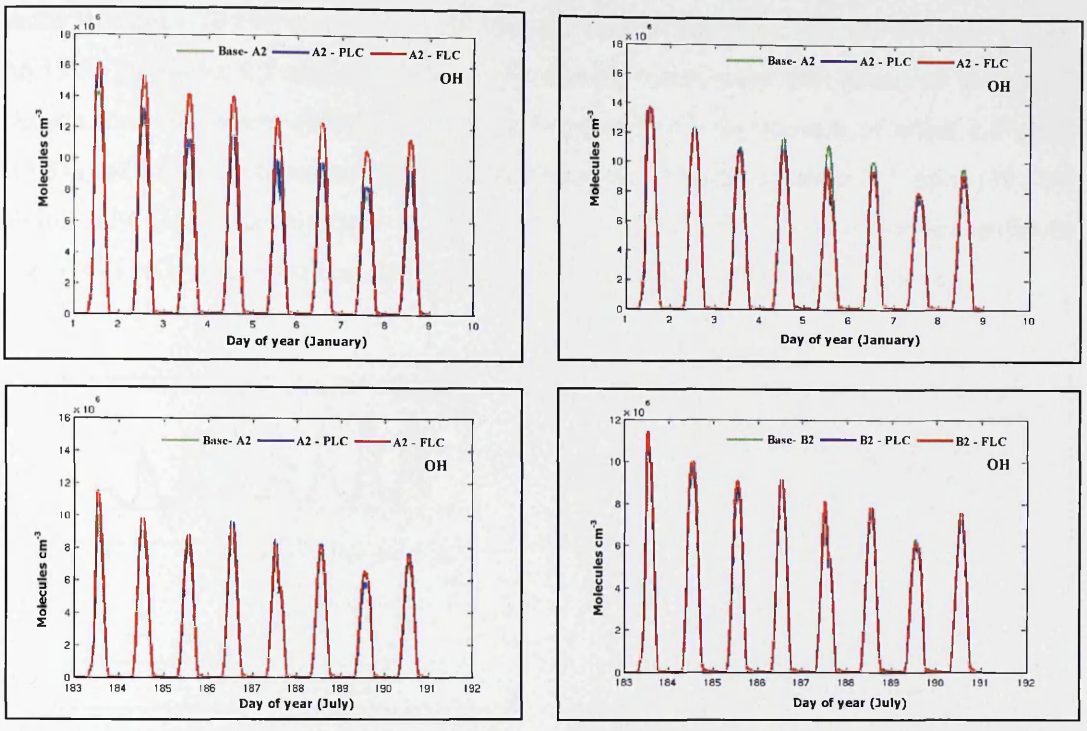

Figure A6.13.1.8: ***Jakarta***: Simulated OH (molecules cm^{-3}) during January and July for the A2 (*left panel*) and B2 (*right panel*) emission scenarios under the present-day (PLC) and modified future landcover (FLC).

A6.13.1.2.3 NOx

The combined effects of climate changes and biogenic emissions on future NO_x concentrations in the present-day landcover scenario (A2PLC and B2PLC) were largely due to climate changes alone. Despite substantial emissions of isoprene observed in Jakarta during both months in both climate scenarios, it showed no changes in NO_x production in without-biogenic emissions in the sensitivity runs (Appendix 6.16). Climate changes alone accounted for the increase of NO_x in both months in the A2 and B2 climate scenarios with the exception of July in the A2 climate scenario (Figure 6.6 and Figure A6.13.9; Appendix 6.7 and Appendix 6.17). However, the impact of climate changes alone were relatively very small; only between 0.3% and 8.2% except during January in A2 with an increase of 2.7 ppbv (24.8%).

Under future landcover scenarios (A2FLC and B2FLC), biogenic emissions impact on future NO_x in Jakarta was also found to be negligible. Climate changes were observed to have a mixture of effects on future NO_x concentrations. Climate changes accounted for the substantial decrease in NO_x about 4.0 (38%) during January and a very small increase of

about 0.1 ppbv (0.1%) during July in the A2 climate scenarios (Figure 6.6 and Figure A6.13.9; Appendix 6.7 and Appendix 6.17). Similar trends were also observed in the B2 climate scenario, where climate change was responsible for the increase of about 1.5 ppbv (15.3%) of NO_x concentrations during January and the decrease of about 1.1 ppbv (11.1%) during July. Comparatively there were much stronger effects from climate changes on future changes of NO_x concentrations during January than in July in both climate scenarios.

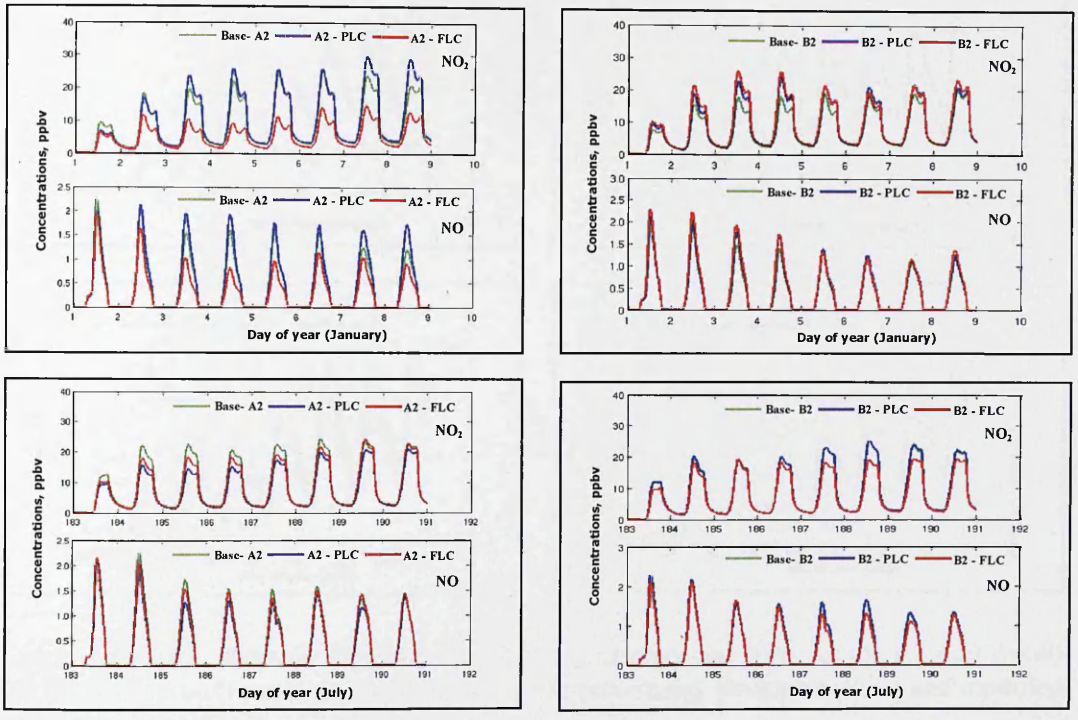

Figure A6.13.9: ***Jakarta***: Simulated NO & NO_2 (ppbv) during January and July for the A2 (*left panel*) and B2 (*right panel*) emission scenarios under the present-day (PLC) and modified future landcover (FLC).

A6.13.1.2.4 PAN

Based on the sensitivity runs, removing the biogenic emissions in the present-day landcover scenarios (A2PLC and B2PLC) in the model was shown to have no effects on the future concentrations of PAN as compared with the runs with-biogenic emissions (Appendix 6.16). Therefore, the small changes of PAN concentrations were also solely due to climate changes. In Jakarta, in both months in the A2 and B2 climate scenarios, climate changes alone were observed to increase the concentrations of PAN by 4.5ppbv (A2) and 6.9 ppbv (B2) during January and to decrease by 0.2ppbv (A2) and 4.4 ppbv (B2) during July (Figure 6.7 and Figure A6.13.10; Appendix 6.8 and Appendix 6.17). Changes in the future climate and in

isoprene emissions in future landcover scenarios have shown a decrease in PAN concentrations in both months for both A2 and B2 climate scenarios, except during January in the A2 climate scenario, where a substantial increase of PAN was observed (6.2 ppbv or about 28.6%) (Figure 6.7 and Figure A6.13.10; Appendix 6.8 and Appendix 6.17).

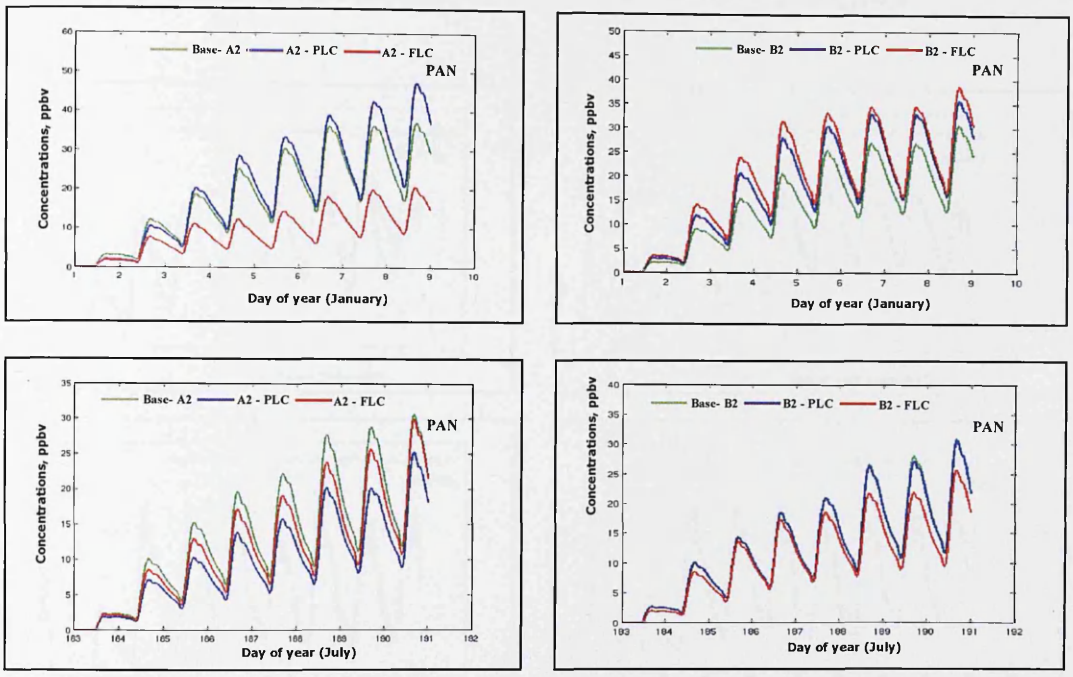

Figure A6.13.10: ***Jakarta***: Simulated PAN during January and July for the A2 (*left panel*) and B2 (*right panel*) emission scenarios under the present-day landcover (PLC) and modified future landcover (FLC).

A6.13.1.2.5 $HONO_2$

The combined effects of climate change and biogenic emissions on future changes of $HONO_2$ concentrations were found to be smaller in Jakarta in both months in the A2 and B2 climate scenarios (Appendix 6.16). Based on the sensitivity runs, it was observed that biogenic emissions have no impact on $HONO_2$ concentrations. As anthropogenic emissions were kept constant in the model runs, the small changes in future $HONO_2$ concentrations were solely due to climate changes. Climate changes were observed to increase $HONO_2$ concentrations by 2.7 ppbv (24.8%) during January and to decrease them by 0.9 ppbv (8.3%) during July in the A2 climate scenario (Figure 6.7 and Figure A6.13.11; Appendix 6.8 and Appendix 6.17). In B2 climate scenarios, climate changes alone were observed to increase $HONO_2$ concentrations by 0.6 ppbv (5.7%) and 0.1 ppbv (0.7%) during January and July respectively. Climate change impact on $HONO_2$ concentrations in future landcover scenarios was also

found to have a mixture of effects. Climate change accounted for the small increase of $HONO_2$ concentrations of between 0.14 ppbv and 1.8 ppbv in the A2 and B2 climate scenarios, except for a very small decrease of about 0.5 ppbv (0.02%) during January in the B2 climate scenario (Figure 6.7 and Figure A6.13.11; Appendix 6.8 and Appendix 6.17). Comparatively, the role of climate change in the increase of $HONO_2$ concentrations in future landcover scenarios was more profound than in present-day landcover scenarios.

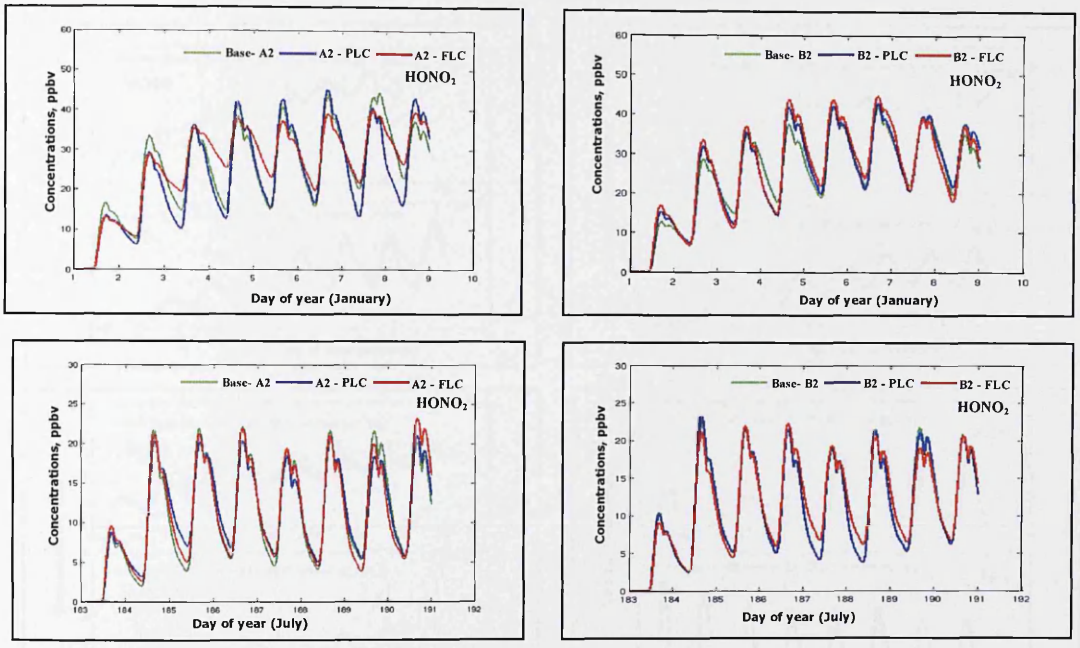

Figure A6.13.11: ***Jakarta***: Simulated $HONO_2$ during January and July for the A2 (*left panel*) and B2 (*right panel*) emission scenarios under the present-day landcover (PLC) and modified future landcover (FLC).

A6.13.1.2.6 HCHO and H_2O_2

Climate changes were found to be responsible for the mixed effects on the future concentrations of HCHO and H_2O_2. In present-day landcover scenarios (A2PLC and B2PLC), climate changes were observed to increase HCHO by 2.5 ppbv (13.8%) during January and to decrease it by 1.8 during July in the A2 climate scenario. Meanwhile, in the B2 climate scenario, climate change was observed to increase HCHO concentrations by 1.7 ppbv (10.7%) and 0.04 ppbv (0.3%) during January and July respectively (Figure 6.8 and Figure A6.13.12; Appendix 6.8 and Appendix 6.17). In future landcover scenarios (A2FLC and B2FLC), HCHO concentrations were observed to decrease by 6.4 ppbv (34.4%) during January in the A2 climate scenario but to increase by 2.5 ppbv (18.5%) during July. In the B2 climate scenario, climate changes were responsible for increases of about 0.7 ppbv (4.5%)

and 1.5 ppbv (10%) during January and July respectively. A mixture of effects of climate changes under the present-day and future landcover scenarios on future concentrations of H_2O_2 were observed. Climate change impacts on H_2O_2 concentration were slightly larger in the future landcover scenario than in that of the present-day, except during January in the B2 climate scenario. In terms of magnitude, the impact was relatively smaller in both landcover scenarios (Figure 6.8 and Figure A6.13.10; Appendix 6.8 and Appendix 6.17).

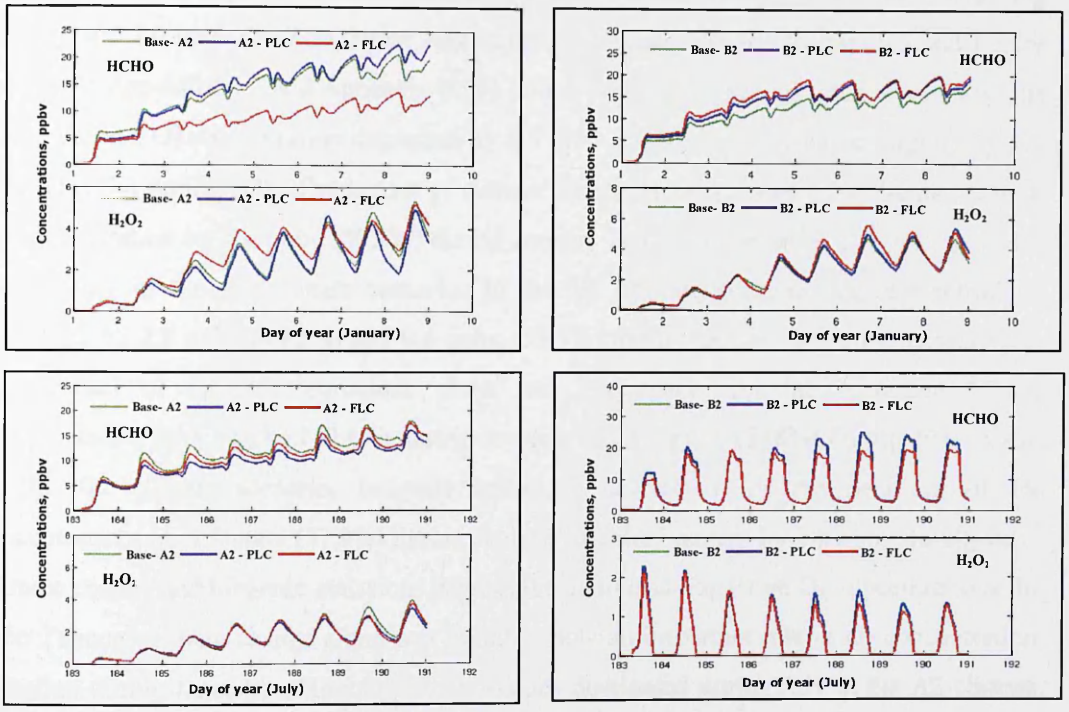

Figure A6.13.12: ***Jakarta***: Simulated HCHO & H_2O_2 (ppbv) during January and July for the A2 (*left panel*) and B2 (*right panel*) emission scenarios under the present-day landcover (PLC) and modified future landcover (FLC).

A6.13.1.3 Koto Tabang

A6.13.1.3.1 O_3

The present-day O_3 concentrations in Koto Tabang during January and July in the present-day landcover scenarios (BaseA2 and BaseB2) were about 15.2 ppbv and 5.3 ppbv for BaselineA2, and 25.9 ppbv and 4.2 ppbv for BaselineB2 (Appendix 6.18). Without a biogenic emissions factor, the baseline O_3 concentration increased significantly to 59.7 ppbv (January) and 51.1 ppbv (July) in BaselineA2; 60.7 ppbv (January) and 54.5 ppbv (July) in BaselineB2. These increases of surface O_3 concentrations were largely due to anthropogenic NOx and

VOCs emissions that were considered as baseline anthropogenic emissions in the CiTTyCAT model input. Similarly in Danum, the increases of surface O_3 in Koto Tabang due to anthropogenic emissions were offset by high isoprene emissions incorporated into the model. In this case, the low NO_x and high isoprene concentrations could actually decrease O_3 concentrations, possibly through sequestering NO_x as organic nitrates and OH titration.

Future simulations to investigate the combined effects of climate change and biogenic emissions on tropospheric O_3 concentrations found a decrease of 6.7 ppbv (44.1%) during January and 2.0 ppbv (36.7%) during July in the A2 climate scenario (Figure 6.5 and Figure A6.13.13; Appendix 6.7 and Appendix 6.19). In the B2 climate scenario during January, the future surface O_3 concentration decreased by 6.3 ppbv (24.3%) but increased slightly by 0.7 ppbv (16.7%) during July. The impact of climate change alone accounted for the decrease in O_3 concentration by 5.4 ppbv (80.6%) during January and the increase by 2.3 ppbv (34.3%) during July in the A2 climate scenario. In the B2 climate scenario, O_3 concentrations decreased by 2.8 ppbv (44.2%) and 0.4 ppbv (52.9%) during January and July respectively. The impact of biogenic emissions alone was responsible for the reduction of O_3 concentrations by 1.3 ppbv (19.4%) during January and 4.3 ppbv (218%) during July in A2. In the B2 climate scenario, biogenic emissions accounted for the decrease of O_3 concentrations by 0.4 ppbv (52.9%) during January and the increase by 1.1 ppbv during July. Climate change and biogenic emissions have shown a diverse impact on O_3 concentrations. In Koto Tabang, climate change alone was found to play an important role in O_3 concentration reduction during January, while biogenic emissions dominated during July in the A2 climate scenario. A balancing impact of climate change and biogenic emissions on the decrease of O_3 concentration was observed during January in the B2 climate scenario. During July in the B2 climate scenario, biogenic emissions were found to contribute significantly to the small increase of O_3 concentrations – by 1.1 ppbv (152.9%).

An investigation of the impact of combined factors on the surface O_3 concentrations in future landcover scenarios were found to cause decreases of smaller magnitude during January in A2 (1.9 ppbv) and B2 (1.4 ppbv) climate scenarios (Figure 6.5 and Figure A6.13.13; Appendix 6.7 and Appendix 6.19). During July, the combined effects were observed to cause an increase in O_3 concentrations by 0.1ppbv (A2) and 0.5 ppbv (B2). The perturbation of future landcover, climate changes alone were responsible for the decrease of O_3 by 10.1 ppbv during January and the increase by 3.8 ppbv during July in the A2 climate scenario. In the B2 climate scenario, climate changes accounted for the increase of about 5 ppbv during January and the decrease of 0.4 ppbv during July. It was also observed that the effects of climate changes were offset by biogenic emissions. In the A2 climate scenario, biogenic emissions

accounted for the increase of O3 by 8.2 ppbv during January and the decrease by 3.7 ppbv during July. In the B2 climate scenario, biogenic emissions were responsible for a decrease of about 6.4 ppbv and an increase of about 0.9 ppbv during January and July respectively.

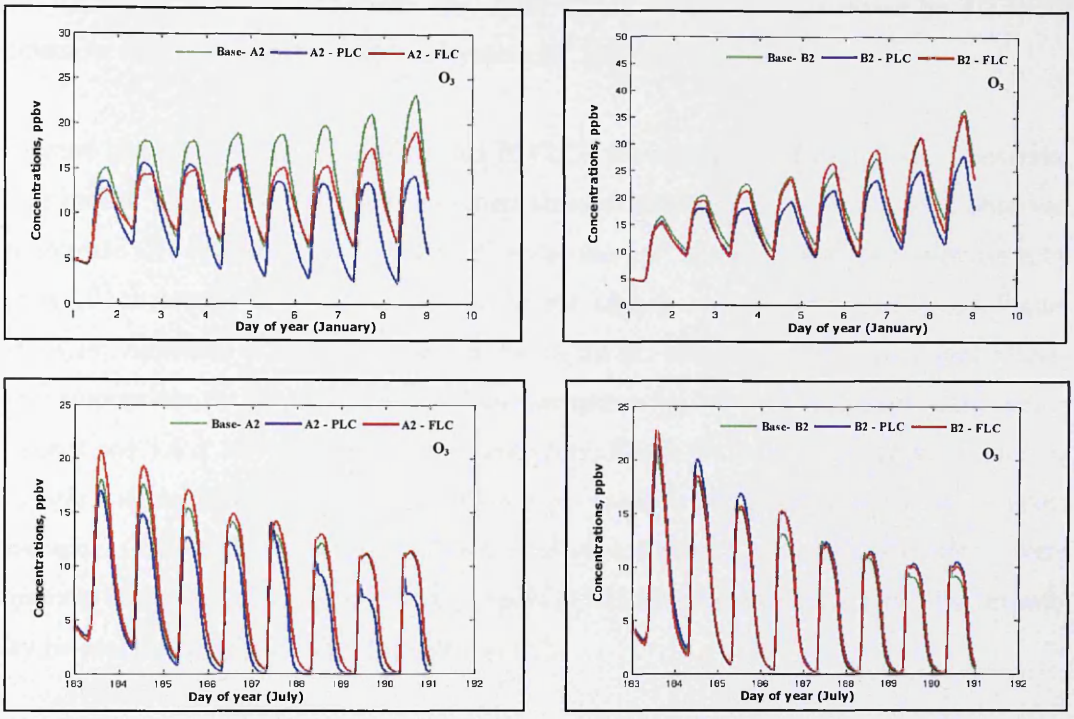

Figure A6.31.13: ***Koto Tabang***: Simulated O_3 (ppbv) during January and July for the A2 (*left panel*) and B2 (*right panel*) emission scenarios under present-day (PLC) and modified future landcover (FLC).

A6.13.1.3.2 OH

In Koto Tabang, under the present-day landcover scenarios (A2PLC and B2PLC), the combined effects of climate changes and biogenic emissions on future OH concentrations have been found to be opposite from those in Danum. The combined effects have been observed to decrease OH concentrations by 2.2 x 10^4 molecules cm^{-3} (45.4%) during January and 0.6 x 10^4 molecules cm^{-3} (45.9%) during July in the A2 climate scenario (Appendix 6.18). Meanwhile, in the B2 climate scenario, OH concentrations decreased by 3.0 x 10^4 molecules cm^{-3} (29.7%) during January but increased during July by 0.2 x 10^4 molecules cm^{-3} (35.7%). In both climate scenarios, the impact of biogenic emissions alone were observed to contribute significantly to the decreases of OH concentrations during January by 2.3 x 10^5 molecules cm^{-}

^{3} (A2) and 3.3 x 10^{5} molecules cm^{-3} (B2), as well as the increases during July by 1.1 x 10^{5} molecules cm^{-3} (A2) and 5.2 x 10^{5} molecules cm^{-3} (B2) respectively (Figure 6.5 and Figure A6.13.14; Appendix 6.7 and Appendix 6.19). On the other hand, climate changes alone accounted for relatively small increases in OH concentrations of about 2.1 x 10^{5} molecules cm^{-3} (A2) and 3.0 x 10^{5} molecules cm^{-3} (B2) during January and decreases by 1.2 x 10^{5} molecules cm^{-3} (A2) and 0.5 x 10^{4} molecules cm^{-3} (B2) during July.

In future landcover scenarios (A2FLC and B2FLC), the combined effects have also observed to be mixed. The combined effects of climate changes and biogenic emissions were observed to decrease OH concentration by 1.3 x 10^{3} molecules cm^{-3} during January and increase it by 0.6 x 10^{3} molecules cm^{-3} during July in the A2 climate scenario (Figure 6.5 and Figure A6.13.14; Appendix 6.7 and Appendix 6.19). In the B2 climate scenario, combined effects were responsible for the decrease in OH concentrations by 1.4 x 10^{4} molecules cm^{-3} during January and 1.6 x 10^{3} molecules cm^{-3} during July. Based on the isolated effect of climate changes and biogenic emissions, both factors were found to offset each other in both climate scenarios. Comparatively, under the future landcover scenarios, the combined effects were observed to have a larger impact on the increase of OH concentrations than under the present-day landcover scenario except during July in B2.

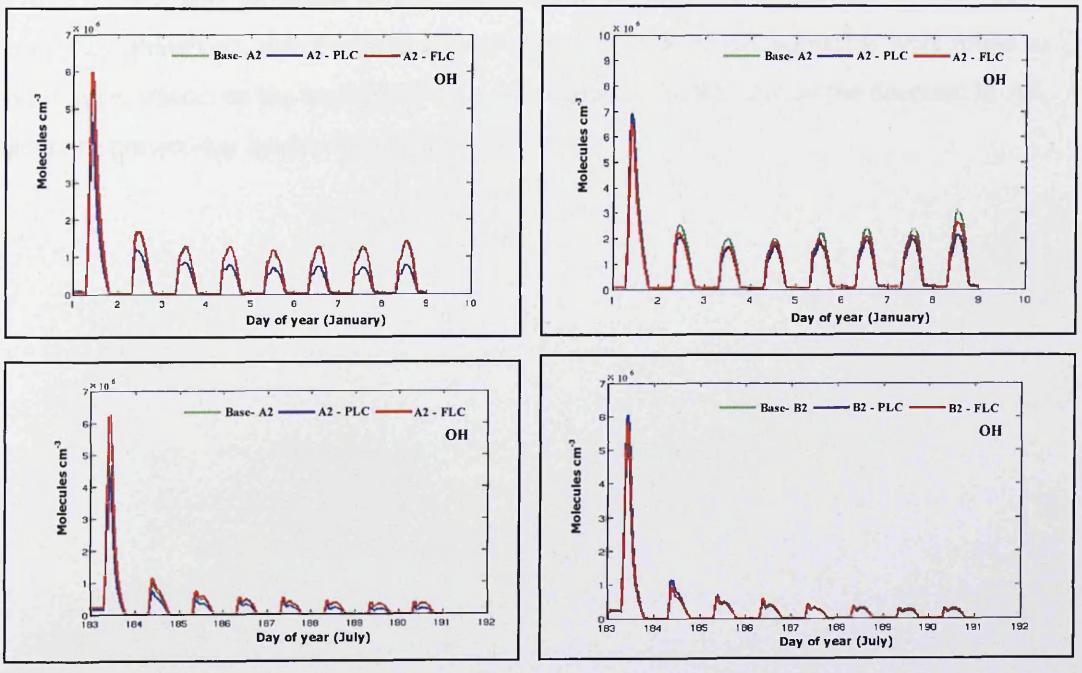

Figure A6.13.14: ***Koto Tabang***: Simulated OH (molecules cm^{-3}) during January and July for the A2 (*left panel*) and B2 (*right panel*) emission scenarios under the present-day (PLC) and modified future landcover (FLC).

A6.13.1.3.3 NO_x

In Koto Tabang, the combined effects of climate changes and biogenic emissions were observed to decrease NO_x concentration in both months for the A2 and B2 climate scenarios (Appendix 6.18). Similarly with Danum, in terms of magnitude of impact on the future changes of NO_x concentrations, climate change and biogenic factors have a balancing effect. Climate changes alone have observed to decrease NO_x concentrations by 0.21 ppbv and 0.1 ppbv during January in the A2 and B2 climate scenarios respectively, and to increase them by 0.03 ppbv during July in the B2 climate scenario (Figure 6.6 and Figure A6.13.15; Appendix 6.7 and Appendix 6.19– shown as NO and NO_2). On the other hand, biogenic emissions alone were observed to increase NO_x by 0.12 ppbv (A2) and 0.01 ppbv (B2) during January, and 1.01 ppbv during July in B2. During July in the A2 climate scenario, biogenic emissions accounted for the decrease in NO_x concentration by 0.33 ppbv.

In the present-day landcover scenarios (A2FLC and B2FLC), the combined effects of climate changes and biogenic emissions were observed to decrease NO_x in both months for the A2 and B2 climate scenarios, except during January in B2 (Figure 6.6 and Figure A6.13.15; Appendix 6.7 and Appendix 6.19). In the A2 climate scenario, the combined effects accounted for the decrease in NO_x concentrations by 0.12 ppbv during January and 0.4 ppbv during July. Meanwhile, in the B2 climate scenario, the combined effects accounted for the increase of NO_x concentrations by 0.03 ppbv during January and a decrease by 1.04 ppbv during July. Relatively, the combined effects in the future landcover scenarios were found to have a larger impact on the increase of NO_x concentrations in B2, and on the decrease in A2, than in the present-day landcover scenario.

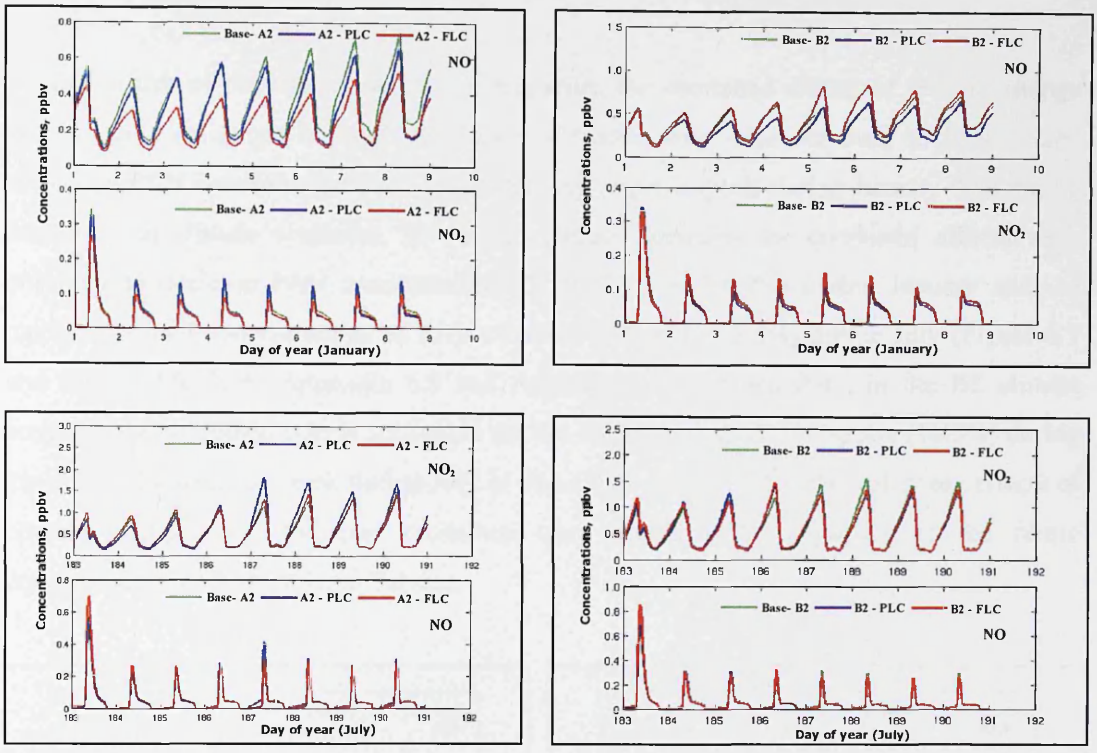

Figure A6.13.15: ***Koto Tabang***: Simulated NO & NO_2 (ppbv) during January and July for the A2 (*left panel*) and B2 (*right panel*) emission scenarios under the present-day (PLC) and modified future landcover (FLC).

A6.13.1.3.4 PAN

In the present-day landcover scenarios (A2PLC and B2PLC), the combined effect of climate changes and biogenic emissions were responsible for the increase of PAN concentrations by 0.23 ppbv (37.7%) during January and 0.04 ppbv (4.8%) during July in the A2 climate scenario (Figure 6.7 and Figure A6.13.16; Appendix 6.8 and Appendix 6.19). In the B2 climate scenario, combined effects accounted for the small decrease of PAN concentrations by about 0.04 ppbv (4.8%) during January and 0.01 ppbv (1.2%) during July. Under this scenario, climate changes and biogenic emissions were observed to have a balancing effect on the future changes of PAN in Koto Tabang. Climate changes alone were found to decrease PAN by 0.13 ppbv (56%) during January and increase by 0.07 ppbv (175%) during July in the A2 climate scenario. In the B2 climate scenario, climate changes were responsible for the decrease of PAN concentrations by 0.10 ppbv and 0.02 ppbv during January and July respectively. At the same time, biogenic emissions were also responsible for the increase of PAN concentrations by 0.36 ppbv (156.5%) during January and the decrease by 0.03 ppbv (75%) during July in the A2 climate scenario. In the B2 climate scenario, biogenic emissions were responsible for the decrease of about 0.08 ppbv (44.4%) and 0.01 ppbv (100%) during January and July respectively.

Similar to that of present-day landcover scenarios, the combined effects of climate change and biogenic emissions in future landcover scenarios were also observed to have mixed effects on PAN concentrations, and comparatively larger impacts during January than during July in both climate scenarios. In the A2 climate scenario, the combined effects were observed to decrease PAN concentrations by 0.31 ppbv (36.9%) during January and to increase a small concentrations of PAN of about 0.02 ppbv (2.4%) during July (Figure 6.7 and Figure A6.13.16; Appendix 6.8 and Appendix 6.19). Meanwhile, in the B2 climate scenario, the combined effects accounted for the increase of about 0.16 ppbv (16.5%) during January and a small decrease during July of about 0.01 ppbv (1.2%). The balancing effects of climate changes and biogenic emissions were found to be important to the future concentrations of PAN in Koto Tabang.

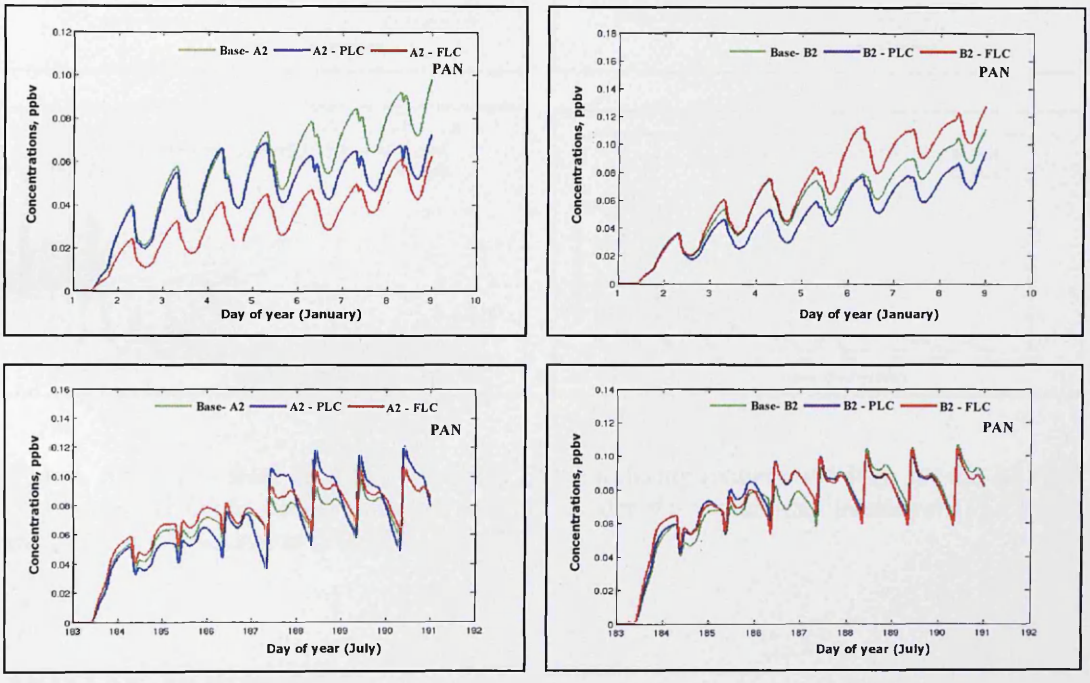

Figure A6.13.16 ***Koto Tabang***: Simulated PAN during January (*top panel*) and July for the A2 (*left panel*) and B2 (*right panel*) emission scenarios under the present-day landcover (PLC) and modified future landcover (FLC).

6.13.1.3.1 $HONO_2$

The small impacts of climate change on future changes of $HONO_2$ concentrations were compensated for by biogenic emissions. Thus, the combined effects were relatively smaller (Figure 6.8 and Figure A6.13.17; Appendix 6.8 and Appendix 6.19). The combined effects of climate changes and biogenic emissions on future $HONO_2$ concentrations in both months for

the A2 and B2 climate scenarios were less than 0.01 ppbv. Generally the combined effects of climate changes and biogenic emissions in future landcover scenarios were small: less than 0.01 ppbv in both climate scenarios. In future landcover scenarios, the combined effects of climate changes and biogenic emissions on $HONO_2$ concentrations were observed to cause a slight increase compared to the effects of the present-day landcover scenarios, except during July in the B2 climate scenario (Figure 6.8 and Figure A6.13.17; Appendix 6.8 and Appendix 6.19).

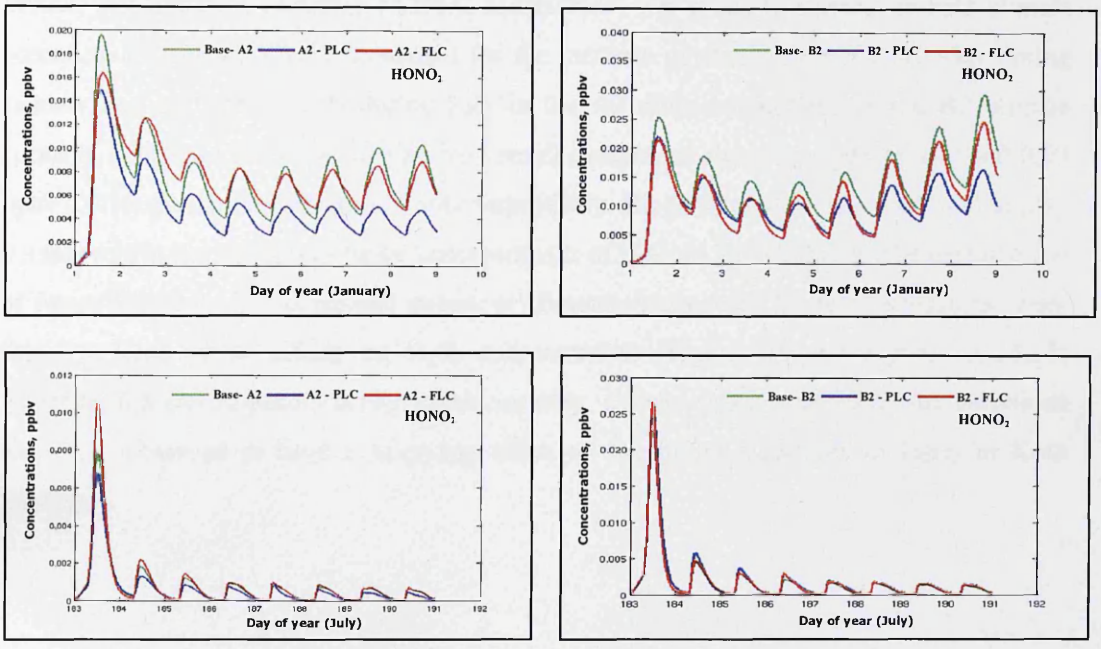

Figure A6.13.17: ***Koto Tabang***: Simulated $HONO_2$ during January and July for the A2 (*left panel*) and B2 (*right panel*) emission scenarios under the present-day landcover (PLC) and modified future landcover (FLC).

A6.13.1.3.6 HCHO and H_2O_2

The combined effects of climate change and biogenic emissions on HCHO and H_2O_2 concentrations were found to be mixed and smaller in magnitude (Appendix 6.18). The biogenic emissions were found to be more important to changes in HCHO concentrations than climate change alone, with exception of some balancing effects from biogenic emissions during January in both climate scenarios. Biogenic emissions alone accounted for the decrease in HCHO concentrations by 0.39 ppbv (47.6%) during July and an increase of 1.0 ppbv (84.2%) during July in the A2 climate scenario. In the B2 climate scenario, biogenic emissions alone were observed to decrease HCHO concentration by 0.16 ppbv (33.3%) and

0.36 ppbv (90%) during January and July respectively (Figure 6.6 and Figure A6.13.18; Appendix 6.8 and Appendix 6.19). Under the future landcover scenarios, the combined effects of climate changes and biogenic emissions also showed a mixture of effects (Figure 6.8 and Figure A6.13.18; Appendix 6.8 and Appendix 6.19). Largely, the future changes in HCHO concentrations were due to biogenic emissions of between 82% and 95% in both climate scenarios.

Meanwhile, for H_2O_2, the combined impact of climate changes and biogenic emissions in the present-day landcover scenarios (A2PLC and B2PLC) was found to increase in both climate scenarios. Combined effects accounted for the increase of about 1.5 ppbv (10.9%) during January and 0.9 ppbv (12.2) during July in the A2 climate scenario. In the B2 climate scenario, combined effects accounted for a small increase of about 0.4 ppbv (3.4%) and 0.03 ppbv (0.4%) during the January and July respectively. Biogenic emissions were found to play a major role in the changes to future concentrations of H_2O_2 in Koto Tabang. The perturbation of future landcover, the combined impact of climate changes and biogenic emissions, were found to have mixed effects on H_2O_2 concentrations (Figure 6.8 and Figure A6.13.18; Appendix 6.8 and Appendix 6.19). In this scenario, climate changes and biogenic emissions were also observed to have a balancing effect on the future emissions of H_2O_2 in Koto Tabang.

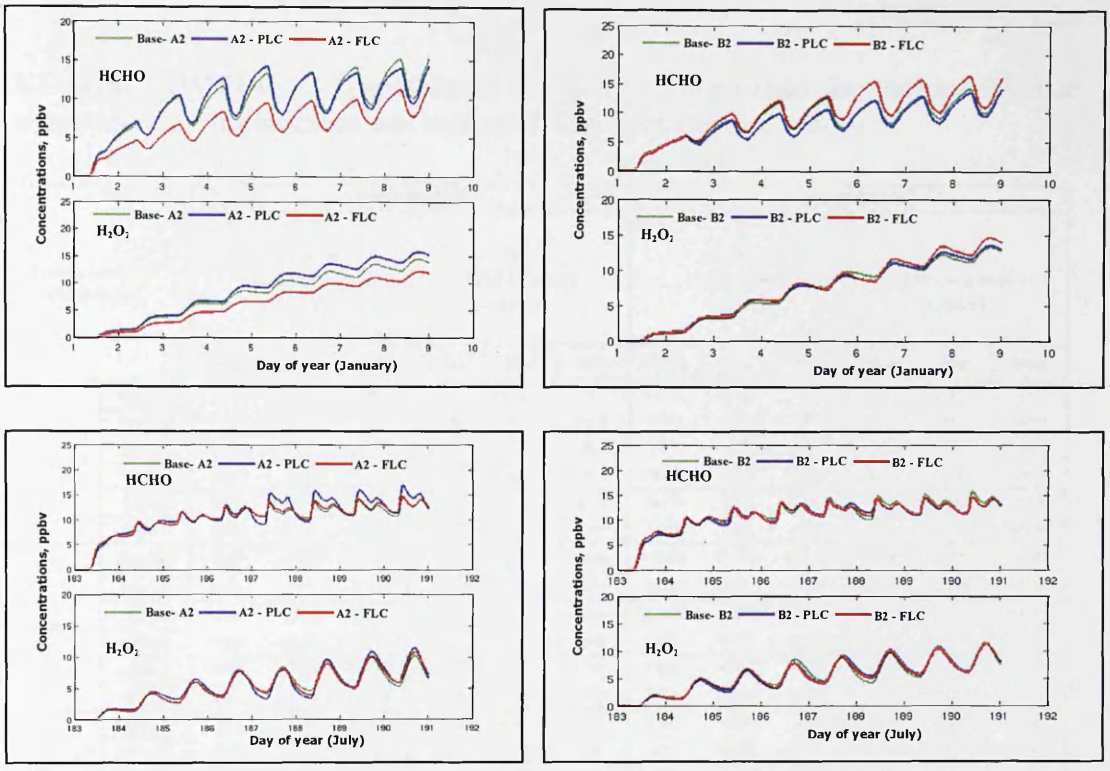

Figure A6.13.18: ***Koto Tabang***: Simulated HCHO & H_2O_2 (ppbv) during January and July for the A2 (*left panel*) and B2 (*right panel*) emission scenarios under the present-day landcover (PLC) and modified future landcover (FLC).

KUALA LUMPUR: Tropospheric chemistry composition in various climate changes, biogenic emissions and landcover during January and July.

Kuala Lumpur (Malaysia)		With BVOC						Without BVOC					
		January (wet season) (ppbv)			July (dry season) (ppbv)			January (wet season) (ppbv)			July (dry season) (ppbv)		
		Mean	Min	Max	Mean	Min	Max	Mean	Min	Max	Mean	Min	Max
O_3	BaseA2	143.80	115.60	174.00	141.5	86.29	203.	143.80	115.60	174.00	141.5	86.29	203.
	BaseB2	143.60	117.8	171.00	137.8	79.51	203.90	143.60	117.8	171.00	137.8	79.51	203.90
	B2PLC	173.0	119.9	229.8	137.3	79.55	203	173.0	119.9	229.8	137.3	79.55	203
	B2FLC	144.1	115.5	174.4	131.7	84.70	184.6	144.1	115.5	174.4	131.7	84.70	184.6
	A2PLC	144.10	115.50	174.40	141.6	90.82	191.9	144.10	115.50	174.40	141.6	90.82	191.9
	A2FLC	138.90	114.5	164.5	129.5	74.05	194.60	138.90	114.5	164.5	129.5	74.05	194.60
OH	BaseA2	2.80E06	3.79E04	1.08E07	2.47E6	2.46E4	9.06E6	2.80E06	3.79E04	1.08E07	2.47E6	2.46E4	9.06E6
	BaseB2	2.81E6	3.69	1.08E7	2.52E6	2.22E4	9.27E6	2.81E6	3.69	1.08E7	2.52E6	2.22E4	9.27E6
	B2PLC	2.36E6	3.31E4	8.95	2.50E6	2.23E4	9.22E6	2.36E6	3.31E4	8.95	2.50E6	2.23E4	9.22E6
	B2FLC	2.96E6	3.87E4	1.13E7	2.64E6	2.68E4	9.84E6	2.96E6	3.87E4	1.13E7	2.64E6	2.68E4	9.84E6
	A2PLC	2.95E6	3.87E4	1.13E7	2.36E6	2.73E4	8.73E6	2.95E6	3.87E4	1.13E7	2.36E6	2.73E4	8.73E6
	A2FLC	2.99E6	3.67E4	1.14E7	2.76E6	2.15E4	1.03E7	2.99E6	3.67E4	1.14E7	2.76E6	2.15E4	1.03E7
NO	BaseA2	0.21	0.001	0.69	0.32	0.001	1.114	0.21	0.001	0.69	0.32	0.001	1.114
	BaseB2	0.19	1.13E-3	0.63	0.36	1.63E-3	1.26	0.19	1.13E-3	0.63	0.36	1.63E-3	1.26
	B2PLC	0.29	1.28E-3	01.00	0.36	1.63E-3	1.26	0.29	1.28E-3	01.00	0.36	1.63E-3	1.26
	B2FLC	0.22	1.20E-3	0.71	0.31	1.49E-3	1.08	0.22	1.20E-3	0.71	0.31	1.49E-3	1.08
	A2PLC	0.22	1.20E-3	0.71	0.27	1.25E-3	0.89	0.22	1.20E-3	0.71	0.27	1.25E-3	0.89
	A2FLC	0.19	1.10E-3	0.62	0.44	2.23E-3	1.59	0.19	1.10E-3	0.62	0.44	2.23E-3	1.59
NO_2	BaseA2	4.92	3.42	7.60	7.02	4.73	9.98	4.92	3.42	7.60	7.02	4.73	9.98
	BaseB2	4.55	3.17	7.08	7.67	5.15	10.98	4.55	3.17	7.08	7.67	5.15	10.98
	B2PLC	6.91	4.91	7.58	7.67	5.16	11.0	7.58	4.91	11.79	0.04	1.56E-3	0.27
	B2FLC	4.96	3.34	7.72	6.51	4.46	9.15	4.96	3.34	7.72	6.51	4.46	9.15
	A2PLC	4.96	3.34	7.72	5.99	4.07	8.70	4.96	3.34	7.72	5.99	4.07	8.70
	A2FLC	4.3	3.13	6.53	8.16	4.67	12.53	4.3	3.13	6.53	8.16	4.67	12.53
$HONO_2$	BaseA2	19.03	17.09	21.46	8.18	5.48	11.91	19.03	17.09	21.46	8.18	5.48	11.91
	BaseB2	19.29	17.55	21.41	7.92	5.00	12.19	19.29	17.55	21.41	7.92	5.00	12.19
	B2PLC	18.22	15.01	21.87	0.58	0.19	1.34	18.22	15.01	21.87	0.58	0.19	1.34
	B2FLC	18.9	16.87	21.36	11.96	1.15	5.55	18.9	16.87	21.36	11.96	1.15	5.55
	A2PLC	18.90	16.87	21.36	8.42	6.14	11.21	18.90	16.87	21.36	8.42	6.14	11.21
	A2FLC	19.41	17.66	21.67	7.45	4.13	12.49	19.41	17.66	21.67	7.45	4.13	12.49
PAN	BaseA2	4.52	3.19	5.97	7.21	5.03	9.78	4.52	3.19	5.97	7.21	5.03	9.78
	BaseB2	4.30	3.03	5.70	7.22	4.94	9.98	4.30	3.03	5.70	7.22	4.94	9.98
	B2PLC	9.18	6.59	11.54	7.37E-4	1.13E-4	1.47E-3	9.18	6.59	11.54	7.37E-4	1.13E-4	1.47E-3
	B2FLC	4.44	3.67	5.99	5.65	3.89	7.81	4.44	3.67	5.99	5.65	3.89	7.81
	A2PLC	4.44	3.06	5.99	6.34	4.51	8.47	4.44	3.06	5.99	6.34	4.51	8.47
	A2FLC	3.86	2.72	5.16	6.33	4.06	9.29	3.86	2.72	5.16	6.33	4.06	9.29
HCHO	BaseA2	5.91	5.54	6.20	7.26	5.98	9.23	5.91	5.54	6.20	7.26	5.98	9.23
	BaseB2	5.71	5.4	5.99	7.28	5.77	9.58	5.71	5.4	5.99	7.28	5.77	9.58
	B2PLC	9.21	8.76	9.83	7.26	5.74	9.55	9.21	8.76	9.83	7.26	5.74	9.55
	B2FLC	5.80	5.33	6.17	6.37	5.27	8.06	5.80	5.33	6.17	6.37	5.27	8.06
	A2PLC	5.79	5.33	6.17	6.85	5.98	8.22	5.79	5.33	6.17	6.85	5.98	8.22
	A2FLC	5.34	5.02	5.57	6.91	5.26	9.46	5.34	5.02	5.57	6.91	5.26	9.46
H_2O_2	BaseA2	3.92	3.30	4.75	2.58	1.63	4.16	3.92	3.30	4.75	2.58	1.63	4.16
	BaseB2	4.35	3.70	5.19	2.30	1.52	3.80	4.35	3.70	5.19	2.30	1.52	3.80
	B2PLC	3.71	2.80	4.99	2.34	1.52	3.75	3.71	2.80	4.99	2.34	1.52	3.75
	B2FLC	4.21	3.59	4.96	2.46	1.74	3.68	4.21	3.59	4.96	2.46	1.74	3.68
	A2PLC	4.21	3.59	4.96	3.07	2.18	4.5	4.21	3.59	4.96	3.07	2.18	4.5
	A2FLC	4.24	3.61	5.08	2.03	1.47	3.00	4.24	3.61	5.08	2.03	1.47	3.00

Note: BaseA2 – Baseline for A2
BaseB2-Baseline for B2
PLC – Present-day landcover
FLC- Modified future landcover

KUALA LUMPUR: Tropospheric chemistry composition changes in various climate changes, biogenic emissions and landcover scenarios during January and July.

Season	Scenarios	O_3 ppbv [%]	NO ppbv [%]	NO_2 ppbv [%]	OH Molecules cm^{-3} [%]	$HONO_2$ ppbv [%]	PAN ppbv [%]	HCHO ppbv [%]	H_2O_2 ppbv [%]
Wet Season (January)	A2PLC-BaseA2	0.3 [0.2]	0.01 [4.8]	0.04 [0.8]	1.5E5 [5.4]	-0.13 [0.7]	-0.08 [1.8]	-0.12 [2.0]	0.29 [7.4]
	A2FLC-BaseA2	-4.9 [3.4]	-0.02 [9.5]	-0.62 [12.6]	1.9E5 [6.8]	0.38 [2.0]	-0.66 [14.6]	-0.57 [9.7]	0.32 [8.2]
	A2FLC-A2PLC	-5.2 [3.6]	-0.03 [13.6]	-0.69 [13.3]	4.0E4 [1.4]	0.51 [2.7]	-0.58 [13.1]	-0.45 [7.8]	0.03 [0.7]
	XA2PLC-XBaseA2	0.3 [0.2]	0.01 [4.8]	0.04 [0.8]	1.5E5 [5.4]	-0.13 [0.7]	-0.08 [1.8]	-0.12 [2.0]	0.29 [7.4]
	B2PLC-BaseB2	29.4 [20.5]	0.10 [52.6]	3.03 [66.6]	-4.5E5 [16.0]	-1.1 [5.6]	4.9 [113.5]	3.5 [61.3]	-0.64 [14.7]
	B2FLC-BaseB2	0.5 [0.35]	0.03 [15.8]	0.44 [9.0]	1.5E5 [5.3]	-0.39 [2.0]	0.14 [3.3]	0.09 [1.6]	-0.14 [3.2]
	B2FLC-B2PLC	-28.9 [16.7]	-0.07 [24.1]	-2.69 [34.6]	6.0E5 [25.4]	0.68 [3.7]	-4.7 [51.6]	-3.4 [37.0]	0.5 [13.5]
	XB2PLC-XBaseB2	29.4 [20.5]	0.10 [52.6]	3.03 [66.6]	-4.5E5 [16.0]	-1.1 [5.6]	4.9 [113.5]	3.5 [61.3]	-0.64 [14.7]
Dry Season (July)	A2PLC-BaseA2	0.10 [0.07]	-0.05 [15.6]	-1.03 [14.7]	-1.1E5 [4.5]	0.24 [2.9]	-0.87 [12.1]	-0.41 [5.6]	0.49 [19.0]
	A2FLC-BaseA2	-12.0 [8.5]	0.12 [37.5]	1.72 [22.7]	2.9E5 [11.7]	-0.73 [8.9]	-0.88 [12.2]	-0.35 [4.8]	-0.55 [21.3]
	A2FLC-A2PLC	-12.1 [0.85]	0.17 [63.0]	2.62 [43.8]	4.0E5 [17.0]	-0.97 [11.5]	-0.01 [0.16]	0.06 [0.88]	-1.0 [33.9]
	XA2PLC-XBaseA2	0.10 [0.07]	-0.05 [15.6]	-1.03 [14.7]	-1.1E5 [4.5]	0.24 [2.9]	-0.87 [12.1]	-0.41 [5.6]	0.49 [19.0]
	B2PLC-BaseB2	-0.50 [0.36]	0.00 [0.00]	0.02 [0.26]	-2.0E4 [0.79]	-0.01 [0.13]	-0.05 [0.69]	-0.02 [0.27]	-0.02 [0.85]
	B2FLC-BaseB2	-6.1 [4.43]	-0.05 [13.9]	-1.21 [15.1]	1.2E5 [4.76]	0.32 [4.04]	-1.6 [21.7]	-0.91 [12.5]	0.10 [4.2]
	B2FLC-B2PLC	-5.6 [4.1]	-0.05 [13.9]	-1.25 [15.3]	1.4E5 [5.6]	0.33 [4.2]	-1.5 [21.2]	-0.89 [12.3]	0.12 [5.1]
	XB2PLC-XBaseB2	-0.50 [0.36]	0.00 [0.00]	0.02 [0.26]	-2.0E4 [0.79]	-0.01 [0.13]	-0.05 [0.69]	-0.02 [0.27]	-0.02 [0.85]

Note: *PLC-present-day landcover*
FLC-Future landcover
A2PLC-BaseA2/B2PLC-BaseB2: Changes due to climate changes and biogenic emissions under present-day landcover
A2FLC-BaseA2/B2FLC-BaseB2: Changes due to climate changes and biogenic emissions under future-day landcover
A2FLC-A2PLC/B2FLC-B2PLC: Changes between present-day landcover and future landcover scenarios

JAKARTA: Tropospheric chemistry composition in various climate, landcover, biogenic emissions during January and July.

Jakarta (Indonesia)		With BVOC						Without BVOC					
		January (wet season) (ppbv)			July (dry season) (ppbv)			January (wet season) (ppbv)			July (dry season) (ppbv)		
		Mean	Min	Max	Mean	Min	Max	Mean	Min	Max	Mean	Min	Max
O_3	BaseA2	269.9	195.3	359.7	216.40	134.3	330	269.90	195.3	359.7	216.40	134.3	330
	BaseB2	243.7	174.3	328.5	219	135.6	333	243.7	174.3	328.5	219	135.6	333
	B2PLC	260.5	183.4	353.9	216.8	133.2	331.7	260.5	183.4	353.9	216.8	133.2	331.7
	B2FLC	260.9	173.6	366.2	207	132.5	308.9	260.9	173.6	366.2	207	132.5	308.9
	A2PLC	278.5	160.2	421.3	198.5	120.4	306.1	278.5	160.2	421.3	198.5	120.4	306.1
	A2FLC	230.6	183.9	285.7	210.7	118.3	334.6	230.6	138.9	285.7	210.7	118.3	334.6
OH	BaseA2	2.31E6	4.26E4	8.77E6	1.78E6	2.57E4	7.10E6	2.31E6	4.26E4	8.77E6	1.78E6	2.57E4	7.10E6
	BaseB2	2.51E6	4.31E4	9.57E6	1.84E6	2.95E4	7.27E6	2.51E6	4.31E4	9.57E6	1.84E6	2.95E4	7.27E6
	B2PLC	2.35E6	4.02E4	8.89E6	1.81E6	2.87E4	7.18E06	2.35E6	4.02E4	8.89E6	1.81E6	2.87E4	7.18E06
	B2FLC	2.44E6	3.94E4	9.18E6	1.90E6	3.03E4	7.60E6	2.44E6	3.94E4	9.18E6	1.90E6	3.03E4	7.60E6
	A2PLC	2.44E6	3.38E4	9.42E6	1.92E6	2.811E4	7.69E6	2.44E6	3.38E4	9.42E6	1.92E6	2.811E4	7.69E6
	A2FLC	2.98E6	4.88E4	1.14E7	1.90E6	2.61E4	7.52E6	2.98E6	4.88E4	1.14E7	1.90E6	2.61E4	7.52E6
NO	BaseA2	0.34	8.11E-5	1.2	0.36	6.11E-5	1.34	0.34	8.11E-5	1.2	0.36	6.11E-5	1.34
	BaseB2	0.34	7.72E-5	1.27	0.36	6.04E-5	1.33	0.34	7.72E-5	1.27	0.36	6.04E-5	1.33
	B2PLC	0.34	8.11E-5	1.21	0.36	6.07E-5	1.34	0.34	8.11E-5	1.21	0.36	6.07E-5	1.34
	B2FLC	0.38	9.2E-5	1.38	0.33	5.74E-5	1.25	0.38	9.2E-5	1.38	0.33	5.74E-5	1.25
	A2PLC	0.45	9.99E-6	1.74	0.361	6.15E-5	1.38	0.45	9.99E-6	1.74	0.361	6.15E-5	1.38
	A2FLC	0.25	5.83E-5	0.92	0.38	6.22E-5	1.44	0.25	5.83E-5	0.92	0.38	6.22E-5	1.44
NO_2	BaseA2	10.37	3.30	20.98	10.06	2.73	22.52	10.37	3.30	20.98	10.06	2.73	22.52
	BaseB2	9.52	2.82	19.92	9.88	2.7	21.99	9.52	2.82	19.92	9.88	2.7	21.99
	B2PLC	10.08	3.17	20.65	9.95	2.68	22.23	10.08	3.17	20.65	9.95	2.68	22.23
	B2FLC	10.98	3.27	23.31	8.78	2.40	19.43	10.98	3.27	23.31	8.78	2.40	19.43
	A2PLC	12.91	3.81	29.33	9.21	2.35	21.01	12.91	3.81	29.33	9.21	2.35	21.01
	A2FLC	6.43	2.33	12.83	10.05	2.64	22.98	6.43	2.33	12.83	10.05	2.64	22.98
$HONO_2$	BaseA2	31.79	22.95	39.48	12.76	5.816	20.19	31.79	22.95	39.48	12.76	5.816	20.19
	BaseB2	28.61	19.57	35.84	13.27	6.20	20.8	28.61	19.57	35.84	13.27	6.20	20.8
	B2PLC	30.51	21.47	37.45	13.20	6.12	20.71	30.51	21.47	37.45	13.20	6.12	20.71
	B2FLC	28.15	17.92	36.8	13.41	6.63	20.66	28.15	17.92	36.8	13.41	6.63	20.66
	A2PLC	29.25	16.15	43	12.92	5.72	21.07	29.25	16.15	43	12.92	5.72	21.07
	A2FLC	33.56	26.56	39.53	13.53	5.43	23.28	33.56	26.56	39.53	13.53	5.43	23.28
PAN	BaseA2	27.74	17.11	37.14	21.21	11.96	30.71	27.74	17.11	37.14	21.21	11.96	30.71
	BaseB2	21.71	12.45	30.48	21.15	11.82	30.82	21.71	12.45	30.48	21.15	11.82	30.82
	B2PLC	26.17	15.82	35.65	20.94	11.65	30.62	26.17	15.82	35.65	20.94	11.65	30.62
	B2FLC	27.91	16.36	38.67	17.44	9.54	25.73	27.91	16.36	38.67	17.44	9.54	25.73
	A2PLC	34.64	20.64	47.42	16.82	8.88	25.29	34.64	20.64	47.42	16.82	8.88	25.29
	A2FLC	14.86	8.83	20.74	20.11	10.84	29.95	14.86	8.83	20.74	20.11	10.84	29.95
HCHO	BaseA2	18.47	15.87	20.7	15.35	13.98	17.88	18.47	15.87	20.7	15.35	13.98	17.88
	BaseB2	16.05	13.70	17.39	15.30	13.91	17.69	16.05	13.70	17.39	15.30	13.91	17.69
	B2PLC	17.76	15.4	19.64	15.26	13.84	17.73	17.76	15.4	19.64	15.26	13.84	17.73
	B2FLC	18.5	16.32	19.98	13.77	12.29	15.88	18.5	16.32	19.98	13.77	12.29	15.88
	A2PLC	21.01	19.33	22.53	13.52	11.96	16.07	21.01	19.33	22.53	13.52	11.96	16.07
	A2FLC	12.12	10.18	13.77	14.65	12.63	17.49	12.12	10.18	13.77	14.65	12.63	17.49
H_2O_2	BaseA2	3.89	2.69	5.33	2.59	1.60	3.19	3.89	2.69	5.33	2.59	1.60	3.19
	BaseB2	3.52	2.55	4.61	2.61	1.58	3.99	3.52	2.55	4.61	2.61	1.58	3.99
	B2PLC	3.88	2.68	5.32	2.56	1.54	3.92	3.88	2.68	5.32	2.56	1.54	3.92
	B2FLC	3.72	2.56	5.10	2.61	1.68	3.81	3.72	2.56	5.10	2.61	1.68	3.81
	A2PLC	3.22	1.85	4.94	2.28	1.40	3.41	3.22	1.85	4.94	2.28	1.40	3.41
	A2FLC	3.99	2.99	5.19	2.35	1.30	3.72	3.99	2.99	5.19	2.35	1.30	3.72

Note: BaseA2 – Baseline for A2
BaseB2-Baseline for B2
PLC – Present-day landcover
FLC- Modified future landcover

JAKARTA: Tropospheric chemistry composition changes in various climate changes, biogenic emissions and landcover scenarios during January and July.

Season	Scenarios	O_3 ppbv [%]	NO ppbv [%]	NO_2 ppbv [%]	OH Molecules cm^{-3} [%]	$HONO_2$ ppbv [%]	PAN ppbv [%]	HCHO ppbv [%]	H_2O_2 ppbv [%]
Wet Season (January)	A2PLC-BaseA2	8.6 [3.2]	0.11 [32.4]	2.54 [24.5]	1.3E5 [5.6]	-2.5 [8.0]	6.9 [24.9]	2.5 [13.8]	-0.7 [17.2]
	A2FLC-BaseA2	-39.3 [14.6]	-0.09 [26.5]	-4.0 [38.0]	6.7E5 [29.0]	1.8 [5.6]	-12.9 [46.4]	-6.4 [34.4]	0.1 [2.6]
	A2FLC-A2PLC	-47.9 [17.2]	-0.2 [44.4]	-6.5 [50.2]	5.4E5 [22.1]	4.3 [14.7]	-19.8 [57.10]	-8.9 [42.3]	0.8 [23.9]
	XA2PLC-XBaseA2	8.6 [3.2]	0.11 [32.4]	2.54 [24.5]	1.3E5 [5.6]	-2.5 [8.0]	6.9 [24.9]	2.5 [13.8]	-0.7 [17.2]
	B2PLC-BaseB2	16.8 [6.9]	0.0 [0.0]	0.56 [5.9]	-1.6E5 [6.4]	1.9 [6.6]	4.5 [20.5]	1.7 [10.7]	0.36 [10.2]
	B2FLC-BaseB2	17.2 [7.1]	0.04 [11.8]	1.54 [15.3]	-7.0E4 [2.8]	-0.5 [0.02]	6.2 [28.6]	2.5 [18.5]	0.2 [5.7]
	B2FLC-B2PLC	0.4 [0.2]	0.04 [11.8]	0.9 [8.9]	9.0E4 [3.8]	-2.4 [7.7]	1.7 [6.6]	0.7 [0.04]	-0.2 [4.1]
	XB2PLC-XBaseB2	16.8 [6.9]	0.0 [0.0]	0.56 [5.9]	-1.6E5 [6.4]	1.9 [6.6]	4.5 [20.5]	1.7 [10.7]	0.36 [10.2]
Dry Season (July)	A2PLC-BaseA2	-17.9 [8.3]	0.001 [0.3]	-0.85 [8.5]	1.4E5 [7.9]	0.2 [1.3]	-4.4 [20.7]	-1.8 [11.9]	-0.3 [12.0]
	A2FLC-BaseA2	-5.7 [2.6]	0.02 [5.6]	-0.01 [0.1]	1.2E5 [6.7]	0.8 [6.0]	-1.1 [5.2]	-0.7 [4.5]	-0.2 [9.3]
	A2FLC-A2PLC	12.2 [6.1]	0.02 [5.6]	0.84 [9.1]	-2.0E4 [1.0]	0.6 [4.7]	3.3 [19.6]	1.1 [8.4]	0.1 [3.1]
	XA2PLC-XBaseA2	-17.9 [8.3]	0.001 [0.3]	-0.85 [8.5]	1.4E5 [7.9]	0.2 [1.3]	-4.4 [20.7]	-1.8 [11.9]	-0.3 [12.0]
	B2PLC-BaseB2	-2.2 [1.0]	0.0 [0.0]	0.07 [0.7]	-3.0E4 [1.6]	-0.07 [0.5]	-0.2 [1.0]	0.04 [0.3]	-0.05 [1.9]
	B2FLC-BaseB2	-12 [5.5]	-0.03 [8.3]	-1.07 [11.1]	6.0E4 [3.3]	0.14 [1.1]	-3.7 [17.5]	-1.5 [10.0]	0.00 [0.0]
	B2FLC-B2PLC	-9.8 [4.5]	-0.03 [8.3]	-1.2 [11.8]	9.0E4 [5.0]	0.21 [1.6]	-3.5 [16.7]	-1.5 [9.8]	0.05 [2.0]
	XB2PLC-XBaseB2	-2.2 [1.0]	0.0 [0.0]	0.07 [0.7]	-3.0E4 [1.6]	-0.07 [0.5]	-0.2 [1.0]	0.04 [0.3]	-0.05 [1.9]

Note: *PLC-present-day landcover*
FLC-Future landcover
A2PLC-BaseA2/B2PLC-BaseB2: Changes due to climate changes and biogenic emissions under present-day landcover
A2FLC-BaseA2/B2FLC-BaseB2: Changes due to climate changes and biogenic emissions under future-day landcover
A2FLC-A2PLC/B2FLC-B2PLC: Changes between present-day landcover and future landcover sceanrios

KOTO TABANG: Tropospheric chemistry composition in various climate changes, biogenic emissions and landcover scenarios during January and July.

Koto Tabang, Sumatera (Indonesia)		With BVOC						Without BVOC					
		January (wet season) (ppbv)			July (dry season) (ppbv)			January (wet season) (ppbv)			July (dry season) (ppbv)		
		Mean	Min	Max	Mean	Min	Max	Mean	Min	Max	Mean	Min	Max
O_3	BaseA2	15.21	6.78	23.27	5.32	0.08	11.35	59.7	5.06	67.31	51.06	35.22	72.16
	BaseB2	25.91	160.05	36.27	4.2	0.02	9.72	60.68	54.1	68.2	54.48	39.74	73.83
	B2PLC	19.64	11.31	27.78	4.90	0.07	10.38	57.91	51.48	63.74	54.11	39.32	73.29
	B2FLC	24.51	13.73	35.54	4.71	0.05	10.02	65.67	58.88	73.34	54.07	39.01	73.51
	A2PLC	8.5	2.39	14.2	3.37	0.002	9.04	54.3	144.1	49.22	53.32	38.22	73.81
	A2FLC	13.36	7.00	19.19	5.45	0.10	11.45	49.65	44.26	55.65	54.84	39.74	73.83
OH	BaseA2	4.91E04	3.02E02	1.44E05	1.22E4	131.9	3.85E4	3.42E4	2.15E4	1.35E7	3.08E6	1.99E4	1.21E7
	BaseB2	1.02E5	8.27E3	3.08E5	9.09E3	70.27	2.87E4	3.40E6	2.11E4	1.34E7	3.01E6	1.99E4	1.18E7
	B2PLC	7.17E4	5.54E3	2.13E5	1.14E4	79.09	3.31E4	3.70E6	2.02E4	1.45E7	2.96E6	1.93E4	1.16E7
	B2FLC	8.80E4	6.85E3	2.62E5	1.07E4	68.49	3.13E04	3.39E6	2.32E4	1.33E7	2.94E6	1.93E4	1.15E7
	A2PLC	2.68E4	869.2	7.78E4	6.64E3	42.17	2.29E4	3.63E6	1.81E4	1.43E7	2.96E6	2.02E4	1.16E7
	A2FLC	1.41E5	2.99E6	3.08E3	1.28E4	110.3	3.80E4	3.81E6	1.66E4	1.51E7	3.03E6	1.99E4	1.18E7
NO	BaseA2	0.03	0.001	0.12	0.42	1.99E-3	0.30	0.09	2.67E-4	0.26	0.15	5.06E-4	0.43
	BaseB2	0.03	6.33E-4	0.09	0.04	1.95E-3	0.29	0.08	2.53E-4	0.25	0.13	4.04E-4	0.40
	B2PLC	0.03	7.55E-4	0.10	0.04	1.56	0.27	0.08	2.48E-4	0.24	0.13	3.66E-4	0.39
	B2FLC	0.03	6.89E-4	0.10	0.04	1.51E-3	0.27	0.09	2.64E-4	0.26	0.13	3.48E-4	0.39
	A2PLC	0.02	9.31E-4	0.14	0.05	2.62E-3	0.31	0.68	2.28E-4	0.22	0.14	3.88E-4	0.43
	A2FLC	0.22	1.18E-3	0.76	0.04	1.73E-3	0.28	0.08	2.46E-4	0.23	0.13	4.04E-4	0.40
NO_2	BaseA2	0.43	0.24	0.73	0.62	0.21	1.47	1.05	0.83	1.51	1.53	1.17	2.14
	BaseB2	0.51	0.34	0.71	1.63	0.19	1.49	1.04	0.83	1.48	1.47	1.13	2.10
	B2PLC	0.42	0.26	0.65	0.58	0.19	1.34	0.94	0.78	1.33	1.43	1.13	2.04
	B2FLC	0.54	0.35	0.79	0.59	0.19	1.35	1.12	0.86	1.65	1.43	1.14	2.05
	A2PLC	0.35	0.16	0.66	0.69	0.20	1.67	0.85	0.72	1.20	1.57	1.16	2.25
	A2FLC	6.44	3.39	10.72	0.60	0.20	1.39	0.79	0.68	1.04	1.47	1.13	2.10
$HONO_2$	BaseA2	0.008	0.005	0.01	7.35E-4	8.49E-5	1.81E-3	2.39	1.79	3.27	0.93	0.26	2.17
	BaseB2	0.02	0.01	0.030	5.78E-4	7.98E-5	1.32E-3	2.47	1.85	3.39	1.02	0.34	2.17
	B2PLC	0.01	8.45E-5	0.02	7.37E-4	1.13E-4	1.47E-3	2.44	1.87	3.24	1.06	0.37	2.21
	B2FLC	0.02	0.01	0.03	7.11E-4	1.05E-4	1.41E-3	2.56	1.92	3.50	1.08	0.38	2.25
	A2PLC	3.76E-3	2.68E-3	4.77E-3	4.21E-4	5.33E-5	1.12 E-3	2.45	1.94	3.17	0.95	0.29	2.10
	A2FLC	21.25	19.08	22.53	7.97E-4	1.19E-4	1.71E-3	2.32	1.78	3.12	1.02	0.34	2.17
PAN	BaseA2	0.84	0.72	0.97	0.84	0.55	1.06	0.47	0.31	0.73	0.69	0.43	1.14
	BaseB2	0.97	0.86	1.10	0.84	0.53	1.10	0.49	0.34	0.74	0.73	0.47	1.16
	B2PLC	0.79	0.68	0.93	0.83	0.58	1.04	0.39	0.26	0.63	0.71	0.46	1.11
	B2FLC	1.13	1.01	1.27	0.83	0.58	1.04	0.59	0.40	0.88	0.71	0.46	1.11
	A2PLC	0.61	0.52	0.71	0.88	0.49	1.21	0.34	0.22	0.54	0.76	0.48	1.23
	A2FLC	9.61	7.49	10.77	0.86	0.6	1.06	0.28	0.18	0.46	0.73	0.47	1.16
HCHO	BaseA2	13.02	10.22	15.23	12.64	10.71	14.67	2.53	2.29	3.07	2.98	2.15	4.63
	BaseB2	12.14	9.93	14.12	13.34	11.4	15.64	2.58	2.40	3.06	3.00	2.34	4.38
	B2PLC	11.66	9.38	13.78	12.94	11.41	14.64	2.26	1.97	2.81	2.96	2.34	4.24
	B2FLC	13.88	11.02	16.43	12.97	11.34	14.69	2.74	2.54	3.25	2.97	2.37	4.25
	A2PLC	12.20	9.57	14.14	13.84	11.32	16.99	2.10	1.88	2.58	3.17	2.43	4.71
	A2FLC	12.71	11.86	13.92	13.03	11.6	14.85	1.96	1.76	2.48	3.00	2.34	4.38
H_2O_2	BaseA2	13.38	12.35	14.54	7.46	5.27	10.14	2.90	2.55	3.36	1.38	0.94	2.09
	BaseB2	12.07	11.07	13.25	8.49	6.08	11.42	2.93	2.54	3.44	1.56	1.07	2.35
	B2PLC	12.490.07	11.55	13.51	8.46	6.16	11.25	3.01	2.67	3.43	1.62	1.12	2.42
	B2FLC	13.36	12.19	14.71	8.40	6.01	11.29	3.16	2.72	3.74	1.59	1.07	2.40
	A2PLC	14.84	13.85	15.89	8.37	5.19	11.38	3.04	2.74	2.42	1.40	0.96	2.13
	A2FLC	6.97	5.07	9.26	8.11	5.90	10.81	0.67	0.59	0.79	1.56	1.07	2.35

Note: BaseA2 – Baseline for A2
BaseB2-Baseline for B2
PLC – Present-day landcover
FLC- Modified future landcover

KOTO TABANG: Tropospheric chemistry composition changes in various climate, biogenic emissions and landcover scenarios during January and July.

Season	Scenarios	O_3 ppbv [%]	NO ppbv [%]	NO_2 ppbv [%]	OH Molecules cm^{-3} [%]	$HONO_2$ ppbv [%]	PAN ppbv [%]	HCHO ppbv [%]	H_2O_2 ppbv [%]
Wet Season (January)	A2PLC-BaseA2	-6.7 [44.1]	-0.01 [33.3]	-0.08 [18.6]	-2.2E4 [45.4]	-4.2E-3 [53.0]	0.23 [37.7]	-0.82 [6.3]	1.46 [10.9]
	A2FLC-BaseA2	-1.85 [12.2]	-0.01 [33.3]	-0.11 [25.6]	-1.3E3 [2.7]	-1.2E-3 [15.3]	-0.31 [36.9]	-3.23 [24.8]	-2.06 [15.4]
	A2FLC-A2PLC	4.9 [57.2]	0.00 [0.00]	-0.03 [8.6]	2.1E5 [78.4]	3.02E-3 [80.3]	-0.08 [13.1]	-2.41 [19.8]	-3.52 [23.7]
	XA2PLC-XBaseA2	-5.4 [9.1]	-0.01 [11.1]	-0.20 [19.0]	2.1E5 [6.1]	0.06 [2.5]	-0.13 [27.7]	-0.43 [17.0]	0.14 [4.8]
	B2PLC-BaseB2	-6.27 [24.2]	0.00 [0.00]	-0.09 [17.7]	-3.03E4 [29.7]	-0.01 [50.0]	-0.18 [18.6]	-0.48 [4.0]	0.42 [3.4]
	B2FLC-BaseB2	-1.4 [5.4]	0.00 [0.00]	0.03 [5.9]	-1.4E4 [13.7]	0.00 [0.00]	0.16 [16.5]	1.74 [0.14]	1.29 [10.7]
	B2FLC-B2PLC	4.9 [24.8]	0.00 [0.00]	0.12 [28.6]	1.6E4 [22.7]	0.01 [100.0]	0.34 [43.0]	2.22 [19.0]	0.87 [7.0]
	XB2PLC-XBaseB2	-3.4 [5.6]	0.00 [0.00]	-0.1 [9.6]	3.0E5 [8.8]	-0.03 [1.2]	-0.10 [20.4]	-0.32 [12.4]	0.08 [2.7]
Dry Season (July)	A2PLC-BaseA2	-2.0 [36.7]	-0.37 [88.1]	0.07 [11.3]	-5.6E3 [45.9]	-3.1E-4 [42.7]	0.04 [4.8]	1.2 [9.5]	0.91 [12.2]
	A2FLC-BaseA2	0.13 [2.4]	-0.38 [90.5]	-0.4 [3.2]	6.0E2 [4.9]	6.2E-5 [8.4]	0.02 [2.4]	0.39 [3.1]	0.65 [8.7]
	A2FLC-A2PLC	2.08 [61.7]	-0.01 [20.0]	-0.10 [13.0]	6.2E3 [92.8]	3.7E-4 [88.6]	-0.02 [2.3]	-0.81 [5.9]	-0.26 [3.1]
	XA2PLC-XBaseA2	2.3 [4.4]	-0.01 [6.7]	0.04 [2.6]	-1.2E5 [3.9]	0.02 [2.2]	0.07 [10.1]	0.19 [6.4]]	0.02 [1.5]
	B2PLC-BaseB2	0.7 [16.7]	0.00 [0.00]	-1.05 [64.4]	2.3E3 [25.4]	1.6E-4 [27.5]	-0.01 [1.2]	-0.40 [3.0]	0.03 [0.4]
	B2FLC-BaseB2	0.51 [12.1]	0.00 [0.00]	-1.04 [63.8]	1.6E3 [17.7]	1.3E-4 [23.0]	-0.01 [1.2]	-0.37 [2.8]	-0.09 [1.1]
	B2FLC-B2PLC	-0.19 [3.9]	0.00 [0.00]	0.01 [1.7]	-7.0E2 [6.1]	-2.6E-5 [3.5]	0.00 [0.00]	0.03 [0.23]	-0.06 [0.71]
	XB2PLC-XBaseB2	-0.37 [0.7]	0.00 [0.00]	-0.04 [2.7]	-5.0E4 [1.7]	0.04 [3.9]	-0.02 [2.7]	-0.04 [1.3]	0.06 [3.9]

Note: *PLC-present-day landcover*
FLC-Future landcover
A2PLC-BaseA2/B2PLC-BaseB2: Changes due to climate changes and biogenic emissions under present-day landcover
A2FLC-BaseA2/B2FLC-BaseB2: Changes due to climate changes and biogenic emissions under future-day landcover
A2FLC-A2PLC/B2FLC-B2PLC: Changes between present-day landcover and future landcover scenarios
XA2PLC-XBaseA2/XB2PLC-Xbaseb2: Changes due to climate changes alone (without biogenic emissions)

LIST OF TRAINING/PUBLICATIONS

1. Regional Climate Model –PRECIS Workshop. *Participant.* Reading University, 1-4 August 2006.

2. Modelling of climate change and tropospheric chemistry in SEA. *PosterI Presentation.* Lancaster Environmental Centre, Lancaster University, June 2006.

3. Modelling of climate change and tropospheric chemistry in SEA. *Oral Presentation.* Climate Change Conference, University of Leeds, RGS-Institute of British Geographer , 29-30 March 2007.

4. Tropical composition: from boiler to freezer. Seminar Participant, University of Leicester, Royal Meteorological Society, 3 April 2007.

5. The past, the present and the future of global weather and climate modelling. Seminar Participant, University of Reading, Royal Meteorological Society, 25 April 2007.

6. Climate change and tropospheric chemistry system in SEA. *Oral Presentation,* Environmental Seminat, Lancaster University, 4 May 2007.

7. Modelling of climate change and tropospheric chemistry in SEA. *PosterII Presentation.* Lancaster Environmental Centre, Lancaster University, June 2007.

8. Atmospheric and land cover forcings effect on climate-tropospheric chemistry system in SEA. *PosterIII Presentation.* Helsingborg, Sweden, IGBP iLEAPS, 15-19 October, 2007.

9. Modelling of climate change and tropospheric chemistry in SEA. *PosterIV Presentation.* Faculty Science and Technology, Lancaster University, 18 December 2007.

10. Statistical Method- Scientific Research. Workshop Participant, Lancaster University, 16-17 April 2008.

11. Modelling of climate change and tropospheric chemistry in SEA. *PosterV Presentation.* Faculty Science and Technology, Lancaster University, 5 June 2008.

12. Landcover impacts on climate change in Southeast Asia. Oral Presentation. OP3 Workshop. Leeds University, 27-28 November 2008.

13. Air quality and Climate Change. Mini-Symposium. Participant. Leeds University, 3 December 2008.

14. Latex Course. Participant. Lancaster University, 16 February 2009.

15. Climate change impacts on biogenic emissions in SEA. *Poster VI Presentation.* Atmospheric Chemistry Forum, Royal Society of Chemistry (RSC). 2 April 2009.

16. The impacts of landcover and atmospheric forcings on regional climate changes in Southeast Asia. *PosterVII Presentation.* iLEAPS-GEWEX Parallel Science Conferences, Melbourne, Australia, 24-28 August 2008 (accepted).